THE DESIGN OF A DEEP WATER CATENARY RISER

VOLUME I

James R. Dingwall, B.Eng(Hons), Diploma

Thesis submitted for the Degree of Doctor of Philosophy

Department of Naval Architecture and Ocean Engineering

University of Glasgow

August 1997

Contents

		Page
Contents		i
List of Figures		ix
List of Tables		xxi
Acknowledgements		xxvi
Dedication		xxvii
Declaration		xxviii
Nomenclature		xxix
Summary		xxxii

VOLUME I

Chapter 1	Introduction	**1-1**
1.1	Offshore Development Trends	1-2
1.2	Deep Water Reserves	1-2
1.3	Deep Water Challenges	1-6
1.4	Project Objective	1-7
1.5	Concept Identification and Description	1-7
1.6	Structure of Thesis	1-11
	References	1-11
Chapter 2	The Selection of a Riser Profile and an Analysis of it's Geometric Characteristics	**2-1**
2.1	General Description	2-2
2.2	Geometric Properties of a Curve	2-3
	2.2.1 Introduction	2-3
	2.2.2 Elliptic Curve	2-5
	2.2.3 Parabolic Curve	2-8
	2.2.4 Catenary Curve	2-10
	2.2.5 Discussion	2-13
2.3	Catenary Line Analysis	2-15

2.3.1 Introduction 2-15
2.3.2 Governing Equations for an Inelastic Catenary Line 2-15
2.3.3 Catenary Characteristics 2-22
2.4 Mooring Characteristics 2-24
2.4.1 Introduction 2-24
2.4.2 Mooring Stiffness - In Plane 2-25
2.4.3 Mooring Stiffness - Out of Plane 2-34
References 2-34
Results (Figures 2.9 - 2.29, Tables 2.12 - 2.20)

Chapter 3 The Design of a Buoyancy Support System for a Catenary Riser **3-1**

3.1 General Description 3-2
3.2 Syntactic Foam Buoyancy 3-5
3.2.1 Introduction 3-5
3.2.2 Syntactic Composite Structure 3-5
3.2.3 Structural Arrangement of the Buoyancy System 3-8
3.2.4 Operational Analysis 3-9
3.2.5 Installation Analysis 3-15
3.3 Nitrogen Gas Buoyancy 3-18
3.3.1 Introduction 3-18
3.3.2 Structural Arrangement of the Buoyancy System 3-19
3.3.3 Operational Analysis 3-19
3.3.4 Installation Analysis 3-29
3.3.5 The Effects of Temperature on Compartment Buoyancy 3-31
3.3.6 The Loss of a Buoyancy Compartment 3-32
References 3-34
Spreadsheets (Spreadsheets 3.1 - 3.5)
Results (Figures 3.10 - 3.44, Table 3.7)

Chapter 4 Production Fluid Heat Loss and Insulation Analysis **4-1**

4.1 General Description 4-2
4.2 Crude Oil Characteristics 4-2

	4.2.1	Viscosity and Gravity	4-2
	4.2.2	Wax Deposition	4-4
	4.2.3	Emulsification	4-4
	4.2.4	Hydration	4-7
4.3	Existing Oil Transportation Methods by Pipeline		4-7
	4.3.1	Introduction	4-7
	4.3.2	Thermal Insulation	4-7
	4.3.3	External Heating	4-12
4.4	Fundamental Heat Transfer Theory for an Annular Section		4-12
	4.4.1	Introduction	4-12
	4.4.2	Heat Transfer Mechanisms	4-13
	4.4.3	Temperature Behaviour of a Pipeline Fluid Subject to Heat Loss	4-15
	4.4.4	The Calculation of a Heat Transfer Coefficient for a Fully Developed Pipe Flow	4-19
	4.4.5	The Calculation of a Heat Transfer Coefficient for an Ambient Fluid	4-22
	4.4.6	The Calculation of a Heat Transfer Coefficient for an Annular Gaseous Layer	4-25
4.5	Insulation Design for a Seabed Pipeline and Catenary Riser		4-27
	4.5.1	Introduction	4-27
	4.5.2	System Modelling	4-27
	4.5.3	Reservoir and Production Flow Data	4-30
	4.5.4	Sea Water Temperatures and Current Velocities	4-30
	4.5.5	Thermal Insulation Characteristics of the Existing Riser Arrangement	4-30
	4.5.6	Alternative Methods of Insulation	4-34
	4.5.7	The Effect of Oil Flow Rate on Temperature Decay	4-37
	4.5.8	The Effect of Oil Viscosity on Temperature Decay	4-38
	4.5.9	The Effect of High Temperatures on Syntactic Foam	4-38
4.6	Thermal Stress Analysis		4-39
	4.6.1	Introduction	4-39
	4.6.2	Thermal Stress Calculations	4-40
	References		4-43
	Spreadsheets (Spreadsheets 4.1 - 4.2)		
	Results (Figures 4.15 - 4.19, Tables 4.2 - 4.4)		

VOLUME II

Chapter 5 Static Installation and Environmental Loading Analysis **5-1**

5.1 General Description 5-2
5.1.1 Functional Loads During Installation 5-2
5.1.2 Functional and Environmental Loads Acting Together During Operation 5-2
5.2 Strength Criteria 5-3
5.2.1 Yielding of the Riser 5-3
5.2.2 Local Buckling of the Riser 5-4
5.3 Loads Exerted During Riser Installation 5-6
5.3.1 Introduction 5-6
5.3.2 Computer Modelling 5-9
5.3.3 Analysis Output 5-9
5.3.4 Lift Trajectory 5-12
5.3.5 Seabed Conditions 5-12
5.3.6 Environmental Loading 5-12
5.3.7 The Loading Characteristics of Catenary and Straight Line Lifting Trajectories 5-13
5.3.8 Failure Analysis 5-16
5.3.9 The Effects of Riser Geometry on Lifting Loads 5-17
5.4 Surface Connection Assembly 5-17
5.5 The Effects on the Riser of a Surface End Surge Displacement 5-29
5.5.1 Introduction 5-29
5.5.2 Computer Modelling 5-31
5.5.3 Analysis Output 5-31
5.5.4 Displacement Definitions 5-31
5.5.5 Seabed Conditions 5-32
5.5.6 Geometric and Loading Characteristics 5-32
5.6 The Effects of Subjecting the Riser to a Current Load 5-38
5.6.1 Introduction 5-38
5.6.2 Current Profiles 5-38
5.6.3 Riser Orientation within the Current Flow 5-46
5.6.4 Finite Element Model 5-46
5.6.5 Current Load Calculation 5-48

5.6.6 Surface and Seabed Boundary Conditions 5-62
5.6.7 Analysis Output 5-63
5.6.8 Discussion of the Results 5-64
5.6.9 The Drag Coefficient Effect 5-68
References 5-68
Results (Figures 5.34 - 5.123, Tables 5.36 - 5.121)

Chapter 6 A Dynamic Analysis to Determine the Characteristics of Natural Vibration **6-1**

6.1 General Description 6-2
6.2 The Formulation of the Dynamic Equation of Motion 6-2
6.2.1 Introduction 6-2
6.2.2 Assumptions 6-3
6.2.3 Equation of Motion 6-3
6.2.4 Finite Difference Numerical Computation 6-5
6.2.5 Applying the Equation of Motion to a Simple Vibration System 6-6
6.2.6 Applying the Equation of Motion to a Catenary Riser 6-9
6.3 Analysis Implementation Using a Computational Program 6-22
6.4 Analysis Input 6-26
6.5 Discussion of the Results 6-27
6.6 Analysis Verification 6-29
6.6.1 Introduction 6-29
6.6.2 Assumptions 6-29
6.6.3 Expressions for Natural Periods and Mode Shapes 6-29
6.6.4 A Comparison of Results 6-35
References 6-37
Results (Figures 6.10 - 6.39)

Chapter 7 Sub-Surface Buoy Conceptual Design Study **7-1**

7.1 General Description 7-2
7.2 Buoy Function 7-3
7.3 Influencing Design Factors 7-3
7.3.1 Maximum Watch Circle Diameter 7-3

	7.3.2 Depth of the Buoy Below the Surface	7-4
	7.3.3 Hydrostatic Pressure	7-7
	7.3.4 Installation	7-7
7.4	Lateral Displacement Stiffness	7-8
7.5	General Description of the Design Proposal	7-10
	7.5.1 Operating Parameters	7-10
	7.5.2 The Compartments	7-15
	7.5.3 Riser Connection Assembly	7-15
	7.5.4 Vertical Mooring Tethers	7-16
	7.5.5 Rigid Flowlines	7-17
	7.5.6 Flexible Risers	7-17
7.6	Calculation to Determine Size and Loading	7-17
	7.6.1 Introduction	7-17
	7.6.2 Buoy Size Calculation	7-18
	7.6.3 Mooring Tether Load Calculation	7-21
	7.6.4 Buoy Weight	7-21
	7.6.5 Loads Imposed by the Risers	7-22
7.7	An Overview of the Design Analysis Spreadsheet	7-22
	7.7.1 Introduction	7-22
	7.7.2 Spreadsheet Input	7-23
7.8	Discussion of the Results	7-24
	7.8.1 Introduction	7-24
	7.8.2 SSB Height and External Volume	7-24
	7.8.3 SSB Weight and Buoyancy	7-25
	7.8.4 Maximum Load Exerted Upon Each Mooring Tether	7-25
	7.8.5 Maximum Current Load Exerted Upon the SSB	7-25
	7.8.6 Component Weights	7-26
7.9	Riser Installation Using a Sub-Surface Buoy	7-26
	7.9.1 Introduction	7-26
	7.9.2 Installation Procedure	7-27
	References	7-31
	Spreadsheets (Spreadsheet 7.1)	
	Results (Figures 7.11 - 7.20, Tables 7.4 - 7.13)	

Chapter 8 Cost Evaluation **8-1**

8.1 General Description 8-2
8.2 Costs Not Included in the Analysis 8-2
8.3 Cost Data 8-2
8.3.1 Syntactic Foam 8-2
8.3.2 Steel - Material 8-3
8.3.3 Steel - Fabrication 8-3
8.3.4 Nitrogen Gas 8-3
8.3.5 Flexible Surface Joints 8-4
8.3.6 Vertical Mooring Tethers 8-4
8.3.7 Flexible Risers 8-4
8.3.8 A Summary of Cost Data Sources 8-4
8.4 Analysis Output 8-5
Spreadsheets (Spreadsheet 8.1)
Results (Figures 8.1 - 8.4)

Chapter 9 Preliminary Design Case Study **9-1**

9.1 General Description 9-2
9.2 Data Gathering 9-2
9.2.1 Field Production Particulars 9-2
9.2.2 Environmental Data 9-6
9.2.3 Engineering Data 9-8
9.2.4 Operational Data 9-8
9.3 Preliminary Design 9-9
9.3.1 Hydraulics 9-9
9.3.2 Geometry and Weight 9-11
9.3.3 Carrier Pipe Diameter 9-11
9.3.4 Flowline Insulation 9-12
9.3.5 Installation - Lift Sequence 9-13
9.3.6 Sub-Surface Buoy Sizing 9-15
References 9-15

Chapter 10 Conclusions **10-1**

10.1 Specific Conclusions of Thesis 10-2
10.1.1 Chapter 2 10-2
10.1.2 Chapter 3 10-3
10.1.3 Chapter 4 10-3
10.1.4 Chapter 5 10-4
10.1.5 Chapter 6 10-5
10.1.6 Chapter 7 10-6
10.1.7 Chapter 8 10-7
10.2 Recommended Future Work 10-7
References 10-9

Appendix A Horizontal Tensions for Catenary Lines with Vertical Offsets of 1400 and 1500 m **A-1**

A.1 Vertical Offset = 1400 m A-2
A.2 Vertical Offset = 1500 m A-3

Appendix B FORTRAN Program Lists for Catenary Riser Lift and Surface Displacement Calculations **B-2**

Appendix C FORTRAN Program Lists for a Catenary Riser Dynamic Analysis and Validation **C-3**

List of Figures

Chapter 1

Figure 1.1 Hydrocarbon Production Maximum Water Depths
Figure 1.2 West of Shetland Oil Fields
Figure 1.3 Riser Cross-Section
Figure 1.4 Catenary Riser Concept (Direct Connection)
Figure 1.5 Catenary Riser Concept (Hybrid Arrangement)

Chapter 2

Figure 2.1 Elliptic, Parabolic and Catenary Curves
Figure 2.2 Definition Diagram for the Catenary
Figure 2.3 Catenary Riser Mooring Behaviour in Surge
Figure 2.4 Catenary Riser Mooring Behaviour in Heave
Figure 2.5 Block Diagram for the Catenary Parameter Calculations
Figure 2.6 In-Plane Catenary Riser Stiffness
Figure 2.7 Out-of-Plane Catenary Riser Stiffness
Figure 2.8 Out-of-Plane Stiffness

Figure 2.9 Bending Moment/Stress Distribution (a = 1000 m)
Figure 2.10 Bending Moment/Stress Distribution (a = 1500 m)
Figure 2.11 Bending Moment/Stress Distribution (a = 2000 m)
Figure 2.12 Elliptic, Parabolic and Catenary Curves (a = 1000 m)
Figure 2.13 Elliptic, Parabolic and Catenary Curves (a = 1500 m)
Figure 2.14 Elliptic, Parabolic and Catenary Curves (a = 2000 m)
Figure 2.15 Catenary Axial/Bending/Total Stress Distributions (a = 1000 m, w = 100 N/m)
Figure 2.16 Catenary Axial/Bending/Total Stress Distributions (a = 1000 m, w = 1000 N/m)
Figure 2.17 Catenary Axial/Bending/Total Stress Distributions (a = 1000 m, w = 2000 N/m)
Figure 2.18 Catenary Axial/Bending/Total Stress Distributions (a = 1500 m, w = 100 N/m)
Figure 2.19 Catenary Axial/Bending/Total Stress Distributions (a = 1500 m, w = 1000 N/m)

Figure 2.20 Catenary Axial/Bending/Total Stress Distributions (a = 1500 m, w = 2000 N/m)
Figure 2.21 Catenary Axial/Bending/Total Stress Distributions (a = 2000 m, w = 100 N/m)
Figure 2.22 Catenary Axial/Bending/Total Stress Distributions (a = 2000 m, w = 1000 N/m)
Figure 2.23 Catenary Axial/Bending/Total Stress Distributions (a = 2000 m, w = 2000 N/m)
Figure 2.24 Horizontal/Vertical/Axial/Bending Load vs Vertical Offset (a = 1000 m)
Figure 2.25 Horizontal/Vertical/Axial/Bending Load vs Vertical Offset (a = 1500 m)
Figure 2.26 Horizontal/Vertical/Axial/Bending Load vs Vertical Offset (a = 2000 m)
Figure 2.27 Surge Disturbance Profiles/Stiffness (a = 1000 m)
Figure 2.28 Surge Disturbance Profiles/Stiffness (a = 1500 m)
Figure 2.29 Surge Disturbance Profiles/Stiffness (a = 2000 m)

Chapter 3

Figure 3.1 Definition of Buoyancy
Figure 3.2 Characteristics of Syntactic Foam
Figure 3.3 Location of Flowlines within the Syntactic Foam Filled Carrier Pipe
Figure 3.4 Cut-away View of the Syntactic Foam Filled Riser
Figure 3.5 Cut-away View of the Syntactic Foam Filled Riser with Ballast Line
Figure 3.6 Location of Flowlines within the Buoyancy Gas Filled Carrier Pipe
Figure 3.7 Cut-away View of the Buoyancy Gas Filled Riser
Figure 3.8 The Layout of Buoyancy Gas Compartments within the Riser
Figure 3.9 Compartmental Ballasting for a Gas Buoyancy Riser

Figure 3.10 Unit Weight and Buoyancy/Submerged Unit Weight (Operational)
Figure 3.11 Submerged Unit Weight - No Ballast Line/With Ballast Line (Installation)
Figure 3.12 Pressure Differences acting Across the Carrier Pipe Wall/Maximum Pressure Difference Across the Carrier Pipe Wall

Figure 3.13 The Influence of C.P. Diameter on Circumferential Stress/Maximum Circumferential Stress
Figure 3.14 Compartmental Unit Weight and Buoyancy/Ballasted Unit Weight and Buoyancy (Operational) - 3 Compartments
Figure 3.15 Compartmental Submerged Unit Weight/Ballasted Submerged Unit Weight (Operational) - 3 Compartments
Figure 3.16 Compartmental Unit Weight and Buoyancy/Ballasted Unit Weight and Buoyancy (Operational) - 4 Compartments
Figure 3.17 Compartmental Submerged Unit Weight/Ballasted Submerged Unit Weight (Operational) - 4 Compartments
Figure 3.18 Compartmental Unit Weight and Buoyancy/Ballasted Unit Weight and Buoyancy (Operational) - 5 Compartments
Figure 3.19 Compartmental Submerged Unit Weight/Ballasted Submerged Unit Weight (Operational) - 5 Compartments
Figure 3.20 Compartmental Unit Weight and Buoyancy/Ballasted Unit Weight and Buoyancy (Operational) - 6 Compartments
Figure 3.21 Compartmental Submerged Unit Weight/Ballasted Submerged Unit Weight (Operational) - 6 Compartments
Figure 3.22 Compartmental Unit Weight and Buoyancy/Ballasted Unit Weight and Buoyancy (Operational) - 10 Compartments
Figure 3.23 Compartmental Submerged Unit Weight/Ballasted Submerged Unit Weight (Operational) - 10 Compartments
Figure 3.24 Compartmental Unit Weight and Buoyancy/Ballasted Unit Weight and Buoyancy (Operational) - 15 Compartments
Figure 3.25 Compartmental Submerged Unit Weight/Ballasted Submerged Unit Weight (Operational) - 15 Compartments
Figure 3.26 Riser Installation - Lift Sequence (3 Compartments)
Figure 3.27 Compartmental Submerged Unit Weight (Installation) - 3 Compartments
Figure 3.28 Riser Installation - Lift Sequence (4 Compartments)
Figure 3.29 Compartmental Submerged Unit Weight (Installation) - 4 Compartments
Figure 3.30 Riser Installation - Lift Sequence (5 Compartments)
Figure 3.31 Compartmental Submerged Unit Weight (Installation) - 5 Compartments
Figure 3.32 Riser Installation - Lift Sequence (6 Compartments)
Figure 3.33 Compartmental Submerged Unit Weight (Installation) - 6 Compartments
Figure 3.34 Riser Installation - Lift Sequence (10 Compartments)

Figure 3.35 Compartmental Submerged Unit Weight (Installation) - 10 Compartments
Figure 3.36 Riser Installation - Lift Sequence (15 Compartments)
Figure 3.37 Compartmental Submerged Unit Weight (Installation) - 15 Compartments
Figure 3.38 The Effects of Gas Temperature on Submerged Unit Weight
Figure 3.39 The Effects of Losing an Individual Compartment/Cumulative Compartment Loss - 3 Compartments
Figure 3.40 The Effects of Losing an Individual Compartment/Cumulative Compartment Loss - 4 Compartments
Figure 3.41 The Effects of Losing an Individual Compartment/Cumulative Compartment Loss - 5 Compartments
Figure 3.42 The Effects of Losing an Individual Compartment/Cumulative Compartment Loss - 6 Compartments
Figure 3.43 The Effects of Losing an Individual Compartment/Cumulative Compartment Loss - 10 Compartments
Figure 3.44 The Effects of Losing an Individual Compartment/Cumulative Compartment Loss - 15 Compartments

Chapter 4

Figure 4.1 Catenary Riser and Seabed Pipeline
Figure 4.2 Crude Oil Viscosity
Figure 4.3 Hydrate Stability Boundary Curves
Figure 4.4 Current Methods of Insulating a Pipeline or Riser
Figure 4.5 An Insulated Flowline
Figure 4.6 Fluid Heat Balance
Figure 4.7 Forced Convection - Normal to the Riser
Figure 4.8 Beckman's Curves for Free Convection Across a Layer of Fluid Between Two Concentric Cylinders
Figure 4.9 Catenary Riser Cross-Section
Figure 4.10 Seabed Pipeline Cross-Section
Figure 4.11 Thermal Model Longitudinal Sections
Figure 4.12 Catenary Riser Cross-Section
Figure 4.13 Thermal Model Longitudinal Section
Figure 4.14 Thermal Stress Model

Figure 4.15 Seabed Pipeline/Catenary Riser Oil Temperature Profile (N2/SF)
Figure 4.16 Seabed Pipeline/Catenary Riser Oil Temperature Profile (HSM Slurry)
Figure 4.17 Seabed Pipeline/Catenary Riser Oil Temperature Profile (SF Sleeve)
Figure 4.18 The Effect of S-Foam Sleeve Thickness/Flow Rate on Oil Temperature
Figure 4.19 Thermal Stressing of the Seabed Pipeline/Catenary Riser

Chapter 5

Figure 5.1 Collapse Form of a Tube Under Pure Bending Conditions
Figure 5.2 Catenary Riser Installation (FPSO)
Figure 5.3 Riser Lift Parameter Definitions
Figure 5.4 Block Calculation Diagram for the Catenary Riser Lift Sequence
Figure 5.5 Flex-Joint
Figure 5.6 Auger TLP Catenary Riser Flex-Joint Unit
Figure 5.7 Auger TLP Production System
Figure 5.8 Upper End of the Riser (Cut-Away View)
Figure 5.9 Surface Connection Assembly
Figure 5.10 Surface Connection Assembly (Cut-Away View)
Figure 5.11 Surface Connection Assembly under Rotation
Figure 5.12 Surface Connection Assembly (Top View)
Figure 5.13 Surge Displacements for Two Production Concepts
Figure 5.14 Drift Displacement Definitions
Figure 5.15 Rotational Definitions
Figure 5.16 Current Profiles Obtained From the Continental Slope Experiment (CONSLEX)
Figure 5.17 CONSLEX Mooring Sites
Figure 5.18 Deep Water Current Profiles - Offshore Brazil
Figure 5.19 Assumed Profile for a Deep Water Drilling Riser Analysis
Figure 5.20 Assumed Current Profile
Figure 5.21 Current Directional Definitions
Figure 5.22 Kirchoff Thin Beam Element in 2-Dimensions
Figure 5.23 Incremental/Iterative Nonlinear Solution Procedure
Figure 5.24 An Example of a LUSAS Input Data File
Figure 5.25 Block Diagram for the LUSAS Input Data File Spreadsheet

Figure 5.26 An Inclined Cylinder Within a Fluid Flow
Figure 5.27 Current Forces Acting Upon a Riser Element
Figure 5.28 Drag Coefficient Versus Reynolds Number for Normal and Tangential Flow
Figure 5.29 Variation of Drag Coefficient With Reynolds Number for a Circular Cylinder at Several Angles of Inclination
Figure 5.30 Typical Distribution of Marine Growth
Figure 5.32 Drag Coefficient Versus Reynolds Number for Normal Flow
Figure 5.33 Flow Around a Cylinder

Figure 5.34 Riser Installation - Lift Sequence Using a Catenary Curve Lift Trajectory (a = 1500 m)
Figure 5.35 Lift Cable Horizontal Load/Vertical Load/Axial Load/Axial Stress at the Top End of the Riser/Axial Stress at the Seabed/Bending Stress Distribution along the Riser

Figure 5.37 Riser Installation - Lift Sequence Using a Straight Line Lift Trajectory (a = 1500 m)
Figure 5.38 Lift Cable Horizontal Load/Vertical Load/Axial Load/Axial Stress at the Top End of the Riser/Axial Stress at the Seabed/Bending Stress Distribution along the Riser

Figure 5.40 Maximum Bending Stress (Seabed)

Figure 5.41 Riser Installation - Lift Sequence (a = 1000 m)
Figure 5.42 Lift Cable Horizontal Load/Vertical Load/Axial Load/Axial Stress at the Top End of the Riser/Axial Stress at the Seabed/Bending Stress Distribution along the Riser

Figure 5.44 Riser Installation - Lift Sequence (a = 2000 m)
Figure 5.45 Lift Cable Horizontal Load/Vertical Load/Axial Load/Axial Stress at the Top End of the Riser/Axial Stress at the Seabed/Bending Stress Distribution along the Riser

Figure 5.47 Surge Displacement (a = 1000 m, b = 1500 m)
Figure 5.49 Surge Displacement (a = 1500 m, b = 1500 m)
Figure 5.51 Surge Displacement (a = 2000 m, b = 1500 m)
Figure 5.53 Surge Displacement (a = 1000 m, b = 1400 m)
Figure 5.55 Surge Displacement (a = 1500 m, b = 1400 m)

Figure 5.57 Surge Displacement (a = 2000 m, b = 1400 m)

Figure 5.59 Current Response (a = 1000 m, w = 100 N/m)
Figure 5.60 Riser Deflection Profiles for a Convex Current
Figure 5.61 Riser Deflection Profiles for a Concave Current
Figure 5.63 Axial Stress Distributions/Surface Forces for a Convex Current
Figure 5.64 Axial Stress Distributions/Surface Forces for a Concave Current

Figure 5.66 Current Response (a = 1000 m, w = 1000 N/m)
Figure 5.67 Riser Deflection Profiles for a Convex Current
Figure 5.68 Riser Deflection Profiles for a Concave Current
Figure 5.70 Axial Stress Distributions/Surface Forces for a Convex Current
Figure 5.71 Axial Stress Distributions/Surface Forces for a Concave Current

Figure 5.73 Current Response (a = 1000 m, w = 2000 N/m)
Figure 5.74 Riser Deflection Profiles for a Convex Current
Figure 5.75 Riser Deflection Profiles for a Concave Current
Figure 5.77 Axial Stress Distributions/Surface Forces for a Convex Current
Figure 5.78 Axial Stress Distributions/Surface Forces for a Concave Current

Figure 5.80 Current Response (a = 1500 m, w = 100 N/m)
Figure 5.81 Riser Deflection Profiles for a Convex Current
Figure 5.82 Riser Deflection Profiles for a Concave Current
Figure 5.84 Axial Stress Distributions/Surface Forces for a Convex Current
Figure 5.85 Axial Stress Distributions/Surface Forces for a Concave Current

Figure 5.87 Current Response (a = 1500 m, w = 1000 N/m)
Figure 5.88 Riser Deflection Profiles for a Convex Current
Figure 5.89 Riser Deflection Profiles for a Concave Current
Figure 5.91 Axial Stress Distributions/Surface Forces for a Convex Current
Figure 5.92 Axial Stress Distributions/Surface Forces for a Concave Current

Figure 5.94 Current Response (a = 1500 m, w = 2000 N/m)
Figure 5.95 Riser Deflection Profiles for a Convex Current
Figure 5.96 Riser Deflection Profiles for a Concave Current
Figure 5.98 Axial Stress Distributions/Surface Forces for a Convex Current
Figure 5.99 Axial Stress Distributions/Surface Forces for a Concave Current

Figure 5.101 Current Response (a = 2000 m, w = 100 N/m)

Figure 5.102 Riser Deflection Profiles for a Convex Current
Figure 5.103 Riser Deflection Profiles for a Concave Current
Figure 5.105 Axial Stress Distributions/Surface Forces for a Convex Current
Figure 5.106 Axial Stress Distributions/Surface Forces for a Concave Current

Figure 5.108 Current Response (a = 2000 m, w = 1000 N/m)
Figure 5.109 Riser Deflection Profiles for a Convex Current
Figure 5.110 Riser Deflection Profiles for a Concave Current
Figure 5.112 Axial Stress Distributions/Surface Forces for a Convex Current
Figure 5.113 Axial Stress Distributions/Surface Forces for a Concave Current

Figure 5.115 Current Response (a = 2000 m, w = 2000 N/m)
Figure 5.116 Riser Deflection Profiles for a Convex Current
Figure 5.117 Riser Deflection Profiles for a Concave Current
Figure 5.119 Axial Stress Distributions/Surface Forces for a Convex Current
Figure 5.120 Axial Stress Distributions/Surface Forces for a Concave Current

Figure 5.122 The Effect of Drag Coefficient on the Deflection Profile
Figure 5.123 The Effect of Drag Coefficient on the Maximum Bending Stress

Chapter 6

Figure 6.1 Centreline of Rod
Figure 6.2 Finite Difference Method
Figure 6.3 A Stretched String in Lateral Vibration
Figure 6.4 Dynamic Model
Figure 6.5 Dynamic Example
Figure 6.6 Block Diagram of the Vibration Analysis FORTRAN Computer Program
Figure 6.7 Definition Diagram for a Profile of an Inclined Cable
Figure 6.8 Symmetric and Antisymmetric In-Plane Cable Modes
Figure 6.9 Mode Shapes of First Symmetric In-Plane Cable Mode

Figure 6.10 The Effect of Diameter on the Riser's Effective Unit Mass/ Horizontal Tension (Syntactic Foam Buoyancy)
Figure 6.11 The Effect of Diameter on the Riser's Effective Unit Mass/ Horizontal Tension (Nitrogen Gas Buoyancy)

Figure 6.12 Natural Period Spectrum - Syntactic Foam Buoyancy (a = 1000 m, D = 1.10 m)
Figure 6.13 Natural Period Spectrum - Syntactic Foam Buoyancy (a = 1000 m, D = 1.20 m)
Figure 6.14 Natural Period Spectrum - Syntactic Foam Buoyancy (a = 1000 m, D = 1.30 m)
Figure 6.15 Natural Period Spectrum - Nitrogen Gas Buoyancy (a = 1000 m, D = 1.0 m)
Figure 6.16 Natural Period Spectrum - Nitrogen Gas Buoyancy (a = 1000 m, D = 1.10 m)
Figure 6.17 Mode Shapes 1 to 6 (a =1000 m)

Figure 6.18 Natural Period Spectrum - Syntactic Foam Buoyancy (a = 1500 m, D = 1.10 m)
Figure 6.19 Natural Period Spectrum - Syntactic Foam Buoyancy (a = 1500 m, D = 1.20 m)
Figure 6.20 Natural Period Spectrum - Syntactic Foam Buoyancy (a = 1500 m, D = 1.30 m)
Figure 6.21 Natural Period Spectrum - Nitrogen Gas Buoyancy (a = 1500 m, D = 1.0 m)
Figure 6.22 Natural Period Spectrum - Nitrogen Gas Buoyancy (a = 1500 m, D = 1.10 m)
Figure 6.23 Mode Shapes 1 to 6 (a =1500 m)

Figure 6.24 Natural Period Spectrum - Syntactic Foam Buoyancy (a = 2000 m, D = 1.10 m)
Figure 6.25 Natural Period Spectrum - Syntactic Foam Buoyancy (a = 2000 m, D = 1.20 m)
Figure 6.26 Natural Period Spectrum - Syntactic Foam Buoyancy (a = 2000 m, D = 1.30 m)
Figure 6.27 Natural Period Spectrum - Nitrogen Gas Buoyancy (a = 2000 m, D = 1.0 m)
Figure 6.28 Natural Period Spectrum - Nitrogen Gas Buoyancy (a = 2000 m, D = 1.10 m)
Figure 6.29 Mode Shapes 1 to 6 (a =2000 m)

Figure 6.30 The Effect of Riser Diameter on the Natural Period of Vibration Syntactic Foam Buoyancy (a = 1000 m)

Figure 6.31 The Effect of Riser Diameter on the Natural Period of Vibration Nitrogen Gas Buoyancy (a = 1000 m)
Figure 6.32 The Effect of Riser Diameter on the Natural Period of Vibration Syntactic Foam Buoyancy (a = 1500 m)
Figure 6.33 The Effect of Riser Diameter on the Natural Period of Vibration Nitrogen Gas Buoyancy (a = 1500 m)
Figure 6.34 The Effect of Riser Diameter on the Natural Period of Vibration Syntactic Foam Buoyancy (a = 2000 m)
Figure 6.35 The Effect of Riser Diameter on the Natural Period of Vibration Nitrogen Gas Buoyancy (a = 2000 m)
Figure 6.36 The Natural Frequency of a Suspended Cable Using Blevin's Analytical Approach
Figure 6.37 The Natural Period of a Suspended Cable Using Blevin's Analytical Approach
Figure 6.38 Antisymmetric and Symmetric Mode Shapes 1 to 8
Figure 6.39 A Comparison of Results

Chapter 7

Figure 7.1 Relative Positioning of Buoy and FPSO Watch Circles
Figure 7.2 Buoy Shape: Long and Slender or Short and Fat
Figure 7.3 Tether Load Components
Figure 7.4 Sub-Surface Buoy (Cross-Sectional View)
Figure 7.5 Sub-Surface Buoy (Top View)
Figure 7.6 Sub-Surface Buoy (Top View)
Figure 7.7 Sub-Surface Buoy (Cut-Away Top View)
Figure 7.8 Sub-Surface Buoy Displacement
Figure 7.9 Catenary Riser Installation Using a Sub-Surface Buoy
Figure 7.10 Sub-Surface Buoy (Tow-Out Condition)
Figure 7.11 Horizontal/Vertical Riser Loads Exerted Upon the Sub-Surface Buoy (w = 100 N/m)
Figure 7.12 Horizontal/Vertical Riser Loads Exerted Upon the Sub-Surface Buoy (w = 500 N/m)
Figure 7.13 Horizontal/Vertical Riser Loads Exerted Upon the Sub-Surface Buoy (w = 1000 N/m)

Figure 7.14 Horizontal/Vertical Riser Loads Exerted Upon the Sub-Surface Buoy (w = 1500 N/m)
Figure 7.15 Horizontal/Vertical Riser Loads Exerted Upon the Sub-Surface Buoy (w = 2000 N/m)
Figure 7.16 Maximum Load Exerted Upon Each Mooring Tether/Maximum Current Load Exerted Upon the Sub-Surface Buoy (w = 100 N/m)
Figure 7.17 Maximum Load Exerted Upon Each Mooring Tether/Maximum Current Load Exerted Upon the Sub-Surface Buoy (w = 500 N/m)
Figure 7.18 Maximum Load Exerted Upon Each Mooring Tether/Maximum Current Load Exerted Upon the Sub-Surface Buoy (w = 1000 N/m)
Figure 7.19 Maximum Load Exerted Upon Each Mooring Tether/Maximum Current Load Exerted Upon the Sub-Surface Buoy (w = 1500 N/m)
Figure 7.20 Maximum Load Exerted Upon Each Mooring Tether/Maximum Current Load Exerted Upon the Sub-Surface Buoy (w = 2000 N/m)

Chapter 8

Figure 8.1 Cost Breakdown of the Sub-Surface Buoy
Figure 8.2 Cost Breakdown of the Riser with Syntactic Foam Buoyancy/ Nitrogen Gas Buoyancy
Figure 8.3 Assembly Cost Breakdown of the Production System (Syntactic Foam/Nitrogen Gas - Riser)
Figure 8.4 Component Cost Breakdown of the Production System (Syntactic Foam/Nitrogen Gas - Riser)

Chapter 9

Figure 9.1 Riser Design Process
Figure 9.2 Deep Water Wellhead Arrangement
Figure 9.3 Catenary Riser and Seabed Pipeline Arrangement
Figure 9.4 Riser Lift Using a Pipe Laying Vessel

Chapter 10

Figure 10.1 Schematic of a Closed Power System
Figure 10.2 Thermal Energy Conversion
Figure 10.3 Cutaway View of an OTEC Plant

List of Tables

Chapter 1

Table 1.1 Potential Deep Water Hydrocarbon Production Areas

Chapter 2

Table 2.1 Cross-Sectional Dimensions

Table 2.2 Bending Moments and Stresses at the Seabed and Surface for a Range of Elliptic Curves

Table 2.3 Elliptic Quadrant Lengths and Surface Slopes

Table 2.4 Bending Moments and Stresses at the Seabed and Surface for a Range of Parabolic Curves

Table 2.5 Parabolic Quadrant Lengths and Surface Slopes

Table 2.6 Catenary Equation Constant Values

Table 2.7 Bending Moments and Stresses at the Seabed and Surface for a Range of Catenary Curves

Table 2.8 Catenary Quadrant Lengths and Surface Slopes

Table 2.9 Surge Stiffnesses for a Horizontal Offset of 1500 m and a Vertical Offset of 1400 m

Table 2.10 Surge Stiffnesses for a Horizontal Offset of 1500 m and a Submerged Weight of 2000 N/m

Table 2.11 Surge Stiffnesses for a Vertical Offset of 1400 m and a Submerged Weight of 2000 N/m

Table 2.12 Bending and Axial Loading at the Surface/Seabed End (w = 100 N/m)

Table 2.13 Bending and Axial Loading at the Surface/Seabed End (w = 500 N/m)

Table 2.14 Bending and Axial Loading at the Surface/Seabed End (w = 1000 N/m)

Table 2.15 Bending and Axial Loading at the Surface/Seabed End (w = 1500 N/m)

Table 2.16 Bending and Axial Loading at the Surface/Seabed End (w = 2000 N/m)

Table 2.17 Shear Loading at the Surface End (maximum)

Table 2.18 Riser Stiffness in Surge (Vertical Offset = 1400 m)
Table 2.19 Riser Stiffness in Surge (Vertical Offset = 1500 m)
Table 2.20 Riser Stiffness in Heave (Vertical Offset = 1500 m)

Chapter 3

Table 3.1 Syntactic Foam Properties
Table 3.2 Submerged Unit Weights for a Selection of Riser Operating Conditions
Table 3.3 Submerged Unit Weights for a Selection of Riser Installation Conditions (No Ballast Line)
Table 3.4 Submerged Unit Weights for a Selection of Riser Installation Conditions (With Ballast Line)
Table 3.5 Buoyancy Gas Pressures for a Riser in 1500 m of Water
Table 3.6 The Effects of an Individual Compartment Loss
Table 3.7 Compartmental Ballast (Steel Rods)

Chapter 4

Table 4.1 The Insulating Capabilities of Various Materials
Table 4.2 Radial Temperature Distributions (N2/SF)
Table 4.3 Radial Temperature Distributions (HSM Slurry)
Table 4.4 Radial Temperature Distributions (SF Sleeve)

Chapter 5

Table 5.1 Buckling Strengths for Various Riser Conditions
Table 5.2 Completed CDTM Projects
Table 5.3 Horizontal Cable Loads for a Catenary Curve and Straight Line Lift Trajectory
Table 5.4 Vertical Cable Loads for a Catenary Curve and Straight Line Lift Trajectory
Table 5.5 Top End Axial Stresses for a Catenary Curve and Straight Line Lift Trajectory

Table 5.6 Examples of Catenary Riser Flex-Joint Installations in Current Usage
Table 5.7 Flex-Joint Design Criteria
Table 5.8 Calculated Rotations for the FPSO System
Table 5.9 Calculated Rotations for the Sub-Surface Buoy System
Table 5.10 Calculated Axial Loads for the FPSO System
Table 5.11 Calculated Axial Loads for the Sub-Surface Buoy System
Table 5.12 NACA Empirical Results Applied to an Inclined Cylinder Exposed to 0.4 m/s Incident Flow
Table 5.13 Limiting Current Velocities for a = 1000 m
Table 5.14 Limiting Current Velocities for a = 1500 m
Table 5.15 Limiting Current Velocities for a = 2000 m

Table 5.36 Bending Stress at the Seabed - Catenary Curve Lift Trajectory (a = 1500 m)
Table 5.39 Bending Stress at the Seabed - Straight Line Lift Trajectory (a = 1500 m)
Table 5.43 Bending Stress at the Seabed - Catenary Curve Lift Trajectory (a = 1000 m)
Table 5.46 Bending Stress at the Seabed - Catenary Curve Lift Trajectory (a = 2000 m)

Table 5.48 Bending Stress at the Seabed - Surge Displacement (a = 1000 m, b = 1500 m)
Table 5.50 Bending Stress at the Seabed - Surge Displacement (a = 1500 m, b = 1500 m)
Table 5.52 Bending Stress at the Seabed - Surge Displacement (a = 2000 m, b = 1500 m)
Table 5.54 Bending Stress at the Seabed - Surge Displacement (a = 1000 m, b = 1400 m)
Table 5.56 Bending Stress at the Seabed - Surge Displacement (a = 1500 m, b = 1400 m)
Table 5.58 Bending Stress at the Seabed - Surge Displacement (a = 2000 m, b = 1400 m)

Table 5.62 Maximum Stress Conditions under Current Loading (a = 1000 m, w = 100 N/m)
Table 5.65 Surface Deflection Angles under Current Loading (a = 1000 m, w = 100 N/m)

Table 5.69 Maximum Stress Conditions under Current Loading (a = 1000 m, w = 1000 N/m)
Table 5.72 Surface Deflection Angles under Current Loading (a = 1000 m, w = 1000 N/m)
Table 5.76 Maximum Stress Conditions under Current Loading (a = 1000 m, w = 2000 N/m)
Table 5.79 Surface Deflection Angles under Current Loading (a = 1000 m, w = 2000 N/m)
Table 5.83 Maximum Stress Conditions under Current Loading (a = 1500 m, w = 100 N/m)
Table 5.86 Surface Deflection Angles under Current Loading (a = 1500 m, w = 100 N/m)
Table 5.90 Maximum Stress Conditions under Current Loading (a = 1500 m, w = 1000 N/m)
Table 5.93 Surface Deflection Angles under Current Loading (a = 1500 m, w = 1000 N/m)
Table 5.97 Maximum Stress Conditions under Current Loading (a = 1500 m, w = 2000 N/m)
Table 5.100 Surface Deflection Angles under Current Loading (a = 1500 m, w = 2000 N/m)
Table 5.104 Maximum Stress Conditions under Current Loading (a = 2000 m, w = 100 N/m)
Table 5.107 Surface Deflection Angles under Current Loading (a = 2000 m, w = 100 N/m)
Table 5.111 Maximum Stress Conditions under Current Loading (a = 2000 m, w = 1000 N/m)
Table 5.114 Surface Deflection Angles under Current Loading (a = 2000 m, w = 1000 N/m)
Table 5.118 Maximum Stress Conditions under Current Loading (a = 2000 m, w = 2000 N/m)
Table 5.121 Surface Deflection Angles under Current Loading (a = 2000 m, w = 2000 N/m)

Chapter 6

Table 6.1 Properties Influencing Vibrational Performance

Table 6.2 Antisymmetric and Symmetric Natural Periods

Chapter 7

Table 7.1 Wave Particle Acceleration versus Depth for a Range of Wave Periods

Table 7.2 The Performance of Fibre Rope from the VIKING 7 STANDARD RANGE

Table 7.3 The SSB's Constituent Component Weights

Table 7.4 Sub-Surface Buoy: Height and External Volume (w = 100 N/m)

Table 7.5 Sub-Surface Buoy: Height and External Volume (w = 500 N/m)

Table 7.6 Sub-Surface Buoy: Height and External Volume (w = 1000 N/m)

Table 7.7 Sub-Surface Buoy: Height and External Volume (w = 1500 N/m)

Table 7.8 Sub-Surface Buoy: Height and External Volume (w = 2000 N/m)

Table 7.9 Sub-Surface Buoy: Weight and Buoyancy (w = 100 N/m)

Table 7.10 Sub-Surface Buoy: Weight and Buoyancy (w = 500 N/m)

Table 7.11 Sub-Surface Buoy: Weight and Buoyancy (w = 1000 N/m)

Table 7.12 Sub-Surface Buoy: Weight and Buoyancy (w = 1500 N/m)

Table 7.13 Sub-Surface Buoy: Weight and Buoyancy (w = 2000 N/m)

Chapter 8

Table 8.1 Cost Data Sources

Acknowledgements

The author is grateful for all the advice, help and support obtained from both the Department of Naval Architecture and Ocean Engineering at the University of Glasgow and BAeSEMA in Glasgow during the research study presented in this thesis.

The author is particularly indebted to:

Professor A. Incecik	for supervising this research and for his assistance, encouragement and support.
Mr N.S. Miller	for all his work and ideas which helped to initiate this research project.
Dr D. Barrie	for all his advice and for being my industrial supervisor at BAeSEMA.
Mr I.C. Smith	for securing BAeSEMA sponsorship for this research.
Mr A. Watters	for all the information and assistance that was provided during the dynamic analysis phase of the research.

Finally, the financial support from the EPSRC (Engineering and Physical Science Research Council) and BAeSEMA is gratefully acknowledged.

Dedicated to my Parents

Declaration

Except where reference is made to the work of others,
this thesis is believed to be original.

Nomenclature

A	Dynamic (or System) Matrix
a	Horizontal Surface Offset
a_y	Vertical Wave Particle Acceleration
B	Buoyancy Force Exerted Upon the Buoy
b	Vertical Offset (Sea Depth)
C_D	Drag Coefficient
C_{DN}	Normal Drag Coefficient
C_{DT}	Tangential Drag Coefficient
C_M	Inertia Coefficient
c	Equation Constant
c_p	Specific Heat Capacity
D	Carrier Pipe Diameter
D	Buoy Diameter
d	Maximum Cable Sag
ds	Elemental Length
E	Elasticity Modulus
F′	Resultant Force on the Cross Section
f	Natural Frequency
f	Friction Factor
g	Gravitational Acceleration
Gr	Grashof Number
H	Horizontal Tension (Horizontal Load Component)
H	Buoy Height
H_w	Wave Height
h	Convective Heat Transfer Coefficient
h_c	Vertical Height of a Buoyancy Compartment
I	Second Moment of Area
I	Unit Matrix
k	Lateral Stiffness
k	Thermal Conductivity
k	Wave Number
L	Total Riser Length
L	Mooring Tether Length
L_c	Buoyancy Compartment Length
M	Bending Moment
m	Mass per Unit Length

m_s	Structural Unit Mass
m_{am}	Added Unit Mass
$\dot{m}$	Fluid Mass Flow Rate
Nu	Nusselt Number
P	Pressure
Pr	Prandtl Number
Q	Rate of Heat Loss
q	Applied Force per Unit Length
q	Rate of Heat Loss per Unit Length
R	Specific Gas Constant
Re	Reynolds Number
r	Profile Radius
r	Position Vector
r	Pipe Surface Radius
1/R	Profile Curvature
s	Distance Along Riser From Origin (usually seabed end)
SF	Shear Force
T	Axial Tension
T	Temperature
Tp	Natural Period of Vibration
Tp	Wave Period
T_T	Total Mooring Tether Load
t	Time
t	Wall Thickness
U	Overall Heat Transfer Coefficient
U	Fluid Velocity
$\dot{U}$	Fluid Acceleration
U_C	Constant Current Velocity (with respect to depth)
U_S	Surface Current Velocity
u_m	Mean Fluid Velocity
V	Vertical Load Component
W_B	Weight (in air) of the Buoy
w	Submerged Unit Length
X_{max}	Maximum Allowable Displacement
x	Horizontal Distance
$\dot{x}$	Horizontal Velocity
$\ddot{x}$	Horizontal Acceleration
y	Vertical Distance

$\dot{y}$	Vertical Velocity
$\ddot{y}$	Vertical Acceleration
y_c	Vertical Distance Up the Buoyancy Compartment
α	Coefficient of Thermal Expansion (solid)
α	Cable Sag Parameter
α	Change in Riser Profile Angle at the Surface (from the horizontal)
β	Coefficient of Thermal Expansion (fluid)
β	Non-Dimensional Natural Frequency Parameter
ε	Axial Strain
φ	Profile Slope (measured from the vertical)
η	Permissible Usage Factor
λ	Eigenvalue
λ	Wave Length
μ	Dynamic Viscosity
θ	Profile Slope (measured from the horizontal)
ρ	Density
ρ_{sw}	Sea Water Density
σ	Stress
υ	Kinematic Viscosity
ω	Natural Frequency (circular)
∇	Volume of Fluid Displaced

Summary

Deep water production more than anything else will sustain the petroleum industry turnaround well into the 21st Century. However the challenges presented by deep water are considerable both commercially and technically especially if the fields are marginal. Engineering solutions must aim to minimise the operator's capital risk and maximise his ability to avoid large capital commitments prior to verification of acceptable reservoir performance.

Among the more daunting technical issues to be addressed is hydrate and paraffin subsea pipeline blockage. Generally considered little more than a nuisance in most shallow water areas, the high flow rates, remoteness and the miles of very low temperature water through which deep water production must pass, make it quite a serious problem for producers. Another physical reality of deep water production are the considerable lengths of riser involved. These generate large riser weights which result in high loads being exerted upon both the riser and surface connection system.

The overall aim of this study is to propose and develop a cost effective production design concept suitable for oil reservoirs situated in deep (1500 m) water which can be quickly and safely installed in areas with limited weather windows. The proposed design is based upon a *steel catenary riser* which will connect an FPSO directly into either a wellhead or seabed pipeline system thereby eliminating both the connection complexities and high cost associated with a central manifold. The catenary geometry will ensure that the structure is inherently compliant whilst a carrier pipe arrangement will provide structural protection and buoyancy to a flowline bundle contained within. The interface between the riser and the surface production vessel is a critical part of any riser system and so for the purposes of this study two design arrangements are considered. The first is based upon a direct connection between an FPSO turret and riser where as the second is a hybrid design in which the riser is supported by a sub-surface buoy which is hydraulically connected to an FPSO using flexible flowlines. This hybrid connection has the advantage of decoupling FPSO and riser motions. Design development is carried out by examining a range of critical areas. Each investigation forms the basis of a chapter as described below.

In Chapter 2, the loading and geometric characteristics of a selection of conceivable riser profiles are examined and compared with one another. The analysis carried out establishes that for all three mathematical curves considered i.e. elliptic, parabolic and catenary, maximum bending moments due to self-weight occur at the seabed, except in the case of an elliptic curve when the profiles horizontal offset exceeds water depth. The

elliptic and parabolic curves, although convenient mathematically would be very difficult to attain on a practical basis, a catenary however describes the form assumed by a perfect flexible inextensible chain of uniform density suspended from two supports.

Chapter 3 is devoted to the design of a buoyancy system which is required in order to support the riser's submerged weight. Two different systems suitable for deep water are investigated. The syntactic foam design provides the riser with a buoyancy system that is simple to use during both riser installation and operation. Its characteristics are not influenced by external factors and it doesn't impose any additional stresses on the riser, however it is very expensive. Nitrogen gas however is relatively cheap, although this is somewhat compromised by a considerably more complex arrangement, involving internal gas tight compartments, high pressure lines and a high pressure gas source.

Chapter 4 examines the problems associated with production oil temperature. A heat loss analysis is carried out using EXCEL spreadsheets. This analysis identifies a requirement for good pipeline and flowline insulation in order for oil transportation problems such as hydration to be avoided within a deep water environment. A structural thermal stress assessment is also undertaken.

In Chapter 5 an installation loading analysis investigates the effects of riser geometry and submerged unit weight on bending stress, axial stress and lifting load. Bending and axial stresses resulting from surface and sub-surface vessel displacements are also calculated along with the corresponding deflection profiles. This chapter also examines the static structural response of the riser to in-plane current loads. The response (in terms of deflection and stress) is characterised by the riser's submerged unit weight, geometry (horizontal surface offset) and the side of the riser on which the current acts i.e. *Concave* or *Convex*. One important characteristic which becomes apparent when a catenary riser is subjected to external forces are the large angular rotations which are generated at the top end. These have to be accommodated in order to avoid creating seriously high bending moments both in the riser as well as in the surface or sub-surface connection assembly. This can be achieved through the use of flexible joints. A design for a surface (or sub-surface) connection system using flexible joints is proposed in this chapter.

In Chapter 6 a resonant period analysis is undertaken using a numerical procedure based upon a finite difference technique and validated by an analytical method developed by Blevin for vibrating stretched strings. From this analysis it is shown that the resonant periods rapidly converge as the mode number is increased. Overall the results suggest that the riser's high natural periods are substantially influenced by carrier pipe diameter and

can therefore be positioned so as to avoid external excitation periods by selecting appropriate diameters.

As an alternative to the direct connection of the riser to the surface production vessel a study to investigate the advantages of a hybrid connection is carried out in Chapter 7. In this study a vertically tethered sub-surface buoy from which a catenary riser is suspended is designed and evaluated. The loads imposed upon the buoy and its tethers along with the lateral stiffness that this arrangement provides are evaluated using spreadsheets.

In Chapter 8 a detailed capital cost analysis for the catenary riser is undertaken. It is found that the economics compare favourably with known production systems designed for the same operational environment.

Chapter 1

Introduction

1.1 Offshore Development Trends

In 1947 oil production began from wells drilled in the Gulf of Mexico from the first offshore platform. The water depth was only 6 metres however this achievement represented the beginning of a technological advancement that has enabled the offshore industry to continually face the challenge of progressively moving into deeper and deeper waters. The driving force behind this drift into deeper water is the fact that reservoirs located in shallower waters are becoming exhausted as result of extensive development over the past three decades. The advancement of production technology since 1947 is summarised in Figure 1.1 in terms of maximum production water depths [1]. In the past decade this advancement has been accelerated with the introduction of TLP platforms. A new world record for production has been set by Shell Oil's Mars Tension Leg Platform which has recently been installed in the Gulf of Mexico in 950 metres of water.

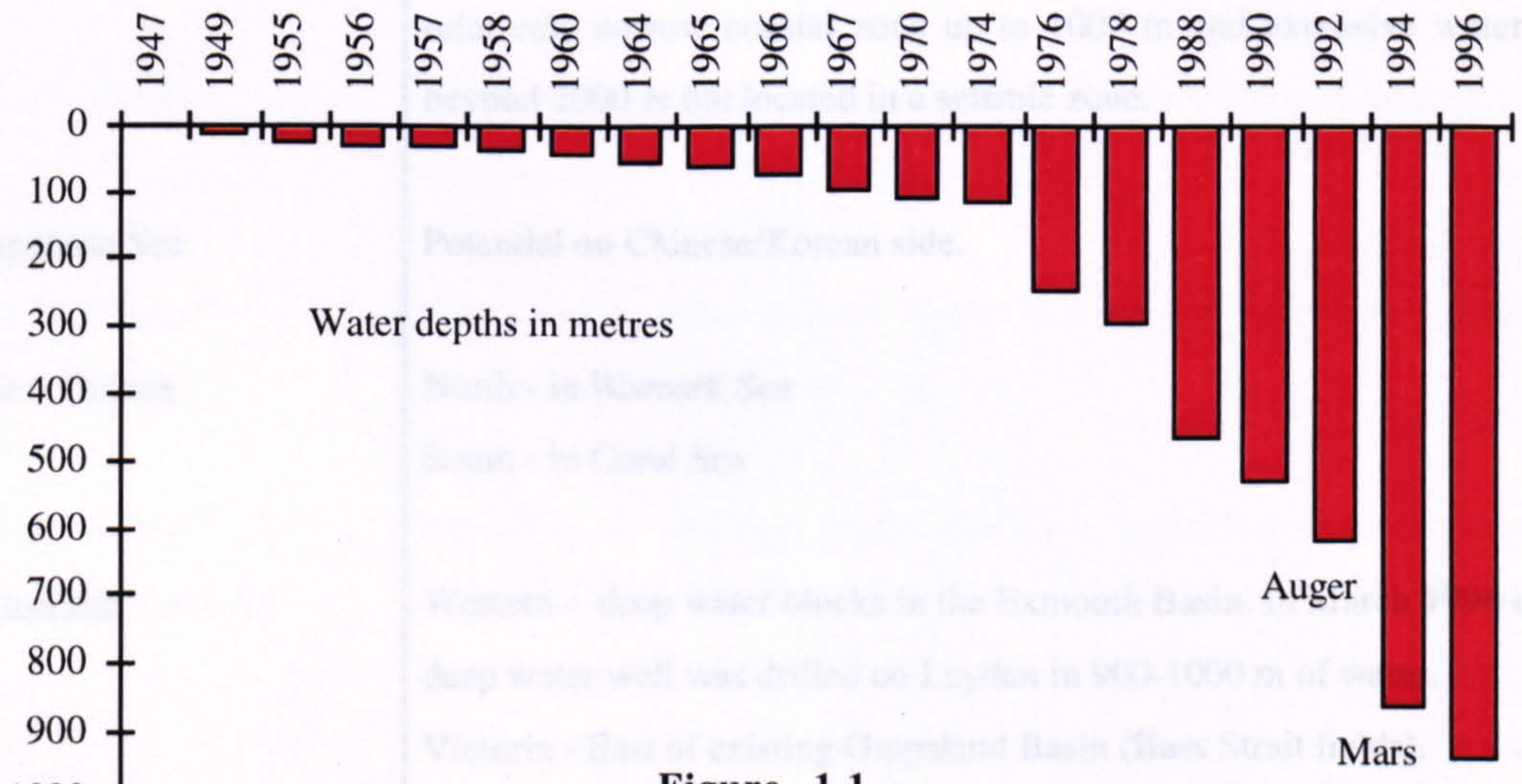

Figure 1.1
Hyrocarbon Production Maximum Water Depths

1.2 Deep Water Reserves

The perception of deep water changes each year as the oil industry continues to step out into increasing offshore locations. Definitions often used today are to classify deep water as 400 m to 2000 m with depths beyond regarded as ultra-deep. Perceptions in the 1970s and early 1980s were somewhat different with many technical papers classifying deep water in the range 200 m to 400 m which coincides with the boundary between the continental shelf and the continental slope. The offshore part of the world's sedimentary basins - those areas likely to contain source rocks for oil and gas is estimated at around 50 million square kilometres. The continental slope and abyssal plains take up

approximately two-thirds of this area and so the undiscovered reserve potential of deep water is considerable. These locations will probably have been supplied plentifully with organically rich sedimentary material, typically by significant runoff from rivers. There are numerous locations around the world where there are hydrocarbon deposits in these waters. In the Gulf of Mexico, reserves exceeding 4 billion barrels have been identified in 500-1800 m waters in the last six years. In Brazil's Campos Basin, oil reserves of over 3 billion barrels are located in water depths of 400-1000 m and over 2 billion barrels in water depths greater than 1000 m.

Location (Boundary)	**Details**
South China Sea	Eastern Area - Philippines/Borneo/S Vietnam has some sea areas extending to 1000+ m. The Philippines seaboard, both E and W has a relatively narrow coastal zone up to 1000 m and extensive waters beyond 2000 m but located in a seismic zone.
Japanese Sea	Potential on Chinese/Korean side.
New Guinea	North - in Bismark Sea South - in Coral Sea
Australia	Western - deep water blocks in the Exmouth Basin. In March 1996 a deep water well was drilled on Leyden in 900-1000 m of water. Victoria - East of existing Gippsland Basin (Bass Strait fields).
Bay of Bengal	Deep water areas extend along the coastal fringe off India, Bangladesh and Myanmar.
Sri Lanka	Extensive area 2000 - 3000 m to West of the Island. Potential to East and up SE Indian Coast, beyond Madras.
West Africa	Extensive areas of Atlantic Ocean beyond 1000 metres water depth: Nigeria/Cameroon/Equatorial Guinea/Gabon Ghana/Ivory Coast/Angola

Table 1.1(a)

Potential Deep Water Hydrocarbon Production Areas [2]

Location (Boundary)	Details
Canada (East Coast)	Areas offshore Nova Scotia and Newfoundland in less than 1000 m presently under development and giving rise to speculation regarding development of areas over 1000 m located further seaward.
Gulf of Mexico	Significant potential for developments southward from existing US coast fields in depths up to 3600 m.
Caribbean Sea	Significant offshore areas which have the potential to have been well supplied with organic material and in water extending beyond 2000 m. Bounded on South by Venezuela.
South Atlantic	Offshore Brazil (only) with potential northward extension from existing areas to include the Amazon Delta.
Bay of Bengal	Deep water areas extend along the coastal fringe off India, Bangladesh and Myanmar.
North Atlantic (West of Shetland)	The West of Shetland region will be a difficult area to develop. Located in the North Atlantic storm channel between the Faeroe Islands and the Scottish archipelago of the Shetland Islands. Heavy rains, wind and waves comparable to those of the North Sea, but often worse, rake the area much of the year and icebergs and ice floes are a winter hazard. Water depths range from 200 - 1500 m and estimated recoverable reserves are put at 5 billion bbl oil and a negligible amount of gas. Altogether, there have been 80 wells drilled in the West of Shetland region since the 1977 discovery well on Clair field. BP has already started developing the Foinhaven field (540 m) using a catenary moored FPSO. Production from Schiehallion (375 m) is scheduled to come on stream later this year using an FPSO which will be the world's purpose built vessel of its kind in terms of hull volume.

Table 1.1(b)

Potential Deep Water Hydrocarbon Production Areas [2]

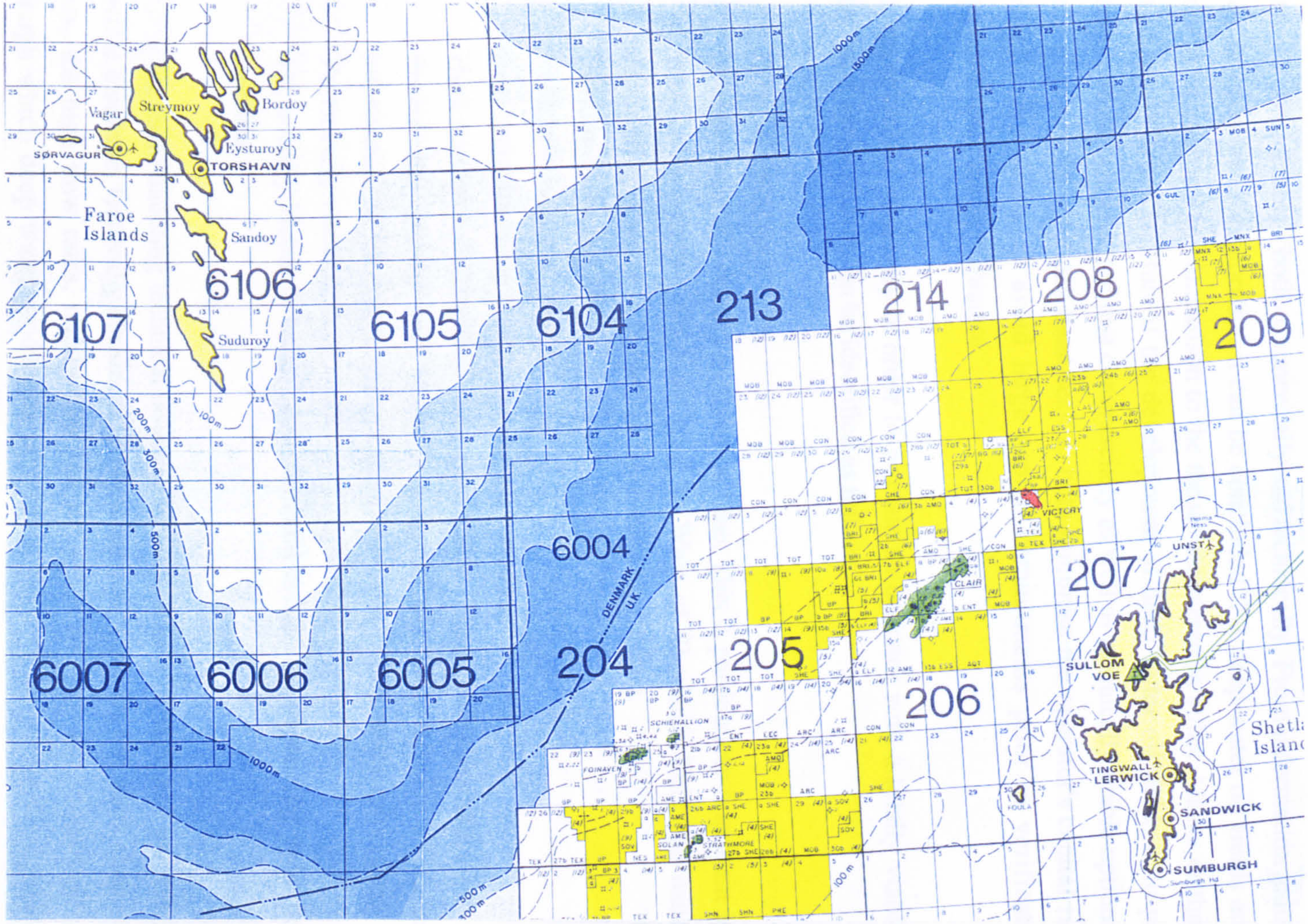

Figure 1.2

West of Shetland Oil Fields

1.3 Deep Water Challenges

Deep water production more than anything else will sustain the petroleum industry turnaround well into the 21st century. However the challenges presented by deep water are considerable - both commercially and technically. From information gained as a result of deep water exploration it can be concluded that deep water oil fields are most likely to be marginal in comparison to the those discovered in either Alaska or the North Sea in the 1970's. Therefore if the development of deep water oil fields is to proceed operators must be convinced that commercially as well as technically viable options exist. These engineering solutions must seek to both minimise the operator's capital risk and maximise his ability to avoid large capital commitments prior to verification of acceptable reservoir performance.

The requirements necessary in order to provide an operator with a totally viable deep water production system can be identified as follows:

- Cost efficient installation
- Minimisation of offshore installation time. This is particularly important in areas with short weather windows such as West of Shetland. This can usually be achieved by maximising onshore fabrication and testing.
- Economic capital cost
- Economic operating cost
- Low maintainability during operational life span.
- High standard of fabrication and manufacture - good quality assurance
- Provide the operator with ability to progressively phase develop a field as more information on the reservoir is gained as a result of continued exploration.
- Technically viable in deep water
- Technically viable in harsh environmental conditions depending upon the field location.

Among the more daunting technical issues to be addressed is hydrate and paraffin subsea pipeline blockage. Generally considered little more than a nuisance in most shallow water areas, the high flow rates, remoteness and the miles of very low temperature water through which deep water production must pass, make it quite a serious problem for producers. Another a physical reality of deep water production are the considerable lengths of riser involved. These generate large riser weights which result in high loads being exerted upon both the riser and surface vessel connection system.

1.4 Project Objective

The overall aim of this study is to develop a production concept suitable for reservoirs situated in deep (1500 m) water. The design will endeavour to incorporate all the requirements specified above so as to provide a cost effective system which can be quickly and safely installed in areas with limited weather windows. The development of this design will be carried out by examining a range of critical areas. These areas are specified in Section 1.6.

1.5 Concept Identification and Description

A fundamental component of this production concept is a passively moored Floating, Production, Storage and Offloading (FPSO) vessel. FPSOs provide a number of practical advantages compared with other surface installations. Based on conventional shipbuilding technology, they are straightforward to build and expensive offshore work is kept to a minimum as most of the construction, hook-up and commissioning can be completed inshore at significantly less cost. Furthermore, FPSOs have the ability to handle heavy payloads and to add equipment incrementally to fit production and reservoir changes. They are also easier to install and decommission and can be used again in other fields. Their versatility is now unquestioned both in the harsh UK West of Shetland environment where two FPSOs will have been installed by 1997 (*Foinhaven* and *Schiehallion*) and in milder environments where two vessels will be installed about the same time in water depths around 800 m (*Barracuda* and *Aquila*).

Many deep water developments will commingle well fluids at the seabed. This will require fewer, but larger production risers connected to the surface production vessel which in this case is an FPSO. Supporting a number of large diameter risers in deep water presents several design challenges. The risers must be compliant enough to allow the surface production vessel some freedom of motion. They must be able to withstand environmental loadings and their weight must be supported.

The *steel catenary riser* concept offers a solution for deep water production. It is intended that the catenary riser will connect the FPSO directly into either a wellhead or seabed pipeline system thereby eliminating both the connection complexities and high cost associated with a central manifold.

The basic features of this riser are

- The riser has catenary profile and is therefore inherently compliant.
- Containment of flowlines and umbilical within a Carrier Pipe (structural protection, buoyancy and potential for thermal insulation), see Figure 1.3 for a cross-sectional illustration. Through the use of heavy bulkheads, the flowlines and Carrier Pipe act integrally to resist tensile and thermally induced loads. This arrangement is similar to the pipeline concept already developed and proven by a number of contractors in the North Sea.
- Use of standard steel flowlines. The number flowlines and their sizing is based upon a maximum design oil output of 70,000 BOPD which is based upon a GOR of 250 SCF/bbl and an oil gravity of 34 °API.
- Costs per metre typically the same as for the current North Sea flexible riser bundles.
- The riser section can be fully fabricated and tested onshore.

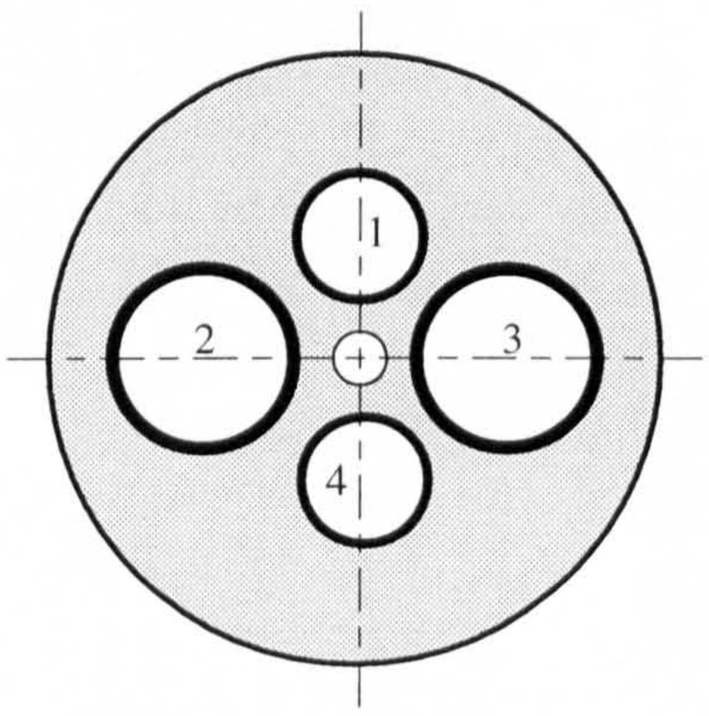

1. Injection Water (8" Line)
2. Production Oil (12" Line)
3. Production Oil (12" Line)
4. Injection Gas (8" Line)

Figure 1.3
Riser Cross-Section

The interface between the riser and the surface production vessel is a critical part of any riser system and so for the purposes of this study two design arrangements will be considered:

1. In this arrangement the top of the catenary riser connects directly into a turret assembly located within the forward section of an FPSO, see Figure 1.4.

2. In this arrangement (commonly referred to as a hybrid design) the risers are supported by a sub-surface buoy which is anchored to the seabed using vertical tethers. A hydraulic connection between the riser and FPSO is provided by flexible flowlines. This type of connection has the advantage of decoupling FPSO and riser motions, see Figure 1.5.

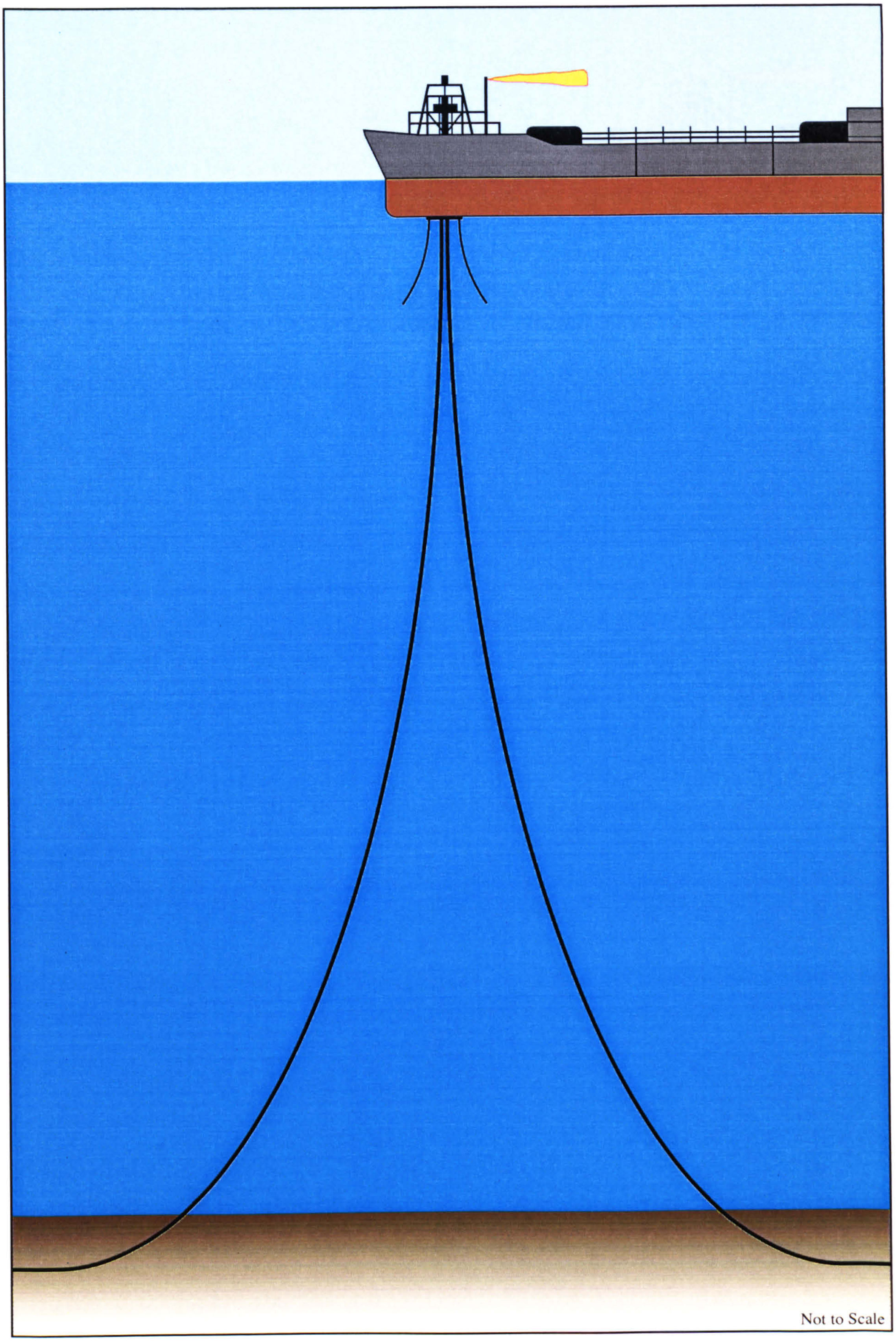

Figure 1.4

Catenary Riser Concept (Direct Connection)

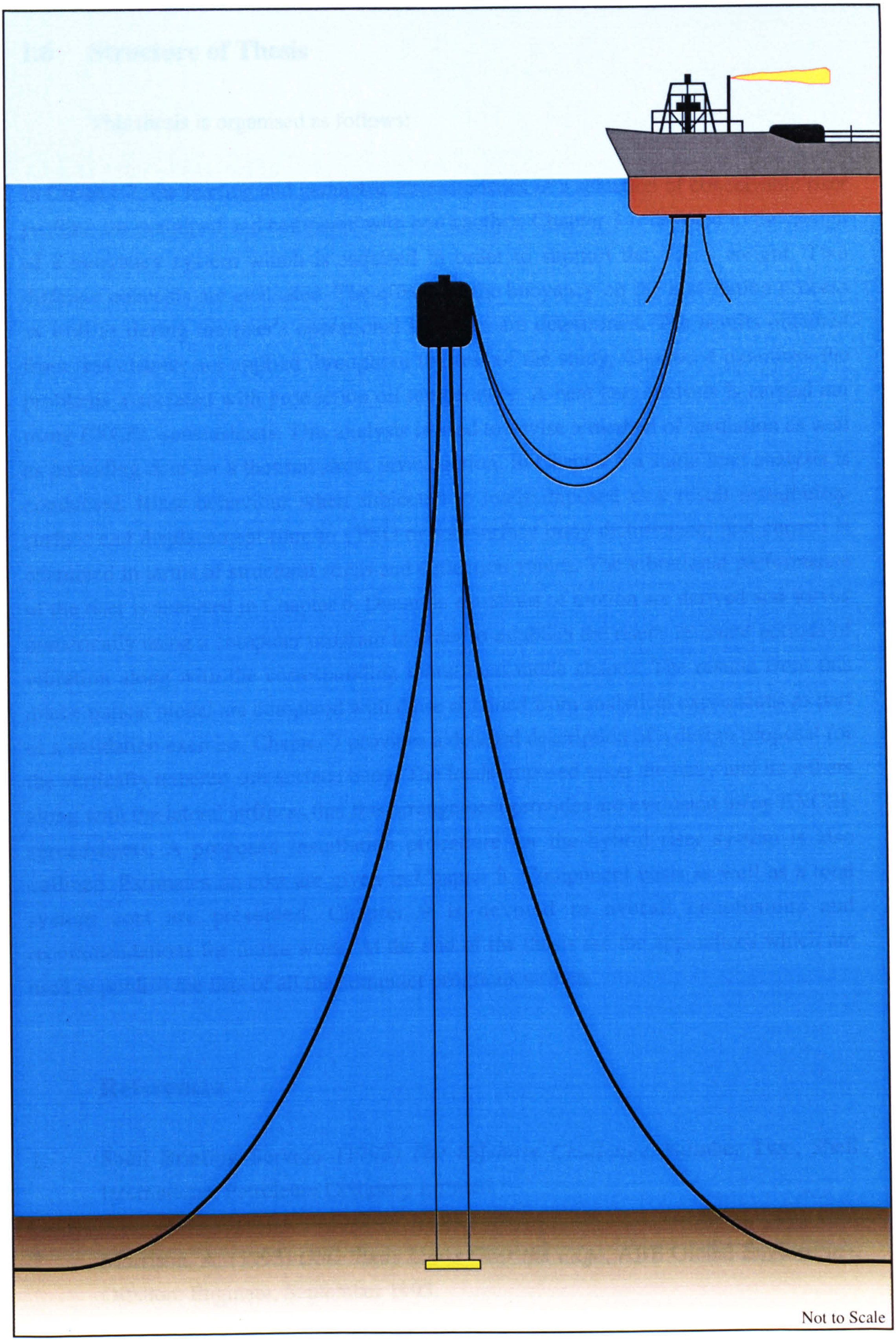

Figure 1.5

Catenary Riser Concept (Hybrid Arrangement)

1.6 Structure of Thesis

This thesis is organised as follows:

In Chapter 2, the loading and geometric characteristics of a selection of conceivable riser profiles are examined and compared with one another. Chapter 3 is devoted to the design of a buoyancy system which is required in order to support the riser's weight. Two different concepts are evaluated. The effects of the buoyancy on the installation process as well as during the riser's operational life span are determined. The results obtained from this chapter are applied throughout the rest of the study. Chapter 4 examines the problems associated with production oil temperature. A heat loss analysis is carried out using EXCEL spreadsheets. This analysis is used to devise a method of insulation as well as providing data for a thermal stress investigation. In Chapter 5 a static load analysis is conducted. Riser behaviour when subjected to loads imposed as a result installation, surface end displacement (due to FPSO or sub-surface buoy disturbance) and current is examined in terms of structural stress and deflection values. The vibrational performance of the riser is analysed in Chapter 6. Dynamic equations of motion are derived and solved numerically using a computer program in order to establish the riser's resonant periods of vibration along with the corresponding vibrational mode shapes. The results from this mathematical model are compared with those obtained from analytical expressions as part of a validation exercise. Chapter 7 provides a detailed description of a design proposal for the vertically tethered sub-surface buoy. The loads imposed upon the buoy and its tethers along with the lateral stiffness that this arrangement provides are evaluated using EXCEL spreadsheets. A proposed installation procedure for the hybrid riser system is also outlined. Estimates on cost are given in Chapter 8. Component costs as well as a total system cost are presented. Chapter 9 is devoted to overall conclusions and recommendations for future work. At the end of the thesis are the appendices which are used to publish the lists of all the computer programs written.

References

1. Shell Briefing Service. (1993) *The Offshore Challenge*, Number Two, Shell International Petroleum Company Limited.

2. Morrison, A. (1993) *OSO Study Looks Over the Edge*, ABB Global Engineering, Offshore Engineer, September 1993.

CHAPTER 2

The Selection of a Riser Profile and an Analysis of its Geometric Characteristics

2.1 General Description

This chapter deals with the loading exerted upon the riser and its connections (surface and seabed) from conditions that are not attributed to sea motions found within its operational environment i.e. sea current and waves. The word 'loading' for the purposes of this chapter and in fact for the entire thesis can be defined so as to include the following:

- Bending moment
- Axial force (tension or compression)
- Shear force

Riser loading for a zero sea motion condition is a characteristic of geometric profile and submerged weight (self-weight) and therefore are parameters that need to be carefully chosen in order that one of the most important considerations involved in the design process, that of structural stress minimisation can be achieved. Over stressing of the riser is as much a problem during its installation as it is during its operational lifetime.

Apart from the structural loading within the riser itself, geometric profile and self-weight inflict many other complexities on the entire production system. These will be examined later in the chapter but can be summarised as follows:

- The imposition of both vertical and horizontal loading on surface or sub-surface connections i.e. FPSO turret or sub-surface buoy
- Riser slope at the surface
- Riser length
- Field development strategy

Submerged weight and profile also combine to give the surface end of the riser a surge and heave stiffness which can be utilised in addition with a conventional mooring system to reduce FPSO/buoy disturbances at the surface. An analysis of this is given in the final section of the chapter.

All axial and bending stress data detailed within this chapter is calculated using the riser cross sectional arrangement defined in the introductory chapter. Diameters and thicknesses of all the flowlines and the carrier pipe are tabulated below:

Component	Outer Diameter (m)	Wall Thickness (mm)
Flowlines		
12"	0.324	25.4
8"	0.219	18.3
Carrier Pipe	1.10	10

Table 2.1.
Cross-Sectional Dimensions

The riser design is based upon the utilisation of high tensile steel as the construction material and therefore an elasticity modulus value of 2.07 E11N/m^2 is used. The choice of diameter and wall thickness for the carrier pipe is severely restricted due to important considerations such as that of riser buoyancy which is examined in considerable detail in Chapter 3. Therefore an estimated outer diameter value of 1.10 m is used along with a wall thickness of 10 mm.

Sea water depth is a critical factor in determining the design of a riser especially when it comes down to calculating the structural loading. In Chapter 1 it was clearly specified that one of the main requirements of the riser was that it could be installed and operated in water depths of between 1000 and 2000 m. For the majority of the calculations presented within this chapter a mean depth of 1500 m has been used, however the loading sensitivity of the system to depth is established and is illustrated graphically.

2.2 Geometric Properties of a Curve

2.2.1 Introduction

This section looks at three different types of curve that could be considered in trying to meet the riser criteria established in the introductory chapter. The curves are:

- Elliptic
- Parabolic
- Catenary

An analysis is conducted so as to establish some basic but important geometric characteristics associated with each of the curves.

This is be done by determining three important characterising features:

- Maximum profile curvature
- Top end (surface) slope
- Curve quadrant length

The curvature at any point on a curve can be expressed analytically as:

$$\frac{1}{R} = \frac{d\theta}{ds} \tag{2.1}$$

in which *ds* is the arc length between two points on the curve. If *ds* is assumed to be very small both the arc and chord lengths between the two points can be considered equal and hence:

$$\frac{dy}{dx} = \tan\theta \tag{2.2}$$

$$\frac{dx}{ds} = \cos\theta \tag{2.3}$$

If Eqn (2.2) is differentiated with respect to *s* an exact relationship between curvature and curve geometry can be obtained:

$$\frac{d\theta}{ds} = \frac{1}{R} = \frac{{}^{d^2y}/_{dx^2}}{\left[1 + \left({}^{dy}/_{dx}\right)^2\right]^{3/2}} \tag{2.4}$$

On knowing the equation $y = f(x)$ of the curve, the first and second differential derivatives can be calculated and subsequently substituted into the above formulae in order to obtain *1/R*. If the riser can be bent elastically so as to attain a curvature *1/R*, the following fundamental relationship can be used:

$$\frac{1}{R} = \frac{M}{EI} \tag{2.5}$$

therefore

$$\frac{M}{EI} = \frac{{}^{d^2y}/_{dx^2}}{\left[1 + \left({}^{dy}/_{dx}\right)^2\right]^{3/2}} \tag{2.6}$$

2.2.2 Elliptic Curve

An ellipse can be defined by the cartesian equation:

$$\frac{x^2}{a^2}+\frac{y^2}{b^2}=1 \tag{2.7}$$

The curve and its co-ordinate axis are illustrated in Figure 2.1(a). On differentiating the following derivatives are found:

$$\frac{dy}{dx}=-\frac{b^2}{a^2}\frac{x}{y} \tag{2.8}$$

$$\frac{d^2y}{dx^2}=-\frac{b^4}{a^2y^3} \tag{2.9}$$

when the differential derivatives are substituted into Eqn (2.6) the following bending moment expression is obtained:

$$\frac{M}{EI}=\frac{b^4a^4}{\left[a^4y^2+b^4x^2\right]^{3/2}} \tag{2.10}$$

Of particular interest are the bending moments at the surface end and at the point of contact with the seabed.

At the **surface** *(y = 0 and x = a)*:

$$\frac{M}{EI}=\frac{a}{b^2} \tag{2.11}$$

At the point of contact with the **seabed** *(y = b and x = 0)*:

$$\frac{M}{EI}=\frac{b}{a^2} \tag{2.12}$$

When the horizontal and vertical offsets are equal *(a = b)* the elliptic curve becomes circular and can therefore be defined by the equation:

$$x^2+y^2=r \tag{2.13}$$

where *r = circle radius (= a = b)*

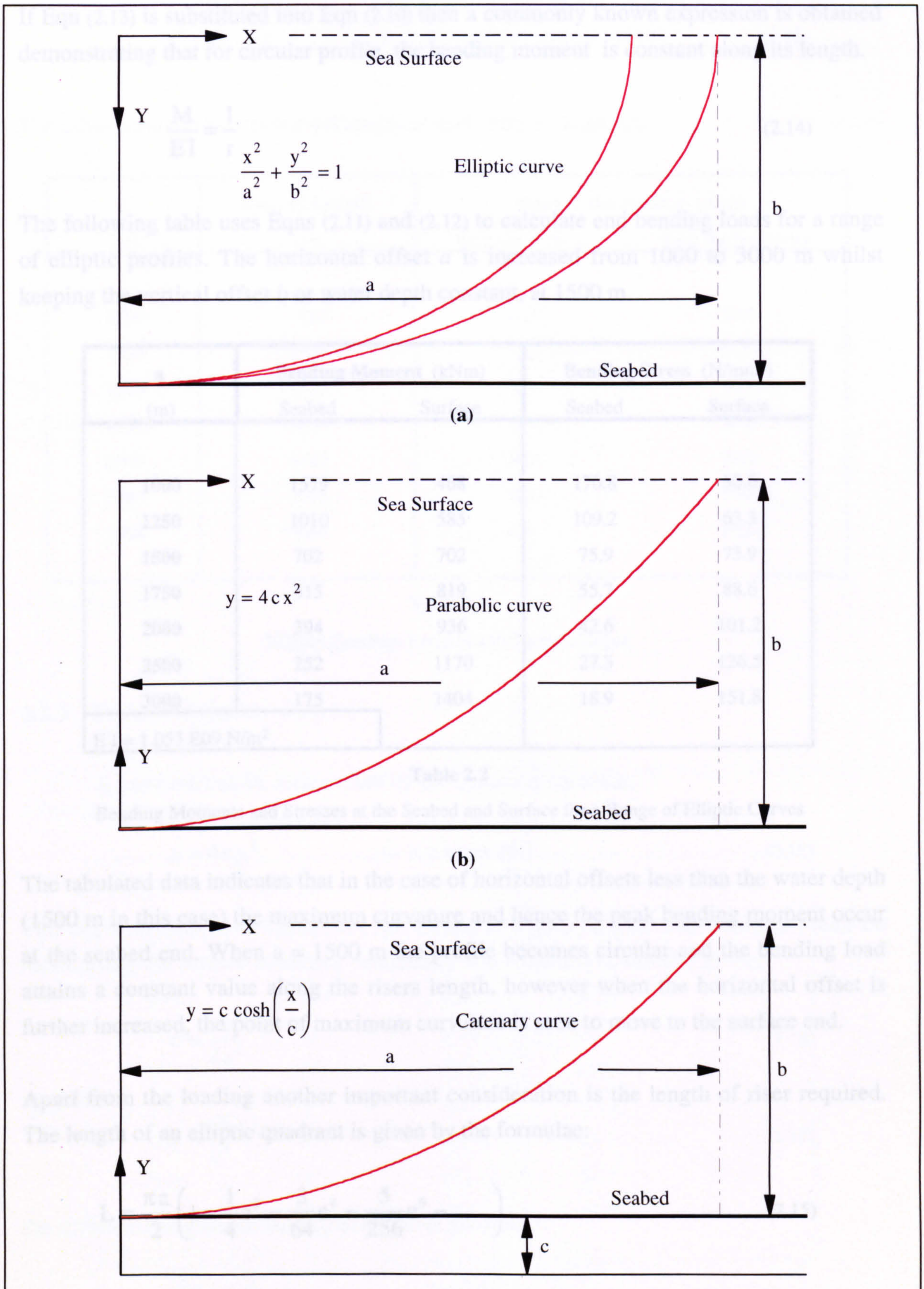
X
Sea Surface
Y
$\frac{x^2}{a^2} + \frac{y^2}{b^2} = 1$
Elliptic curve
a
b
Seabed
(a)
X
Sea Surface
$y = 4cx^2$
Parabolic curve
a
b
Y
Seabed
(b)
X
Sea Surface
$y = c\cosh\left(\frac{x}{c}\right)$
Catenary curve
a
b
Y
Seabed
c
(c)

Figure 2.1

If Eqn (2.13) is substituted into Eqn (2.10) then a commonly known expression is obtained demonstrating that for circular profile, the bending moment is constant along its length.

$$\frac{M}{EI} = \frac{1}{r} \qquad (2.14)$$

The following table uses Eqns (2.11) and (2.12) to calculate end bending loads for a range of elliptic profiles. The horizontal offset a is increased from 1000 to 3000 m whilst keeping the vertical offset b or water depth constant, at 1500 m.

a (m)	**Bending Moment** (kNm)		**Bending Stress** (N/mm^2)	
	Seabed	Surface	Seabed	Surface
1000	1579	468	170.8	50.6
1250	1010	585	109.2	63.3
1500	702	702	75.9	75.9
1750	515	819	55.7	88.6
2000	394	936	42.6	101.2
2500	252	1170	27.3	126.5
3000	175	1404	18.9	151.8
E I = 1.053 E09 N/m^2				

Table 2.2

Bending Moments and Stresses at the Seabed and Surface for a Range of Elliptic Curves

The tabulated data indicates that in the case of horizontal offsets less than the water depth (1500 m in this case) the maximum curvature and hence the peak bending moment occur at the seabed end. When a = 1500 m the profile becomes circular and the bending load attains a constant value along the risers length, however when the horizontal offset is further increased, the point of maximum curvature is seen to move to the surface end.

Apart from the loading another important consideration is the length of riser required. The length of an elliptic quadrant is given by the formulae:

$$L = \frac{\pi a}{2}\left(1 - \frac{1}{4}e^2 - \frac{3}{64}e^4 - \frac{5}{256}e^6 - .....\right) \qquad (2.15)$$

in which the term outside the bracket gives the length of an arc of a circle and

$$e^2 = 1 - \frac{b^2}{a^2} \qquad (a \text{ is always the largest offset}) \qquad (2.16)$$

The table below gives the curved length of each elliptic quadrant.

a (m)	**Curved Length** (m)	**Slope at the Surface** (degs) from the vertical	from the horizontal
1000	1987	0.0	90.0
1250	2164	0.0	90.0
1500	2356	0.0	90.0
1750	2558	0.0	90.0
2000	2765	0.0	90.0
2500	3203	0.0	90.0
3000	3666	0.0	90.0

Table 2.3

Elliptic Quadrant Lengths and Surface Slopes

2.2.3 Parabolic Curve

A parabola can be represented by the cartesian equation:

$$y = 4cx^2 \qquad (c \text{ is a constant}) \qquad (2.17)$$

The curve and its co-ordinate axis are shown in Figure 2.1(b). The constant c can be found using the surface boundary condition $y = b$ when $x = a$, thereby giving:

$$c = \frac{b}{4a^2} \qquad (2.18)$$

therefore:

$$y = \frac{b}{a^2} x^2 \qquad (2.19)$$

On differentiating the following derivatives are found:

$$\frac{dy}{dx} = 2\frac{b}{a^2} x \qquad (2.20)$$

$$\frac{d^2y}{dx^2} = 2\frac{b}{a^2} \tag{2.21}$$

When the differential derivatives are substituted into Eqn (2.6) a bending moment expression is obtained:

$$\frac{M}{EI} = \frac{2ba^4}{\left[a^4 + 4b^2x^2\right]^{3/2}} \tag{2.22}$$

As in the case of the elliptic curve, maximum and minimum bending load values can be found at the surface and seabed ends.

At the **surface** *(x = a)*:

$$\frac{M}{EI} = \frac{2ba}{\left[a^2 + 4b^2\right]^{3/2}} \tag{2.23}$$

At the **seabed** *(x = 0)*:

$$\frac{M}{EI} = \frac{2b}{a^2} \tag{2.24}$$

The following table uses Eqns (2.23) and (2.24) to calculate end bending loads for a range of parabolic profiles.

a (m)	**Bending Moment** (kNm) Seabed	Surface	**Bending Stress** (N/mm^2) Seabed	Surface
1000	3159	100	341.6	10.8
1250	2022	115	218.6	12.4
1500	1404	126	151.8	13.6
1750	1032	132	111.5	14.3
2000	790	135	85.4	14.6
2500	505	133	54.7	14.3
3000	351	124	38.0	13.4
E I = 1.053 E09 N/m^2				

Table 2.4

Bending Moments and Stresses at the Seabed and Surface for a Range of Parabolic Curves

The results clearly illustrate the big difference in curvature between seabed and surface. The top end is characterised by a very flat profile thereby creating a low bending stress region and as the surface offset is increased this loading is seen to peak at an offset of about 2000 m.

The length of the parabola from the seabed to the surface is calculated using the formula:

$$L = b\left[\left(\frac{a^2}{4b^2}+1\right)^{1/2} + \frac{a^2}{4b^2}\sinh^{-1}\left(\frac{2b}{a}\right)\right] \qquad (2.25)$$

and the profiles surface slope (measured from the horizontal) is found by letting $x = a$ in Eqn (2.20) i.e.

$$\theta_s = \tan^{-1}\left(\frac{2b}{a}\right) \qquad (2.26)$$

a (m)	**Curved Length** (m)	**Slope at the Surface** (degs) from the vertical	from the horizontal
1000	1884	18.4	71.6
1250	2044	22.6	67.4
1500	2218	26.6	63.4
1750	2404	30.3	59.7
2000	2600	33.7	56.3
2500	3011	39.8	50.2
3000	3442	45.0	45.0

Table 2.5

Parabolic Quadrant Lengths and Surface Slopes

2.2.4 Catenary Curve

A catenary can be defined by the equation:

$$y = c\cosh\left(\frac{x}{c}\right) \qquad (c \text{ is a constant}) \qquad (2.27)$$

The curve and co-ordinate system used are illustrated in Figure 2.1(c). The constant is determined by iteration using the surface boundary condition $y = c + b$ when $x = a$. All iterations are carried out using an EXCEL spreadsheet. Table 2.6 lists a selection of catenary equation constants for a range of horizontal and vertical offsets.

a	**Catenary Constant**		
(m)	b = 1000 m	b = 1500 m	b = 2000 m
1000	618.76	475.68	404.43
1250	911.60	683.29	572.61
1500	1263.50	928.14	766.54
1750	1675.60	1211.24	987.96
2000	2148.64	1533.40	1237.52
2500	3279.31	2297.24	1823.19
3000	4657.74	3222.96	2526.99

Table 2.6

Catenary Equation Constant Values

On differentiating Eqn (2.27) the following derivatives are obtained:

$$\frac{dy}{dx} = \sinh\left(\frac{x}{c}\right) \tag{2.28}$$

$$\frac{d^2y}{dx^2} = \frac{1}{c}\cosh\left(\frac{x}{c}\right) \tag{2.29}$$

When these derivatives are substituted into Eqn (2.6) a bending moment expression is obtained:

$$\frac{M}{EI} = \frac{1}{c\cosh^2\left(\frac{x}{c}\right)} \tag{2.30}$$

At the **seabed** *(x = 0)*:

$$\frac{M}{EI} = \frac{1}{c} \tag{2.31}$$

At the **surface** *(x = a)*:

$$\frac{M}{EI} = \frac{1}{c \cosh\left(\frac{a}{c}\right)} \tag{2.32}$$

The following table uses Eqns (2.31) and (2.32) to calculate end bending loads for a range of parabolic profiles. The horizontal offset *a* is increased from 1000 to 3000 m whilst keeping the vertical offset *b* constant at 1500 m.

a (m)	**Bending Moment** (kNm) Seabed	Surface	**Bending Stress** (N/mm^2) Seabed	Surface
1000	2214	533	239.4	57.6
1250	1541	482	166.7	52.2
1500	1135	433	122.7	46.9
1750	869	388	94.0	42.0
2000	687	347	74.3	37.5
2500	458	277	49.6	30.0
3000	327	223	35.3	24.1
E I = 1.053 E09 N/m^2				

Table 2.7

Bending Moments and Stresses at the Seabed and Surface for a Range of Catenary Curves

The results of the analysis demonstrate that in the case of a catenary profile the behaviour between bending load and an increase in surface offset is fairly straightforward. As *a* is increased curvatures at both surface and seabed ends reduce resulting in a decrease in bending stress.

The length of a catenary arc from $x = 0$ to $x = a$ is attained by using the following hyperbolic expression:

$$L = c \sinh\left(\frac{a}{c}\right) \tag{2.33}$$

and the surface slope is found from Eqn (2.28):

$$\theta_s = \tan^{-1}\left[\sinh\left(\frac{a}{c}\right)\right] \tag{2.34}$$

a (m)	**Curved Length** (m)	**Slope at the Surface** (degs) from the vertical	from the horizontal
1000	1918	13.9	76.1
1250	2074	18.2	71.8
1500	2244	22.5	67.5
1750	2426	26.5	63.5
2000	2617	30.4	59.6
2500	3024	37.2	52.8
3000	3452	43.0	47.0

Table 2.8

Catenary Quadrant Lengths and Surface Slopes

2.2.5 Discussion

The geometric analysis undertaken has established that for all three mathematical curves considered maximum bending moments occur at the seabed, except in the case of an elliptic profile when horizontal offset exceeds vertical offset. For the selection of surface offsets considered (1000 to 3000 m) bending stresses at the seabed are found to be lowest in the case of the ellipse and highest for the parabola. However when the conditions at the surface end are examined the converse is found, with the largest stresses corresponding to the elliptic curve and the smallest with the parabolic. At both ends of the curve and in fact along the entire length the catenary is shown to offer an almost mean bending stress between those of the ellipse and parabola. Bending load distributions for all three curves are illustrated graphically in Figures 2.9 to 2.11 for horizontal offsets of 1000, 1500 and 2000 m.

The parabola and catenary both suffer from having a significant slope at the sea surface creating potential problems in terms of connection to either a turret or sub-surface buoy. The ellipse however avoids any connection problems with the ideal end condition of infinite slope. These geometric features are illustrated in Figures 2.12 to 2.14.

Curve length follows the same behaviour as that shown for both bending load and surface slope, in that the catenary profile possesses a length that is somewhere in between that offered by the parabola and ellipse. For the range of surface offset values analysed the elliptic quadrant possesses the greatest length and the parabolic the least and as found in the case of slope, the difference between catenary and parabola is considerably smaller than that between catenary and ellipse. It should be noted that any reduction in length will ultimately be beneficial for three reasons:

- Limits the length exposed to current
- Reduces material and fabrication costs
- Makes the installation of the riser easier

In general the catenary appears to offer a compromise between the parabola and ellipse in terms of its geometric characteristics. The results also suggest that for a given sea depth, horizontal surface offset is a critical factor in determining the profile load, length and surface slope and so in the next section this will be one aspect that will be looked at in more detail.

The elliptic and parabolic curves, although convenient mathematically would be very difficult to attain on a practical basis. It would require an exact buoyancy load distribution to be imposed along the riser and due to the bending flexibility of the system very little tolerance in either weight or buoyancy could be accommodated. Any benefits would be significantly out weighed by an inevitable increase in fabrication complexity and cost. A catenary however describes the form assumed by a perfect flexible inextensible chain of uniform density suspended from two supports. Therefore a riser with a negligible bending stiffness, uniform submerged unit weight and supported at surface and seabed could accurately be assumed to take up a catenary profile. Therefore on a practical installation and production basis a catenary curve appears to offer the only real option in terms of riser profile. As a result of this it will be a catenary geometry that is taken up and analysed in detail throughout the rest of this chapter with the objective of using the subsequent results throughout the rest of the production systems design detailed in this thesis.

2.3 Catenary Line Analysis

2.3.1 Introduction

The behaviour of a catenary riser operating in an deep water environment where depths range from between 1000 and 2000 m can accurately be modelled as a common mooring line. This usually comprises of a freely hanging pre-tensioned wire or chain line connecting a surface platform to an anchor on a seabed some distance from the platform. If the wire line is replaced by a pipe or bundle of pipes and an anchor substituted for a seabed connection unit the entire assembly then effectively becomes a catenary riser production system. A catenary riser operating in deep water will have an overall length of between 2 and 3km depending upon length of offsets and will therefore have negligible stiffness in bending even though the riser is of a rigid steel fabrication i.e. it is not a flexible riser.

The basic theory underlying the behaviour of catenary lines is well known - see, for example, *O' Brien and Francis (1964)* [3]. However this section will review the basic mechanics of a catenary and derive its governing equations.

2.3.2 Governing Equations for an Inelastic Catenary Line [4].

Figure 2.2(b) shows an element of a line (assumed to be inextensible) of constant submerged weight per unit length w hanging freely as shown in Figure 2.2(a). The element weight of $w\,ds$ is supported by a variation in tension along the line. A differential equation for this variation is obtained by taking both vertical and horizontal equilibrium of the forces acting on the line element of Figure 2.2(b). Thus

vertically:

$$T\sin\theta + \frac{d}{ds}(T\sin\theta)ds - w\,ds - T\sin\theta = 0 \qquad (2.35)$$

$$\frac{d}{ds}(T\sin\theta) = w \qquad (2.36)$$

horizontally:

$$\frac{d}{ds}(T\cos\theta) = 0 \qquad (2.37)$$

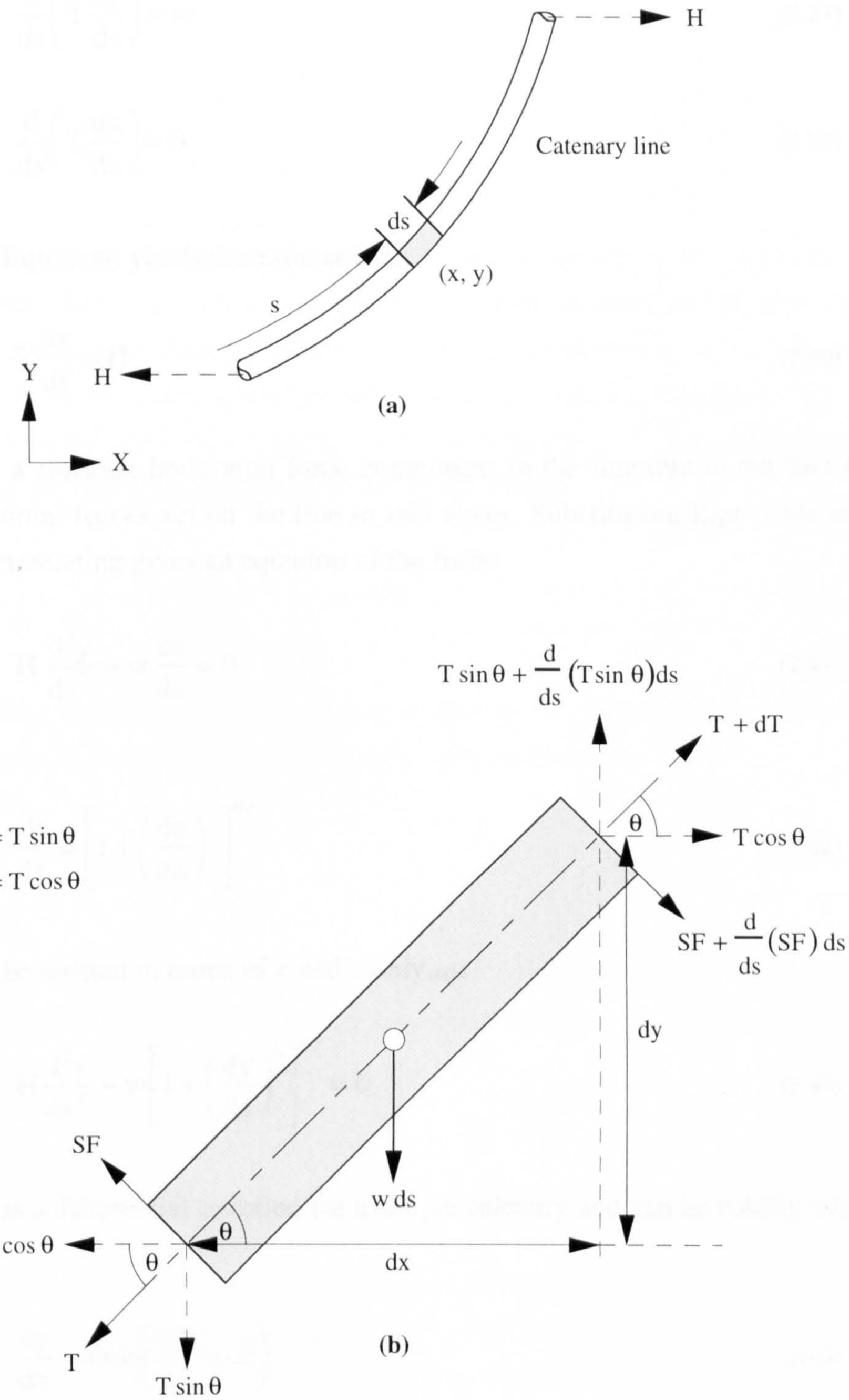

Figure 2.2

Definition Diagram for the Catenary

Taking $sin\,\theta = dy/ds$ and $cos\,\theta = dx/ds$ and substituting them into Eqns (2.36) and (2.37) respectively gives:

$$\frac{d}{ds}\left(T\frac{dy}{ds}\right) = w \tag{2.38}$$

and

$$\frac{d}{ds}\left(T\frac{dx}{ds}\right) = 0 \tag{2.39}$$

Integration of Eqn (2.39) yields the expression:

$$T\frac{dx}{ds} = H \tag{2.40}$$

in which H is a constant horizontal force component in the line due to the fact that no external horizontal forces act on the line in still water. Substituting Eqn (2.40) into Eqn (2.38) and differentiating gives an equation of the form:

$$H\frac{d^2y}{dx^2} - w\frac{ds}{dx} = 0 \tag{2.41}$$

Since

$$\frac{ds}{dx} = \left[1 + \left(\frac{dy}{dx}\right)^2\right]^{1/2} \tag{2.42}$$

Eqn (2.41) can be written in terms of x and y only as:

$$H\frac{d^2y}{dx^2} - w\left[1 + \left(\frac{dy}{dx}\right)^2\right]^{1/2} = 0 \tag{2.43}$$

This equation is a differential equation for a simple catenary and can be readily integrated to yield:

$$\frac{dy}{dx} = \sinh\left(\frac{wx}{H} + \vartheta\right) \tag{2.44}$$

in which the constant of integration ϑ is given by using boundary conditions which constrain the line to go through points $x = 0, y = 0$ (seabed) and $x = a, y = b$ (surface).

When this condition is applied:

$$\vartheta = \sinh^{-1}\left[\frac{\lambda(b/a)}{\sinh\lambda}\right] + \lambda \tag{2.45}$$

in which

$$\lambda = \frac{wa}{2H} \tag{2.46}$$

It should be noted that if a catenary riser is to have zero slope at the point of seabed contact then from Eqn (2.44) it is shown that the constant ϑ must also be zero. In order for seabed connections to either a wellhead or other subsea assembly to be made possible the riser has to attain a horizontal orientation at the seabed. Therefore all profile calculations are based upon zero slope at $x = 0$ and hence $\vartheta = 0$. Integrating Eqn (2.44) again and using the boundary conditions given above yields:

$$y = \frac{H}{w}\left[\cosh\left(\frac{wx}{H} + \vartheta\right) - \cosh\vartheta\right] \tag{2.47}$$

This equation can be cross checked by applying the zero slope condition, which is done (as previously mentioned) by putting ϑ equal to zero and hence:

$$y = \frac{H}{w}\cosh\left(\frac{wx}{H}\right) \tag{2.48}$$

The component H/w is constant along the catenary line and if it is replaced by the constant c, Eqn (2.47) then becomes identical to the mathematical expression defining a catenary curve given in Section 2.2 i.e.

$$y = c\cosh\left(\frac{x}{c}\right) \tag{2.49}$$

This is useful since the equation constant values already calculated using an iterative procedure and tabulated in Table 2.6 can be used to obtain horizontal forces for catenary lines with submerged unit weights w and horizontal and vertical offsets a and b respectively i.e. $H = cw$. Horizontal forces for a range of submerged unit weights (100, 500, 1000, 1500 and 2000 N/m), horizontal offsets (1000, 1250, 1500, 1750 and 2000 m) and vertical offsets (1000, 1400 m) are given in Appendix A.

A number of important results can be derived from these equations. The length of a catenary line from its origin (seabed) to a position *(x, y)* can be obtained as:

$$s = \int_0^x \frac{ds}{dx}\,dx \tag{2.50}$$

From Eqn (2.42)

$$\frac{ds}{dx} = \cosh\left(\frac{wx}{H} + \vartheta\right) \tag{2.51}$$

therefore:

$$s = \int_0^x \cosh\left(\frac{wx}{H} + \vartheta\right) dx$$

$$s = \left[\frac{H}{w}\sinh\left(\frac{wx}{H} + \vartheta\right)\right]_0^x$$

$$s = \frac{H}{w}\left[\sinh\left(\frac{wx}{H} + \vartheta\right) - \sinh\vartheta\right] \tag{2.52}$$

The total length can be found by letting $x = a$

$$L = \frac{H}{w}\left[\sinh\left(\frac{wa}{H} + \vartheta\right) - \sinh\vartheta\right]$$

$$L = \frac{2H}{w}\sinh\lambda\cosh(\vartheta + \lambda) \tag{2.53}$$

This equation can be verified by putting $H/w = c$ and $\vartheta = 0$, it is then shown to be equal to Eqn (2.33). Substituting $x = a$ and $y = b$ into Eqn (2.47) and simplifying also gives:

$$b = \frac{2H}{w}\sinh\lambda\sinh(\vartheta + \lambda) \tag{2.54}$$

Squaring Eqns (2.53) and (2.54) and subtracting yields the relationship:

$$L^2 = b^2 + \frac{a^2 \sinh^2 \lambda}{\lambda^2} \tag{2.55}$$

and if the term

$$\lambda = \frac{wa}{2H}$$

is inserted, then:

$$\left(L^2 - b^2\right) w^2 = 4H^2 \sinh^2\left(\frac{wa}{2H}\right) \tag{2.56}$$

which is a useful expression for determining H by iteration from known variables a, b, w and L. The loads exerted on the riser due to its geometry and submerged weight can now be obtained easily from the work outlined above.

Axial Tension

The axial tension distribution along the catenary can be written as:

$$T = H\left(\frac{ds}{dx}\right)_x$$

$$T = H \cosh\left(\frac{wx}{H} + \vartheta\right) \tag{2.57}$$

Vertical Force

The vertical component of tension can be given by:

$$V = H\left(\frac{dy}{dx}\right)_x$$

$$V = H \sinh\left(\frac{wx}{H} + \vartheta\right) \tag{2.58}$$

Bending Moment/Stress

An expression for bending moment can be formulated by substituting Eqn (2.44) and its differential derivative:

$$\frac{d^2y}{dx^2} = \frac{w}{H}\cosh\left(\frac{wx}{H} + \vartheta\right) \tag{2.59}$$

into Eqn (2.6) and hence:

$$M = \frac{w\cosh\left({}^{wx}/_{H} + \vartheta\right)}{H\left[1 + \sinh^2\left({}^{wx}/_{H} + \vartheta\right)\right]^{3/2}} EI$$

$$M = \frac{wEI}{H\cosh^2\left({}^{wx}/_{H} + \vartheta\right)} \tag{2.60}$$

This again can be checked by first substituting $c = H/w$ and $\vartheta = 0$ and then comparing it to Eqn (2.32).

The bending stress resulting from this moment can be established using the fundamental relationship:

$$\frac{\sigma_b}{z} = \frac{M}{I} \tag{2.61}$$

in which z is the transverse distance from the neutral axis and I is the second moment of area. If this equation is substituted into Eqn (2.60) then:

$$\sigma_z = \frac{wEz}{H\cosh^2\left({}^{wx}/_{H} + \vartheta\right)} \tag{2.62}$$

Shear Force

The shear force exerted across the riser cross section can be obtained by calculating the transverse component of horizontal force, see Figure 2.2(b).

$$SF = H\left(\frac{dy}{ds}\right)_x = H\left(\frac{dx}{ds}\frac{dy}{dx}\right)_x$$

$$SF = H \tanh\left(\frac{wx}{H} + \vartheta\right) \tag{2.63}$$

2.3.3 Catenary Characteristics

The equations set out above are utilised in several EXCEL spreadsheets to derive riser loads and profile features such as slope and length for a selection of catenary geometries. In order to enable optimum weights and profiles to be chosen several determining parameters are varied and the system's sensitivity towards them established. Parameters varied include:

- Horizontal offset *(1000, 1500 and 2000 m)*
- Submerged unit weight *(100, 500, 1000, 1500 and 2000 N/m)*

Figures 2.15 to 2.23 utilise Eqns (2.57) to (2.63) to illustrate the loading exerted upon the catenary riser as a result of its geometry only. The axial and shear loads shown in graphs (a) and (b) attain a maximum value at the surface whilst the bending loads reach a peak at the seabed.

Axial stress results shown in graph (b) are calculated using two cross-sectional areas:

- C.P csa only - cross-sectional area of the carrier pipe only
- C.P plus Flowlines csa - total cross-sectional area of the carrier pipe and flowlines with dimensions as tabulated in Table 2.1

This is done to illustrate the effect of allowing the flowline bundle to become an integral part of the riser structure. The conclusion being that the flowlines reduce the axial stressing by virtually trebling the steel cross-sectional area. Bending stresses however, are not influenced by the flowlines since they are a function of distance from the neutral axis z as opposed to cross-sectional area, see Eqn (2.62). All the bending stress data presented is based upon $z = D/2$ where D is the carrier pipe outer diameter. Maximum stresses along the riser are obtained by summing together both the bending and axial stress contributions as shown in graph (e). These results are again presented for the two cross-sectional area conditions. If the risers submerged unit weight is increased (assumed to be constant along the entire length) from 100 through 1000 to 2000 N/m the axial loading is shown to also increase as expected, however the bending stress remains un-affected since the profile geometry is independent of unit weight. Another parameter that is varied is the horizontal surface offset which in the Figures 2.15 to 2.23 is increased from 1000 through 1500 to 2000 m.

The effects of this on the stress condition are twofold:

- Increases the axial loading due to a greater suspended length of riser
- Reduces the bending load at the seabed as a result of less curvature; the whole profile becomes much flatter.

As an example, an offset of 1000 m delivers a maximum stress of approximately 230 N/mm² which in relation to a working stress of 270 N/mm² (0.6 of yield strength) is obviously too high given that environmental loading has yet to be considered. However an offset of 2000 m yields a maximum stress of approximately 100 N/mm² which would be deemed acceptable since it leaves enough strength capacity to hopefully accommodate current and wave loading. Another important consideration is that of riser slope, as the horizontal offset is increased the slope at the surface (from the horizontal) decreases. A shallow riser profile at this point could cause connection problems at the surface vessel.

All the loading and geometric characteristics associated with both the seabed and surface ends are summarised in tabular format in Tables 2.12 to 2.17 for a comprehensive range of riser conditions created by altering selected parameters as detailed above.

Figures 2.24 to 2.26 illustrate the sensitivity of the system to sea depth by plotting selected riser loads against sea depths of 1000, 1400, 1500 and 2000 m. A value of 1400 m has been included since the results will then correspond to a sub-surface buoy arrangement operating in 1500 m of water as already detailed .i.e. the risers vertical offset = 1400 m. An increase in water depth requires a greater length of riser and hence a greater suspended weight. If this characteristic is coupled with the fact that as the sea depth is increased, the risers inclination with the horizontal also increases then the outcome is a reduced horizontal force and a greater vertical load acting upon the riser as shown in graphs (a) and (b) respectively. The resultant of these two load components acting perpendicular to one another is a tensile force acting axially along the riser. For a relatively small horizontal offset such as 1000 m, it is shown that axial tension significantly increases with vertical offset, see Figure 2.24(c). This is due to the dominance of the increasing vertical load component over the declining horizontal load component, since the riser has a relatively steep slope, however this dominance reduces as the horizontal offset is increased and the gradient becomes increasingly shallow. For a horizontal offset of 2000 m the reduction in horizontal force becomes the dominate characteristic in going from a sea depth of 1000 to 1400 m to such an extent that the resultant axial tension at the surface actually decreases slightly. If the sea depth is further increased up to 2000 m then the axial tension is also increased and so it is then apparent from Figure 2.26(c) that an optimum sea depth of approximately 1400 m can be

established, however more data points are required in order to attain a more accurate behavioural picture.

2.4 Mooring Characteristics

2.4.1 Introduction

As previously stated a catenary riser is effectively a mooring line and will therefore introduce a stiffness composed of an elastic and geometric stiffness on both heave and surge surface vessel motions. Surge is taken in this analysis to describe horizontal motion within the plane of the riser i.e. along the X-axis, see Figure 2.6(a). As the vessel moves in response to environmental loads such as waves and current, surface restoring forces are generated from a change in tension, brought about by the varying riser geometry. These forces are non-linear and are solely dependent upon catenary configuration i.e. offset length (vertical and horizontal) and submerged weight. This section therefore aims to examine the mooring potential of both riser systems in both heave and surge by calculating stiffnesses for a range of offsets and submerged unit weights. The two production system concepts in question both consist of an in-plane double catenary riser arrangement as proposed in Chapter 1, and can be summarised as follows :

- Hybrid Concept - two risers connecting to a sub-surface buoy 100 m below the sea surface
  catenary vertical offset = sea depth - 100 m = 1400 m

- Two risers connecting to an FPSO turret on the sea surface
  catenary vertical offset = sea depth = 1500 m

For the purposes of this study stiffness values are calculated using surface or near surface horizontal displacements of up to 100 m which is approximately 7% of water depth. For a tethered sub-surface buoy a drift displacement of 7% would considered a maximum, however for a surface moored vessel (FPSO) excursions of up to 25% of water depth may need to be designed for in order to accommodate the simultaneous scenario of a 100 year current with a damaged mooring system. The bending and axial loading exerted on the risers as a consequence of in-plane surface displacements are investigated in Chapter 5.

The following analysis neglects the effect of elasticity on the grounds that it will be small due to the risers large axial stiffness *(AE)* generated by the relatively high combined cross-sectional area of the carrier pipe and flowline bundle. The riser is assumed to have a constant submerged weight per unit length *w*.

2.4.2 Mooring Stiffness - In Plane

Figure 2.3 shows a catenary riser deployed from a connecting point *A* on the underside of a sub-surface buoy or FPSO to a point *B* on the seabed with horizontal and vertical offsets *a* and *b* respectively. Points *A* and *B* represent catenary riser end positions for an undisplaced condition i.e. point *A* can be considered as the centre of a surface excursion watch circle. As the surface vessel is disturbed from point *A*, through A_3, to A_4, the length of catenary riser lying on the seabed progressively increases resulting in a reduction in suspended length. The tension load in the riser at the surface end position A_i is a function of the total submerged weight of the suspended length and so as this decreases so does the tension. This feature coupled with the simultaneous increase in riser angle to the horizontal causes the horizontal force H_i on the vessel to decrease in a non-linear manner. If the surface end is shifted in the opposite direction i.e. from *A*, through A_2, to A_1 then the riser is lifted off the seabed and the suspended length is subsequently increased. The tension increases due to the extra riser weight and coupled with a reduction in riser inclination at the buoy connection the horizontal force is increased. Vertical displacements exhibit exactly the same behaviour. If the surface end is shifted upwards from A_1 through to A_4 the riser is progressively lifted off the seabed and the downward vertical force Vs_i exerted on the surface vessel increases, see Figure 2.4. However if it is shifted downwards the opposite occurs i.e. the vertical surface force decreases.

A mooring analysis is carried out utilising the equations developed in Section 2.3 within a FORTRAN computer program thus enabling the many iterations required to be carried out quickly and easily. Calculations are set up initially to ascertain the horizontal and vertical forces exerted on the surface vessel at prescribed displacements from an initial undisplaced position *A*.

- up to ±100 m in 25 m increments - horizontally
- up to ±50 m in 25 m increments - vertically

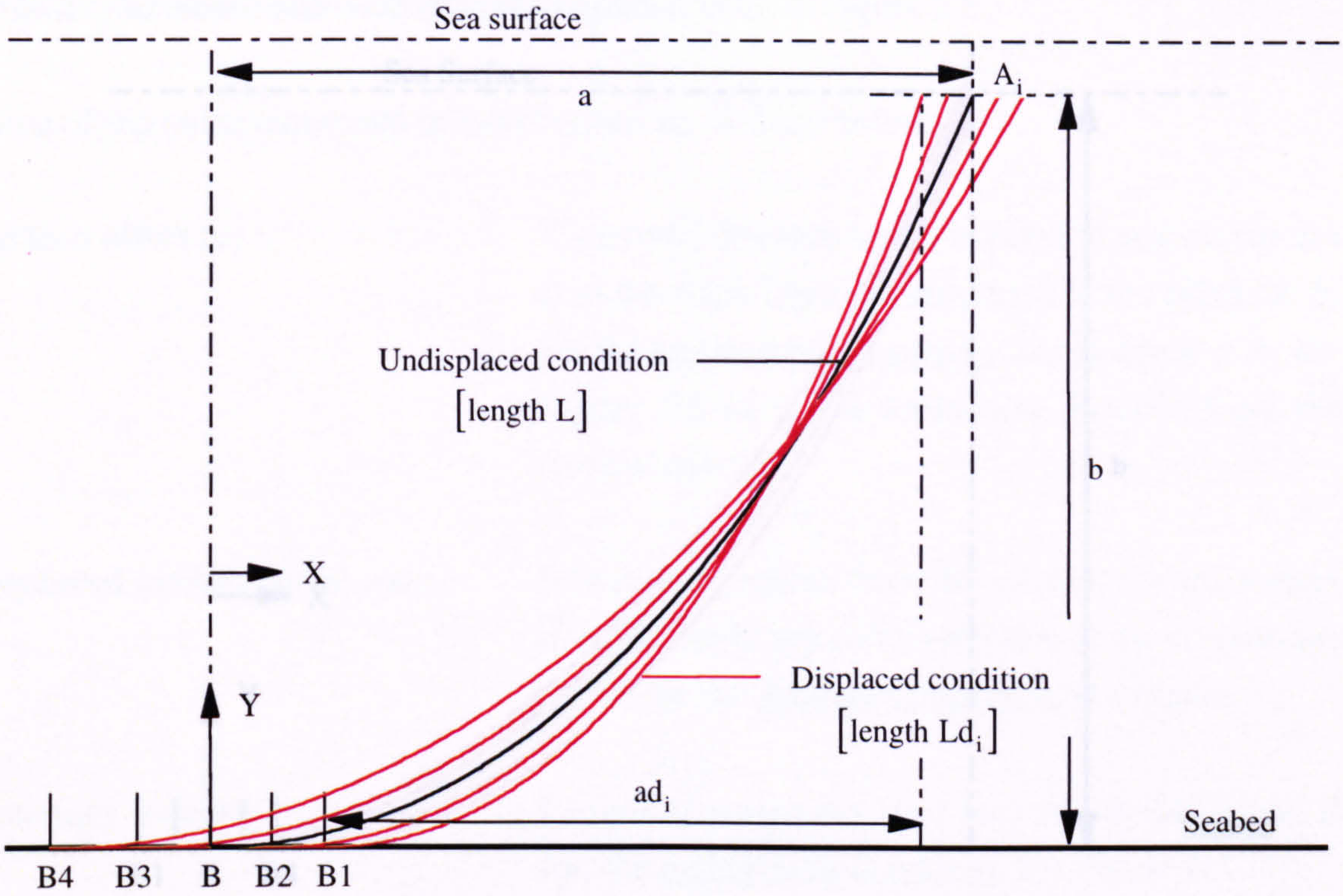

(a)

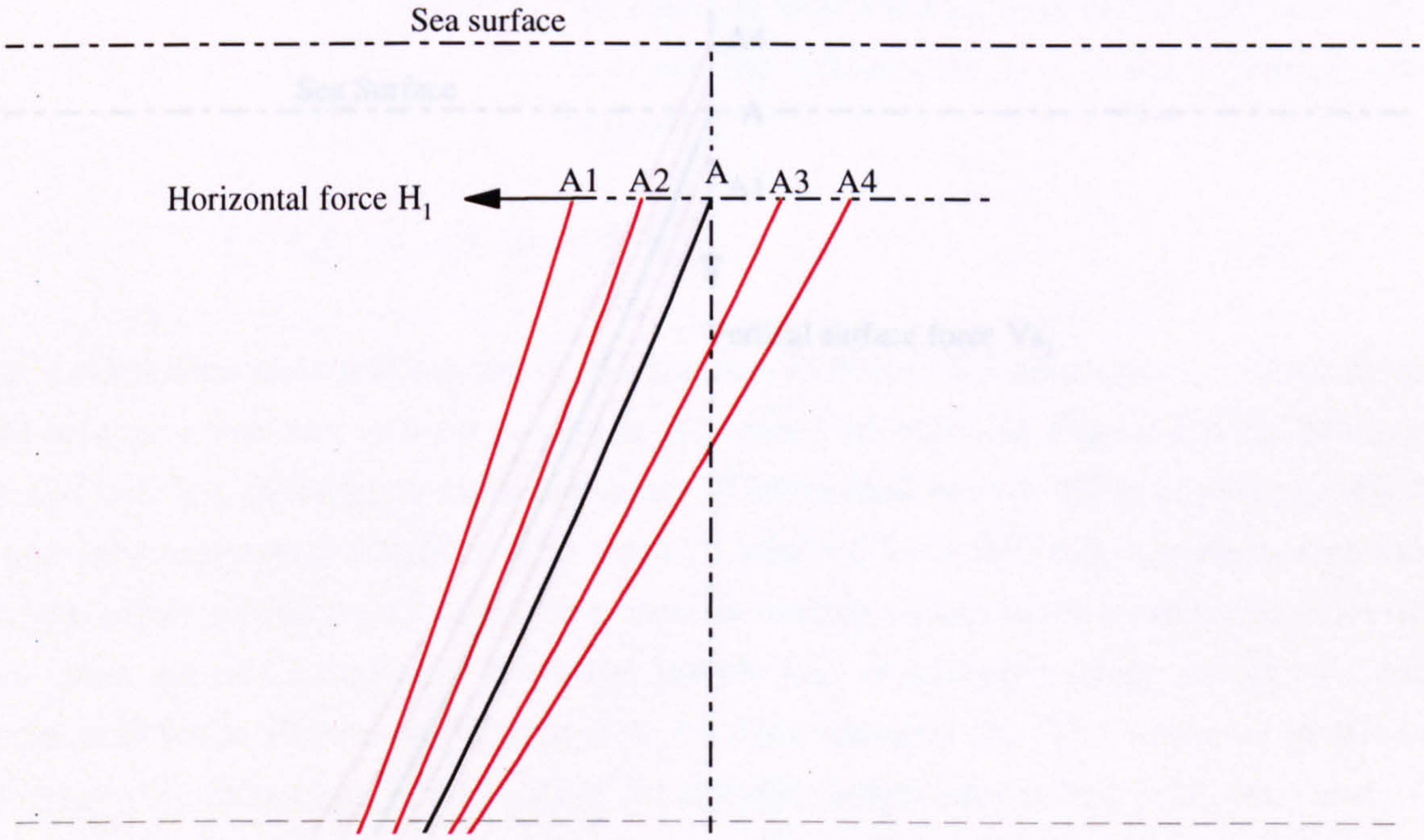

(b)

Figure 2.3
Catenary Riser Mooring Behaviour in Surge

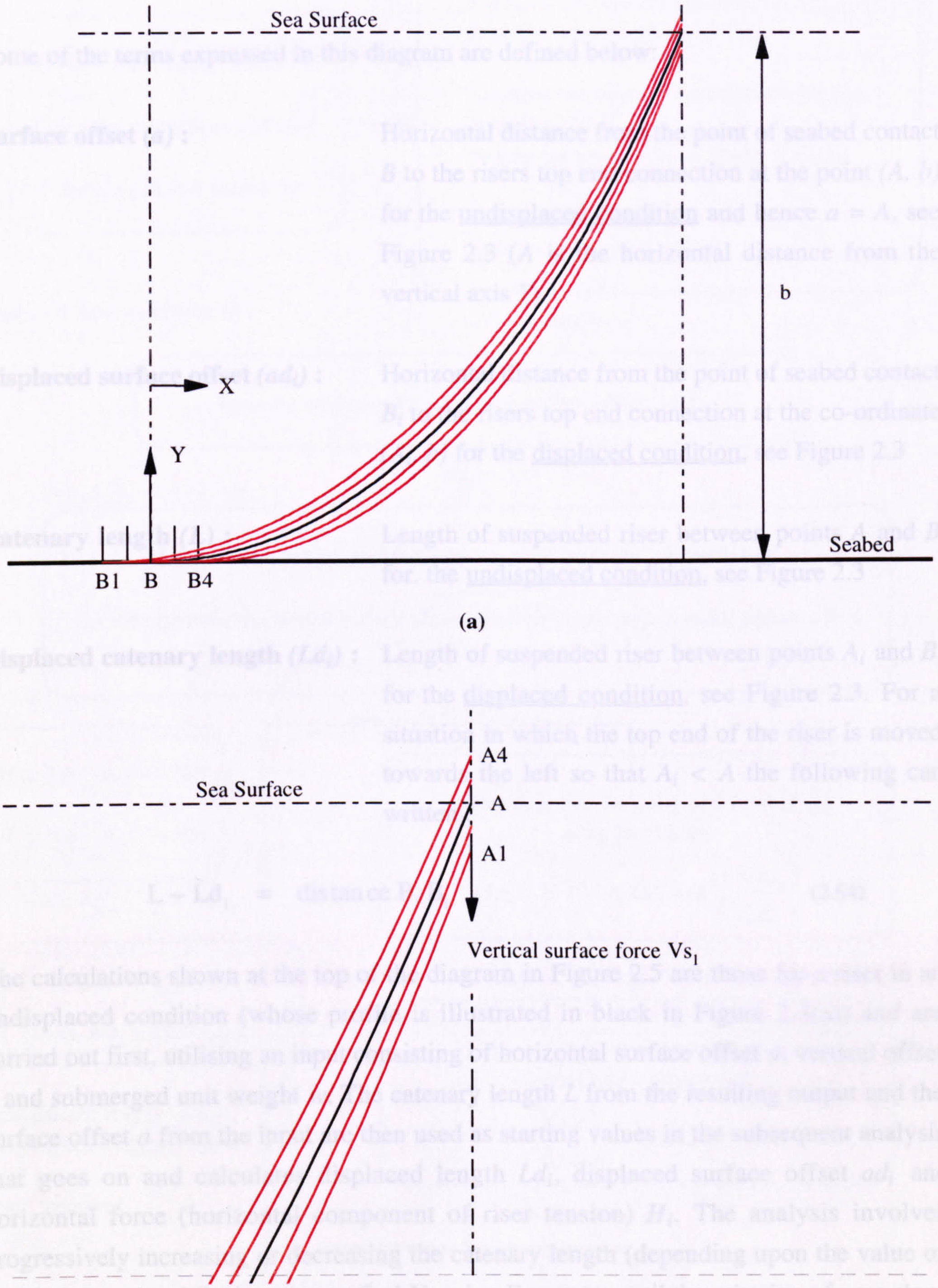

Figure 2.4
Catenary Riser Mooring Behaviour in Heave

The analytical process can be represented in block diagram form and as an example, the surge displacement case is displayed diagramatically in Figure 2.5.

Some of the terms expressed in this diagram are defined below:

Surface offset *(a)* : Horizontal distance from the point of seabed contact B to the risers top end connection at the point (A, b) for the undisplaced condition and hence $a = A$, see Figure 2.3 (A is the horizontal distance from the vertical axis Y).

Displaced surface offset (ad_i) : Horizontal distance from the point of seabed contact B_i to the risers top end connection at the co-ordinate (A_i, b) for the displaced condition, see Figure 2.3

Catenary length *(L)* : Length of suspended riser between points A and B for. the undisplaced condition, see Figure 2.3

Displaced catenary length (Ld_i) : Length of suspended riser between points A_i and B_i for the displaced condition, see Figure 2.3. For a situation in which the top end of the riser is moved towards the left so that $A_i < A$ the following can written :

$$L - Ld_i = \text{distance } B, B_i \qquad (2.64)$$

The calculations shown at the top of the diagram in Figure 2.5 are those for a riser in an undisplaced condition (whose profile is illustrated in black in Figure 2.3(a)) and are carried out first, utilising an input consisting of horizontal surface offset a, vertical offset b and submerged unit weight w. The catenary length L from the resulting output and the surface offset a from the input are then used as starting values in the subsequent analysis that goes on and calculates displaced length Ld_i, displaced surface offset ad_i and horizontal force (horizontal component of riser tension) H_i. The analysis involves progressively increasing or decreasing the catenary length (depending upon the value of A_i relative to A) whilst iterating to find H_i using Eqn (2.51) until the criterion of zero slope at the seabed is satisfied.

Undisplaced riser condition :

Input

1. Horizontal surface offset (a)
   (as = a)
2. Vertical offset/Sea depth (b)
3. Submerged unit weight (w)

Calculate the catenary constant (c)
from the iteration of Eqn (2.27)

Calculate the catenary riser total length (L)
from Eqn (2.33)
Suspended length = Total length (Ls = L)

Calculate the horiziontal force (H)
from c = H/w (see Eqn 2.49)

Displaced riser condition (i) :

Input the displacement horizontal surface offset (a_i)

Let the displaced suspended length equal the undisplaced total length

$$Ls_i = L$$

Let the suspended horizontal surface offset equal the displaced horizontal surface offset

$$as_i = a_i$$

Iterate to find the horizontal force (H_i)
using Eqn (2.56)

$$\left(Ls_i - b^2\right) w^2 = 4 H_i \sinh^2\left(\frac{w\, as_i}{2 H_i}\right)$$

Calculate the riser slope at the seabed
using Eqn (2.44) at x = 0

$$\left(\frac{dy}{dx}\right)_0 = \sinh(\vartheta)$$

Is the seabed slope zero ?

No

If $a_i > a$ $\quad n = +0.001$

If $a_i < a$ $\quad n = -0.001$

$Ls_i = Ls_i + n$

$as_i = a_i - (L - Ls_i)$

Suspended length (Ls_i)
is progressively decreased
if $a_i < a$
and increased
if $a_i > a$

Yes

Output

$(H_i, Ls_i$ and $as_i)$

Figure 2.5

Block diagram for the catenary parameter calculations

If the surface forces are plotted against vessel or buoy offset a non-linear curve is obtained and since the stiffness is equal to the differential of the curve then it can be considered as behaving linearly over the displacement range. For a single riser arrangement the horizontal and vertical forces are always in the same direction and hence the stiffness is uni-directional i.e. it only acts left to right horizontally (for the configuration shown in Figure 2.3) and upwards vertically. For the purposes of a comparative study the risers stiffness at the zero displacement position is calculated, which is done by assuming the force curve to be linear between prescribed displacements lying either side of this position i.e. 25 and -25 m. In most situations this stiffness value will be a good approximate to the mean for the entire displacement range. Surge displacement profiles and force curves for the sub-surface buoy system with varying horizontal offsets and unit weights are illustrated in Figures 2.27 to 2.29. Three main conclusions can be drawn from these results:

For a given displacement

- Curve gradient increases with unit weight
- Curve gradient increases with a reduction in vertical offset
- Restoring force increases with horizontal offset

The first point can be explained by noting that as the top end of the riser is displaced from A to A_i the same amount of riser is either lifted off or deposited on the seabed irrespective of its submerged weight. However the resulting increase or decrease in riser tension and hence restoring force is a function of unit weight and therefore varies. This observation is demonstrated more clearly if the stiffness k is tabulated against a selection of riser unit weights, see Table 2.6.

Submerged unit weight (N/m)	Stiffness for a Single Riser Arrangement (kN/m)	Stiffness for a Double Riser Arrangement (kN/m)
100	0.427	0.854
500	2.134	4.268
1000	4.267	8.534
1500	6.401	12.802
2000	8.534	17.068

Table 2.9

Surge Stiffnesses for a Horizontal Offset of **1500 m** and a Vertical Offset of **1400 m.**

The second conclusion can be demonstrated in Table 2.10. As the vertical offset is reduced the riser curvature at the seabed end decreases with the consequence that a greater length of riser is either deposited on or lifted off the seabed for a given displacement. This results in a greater curve gradient and hence a higher stiffness.

Vertical offset (m)	Stiffness for a Single Riser Arrangement (kN/m)	Stiffness for a Double Riser Arrangemnt (kN/m)
1400	8.534	17.068
1500	7.437	14.874

Table 2.10

Surge Stiffnesses for a Horizontal Offset of **1500 m** and a Submerged Weight of **2000 N/m.**

Finally, Table 2.11 shows the effect of horizontal offset on surge stiffness, from which it is shown that stiffness increases with offset. The reasons for this are identical to those given above concerning the effects of a reduction in vertical offset. Increasing the horizontal offset for a given vertical offset has the same effect geometrically as reducing the vertical offset whilst keeping *a* constant. A comprehensive set of stiffness results for both surge and heave displacements are tabulated in Tables 2.18 to 2.20.

Horizontal offset (m)	Stiffness for a Single Riser Arrangement (kN/m)	Stiffness for a Double Riser Arrangement (kN/m)
1000	4.237	8.474
1250	6.091	12.182
1500	8.534	17.068
1750	11.697	23.394
2000	15.719	31.438

Table 2.11

Surge Stiffnesses for a Vertical Offset of **1400 m** and Submerged Weight of **2000 N/m**

The analysis so far has concentrated on calculating the in-plane stiffness associated with a single riser arrangement as shown in Figure 2.3, however both the sub-surface buoy and FPSO concepts involve two in-plane risers as illustrated in Figure 2.6(a). The combined bi-directional stiffness can be calculated by first modelling the system as an equivalent spring arrangement in which two identical springs are attached in tandem to opposite

sides of a block, see Figure 2.6(b). Both springs are subjected to a pretension F_0 and represent the two risers with a horizontal tension H, attached to a buoy or surface vessel (modelled as a simple block) at zero displacement. In this condition there are no external forces exerted on the system and so an equation of static equilibrium can be expressed simply as:

$$F_0 - F_0 = 0 \tag{2.65}$$

If the surface vessel or block is displaced a distance x by an external force F_{ext} then the static equilibrium equation is as follows:

$$(F_0 - kx) + F_{ext} - (F_0 + kx) = 0 \tag{2.67}$$

where k is the stiffness of a single riser arrangement. F_0 cancels out and therefore:

$$-kx + F_{ext} - kx = 0$$

$$F_{ext} = 2kx \tag{2.68}$$

This expression shows that the total stiffness of the two riser system is simply twice that of the single riser arrangement i.e.

$$k_T = 2k \tag{2.69}$$

This expression also applies in the case of vertical displacements.

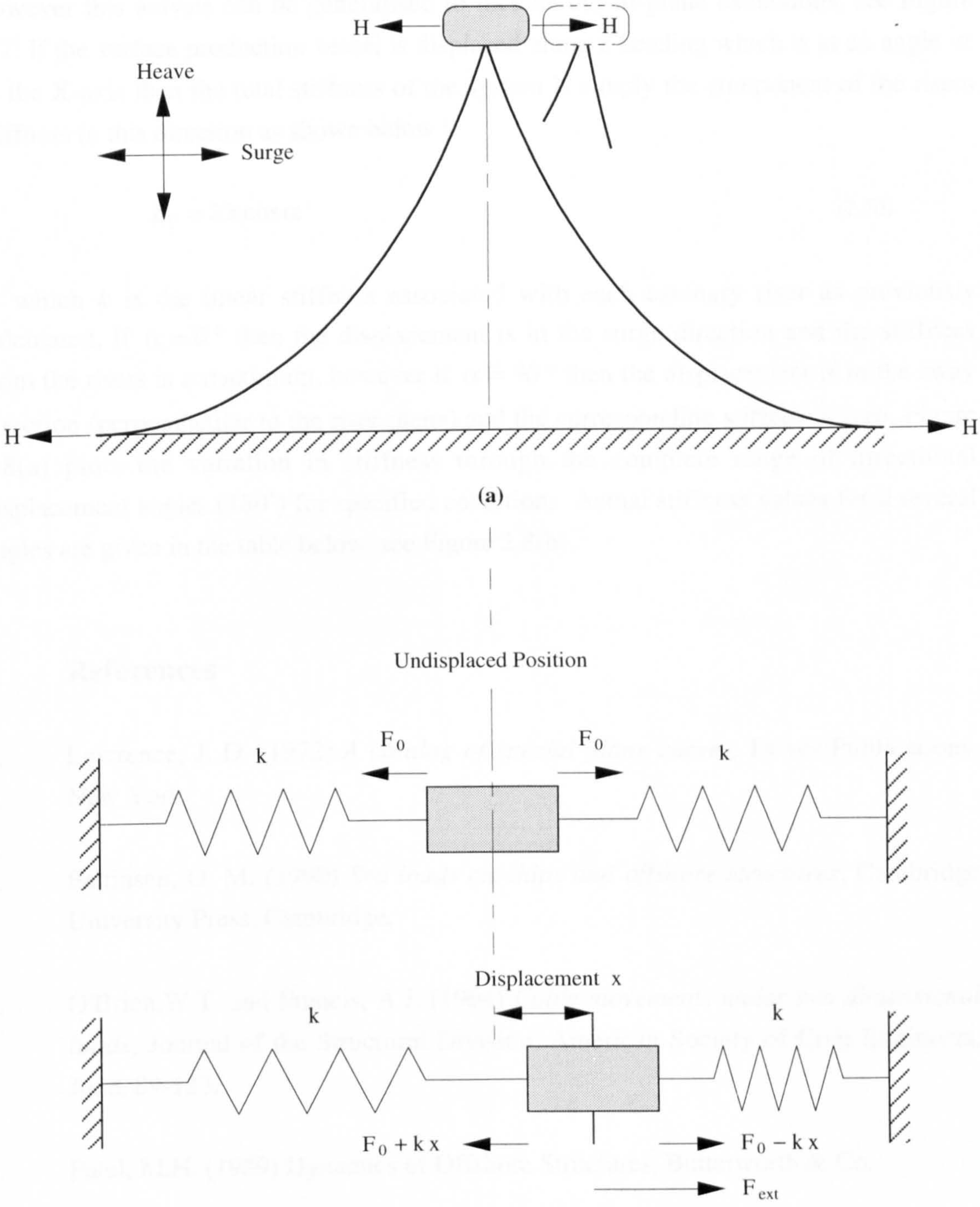

Figure 2.6

In-Plane Catenary Riser Stiffness

2.4.3 Mooring Stiffness - Out of Plane

The mooring behaviour of the riser arrangement has so far been based upon surface or near-surface displacements within the same plane i.e. heave and surge, however this anlysis can be generalised to include out-of-plane excursions, see Figure 2.7. If the surface production vessel is displaced along a heading which is at an angle α to the X-axis then the total stiffness of the system is simply the component of the risers stiffness in this direction as shown below :

$$k_T = 2k\cos\alpha \qquad (2.70)$$

in which k is the linear stiffness associated with each catenary riser as previously calculated. If $\alpha = 0°$ then the displacement is in the surge direction and the stiffness from the risers is a maximum, however if $\alpha = 90°$ then the displacement is in the sway direction (perpendicular to the riser plane) and the corresponding stiffnes is zero. Figure 2.8(a) plots the variation in stiffness through the complete range of directional displacement angles (180°) for specified conditions. Actual stiffness values for a several angles are given in the table below, see Figure 2.8(b).

References

1. Lawrence, J. D. (1972) *A catalog of special plane curves*, Dover Publications, New York.

2. Faltinsen, O. M. (1990) *Sea loads on ships and offshore structures*, Cambridge University Press, Cambridge.

3. O'Brien,W.T. and Francis, A.J. (1964) *Cable movements under two dimensional loads*, Journal of the Structural Division, American Society of Civil Engineers, June, 89-123.

4. Patel, M.H. (1989) Dynamics of Offshore Structures, Butterworth & Co.

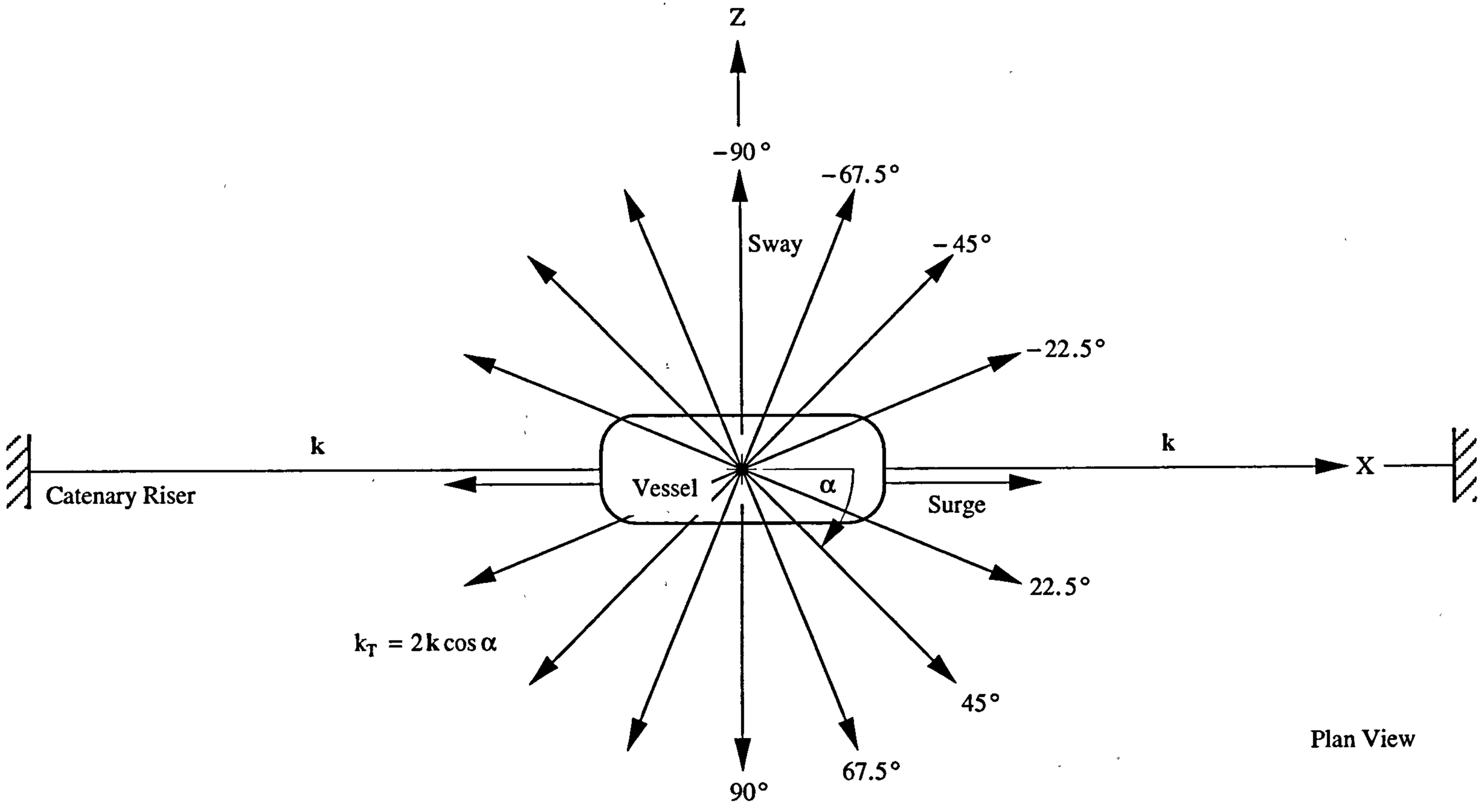

Figure 2.7

Out-of-Plane Catenary Riser Stiffness

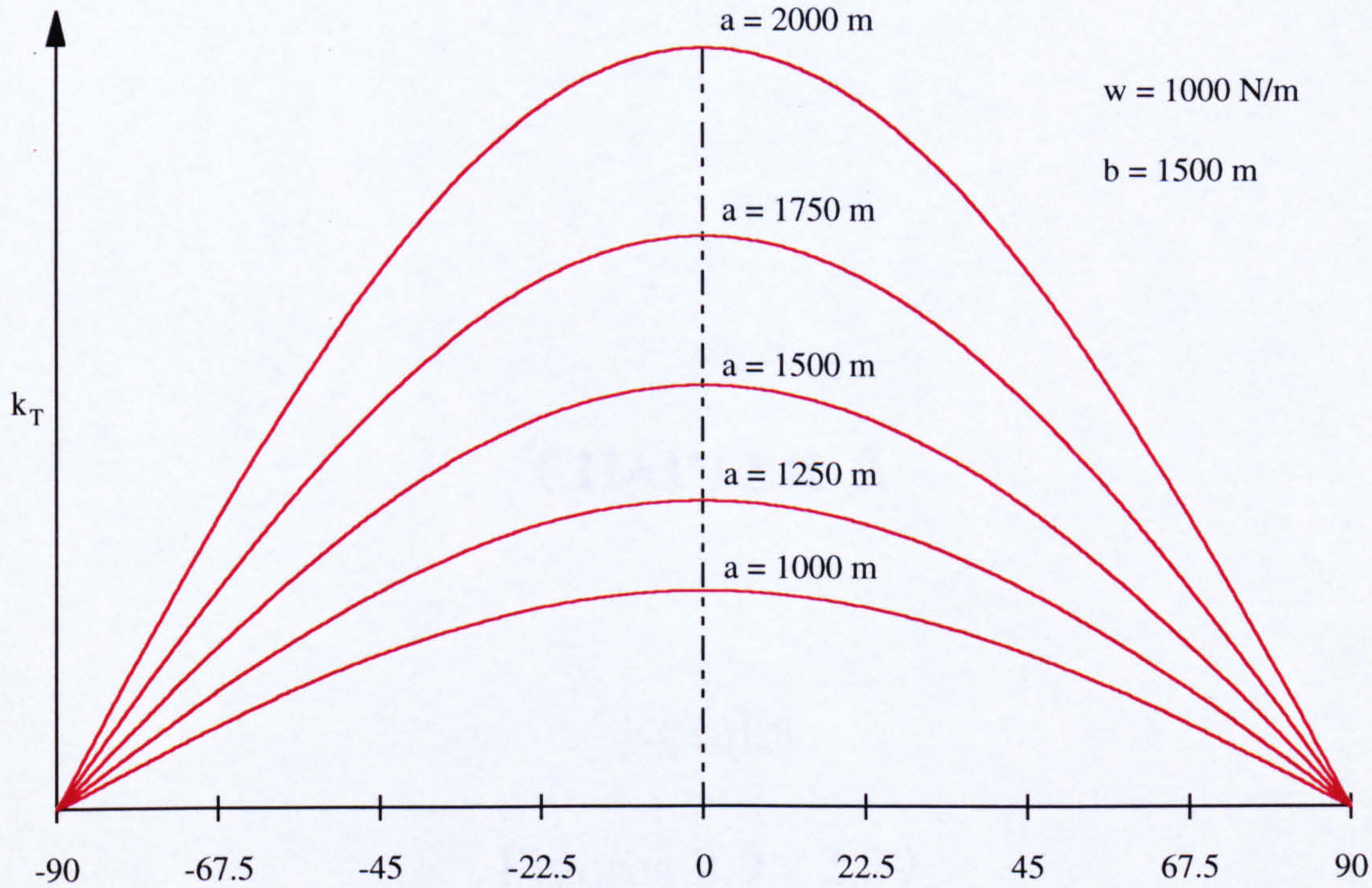

(a)

Horizontal Offset (m)	k	Total Horizontal Stiffness k_T 0°	22.5°	45°	67.5°	90°
1000	**1.906**	3.812	3.522	2.695	1.459	0.000
1250	**2.694**	5.388	4.978	3.810	2.062	0.000
1500	**3.718**	7.436	6.870	5.258	2.846	0.000
1750	**5.028**	10.056	9.291	7.111	3.848	0.000
2000	**6.675**	13.350	12.334	9.440	5.109	0.000
		surge				sway

(b)

Figure 2.8
Out-of-Plane Stiffness

CHAPTER 2

Results

Figures 2.9 - 2.29

Tables 2.12 - 2.20

Bending Moment Distribution (a = 1000 m)

(a)

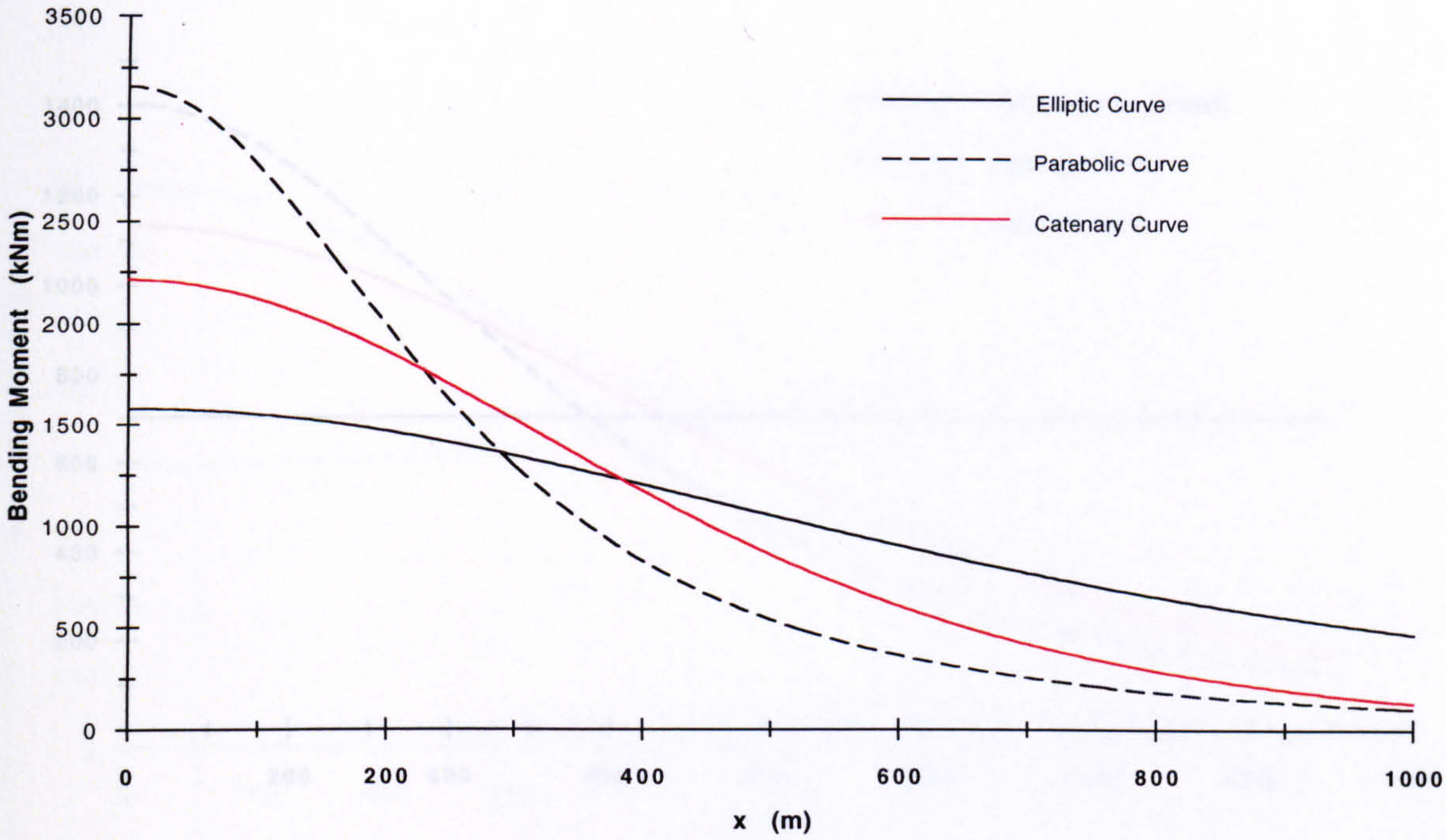

Bending Stress Distribution (a = 1000 m)

(b)

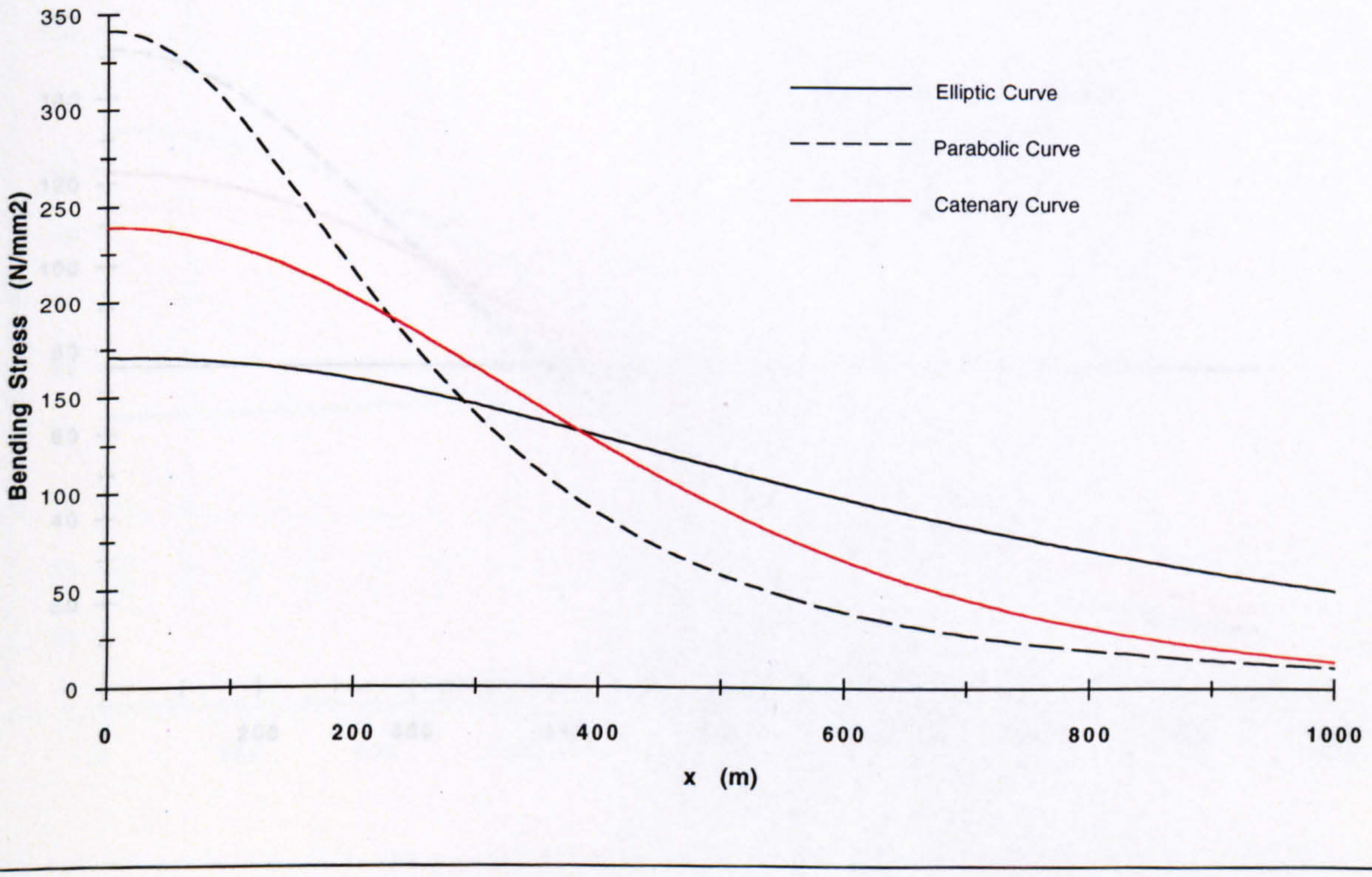

Horizontal Surface Offset = 1000 m

Carrier Pipe Outer Diameter = 1.10 m

Sea Depth = 1500 m

Carrier Pipe Wall Thickness = 10 mm

Figure 2.9

Bending Moment Distribution (a = 1500 m)

(a)

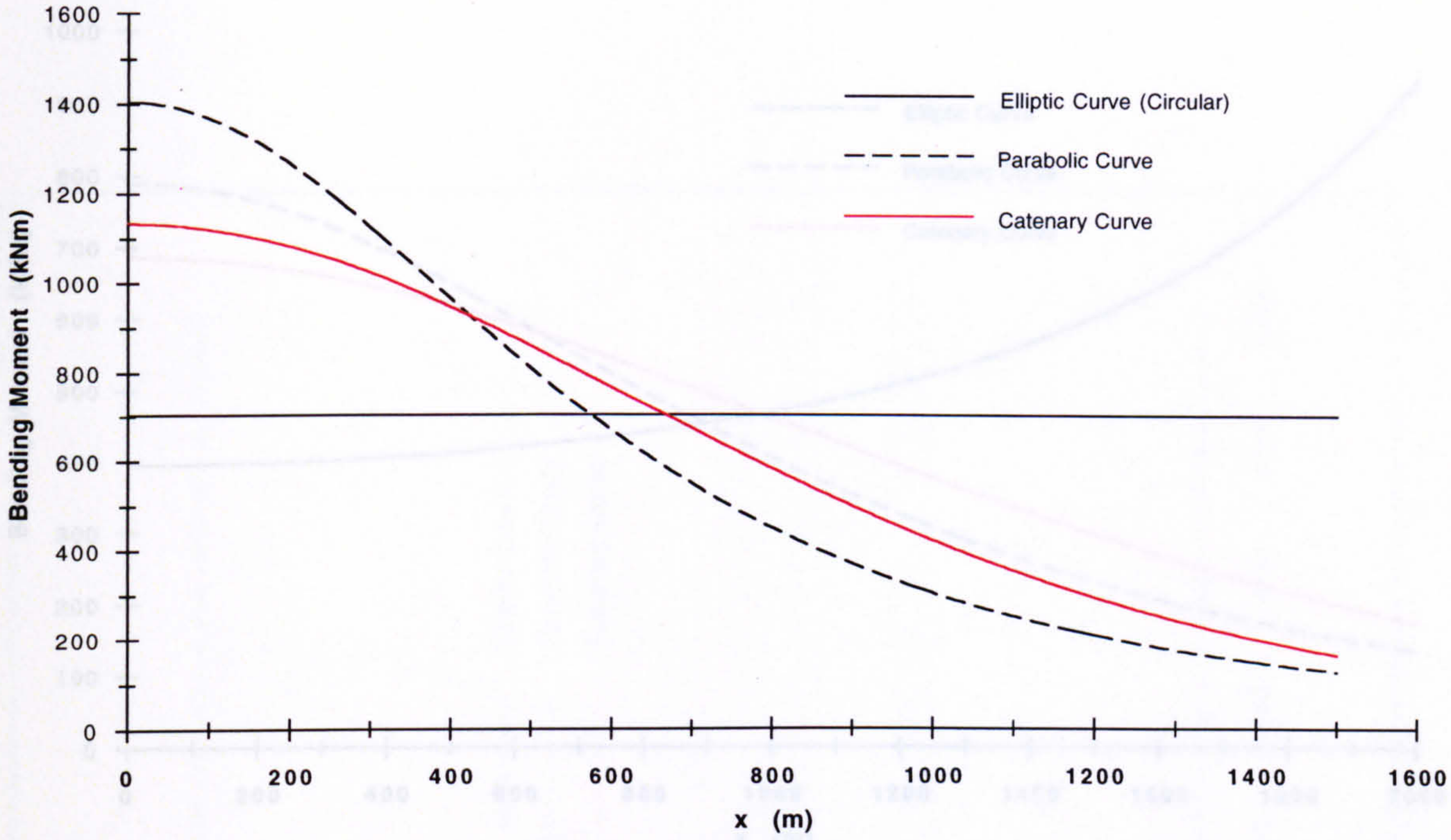

Bending Stress Distribution (a = 1500 m)

(b)

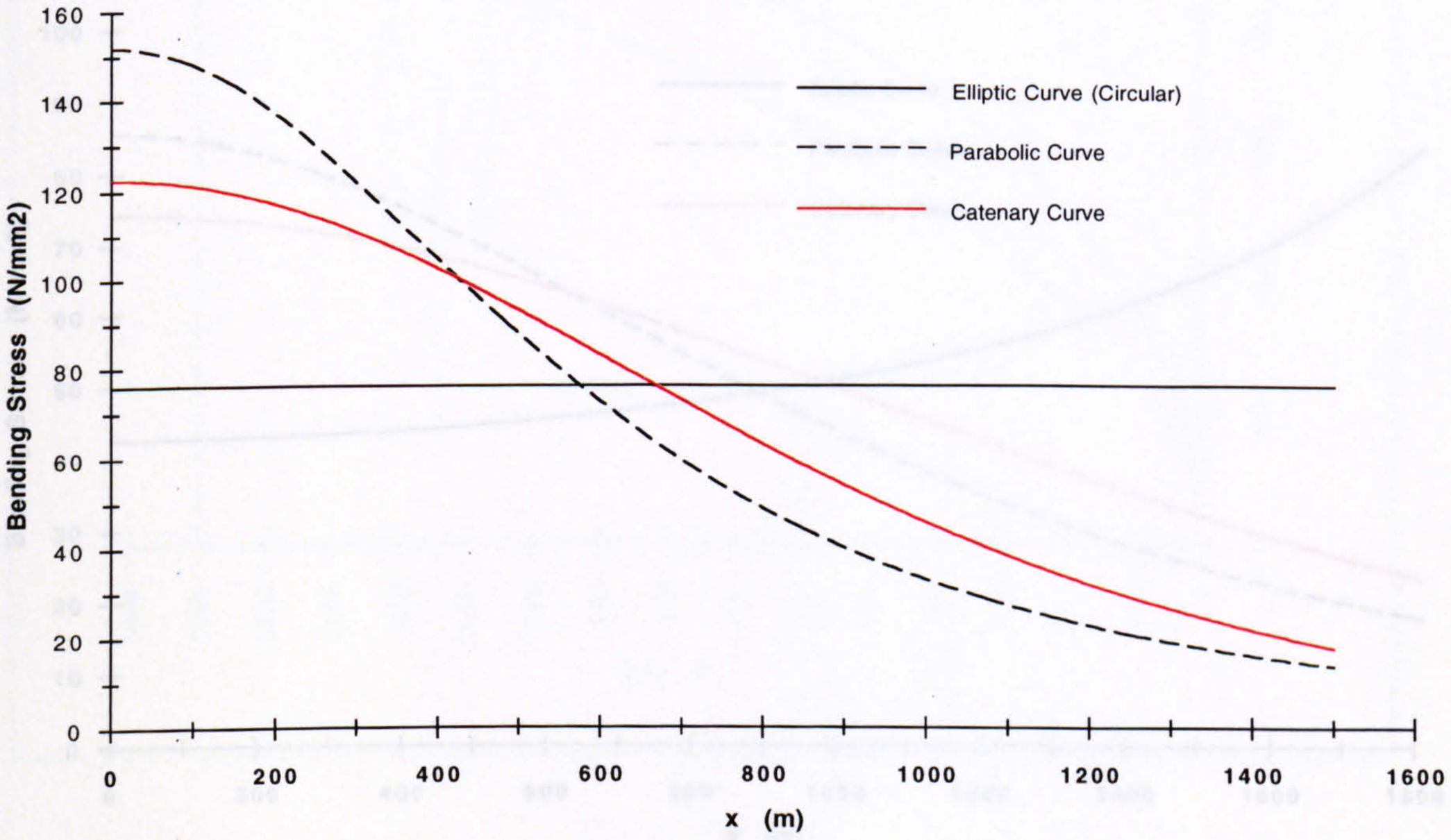

Horizontal Surface Offset = 1500 m

Sea Depth = 1500 m

Carrier Pipe Outer Diameter = 1.10 m

Carrier Pipe Wall Thickness = 10 mm

Figure 2.10

Bending Moment Distribution (a = 2000 m)

(a)

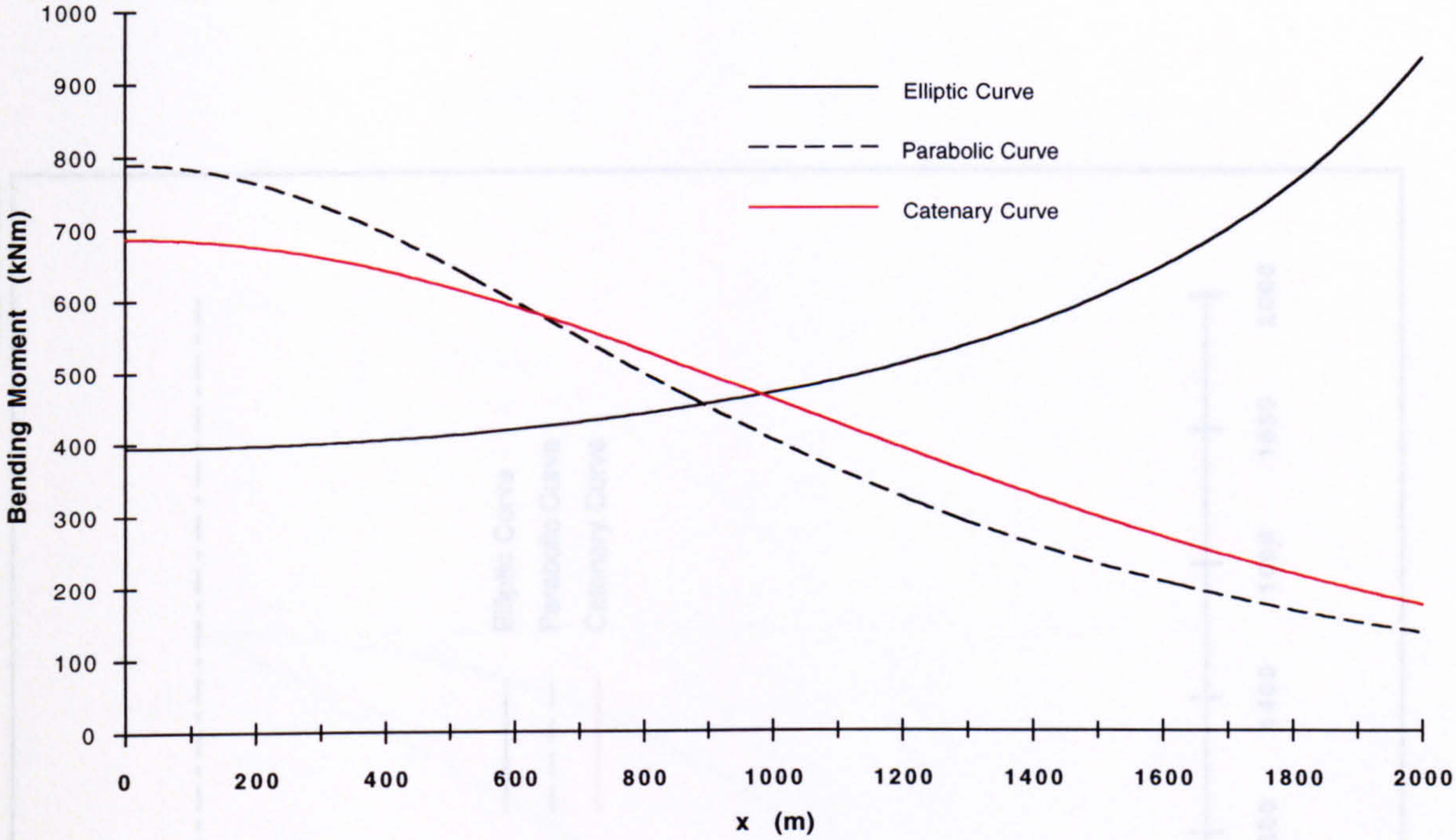

Bending Stress Distribution (a = 2000 m)

(b)

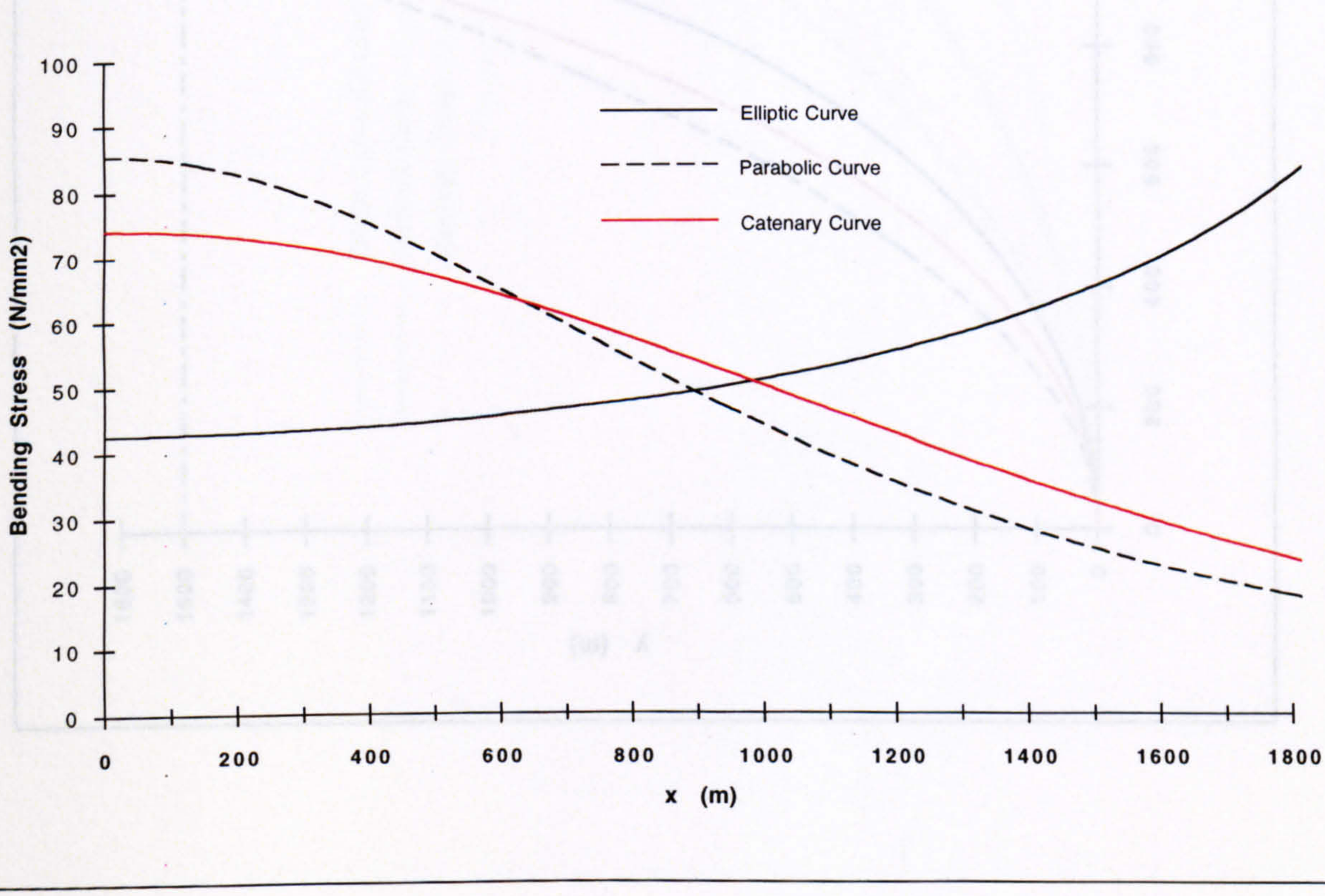

Horizontal Surface Offset = 2000 m

Sea Depth = 1500 m

Carrier Pipe Outer Diameter = 1.10 m

Carrier Pipe Wall Thickness = 10 mm

Figure 2.11

Elliptic, Parabolic and Catenary Curves (a = 1000 m)

Axes to Scale

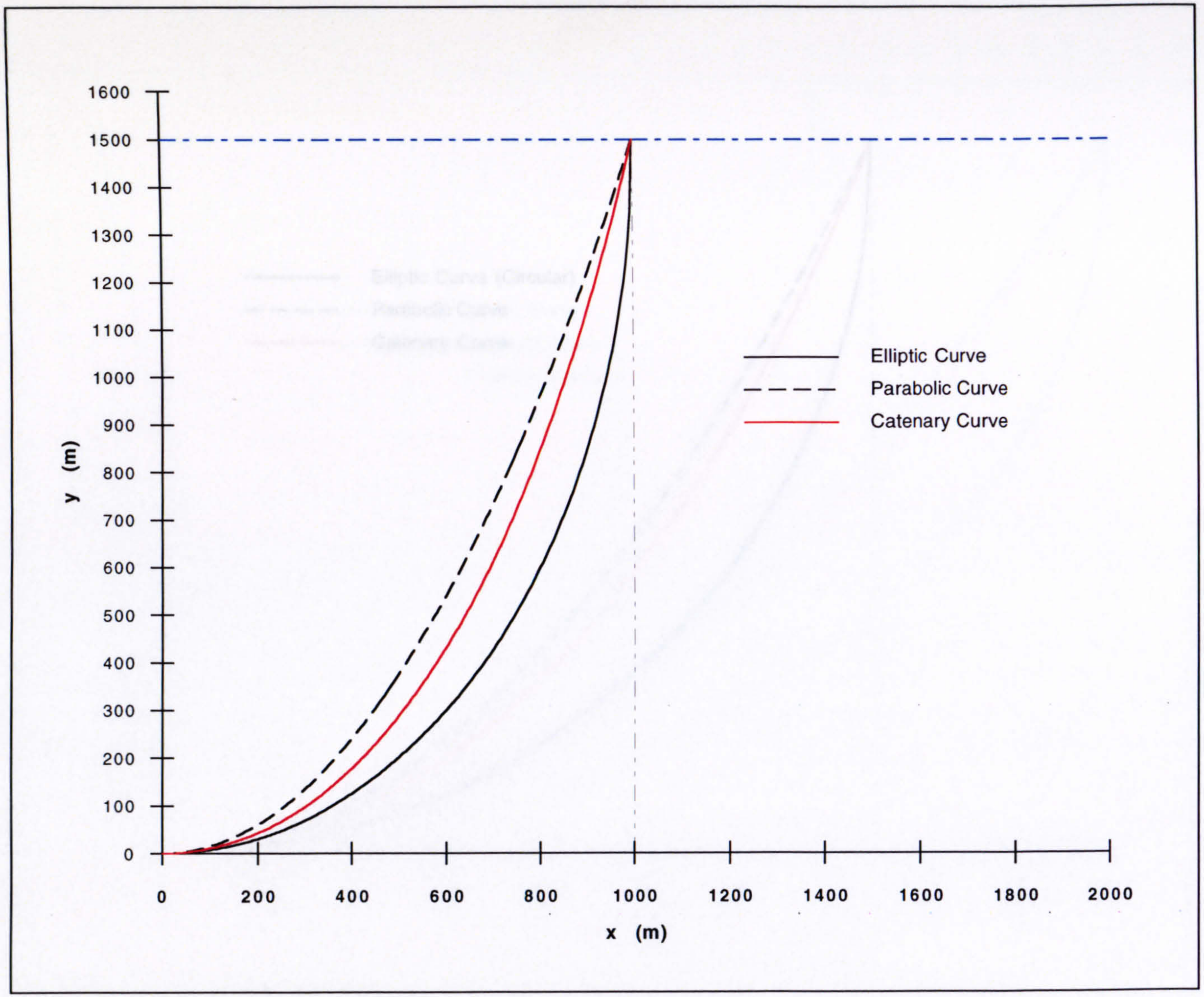

Horizontal Surface Offset = 1000 m

Sea Depth = 1500 m

Figure 2.12

Elliptic, Parabolic and Catenary Curves (a = 1500 m)

Axes to Scale

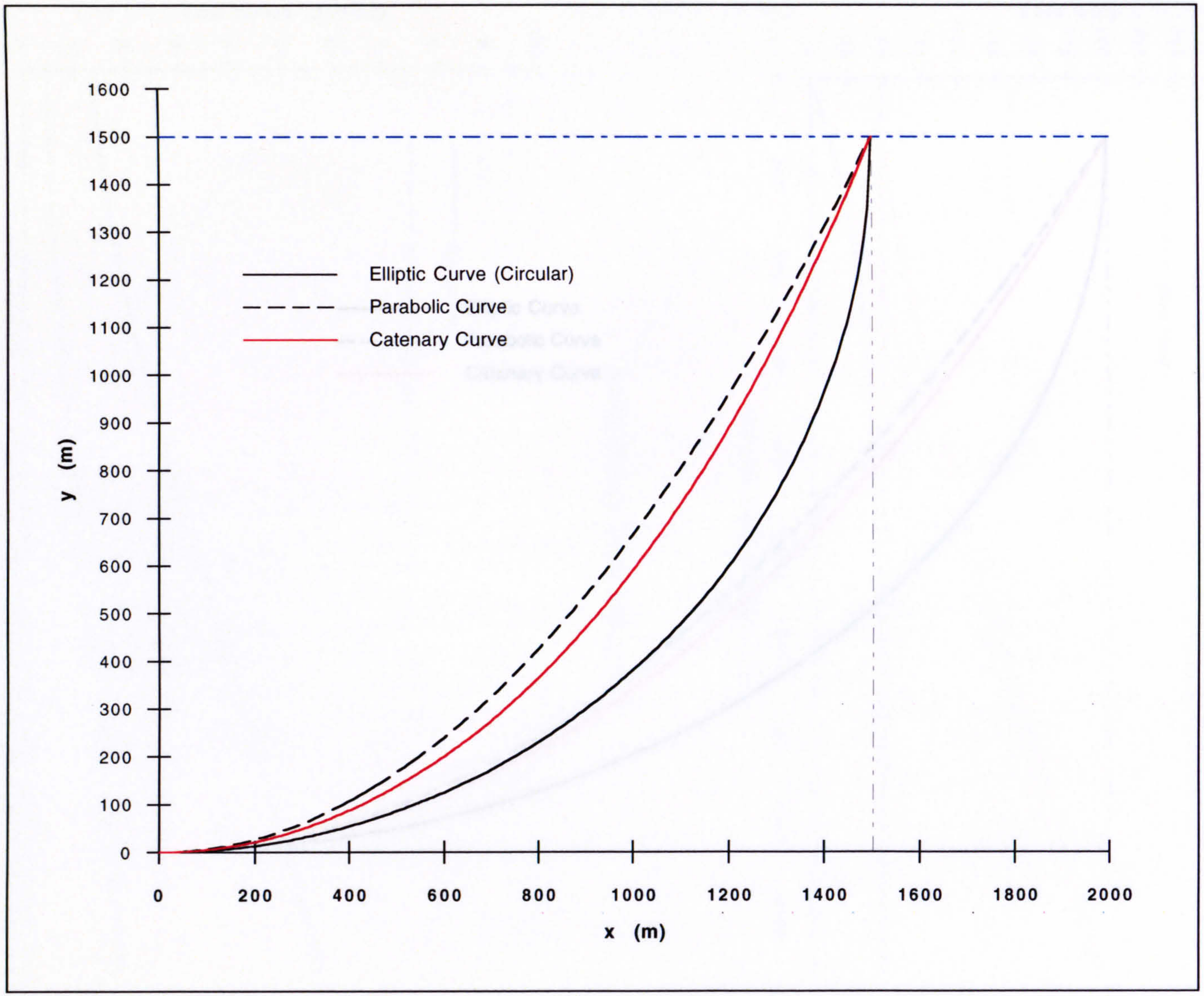

Horizontal Surface Offset = 1500 m

Sea Depth = 1500 m

Figure 2.13

Elliptic, Parabolic and Catenary Curves (a = 2000 m)

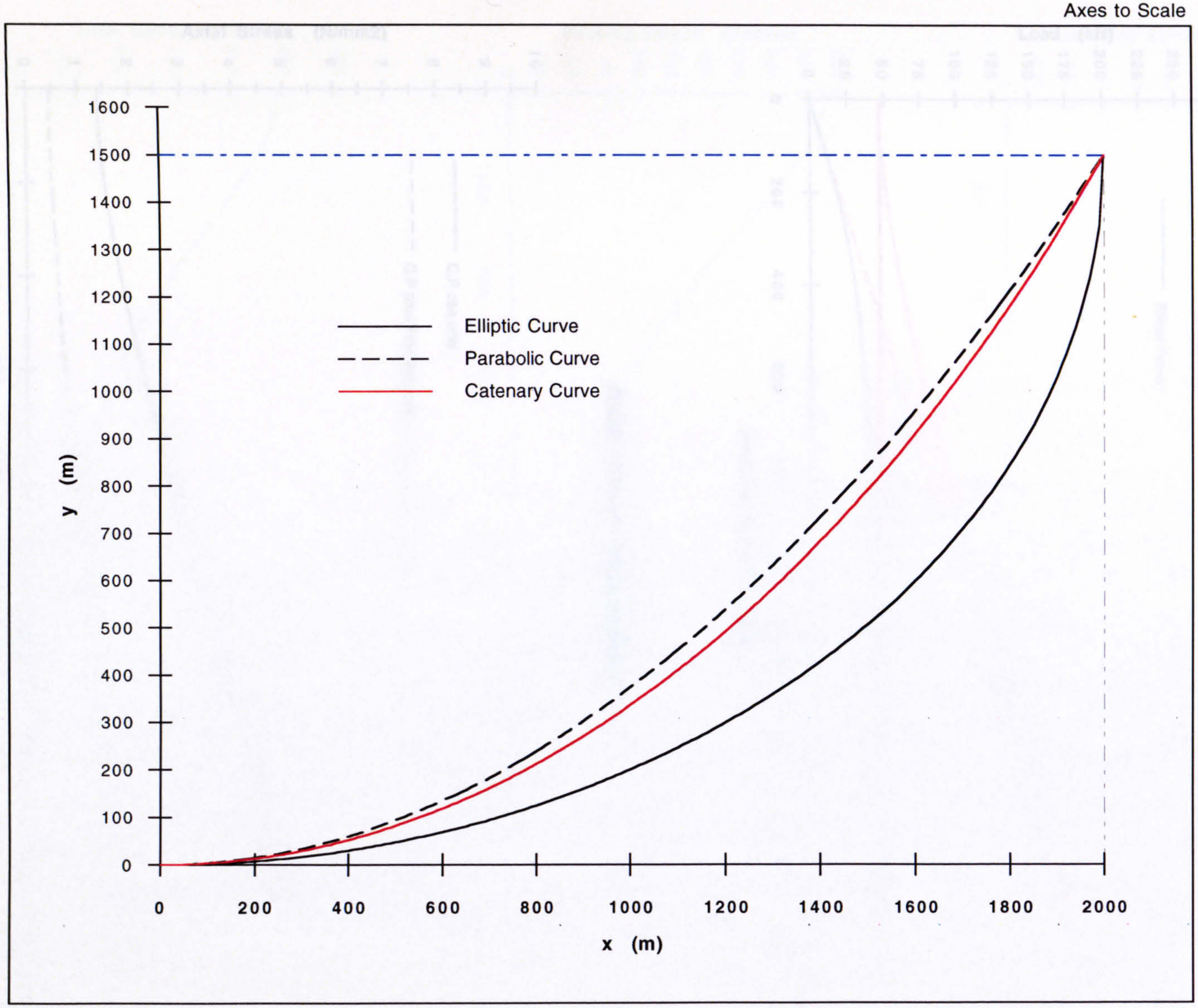

Horizontal Surface Offset = 2000 m

Sea Depth = 1500 m

Figure 2.14

Axial Load Distributions

(a)

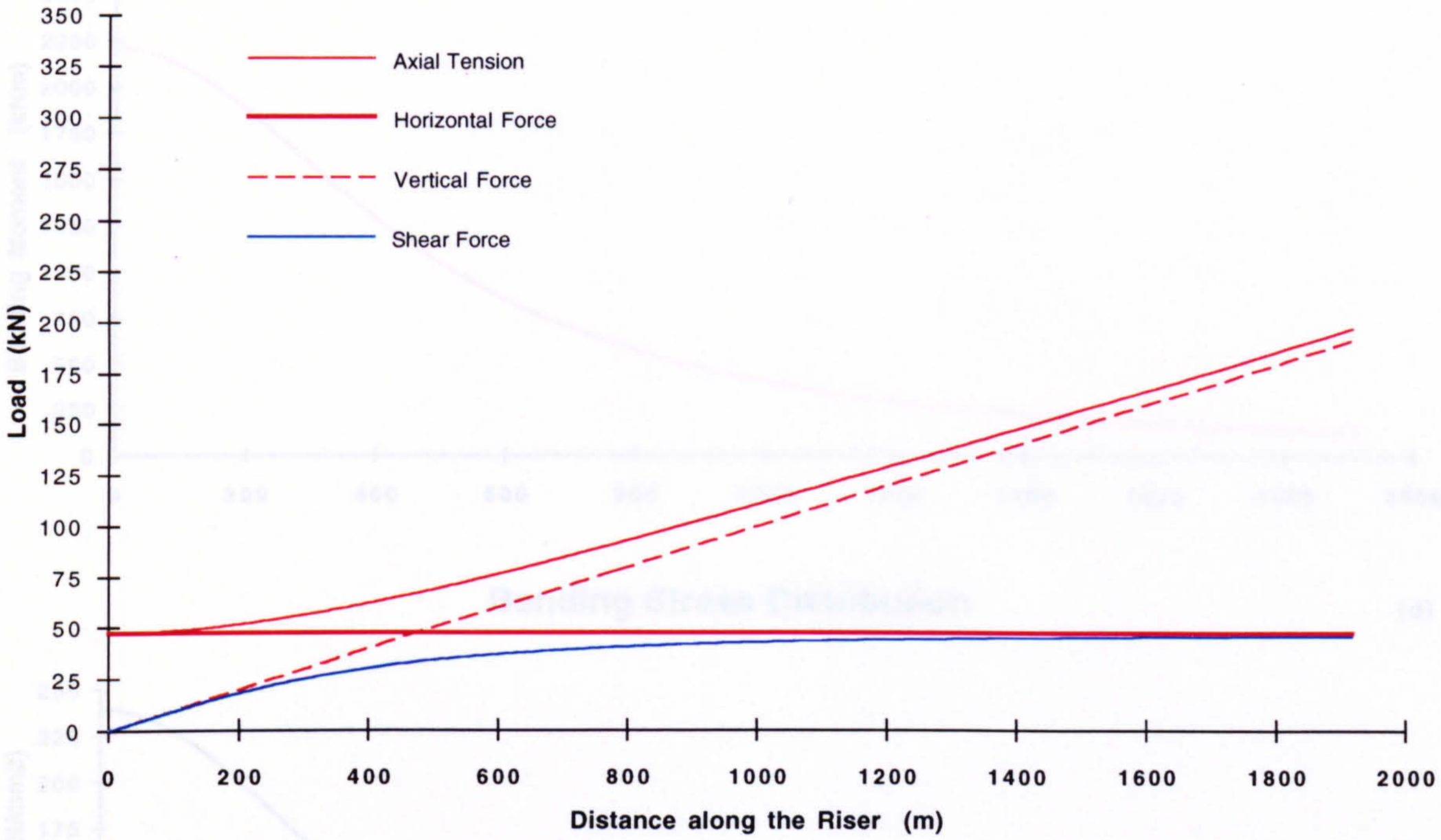

Axial Stress Distributions

(b)

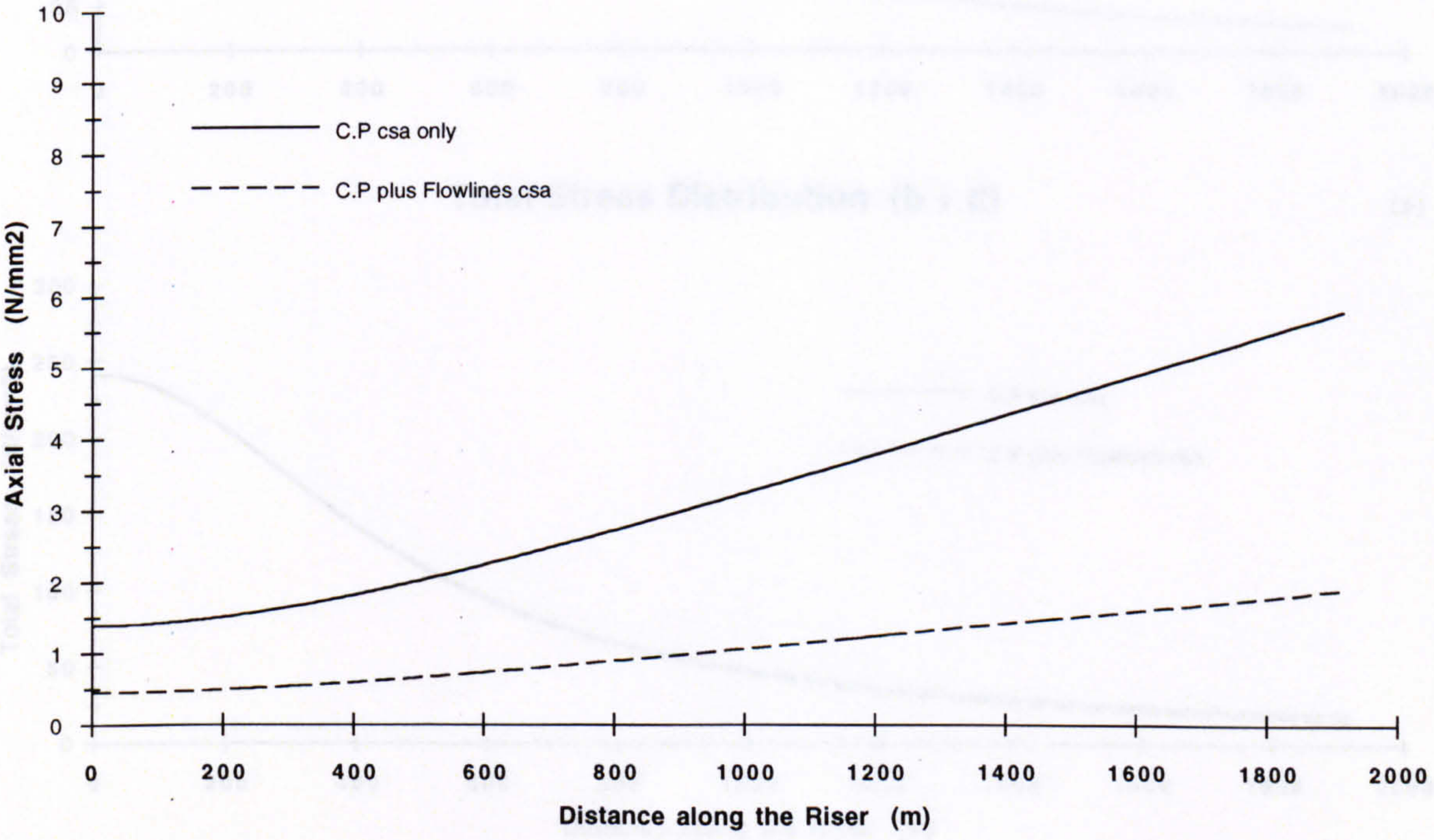

Horizontal Surface Offset = 1000 m

Submerged Unit Weight = 100 N/m

Sea Depth = 1500 m

Carrier Pipe Outer Diameter = 1.10 m

Carrier Pipe Wall Thickness = 10 mm

Figure 2.15

Bending Moment Distribution

(c)

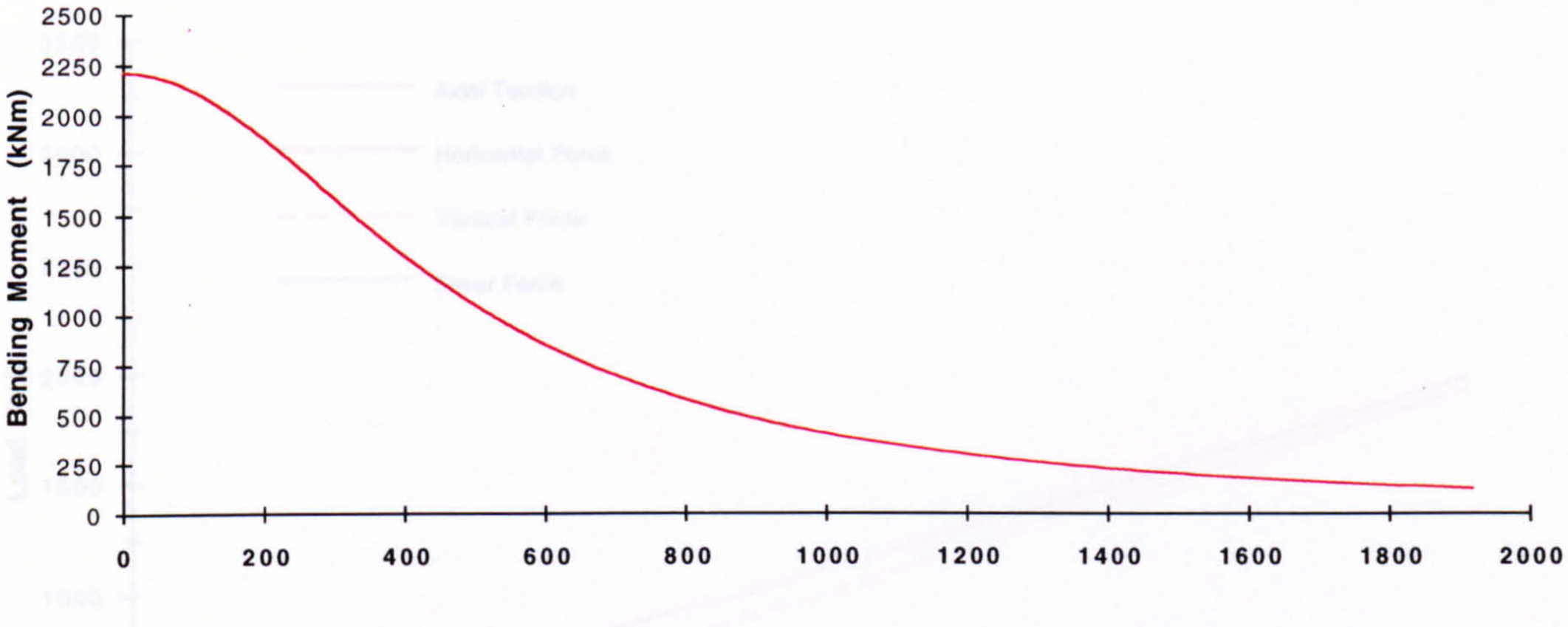

Bending Stress Distribution

(d)

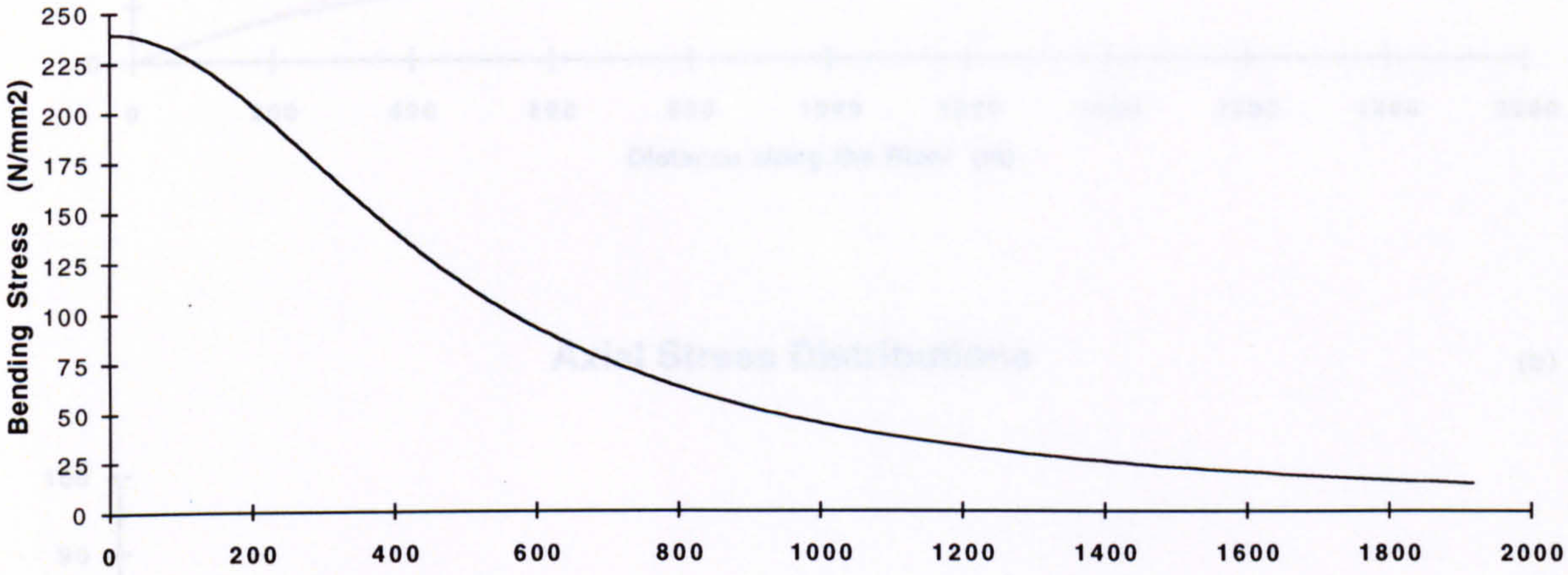

Total Stress Distribution (b + d)

(e)

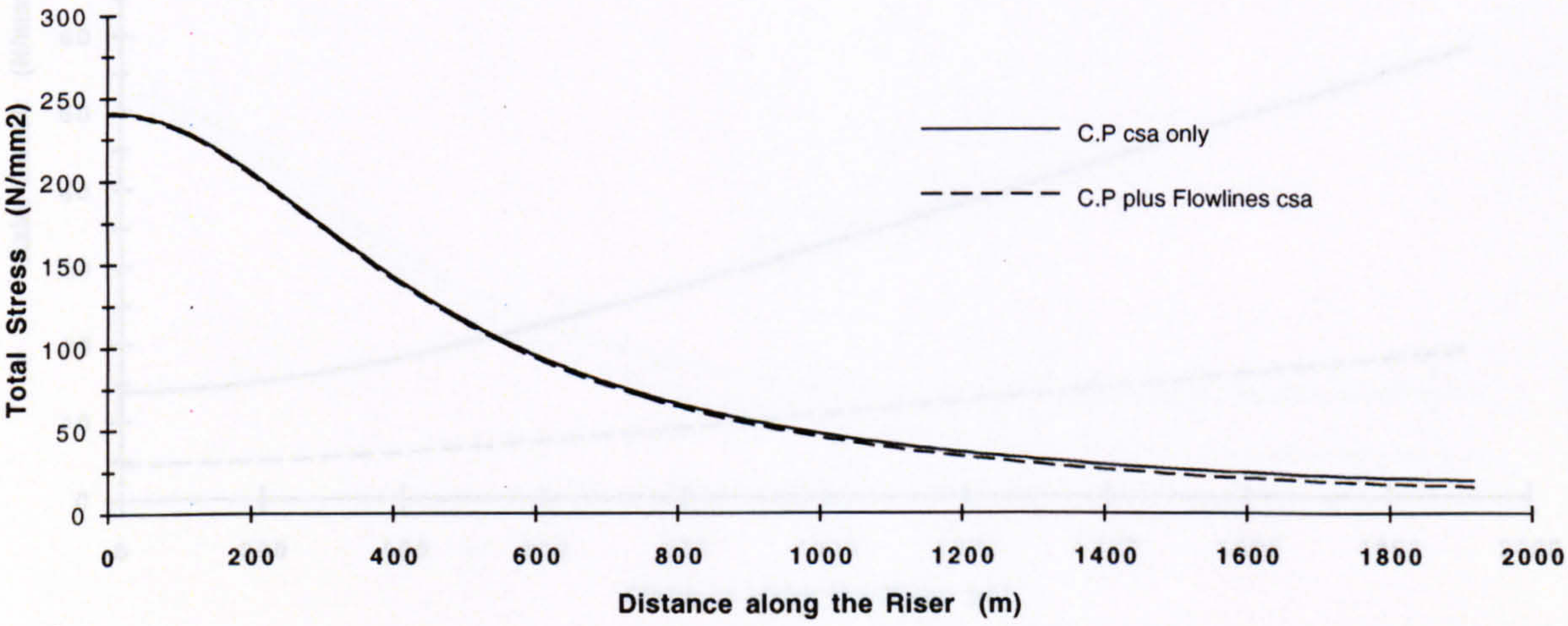

Horizontal Surface Offset = 1000 m

Submerged Unit Weight = 100 N/m

Sea Depth = 1500 m

Carrier Pipe Outer Diameter = 1.10 m

Carrier Pipe Wall Thickness = 10 mm

Figure 2.15

Load Distributions

(a)

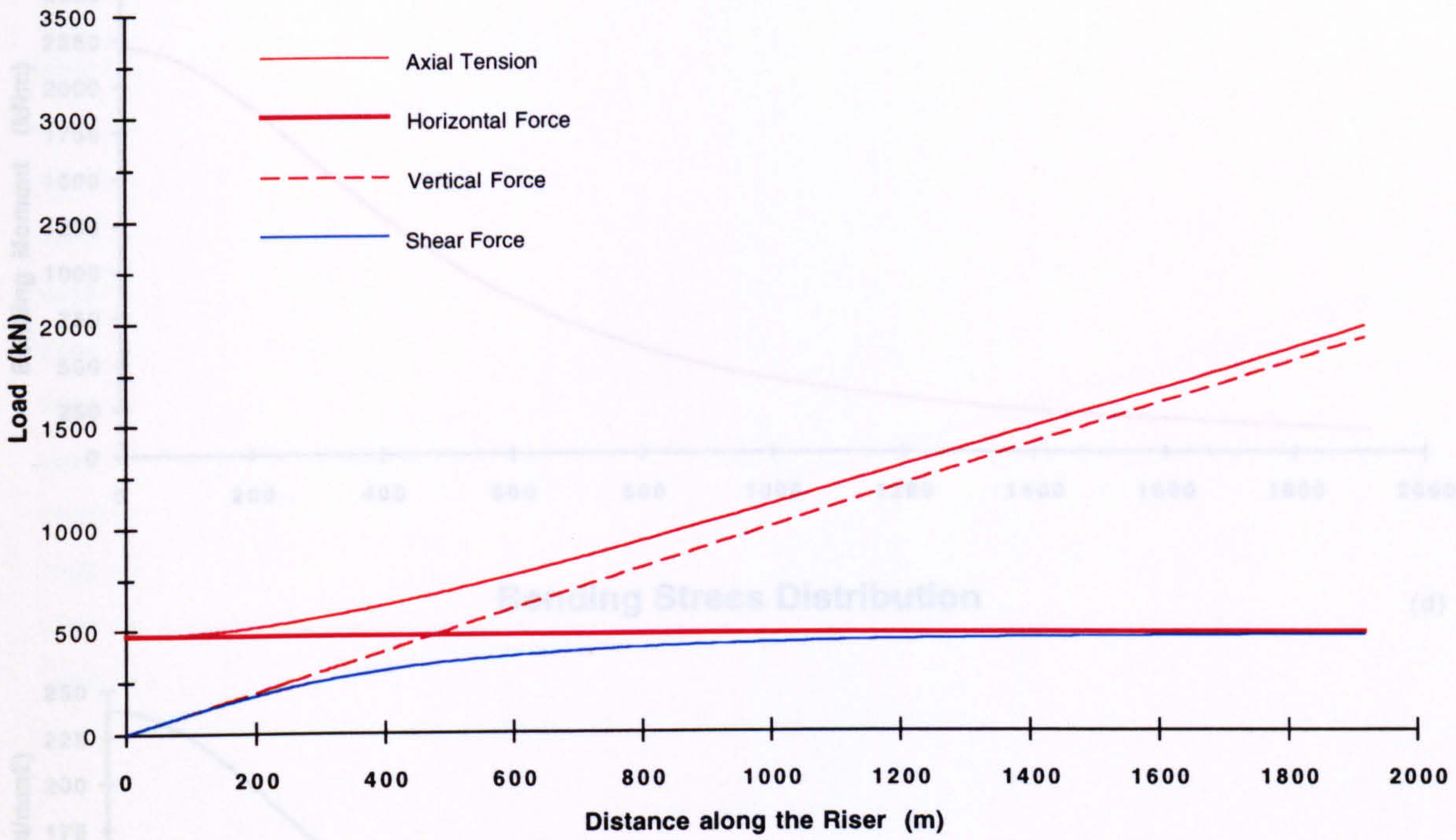

Axial Stress Distributions

(b)

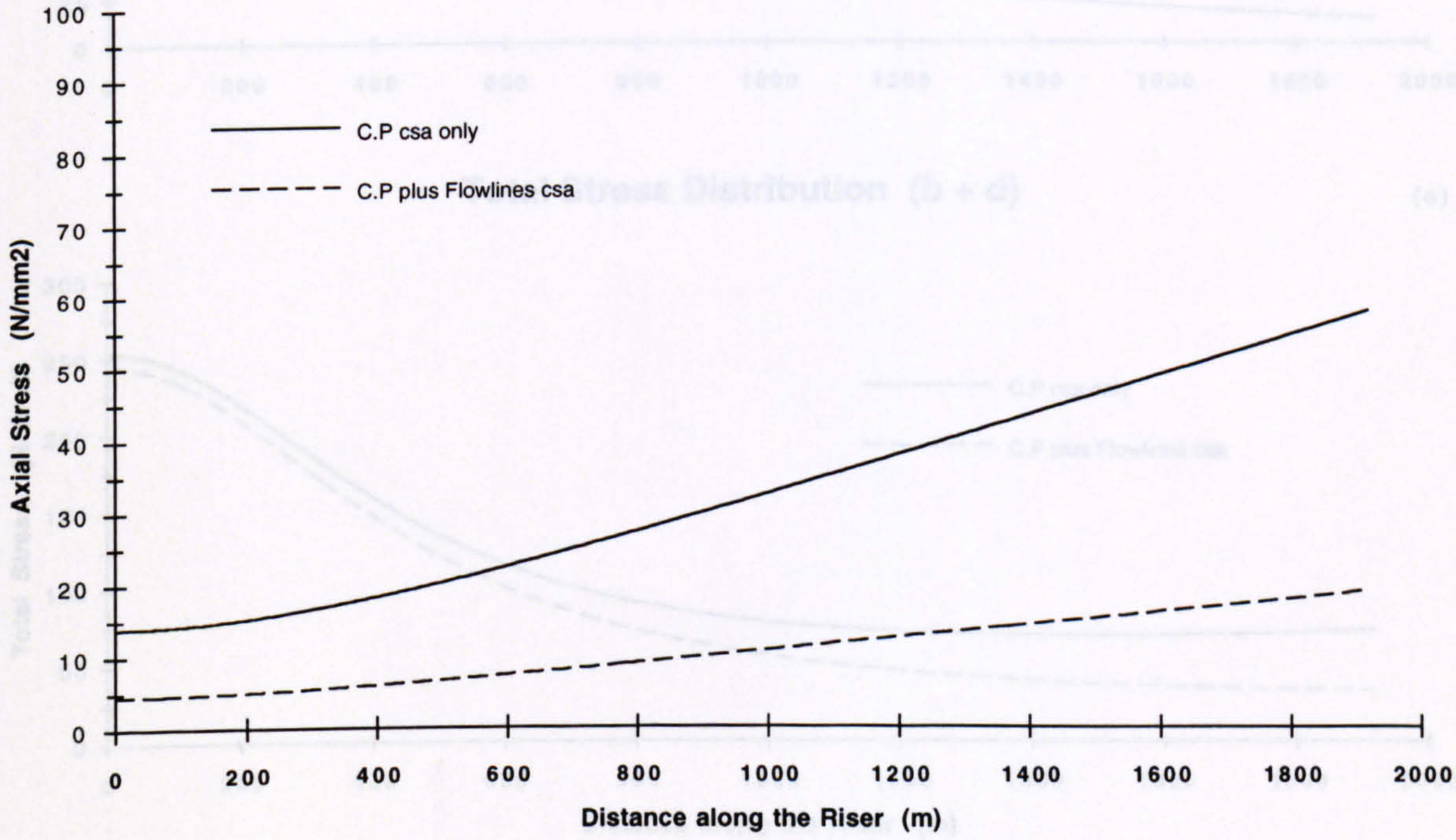

Horizontal Surface Offset = 1000 m

Submerged Unit Weight = 1000 N/m

Sea Depth = 1500 m

Carrier Pipe Outer Diameter = 1.10 m

Carrier Pipe Wall Thickness = 10 mm

Figure 2.16

Bending Moment Distribution (c)

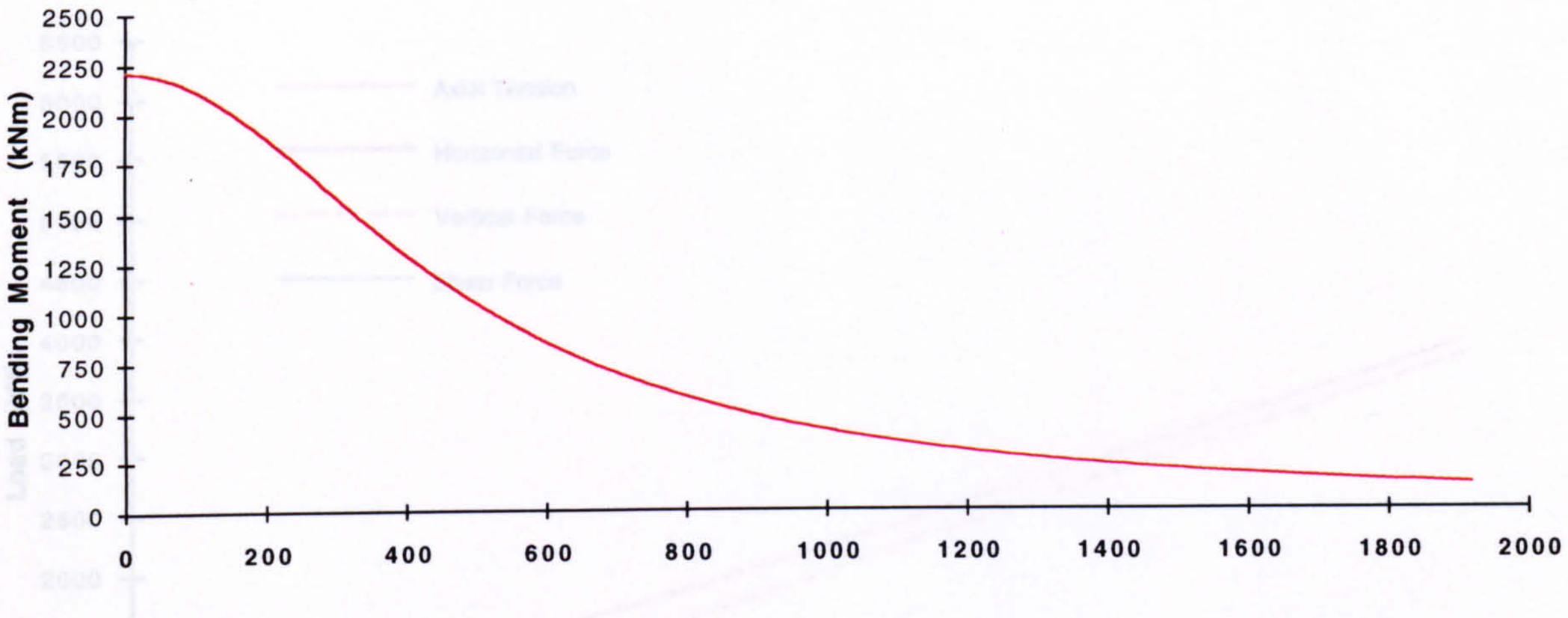

Bending Stress Distribution (d)

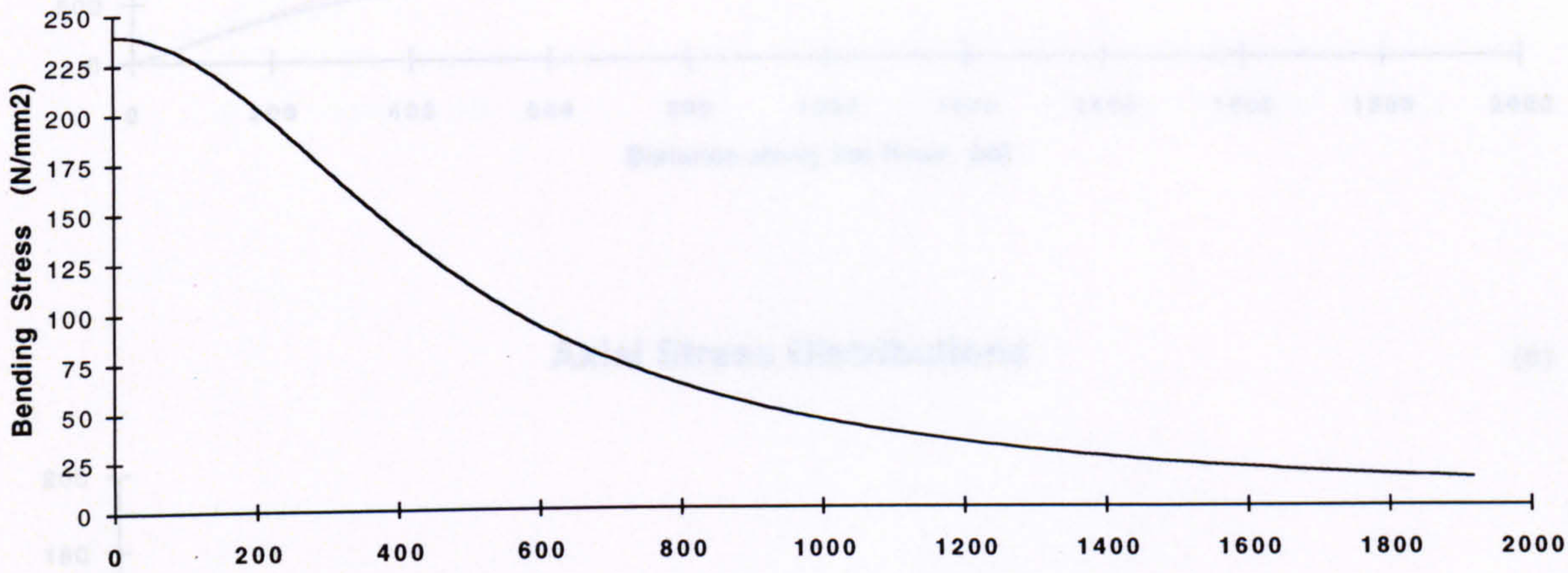

Total Stress Distribution (b + d) (e)

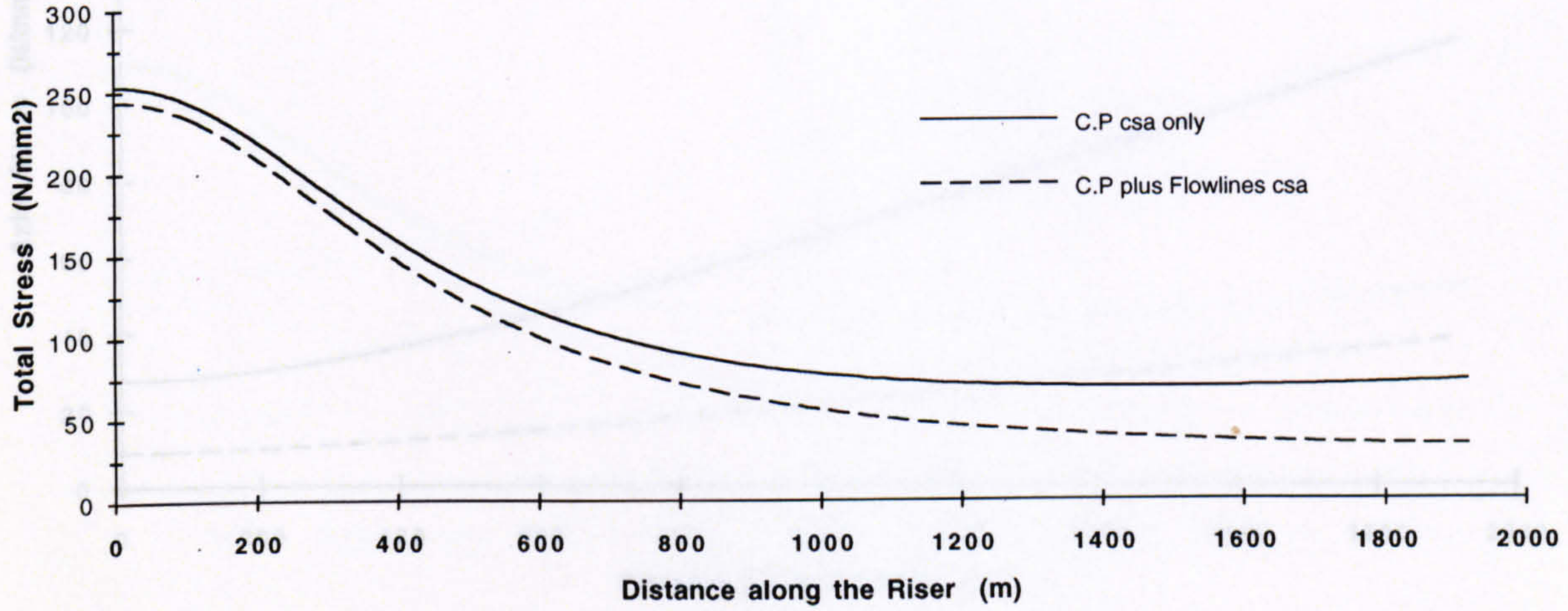

Horizontal Surface Offset = 1000 m

Submerged Unit Weight = 1000 N/m

Sea Depth = 1500 m

Carrier Pipe Outer Diameter = 1.10 m

Carrier Pipe Wall Thickness = 10 mm

Figure 2.16

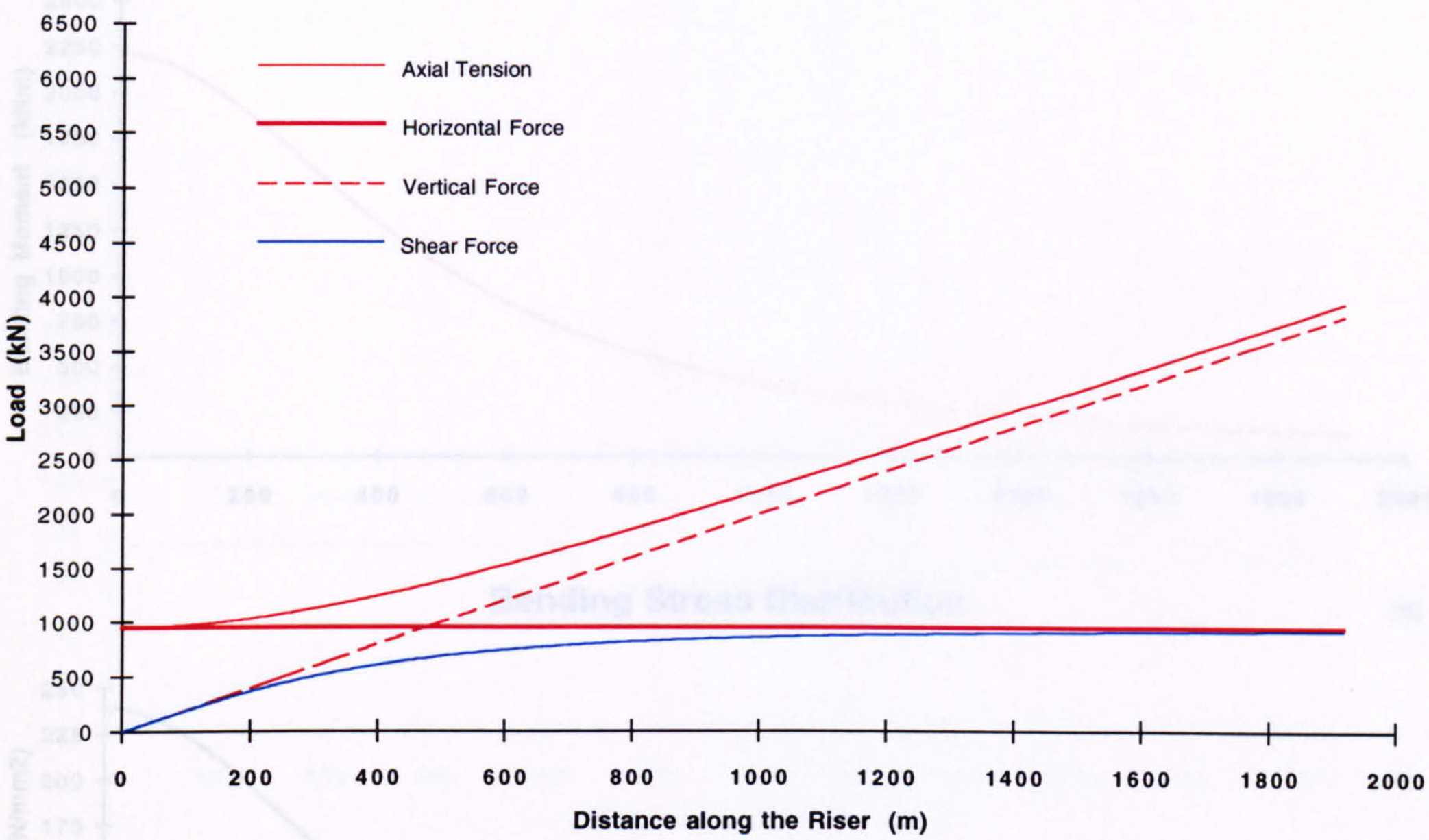

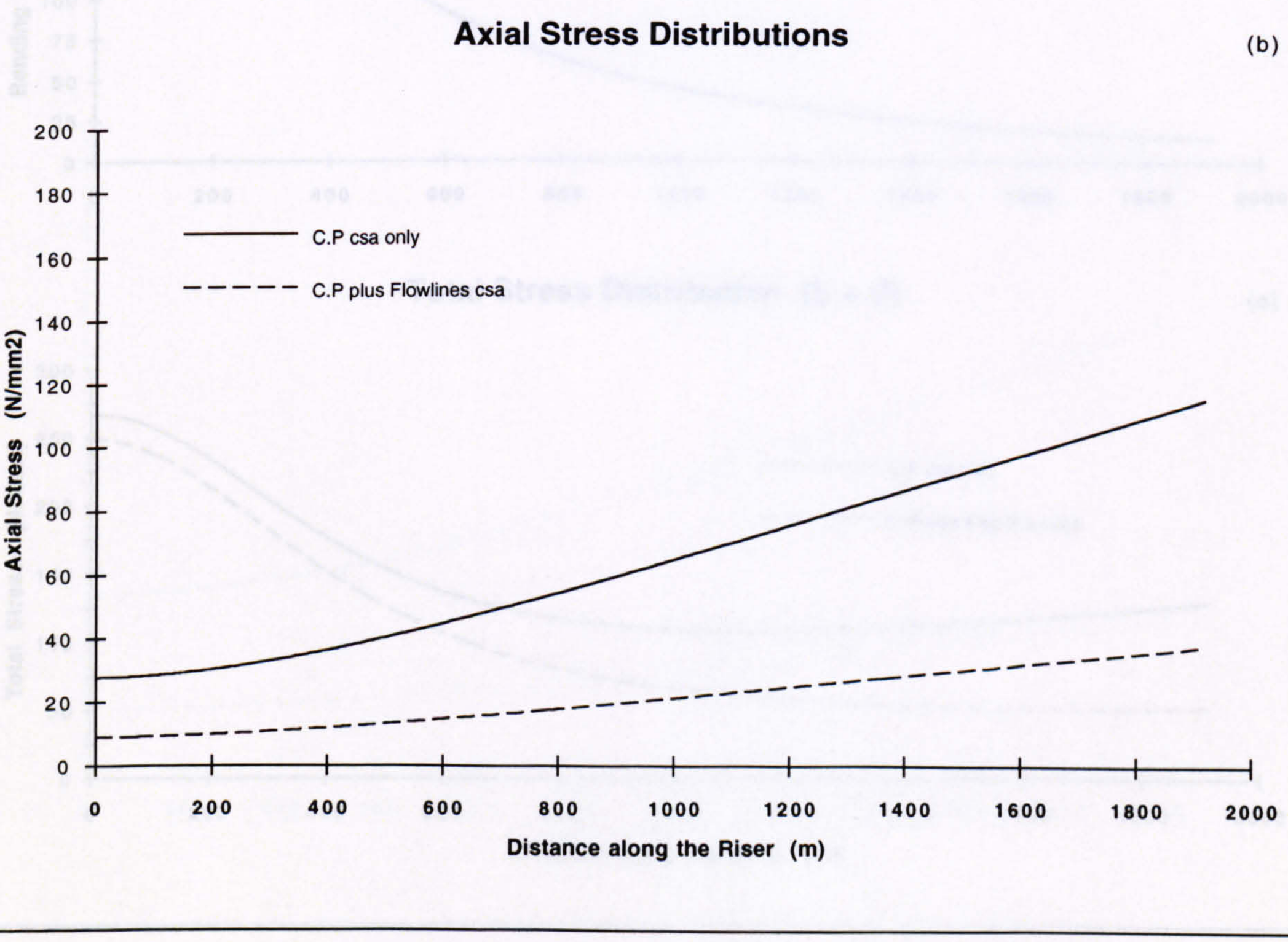

Horizontal Surface Offset = 1000 m

Submerged Unit Weight = 2000 N/m

Sea Depth = 1500 m

Carrier Pipe Outer Diameter = 1.10 m

Carrier Pipe Wall Thickness = 10 mm

Figure 2.17

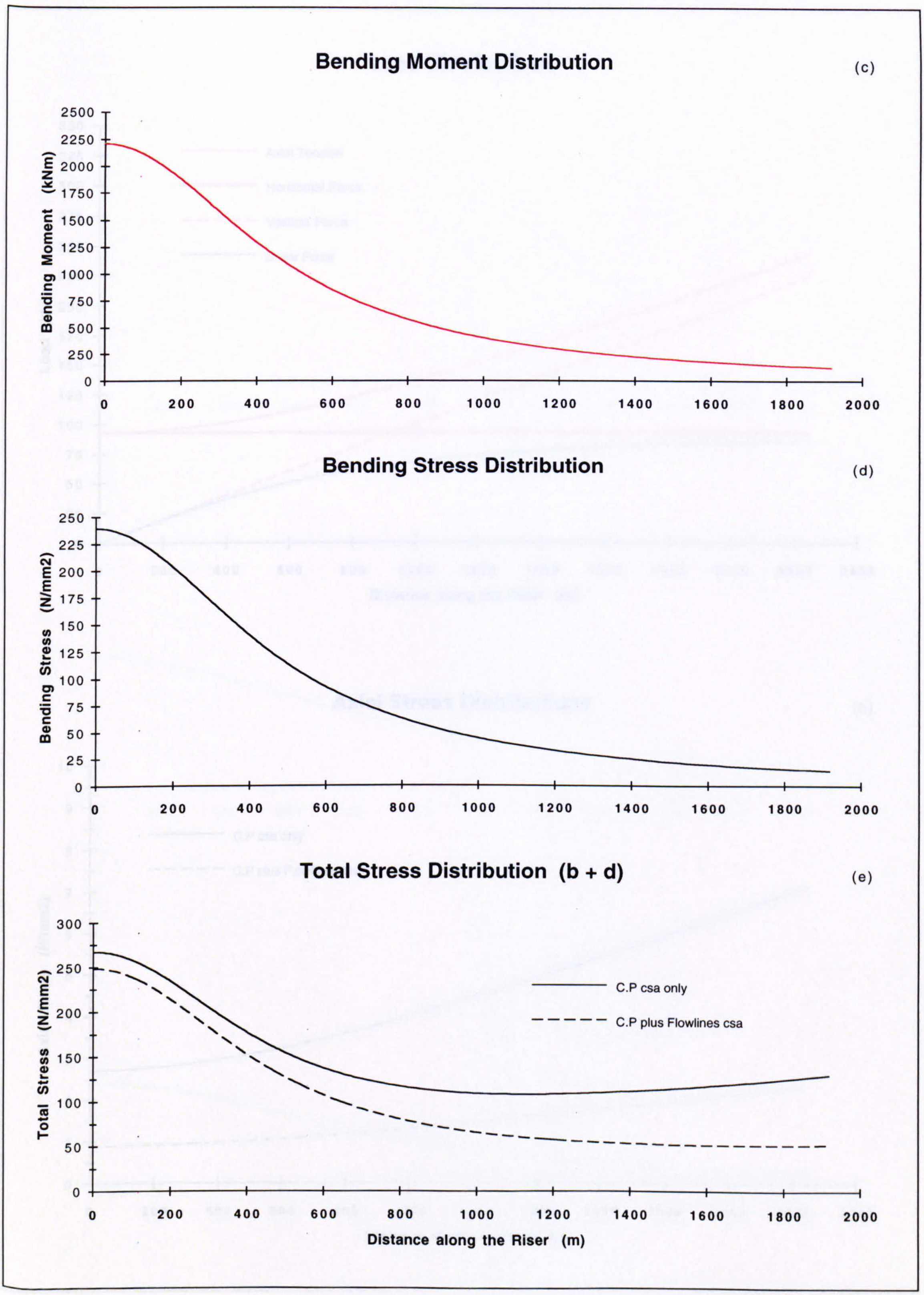

Horizontal Surface Offset = 1000 m

Submerged Unit Weight = 2000 N/m

Sea Depth = 1500 m

Carrier Pipe Outer Diameter = 1.10 m

Carrier Pipe Wall Thickness = 10 mm

Figure 2.17

Load Distributions

(a)

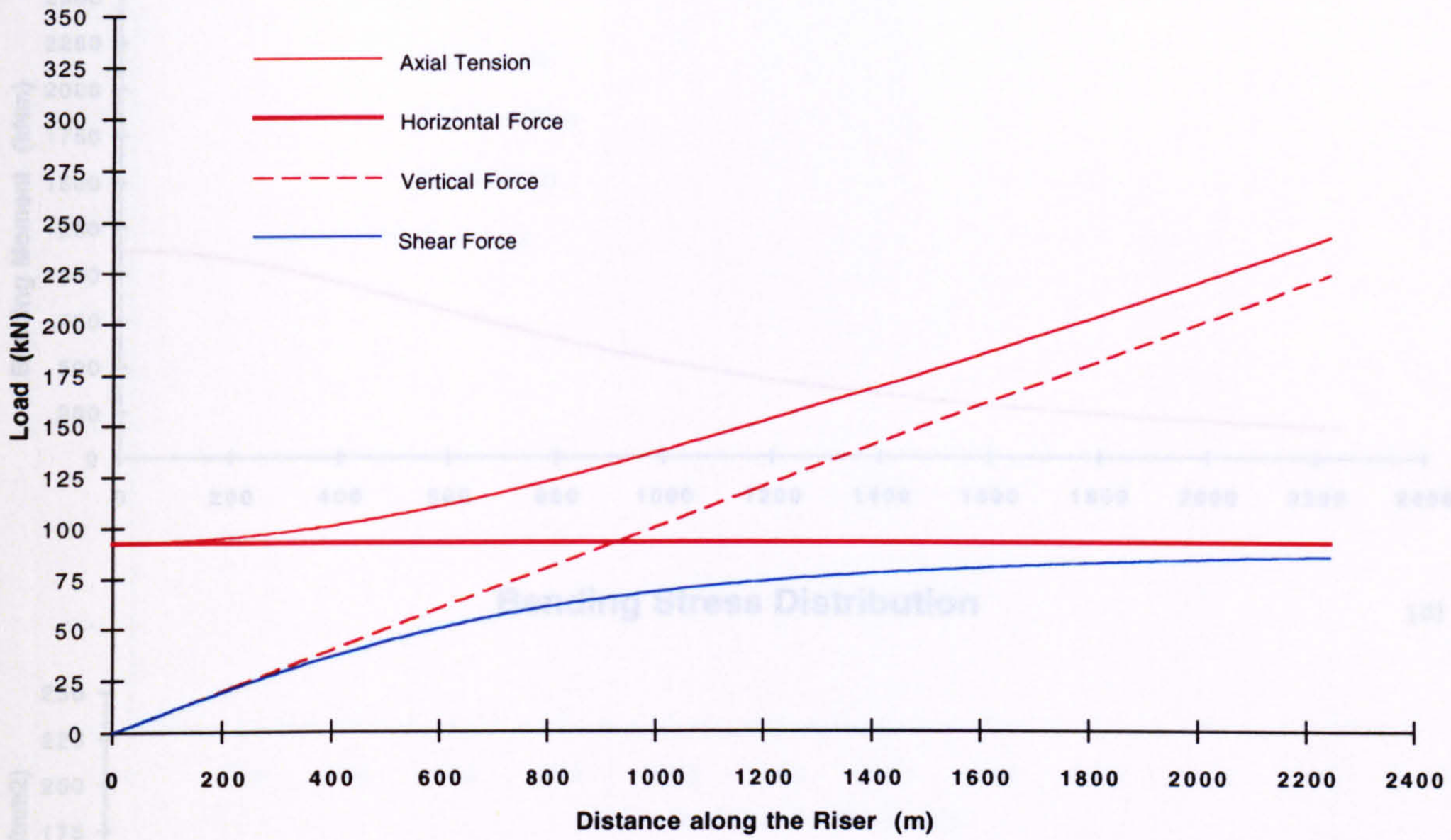

Axial Stress Distributions

(b)

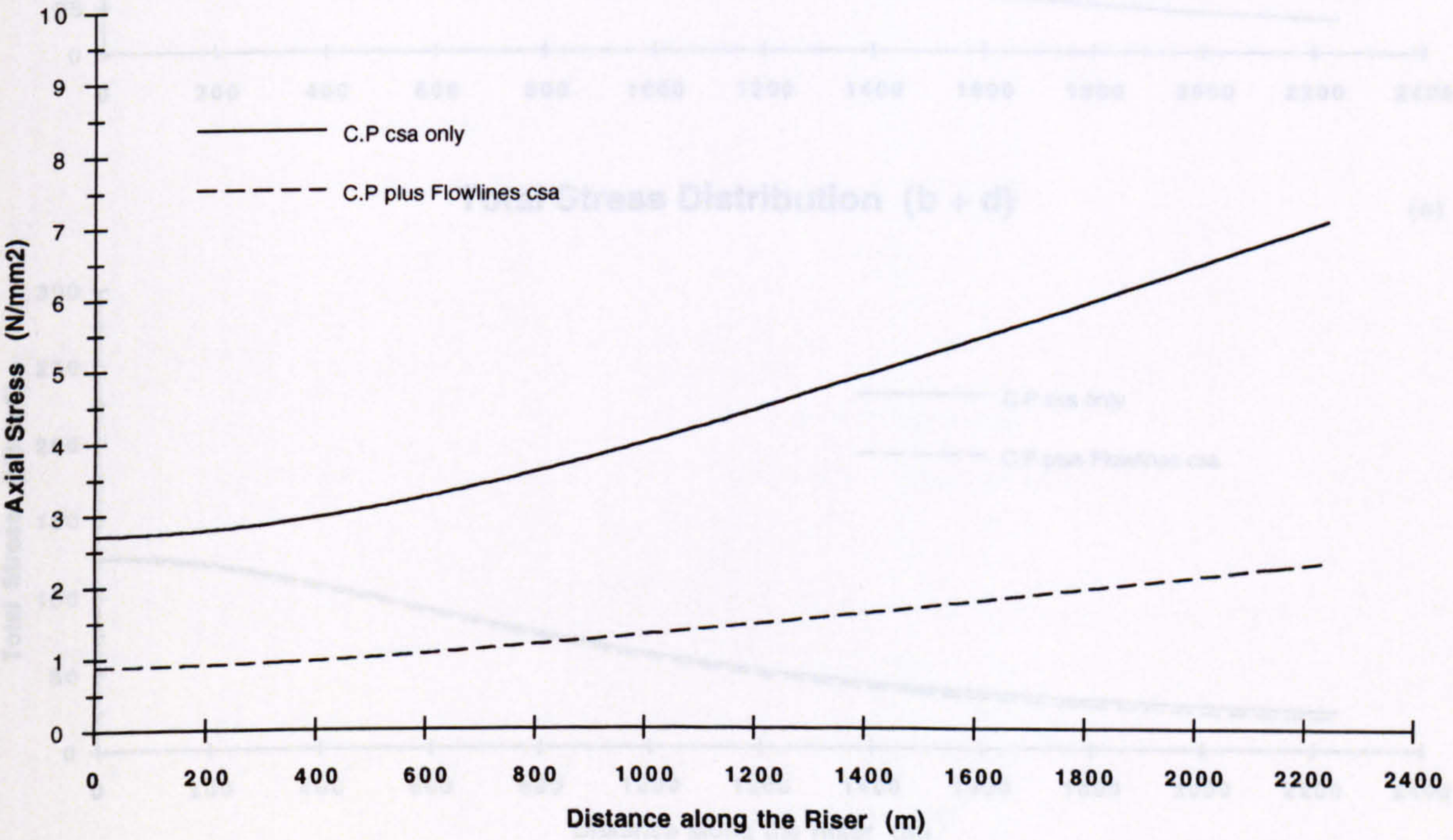

Horizontal Surface Offset = 1500 m

Submerged Unit Weight = 100 N/m

Sea Depth = 1500 m

Carrier Pipe Outer Diameter = 1.10 m

Carrier Pipe Wall Thickness = 10 mm

Figure 2.18

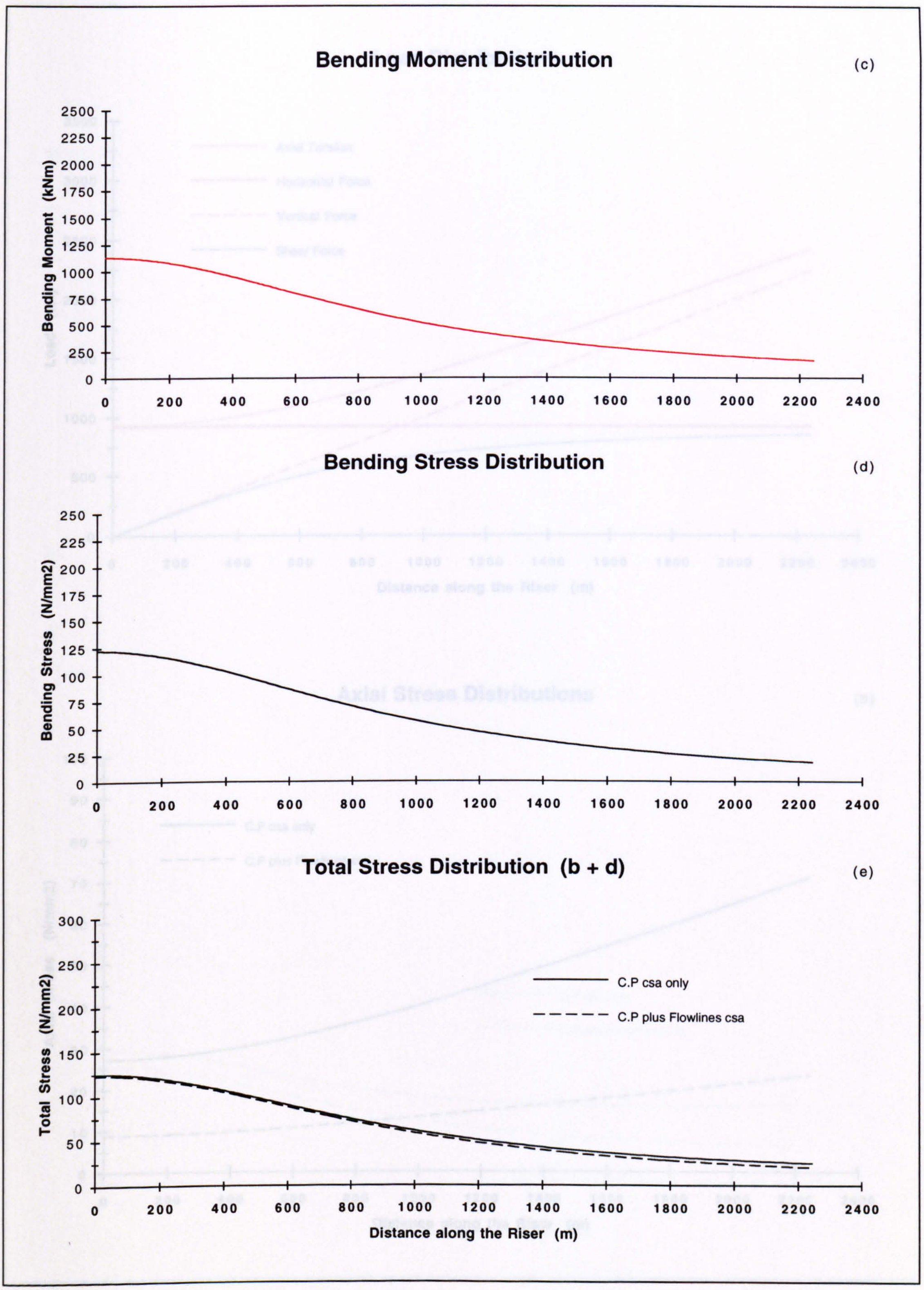

Horizontal Surface Offset = 1500 m

Submerged Unit Weight = 100 N/m

Sea Depth = 1500 m

Carrier Pipe Outer Diameter = 1.10 m

Carrier Pipe Wall Thickness = 10 mm

Figure 2.18

Load Distributions

(a)

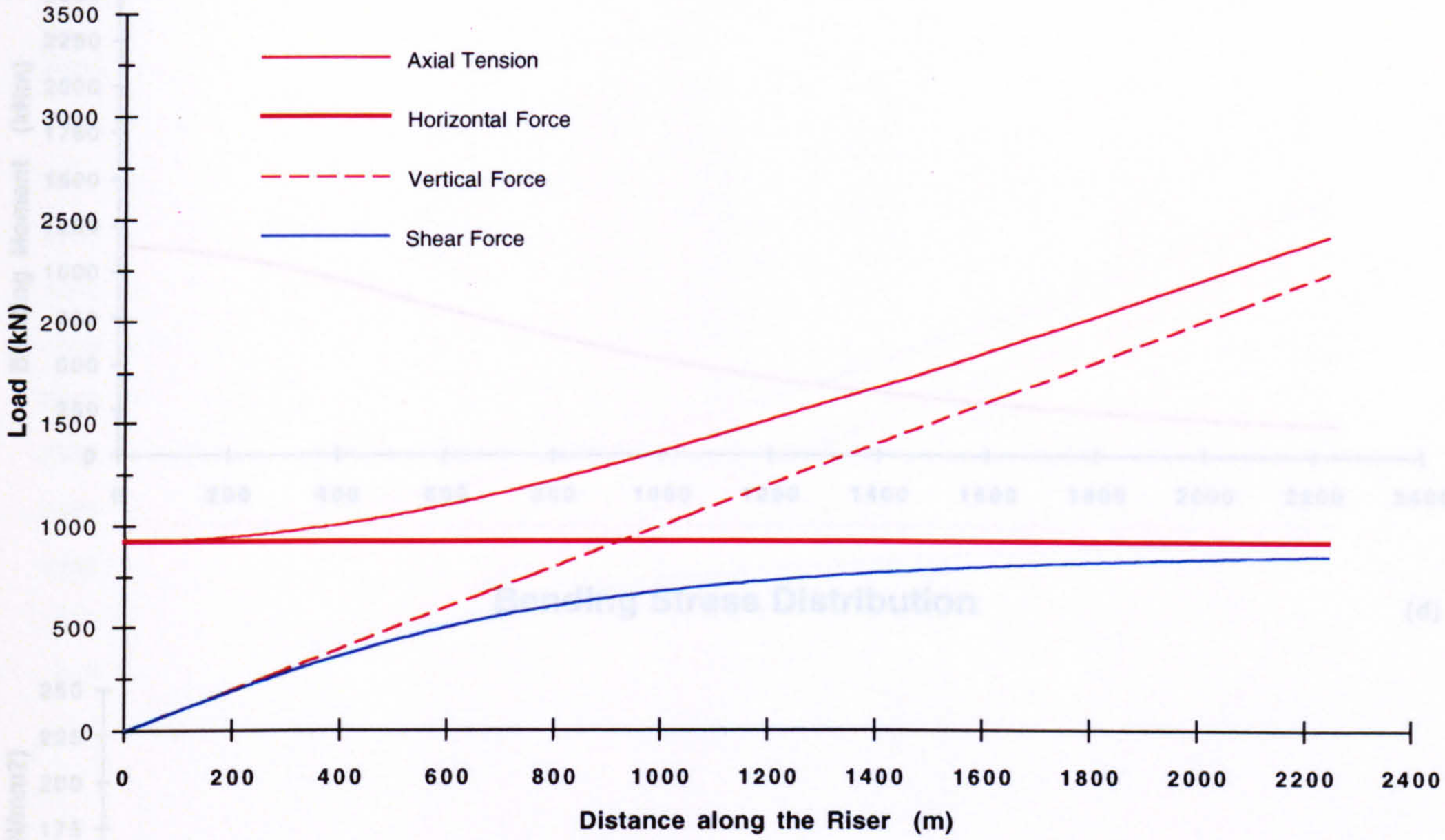

Axial Stress Distributions

(b)

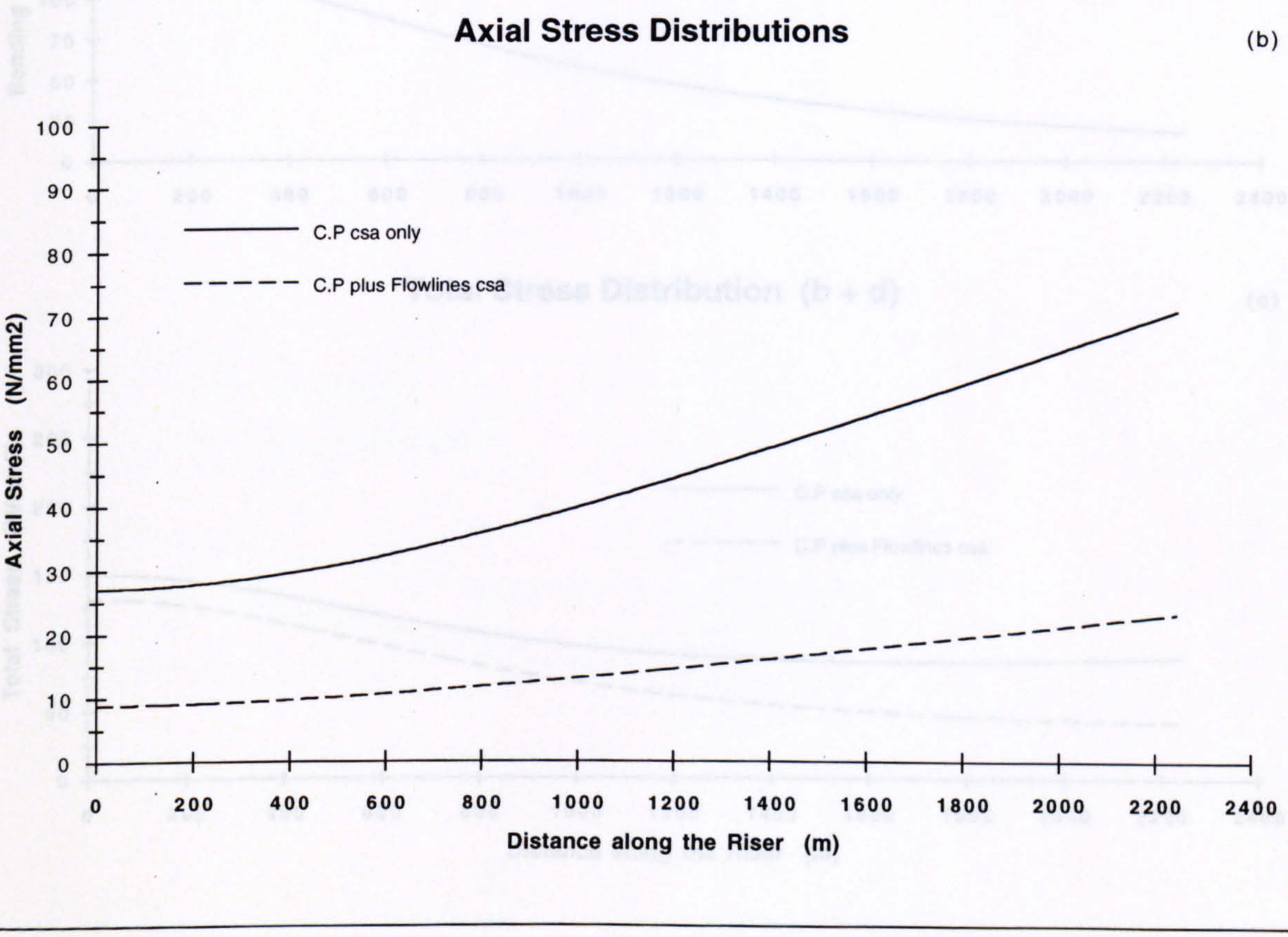

Horizontal Surface Offset = 1500 m

Submerged Unit Weight = 1000 N/m

Sea Depth = 1500 m

Carrier Pipe Outer Diameter = 1.10 m

Carrier Pipe Wall Thickness = 10 mm

Figure 2.19

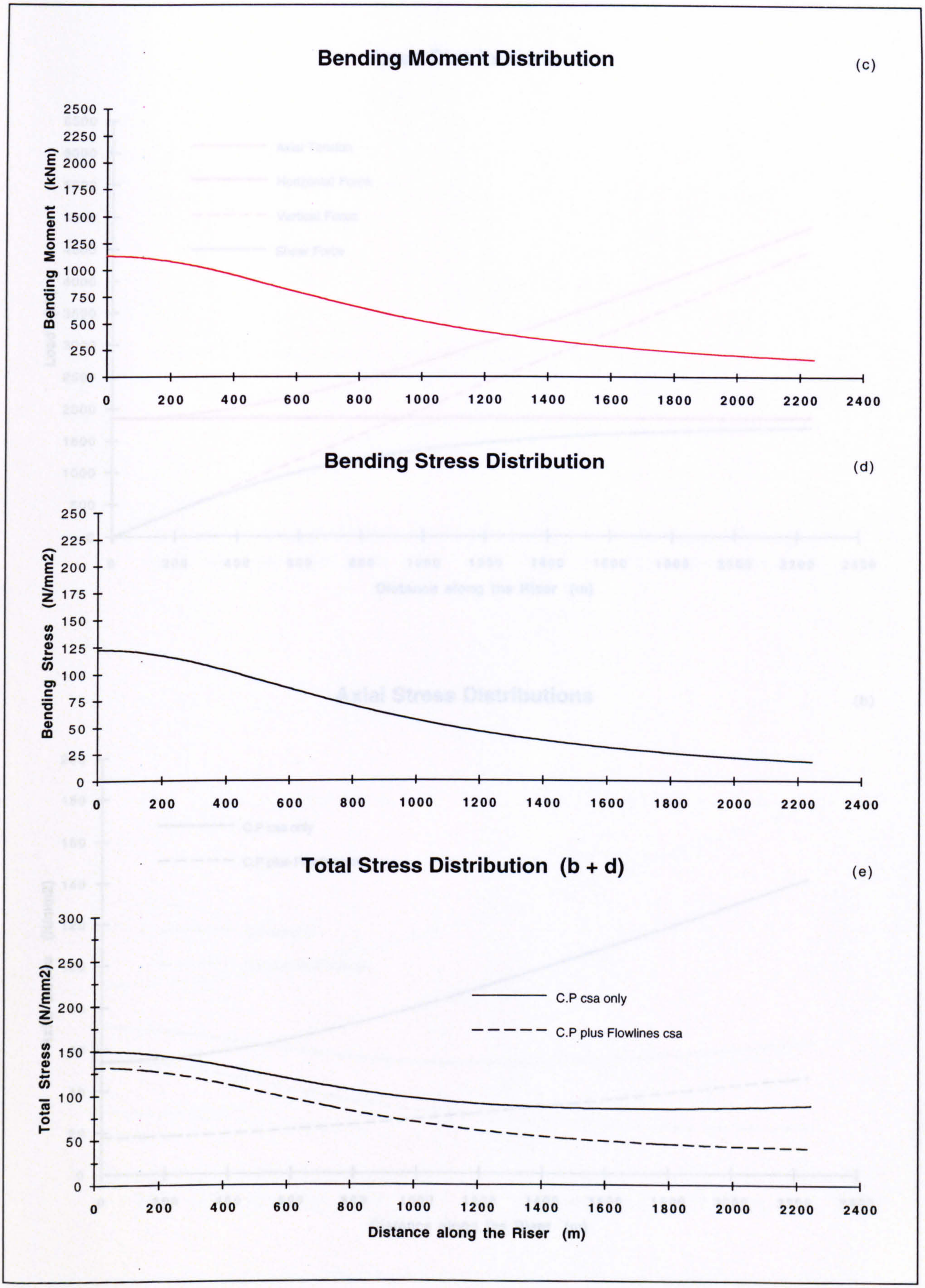

Horizontal Surface Offset = 1500 m

Submerged Unit Weight = 1000 N/m

Sea Depth = 1500 m

Carrier Pipe Outer Diameter = 1.10 m

Carrier Pipe Wall Thickness = 10 mm

Figure 2.19

Load Distributions

(a)

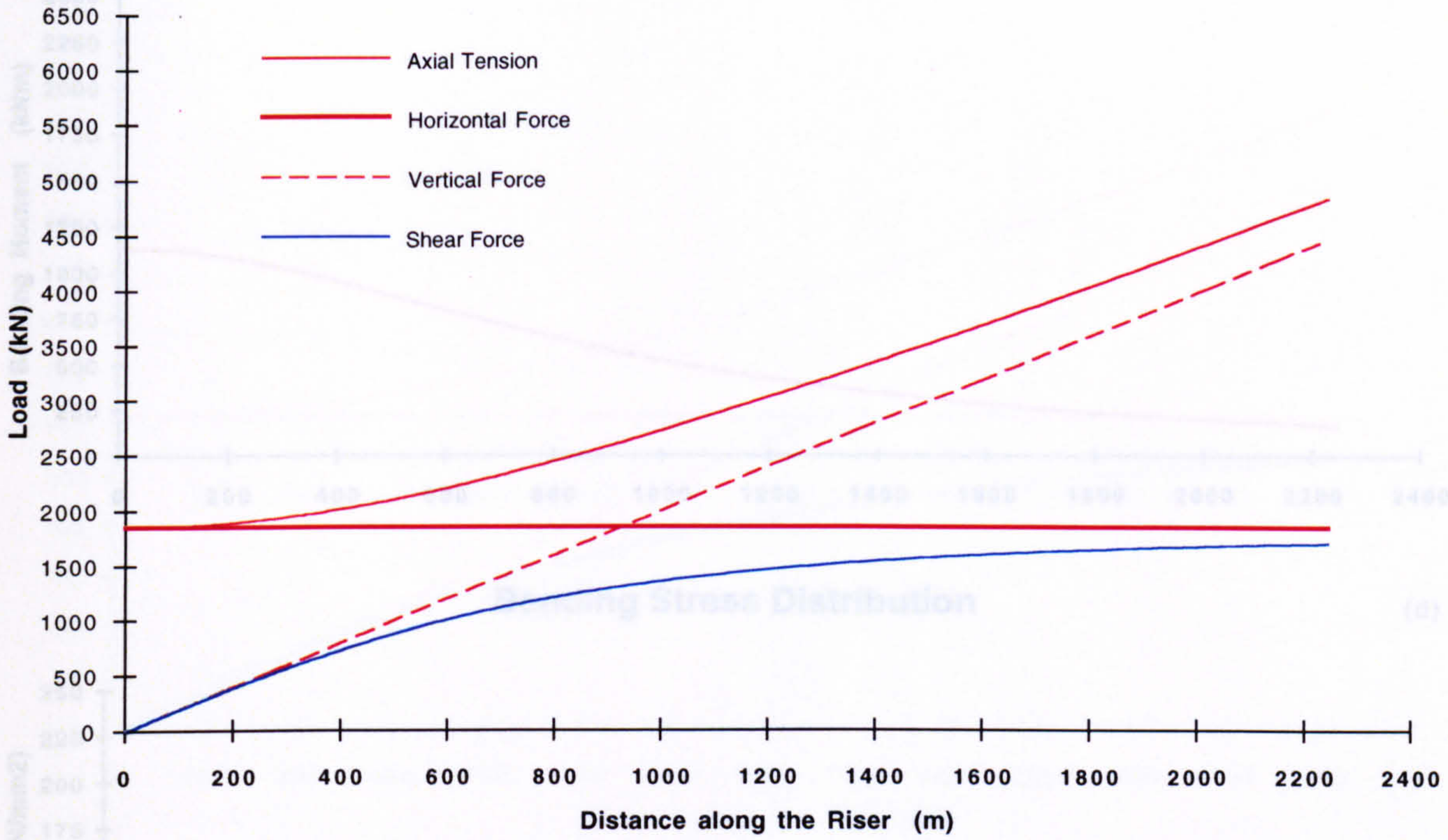

Axial Stress Distributions

(b)

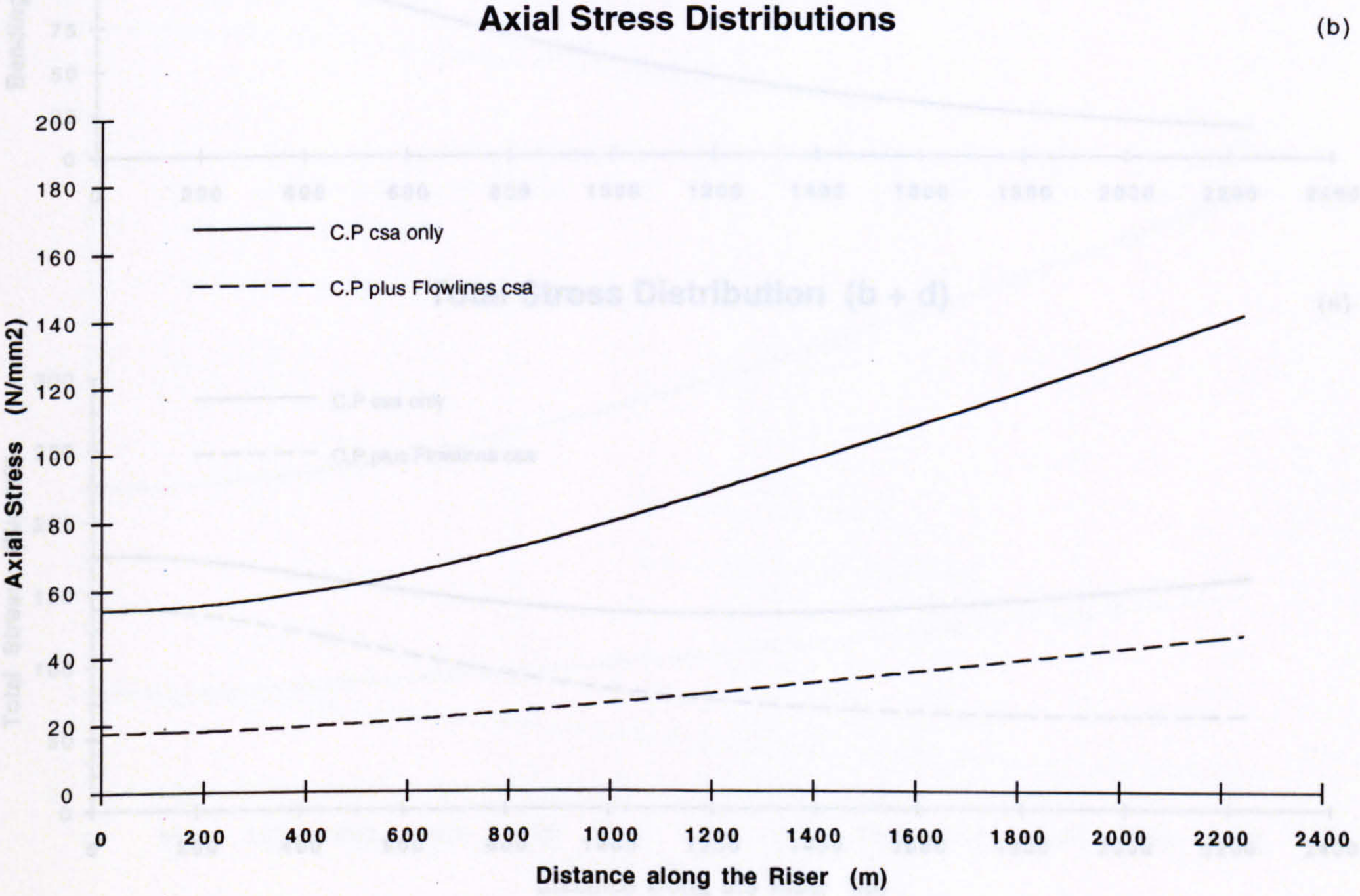

Horizontal Surface Offset = 1500 m

Submerged Unit Weight = 2000 N/m

Sea Depth = 1500 m

Carrier Pipe Outer Diameter = 1.10 m

Carrier Pipe Wall Thickness = 10 mm

Figure 2.20

Bending Moment Distribution (c)

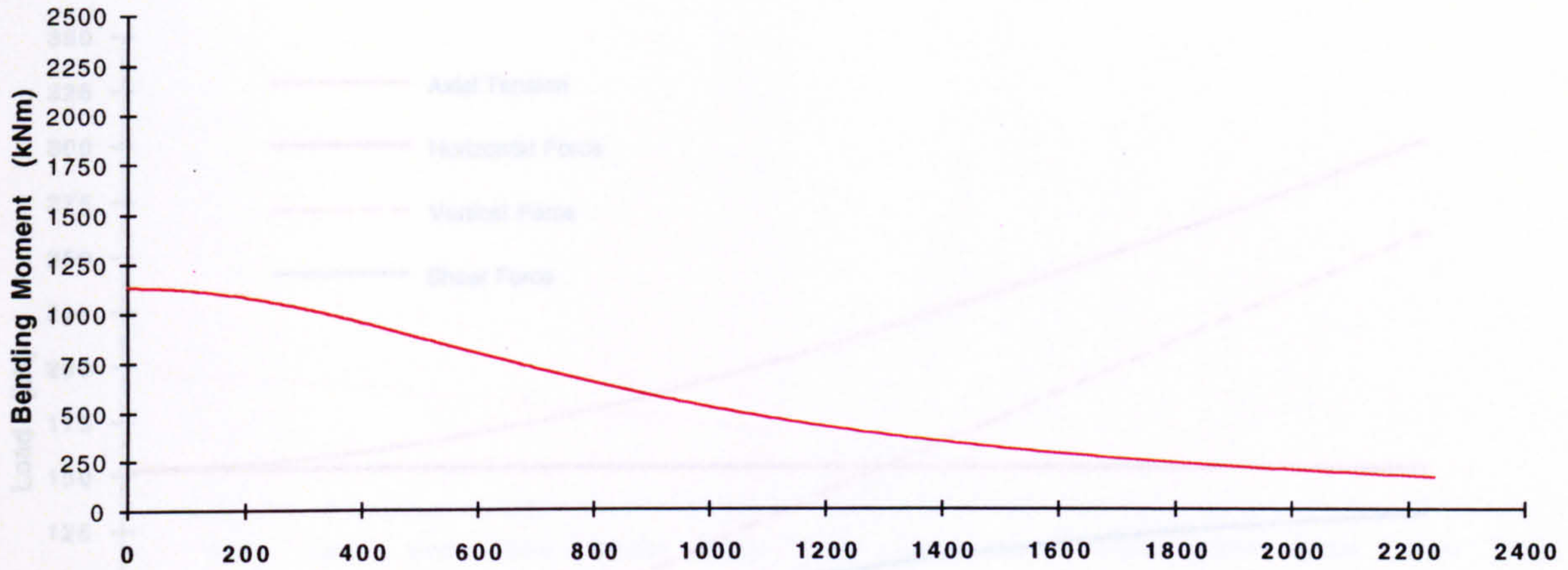

Bending Stress Distribution (d)

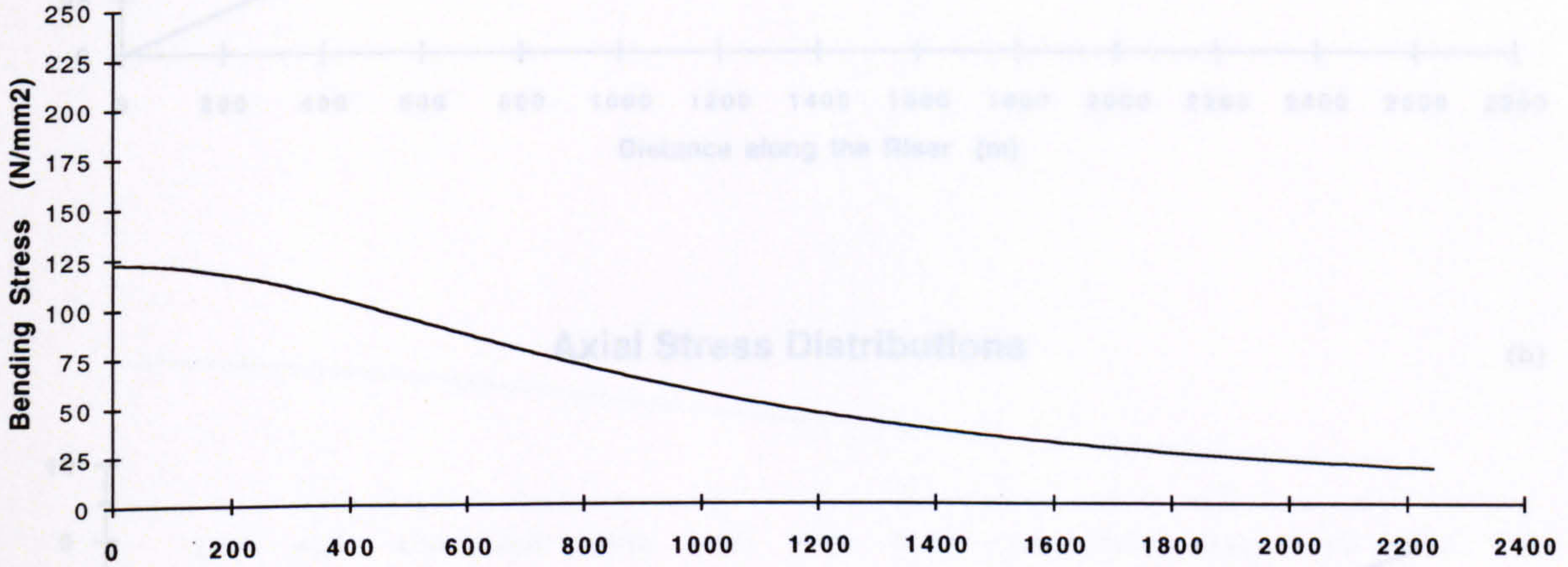

Total Stress Distribution (b + d) (e)

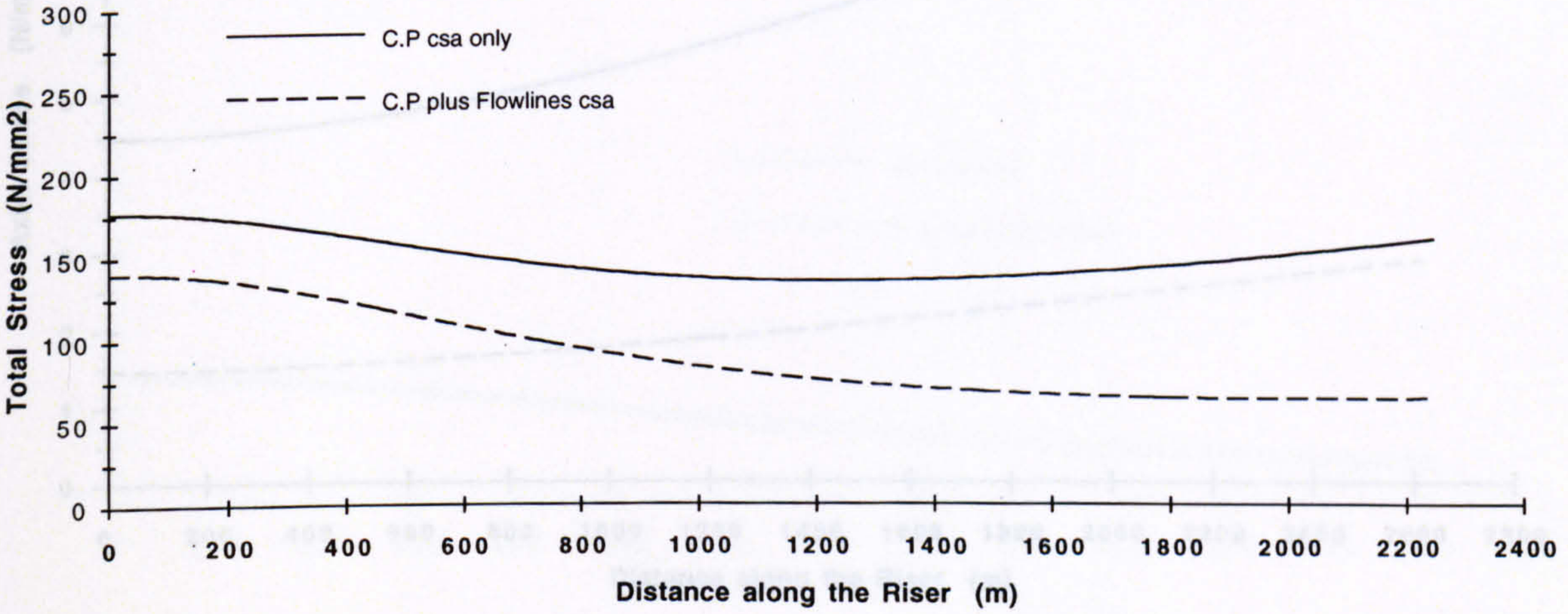

Horizontal Surface Offset = 1500 m

Submerged Unit Weight = 2000 N/m

Sea Depth = 1500 m

Carrier Pipe Outer Diameter = 1.10 m

Carrier Pipe Wall Thickness = 10 mm

Figure 2.20

Load Distributions

(a)

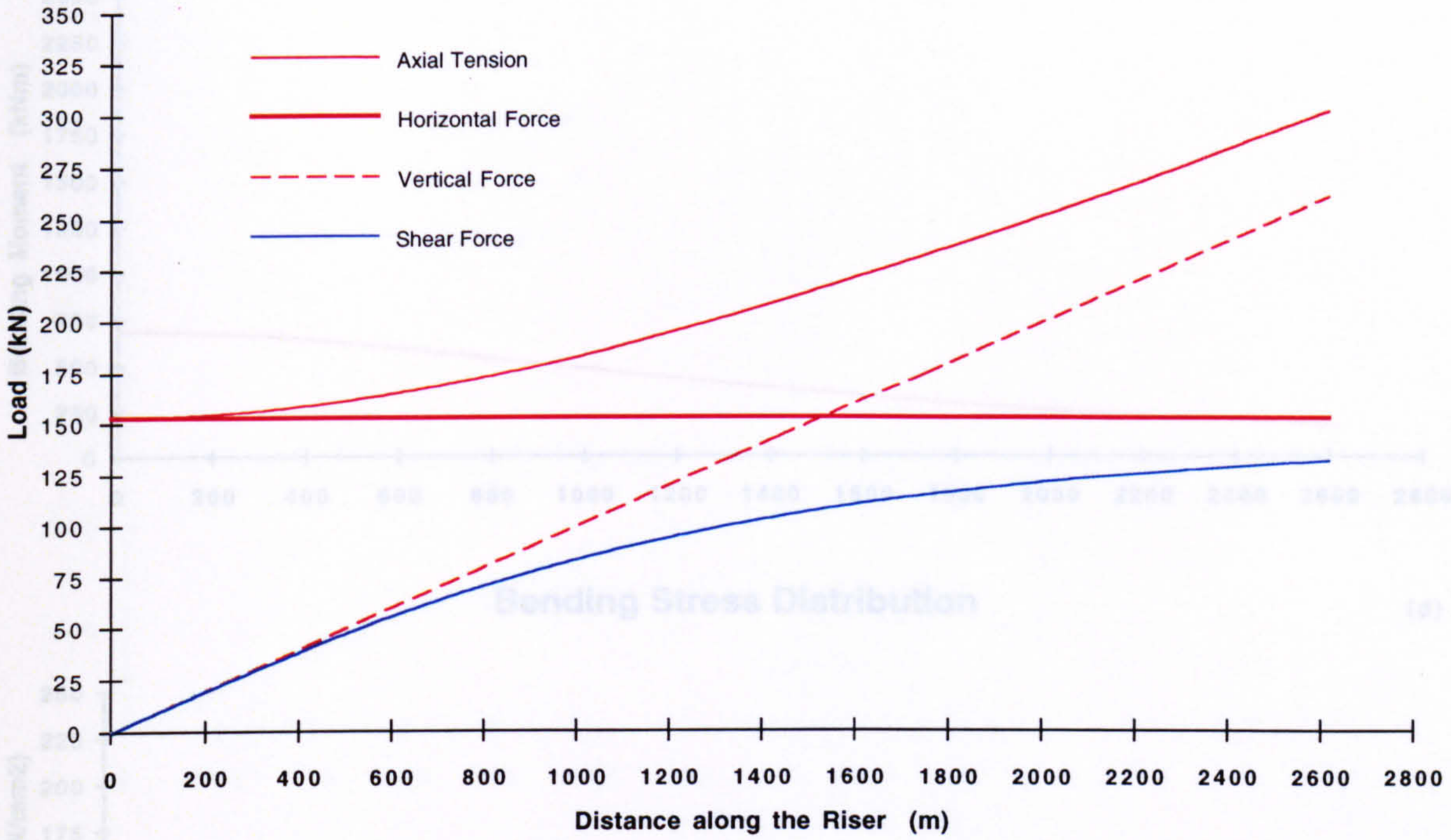

Axial Stress Distributions

(b)

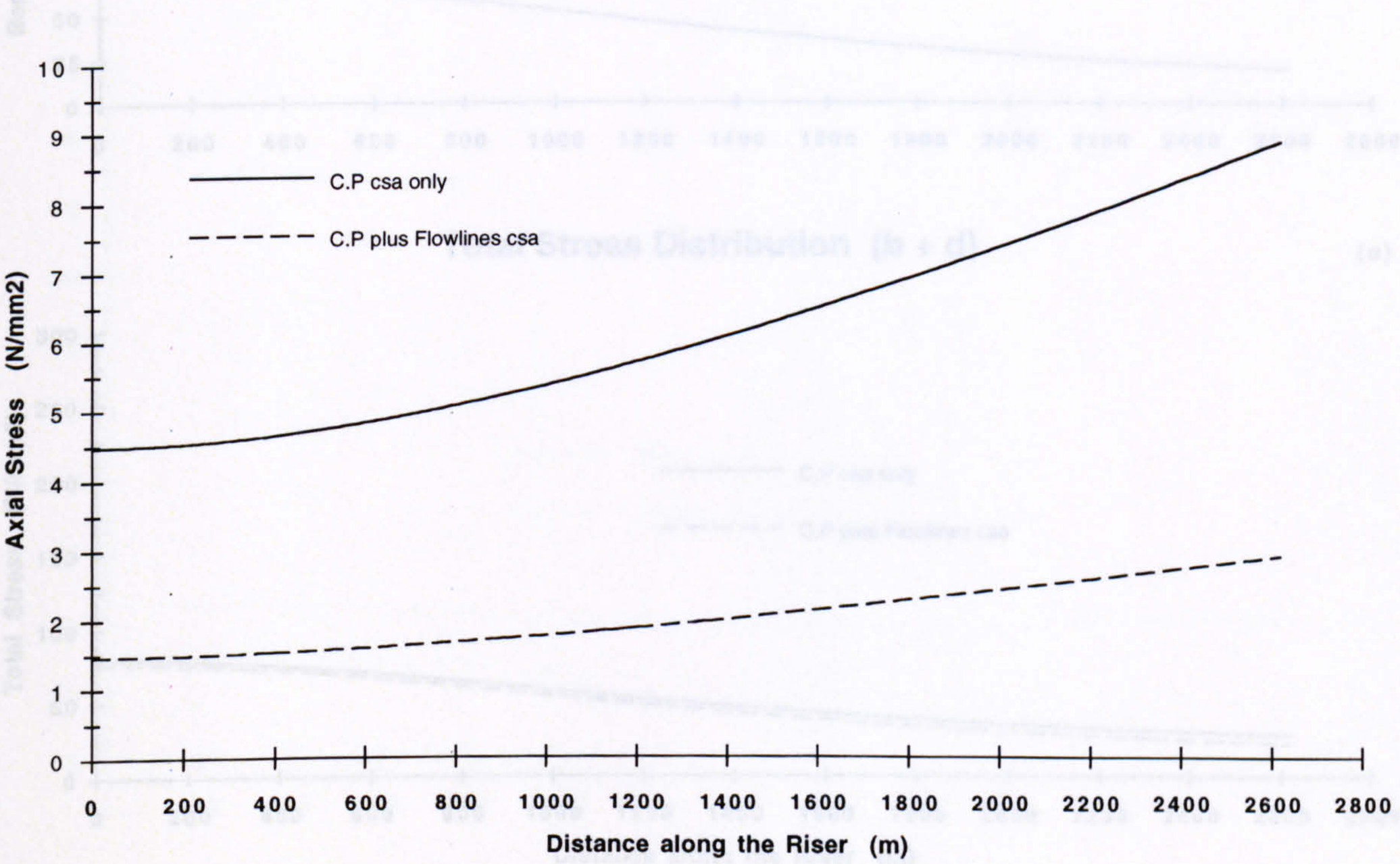

Horizontal Surface Offset = 2000 m

Submerged Unit Weight = 100 N/m

Sea Depth = 1500 m

Carrier Pipe Outer Diameter = 1.10 m

Carrier Pipe Wall Thickness = 10 mm

Figure 2.21

Bending Moment Distribution

(c)

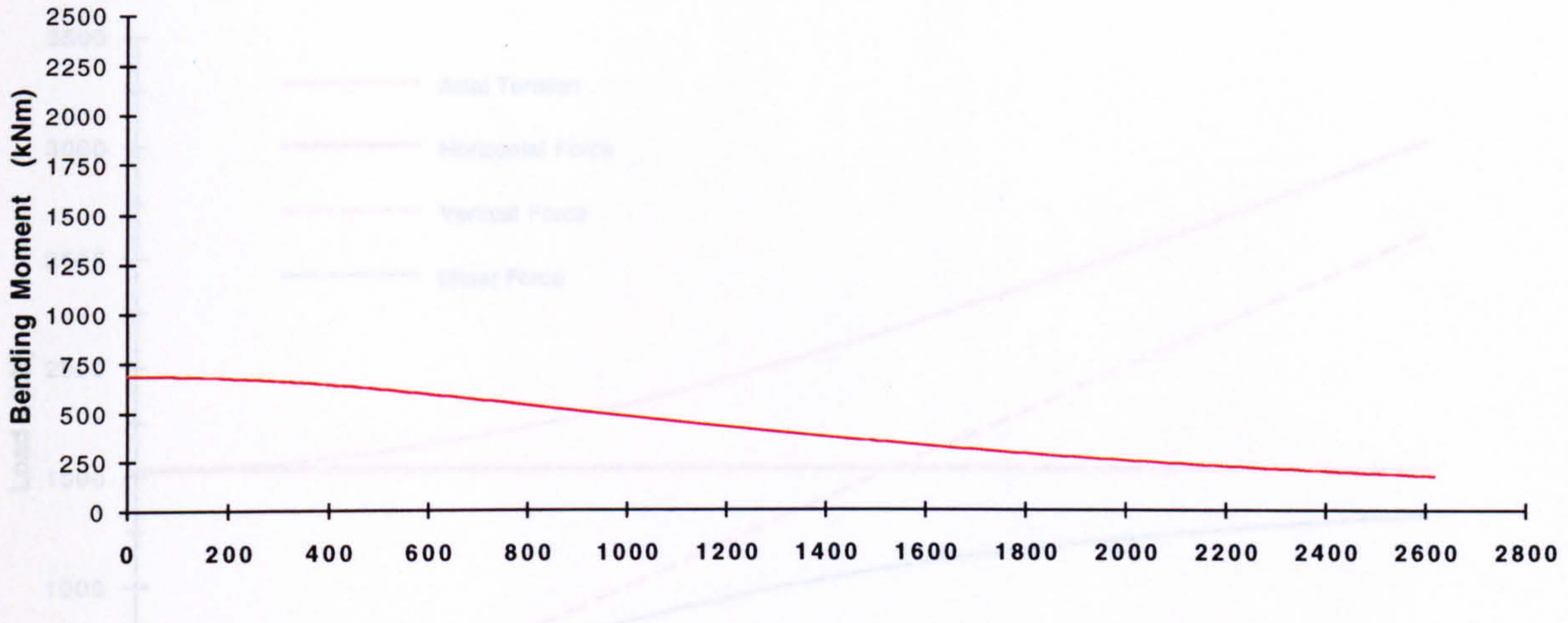

Bending Stress Distribution

(d)

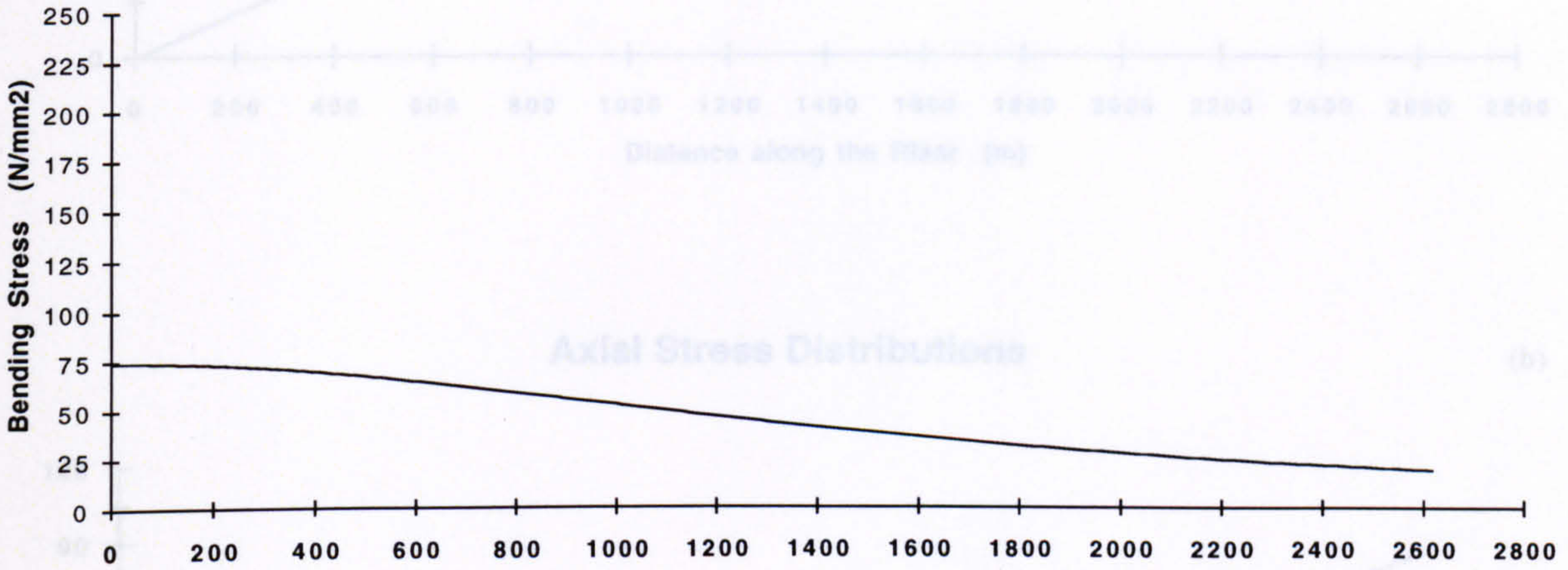

Total Stress Distribution (b + d)

(e)

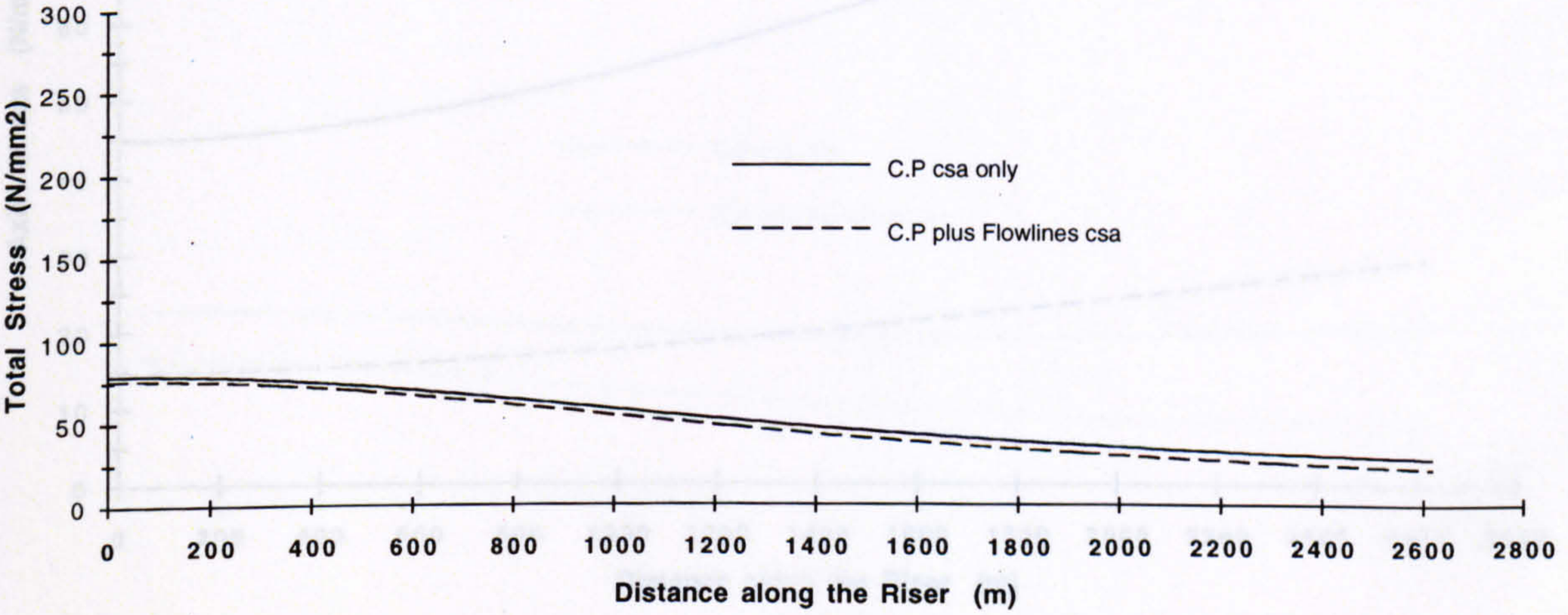

Horizontal Surface Offset = 2000 m

Submerged Unit Weight = 100 N/m

Sea Depth = 1500 m

Carrier Pipe Outer Diameter = 1.10 m

Carrier Pipe Wall Thickness = 10 mm

Figure 2.21

Load Distributions

(a)

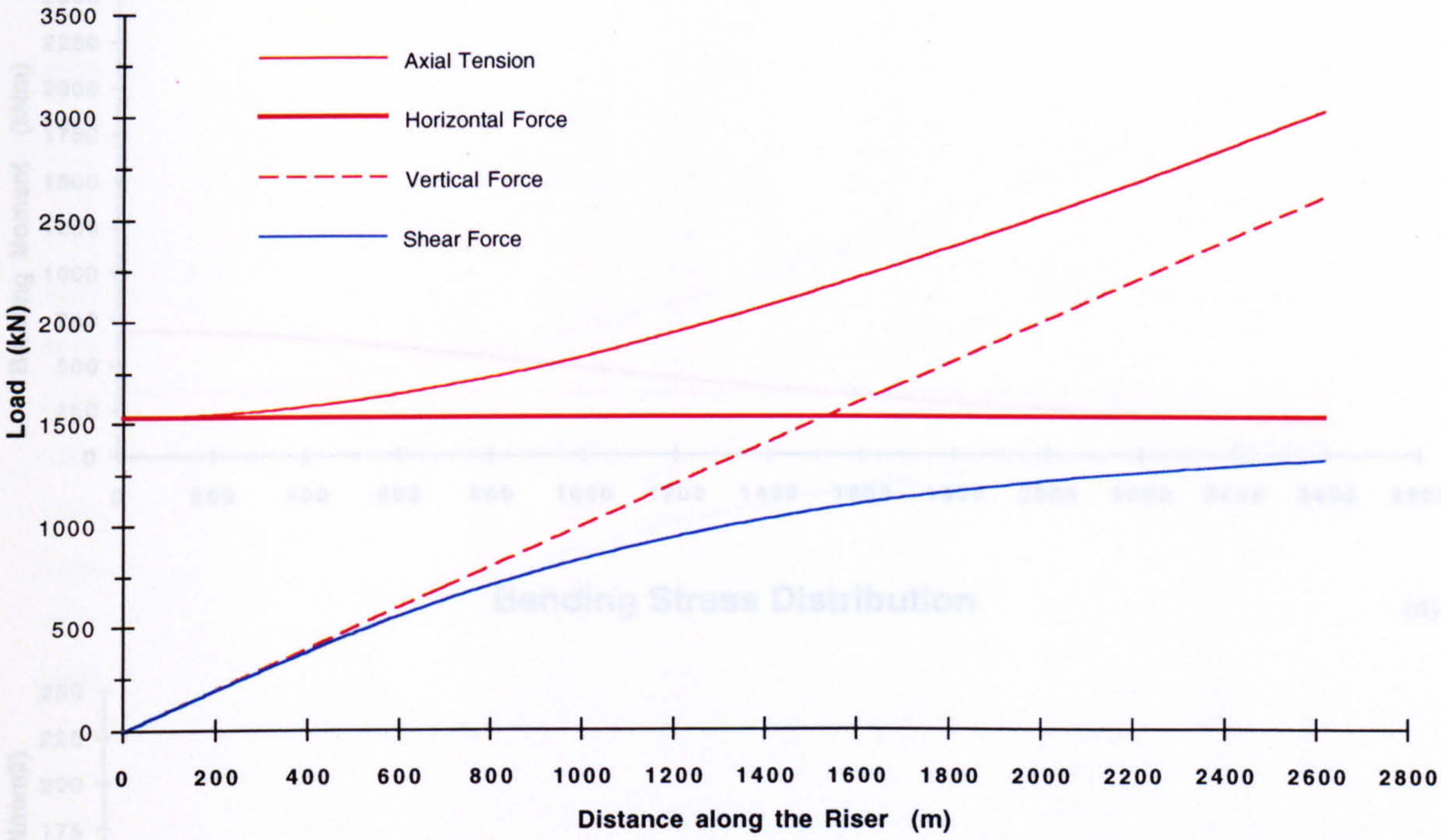

Axial Stress Distributions

(b)

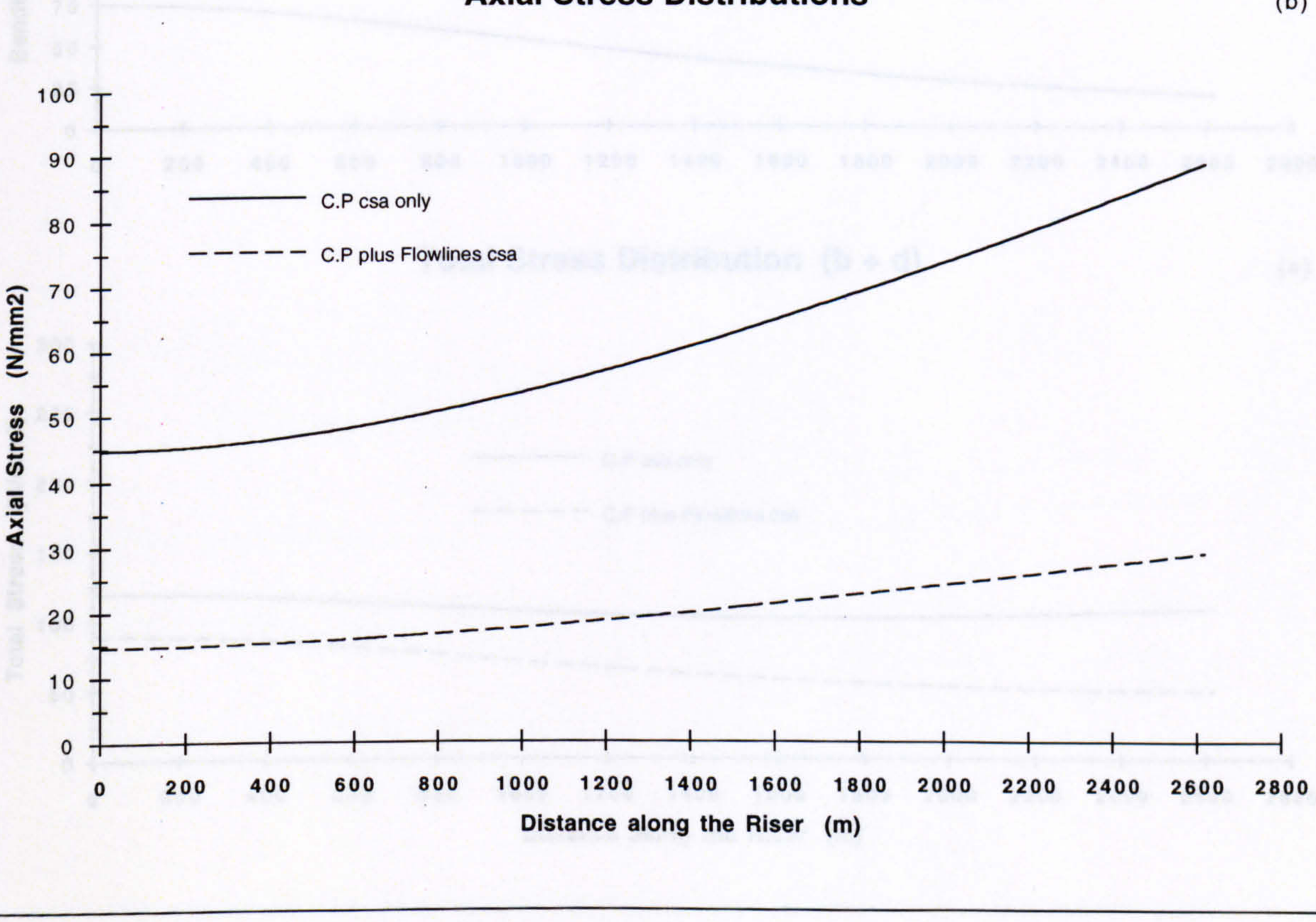

Horizontal Surface Offset = 2000 m

Submerged Unit Weight = 1000 N/m

Sea Depth = 1500 m

Carrier Pipe Outer Diameter = 1.10 m

Carrier Pipe Wall Thickness = 10 mm

Figure 2.22

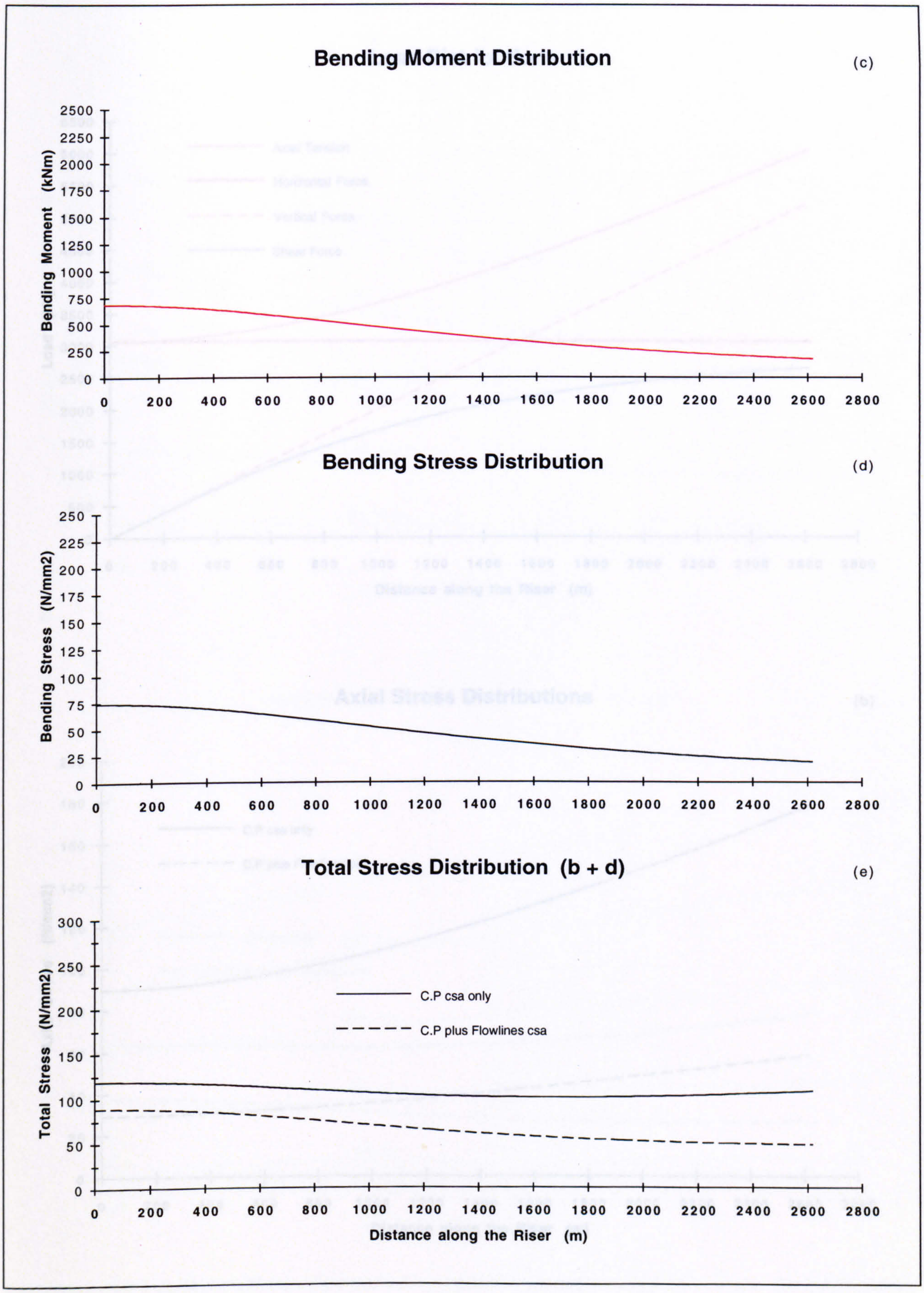

Horizontal Surface Offset = 2000 m

Submerged Unit Weight = 1000 N/m

Sea Depth = 1500 m

Carrier Pipe Outer Diameter = 1.10 m

Carrier Pipe Wall Thickness = 10 mm

Figure 2.22

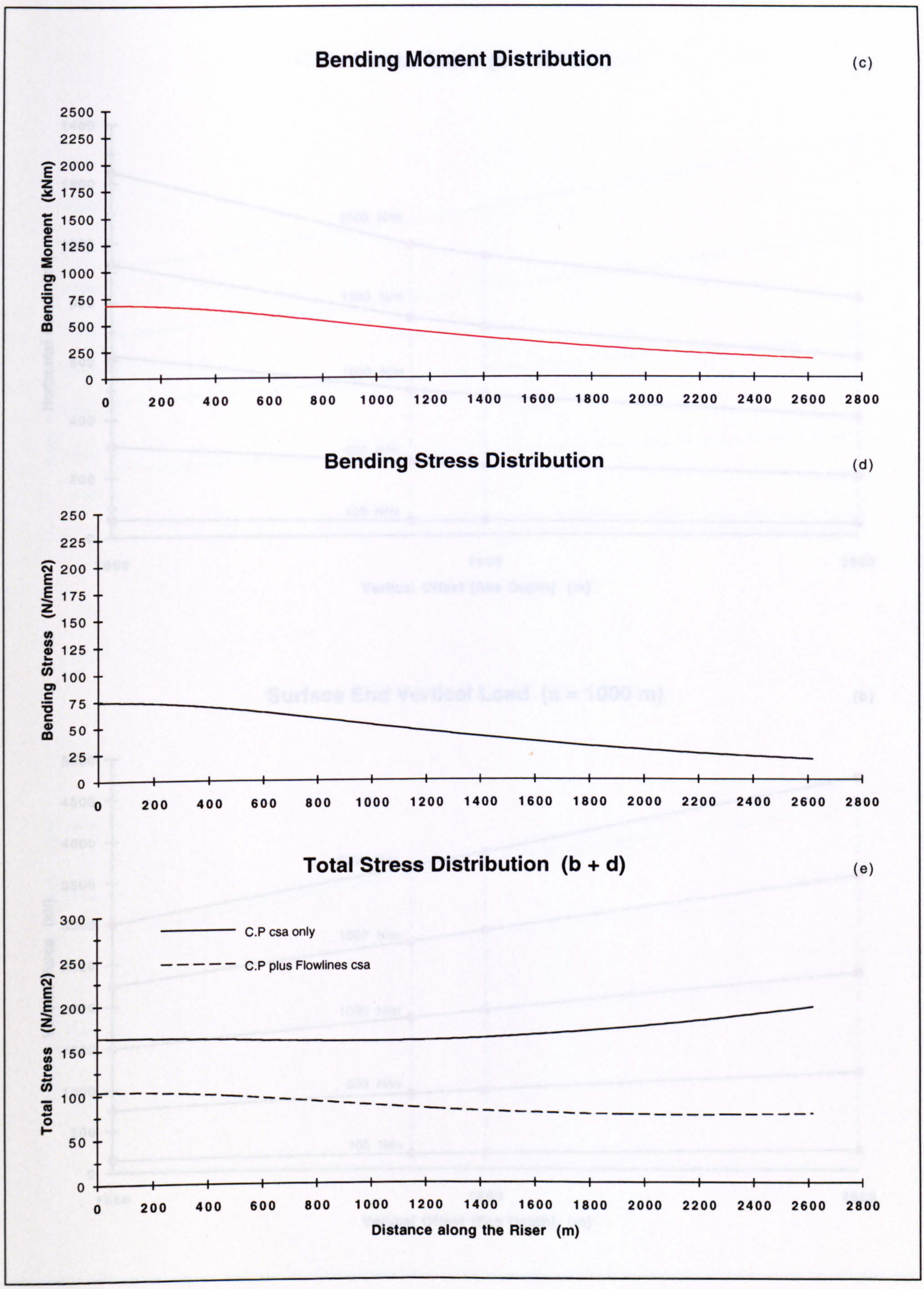

Horizontal Surface Offset = 2000 m

Submerged Unit Weight = 2000 N/m

Sea Depth = 1500 m

Carrier Pipe Outer Diameter = 1.10 m

Carrier Pipe Wall Thickness = 10 mm

Figure 2.23

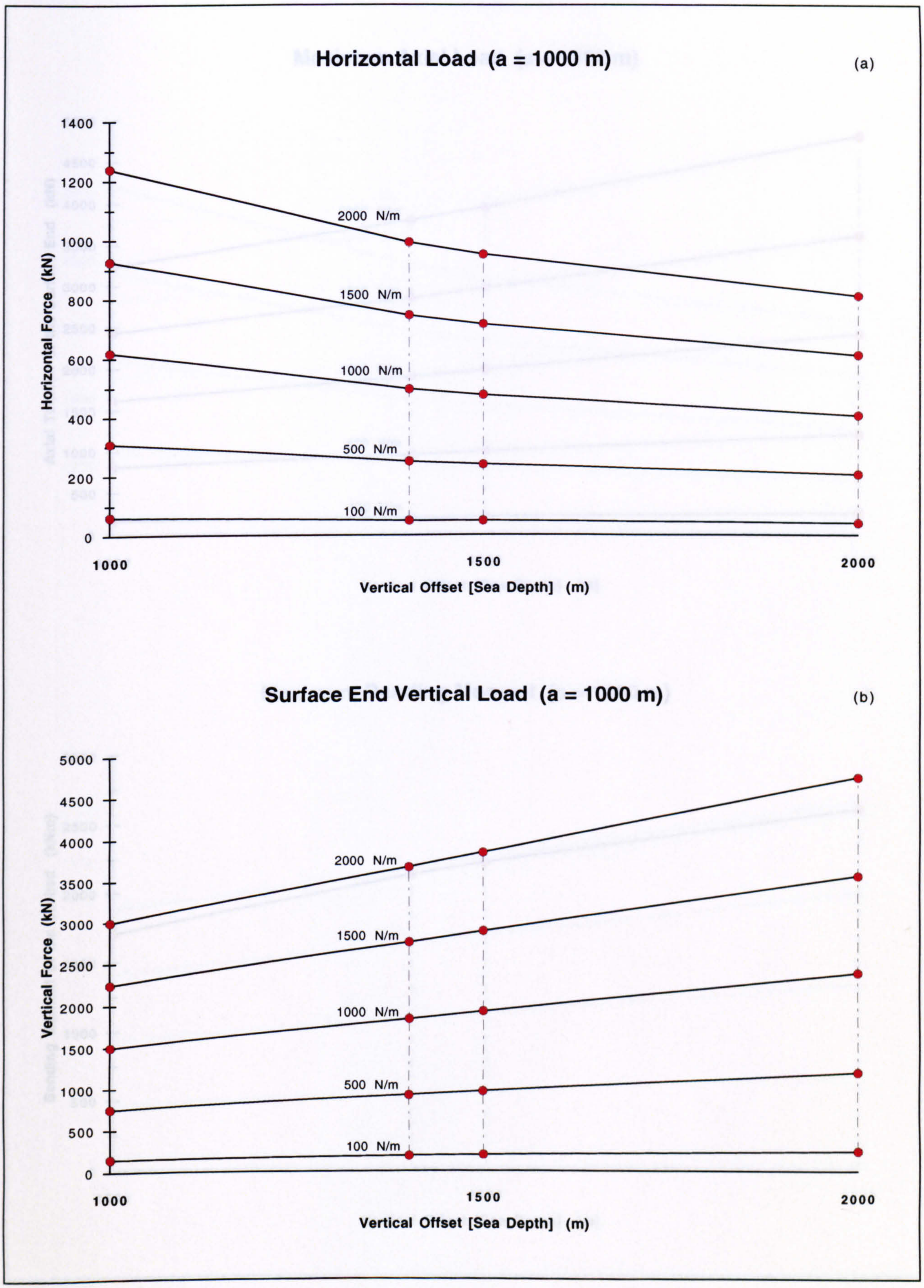

Horizontal Surface Offset = 1000 m

Figure 2.24

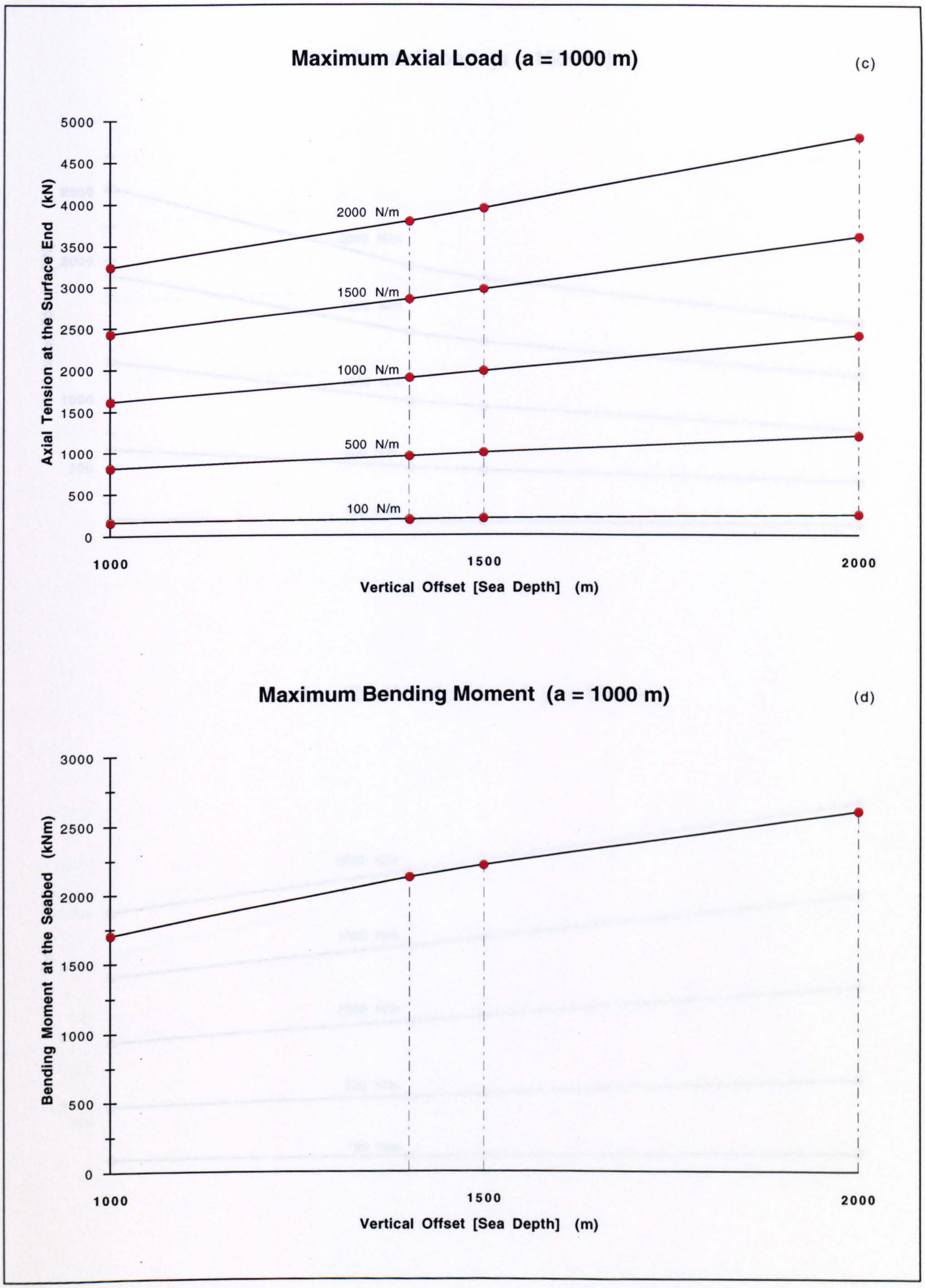

Horizontal Surface Offset = 1000 m

Figure 2.24

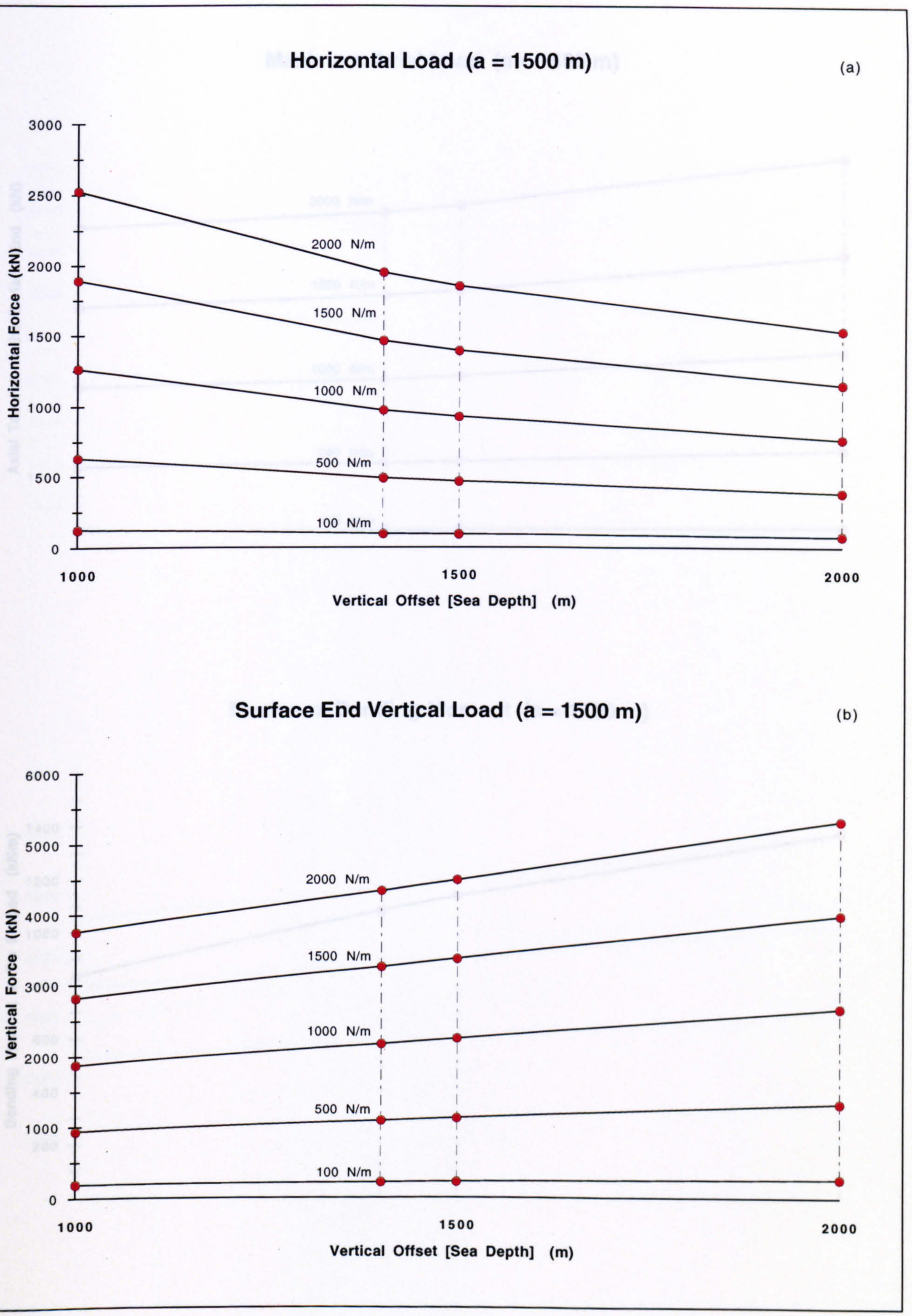

Horizontal Surface Offset = 1500 m

Figure 2.25

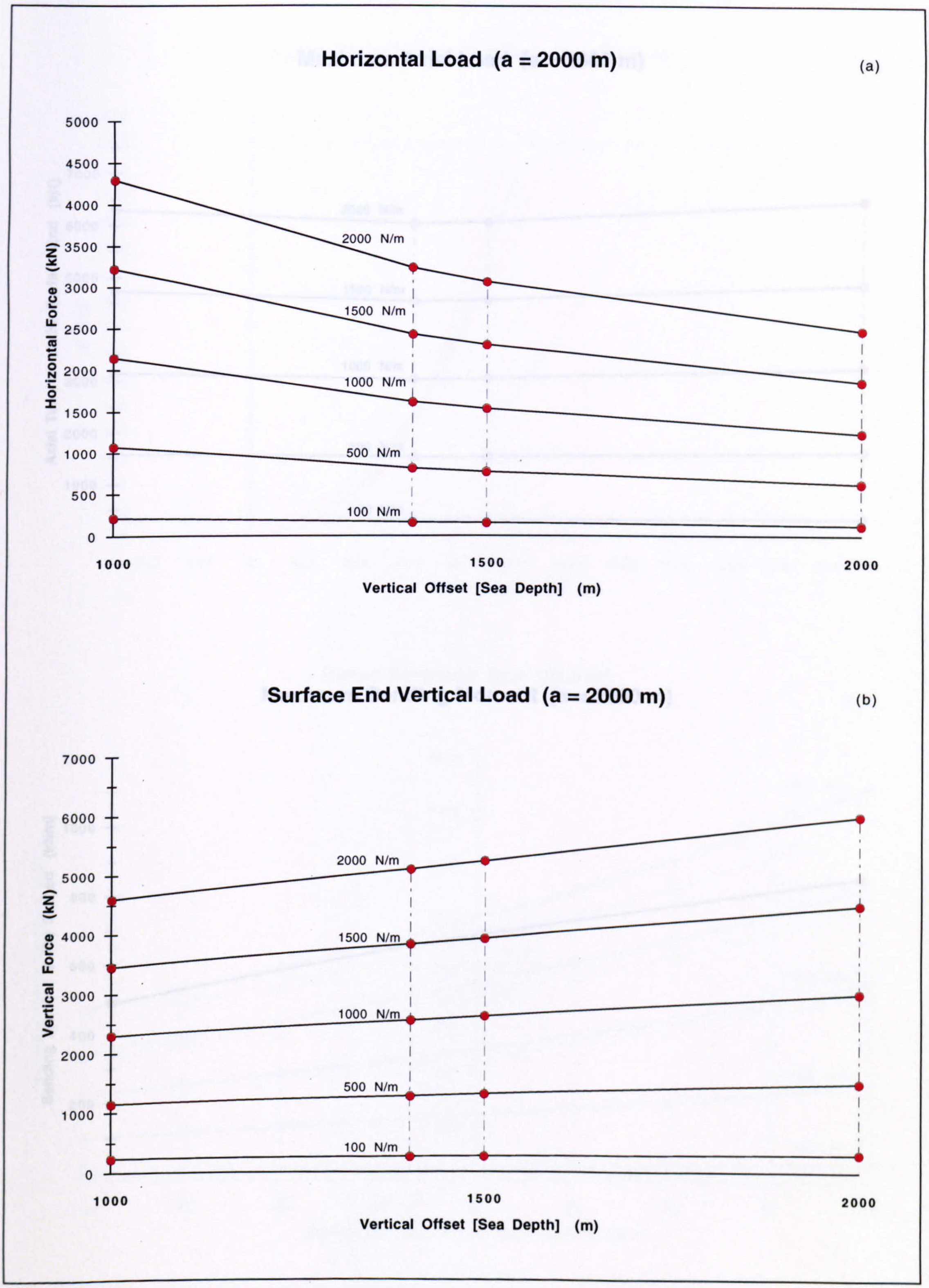

Horizontal Surface Offset = 2000 m

Figure 2.26

Maximum Axial Load (a = 2000 m)

(c)

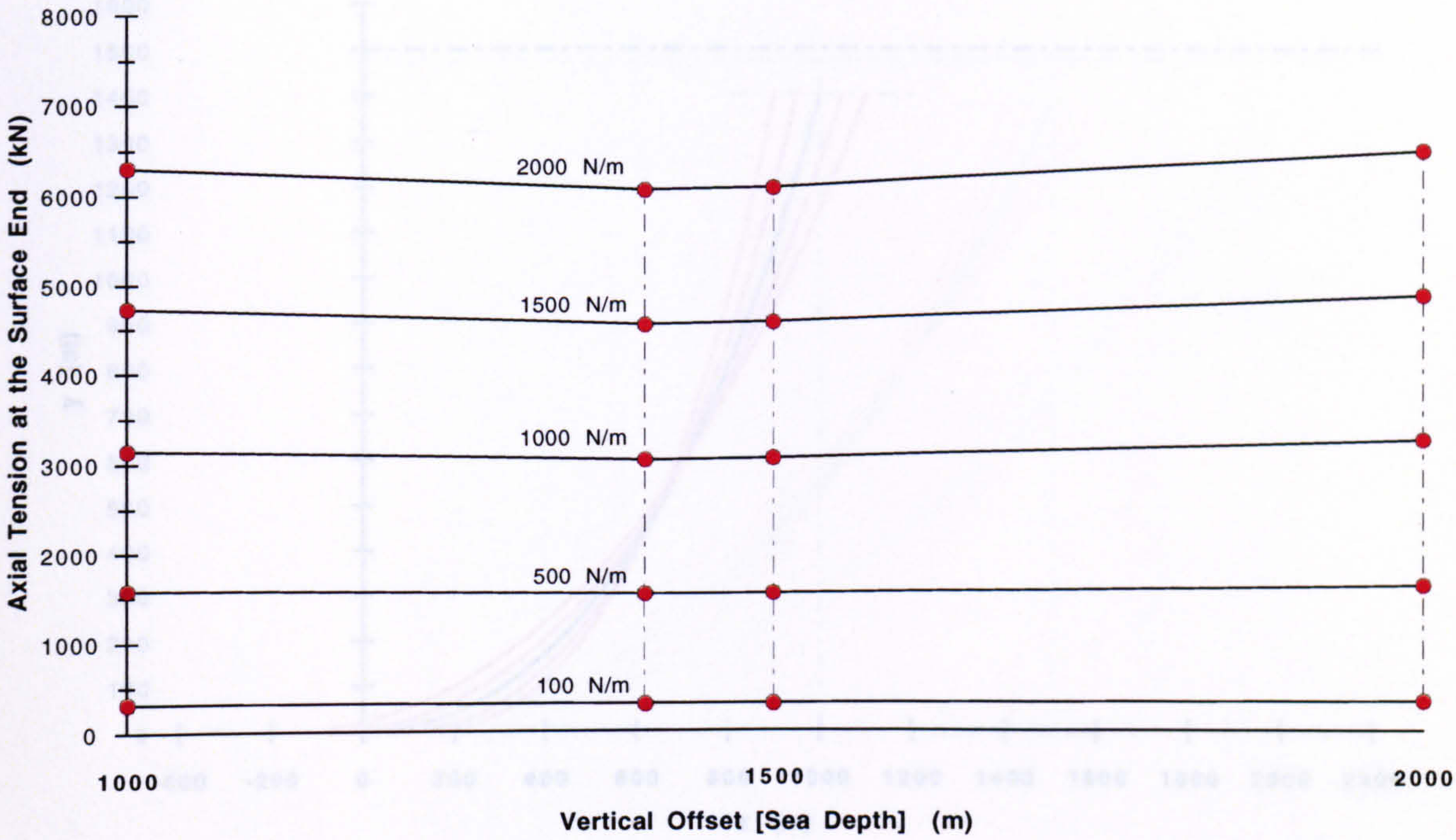

Maximum Bending Moment (a = 2000 m)

(d)

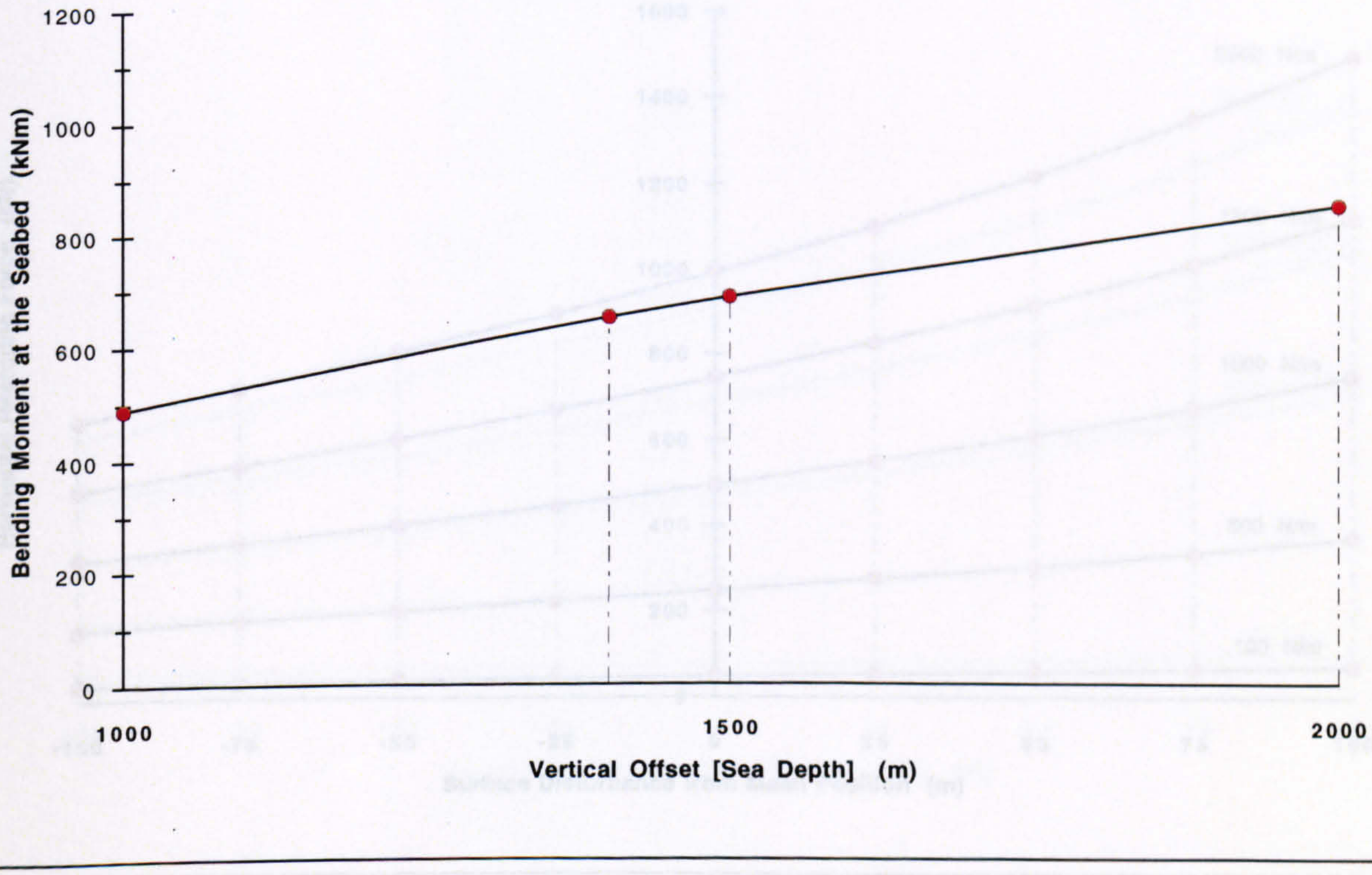

Horizontal Surface Offset = 2000 m

Figure 2.26

Surge Disturbance Profiles (a = 1000 m)

(a)

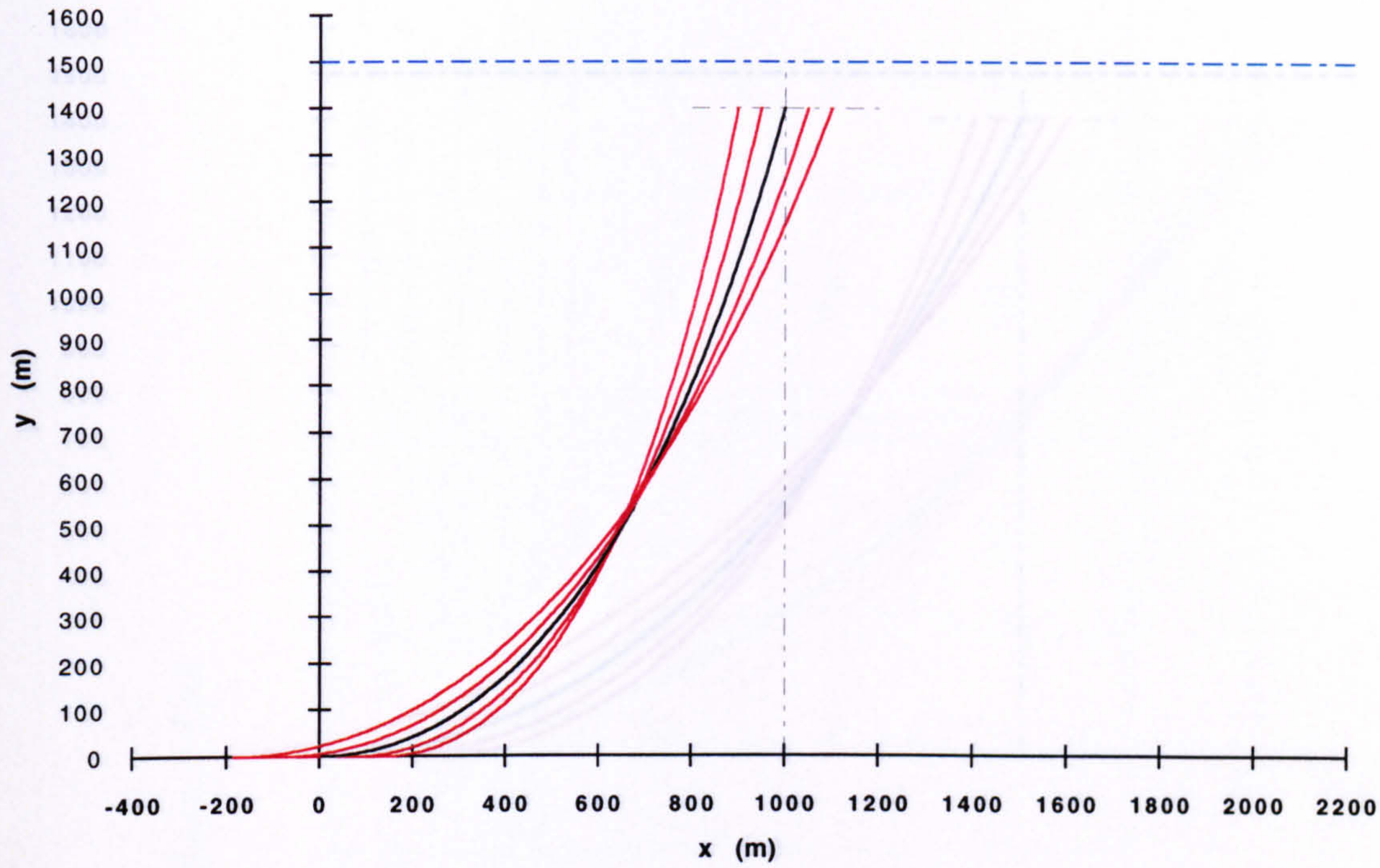

Surge Stiffness (a = 1000 m)

(b)

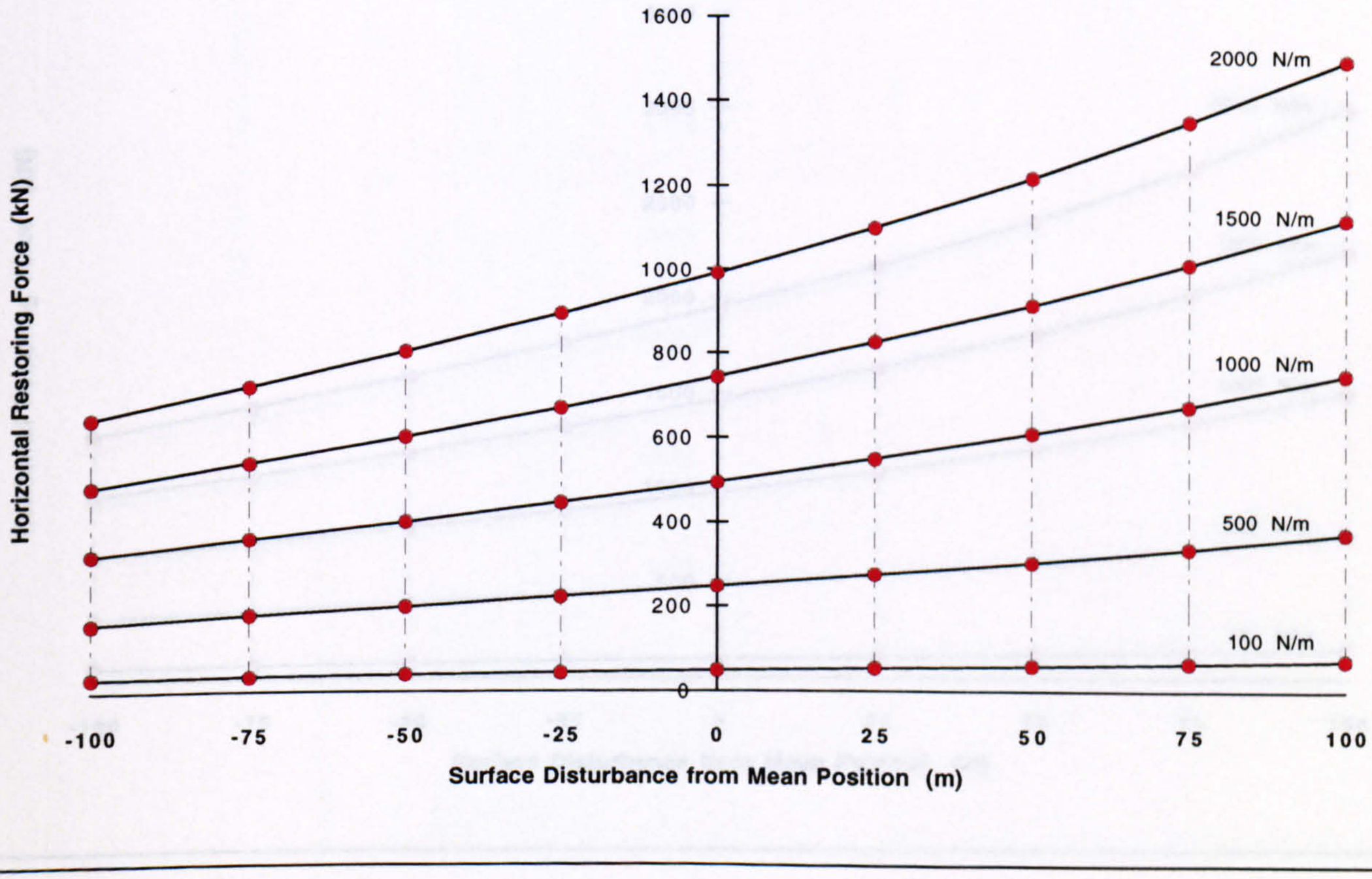

Mean Horiz Surface Offset = 1000 m

Sea Depth = 1500 m

Vertical Offset = 1400 m

Carrier Pipe Outer Diameter = 1.10 m

Carrier Pipe Wall Thickness = 10 mm

Figure 2.27

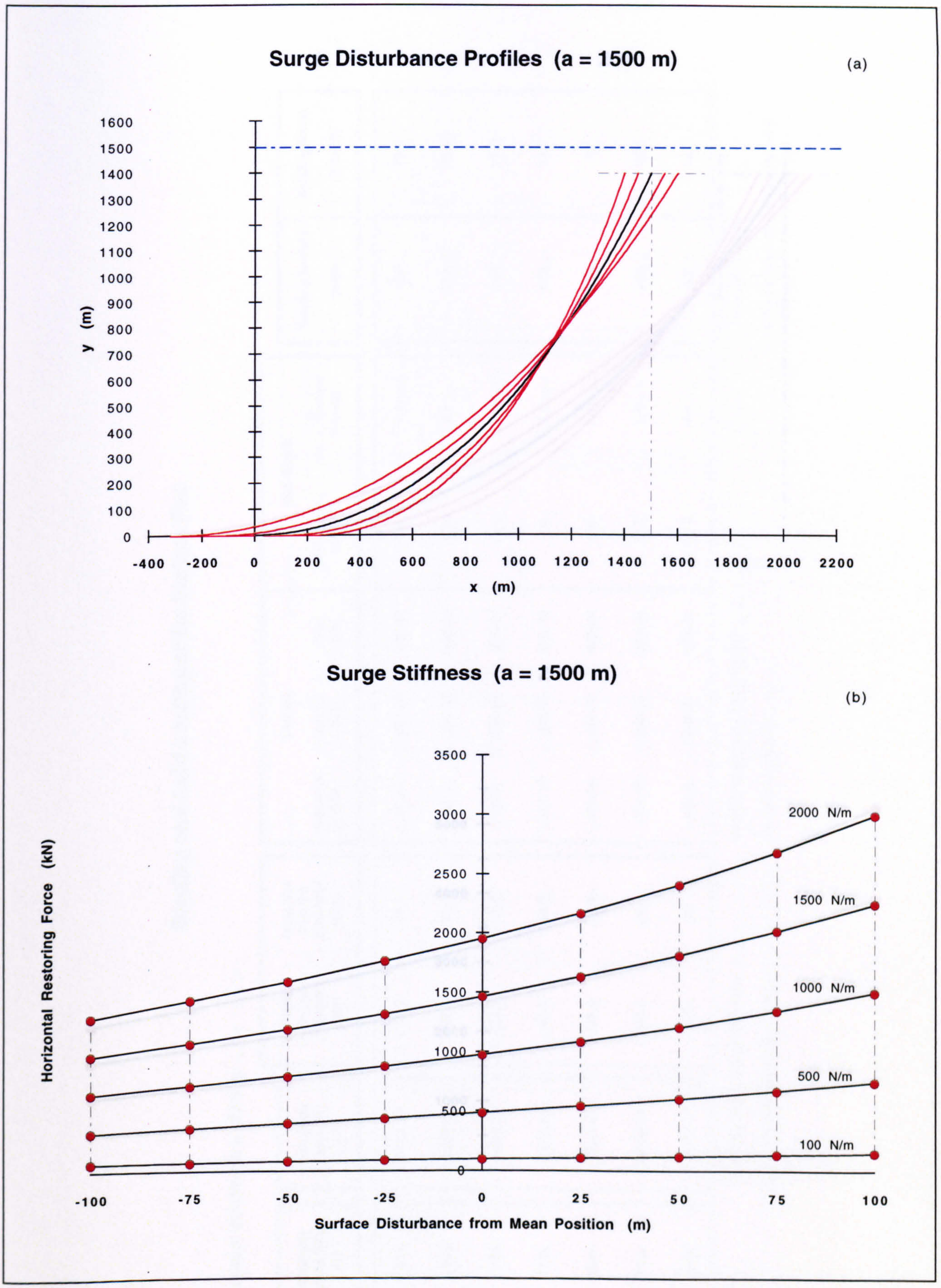

Mean Horiz Surface Offset = 1500 m

Sea Depth = 1500 m

Vertical Offset = 1400 m

Carrier Pipe Outer Diameter = 1.10 m

Carrier Pipe Wall Thickness = 10 mm

Figure 2.28

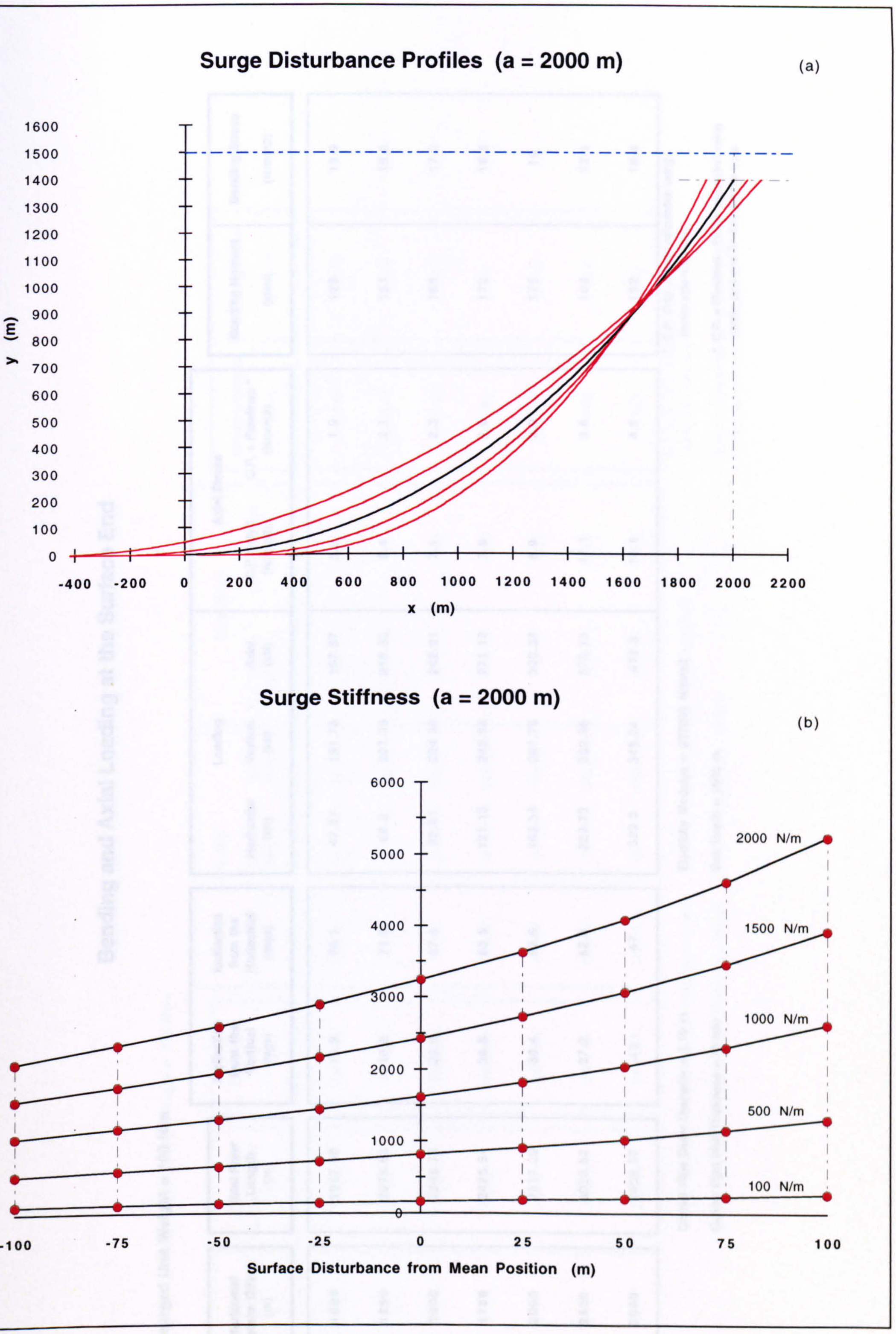

Mean Horiz Surface Offset = 2000 m

Sea Depth = 1500 m

Vertical Offset = 1400 m

Carrier Pipe Outer Diameter = 1.10 m

Carrier Pipe Wall Thickness = 10 mm

Figure 2.29

Bending and Axial Loading at the Surface End

Submerged Unit Weight = 100 N/m

Horizontal Surface Offset (m)	Total Riser Length (m)	Inclination from the Vertical (degs)	Inclination from the Horizontal (degs)	Loading			Axial Stress		Bending Moment	Bending Stress
				Horizontal (kN)	Vertical (kN)	Axial (kN)	C.P. only * (N/mm2)	C.P. + Flowlines * (N/mm2)	(kNm)	(N/mm2)
1000	1917.56	13.9	76.1	47.57	191.76	197.57	5.8	1.9	128	13.9
1250	2073.63	18.2	71.8	68.3	207.36	218.33	6.4	2.1	151	16.3
1500	2243.75	22.5	67.5	92.81	224.38	242.81	7.1	2.3	166	17.9
1750	2425.64	26.5	63.5	121.12	242.56	271.12	7.9	2.6	173	18.8
2000	2617.29	30.4	59.6	153.34	261.73	303.34	8.9	2.9	175	19
2500	3023.52	37.2	52.8	229.73	302.36	379.73	11.1	3.6	168	18.1
3000	3452.37	43	47	322.3	345.24	472.3	13.8	4.5	152	16.4

Carrier Pipe Outer Diameter = 1.10 m

Carrier Pipe Wall Thickness = 10 mm

Elasticity Modulus = 207000 N/mm2

Sea Depth = 1500 m

* C.P. Only - Stress calculation using carrier pipe c.s.a only

* C.P. + Flowlines - Stress calculation using carrier pipe and flowline bundle c.s.a

Table 2.12(a)

Bending and Axial Loading at the Seabed End

Submerged Unit Weight = 100 N/m

Horizontal Surface Offset (m)	Total Riser Length (m)	Loading			Axial Stress		Bending Moment	Bending Stress
		Horizontal (kN)	Vertical (kN)	Axial (kN)	C.P. csa only * (N/mm2)	C.P. + Flowlines * (N/mm2)	(kNm)	(N/mm2)
1000	1917.56	47.57	0	47.57	1.4	0.5	2213	239.3
1250	2073.63	68.33	0	68.33	2	0.7	1541	166.6
1500	2243.75	92.81	0	92.81	2.7	0.9	1134	122.7
1750	2425.64	121.12	0	121.12	3.5	1.2	869	94
2000	2617.29	153.34	0	153.34	4.5	1.5	687	74.2
2500	3023.52	229.73	0	229.73	6.2	2.2	458	49.6
3000	3452.37	322.3	0	322.3	9.4	3.1	327	35.3

Carrier Pipe Outer Diameter = 1.10 m

Carrier Pipe Wall Thickness = 10 mm

Elasticity Modulus = 207000 N/mm2

Sea Depth = 1500 m

* C.P. Only - Stress calculation using carrier pipe c.s.a only

* C.P. + Flowlines - Stress calculation using carrier pipe and flowline bundle c.s.a

Table 2.12(b)

Bending and Axial Loading at the Surface End

Submerged Unit Weight = 500 N/m

Horizontal Surface Offset (m)	Total Riser Length (m)	Inclination from the Vertical (degs)	Inclination from the Horizontal (degs)	Loading			Axial Stress		Bending Moment	Bending Stress
				Horizontal (kN)	Vertical (kN)	Axial (kN)	C.P. only * (N/mm2)	C.P. + Flowlines * (N/mm2)	(kNm)	(N/mm2)
1000	1917.56	13.9	76.1	237.84	958.78	987.84	28.8	9.4	128	13.9
1250	2073.63	18.2	71.8	341.63	1036.79	1091.63	31.9	10.4	151	16.3
1500	2243.75	22.5	67.5	464.07	1121.88	1214.07	35.5	11.6	166	17.9
1750	2425.64	26.5	63.5	605.61	1212.82	1355.61	39.6	12.9	173	18.8
2000	2617.29	30.4	59.6	766.7	1308.65	1516.7	44.3	14.5	175	19
2500	3023.52	37.2	52.8	1148.65	1511.78	1898.65	55.4	18.1	168	18.1
3000	3452.37	43	47	1611.51	1726.2	2361.51	69	22.5	152	16.4

Carrier Pipe Outer Diameter = 1.10 m

Carrier Pipe Wall Thickness = 10 mm

Elasticity Modulus = 207000 N/mm2

Sea Depth = 1500 m

* C.P. Only - Stress calculation using carrier pipe c.s.a only

* C.P. + Flowlines - Stress calculation using carrier pipe and flowline bundle c.s.a

Table 2.13(a)

Bending and Axial Loading at the Seabed End

Submerged Unit Weight = 500 N/m

Horizontal Surface Offset (m)	Total Riser Length (m)	Loading			Axial Stress		Bending Moment	Bending Stress
		Horizontal (kN)	Vertical (kN)	Axial (kN)	C.P. csa only * (N/mm2)	C.P. + Flowlines * (N/mm2)	(kNm)	(N/mm2)
1000	1917.56	237.84	0	237.84	6.9	2.3	2213	239.3
1250	2073.63	341.63	0	341.63	10	3.3	1541	166.6
1500	2243.75	464.07	0	464.07	13.6	4.4	1134	122.7
1750	2425.64	605.61	0	605.61	17.7	5.8	869	94
2000	2617.29	766.7	0	766.7	22.4	7.3	687	74.2
2500	3023.52	1148.65	0	1148.65	33.5	11	458	49.6
3000	3452.37	1611.51	0	1611.51	47.1	15.4	327	35.3

Carrier Pipe Outer Diameter = 1.10 m

Carrier Pipe Wall Thickness = 10 mm

Elasticity Modulus = 207000 N/mm2

Sea Depth = 1500 m

* C.P. Only - Stress calculation using carrier pipe c.s.a only

* C.P. + Flowlines - Stress calculation using carrier pipe and flowline bundle c.s.a

Table 2.13(b)

Bending and Axial Loading at the Surface End

Submerged Unit Weight = 1000 N/m

Horizontal Surface Offset (m)	Total Riser Length (m)	Inclination from the Vertical (degs)	Inclination from the Horizontal (degs)	Loading			Axial Stress		Bending Moment	Bending Stress
				Horizontal (kN)	Vertical (kN)	Axial (kN)	C.P. csa only * (N/mm2)	C.P. + Flowlines * (N/mm2)	(kNm)	(N/mm2)
1000	1917.56	13.9	76.1	475.68	1917.56	1975.68	57.7	18.8	128	13.9
1250	2073.63	18.2	71.8	683.26	2073.59	2183.26	63.8	20.8	151	16.3
1500	2243.75	22.5	67.5	928.14	2243.75	2428.14	70.9	23.2	166	17.9
1750	2425.64	26.5	63.5	1211.23	2425.63	2711.23	79.2	25.9	173	18.8
2000	2617.29	30.4	59.6	1533.4	2617.29	3033.4	88.6	28.9	175	19
2500	3023.52	37.2	52.8	2297.29	3023.55	3797.9	110.9	36.2	168	18.1
3000	3452.37	43	47	3233.01	3452.4	4723.01	137.9	45	152	16.4

Carrier Pipe Outer Diameter = 1.10 m

Carrier Pipe Wall Thickness = 10 mm

Elasticity Modulus = 207000 N/mm2

Sea Depth = 1500 m

* C.P. Only - Stress calculation using carrier pipe c.s.a only

* C.P. + Flowlines - Stress calculation using carrier pipe and flowline bundle c.s.a

Table 2.14(a)

Bending and Axial Loading at the Seabed End

Submerged Unit Weight = 1000 N/m

Horizontal Surface Offset (m)	Total Riser Length (m)	Loading			Axial Stress		Bending Moment	Bending Stress
		Horizontal (kN)	Vertical (kN)	Axial (kN)	C.P. csa only * (N/mm2)	C.P. + Flowlines * (N/mm2)	(kNm)	(N/mm2)
1000	1917.56	475.68	0	475.68	13.9	4.5	2213	239.3
1250	2073.63	683.26	0	683.26	20	6.5	1541	166.6
1500	2243.75	928.14	0	928.14	27.1	8.9	1134	122.7
1750	2425.64	1211.23	0	1211.23	35.4	11.6	869	94
2000	2617.29	1533.4	0	1533.4	44.8	14.6	687	74.2
2500	3023.52	2297.29	0	2297.29	67.1	21.9	458	49.6
3000	3452.37	3223.01	0	3223.01	94.1	30.7	327	35.3

Carrier Pipe Outer Diameter = 1.10 m

Carrier Pipe Wall Thickness = 10 mm

Elasticity Modulus = 207000 N/mm2

Sea Depth = 1500 m

* C.P. Only - Stress calculation using carrier pipe c.s.a only

* C.P. + Flowlines - Stress calculation using carrier pipe and flowline bundle c.s.a

Table 2.14(b)

Bending and Axial Loading at the Surface End

Submerged Unit Weight = 1500 N/m

Horizontal Surface Offset (m)	Total Riser Length (m)	Inclination from the Vertical (degs)	Inclination from the Horizontal (degs)	Loading			Axial Stress		Bending Moment	Bending Stress
				Horizontal (kN)	Vertical (kN)	Axial (kN)	C.P. csa only * (N/mm2)	C.P. + Flowlines * (N/mm2)	(kNm)	(N/mm2)
1000	1917.56	13.9	76.1	713.52	2876.35	2963.52	86.5	28.3	128	13.9
1250	2073.63	18.2	71.8	1024.89	3110.38	3274.89	95.6	31.2	151	16.3
1500	2243.75	22.5	67.5	1392.21	3365.63	3642.21	106.4	34.7	166	17.9
1750	2425.64	26.5	63.5	1816.84	3638.45	4066.84	118.8	38.8	173	18.8
2000	2617.29	30.4	59.6	2300.1	3925.94	4550.1	132.9	43.4	175	19
2500	3023.52	37.2	52.8	3445.94	4535.33	5695.94	166.3	54.3	168	18.1
3000	3452.37	43	47	4834.52	5178.6	7084.52	206.9	67.6	152	16.4

Carrier Pipe Outer Diameter = 1.10 m

Carrier Pipe Wall Thickness = 10 mm

Elasticity Modulus = 207000 N/mm2

Sea Depth = 1500 m

* C.P. Only - Stress calculation using carrier pipe c.s.a only

* C.P. + Flowlines - Stress calculation using carrier pipe and flowline bundle c.s.a

Table 2.15(a)

Bending and Axial Loading at the Seabed End

Submerged Unit Weight = 1500 N/m

Horizontal Surface Offset (m)	Total Riser Length (m)	Loading			Axial Stress		Bending Moment	Bending Stress
		Horizontal (kN)	Vertical (kN)	Axial (kN)	C.P. csa only * (N/mm2)	C.P. + Flowlines * (N/mm2)	(kNm)	(N/mm2)
1000	1917.56	713.52	0	713.52	20.8	6.8	2213	239.3
1250	2073.63	1024.89	0	1024.89	29.9	9.8	1541	166.6
1500	2243.75	1392.21	0	1392.21	40.7	13.3	1134	122.7
1750	2425.64	1816.84	0	1816.84	53.1	17.3	869	94
2000	2617.29	2300.1	0	2300.1	67.2	21.9	687	74.2
2500	3023.52	3445.94	0	3445.94	100.6	32.9	458	49.6
3000	3452.37	4834.52	0	4834.52	141.2	46.1	327	35.3

Carrier Pipe Outer Diameter = 1.10 m

Carrier Pipe Wall Thickness = 10 mm

Elasticity Modulus = 207000 N/mm2

Sea Depth = 1500 m

* C.P. Only - Stress calculation using carrier pipe c.s.a only

* C.P. + Flowlines - Stress calculation using carrier pipe and flowline bundle c.s.a

Table 2.15(b)

Bending and Axial Loading at the Surface End

Submerged Unit Weight = 2000 N/m

Horizontal Surface Offset (m)	Total Riser Length (m)	Inclination from the Vertical (degs)	Inclination from the Horizontal (degs)	Loading			Axial Stress		Bending Moment	Bending Stress
				Horizontal (kN)	Vertical (kN)	Axial (kN)	C.P. csa only * (N/mm2)	C.P. + Flowlines * (N/mm2)	(kNm)	(N/mm2)
1000	1917.56	13.9	76.1	951.37	3835.13	3951.37	115.4	37.7	128	13.9
1250	2073.63	18.2	71.8	1366.51	4147.18	4366.51	127.5	41.6	151	16.3
1500	2243.75	22.5	67.5	1856.28	4487.5	4856.28	141.8	46.3	166	17.9
1750	2425.64	26.5	63.5	2422.46	4851.26	5422.46	158.4	51.7	173	18.8
2000	2617.29	30.4	59.6	3066.81	5234.58	6066.81	177.2	57.9	175	19
2500	3023.52	37.2	52.8	4594.58	6047.11	7594.58	221.8	72.4	168	18.1
3000	3452.37	43	47	6446.03	6904.79	9446.03	275.8	90.1	152	16.4

Carrier Pipe Outer Diameter = 1.10 m

Carrier Pipe Wall Thickness = 10 mm

Elasticity Modulus = 207000 N/mm2

Sea Depth = 1500 m

* C.P. Only - Stress calculation using carrier pipe c.s.a only

* C.P. + Flowlines - Stress calculation using carrier pipe and flowline bundle c.s.a

Table 2.16(a)

Bending and Axial Loading at the Seabed End

Submerged Unit Weight = 2000 N/m

Horizontal Surface Offset (m)	Total Riser Length (m)	Loading			Axial Stress		Bending Moment	Bending Stress
		Horizontal (kN)	Vertical (kN)	Axial (kN)	C.P. csa only * (N/mm2)	C.P. + Flowlines * (N/mm2)	(kNm)	(N/mm2)
1000	1917.56	951.37	0	951.37	27.8	9.1	2213	239.3
1250	2073.63	1366.51	0	1366.51	39.9	13	1541	166.6
1500	2243.75	1856.28	0	1856.28	54.2	17.7	1134	122.7
1750	2425.64	2422.46	0	2422.46	70.7	23.1	869	94
2000	2617.29	3066.81	0	3066.81	89.6	29.3	687	74.2
2500	3023.52	4594.58	0	4594.58	134.2	43.8	458	49.6
3000	3452.37	6446.03	0	6446.03	188.2	61.5	327	35.3

Carrier Pipe Outer Diameter = 1.10 m

Carrier Pipe Wall Thickness = 10 mm

Elasticity Modulus = 207000 N/mm2

Sea Depth = 1500 m

* C.P. Only - Stress calculation using carrier pipe c.s.a only

* C.P. + Flowlines - Stress calculation using carrier pipe and flowline bundle c.s.a

Table 2.16(b)

Shear Loading at the Surface End (maximum)

Carrier Pipe Outer Diameter = 1.10 m

Carrier Pipe Wall Thickness = 10 mm

Horizontal Surface Offset (m)	Submerged Unit Weight (N/m)	Shear Force (kN)	Shear Stress (N/mm2)
1000	100	46	1.3
	500	231	6.7
	1000	462	13.5
	1500	693	20.2
	2000	923	27.0
1250	100	65	1.9
	500	324	9.5
	1000	649	19.0
	1500	973	28.4
	2000	1298	37.9
1500	100	86	2.5
	500	429	12.5
	1000	858	25.0
	1500	1286	37.6
	2000	1712	50.1
1750	100	108	3.2
	500	542	15.8
	1000	1084	31.6
	1500	1625	47.5
	2000	2167	63.3
2000	100	132	3.9
	500	662	19.3
	1000	1323	38.6
	1500	1985	58.0
	2000	2646	77.3
2500	100	183	5.3
	500	915	26.7
	1000	1829	53.4
	1500	2744	80.1
	2000	3658	106.8
3000	100	236	6.9
	500	1178	34.4
	1000	2356	68.8
	1500	3534	103.2
	2000	4712	137.6

Table 2.17

Riser Stiffness in Surge

Vertical Offset = 1400 m

Horizontal Surface Offset (m)	Submerged Unit Weight (N/m)	Stiffness for a Single Riser Arrangement (kN/m)	Stiffness for a Double Riser Arrangement (kN/m)
1000	100	0.2	0.4
	500	1.1	2.1
	1000	2.1	4.2
	1500	3.2	6.4
	2000	4.2	8.5
1250	100	0.3	0.6
	500	1.5	3.0
	1000	3.0	6.1
	1500	4.6	9.1
	2000	6.1	12.2
1500	100	0.4	0.9
	500	2.1	4.3
	1000	4.3	8.5
	1500	6.4	12.8
	2000	8.5	17.1
1750	100	0.6	1.2
	500	2.9	5.8
	1000	5.8	11.7
	1500	8.8	17.5
	2000	11.7	23.4
2000	100	0.8	1.6
	500	3.9	7.9
	1000	7.9	15.9
	1500	11.8	23.6
	2000	15.7	31.4

Table 2.18

Riser Stiffness in Surge

Vertical Offset = 1500 m

Horizontal Surface Offset (m)	Submerged Unit Weight (N/m)	Stiffness for a Single Riser arrangement (kN/m)	Stiffness for a Double Riser Arrangement (kN/m)
1000	100	0.2	0.4
	500	1.0	1.9
	1000	1.9	3.8
	1500	2.9	5.7
	2000	3.8	7.6
1250	100	0.3	0.5
	500	1.3	2.7
	1000	2.7	5.4
	1500	4.0	8.1
	2000	5.4	10.8
1500	100	0.4	0.7
	500	1.9	3.7
	1000	3.7	7.4
	1500	5.6	11.2
	2000	7.4	14.9
1750	100	0.5	1.0
	500	2.5	5.0
	1000	5.0	10.1
	1500	7.5	15.1
	2000	10.1	20.1
2000	100	0.7	1.3
	500	3.3	6.7
	1000	6.7	13.4
	1500	10.0	20.0
	2000	13.4	26.7

Table 2.19

Riser Stiffness in Heave

Vertical Offset = 1500 m

Horizontal Surface Offset (m)	Submerged Unit Weight (N/m)	Stiffness for a Single Riser Arrangement (kN/m)	Stiffness for a Double Riser Arrangement (kN/m)
1000	100	0.2	0.4
	500	1.1	2.2
	1000	2.2	4.3
	1500	3.3	6.5
	2000	4.3	8.7
1250	100	0.2	0.5
	500	1.2	2.4
	1000	2.4	4.8
	1500	3.6	7.3
	2000	4.8	9.7
1500	100	0.3	0.5
	500	1.3	2.7
	1000	2.7	5.4
	1500	4.0	8.1
	2000	5.4	10.7
1750	100	0.3	0.6
	500	1.5	3.0
	1000	3.0	5.9
	1500	4.4	8.9
	2000	5.9	11.8
2000	100	0.3	0.6
	500	1.6	3.2
	1000	3.2	6.5
	1500	4.9	9.7
	2000	6.5	12.9

Table 2.20

CHAPTER 3

The Design of a Buoyancy Support System for a Catenary Riser

3.1 General Description

The design of a production riser for ultra-deep water operations has to take into consideration the effects of its considerable self-weight resulting from the choice of steel as the fabrication material and a suspended length which could be anywhere between 1000 and 3000 m depending upon the sea depth and the horizontal surface offset chosen. The weight of the riser assembly can be limited or even eliminated by the addition of support, either in discrete or continuous amounts along the risers length. The minimisation of a risers weight is critical if it is to be considered technically feasible for environmentally harsh oceanic conditions such as those experienced West of Shetland. Two very important reasons for this can be summarised as follows:

- Limiting the axial stress exerted upon the riser due to its own weight enables the system to retain a greater ability to safely withstand loads generated by prevailing environmental conditions.

- The connection assembly between riser and surface vessel or sub-surface buoy is a critical component within the system. To ensure that this component is technically feasible in terms of its required strength at a cost that is economic compels the combined forces of self-weight and environmental loading acting upon it to be minimised.

Riser support is achieved through the addition of a buoyancy system which works on the basis of a principle laid down by the Greek physicist and mathematician Archimedes (c.287 - 212 B.C.). The *buoyancy* of a body immersed in a fluid is the vertical upthrust it experiences due to the displacement of the fluid, see Figure 3.1(a). It is therefore the resultant of all the hydrostatic pressure forces (which increase with depth) acting perpendicular to the sides of the immersed body, see Figure 3.1(b) and can be expressed analytically as:

$$\text{Buoyancy} = \nabla g \rho_f \qquad (3.1)$$

where: ∇ = volume of fluid displaced

ρ_f = fluid density

If the body is fully immersed as illustrated in Figure 3.1 then ∇ will also be equal to the external volume of the body.

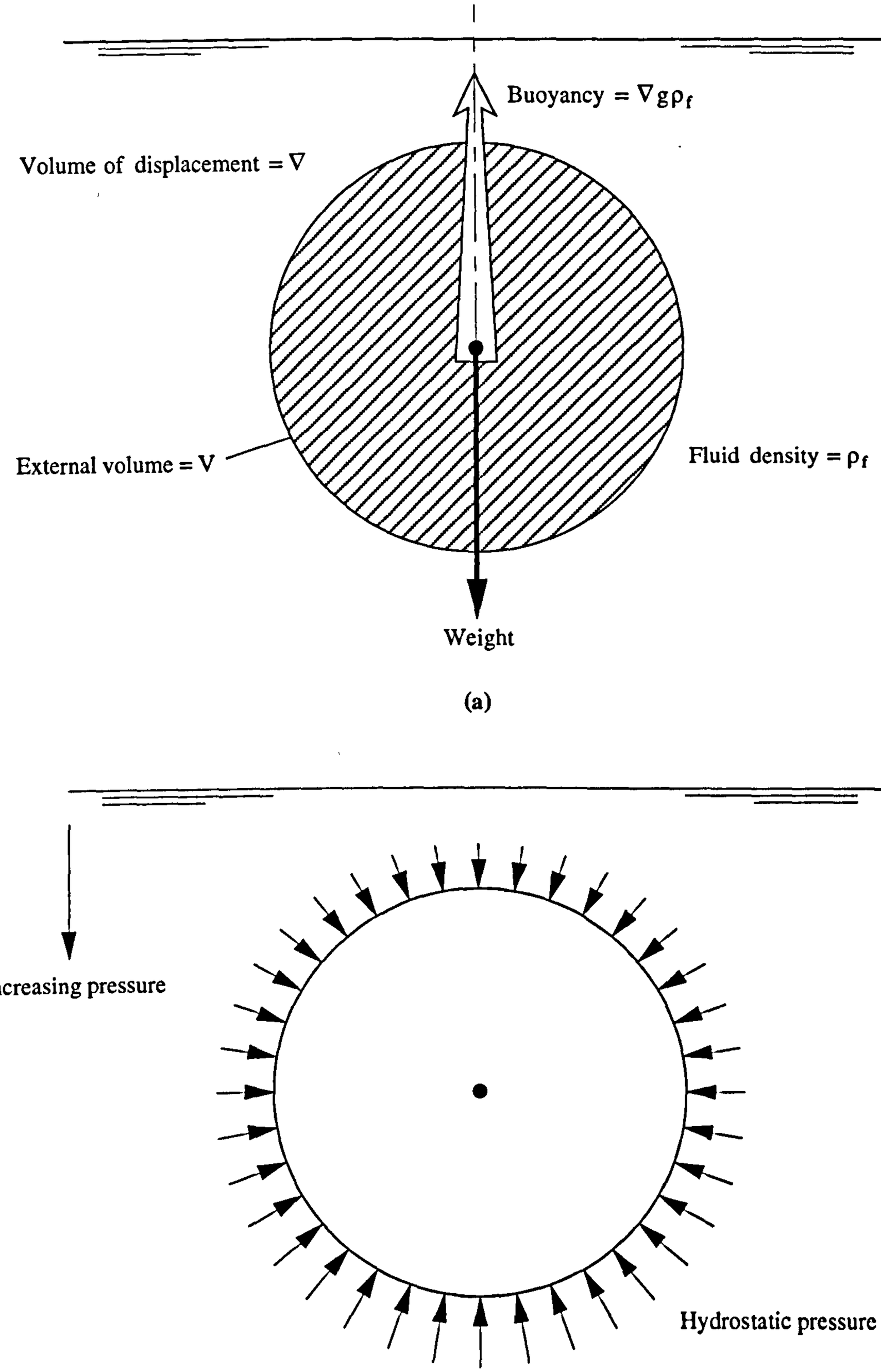

Figure 3.1

Definition of Buoyancy

The *submerged weight* of a body which was a term used frequently in Chapter 2 can now be fully defined as being equal to the weight of the body in air minus the buoyancy exerted upon it when immersed i.e.

$$\text{Submerged weight} = \text{Weight in air} - \text{Buoyancy}$$

A buoyancy system simply reduces the submerged weight of a riser structure by increasing its external volume thereby increasing the buoyancy force exerted upon it. An effective buoyancy system will greatly enhance the volume at the expense of very little gain in weight.

Any buoyancy system under consideration for a deep water riser has to posses certain attributes:

- Sufficient compression strength. The hydrostatic pressure at a water depth of 1500 m is 151 bar (2189 psi). If the buoyancy material is very compressible it will contract under pressure losing volume and hence buoyancy. Ordinary expanded polystyrene foam for example is useless at any depth in excess of 50 m for this reason.
- Low density and therefore a high buoyancy/weight ratio
- Very low or preferably zero rate of water absorption over long periods of time. The gradual intrusion of water in to a buoyancy system or material causes an increase in density and therefore weight. The magnitude of this increase may have a negligible effect for short term usage, however for long term exposure the weight gain may accumulate to an unacceptable level.
- Low maintenance over the operational lifetime of the production system.
- Economical
- Low fabrication complexity

The objective of this chapter is to examine two buoyancy systems that have the potential capability of providing continuous support to a deep water production riser. This chapter discusses the main features of each system and how they effect the riser in terms of the following :

- Manufacture and fabrication
- Riser loading
- Performance during installation
- Performance during operational life span

3.2 Syntactic Foam Buoyancy

3.2.1 Introduction

Syntactics, because of their low density, were recognised as being ideal for deepsea buoyancy from the start. In addition to their low density, they are characterised by high hydrostatic strength and a low water absorption. For these reasons syntactic foam has long been the most commonly used buoyancy material for supporting marine risers in offshore oil exploration. Many drilling depth records have been set with risers equipped with syntactic foam, however exploration risers tend to be used for only short periods, from a few weeks to a few months at a time, so that most experience is limited to short term exposure to hydrostatic pressure. In recent years, however the emphasis has shifted to production, the industry needs assurance of 10-, 20- and even 30 year survivability during continuous deployment at depth, with buoyancy losses typically less than 3 - 5% over the entire time span. To fully understand both the benefits and limitations that syntactic foam brings to deepsea buoyancy requires a basic knowledge of its unique structure and this is given in the next section.

3.2.2 Syntactic Composite Structure

Syntactic composites are unique materials formed by combining hollow, thin-walled glass microspheres with polymeric resins, which are the cured to produce solids with specific properties. Theoretically, the concept of introducing reinforced air in to a polymer matrix could include any hollow particle. But from the beginning, the material universally used in deepsea applications has been glass, since it is much stronger than any other medium available, and strength is the key requirement for withstanding hydrostatic pressures. Although glass spheres and resin are the fundamental ingredients, two other materials are usually incorporated - macrospheres and external skins. These are the four ingredients which form the traditional image of syntactic materials. The composition of syntactic foam is illustrated in Figure 3.2(a).

Microspheres

Microballon microspheres range from 6 to 120 microns in diameter and are made of high strength water glass feed stock. Internal atmosphere is inert.

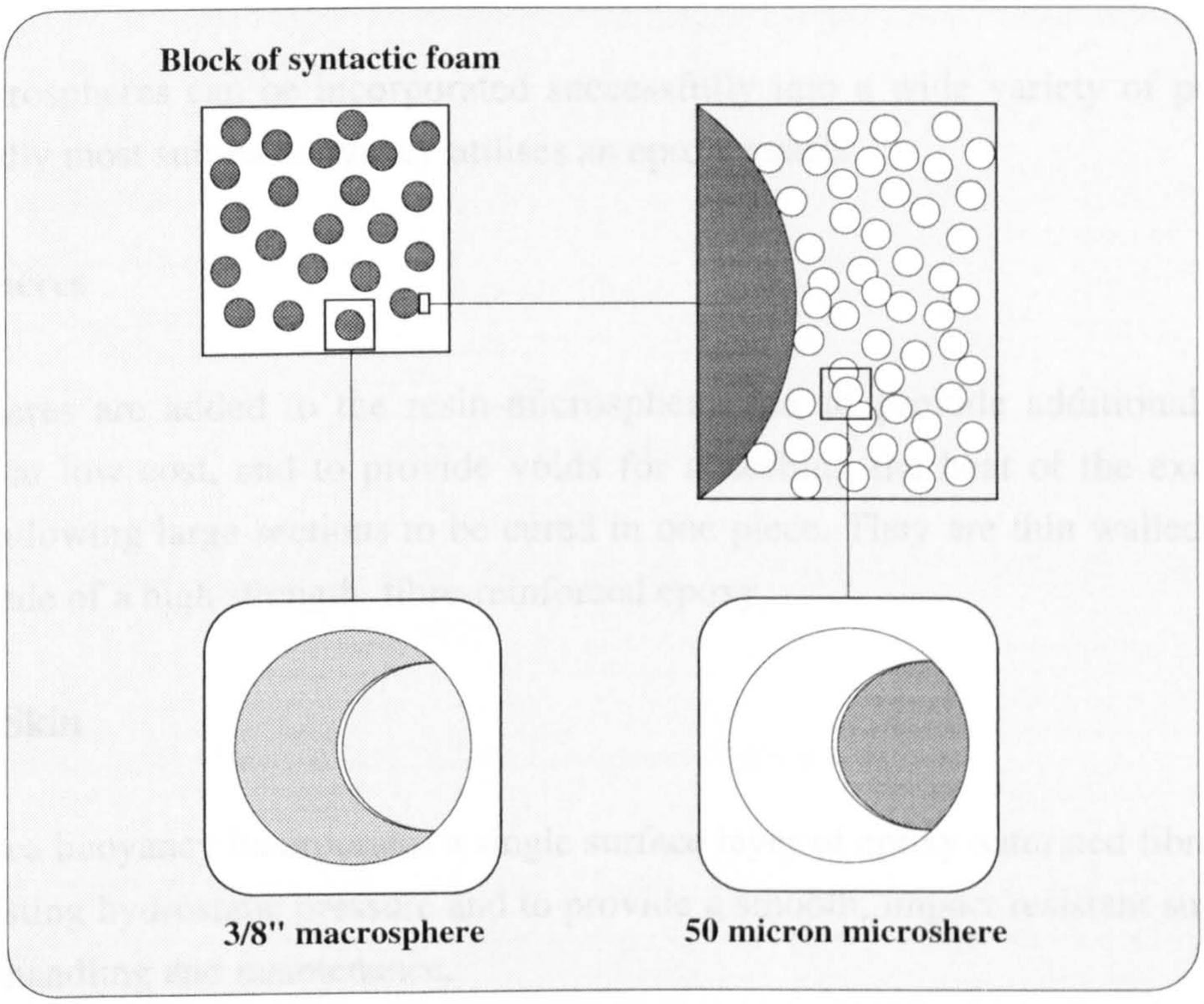

A sample of syntactic foam is composed of trillions of microscopic microspheres and a few macrospheres, all immobilised in epoxy resin

(a)

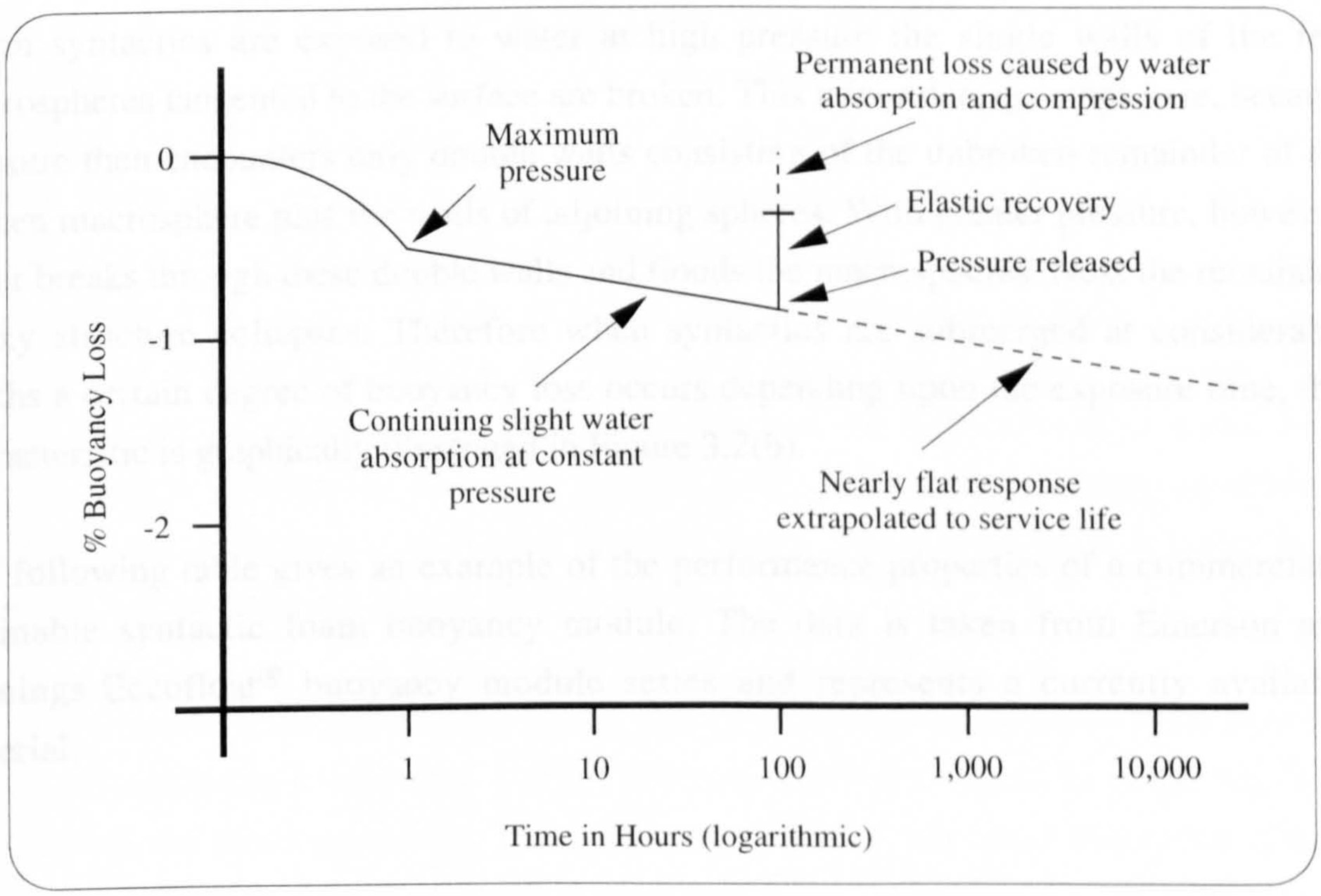

(b)

Figure 3.2

Characteristics of Syntactic Foam

Resins

Glass microspheres can be incorporated successfully into a wide variety of polymers. Traditionally most subsea buoyancy utilises an epoxy matrix.

Macrospheres

Macrospheres are added to the resin-microsphere mix to provide additional density reduction at low cost, and to provide voids for absorbing the heat of the exothermic reaction, allowing large sections to be cured in one piece. They are thin walled and are usually made of a high strength, fibre-reinforced epoxy.

External Skin

Most subsea buoyancy incorporates a single surface layer of epoxy-saturated fibreglass to aid in resisting hydrostatic pressure and to provide a smooth, impact resistant surface for finishing, handling and maintenance.

Performance

When syntactics are exposed to water at high pressure the single walls of the few macrospheres tangential to the surface are broken. This minor damage stops here, because pressure then encounters only double walls consisting of the unbroken remainder of the broken macrosphere plus the walls of adjoining spheres. With greater pressure, however, water breaks through these double walls and floods the macrospheres. Next the remaining epoxy structure collapses. Therefore when syntactics are submerged at considerable depths a certain degree of buoyancy loss occurs depending upon the exposure time, this characteristic is graphically illustrated in Figure 3.2(b).

The following table gives an example of the performance properties of a commercially attainable syntactic foam buoyancy module. The data is taken from Emerson and Cumings Eccofloat® buoyancy module series and represents a currently available material.

Performance Properties (Eccofloat® RG - 24)	
Nominal Density (kg/m3)	384.4
Crush Pressure (bar)	151.7
Crush Pressure Depth (m)	1506
Rated Service Pressure (bar)	91.9
Rated Service Depth (m)	914

Table 3.1

Syntactic Foam Properties

A higher specification foam is available in terms of its pressure rating, however this is compromised by an increase in density.

3.2.3 Structural Arrangement of the Buoyancy System

The proposed design encases the flowline bundle, comprising of two production and two fluid injection lines plus an umbilical within syntactic foam. The whole assembly is then sleeved by a large diameter steel pipe known as a carrier pipe. The carrier pipe is fabricated so as ensure that the contents enclosed within it are not exposed to sea water, however because of the pipes inherently small wall thickness to radius ratio (≈ 0.02) it simply acts a shell membrane and is therefore unable to provide resistance to the high external hydrostatic pressures experienced in deep water. It therefore relies on the foams substantial compressive strength to support the carrier pipe wall so as to avoid failure through buckling. A structural connection between carrier pipe and flowline bundle is created by transversely sub-dividing the riser assembly along its length with bulkheads. These ensure that the carrier pipe and flowlines act integrally to resist tensile loads generated by self-weight, external environmental forces and thermal expansion. High density polyurethane foam sleeves are inserted between the flowlines and syntactic foam in an attempt to insulate the buoyancy material from the potentially damaging effect of high temperatures generated by the hot flowline fluids. This phenomenon is investigated in more detail in the next chapter (Section 4.5.9).

The main reason for introducing the carrier pipe, is to protect the syntactic foam from the effects of a prolonged exposure to high pressure sea water which have already been discussed in the previous section. The carrier pipe ensures that water absorption doesn't occur and despite its limited strength in circumferential compression it will offer some degree of structural protection against the high hydrostatic pressures. The result of this being that a lower density foam can be used which ultimately benefits the economics of

the system, the use of a carrier pipe also offers the operators more assurance in terms of buoyancy performance over the life span of the assembly.

3.2.4 Operational Analysis

The proceeding analysis uses an operational spreadsheet (Spreadsheet 3.1) constructed in EXCEL in order to evaluate the effect that the carrier pipe diameter has on the risers weight and buoyancy. The results should then enable a designer to select optimum dimensions on the basis of operational performance as well as cost. The analysis is conducted using two riser arrangements as shown in Figures 3.3, 3.4 and 3.5. The first arrangement has a carrier pipe enclosing the standard four flowline bundle as previously detailed, where as the second arrangement has an additional flowline. This flowline provides the operator with greater flexibility in terms of adjusting the weight of the system. Filling the flowline with either water or air (at different pressures) can either ballast or de-ballast the riser. This is an extremely useful attribute especially during oil production, since it is common for wellhead production fluids to change in composition and therefore density over the life span of the reservoir. This change could be substantial enough to alter the submerged weight of the system to an extent which could be detrimental in terms of both the risers behaviour under environmental loading and the forces exerted upon a surface (or sub-surface) vessel. The ability to trim the risers weight during its operational life is therefore of great benefit.

The spreadsheet breaks the riser up into six equal length compartments and for each of these the buoyancy and weight are calculated. At this stage it is assumed that the risers cross-sectional geometry along with the properties of the flowline fluids remain constant along the entire length. As a result both unit buoyancy and weight are uniform along the complete length of the riser.

Note: Numbers in brackets correspond to columns or boxes displayed within the spreadsheet.

The **buoyancy** (5) of each compartment is attained using the following expression:

$$\text{Buoyancy} = \left(\frac{\pi}{4}\right) D^2 \, g \, L_c \, \rho_{sw} \qquad (3.2)$$

where D = outer diameter of the carrier pipe
L_c = compartment length
ρ_{sw} = sea water density

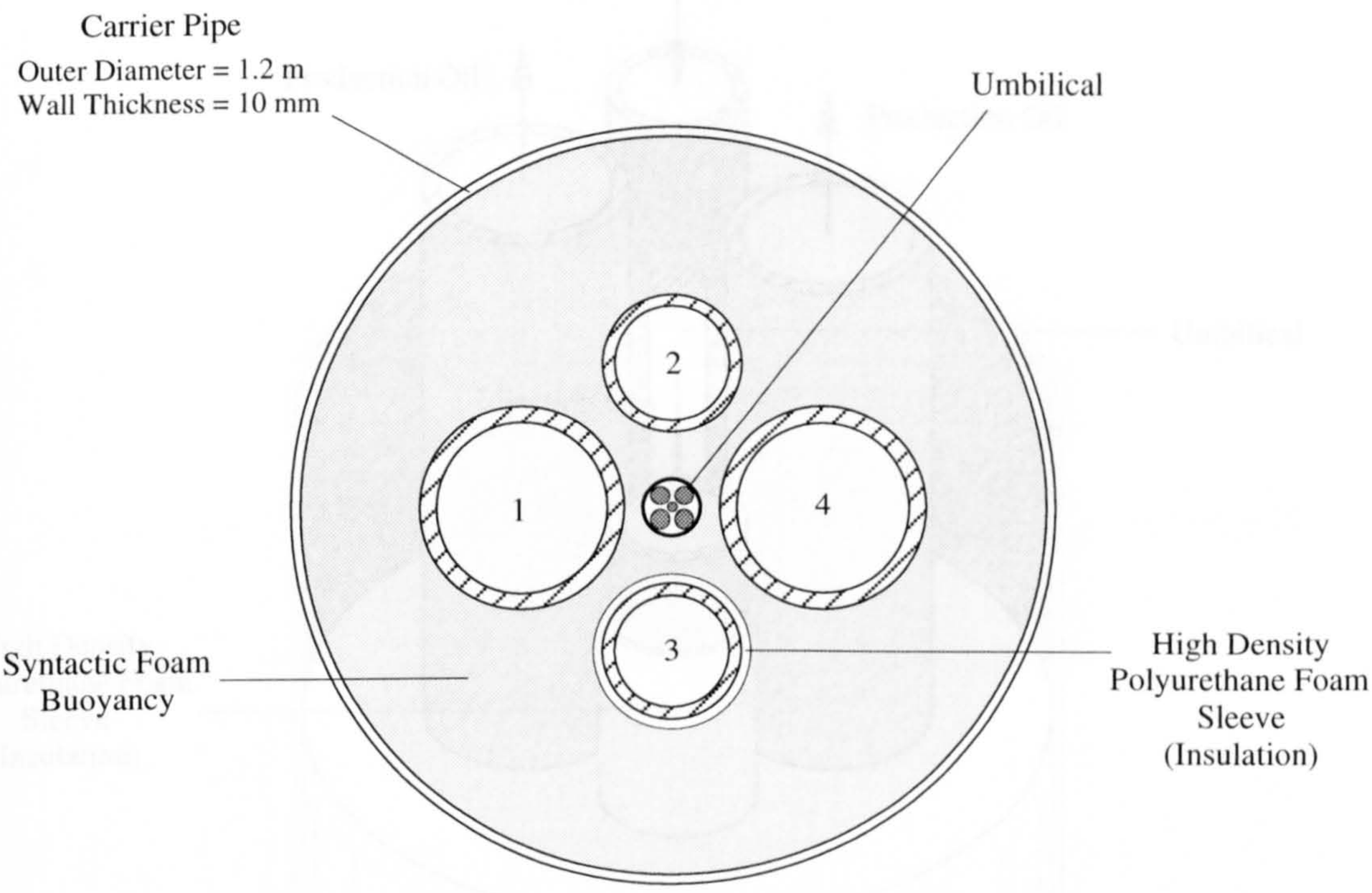

(a)

1 12" Production Oil Flowline

2 8" Injection Water Flowline

3 8" Injection Gas Flowline

4 12" Production Oil Flowline

5 8" Ballast Line

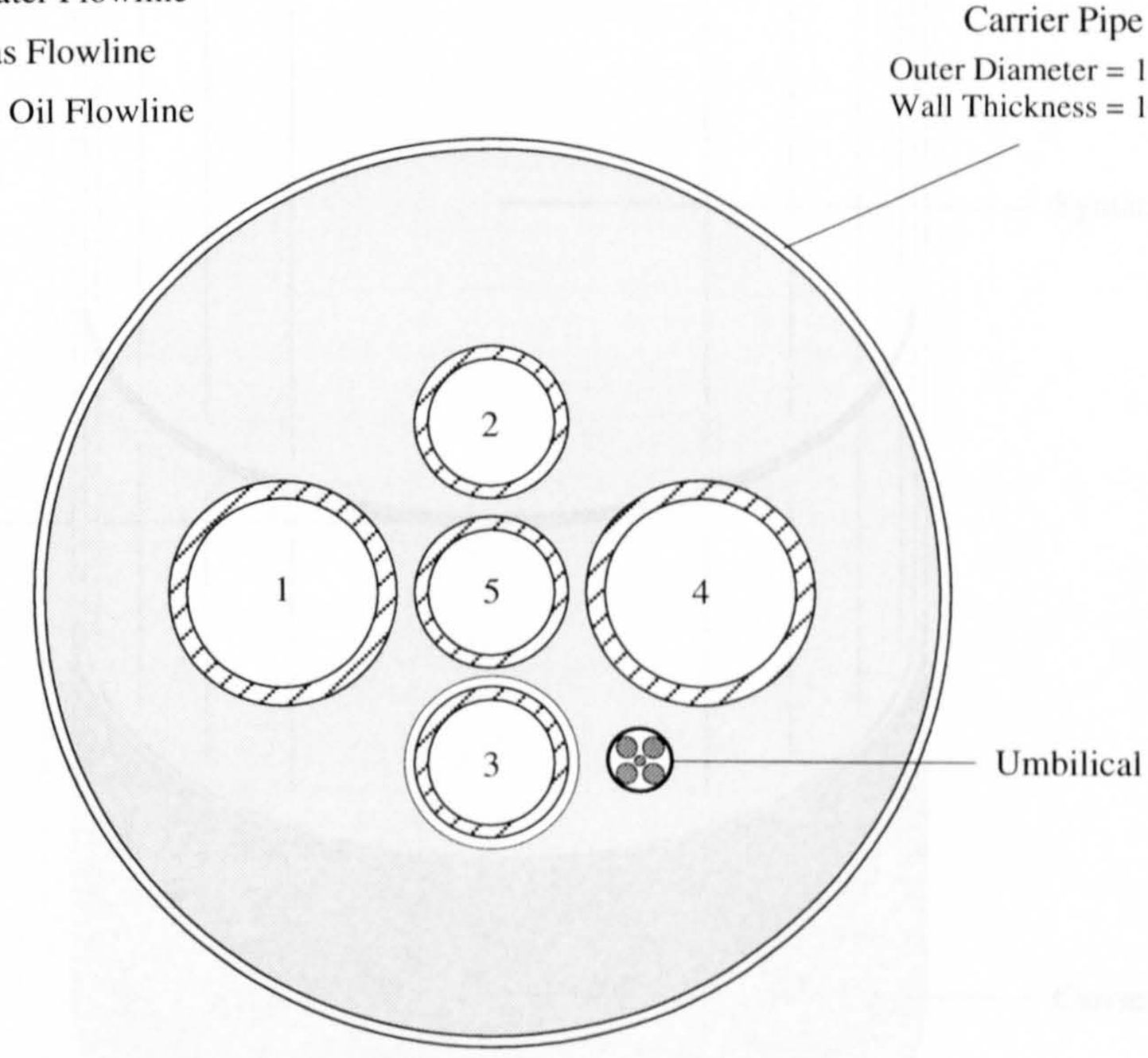

(b) **Scale 1:15**

Figure 3.3

Location of Flowlines within the Syntactic Foam Filled Carrier Pipe

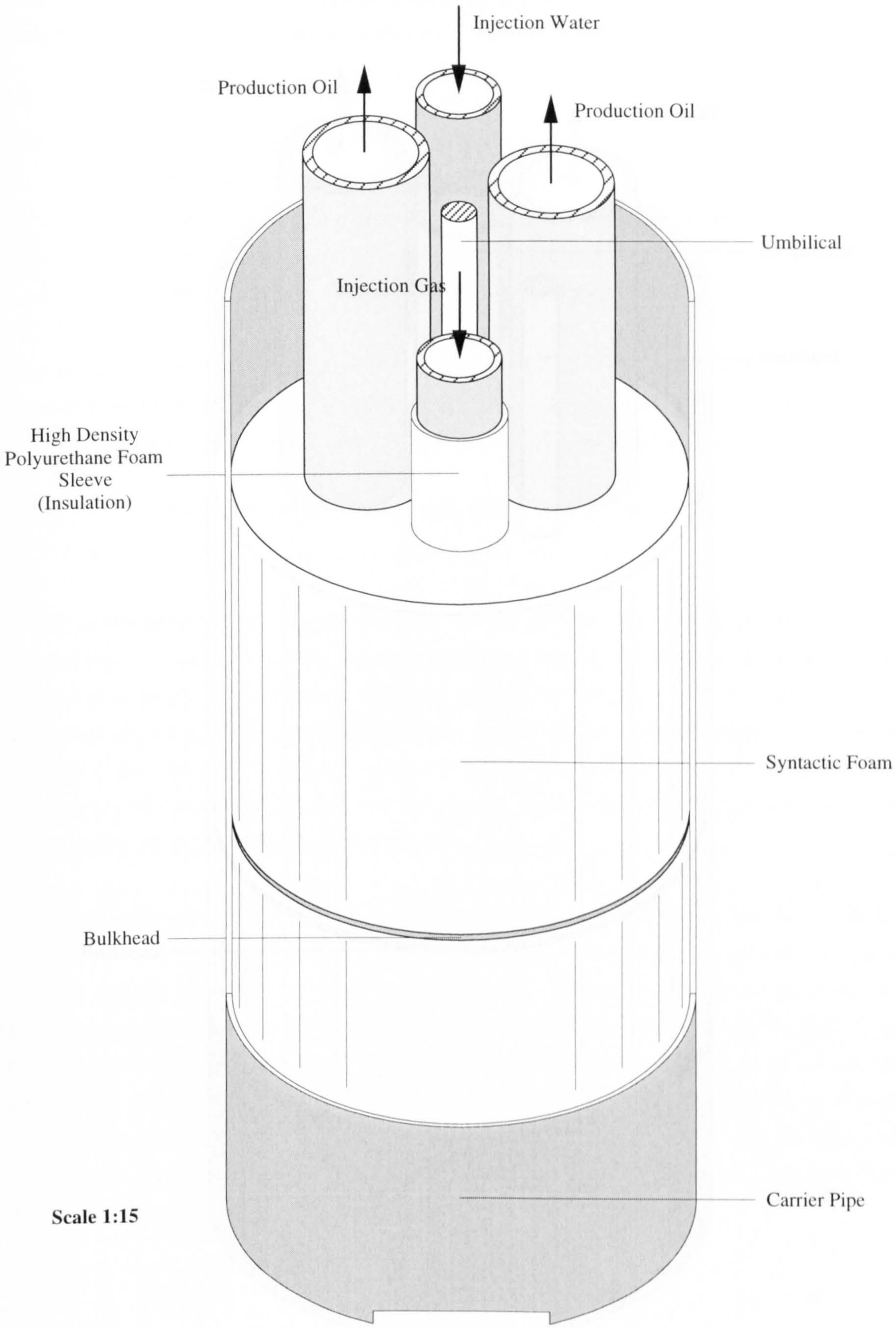

Figure 3.4

Cut-away View of the Syntactic Foam Filled Riser

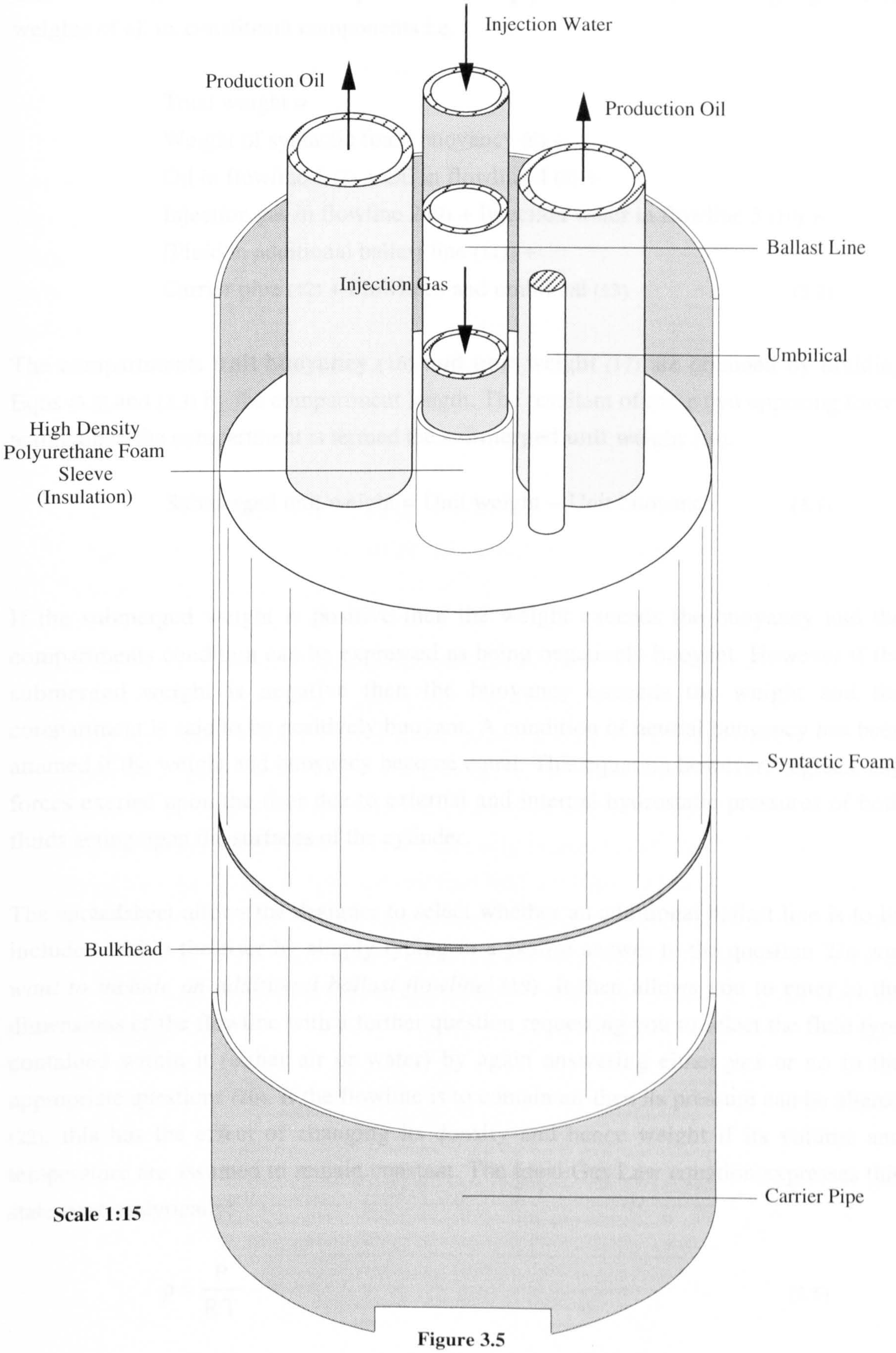

Figure 3.5

Cut-Away View of the Syntactic Foam Filled Riser with Ballast Line

The **total weight** (15) of each compartment is simply calculated by summing together the weights of all its constituent components i.e.

Total weight =
Weight of syntactic foam buoyancy (6) +
Oil in flowline 1 (7) + Oil in flowline 4 (8) +
Injection gas in flowline 2 (9) + Injection water in flowline 3 (10) +
[Fluid in additional ballast line (11)] +
Carrier pipe (12) + Flowlines and umbilical (13) (3.3)

The compartments **unit buoyancy** (16) **and unit weight** (17) are obtained by dividing Eqns (3.2) and (3.3) by the compartment length. The resultant of these two opposing forces acting upon the compartment is termed the **submerged unit weight** (19).

Submerged unit weight = Unit weight – Unit buoyancy (3.4)

If the submerged weight is positive then the weight exceeds the buoyancy and the compartments condition can be expressed as being negatively buoyant. However if the submerged weight is negative then the buoyancy exceeds the weight and the compartment is said to be positively buoyant. A condition of neutral buoyancy has been attained if the weight and buoyancy become equal. This equation however, neglects any forces exerted upon the riser due to external and internal hydrostatic pressures of both fluids acting upon the surfaces of the cylinder.

The spreadsheet allows the designer to select whether an additional ballast line is to be included within the riser by simply typing in a *yes/no* answer to the question *'Do you want to include an additional ballast flowline'* (19). It then allows you to enter in the dimensions of the flowline with a further question requesting you to select the fluid type contained within it (either air or water) by again answering either *yes* or *no* to the appropriate questions (20). If the flowline is to contain air then its pressure can be altered (22), this has the effect of changing its density and hence weight if its volume and temperature are assumed to remain constant. The Ideal Gas Law equation expresses this statement analytically:

$$\rho = \frac{P}{RT} \tag{3.5}$$

where ρ = gas density

P = gas pressure

R = specific gas constant

T = gas temperature

Results obtained from Spreadsheet 3.1 are illustrated in graphical format in Figure 3.10. Figure 3.10(a) plots the risers unit buoyancy and unit weight against carrier pipe outer diameter which is varied from 0.9 m to 1.7 m. A diameter of 0.9 m represents the smallest carrier pipe (in terms of its cross-section) that could used to completely surround the pre-defined flowline bundle. A carrier pipe plating thickness of 10 mm is selected from fabrication considerations and is therefore kept constant throughout the analysis. In the case of unit weight, three curves (**1, 2** and **3**) are plotted corresponding to three different ballast conditions:

1. Riser with a ballast line full of sea water
2. Riser with a ballast line full of air at atmospheric pressure (1 bar)
3. Riser with no ballast line

The submerged unit weight which is the resultant of the two unit forces shown in Figure 3.10(a) is illustrated in Figure 3.10(b). For carrier pipe diameters less than 1.3 to 1.4 depending upon ballast line conditions, the risers submerged weight is positive resulting in a negative buoyancy condition, however if the carrier pipes diameter is greater than 1.4 then the riser becomes positively buoyant. Since most surface connection assemblies are designed for use under a tensile load a negatively buoyant riser should be the principle aim throughout the design as opposed to a riser with a positively buoyant condition which would consequently create compressive a load. Negative buoyancy also enables the riser to resist significant deformation when exposed to environmental loading such as an ocean current. These considerations therefore constrain the designer to using only the left hand side of the graph.

Carrier Pipe Diameter (m)	Submerged Unit Weight (N/m)					
	Ballast Line Fluid Content					No Ballast Line
	Sea Water	Air				
		150 bar	**100 bar**	**50 bar**	**1 bar**	
1.0	3944	3728	3712	3697	3681	2934
1.1	3137	2922	2906	2890	2875	2128
1.2	2232	2016	2001	1985	1970	1222
1.3	1228	1013	997	981	966	219
1.4	126	-90	-106	-121	-137	-884

Table 3.2

Submerged Unit Weights for a Selection of Riser Operating Conditions

Both graphs clearly show the effect of having a ballast line within the riser and the extra weight it can add to the system when water is pumped in to replace the air. The table above highlights this characteristic by tabulating actual submerged unit weight values for the three ballast line conditions stated above, however in this case the air pressure has been varied to illustrate its influence.

3.2.5 Installation Analysis

Up until now a buoyancy analysis has been conducted with the riser in its operational condition defined as being a situation in which fluids such as production oil and injection water are being transported between wellhead and production vessel (or vice versa) through the riser. However the risers buoyancy performance during its installation is just as important if failure of the riser or auxiliary installation equipment through excessive loading is to be avoided. Riser installation is dealt with in considerable detail later on in the thesis however the procedure can be summarised in three stages:

- **Tow-out** - Sub-Surface tow (CDTM) from assembly yard to oil field
- **Sinkage** - Lowering of the riser on to the seabed
- **Lift** - Securing one end to the seabed production unit whilst lifting the other end to the surface for connection to either a surface vessel or sub-surface buoy.

All three stages of riser installation require an optimum submerged weight condition. This is achieved by flooding some of the flowlines with sea water whilst leaving the rest filled with air. The proceeding analysis examines the effects that a selection of possible flowline fluid ballast scenarios have on the risers submerged unit weight during the lift

installation phase by utilising an EXCEL spreadsheet that has been adapted from that used to calculate operational buoyancy and weight conditions. The installation spreadsheet (Spreadsheet 3.2) allows the designer to select whether the fluid content of each flowline is either air at atmospheric pressure or sea water by just typing in either a *yes* or *no* input (20), this information is then used as before to calculate the submerged weight condition. The results obtained from the spreadsheet for various flowline fluid arrangements are then plotted against a range of carrier pipe outer diameters, see Figure 3.11.

Eight ballast conditions (denoted by bold type) are analysed:

No ballast line

1. All flowlines full of sea water
2. Flowlines 1 and 4 full of sea water
3. Flowline 1 only full of water
4. All flowlines full of air

With ballast line

1. All flowlines + ballast line full of sea water
2. Flowlines 1 and 4 full of sea water
3. Flowline 1 only full of water
4. All flowlines full of air

It should be noted that any flowlines not flooded with sea water are filled with air at atmospheric pressure (1 bar). At a depth of 1500 m for example, the riser is exposed to a hydrostatic pressure of approximately 151 bar ($1.51\times10^7 N/m^2$) resulting in a pressure differential acting across the risers section of 150 bar, however it is thought that the flowlines and foam are of sufficient strength to sustain this. The maximum circumferential stress that the 12" flowline would experience due this condition can be calculated by assuming that the foam offers zero strength resistance thereby allowing the following equation to be used.

$$\sigma_c = \frac{PD}{2t} \tag{3.6}$$

where σ_c = circumferential stress
P = external hydrostatic force
D = mean diameter of the flowline
t = wall thickness of flowline

For a 12" flowline the circumferential stress is found to be 88.1 N/mm^2 which is approximately 19% of yield. The flowline would be expected to yield before buckling in the circumferential direction.

To help emphasise the effects of selective flowline flooding during installation, extracts of data have been taken from the graphs and tabulated in Tables 3.3 and 3.4 below.

No ballast line

Carrier Pipe Diameter (m)	**Submerged Unit Weight** (N/m)			
	Flowline Condition			
	1	**2**	**3**	**4**
1.0	3557	3032	2444	1855
1.1	2751	2226	1637	1049
1.2	1846	1320	732	144
1.3	842	317	-272	-860
1.4	-260	-786	-1374	-1963

Table 3.3

Submerged Unit Weights for a Selection of Riser Installation Conditions

The shaded areas of the tables highlight a positive buoyancy condition.

With ballast line

Carrier Pipe Diameter (m)	**Submerged Unit Weight** (N/m)			
	Flowline Condition			
	1	**2**	**3**	**4**
1.0	4567	3779	3191	2603
1.1	3761	2973	2384	1796
1.2	2856	2068	1479	891
1.3	1852	1064	475	-113
1.4	749	-39	-627	-1215

Table 3.4

Submerged Unit Weights for a Selection of Riser Installation Conditions

Both the graphs and the tables show up three important characteristics:

- The ability to flood flowlines with sea water offers the operator a range of riser submerged weights during the critical installation phase.

- The inclusion of an additional ballast line within the flowline bundle increases the submerged weight of the riser (for a given carrier pipe diameter) for all four flooding scenarios.
- A ballast line increases the range of weights that can be attained by either flooding or de-flooding lines.

The design of a syntactic foam filled riser using both the operational and installation spreadsheets can be summarised as follows:

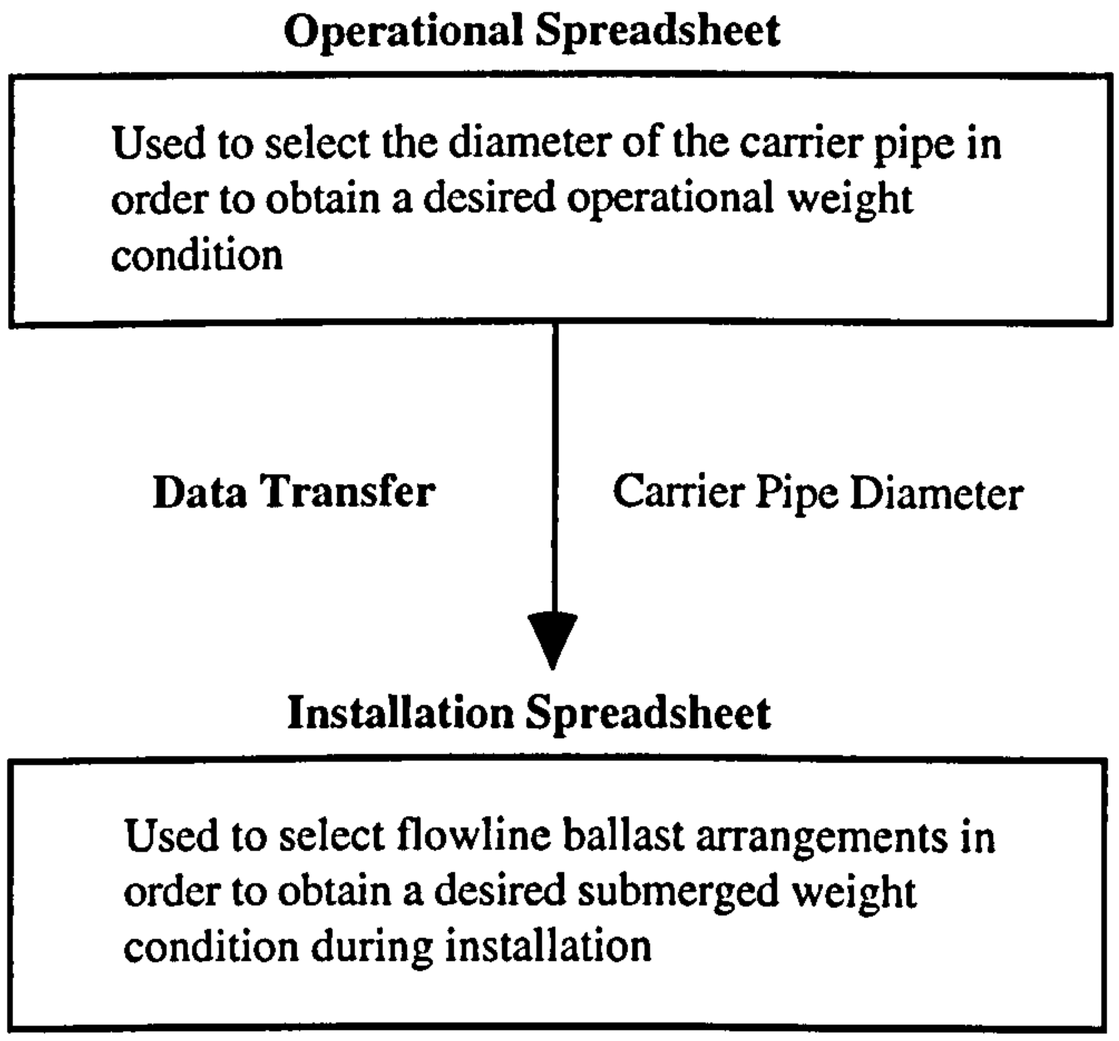

3.3 Nitrogen Gas Buoyancy

3.3.1 Introduction

The principle ingredient of most buoyancy systems is a gas such as air or nitrogen since both are light and cheap. A good vacuum weighs a bit less, but is much more expensive. Unfortunately gasses are highly compressible and so experience considerable changes in density with pressure. Differences between various buoyancy systems devolve into distinctions between the various ways in which the gas can be packaged. This section

outlines the details of a buoyancy design using pressurised nitrogen gas encapsulated within a carrier pipe.

3.3.2 Structural Arrangement of the Buoyancy System.

The objective of the proposed study is to devise an underwater system in which the flowline bundle is provided with mutually independent gas buoyancy compartments along its entire suspended length. Each compartment is to be supplied with a pressure fluid such as nitrogen to provide an amount of buoyancy appropriate for that compartment. The cross-section of the riser is illustrated in Figure 3.6 These compartments are created by enclosing the flowlines within an outer jacket or carrier pipe, the whole assembly is then transversely subdivided using a series of gas tight bulkheads. As in the case of the syntactic foam system, these bulkheads also ensure that the carrier pipe and flowline bundle act as a continuous structural unit when subjected to axial loading. Pressurised gas can be supplied to each compartment independently by utilising gas injection lines which run from the surface production vessel along the riser to the corresponding compartments, they are arranged in a cluster formation around the umbilical which situated in the centre of the riser (Figure 3.7). Fluids can be expelled from the compartment by means of a control valve situated within the carrier pipe at the bottom of each compartment, just above the bulkhead. This valve can also be used as an intake allowing the ambient sea water access to a compartment thereby providing the system with a flooding capability.

3.3.3 Operational Analysis

The whole buoyancy system works on the basis that the carrier pipe as in the syntactic foam case effectively acts as a membrane in that it lacks the strength capability required to sustain the high hydrostatic loads experienced in deep water. It therefore requires support and this can be achieved by ensuring that the compartmental gas pressure is either equal or very close to that of the water which surrounds it, whatever its depth. The carrier pipe therefore acts as a container and not as a pressure vessel.

During the installation of the riser all of the compartments are flooded so as to provide sufficient ballast for the riser to be dropped down on to the seabed. When it is desired to connect the riser up to the surface production unit buoyancy has to be created in order to avoid over loading both the riser and lifting unit. Compartment de-ballasting is done simultaneously and is achieved by injecting in sufficiently pressurised nitrogen gas so as to force the water out through the control valve.

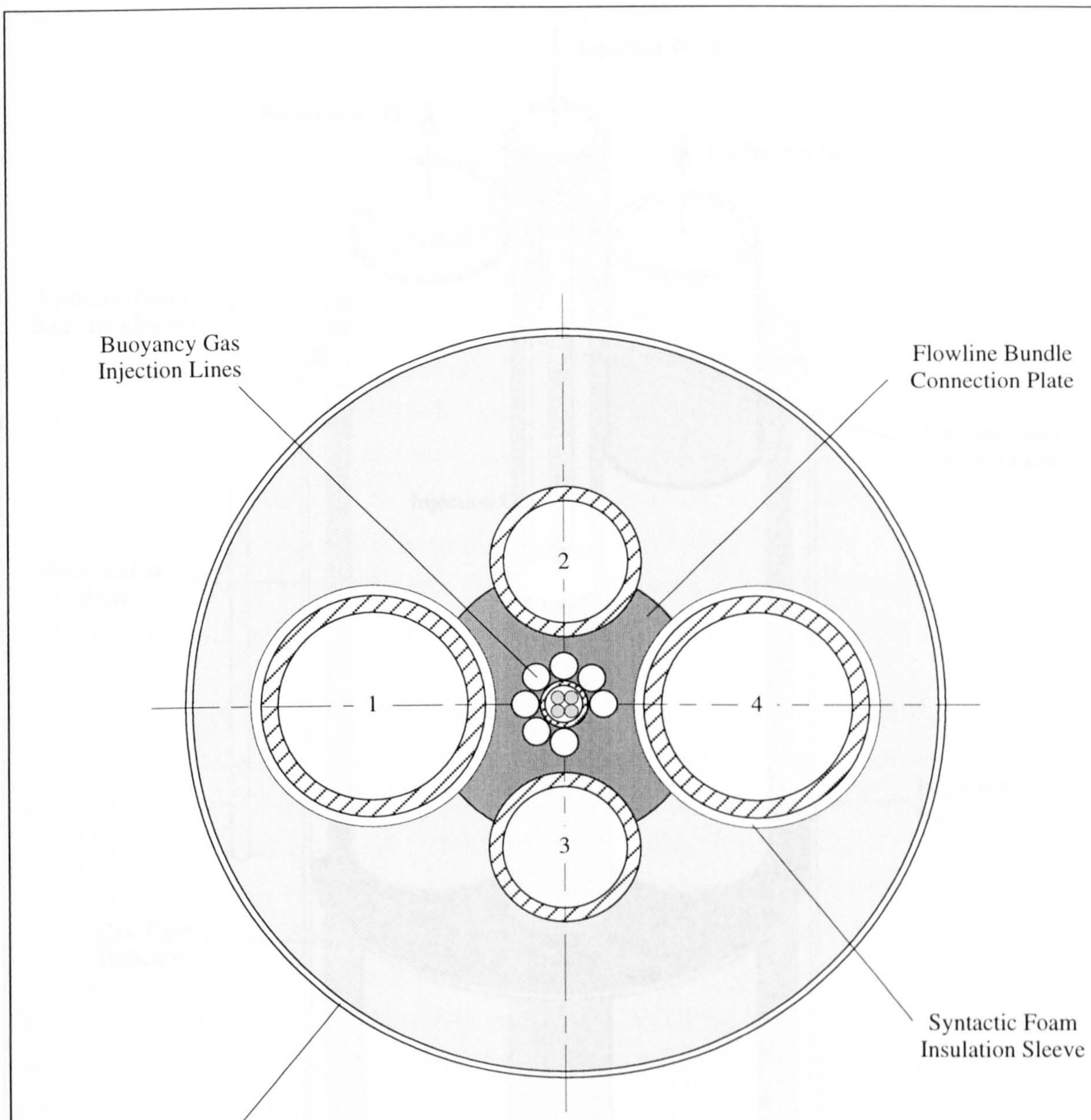

1 12" Production Oil Flowline

2 8" Injection Water Flowline

3 8" Injection Gas Flowline

4 12" Production Oil Flowline

Scale 1:10

Figure 3.6

Location of Flowlines within the Buoyancy Gas Filled Carrier Pipe

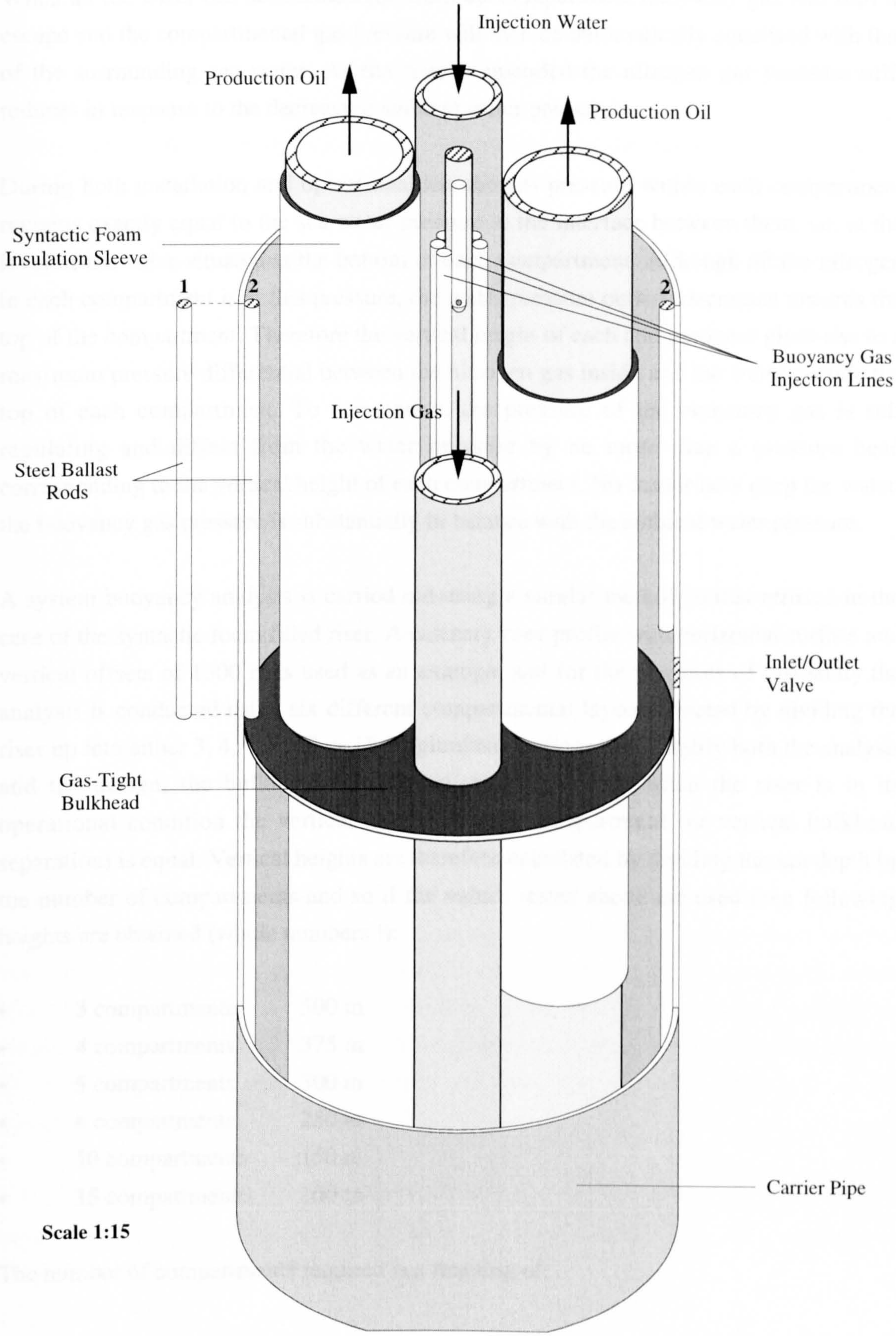

Figure 3.7

Cut-away View of the Buoyancy Gas Filled Riser

When all the water has been exhausted from the compartment buoyancy gas will start to escape and the compartmental gas pressure will then be automatically equalised with that of the surrounding sea water. As the riser is upended the nitrogen gas pressure self-reduces in response to the decreasing ambient water pressure.

During both installation and operational life the gas pressure within each compartment remains exactly equal to the sea water pressure at the interface between them, i.e. at the level of the valve situated at the bottom of each compartment. Although all the nitrogen in each compartment is at this pressure, the water pressure outside decreases towards the top of the compartment. Therefore the vertical height of each compartment gives rise to a maximum pressure differential between the nitrogen gas inside and the water outside the top of each compartment. To summarise, the pressure of the buoyancy gas is self regulating and differs from the water pressure by no more than a pressure head corresponding to the vertical height of each compartment. No matter how deep the water, the buoyancy gas pressure is substantially in balance with the ambient water pressure.

A system buoyancy analysis is carried out using a similar method to that utilised in the case of the syntactic foam filled riser. A catenary riser profile with horizontal surface and vertical offsets of 1500 m is used as an example and for the purposes of this study the analysis is conducted using six different compartmental layouts created by dividing the riser up into either 3, 4, 5, 6, 10 or 15 longitudinal sections. To simplify both the analysis and the design, the bulkheads have been situated so that when the riser is in its operational condition the vertical height of each compartment (or vertical bulkhead separation) is equal. Vertical heights are therefore calculated by dividing the sea depth by the number of compartments and so if the values stated above are used then following heights are obtained (whole numbers !):

- **3** compartments 500 m
- **4** compartments 375 m
- **5** compartments 300 m
- **6** compartments 250 m
- **10** compartments 150 m
- **15** compartments 100 m

The number of compartments required is a function of:

- Cost
- Operating complexity
- Pressure difference induced stress

- Compartment loss vulnerability

More compartments will increase the cost of fabrication as well as making the installation and operation of the riser more complex through the greater use of gas injectors and valves. The effects on riser stressing are ascertained by examining the pressure differentials that are inherent within the system.

The pressure differential acting across the carrier pipe wall can be expressed using the following hydrostatic equation:

$$\Delta P = \rho_{sw} g y_c \tag{3.7}$$

where ρ_{sw} = sea water density
g = gravitational acceleration
y_c = vertical distance up the compartment

This is illustrated in Figure 3.8 from where it is shown that the maximum pressure difference occurs at the top of the compartment i.e.

$$\Delta P_{max} = \rho_{sw} g h_c \tag{3.8}$$

where h_c = vertical height of the compartment

The above equations are used to graphically demonstrate the pressure loading behaviour up the compartment, see Figure 3.12(a). Since the maximum pressure loading is a direct function of compartment height it is then also a function of compartment number assuming a constant water depth and a uniform compartment height for all compartments. This allows the pressure maximum loading to be plotted against the number of compartments as shown in Figure 3.12(b). Compartment height is reduced as the number of compartments is increased, thereby reducing the pressure difference at the compartments top end.

The pressure difference across the carrier pipe sets up a circumferential stress σ_c which is tensile since the internal pressure will always be greater than the outer. This stress can be obtained as follows:

$$\sigma_c = \frac{\Delta p D}{2t} \tag{3.9}$$

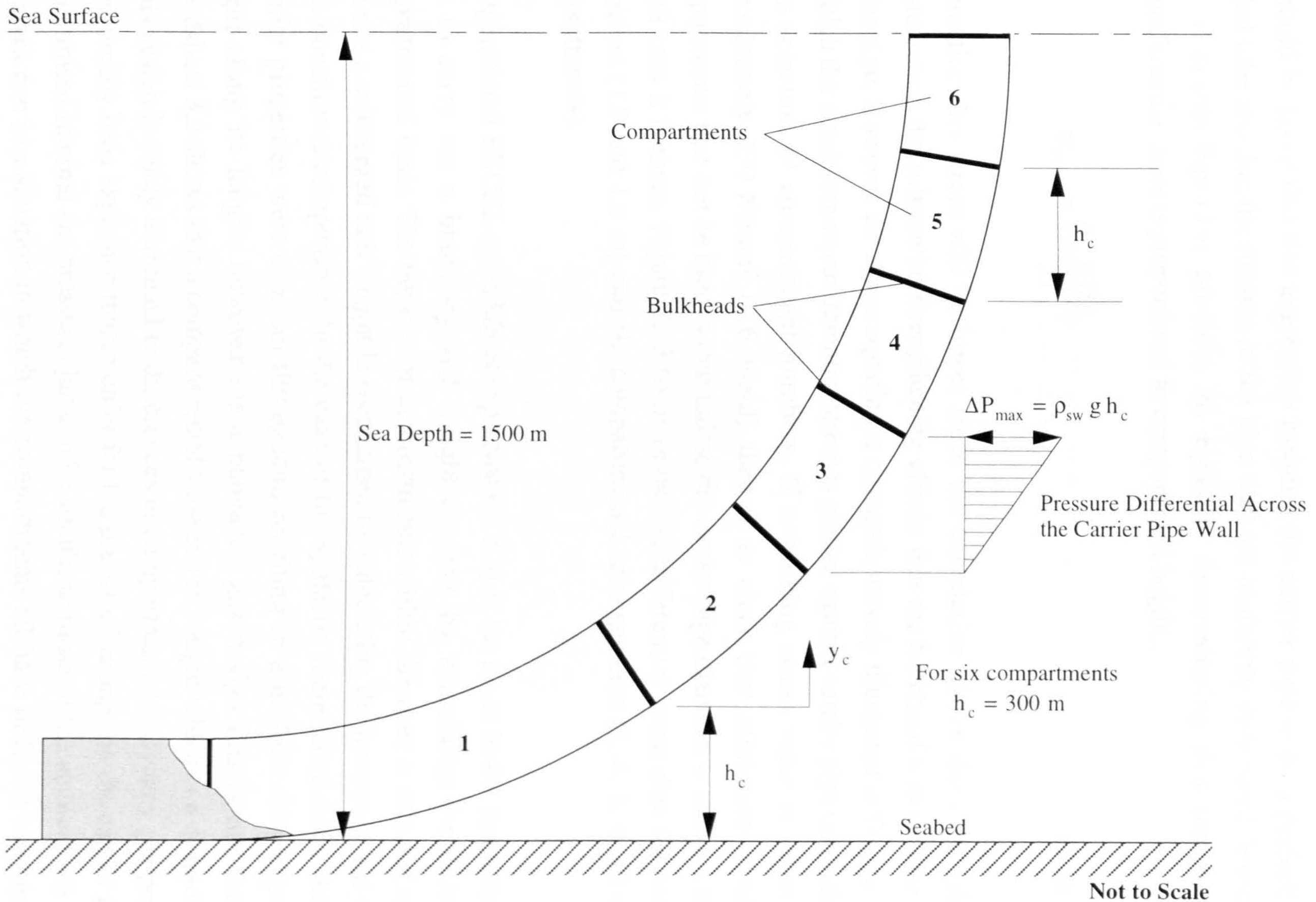

Figure 3.8

The Layout of Buoyancy Gas Compartments within the Riser

where D = diameter of the carrier pipe

t = wall thickness

It should be noted that this expression assumes the carrier pipe to be a perfectly thin-walled tube and that the stresses in the pipe wall are uniformly distributed. Substituting Eqn (3.8) into Eqn (3.9) provides an equation demonstrating that the maximum circumferential stress is proportional to compartment height .

$$\sigma_{c\,max} = \frac{\rho_{sw}\, g D h_c}{2t} \qquad (3.10)$$

In practice this stress will be lower since the calculation above does not take into consideration the substantial strengthening effects that the bulkhead will impose on the carrier pipe. However the above equation is comprehensively illustrated in Figure 3.13(a) in which the maximum circumferential stress is plotted against carrier pipe outer diameter for a selection of compartment numbers. If a working stress value is taken to be approximately 270 N/mm^2 (0.6 yield) then it is clear that minimum number of compartments that can be used is four unless the carrier pipe diameter is above 1.05 m in which case it is three. Figure 3.13(b) presents circumferential stress data for two riser diameters (1.0 and 1.1 m) and six compartmental arrangements (3, 4, 5, 6, 10 and 15 compartments).

An operational EXCEL spreadsheet (Spreadsheet 3.3) is set up as in the syntactic foam case to carry out a buoyancy and weight analysis by examining the riser on a compartmental basis. The number of compartments within the riser is selected and for each one a submerged unit weight is ascertained by calculating the buoyancy and weight of its constituent components. In the case of the syntactic foam filled riser, fluid and material properties were constant throughout, resulting in a uniform submerged unit weight along its length, however for a buoyancy gas design this is not the case. Spreadsheet 3.3 shows that a compartmental variation in weight which is a characteristic of this design is solely attributed to differences in compartmental buoyancy gas pressure. It has already been explained that in order for the pressure loadings on the carrier pipe to be minimised internal gas pressures have to be similar to those of the ambient sea water, this gives rise to a situation in which the compartments all have different buoyancy gas pressures. These compartmental gas pressures reduce along the riser from seabed to surface in response to the sea water pressure. Table 3.5 tabulates buoyancy gas pressures corresponding to both the *compartment no.* and the *number of compartments* within the riser.

Compartment No.	Compartmental Buoyancy Gas Pressure (bar)					
	Number of Compartments					
	3	4	5	6	10	15
1	151	151	151	151	151	151
2	101	113	121	126	136	141
3	50	75	90	101	121	131
4		38	60	75	106	121
5			30	50	90	111
6				25	75	101
7					60	90
8					45	80
9					30	70
10					15	60
11						50
12						40
13						30
14						20
15						10

Table 3.5
Buoyancy Gas Pressures for a Riser in 1500 m of Water

If a gas can be assumed to be ideal then its unit mass can be related to its pressure by the fundamental Ideal Gas Law equation:

$$m = \frac{P_{gas} A}{RT} \tag{3.11}$$

where m = mass per unit length
P_{gas} = gas pressure
A = internal compartment area
R = specific gas constant
T = gas temperature

The unit mass is shown to be proportional to pressure and so will decrease compartmentally up the riser, however the unit buoyancy remains constant since the carrier pipe diameter and hence volume remain constant along its length. If the unit buoyancy is subtracted from the unit weight a submerged unit weight is obtained and from Figures 3.14 to 3.25 this is shown to decrease compartmentally up the riser i.e. the riser becomes progressively more buoyant.

To counteract the decrease in compartmental weight it proposed to add additional steel weight (or ballast) to the riser with the aim of creating a uniform weight distribution along its entire length as detailed in Figures 3.14 to 3.25. The operational spreadsheet (Spreadsheet 3.3) is used to calculate the compartmental increase in steel cross-sectional area required for the riser to attain a uniform submerged weight distribution equal to that of the first compartment (seabed end). The results obtained from this analysis are tabulated in Tables 3.7 and 3.8. The additional steel area could be created by progressively thickening the carrier pipes walls in compartmental steps, however this would undoubtedly cause difficulties during fabrication and manufacture and hence increase the cost. This study therefore proposes to add additional area either externally or internally by attaching steel rods longitudinally to the carrier pipe as illustrated in Figures 3.7 and 3.9. They could be manufactured easily and cheaply to an accurate tolerance and welded to the carrier pipe and would run the entire length of each compartment. The cross-sectional area of the rods would increase in compartmental steps along the riser (going from seabed to surface). In order to demonstrate this Tables 3.7 and 3.8 also provide cross-sectional area data for a four rod arrangement attached to a riser of differing diameter and compartmental layout.

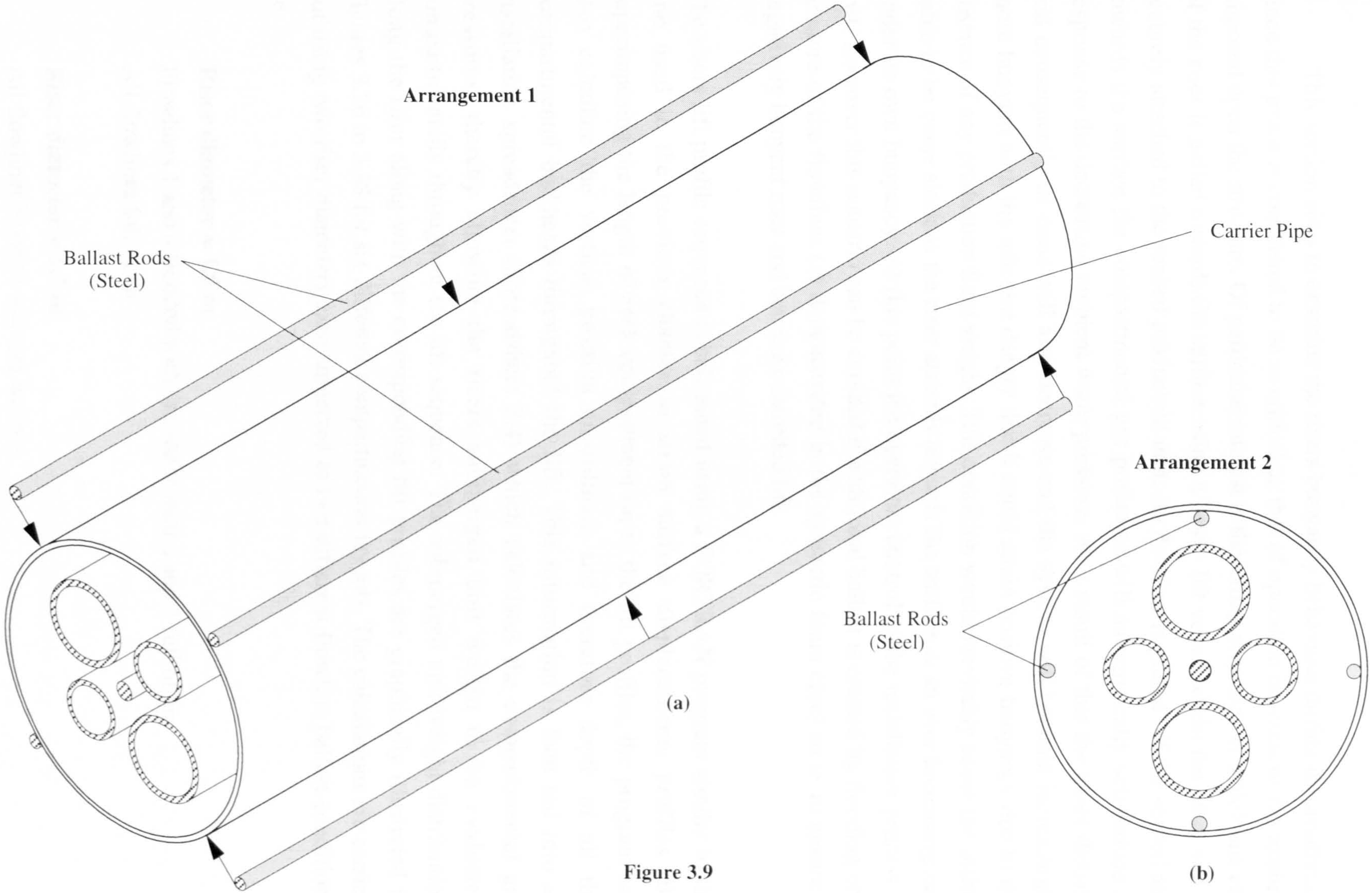

Figure 3.9

Compartmental Ballasting for a Gas Buoyancy Riser

3.3.4 Installation Analysis

This section aims to examine the risers buoyancy behaviour during its installation since this phase is considered to be as critical as that of operation in terms of the loading imposed upon the structure. Of particular interest is the lifting sequence in which one end of the riser is pulled towards the surface using a heavy lift vessel whilst the other end is securely attached to the seabed production unit. As the riser is pulled off the seabed and towards the surface the compartmental gas pressures will automatically self-reduce in response to the decreasing ambient water pressure. As a result of this the gases density and consequently its mass will also decrease and the system will become increasingly more buoyant with the inherent danger that it could attain positive buoyancy due to the absence of any production fluid weight. This condition would inevitably cause the lifting cable to be come slack as the riser ascends towards the surface at an ever increasing rate under its own buoyancy. At this point the operators control of the installation process is lost. However this scenario can be avoided if additional ballast is created by flooding one or more of the flowlines (as demonstrated in the syntactic foam case) so as to ensure a negatively buoyant riser and hence a controlled lift.

The risers lift profile sequence is calculated using a FORTRAN program similar to the one used in the previous chapter to attain surface displacements profiles. By superimposing the length of each compartment on to the lift profiles, the program can also calculate the vertical position co-ordinate and therefore depth of all the compartmental bulkheads throughout the lift. This information is then fed into an installation spreadsheet (Spreadsheet 3.4) which calculates the compartmental gas pressures, thereby allowing the risers submerged unit weight to be evaluated compartmentally throughout the lift sequence. The submerged unit weight distribution along the riser along with the corresponding lift profiles are graphically illustrated in Figures 3.26 to 3.38 for six different compartmental layouts. The calculations are carried out using two riser diameters each subjected to two different flowline ballast conditions i.e.

Riser diameter = 1.0 m

- Flowlines 1 and 4 flooded with sea water with 2 and 3 full of air
- All flowlines full of air

Riser diameter = 1.1 m

- All flowlines flooded with sea water
- Flowline 1 flooded with sea water and 2, 3 and 4 full of air

The flowline fluid ballast arrangement is determined by inputting either a *yes* or *no* answer to the relevant questions in box (20) in the installation spreadsheet (Spreadsheet 3.4).

The top black line shown in the submerged unit weight graphs and denoted by the word *Seabed* corresponds to the risers submerged unit weight condition when lying flat on the seabed prior to lift. In this condition all the compartmental gas pressures equal the ambient sea water pressure at 1500 m, however the graph clearly shows a compartmental step increase in submerged unit weight along the riser. This characteristic is a result of the additional steel added in order for the riser to attain a uniform submerged unit weight when in its operational condition. The required compartmental increase in steel cross-sectional area for a given carrier pipe diameter is evaluated using the operational spreadsheet (Spreadsheet 3.3), this information is then fed through into the calculations carried out within the installation spreadsheet (Spreadsheet 3.4).

This whole procedure can be as summarised as follow.

The lift sequence is represented in five stages which are shown up in red on both the profile and submerged unit weight graphs. The results clearly show that during the risers ascent towards the surface the difference in unit weight between compartments progressively decreases until a condition of uniform submerged unit weight is attained. At this point the top end of the riser has reached the surface at the correct horizontal offset and is depicted on the graph by a flat black line denoted by the word *Surface*.

When the sea water and air have been evacuated from the flowlines and production fluids such as oil and injection water allowed to flow, the riser attains its operational condition and is represented on the graph by the flat blue line. The graphs demonstrate the need for different flowline ballasting arrangements depending upon the riser diameter so as to ensure negative buoyancy throughout the lift as previously mentioned. A riser with a diameter of 1.1 m generates more buoyancy force than a riser with a diameter of 1.0 m with the result that more flowlines have to be flooded with sea water in order to add more weight. However too much weight causes an unnecessarily high load to be exerted on both the riser and lifting cable/vessel leading to an outcome that could include either higher installation costs or a greater risk of technical failure. Cable and riser loading throughout the lift sequence is examined in a later chapter.

3.3.5 The Effects of Temperature on Compartment Buoyancy

It has already been shown through the use of the Ideal Gas equation (Eqn (3.11)) that the mass of gas is a directly proportional to pressure, volume and inversely proportional to temperature. Since volume can be assumed to be constant and the effects of a variable pressure have been dealt with during the installation analysis this section aims to demonstrate the influence temperature has on the riser submerged weight condition. Buoyancy gas temperature is dependent upon three aspects:

- Flowline temperature - can vary from 0 °C to 90 °C depending upon the fluid flowing through it i.e. production oil or ballast sea water
- Ambient sea water temperature - at 1500 m it can be as low -1 °C
- Thermal insulation within the riser.

The average temperature which a buoyancy gas attains under operational conditions is examined in detail in the next chapter, however for the purposes of a buoyancy study a gas temperature of 20 °C is assumed. This is an attempt to emulate the gases thermal condition when exposed to heat generated by the warm wellhead production fluids. The installation calculations are based upon a gas temperature of 0 °C, this aims to take into account the temperature of the sea water ballast within the flowlines as well as the fact that the riser may well have been lying on the cold seabed for a considerable amount of time before it is lifted.

The effect that a variation in gas temperature would have on the risers submerged unit weight is determined using the operational spreadsheet. The results from this analysis are presented graphically in Figure 3.38 for two risers of different diameters, 1.0 m and 1.1 m. The results suggest that an increase in gas temperature is accompanied by relatively

small drop in submerged weight. For example in the case of a riser with a carrier pipe diameter of 1.0 m a 40 °C increase in temperature only generates a 6% drop in submerged unit weight. For an increased diameter of 1.1 m and hence a greater volume of gas the reduction is slightly higher at approximately 18%.

3.3.6 The Loss of a Buoyancy Compartment

The inherent risk with all gas buoyancy systems is that of compartmental structural failure with the inevitable consequence of an often rapid displacement of buoyancy gas with ambient sea water. This results in a reduction of buoyancy volume leading to an increase in the submerged weight of the system, the only buoyancy in the system would now be generated from the external volume of the flowline bundle. Various scenarios which could cause this condition are outlined below:

- Excessive carrier pipe corrosion leading to a sea water leakage
- Damaged inlet/outlet valve
- Pressure difference across carrier pipe exceeds critical value resulting in pipe collapse or rupture depending upon whether the sea water or the gas is at the higher pressure (respectively).
- Compartment puncture from an external object such as a ship hull or torpedo hitting the riser.

The proceeding analysis evaluates the effects of a compartment loss on the riser in an operational condition in terms of both the axial loading exerted upon the riser and vertical loading exerted upon a surface or sub-surface vessel. The evaluation is conducted using a EXCEL spreadsheet that has been adapted from the one used during the operational analysis. The buoyancy loss spreadsheet (Spreadsheet 3.5) allows the designer to model a compartmental loss by filling either single or multiple compartments with sea water by again responding to the appropriate questions. On the basis of this input the spreadsheet calculates a total submerged weight for the riser which is equal to the vertical loading exerted upon the surface production unit, however the risers axial loading at the surface is obtained from expressions formulated in Chapter 2. Axial tension can be expressed as a function of vertical force by combining Eqns (2.57) and (2.58) respectively i.e.

$$T = H\left(\frac{ds}{dx}\right)_x$$

$$V = H\left(\frac{dy}{dx}\right)_x$$

Substituting Eqn (2.58) into Eqn (2.57) in order to eliminate H creates the following expression:

$$T = V\left(\frac{ds}{dy}\right)_x \tag{3.12}$$

From Figure 2.2(b) it is shown that $\sin\theta = dy/ds$ and hence:

$$T_{surface} = \left(\frac{V}{\sin\theta}\right)_{surface} \tag{3.13}$$

where V = vertical load at the surface (= total submerged weight)
θ = riser inclination from the horizontal at the surface

Results from this analysis are presented in Figures 3.39 to 3.44 for risers with 3, 4, 5, 6, 10 and 15 compartments and diameters of 1.0 m and 1.1 m.

Graph (a) Demonstrates the effect on both vertical and axial loading of losing a single compartment

Graph (b) Illustrates the effect on axial stress of losing a single compartment

Graph (c) Demonstrates the effect on both vertical and axial loading of cumulative compartment loss going from surface to seabed

Graph (d) Illustrates the effect on axial stress of a cumulative compartment loss going from surface to seabed

The results clearly demonstrate that the greatest impact on loading is attained when the seabed compartment (1) is lost where as the flooding of the other compartments all create smaller additional loads very similar to one another. These characteristics are attributed to the length of each compartment which has already been determined using an equal compartment height arrangement ensuring that compartment (1) is the longest with the rest significantly shorter and decreasing in length up the riser. This decrease is however marginal which explains why the difference in loading between them is almost negligible. The table below summarises the effects of buoyancy loss for various compartmental layouts and helps to illustrate the difference between losing compartment (1) and any one of the others.

No. of Compartments	% Increase in Axial Stress	
	Compartment (1)	Other Compartments
3	108	62
4	91	47
5	80	38
6	72	31
10	54	19
15	44	13

Table 3.6

The Effects of an Individual Compartment Loss

One of the most important features to note is the way the increase in axial stress decreases with an increase in the number of compartments. Increasing the number of compartments reduces their length and therefore their impact on overall buoyancy if one of them is lost. This is one of the main benefits to increasing the number of buoyancy compartments.

Graphs (c) and (d) illustrate the effects of losing more than one compartment. A progressive increase in both axial and vertical loading is demonstrated as compartments are systematically flooded from surface to seabed i.e. from compartment (6) to compartment (1) in the case of a riser with six compartments. These graphs also help to underline the benefits of riser buoyancy in terms of minimising self-weight stress. If all the buoyancy compartments are intact, then the maximum axial stress (at the surface) is found to be 45 N/mm^2 for a carrier pipe diameter of 1.0 m or 17.3 N/mm^2 if the diameter is 1.1 m. However if all the compartments are flooded then this stress increases to 153 N/mm^2 in the case of a 1.0 m diameter carrier pipe and 156 N/mm^2 for a diameter of 1.1 m. The differences in both cases is well over 100 N/mm^2 which is substantial when set against an overall working stress of approximately 270 N/mm^2.

References

1. Emerson & Cuming®. (1994) *Syntactics, Unique Composites for the Uniform Entrainment of Reinforced Air*, Technical Brochure.

2. Benham, P.P. and Crawford, R.J. (1987) *Mechanics of Engineering Materials*, Longman Scientific & Technical.

CHAPTER 3

Analysis Spreadsheets

Spreadsheets 3.1 - 3.5

Buoyancy and Weight - Syntactic Foam (Operational)

Catenary Parameters

Horizontal Surface Offset =	1500	m
Sea Depth =	1500	m
Approx Submerged Weight =	100	N/m
Horizontal Tension =	9.2814E+04	N
Total Riser Length =	2243.75	m
Suspended Riser Length =	2243.75	m
Lamda =	0.8081	
Integration Constant =	0.0000	

Note :

Spreadsheet Input - Blue

Spreadsheet Output - Red

22

Air Pressure =	1	bar

Carrier Pipe Geometry

Outer Diameter =	1.2	m
Wall Thickness =	10	mm
Bulkhead Thickness =	10	mm

External Cross Sectional Area =	1.131	m2
Steel Cross Sectional Area =	0.037	m2
Internal Cross Sectional Area =	1.094	m2

Material and Fluid Densities

Air (at 275 K) =	1.226	kg/m3
Syntactic Foam =	384.4	kg/m3
Production Oil =	855	kg/m3
Injection Water =	1030	kg/m3
Injection Gas =	270	kg/m3
Sea Water =	1025	kg/m3
Steel Density =	7850	kg/m3

Flowline Geometries

	No.	Inner Diameter (mm)	Outer Diameter (mm)	External c.s.a (m)	Internal c.s.a (m)	Steel c.s.a (m)
12" Flowline	2	273.1	323.9	0.082	0.059	0.024
8" Flowline	2	182.5	219.1	0.038	0.026	0.012
Umbilical	1	-	100	0.008	-	
Additional Flowline	0	182.5	219.1	0.038	0.026	0.012

Total External c.s.a =	0.248	m2
Total Steel c.s.a =	0.071	m2

19

Do you want include an addtional ballast flowline (Yes/No)	No

20

Water in Ballast Flowline	No
Air in Ballast Flowline	Yes

Buoyancy and Weight

Measured at the bottom of each compartment

1	2		3	4	5	6	7	8	9	10	11	12	13	14
Compartment No.	Bulkhead Co-ordinates x (m)	y (m)	Compartment Length (m)	Hydrostatic Pressure (bar)	Compartment Buoyancy (kN)	Weight of Syntactic Foam in Riser (kN)	Weight of Oil in Flowline 1 (kN)	Weight of Oil in Flowline 4 (kN)	Weight of Injection Gas in Flowline 2 (kN)	Weight of Injection Water in Flowline 3 (kN)	Weight of Water/Air in Ballast Flowline (kN)	Weight of Carrier Pipe (kN)	Weight of Flowlines plus Umbilical (kN)	Total Compartment Weight (kN)
1	364.5	72.5	373.96	151	4253	1192	140	140	26	99	0.00	1077	2037	4710
2	684.2	1067.2	373.96	114	4253	1192	140	140	26	99	0.00	1077	2037	4710
3	948.1	1233.8	373.96	82	4253	1192	140	140	26	99	0.00	1077	2037	4710
4	1164.9	1348.7	373.96	55	4253	1192	140	140	26	99	0.00	1077	2037	4710
5	1345.9	1433.8	373.96	34	4253	1192	140	140	26	99	0.00	1077	2037	4710
6	1500.0	1500.0	373.96	15	4253	1192	140	140	26	99	0.00	1077	2037	4710
	Total :		2243.8		25516	7154	838	838	155	593	0	6460	12221	28259

15	16	17	18
Compartment No.	Buoyancy per metre (N/m)	Weight per metre (N/m)	Submerged Unit Weight (N/m)	Buoyancy as a % of Weight
1	11372	12595	1222	0.90
2	11372	12595	1222	0.90
3	11372	12595	1222	0.90
4	11372	12595	1222	0.90
5	11372	12595	1222	0.90
6	11372	12595	1222	0.90

Additional Information

Total Steel Cross-Sectional Area =	0.108	m2
Mass per Unit Length =	1284	kg/m

Spreadsheet 3.1

Buoyancy and Weight - Syntactic Foam (Installation)

Catenary Parameters

Horizontal Surface Offset =	1500	m
Sea Depth =	1500	m
Approx Submerged Weight =	100	N/m
Horizontal Tension =	9.2814E+04	N
Total Riser Length =	2243.75	m
Suspended Riser Length =	2243.75	m
Lamda =	0.8081	
Integration Constant =	0.0000	

Note :

Spreadsheet Input - Blue

Spreadsheet Output - Red

Carrier Pipe Geometry

Outer Diameter =	1.2	m
Wall Thickness =	10	mm
Bulkhead Thickness =	10	mm

External Cross Sectional Area =	1.131	m2
Steel Cross Sectional Area =	0.037	m2
Internal Cross Sectional Area =	1.094	m2

21

Air Pressure =	1	bar

Material and Fluid Densities

Air (at 275 K) =	1.226	kg/m3
Syntactic Foam =	384.4	kg/m3
Production Oil =	855	kg/m3
Injection Water =	1030	kg/m3
Injection Gas =	270	kg/m3
Sea Water =	1025	kg/m3
Steel Density =	7850	kg/m3

Flowline Geometries

	No.	Inner Diameter (mm)	Outer Diameter (mm)	External c.s.a (m)	Internal c.s.a (m)	Steel c.s.a (m)
12" Flowline	2	273.1	323.9	0.082	0.059	0.024
8" Flowline	2	182.5	219.1	0.038	0.026	0.012
Umbilical	1	-	100	0.008	-	
Additional Flowline	0	182.5	219.1	0.038	0.026	0.012

Total External c.s.a =	0.248	m2
Total Steel c.s.a =	0.071	m2

19

Do you want include an addtional ballast flowline (Yes/No) : No

20

Water	Yes	Yes	No	No	No
Air (1 bar)	No	No	Yes	Yes	Yes

Buoyancy and Weight

Measured at the bottom of each compartment

1 Compartment No.	2 Bulkhead Co-ordinates x (m)	y (m)	3 Compartment Length (m)	4 Hydrostatic Pressure (bar)	5 Compartment Buoyancy (kN)	6 Weight of Syntactic Foam in Riser (kN)	7 Weight of Fluid in Flowline 1 (kN)	8 Weight of Fluid in Flowline 4 (kN)	9 Weight of Fluid Flowline 2 (kN)	10 Weight of Fluid in Flowline 3 (kN)	11 Weight of Fluid in Ballast Flowline (kN)	12 Weight of Carrier Pipe (kN)	13 Weight of Flowlines plus Umbilical (kN)	14 Total Compartment Weight (kN)
1	364.5	72.5	373.96	151	4253	1192	220.27	220.27	0.12	0.12	0.00	1077	2037	4747
2	684.2	1067.2	373.96	114	4253	1192	220.27	220.27	0.12	0.12	0.00	1077	2037	4747
3	948.1	1233.8	373.96	82	4253	1192	220.27	220.27	0.12	0.12	0.00	1077	2037	4747
4	1164.9	1348.7	373.96	55	4253	1192	220.27	220.27	0.12	0.12	0.00	1077	2037	4747
5	1345.9	1433.8	373.96	34	4253	1192	220.27	220.27	0.12	0.12	0.00	1077	2037	4747
6	1500.0	1500.0	373.96	15	4253	1192	220.27	220.27	0.12	0.12	0.00	1077	2037	4747
	Total :		2243.8		25516	7154	1322	1322	1	1	0	6460	12221	28479

Compartment No.	15 Buoyancy per metre (N/m)	16 Weight per metre (N/m)	17 Submerged Unit Weight (N/m)	18 Buoyancy as a % of Weight
1	11372	12693	1320	0.90
2	11372	12693	1320	0.90
3	11372	12693	1320	0.90
4	11372	12693	1320	0.90
5	11372	12693	1320	0.90
6	11372	12693	1320	0.90

Additional Information

Total Steel Cross-Sectional Area =	0.108	m2
Mass per Unit Length =	1294	kg/m

Spreadsheet 3.2

Buoyancy and Weight - Nitrogen Gas (Operational)

Catenary Parameters

Horizontal Surface Offset =	1500	m
Sea Depth =	1500	m
Approx Submerged Weight =	100	N/m
Horizontal Tension =	9.2814E+04	N
Total Riser Length =	2243.75	m
Suspended Riser Length =	2243.75	m
Lamda =	0.8081	
Integration Constant =	0.0000	
No of Compartments =	6	

Note :

Spreadsheet Input - Blue

Spreadsheet Output - Red

Carrier Pipe Geometry

Outer Diameter =	1.0	m
Wall Thickness =	10	mm
Bulkhead Thickness =	10	mm

External Cross Sectional Area =	0.785	m2
Steel Cross Sectional Area =	0.031	m2
Internal Cross Sectional Area =	0.754	m2

Material and Fluid Densities

Production Oil =	855	kg/m3
Injection Water =	1030	kg/m3
Injection Gas =	270	kg/m3
Sea Water =	1025	kg/m3
Steel Density =	7850	kg/m3

Flowline Geometries

	No.	Inner Diameter (mm)	Outer Diameter (mm)	External c.s.a (m)	Internal c.s.a (m)	Steel c.s.a (m)
12" Flowline	2	273.1	323.9	0.082	0.059	0.024
8" Flowline	2	182.5	219.1	0.038	0.026	0.012
Umbilical	1	-	100	0.008	-	

Total External c.s.a =	0.248	m2
Total Steel c.s.a =	0.071	m2

Buoyancy and Weight

Measured at the bottom of each compartment

1	2		3	4	5	6	7	8	9	10	11	12	13	14
Compartment No.	Bulkhead Co-ordinates x (m)	y (m)	Compartment Length (m)	Hydrostatic Pressure (bar)	Compartment Buoyancy (kN)	Temperature of Nitrogen Gas (degs C)	Weight of Nitrogen Gas in Riser (kN)	Weight of Oil in Flowline 1 (kN)	Weight of Oil in Flowline 4 (kN)	Weight of Injection Gas in Flowline 2 (kN)	Weight of Injection Water in Flowline 3 (kN)	Weight of Carrier Pipe (kN)	Weight of Flowlines plus Umbilical (kN)	Total Compartment Weight (kN)
1	666.8	250.0	725.65	151	5731	20	625	271	271	50	192	1738	3952	7100
2	924.7	500.0	359.77	126	2841	20	258	134	134	25	95	862	1960	3468
3	1112.2	750.0	312.69	101	2469	20	180	117	117	22	83	749	1703	2970
4	1262.8	1000.0	291.94	75	2306	20	126	109	109	20	77	699	1590	2731
5	1389.8	1250.0	280.44	50	2215	20	81	105	105	19	74	672	1527	2583
6	1500.0	1500.0	273.26	25	2158	20	39	102	102	19	72	654	1488	2477
	Total :		2243.8		17720		1309	838	838	155	593	5374	12221	21328

15	16	17	18	19		20	21	22
Compartment No.	Buoyancy per metre (N/m)	Weight per metre (N/m)	Submerged Unit Weight (N/m)	Buoyancy as a % of Weight	Difference in SUW (N/m)	**Additional steel area required to equalise the submerged unit weight to that of compartment no. 1**	Steel Area Increase (m2)	Equiv to four Steel Rods with a Diameter (mm)	New Submerged Unit Weight (N/m)
1	7897	9784	1887	0.81	0		0	0	1887
2	7897	9640	1743	0.82	144		0.0019	24	1887
3	7897	9497	1599	0.83	287		0.0037	34	1887
4	7897	9353	1456	0.84	431		0.0056	42	1887
5	7897	9210	1312	0.86	574		0.0075	49	1887
6	7897	9066	1169	0.87	718		0.0093	54	1887

Spreadsheet 3.3

Buoyancy and Weight - Nitrogen Gas (Installation)

Catenary Parameters

Horizontal Surface Offset =	1500	m
Sea Depth =	1500	m
Approx Submerged Weight =	100	N/m
Horizontal Tension =	9.2814E+04	N
Total Riser Length =	2243.75	m
Suspended Riser Length =	2243.75	m
Lamda =	0.8081	
Integration Constant =	0.0000	
No of Compartments =	6	
Gas Temperature =	0	degs C

Note :

Spreadsheet Input - Blue

Spreadsheet Output - Red

Air Pressure =	1	bar

Carrier Pipe Geometry

Outer Diameter =	1.0	m
Wall Thickness =	10	mm
Bulkhead Thickness =	10	mm

External Cross Sectional Area =	0.785	m2
Steel Cross Sectional Area =	0.031	m2
Internal Cross Sectional Area =	0.754	m2

Material and Fluid Densities

Air (at 275 K) =	1.226	kg/m3
Production Oil =	855	kg/m3
Injection Water =	1030	kg/m3
Injection Gas =	270	kg/m3
Sea Water =	1025	kg/m3
Steel Density =	7850	kg/m3

Flowline Geometries

	No.	Inner Diameter (mm)	Outer Diameter (mm)	External c.s.a (m)	Internal c.s.a (m)	Steel c.s.a (m)
12" Flowline	2	273.1	323.9	0.082	0.059	0.024
8" Flowline	2	182.5	219.1	0.038	0.026	0.012
Umbilical	1	-	100	0.008	-	

Total External c.s.a =	0.248	m2
Total Steel c.s.a =	0.071	m2

Buoyancy and Weight

	1	2		3	4	5	6	7	8	9	10	11	12	13	14
	Compartment No.	Bulkhead Co-ordinates x (m)	y (m)	Compartment Length (m)	Compartment Buoyancy (kN)	Compartment Depth (m)	Buoyancy Gas Pressure (bar)	Weight of Nitrogen Gas in Riser (kN)	Weight of Fluid in Flowline 1 (kN)	Weight of Fluid in Flowline 4 (kN)	Weight of Fluid in Flowline 2 (kN)	Weight of Fluid in Flowline 3 (kN)	Weight of Carrier Pipe (kN)	Weight of Flowlines plus Umbilical (kN)	Total Compartment Weight (kN)
							20								
		Water						Yes	Yes	Yes	No	No			
		Air (1 bar)						No	No	No	Yes	Yes			
1	1	666.8	250.0	725.65	5731	1500	151	671	427.42	427.42	0.23	0.23	1738	3952	7217
2	2	924.7	500.0	359.77	2841	1480	149	328	211.91	211.91	0.11	0.11	862	1960	3574
3	3	1112.2	750.0	312.69	2469	1448	146	279	184.18	184.18	0.10	0.10	749	1703	3100
4	4	1262.8	1000.0	291.94	2306	1409	142	254	171.96	171.96	0.09	0.09	699	1590	2887
5	5	1389.8	1250.0	280.44	2215	1363	137	236	165.18	165.18	0.09	0.09	672	1527	2765
6	6	1500.0	1500.0	273.26	2158	1310	132	221	160.95	160.95	0.09	0.09	654	1488	2686
		Total :		2243.8	17720			1988	1322	1322	1	1	5374	12221	22228

	15	16	17	18	19
Compartment No.	Buoyancy per metre (N/m)	Weight per metre (N/m)	Additional Steel C.S.A (m2)	Additional Unit Weight (N/m)	Submerged Unit Weight (N/m)
1	7897	9945	0	0	2048
2	7897	9933	0.0019	146	2182
3	7897	9913	0.0037	285	2301
4	7897	9889	0.0056	431	2423
5	7897	9861	0.0075	578	2541
6	7897	9828	0.0093	716	2647

Spreadsheet 3.4

CHAPTER 3

Results

Figures 3.10 - 3.44

Table 3.7

Unit Weight and Buoyancy (Operational)

(a)

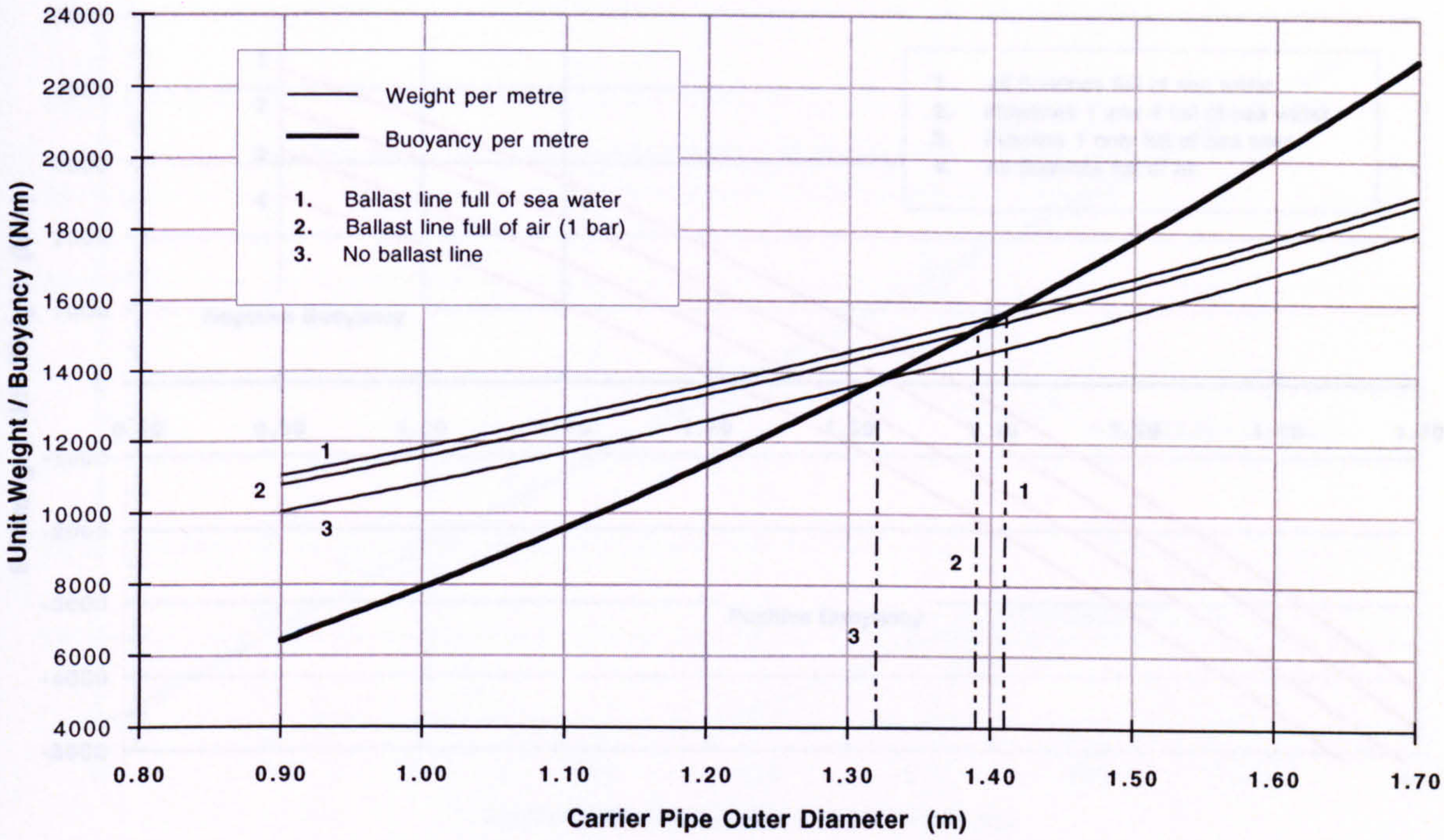

Submerged Unit Weight (Operational)

(b)

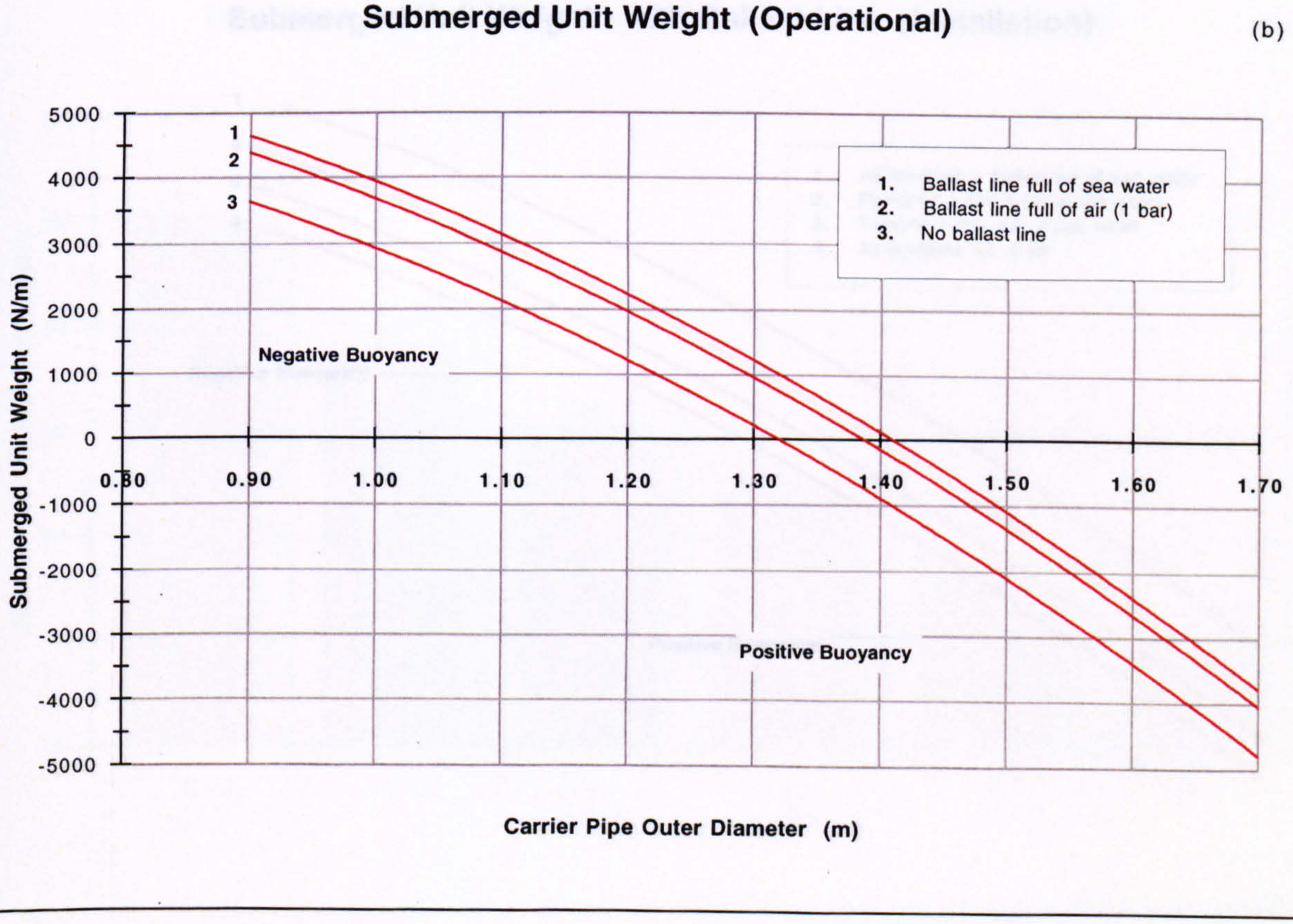

Horizontal Surface Offset = 1500 m

Carrier Pipe Wall Thickness = 10 mm

Sea Depth = 1500 m

Figure 3.10

Submerged Unit Weight (Installation)

(a)

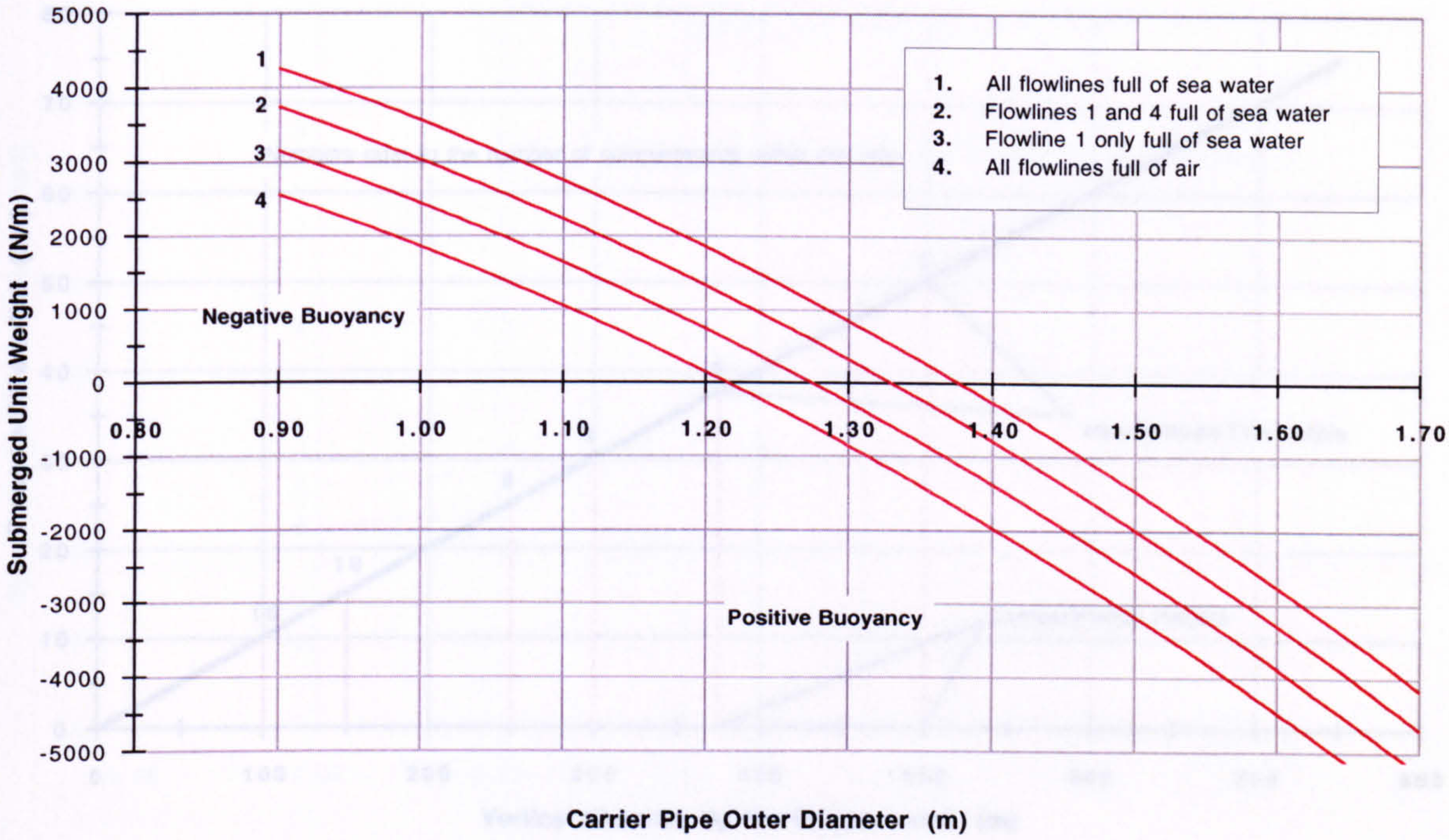

Submerged Unit Weight - with Ballast Line (Installation)

(b)

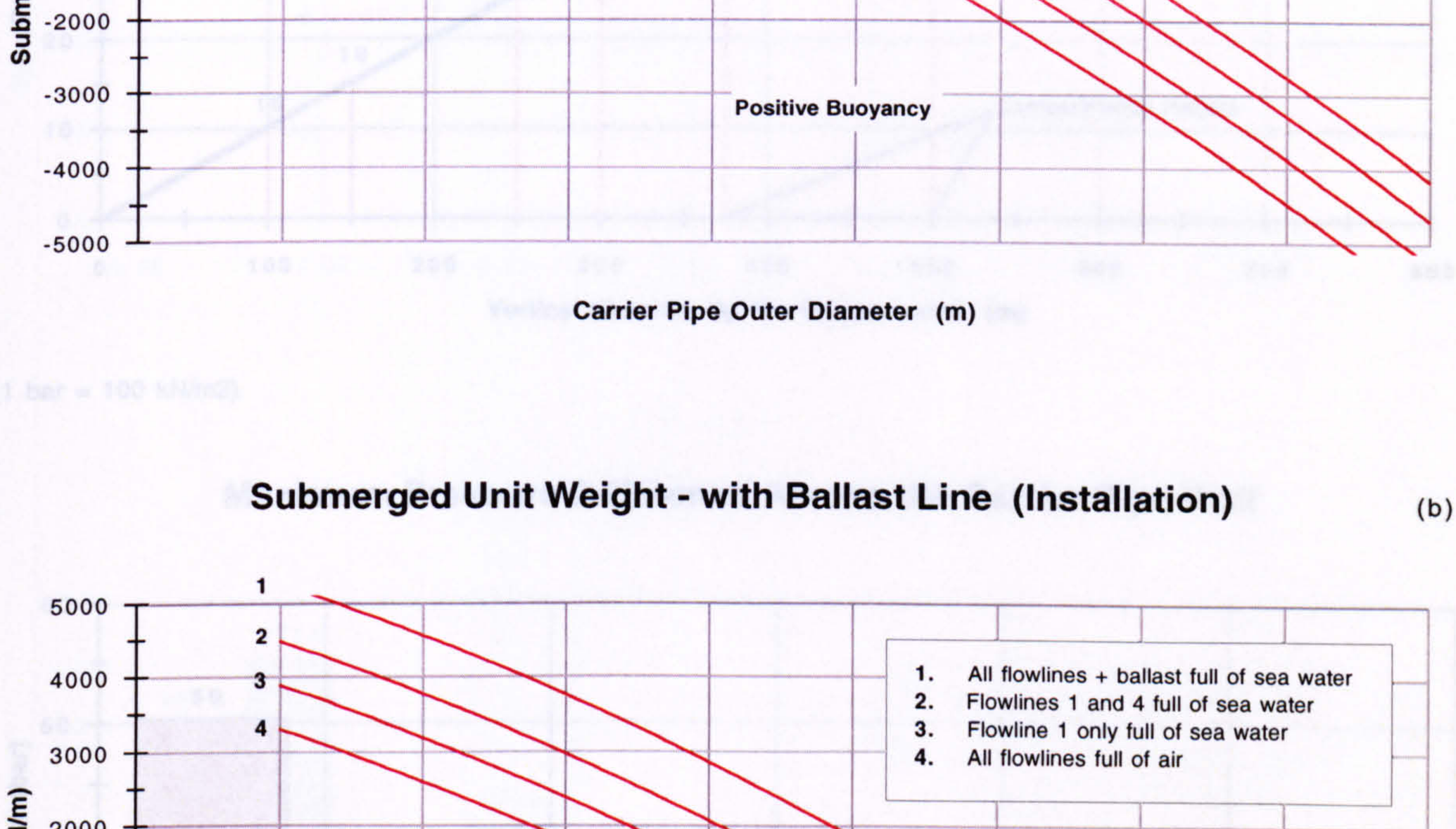

Horizontal Surface Offset = 1500 m

Carrier Pipe Wall Thickness = 10 mm

Sea Depth = 1500 m

Figure 3.11

Pressure Differences Acting Across the Carrier Pipe Wall

(a)

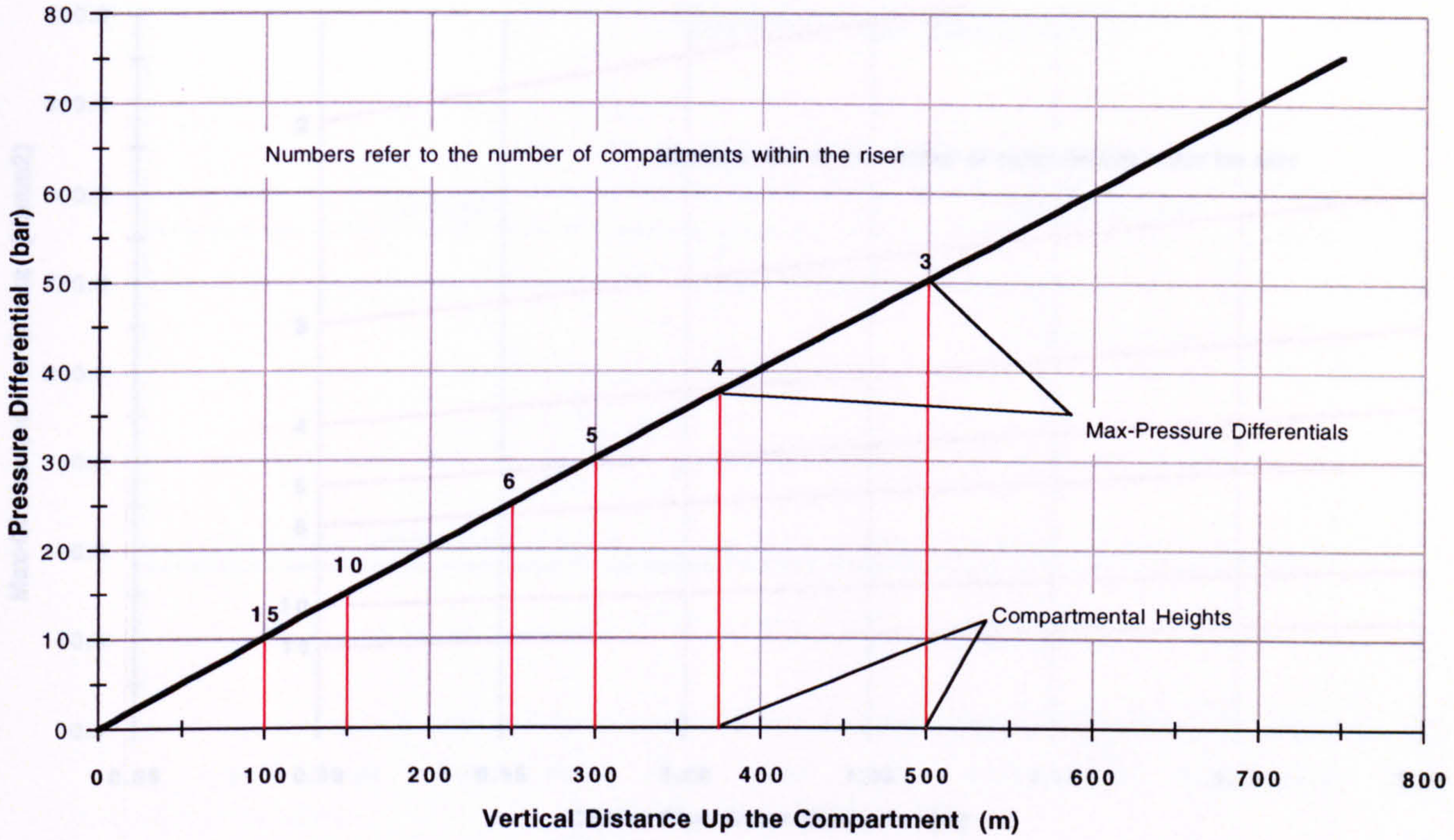

(1 bar = 100 kN/m2)

Maximum Pressure Difference Across the Carrier Pipe Wall

(b)

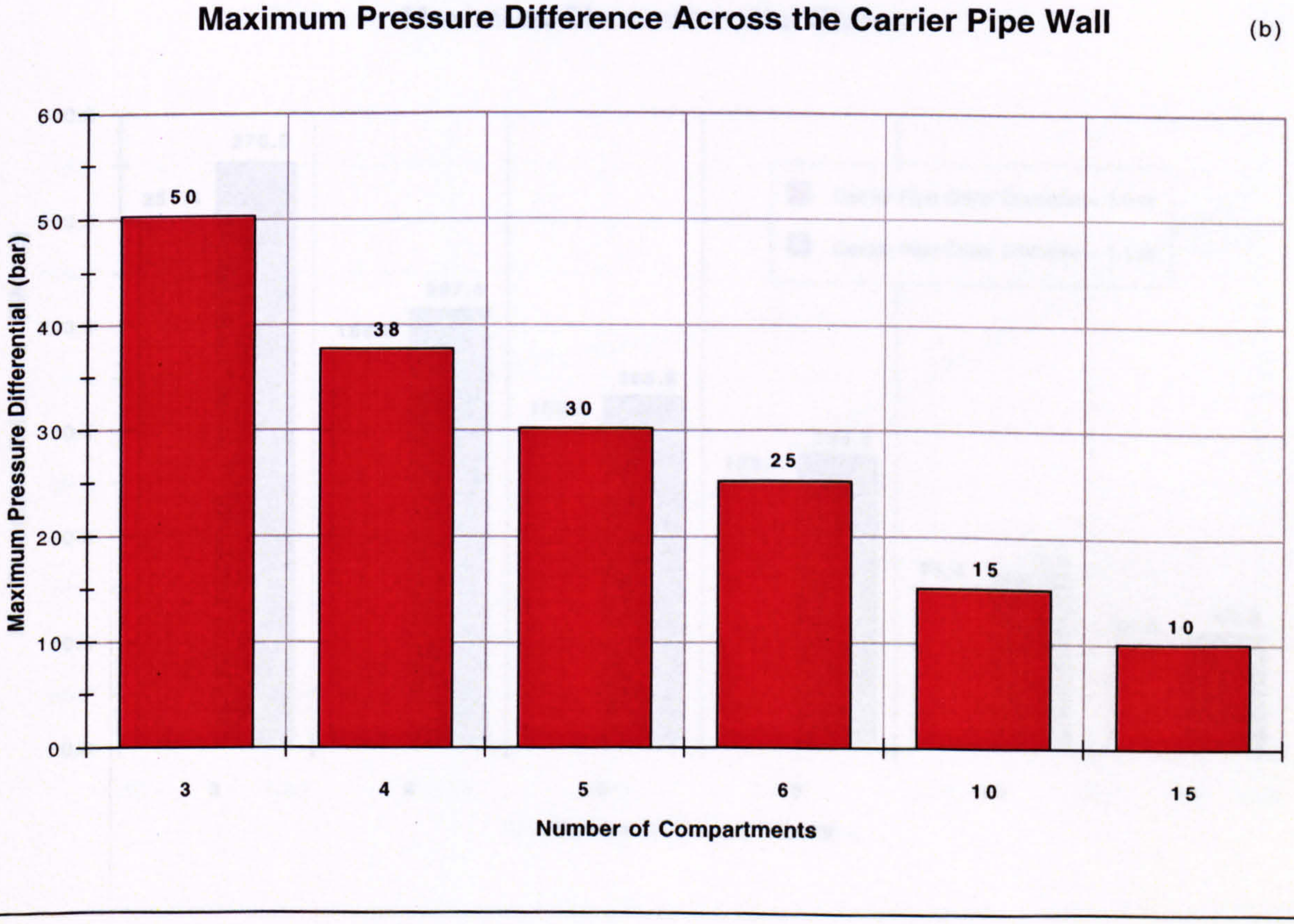

Horizontal Surface Offset = 1500 m

Carrier Pipe Wall Thickness = 10 mm

Sea Depth = 1500 m

Figure 3.12

The Influence of C.P. Diameter on Circumferential Stress

(a)

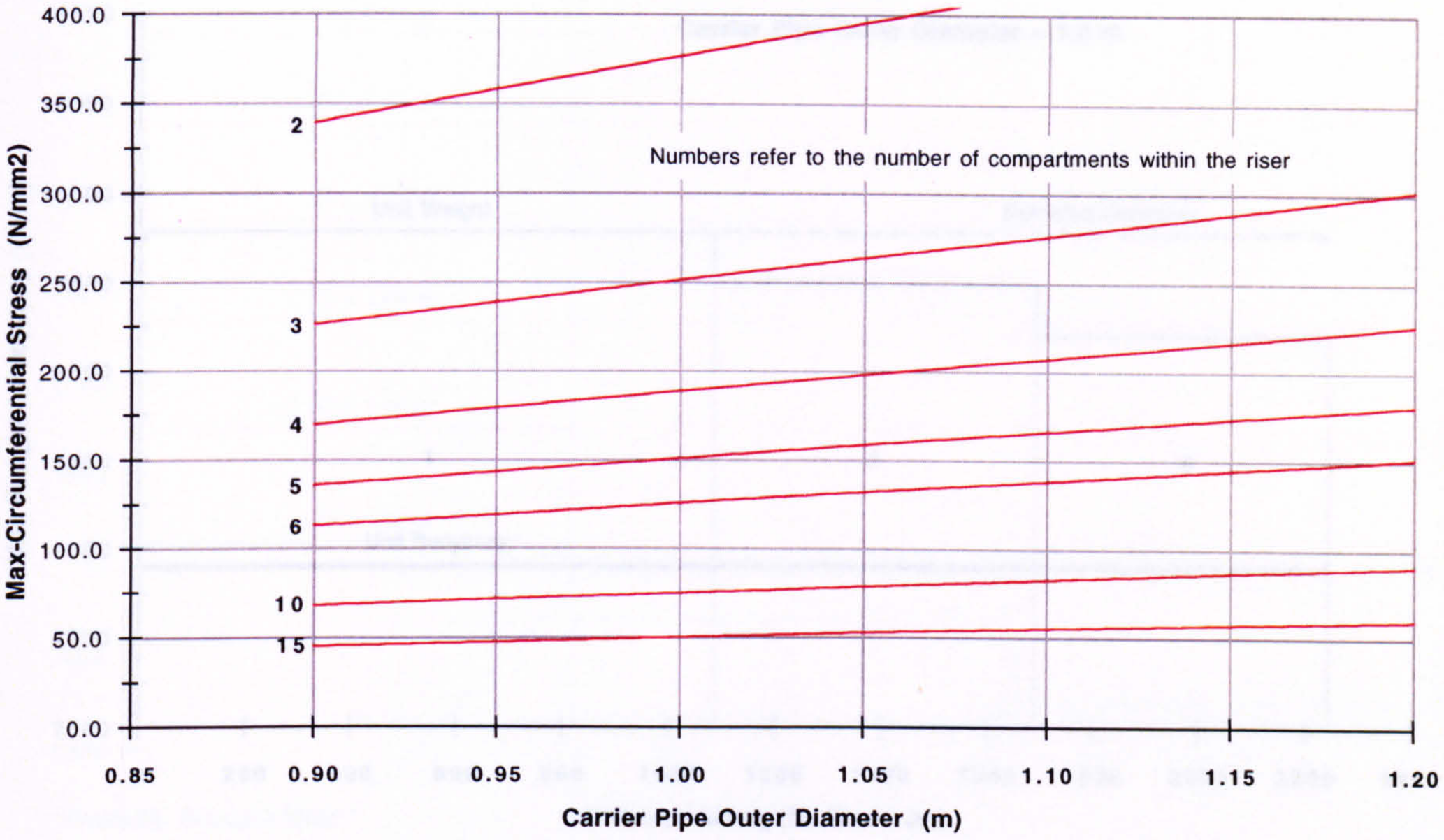

Maximum Circumferential Stress

(b)

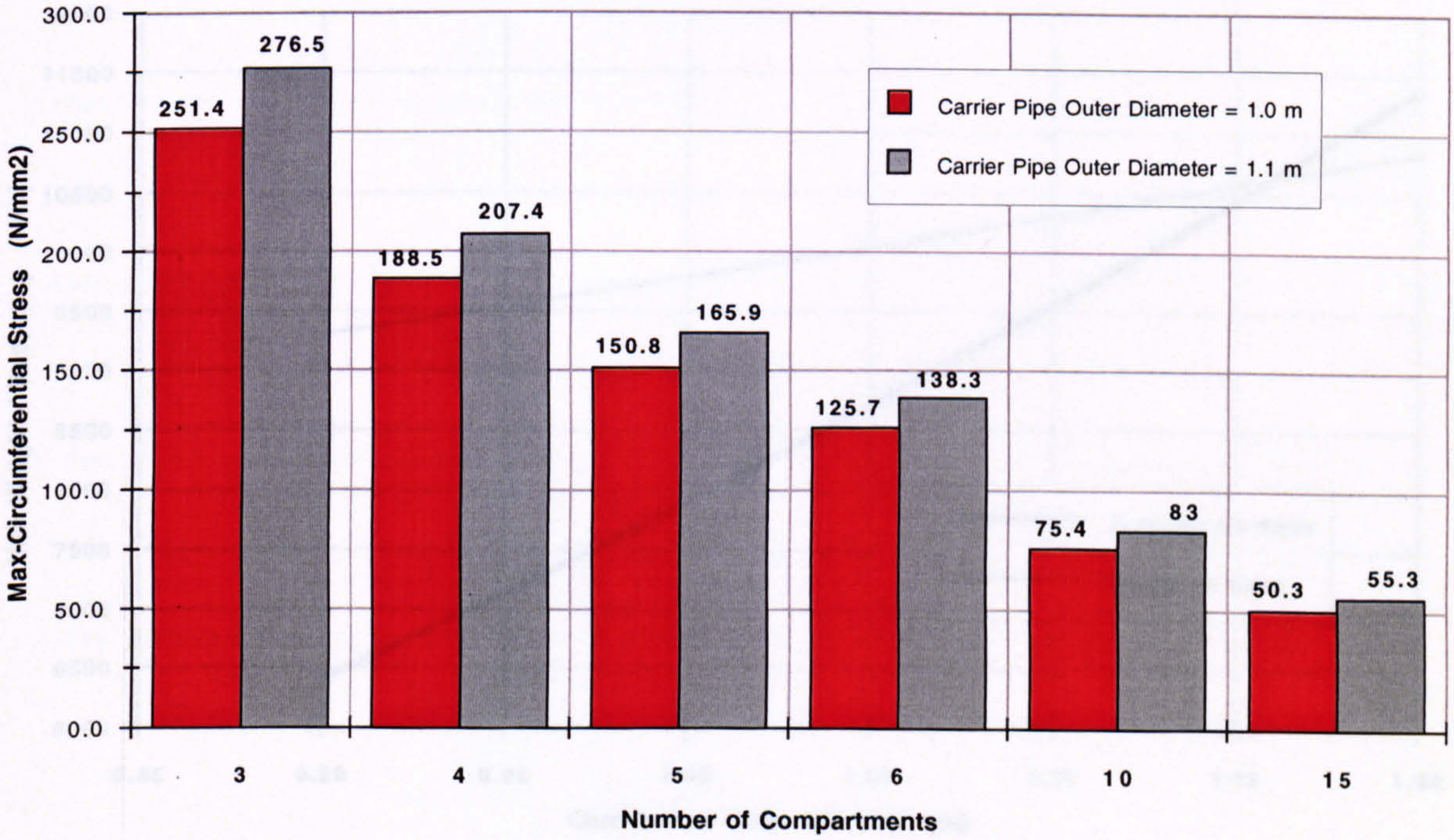

Horizontal Surface Offset = 1500 m

Carrier Pipe Wall Thickness = 10 mm

Sea Depth = 1500 m

Figure 3.13

Compartmental Unit Weight and Buoyancy (Operational) (a)

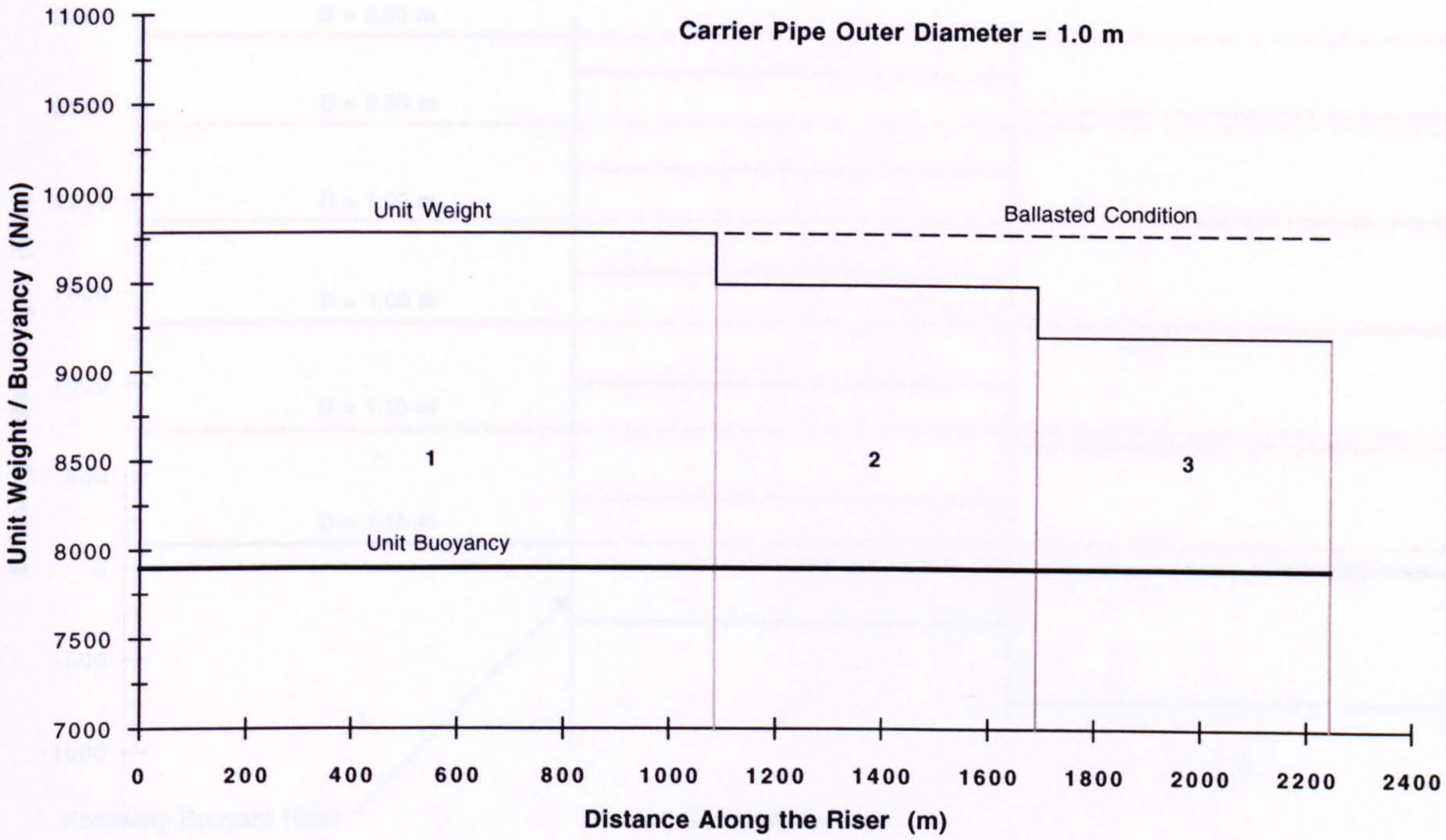

3 Compartments

Ballasted Unit Weight and Buoyancy (Operational) (b)

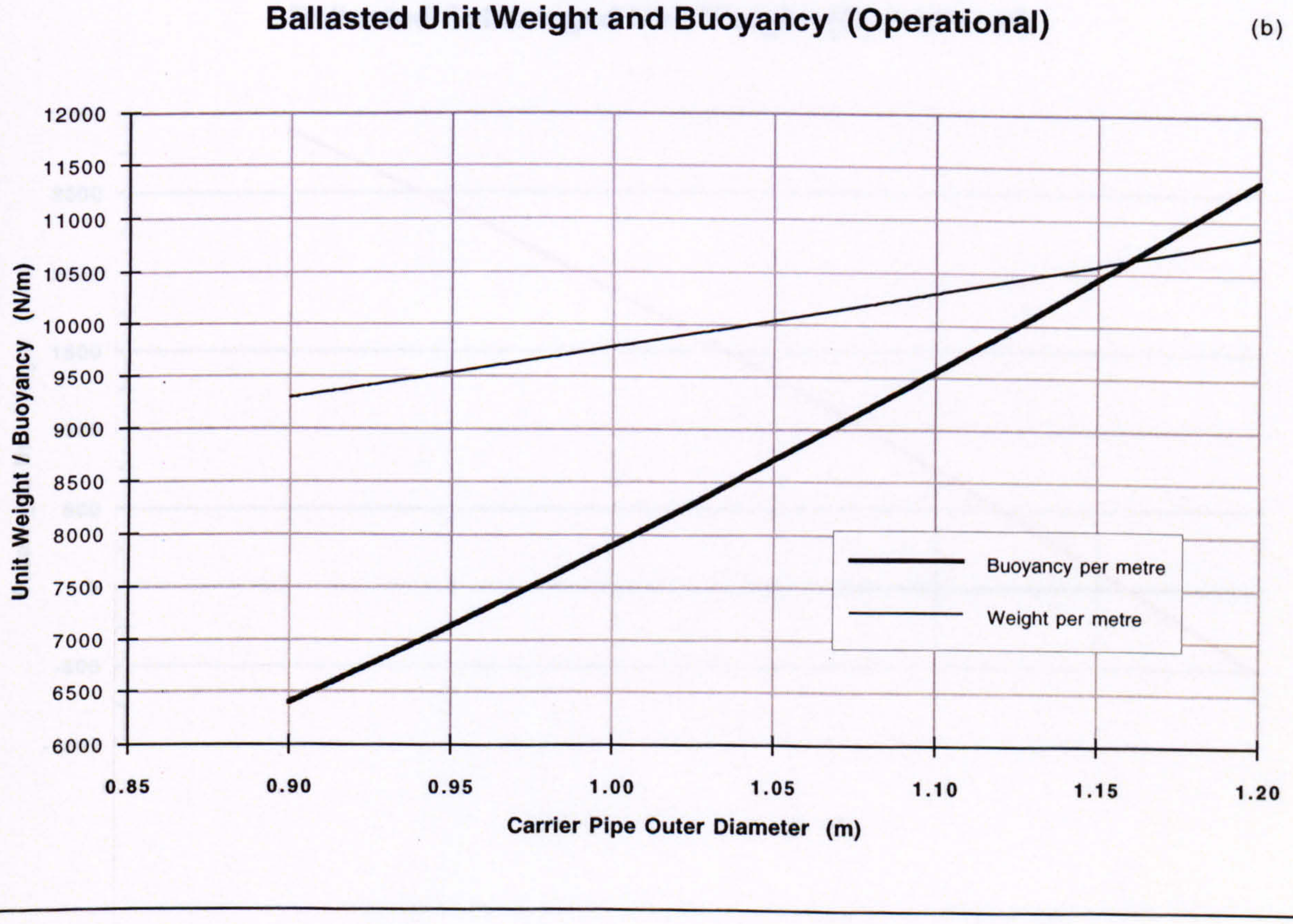

Horizontal Surface Offset = 1500 m

Sea Depth = 1500 m

Carrier Pipe Wall Thickness = 10 mm

Nitrogen Gas Temperature = 20 degs C

Figure 3.14

Compartmental Submerged Unit Weight (Operational)

(a)

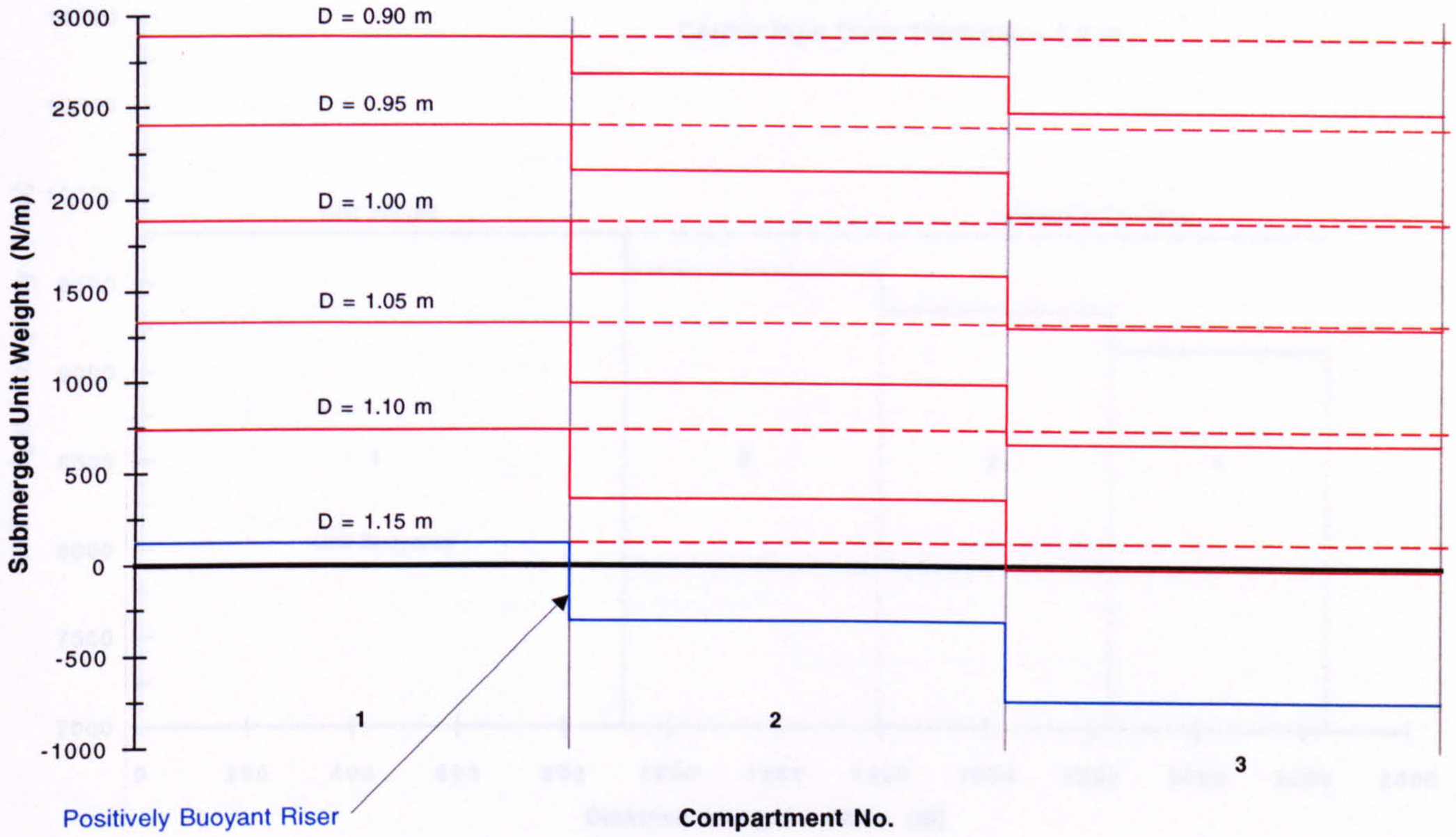

3 Compartments

Ballasted Submerged Unit Weight (Operational)

(b)

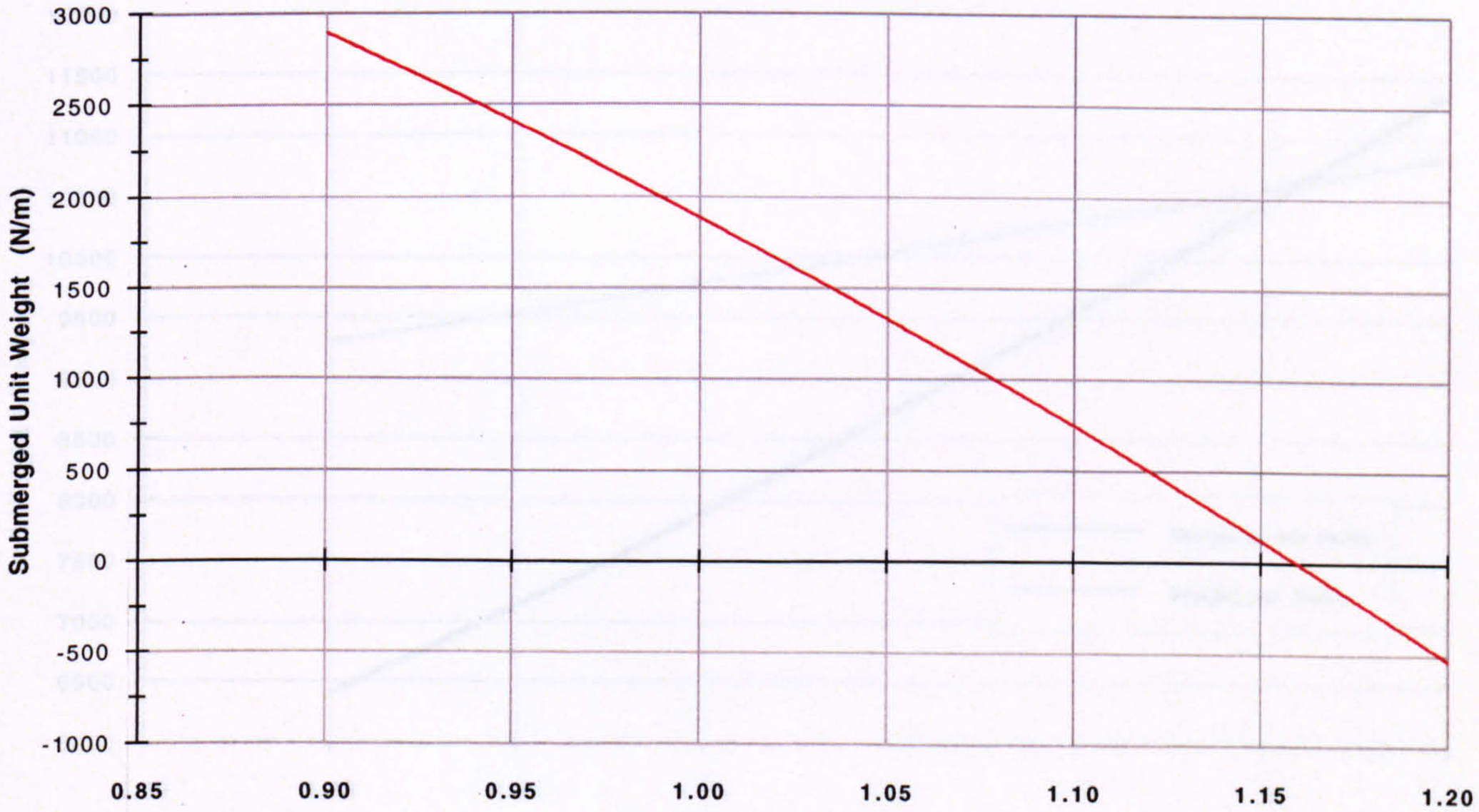

Horizontal Surface Offset = 1500 m

Sea Depth = 1500 m

Carrier Pipe Wall Thickness = 10 mm

Nitrogen Gas Temperature = 20 degs C

Figure 3.15

Compartmental Unit Weight and Buoyancy (Operational)

(a)

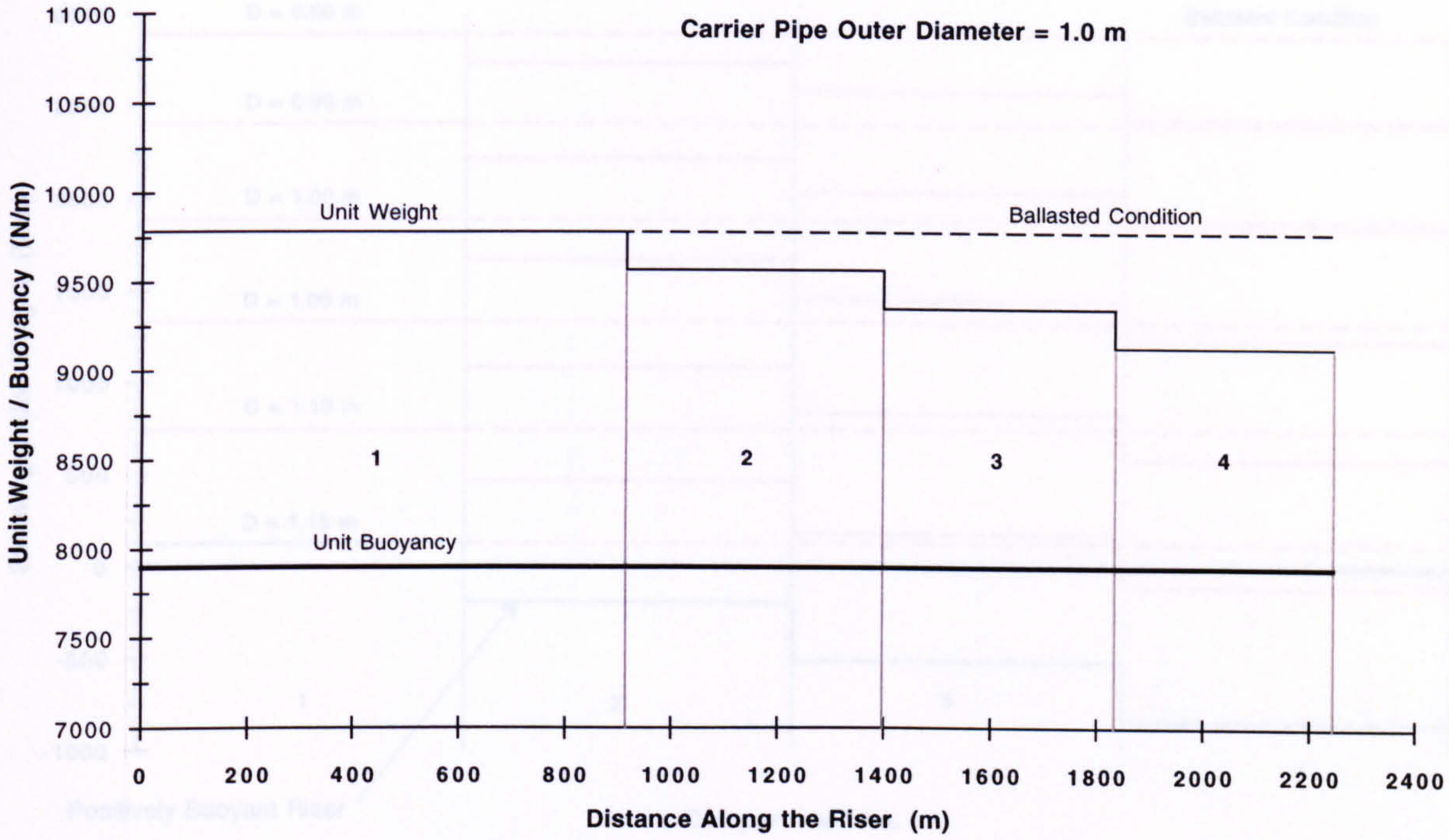

4 Compartments

Ballasted Unit Weight and Buoyancy (Operational)

(b)

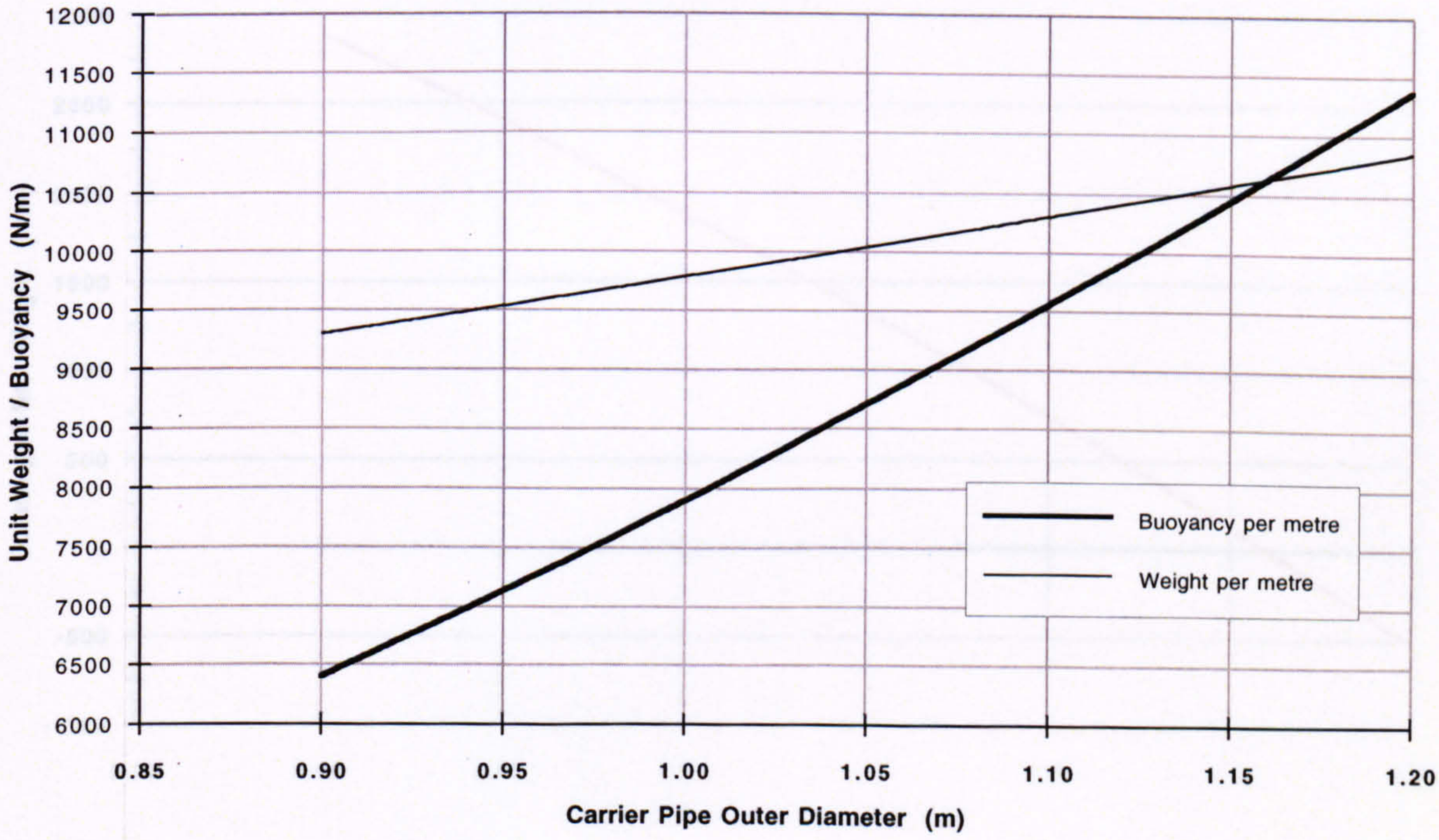

Horizontal Surface Offset = 1500 m

Sea Depth = 1500 m

Carrier Pipe Wall Thickness = 10 mm

Nitrogen Gas Temperature = 20 degs C

Figure 3.16

Compartmental Submerged Unit Weight (Operational)

(a)

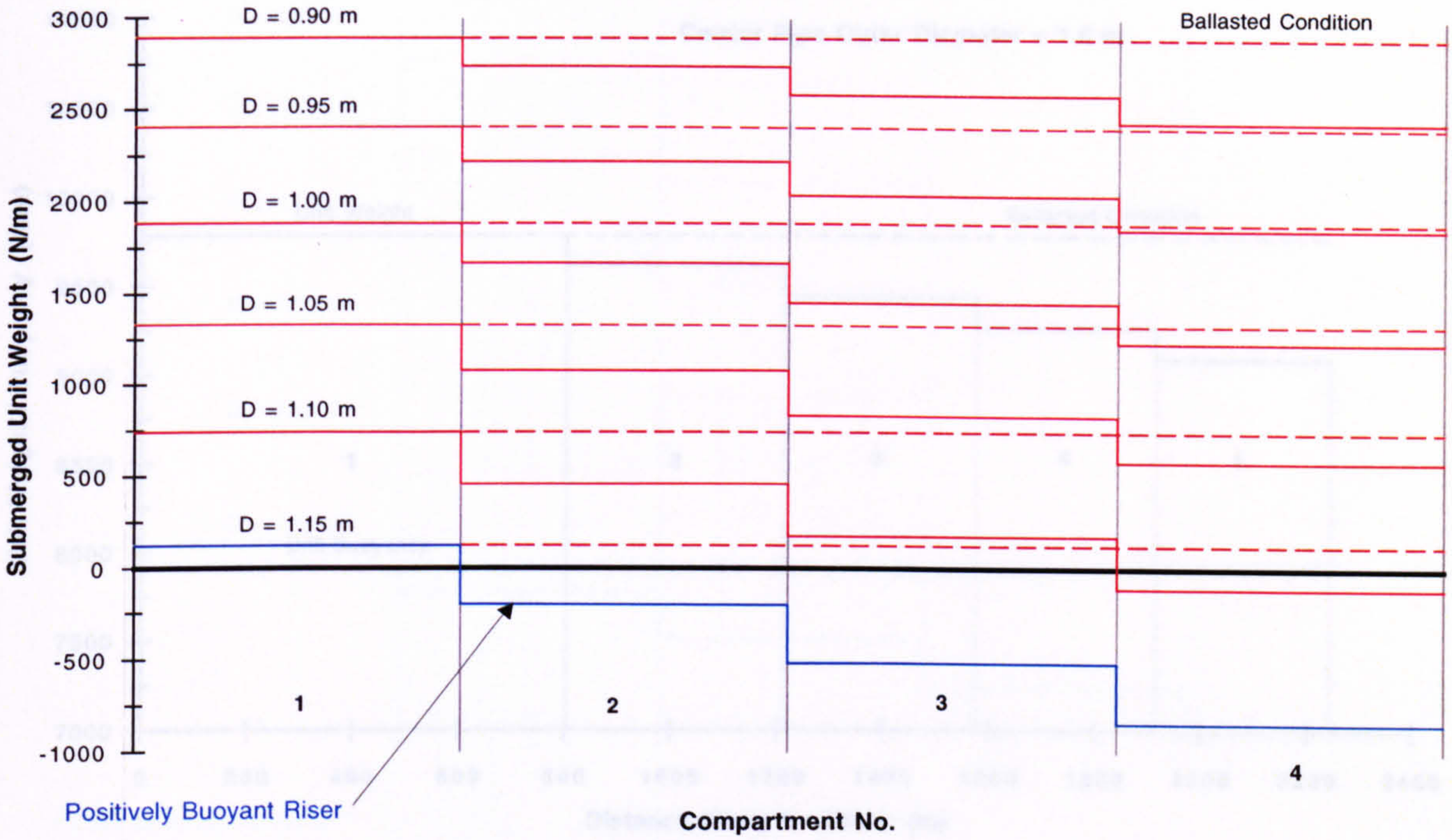

4 Compartments

Ballasted Submerged Unit Weight (Operational)

(b)

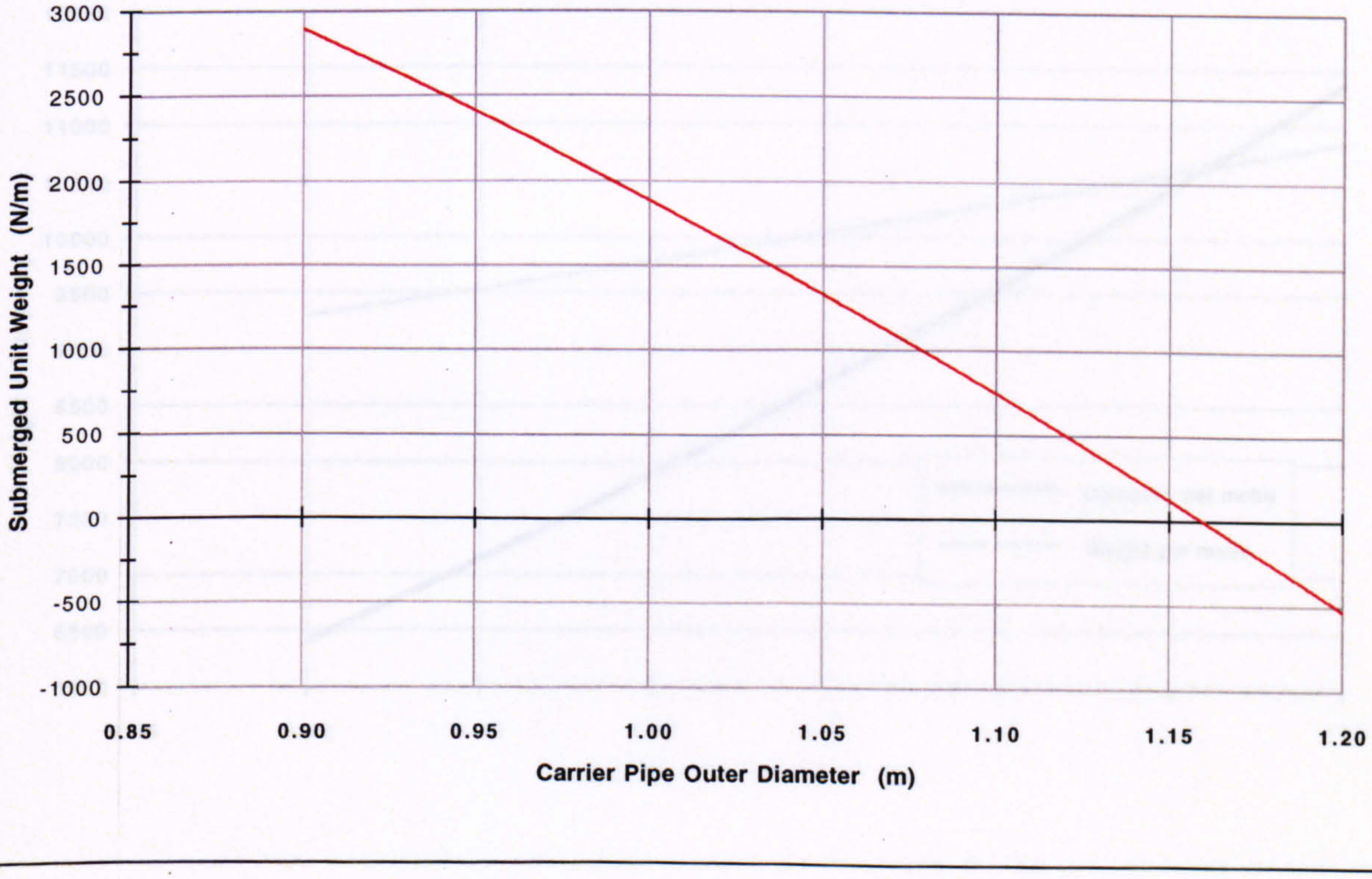

Horizontal Surface Offset = 1500 m

Sea Depth = 1500 m

Carrier Pipe Wall Thickness = 10 mm

Nitrogen Gas Temperature = 20 degs C

Figure 3.17

Compartmental Unit Weight and Buoyancy (Operational) (a)

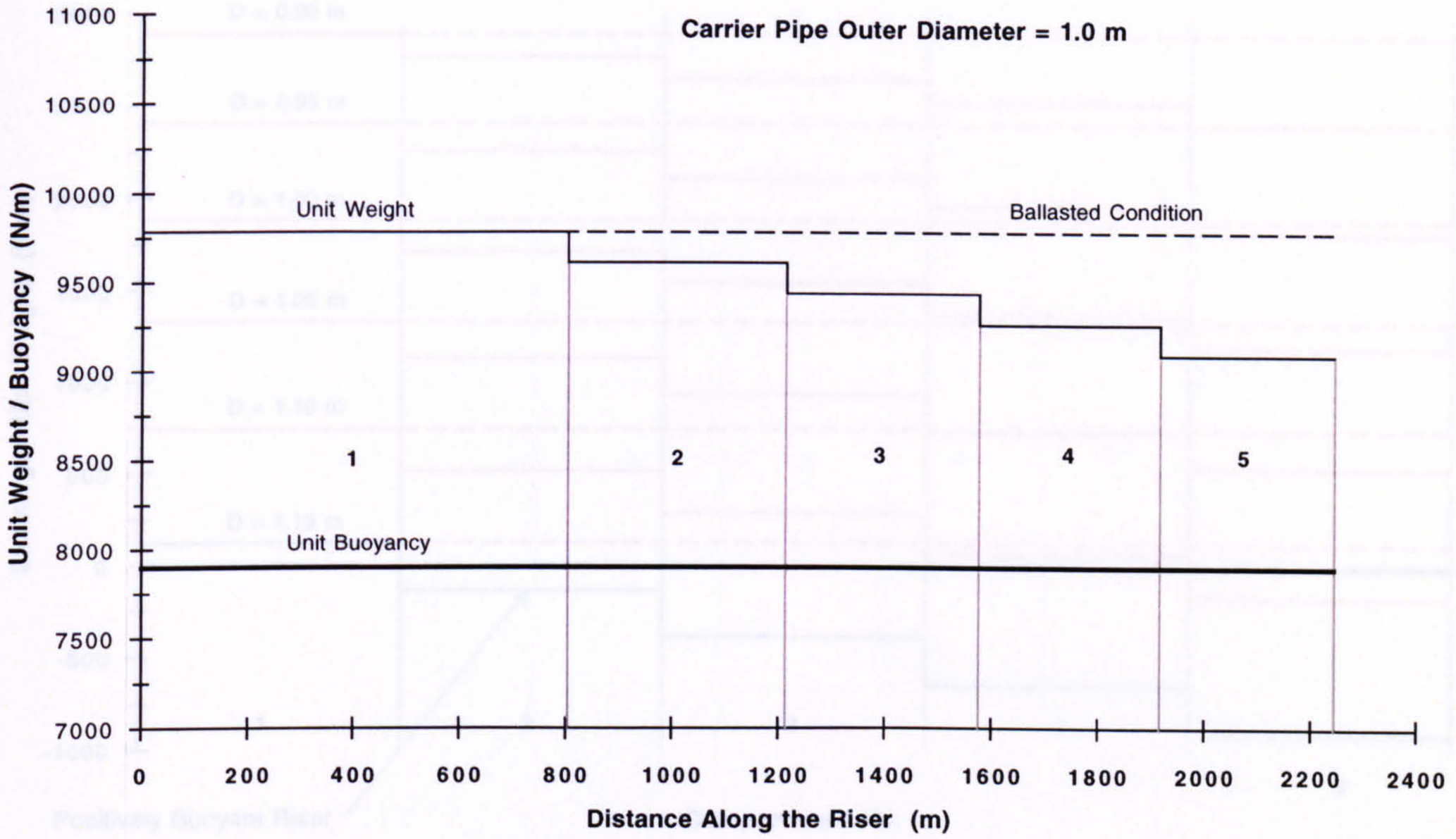

5 Compartments

Ballasted Unit Weight and Buoyancy (Operational) (b)

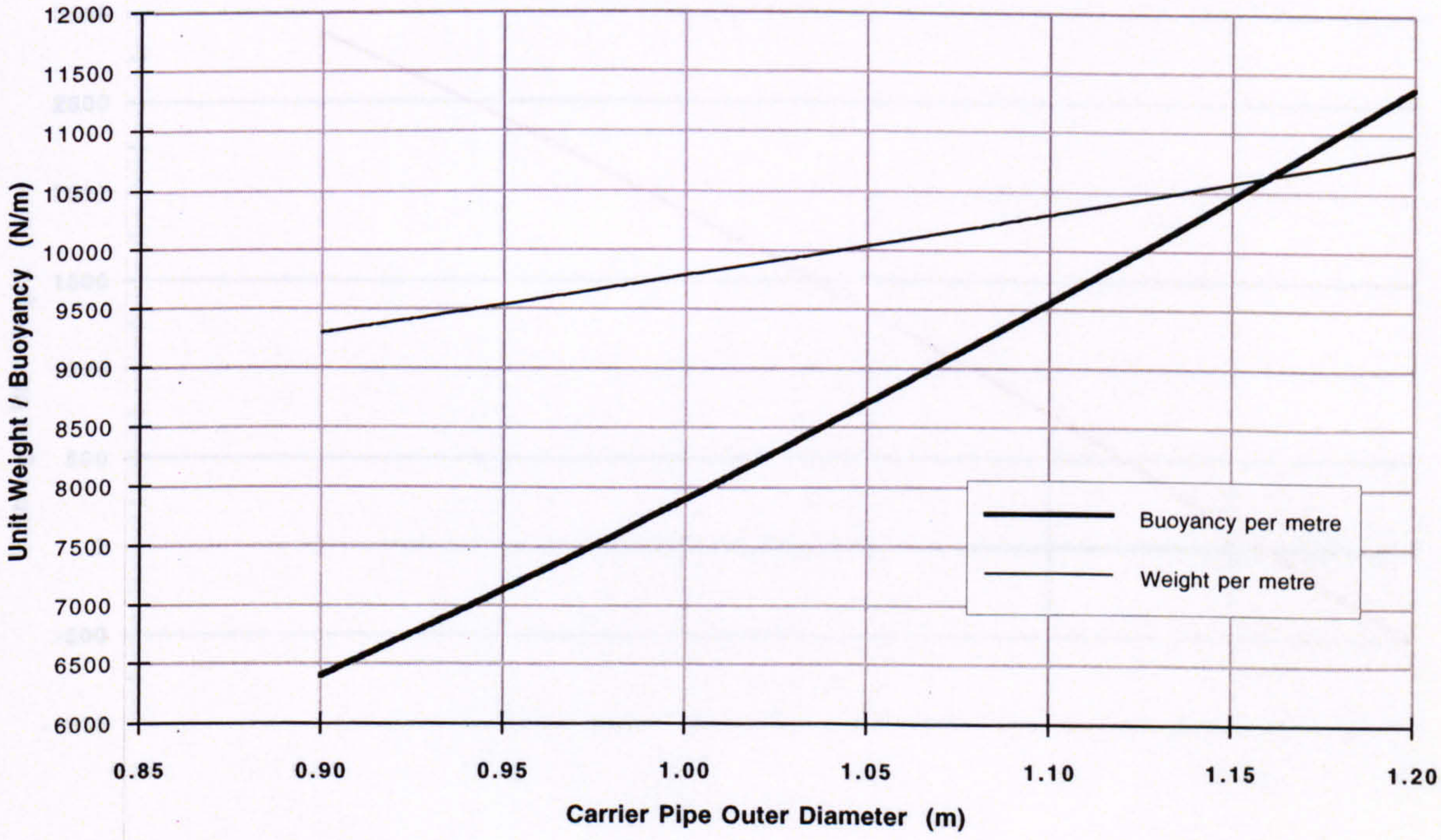

Horizontal Surface Offset = 1500 m

Sea Depth = 1500 m

Carrier Pipe Wall Thickness = 10 mm

Nitrogen Gas Temperature = 20 degs C

Figure 3.18

Compartmental Submerged Unit Weight (Operational)

(a)

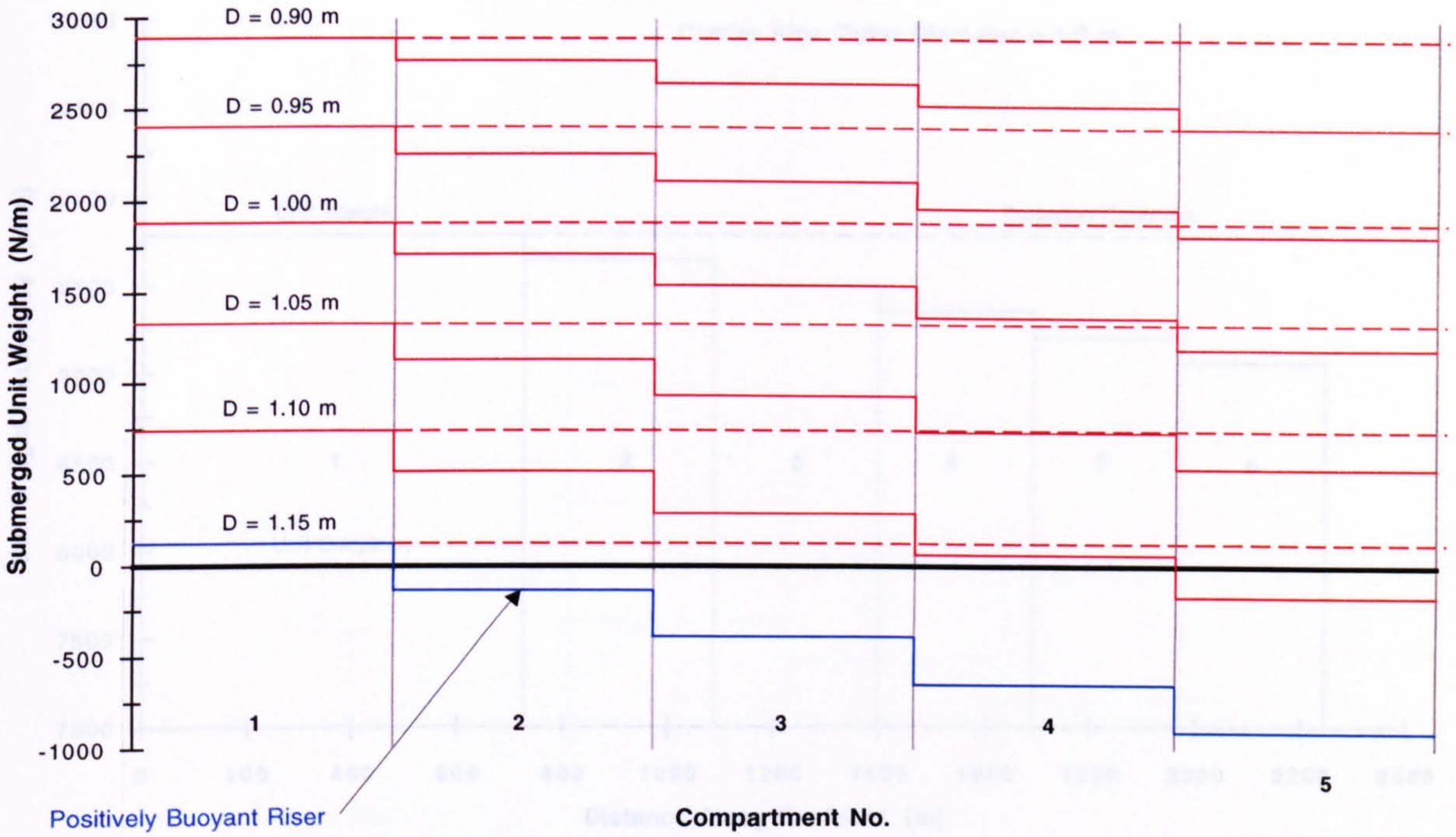

5 Compartments

Ballasted Submerged Unit Weight (Operational)

(b)

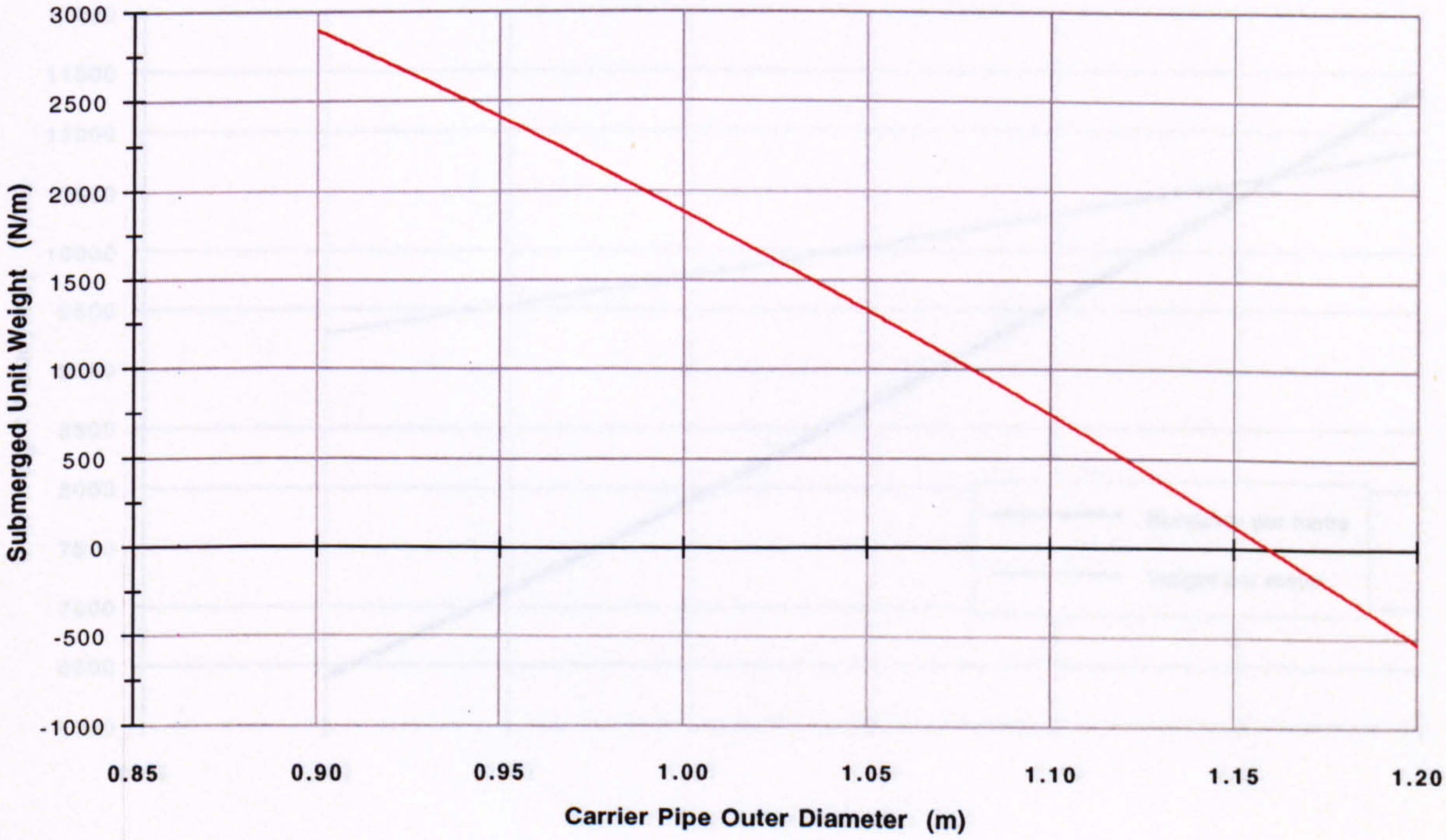

Horizontal Surface Offset = 1500 m

Sea Depth = 1500 m

Carrier Pipe Wall Thickness = 10 mm

Nitrogen Gas Temperature = 20 degs C

Figure 3.19

Compartmental Unit Weight and Buoyancy (Operational) (a)

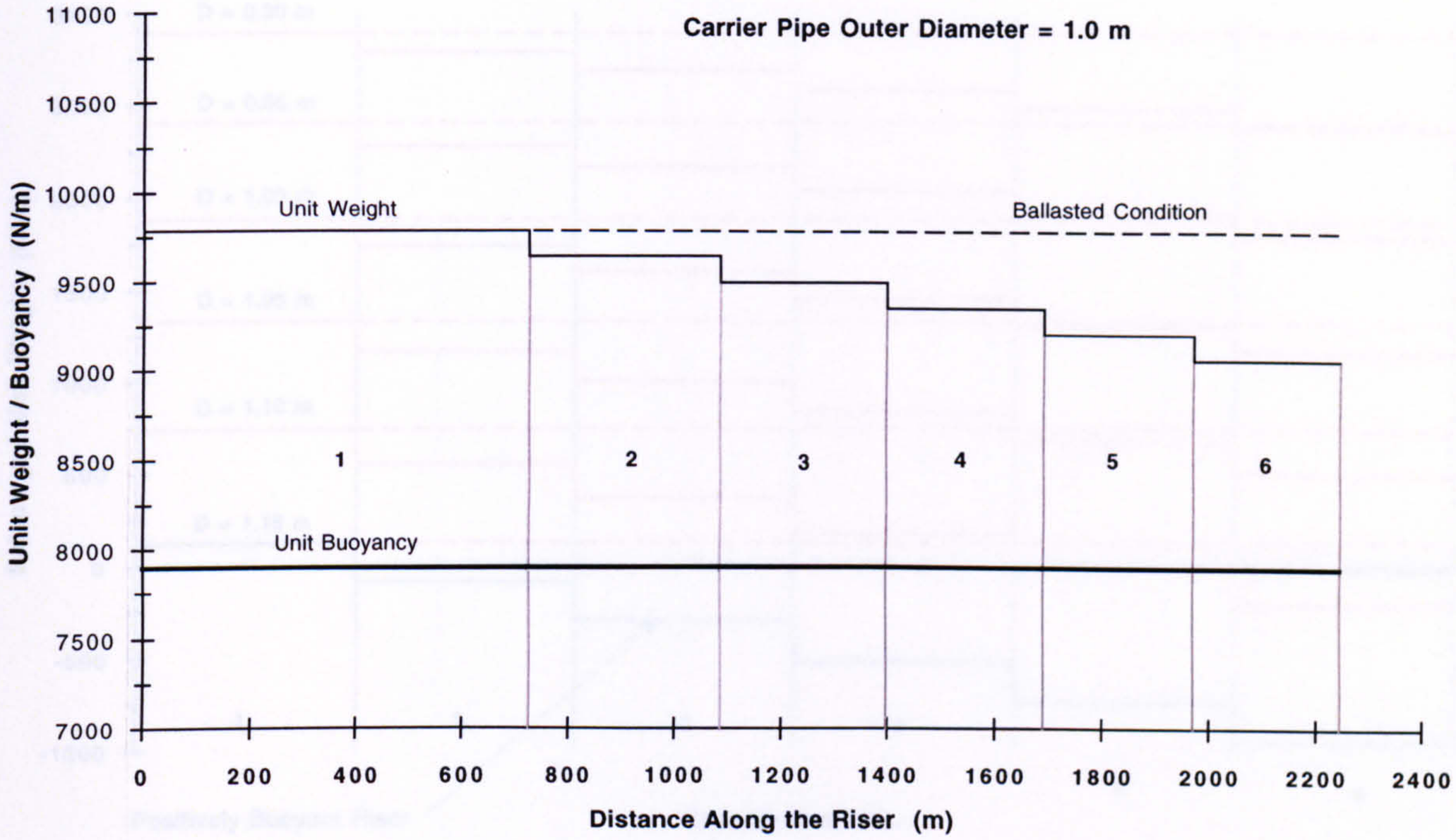

6 Compartments

Ballasted Unit Weight and Buoyancy (Operational) (b)

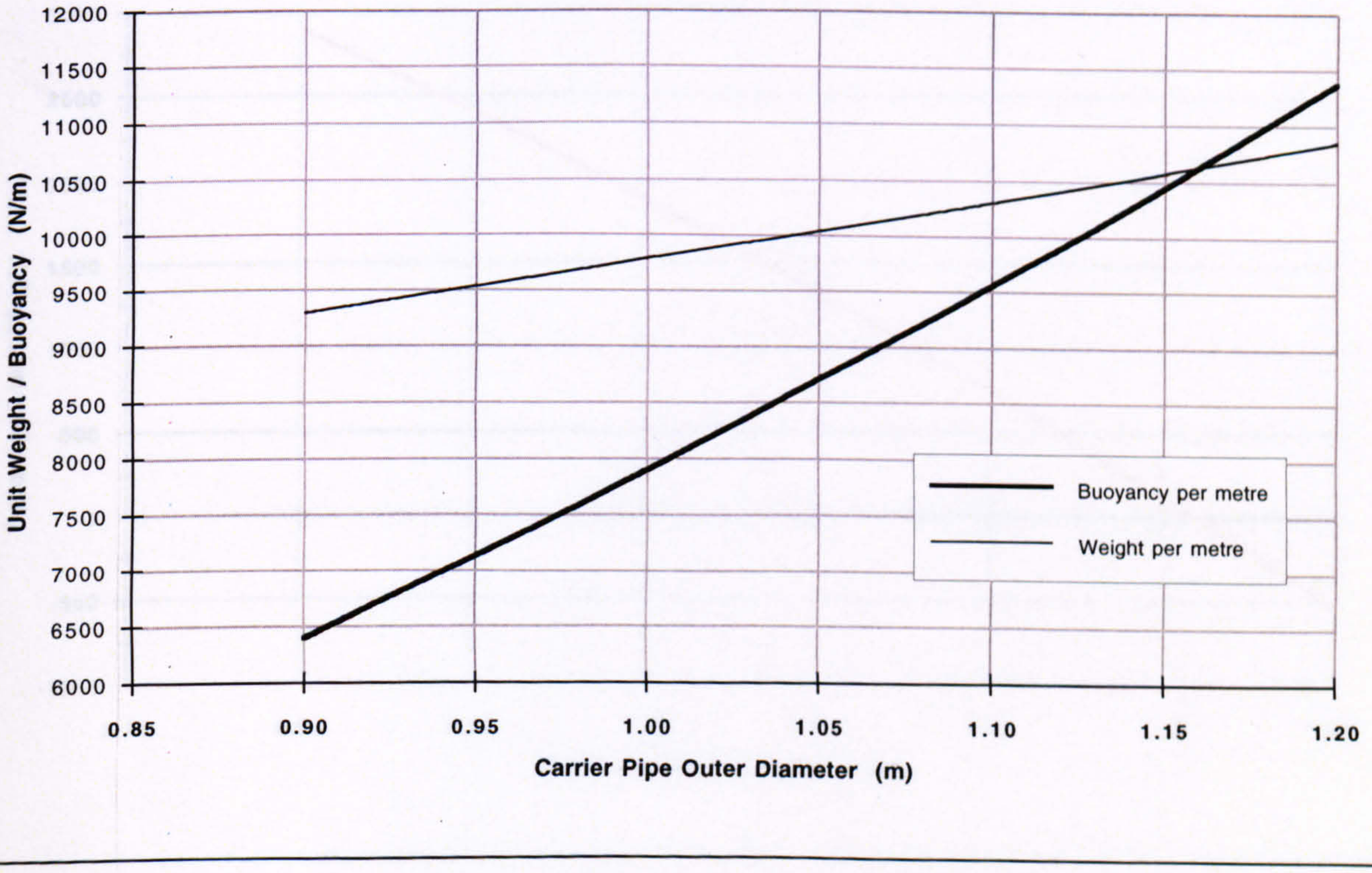

Horizontal Surface Offset = 1500 m

Sea Depth = 1500 m

Carrier Pipe Wall Thickness = 10 mm

Nitrogen Gas Temperature = 20 degs C

Figure 3.20

Compartmental Submerged Unit Weight (Operational)

(a)

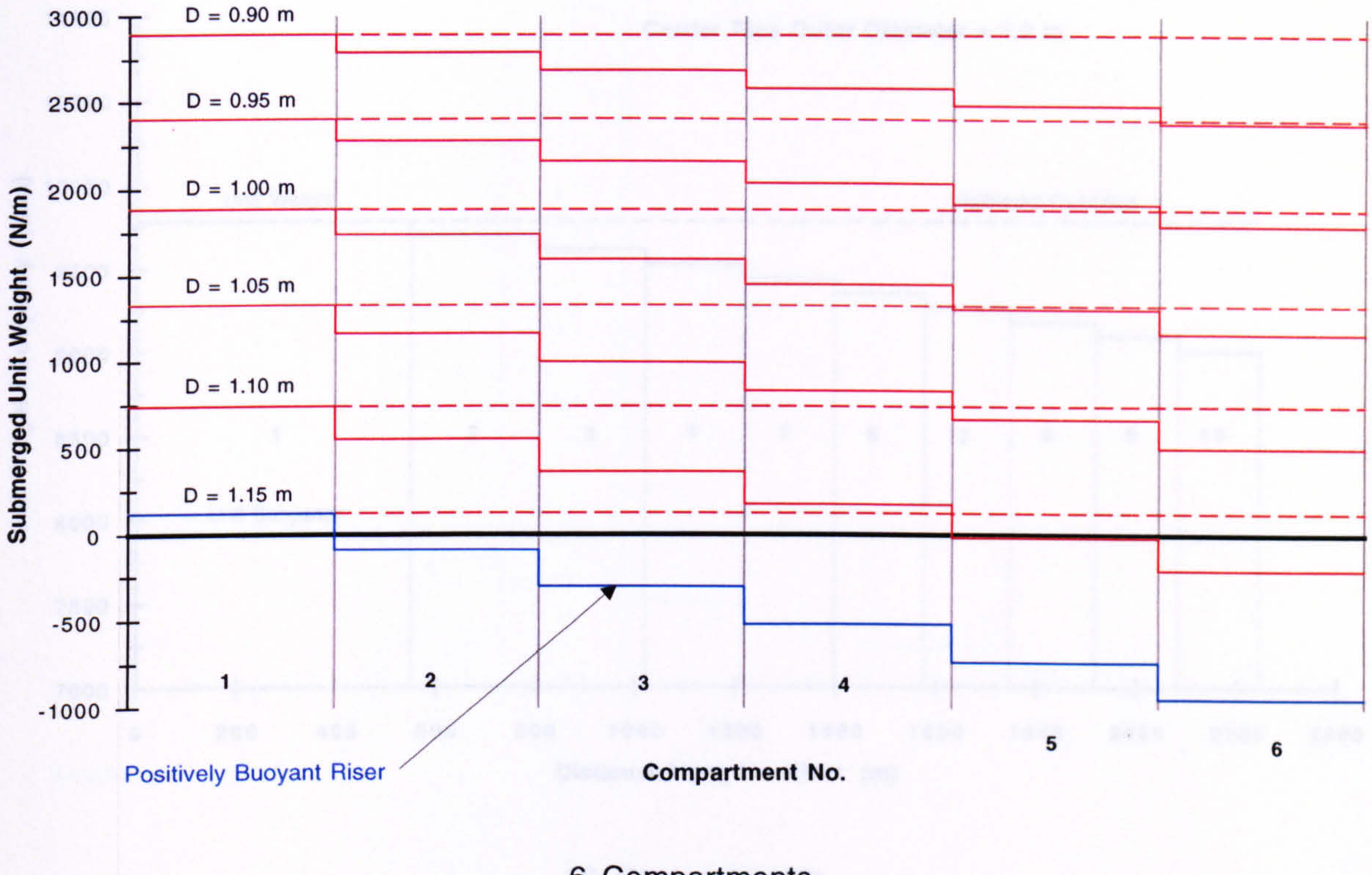

6 Compartments

Ballasted Submerged Unit Weight (Operational)

(b)

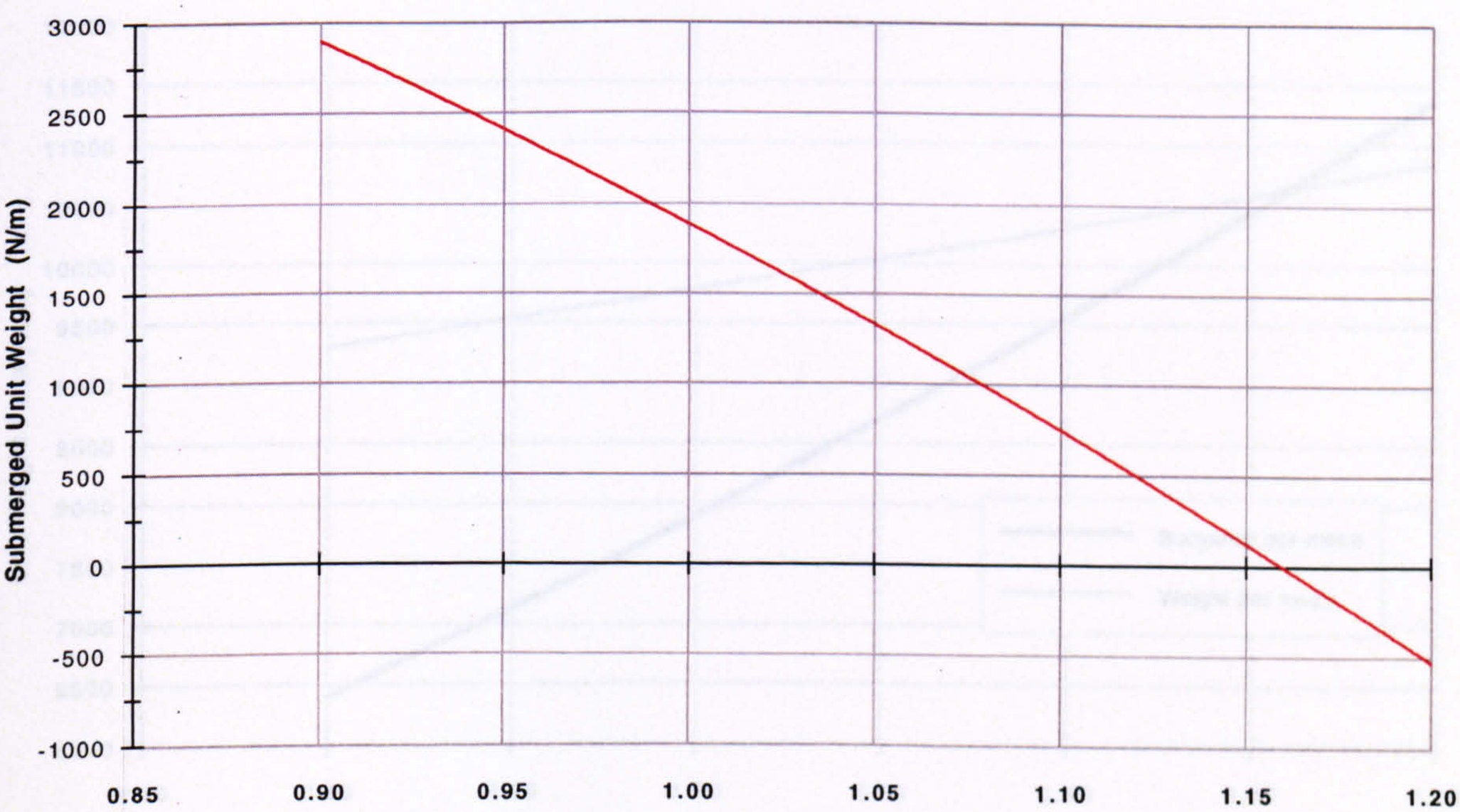

Horizontal Surface Offset = 1500 m

Sea Depth = 1500 m

Carrier Pipe Wall Thickness = 10 mm

Nitrogen Gas Temperature = 20 degs C

Figure 3.21

Compartmental Unit Weight and Buoyancy (Operational) (a)

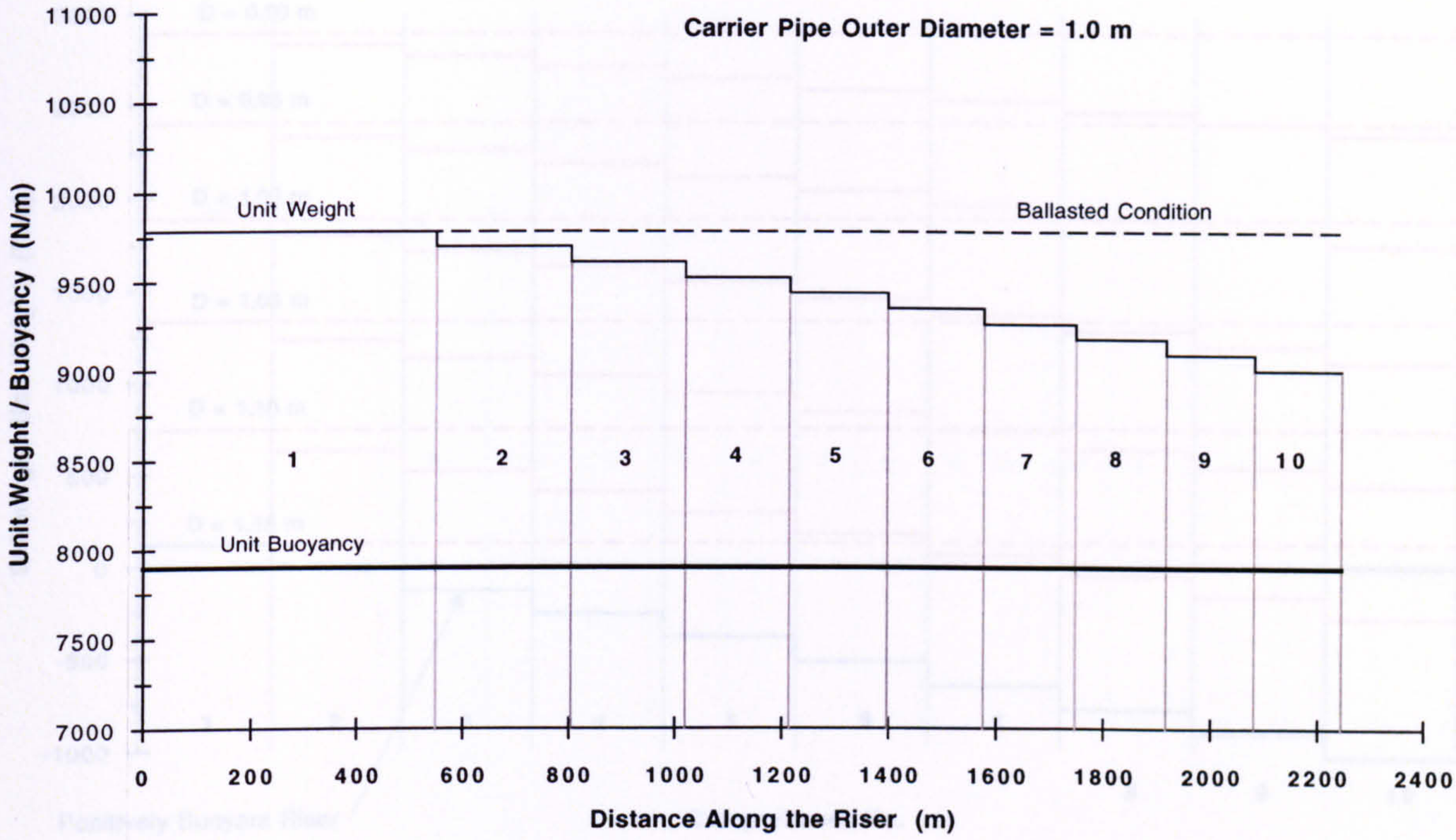

10 Compartments

Ballasted Unit Weight and Buoyancy (Operational) (b)

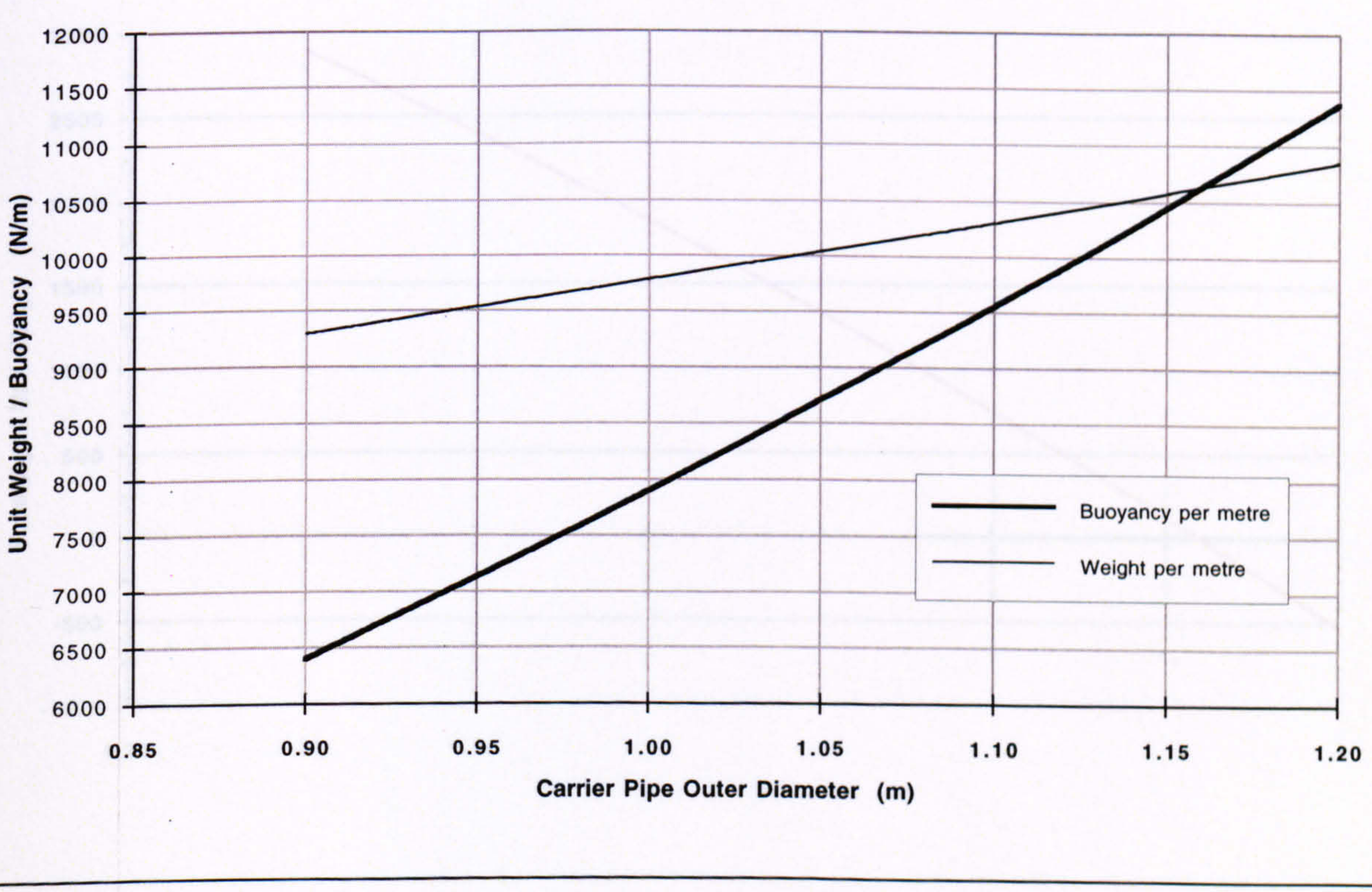

Horizontal Surface Offset = 1500 m

Sea Depth = 1500 m

Carrier Pipe Wall Thickness = 10 mm

Nitrogen Gas Temperature = 20 degs C

Figure 3.22

Compartmental Submerged Unit Weight (Operational) (a)

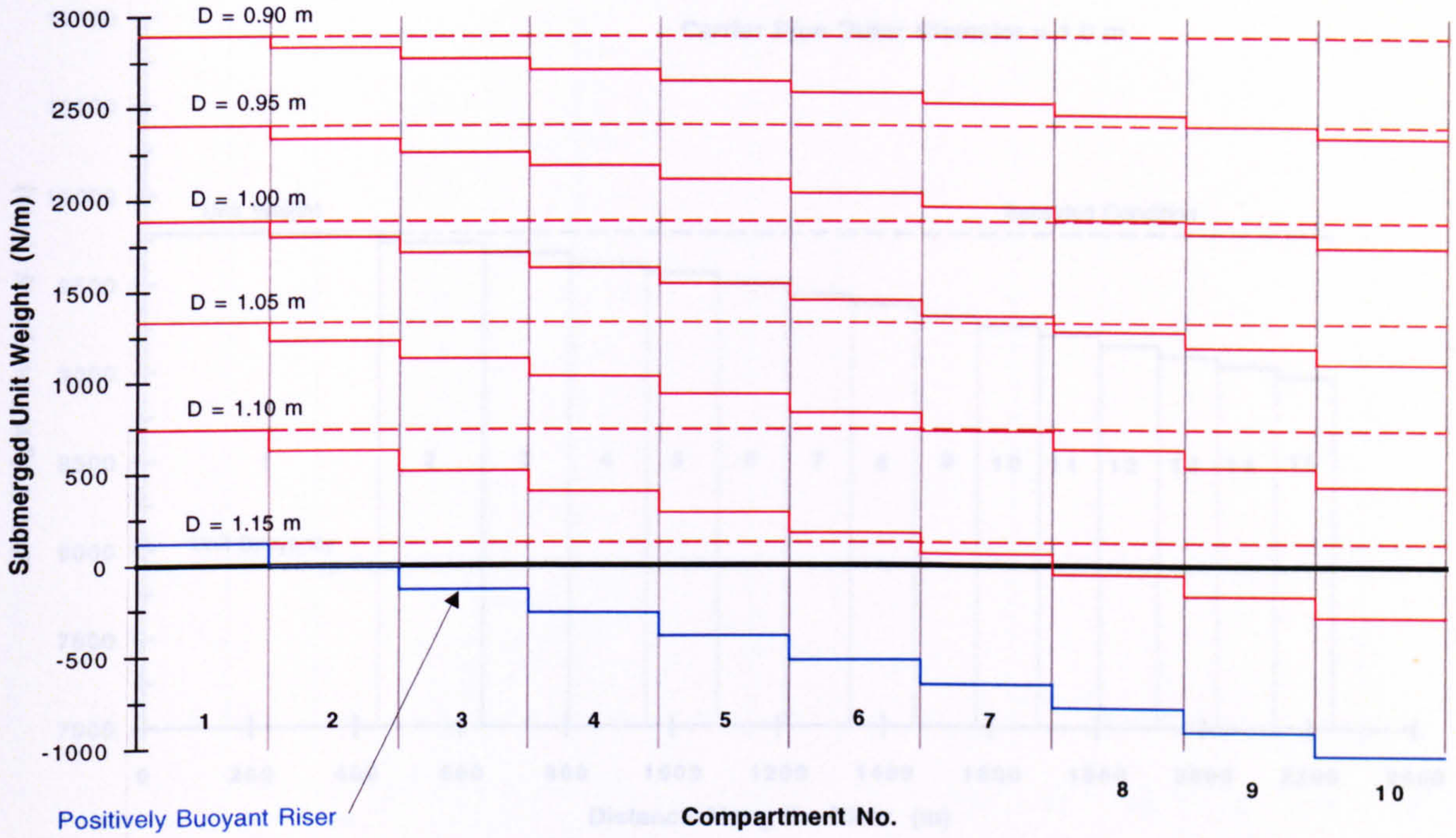

10 Compartments

Ballasted Submerged Unit Weight (Operational) (b)

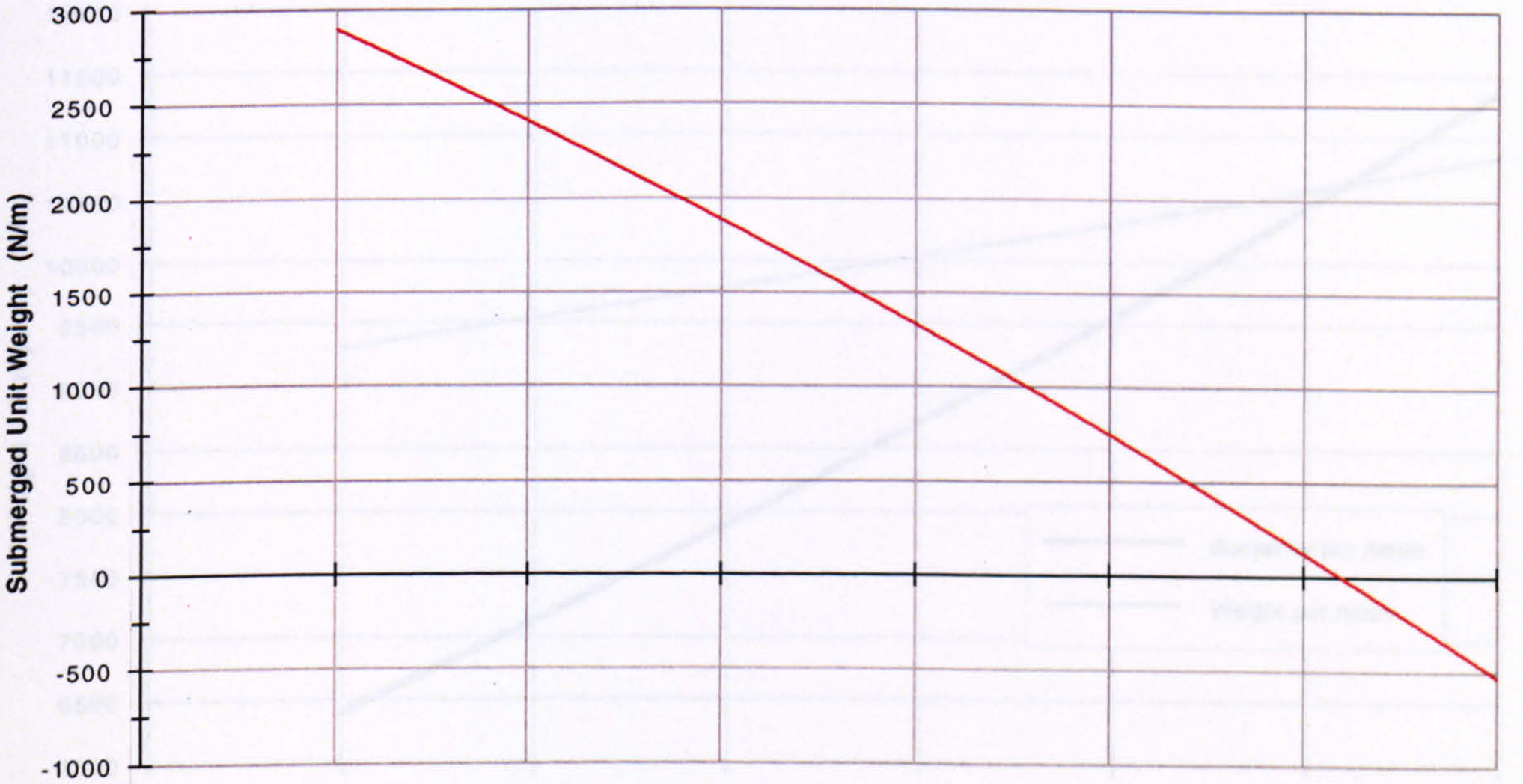

Horizontal Surface Offset = 1500 m

Sea Depth = 1500 m

Carrier Pipe Wall Thickness = 10 mm

Nitrogen Gas Temperature = 20 degs C

Figure 3.23

Compartmental Unit Weight and Buoyancy (Operational) (a)

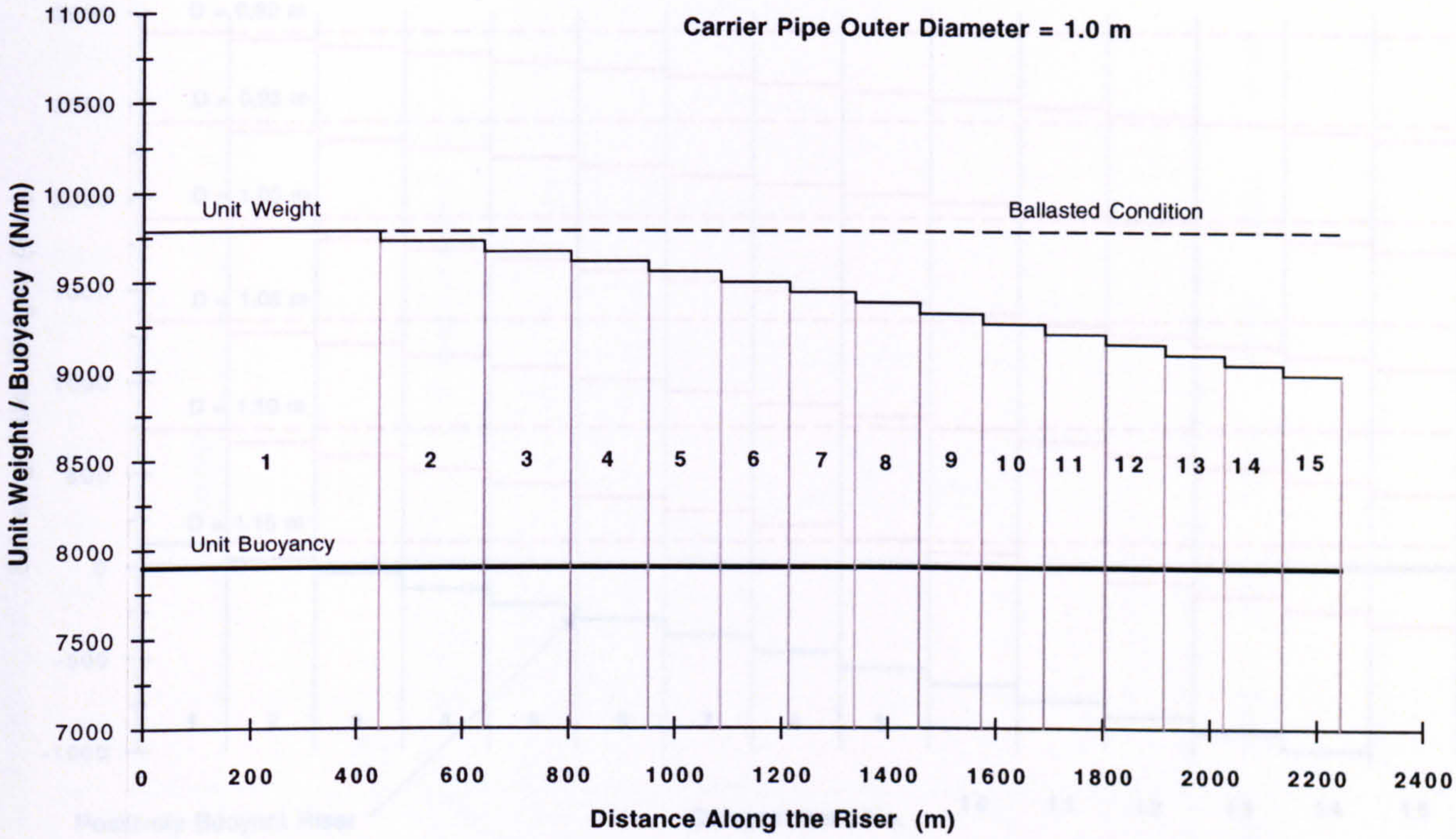

15 Compartments

Ballasted Unit Weight and Buoyancy (Operational) (b)

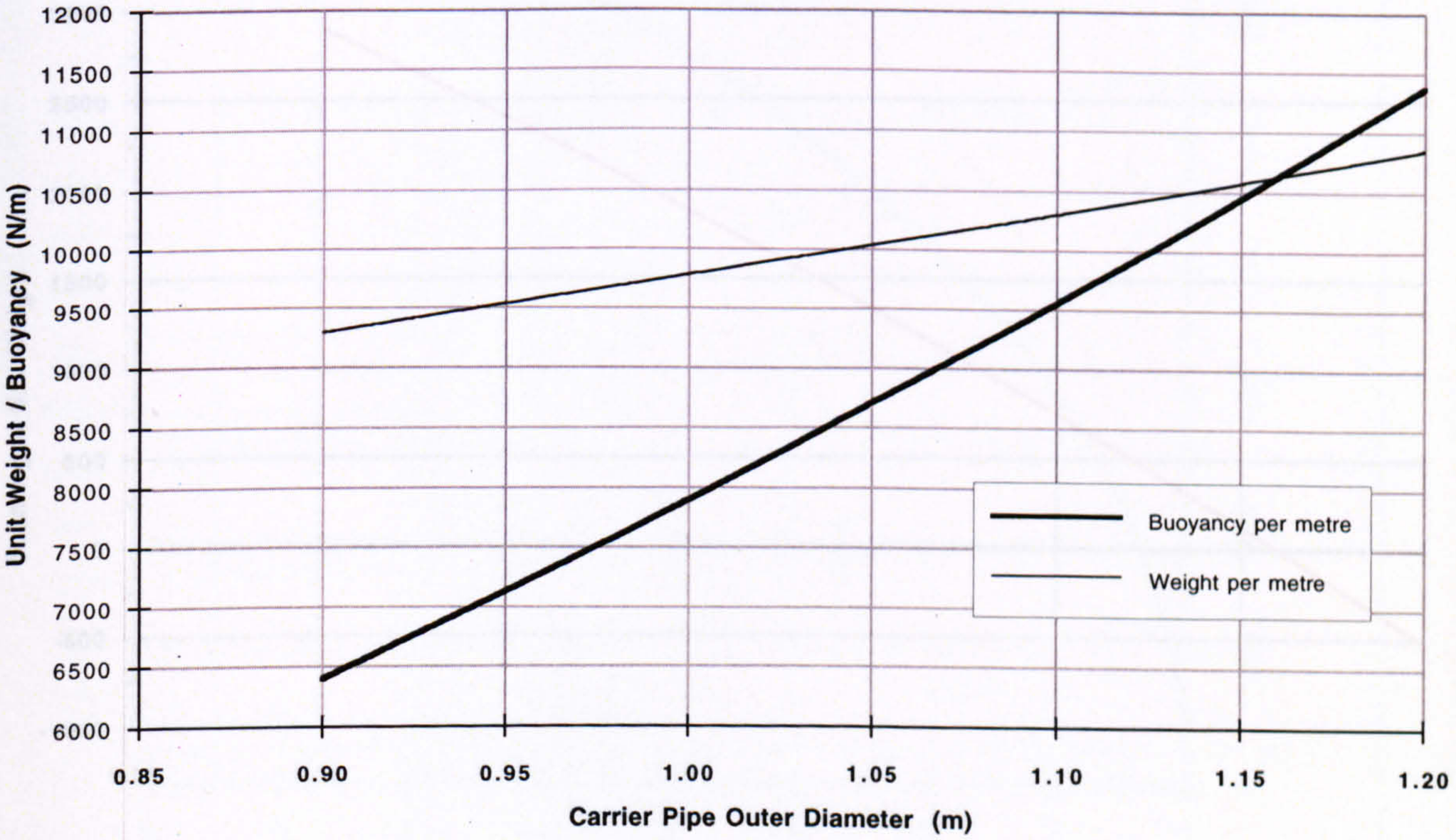

Horizontal Surface Offset = 1500 m

Carrier Pipe Wall Thickness = 10 mm

Sea Depth = 1500 m

Nitrogen Gas Temperature = 20 degs C

Figure 3.24

Compartmental Submerged Unit Weight (Operational) (a)

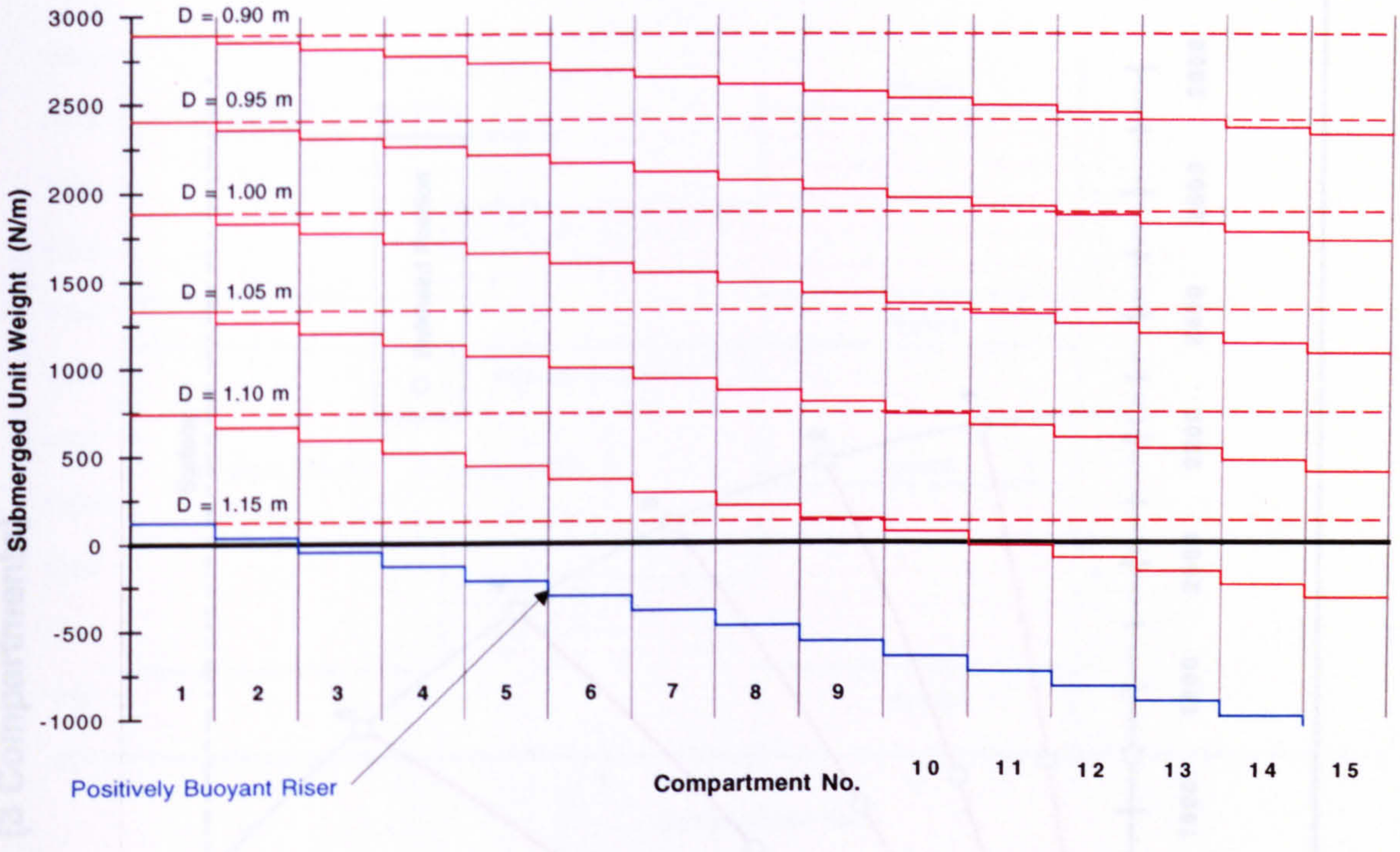

15 Compartments

Ballasted Submerged Unit Weight (Operational) (b)

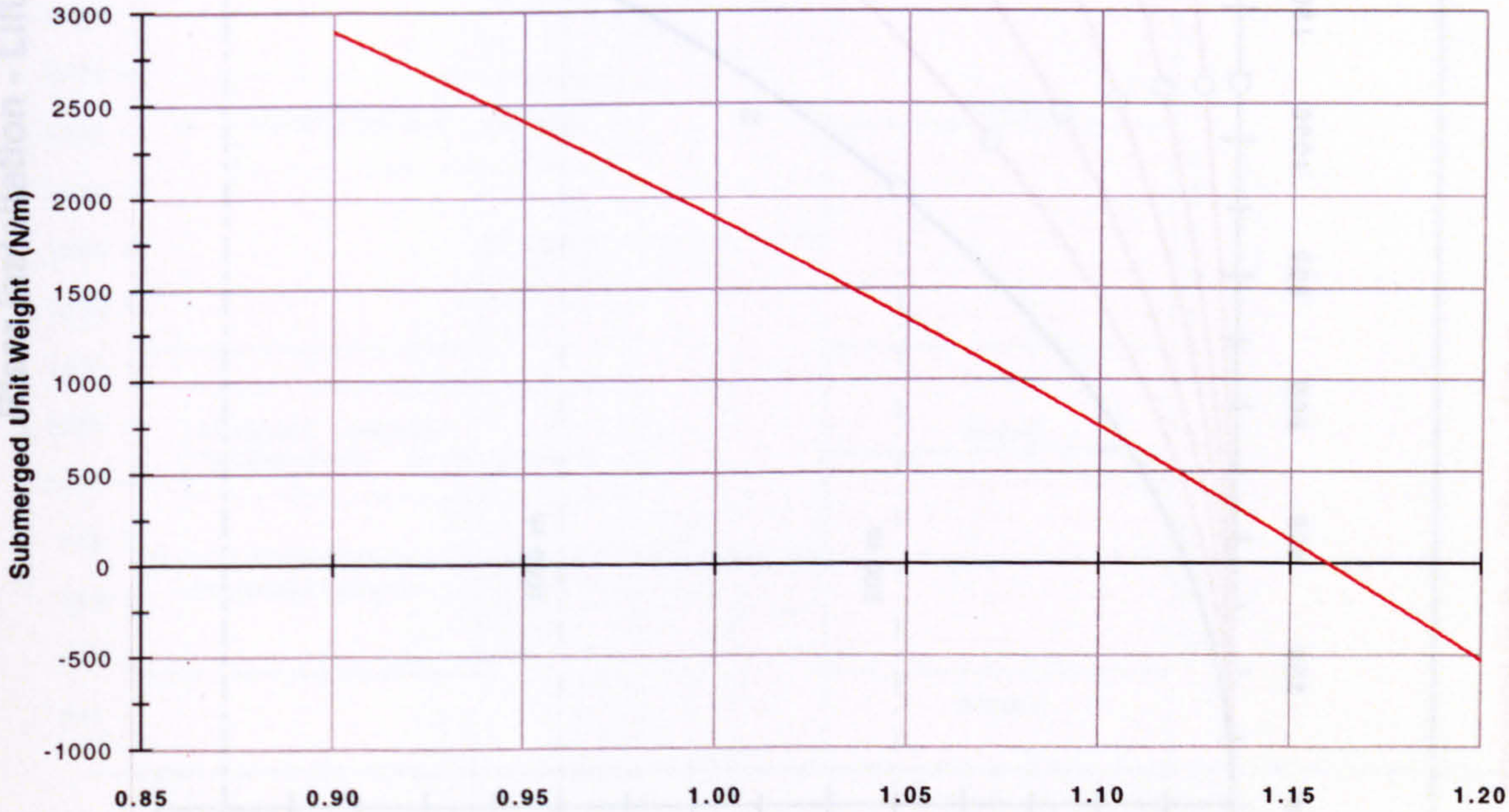

Horizontal Surface Offset = 1500 m

Carrier Pipe Wall Thickness = 10 mm

Sea Depth = 1500 m

Nitrogen Gas Temperature = 20 degs C

Figure 3.25

Riser Installation - Lift Sequence (3 Compartments)

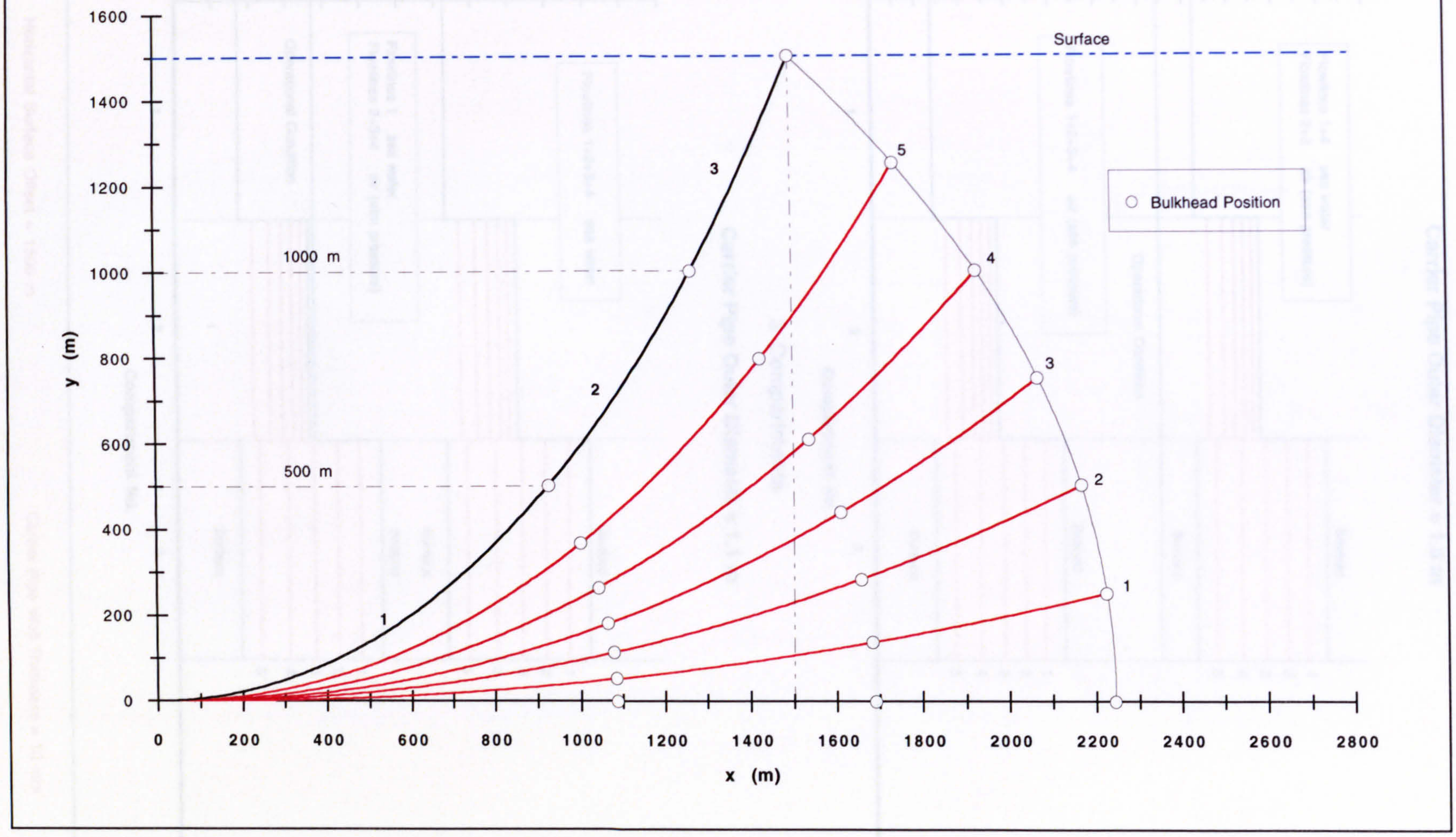

Horizontal Surface Offset = 1500 m

Sea Depth = 1500 m

Figure 3.26

Compartmental Submerged Unit Weight (Installation)

Carrier Pipe Outer Diameter = 1.0 m

(a)

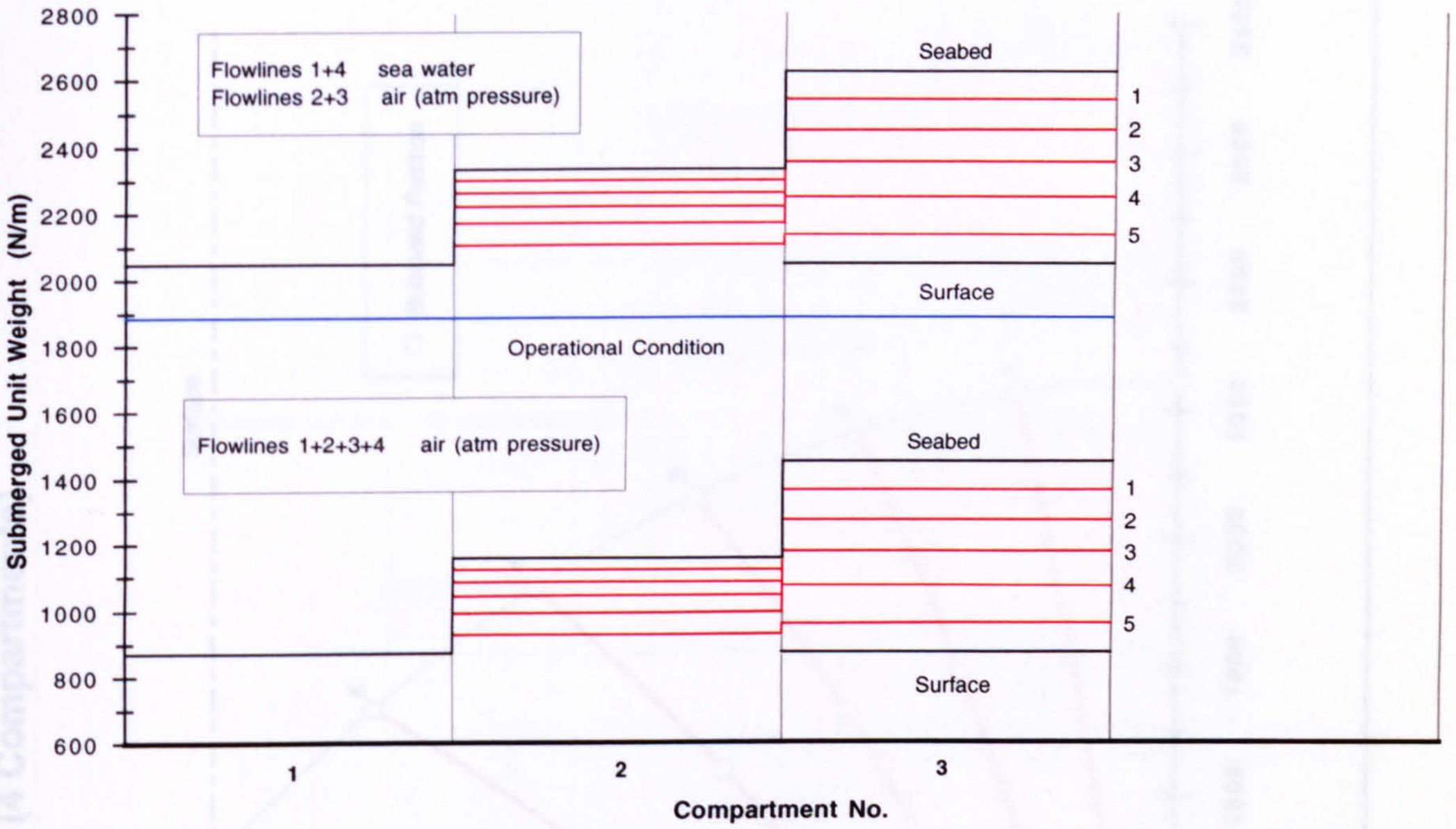

3 Compartments

Carrier Pipe Outer Diameter = 1.1 m

(b)

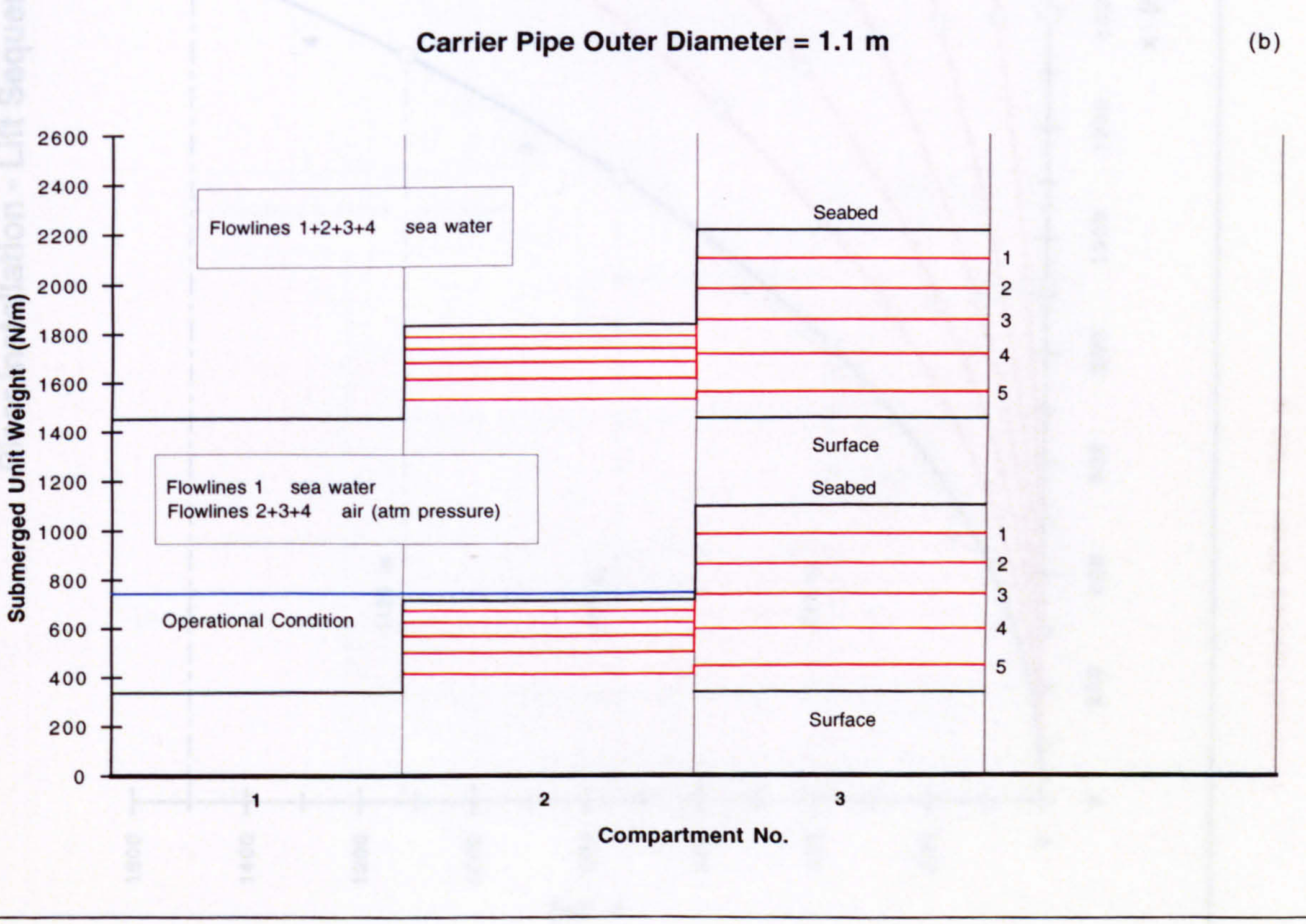

Horizontal Surface Offset = 1500 m

Carrier Pipe Wall Thickness = 10 mm

Sea Depth = 1500 m

Nitrogen Gas Temperature = 0 degs C

Figure 3.27

Riser Installation - Lift Sequence (4 Compartments)

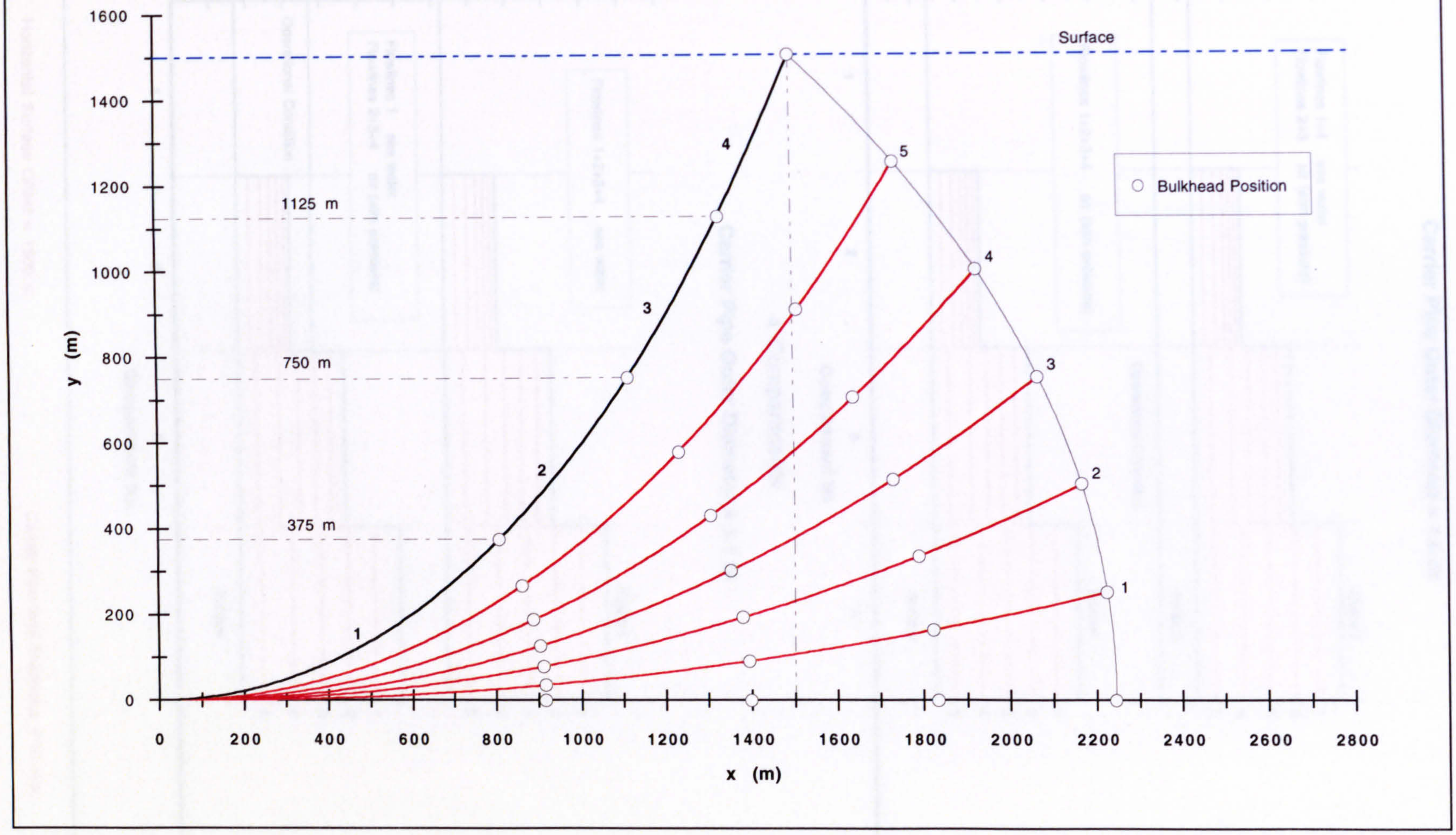

Horizontal Surface Offset = 1500 m

Sea Depth = 1500 m

Figure 3.28

Compartmental Submerged Unit Weight (Installation)

Carrier Pipe Outer Diameter = 1.0 m

(a)

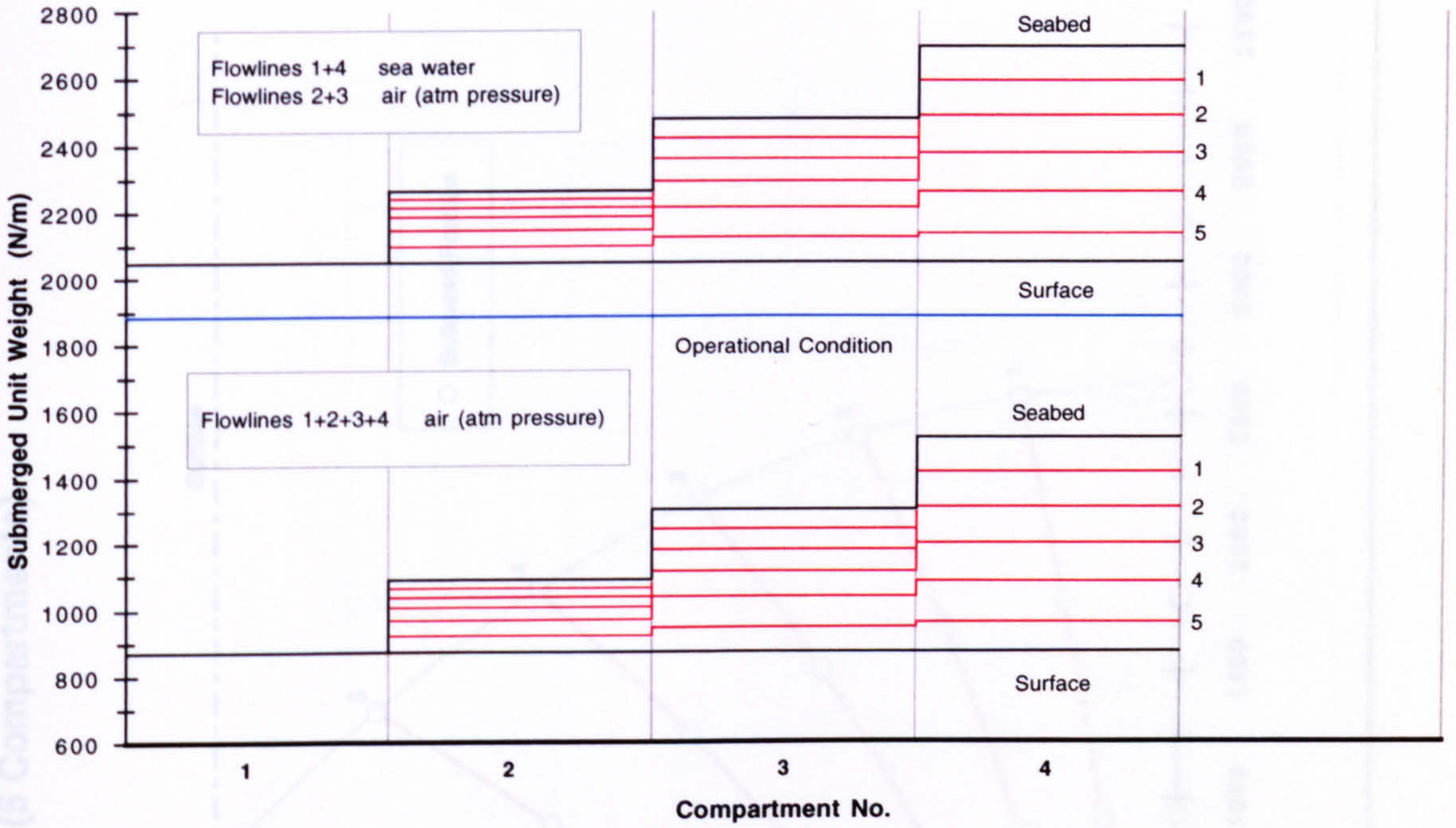

4 Compartments

Carrier Pipe Outer Diameter = 1.1 m

(b)

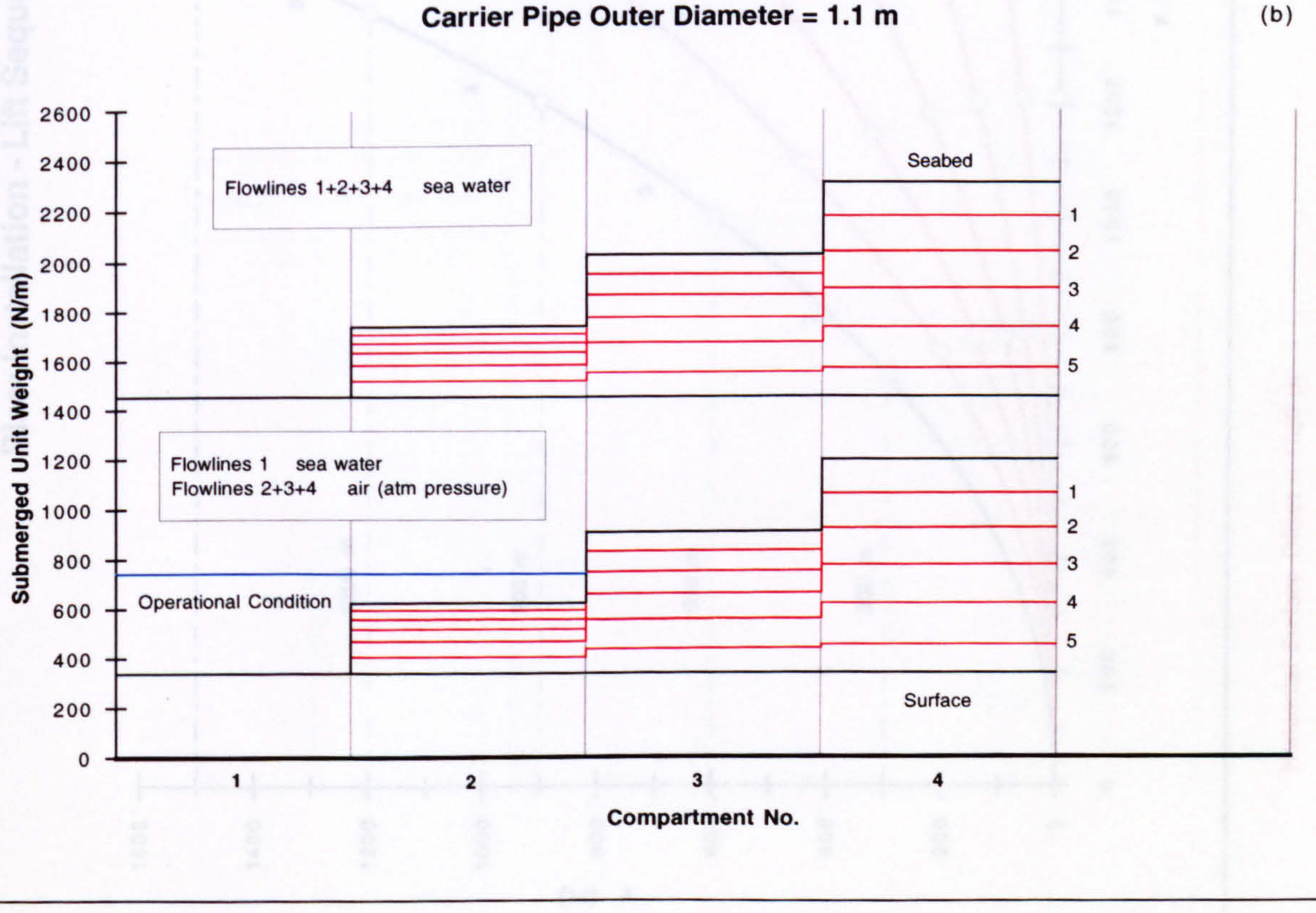

Horizontal Surface Offset = 1500 m

Carrier Pipe Wall Thickness = 10 mm

Sea Depth = 1500 m

Nitrogen Gas Temperature = 0 degs C

Figure 3.29

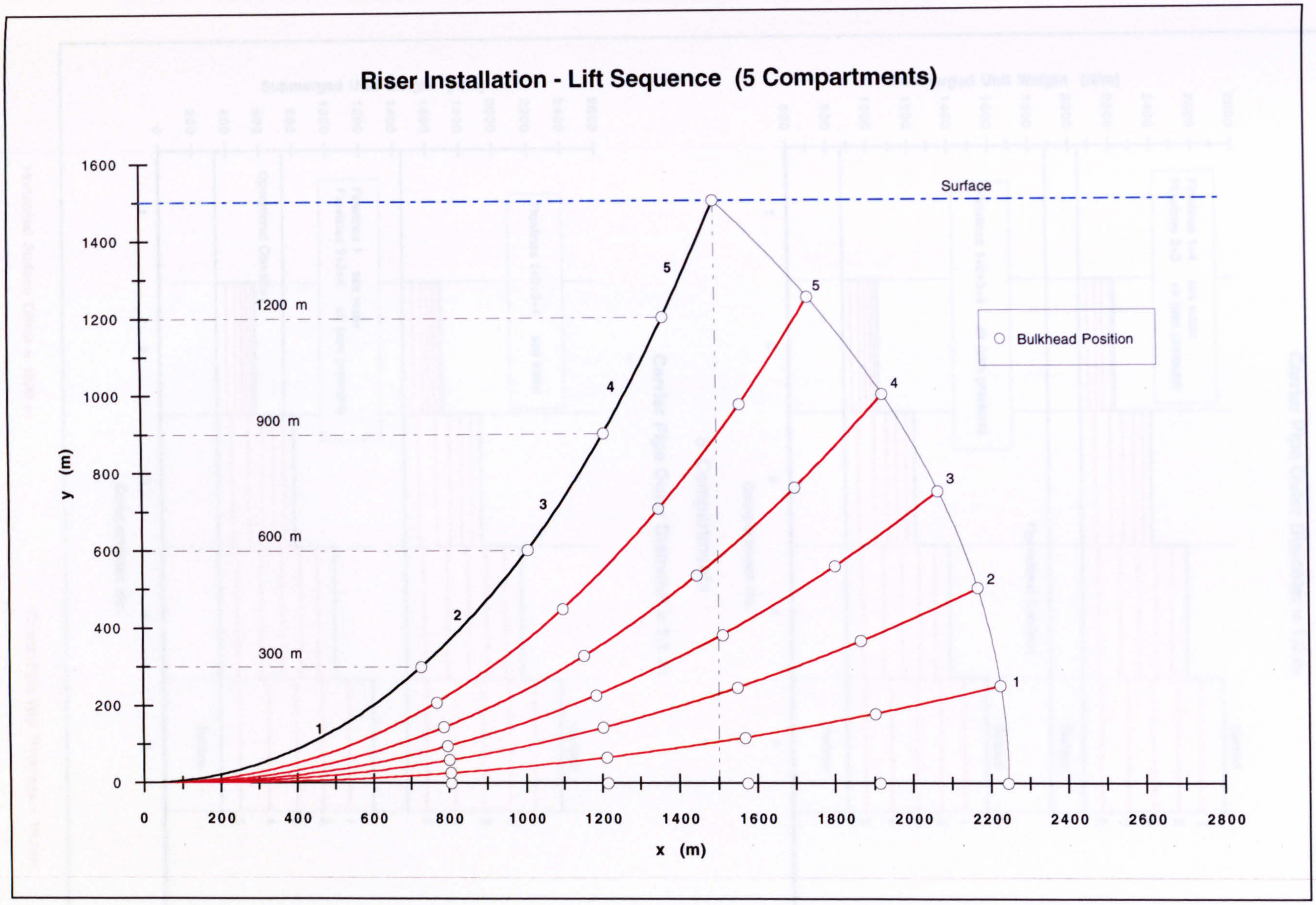

Horizontal Surface Offset = 1500 m

Sea Depth = 1500 m

Figure 3.30

Compartmental Submerged Unit Weight (Installation)

Carrier Pipe Outer Diameter = 1.0 m

(a)

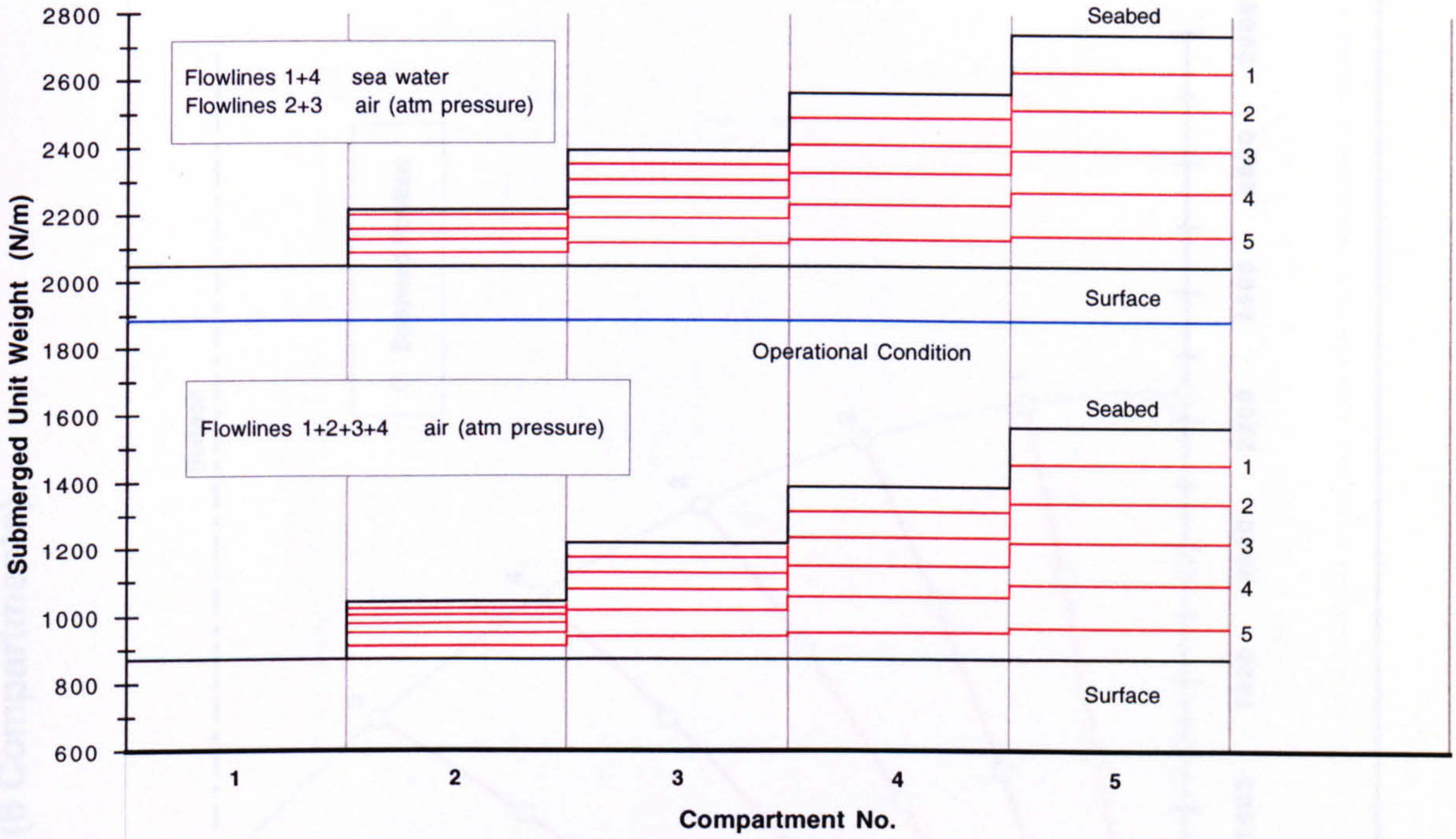

5 Compartments

Carrier Pipe Outer Diameter = 1.1 m

(b)

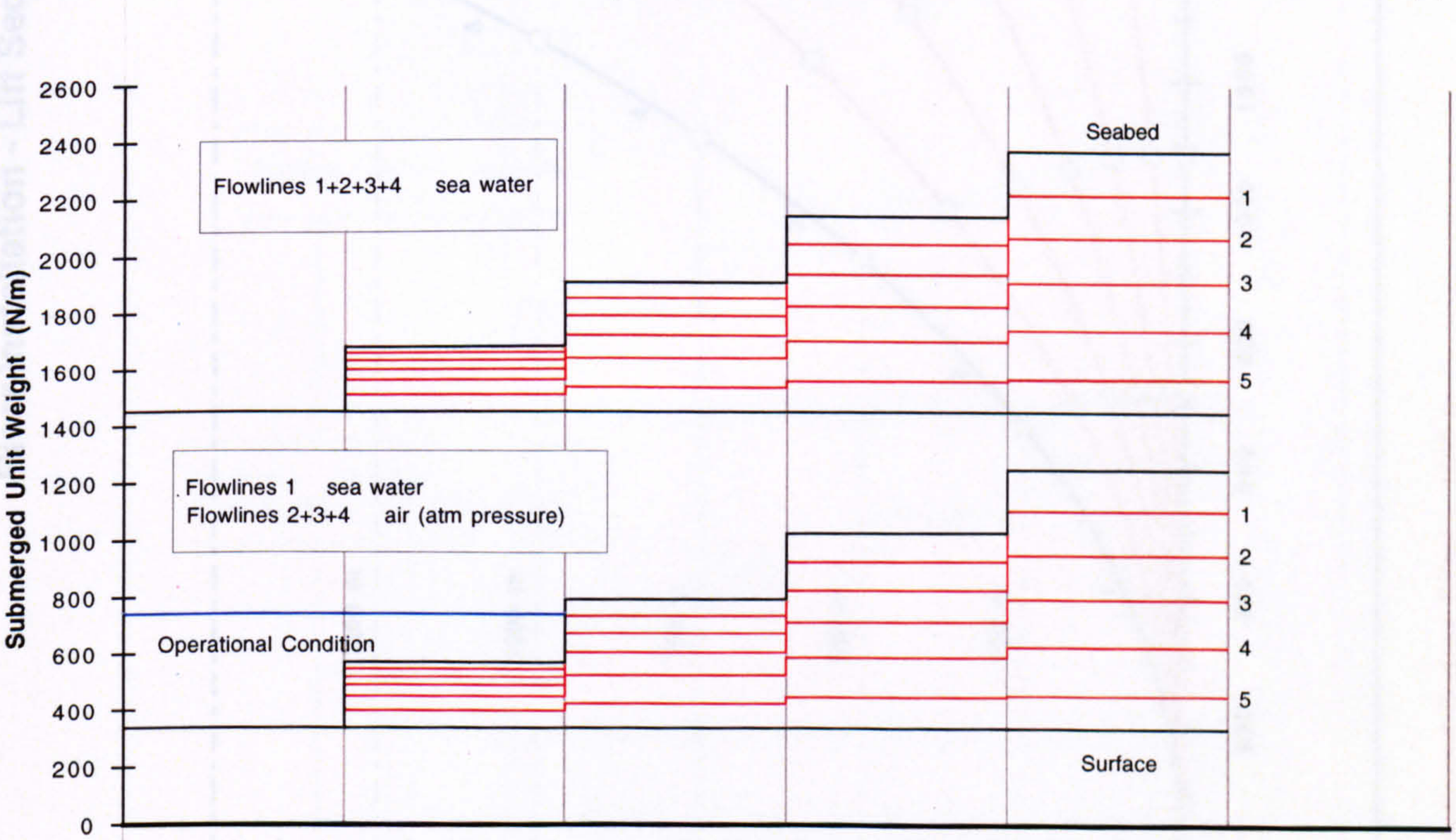

Horizontal Surface Offset = 1500 m

Carrier Pipe Wall Thickness = 10 mm

Sea Depth = 1500 m

Nitrogen Gas Temperature = 0 degs C

Figure 3.31

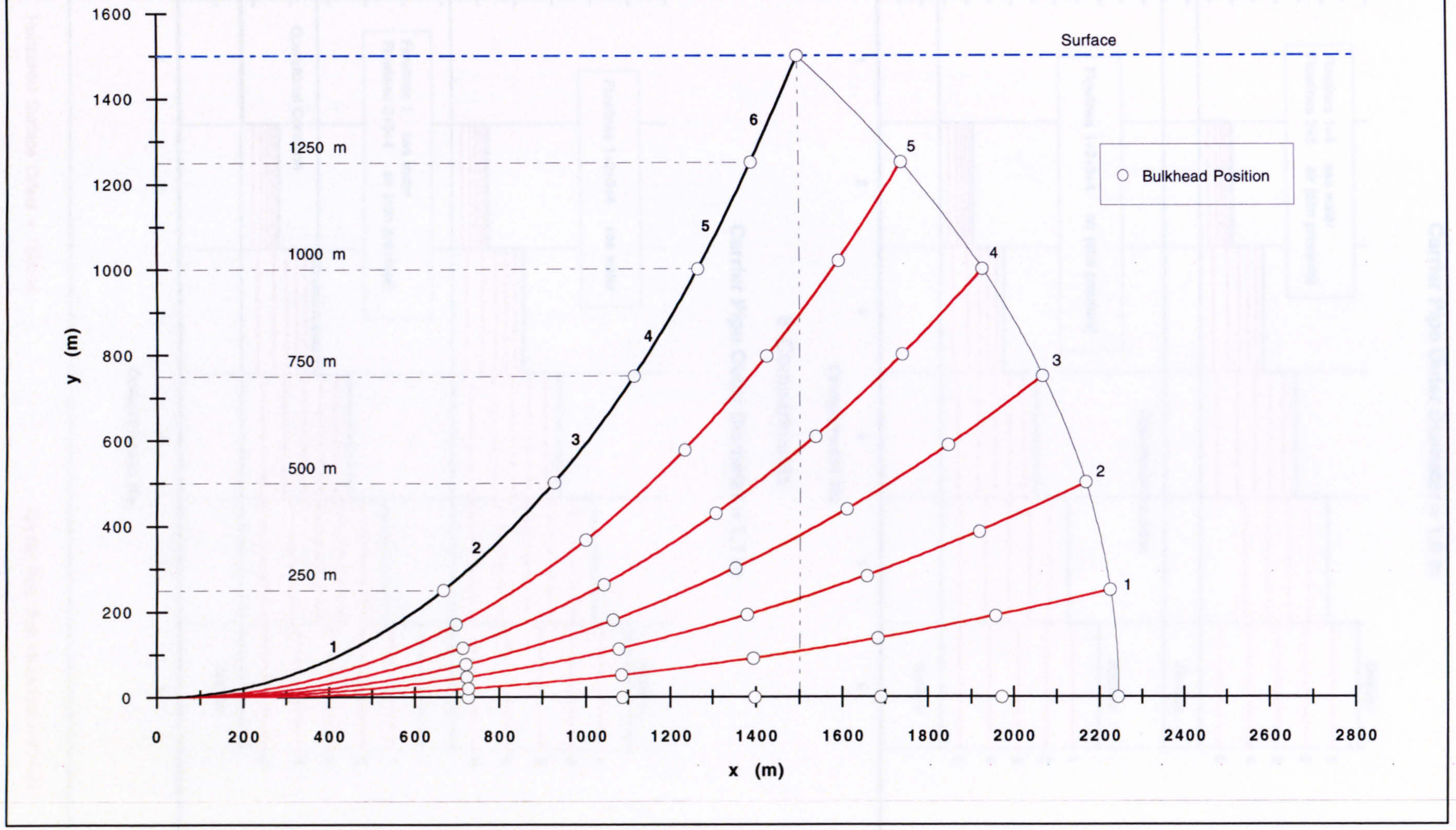

Horizontal Surface Offset = 1500 m

Sea Depth = 1500 m

Figure 3.32

Compartmental Submerged Unit Weight (Installation)

Carrier Pipe Outer Diameter = 1.0 m

(a)

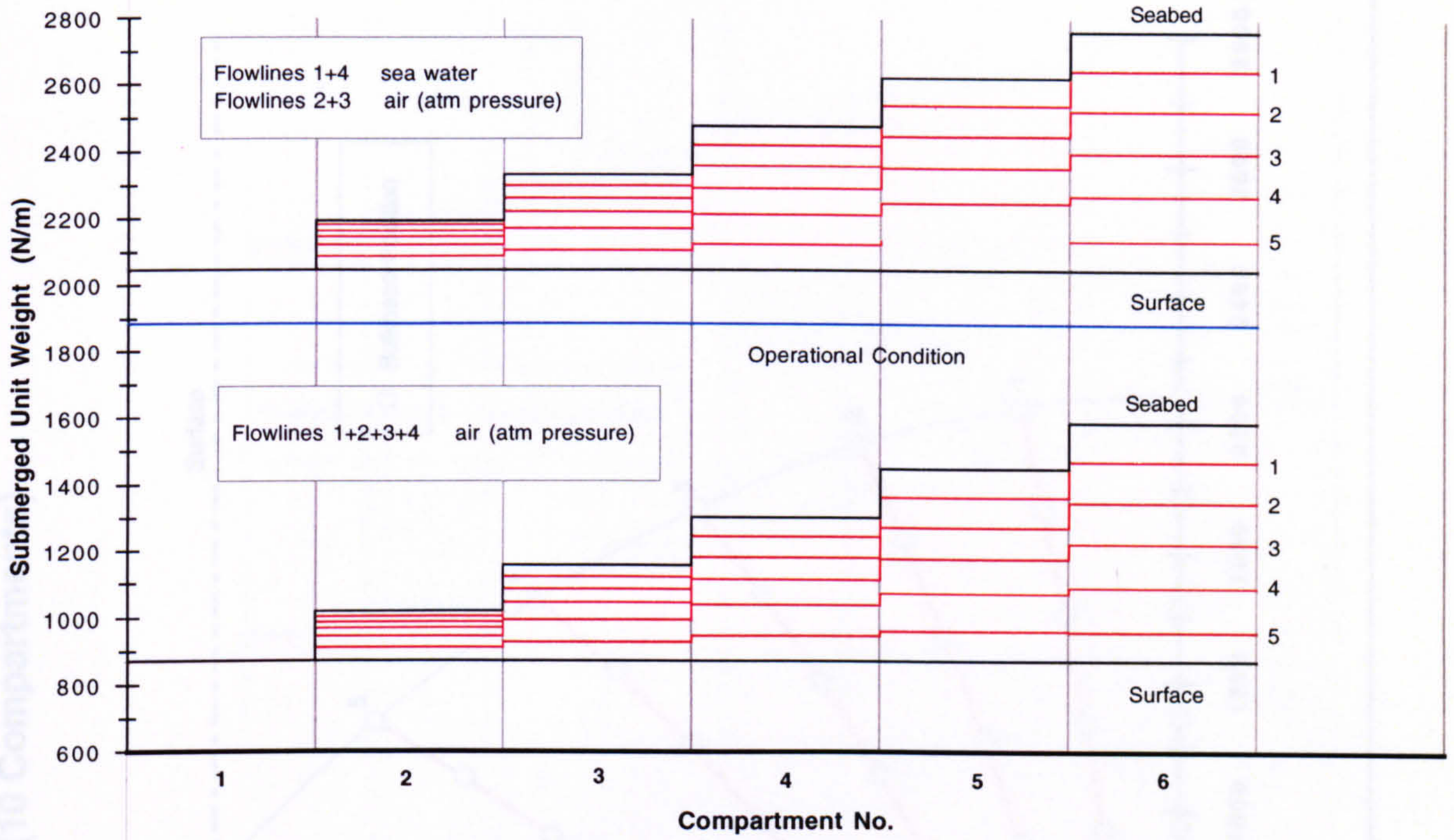

6 Compartments

Carrier Pipe Outer Diameter = 1.1 m

(b)

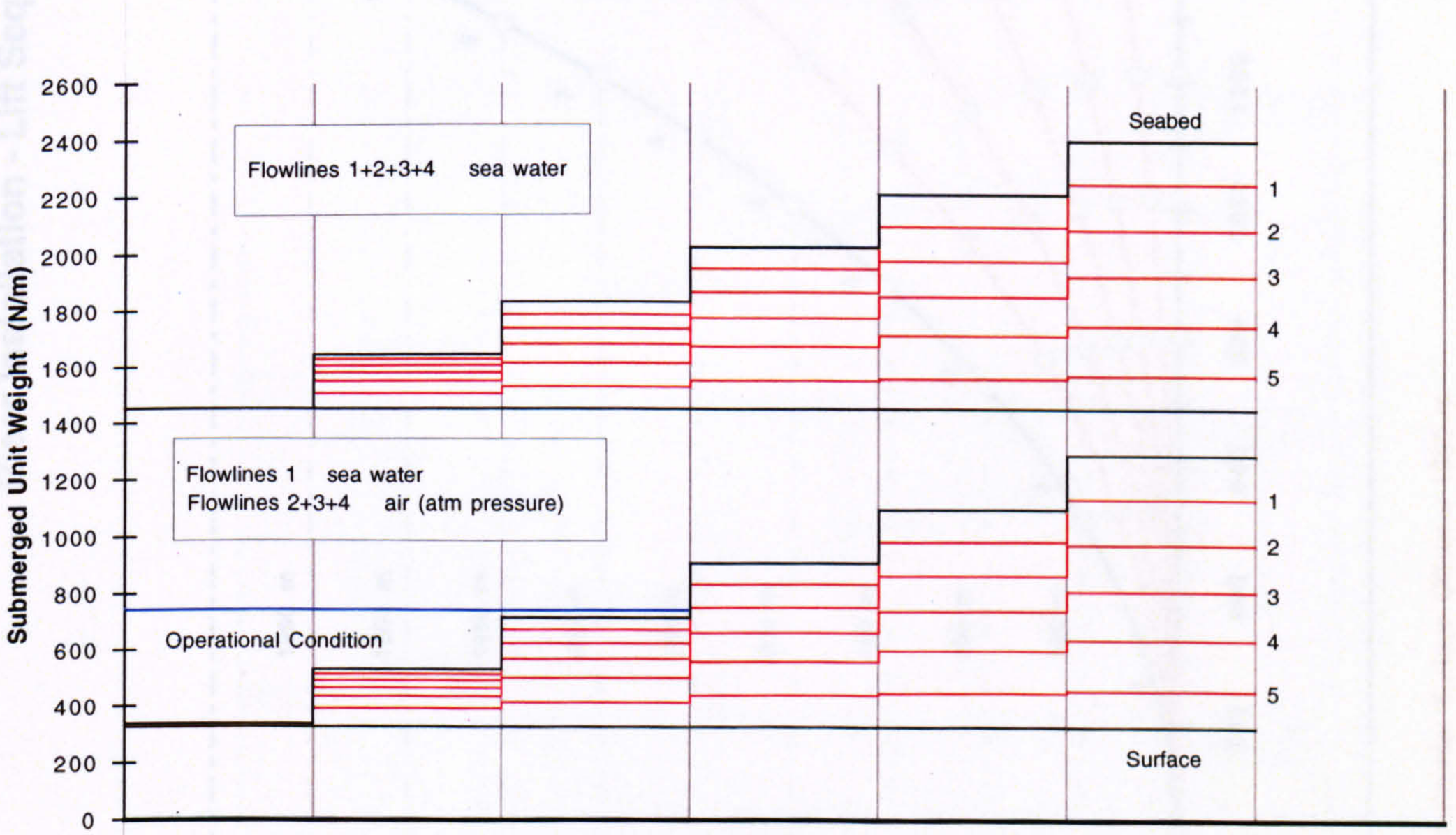

Horizontal Surface Offset = 1500 m

Carrier Pipe Wall Thickness = 10 mm

Sea Depth = 1500 m

Nitrogen Gas Temperature = 0 degs C

Figure 3.33

Riser Installation - Lift Sequence (10 Compartments)

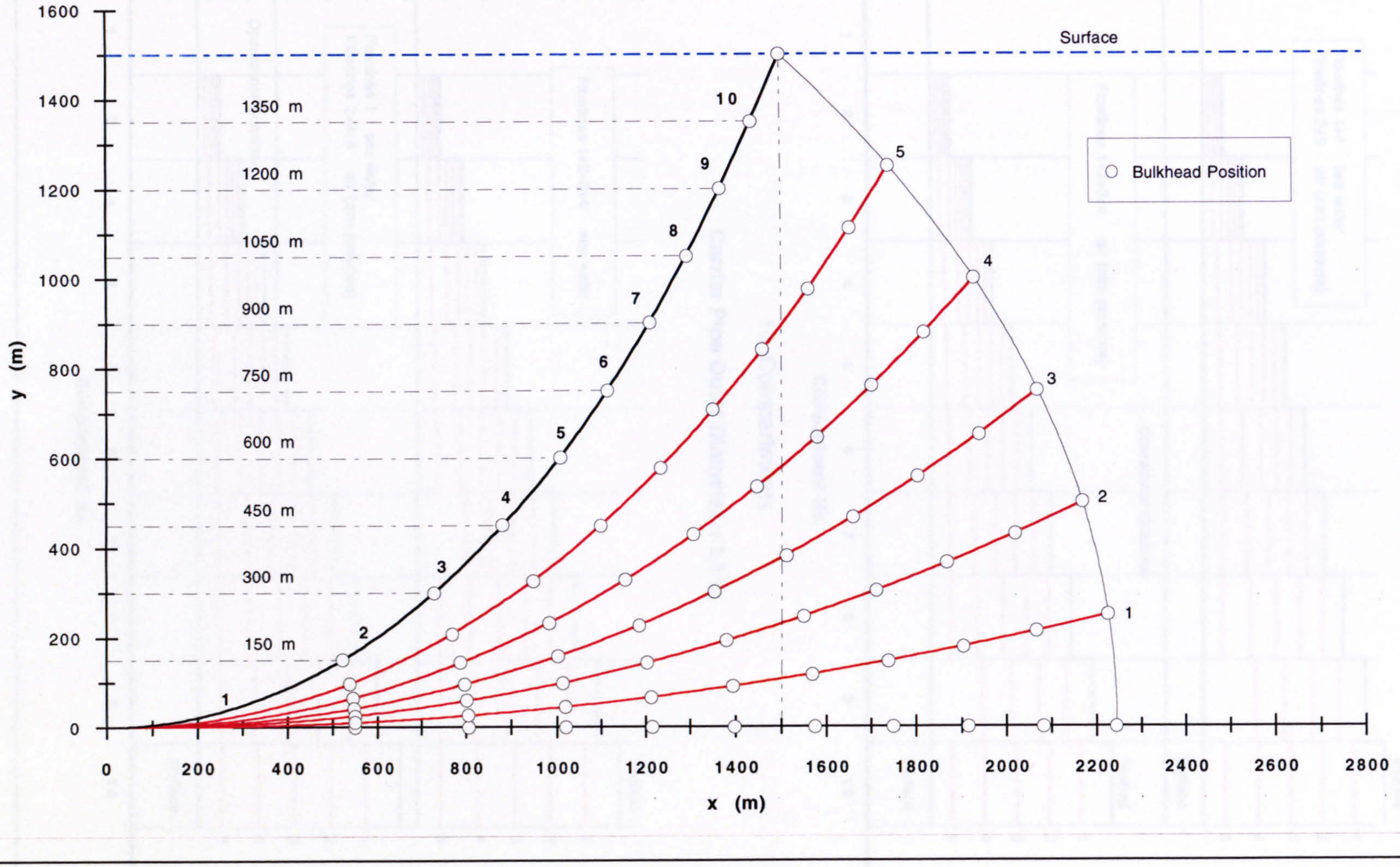

Horizontal Surface Offset = 1500 m

Sea Depth = 1500 m

Figure 3.34

Compartmental Submerged Unit Weight (Installation)

Carrier Pipe Outer Diameter = 1.0 m

(a)

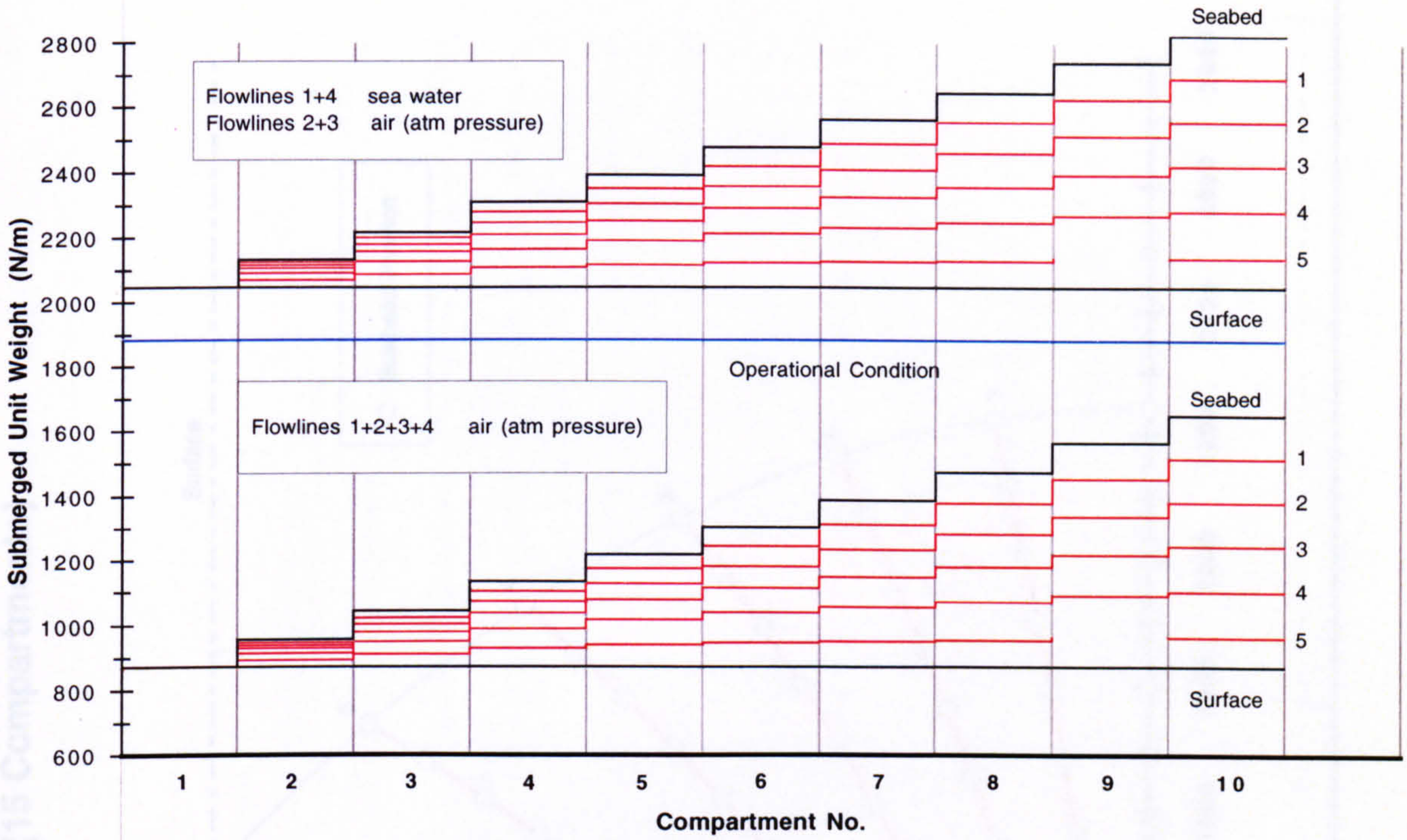

10 Compartments

Carrier Pipe Outer Diameter = 1.1 m

(b)

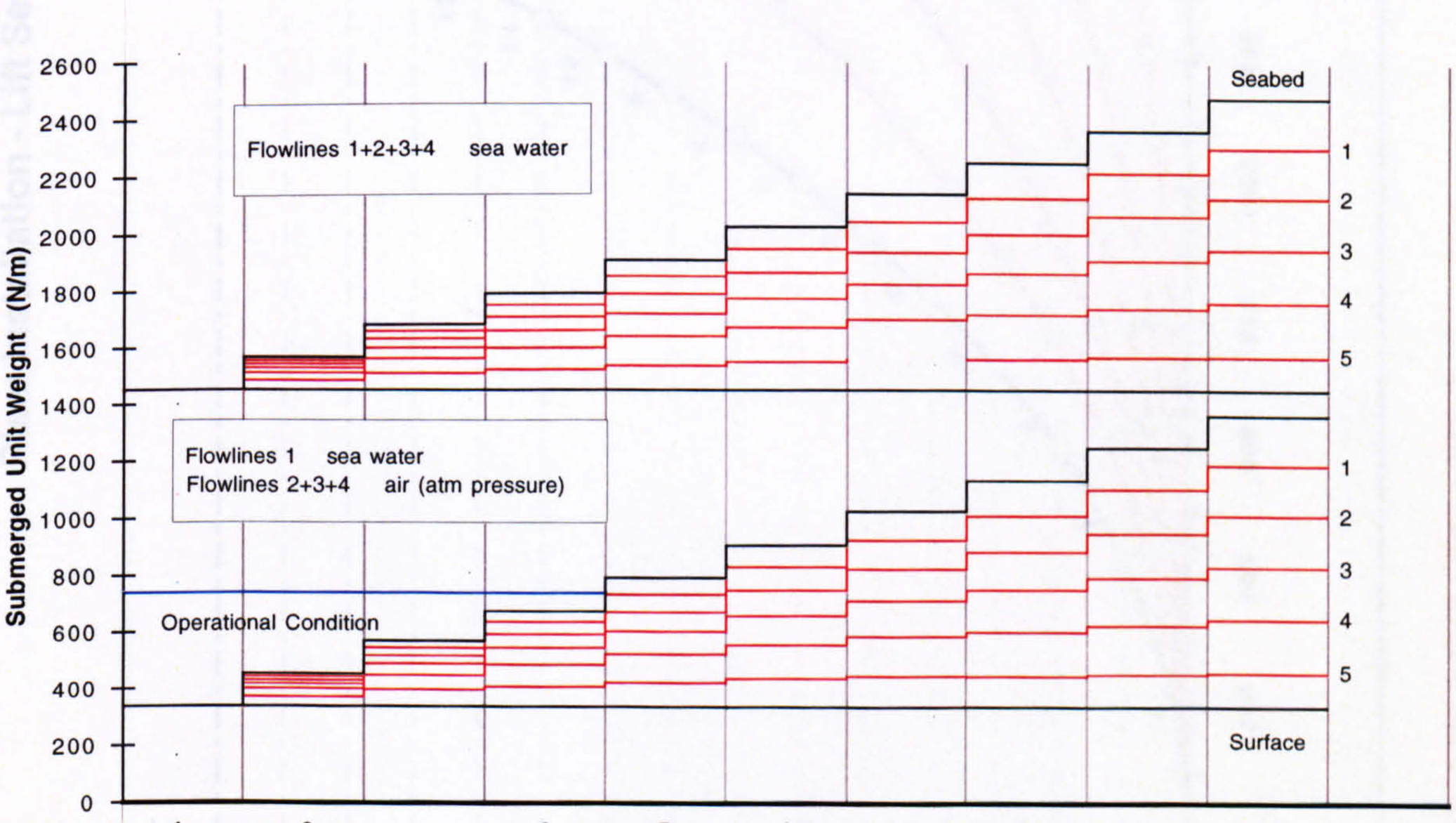

Horizontal Surface Offset = 1500 m

Carrier Pipe Wall Thickness = 10 mm

Sea Depth = 1500 m

Nitrogen Gas Temperature = 0 degs C

Figure 3.35

Riser Installation - Lift Sequence (15 Compartments)

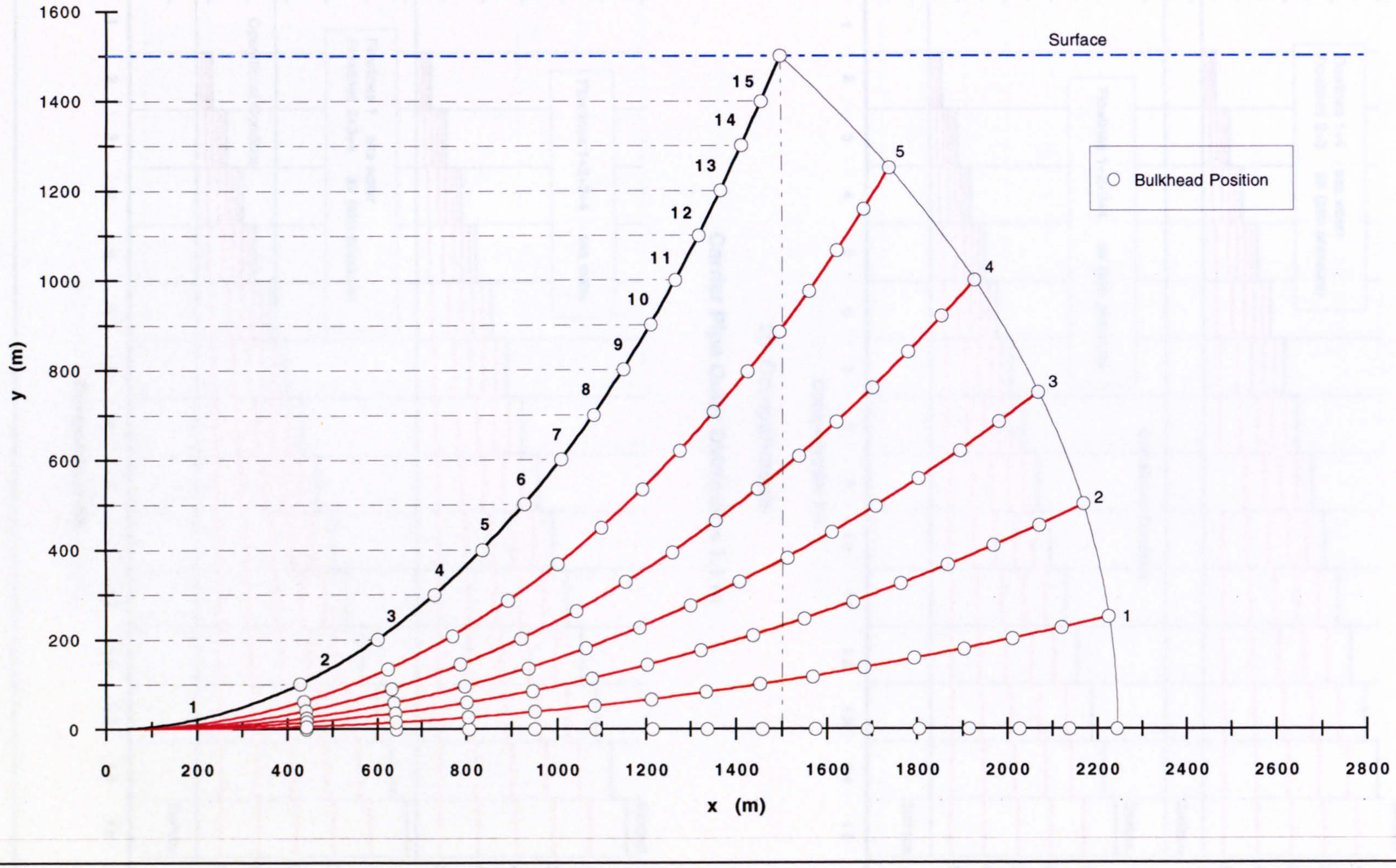

Horizontal Surface Offset = 1500 m

Sea Depth = 1500 m

Figure 3.36

Compartmental Submerged Unit Weight (Installation)

Carrier Pipe Outer Diameter = 1.0 m

(a)

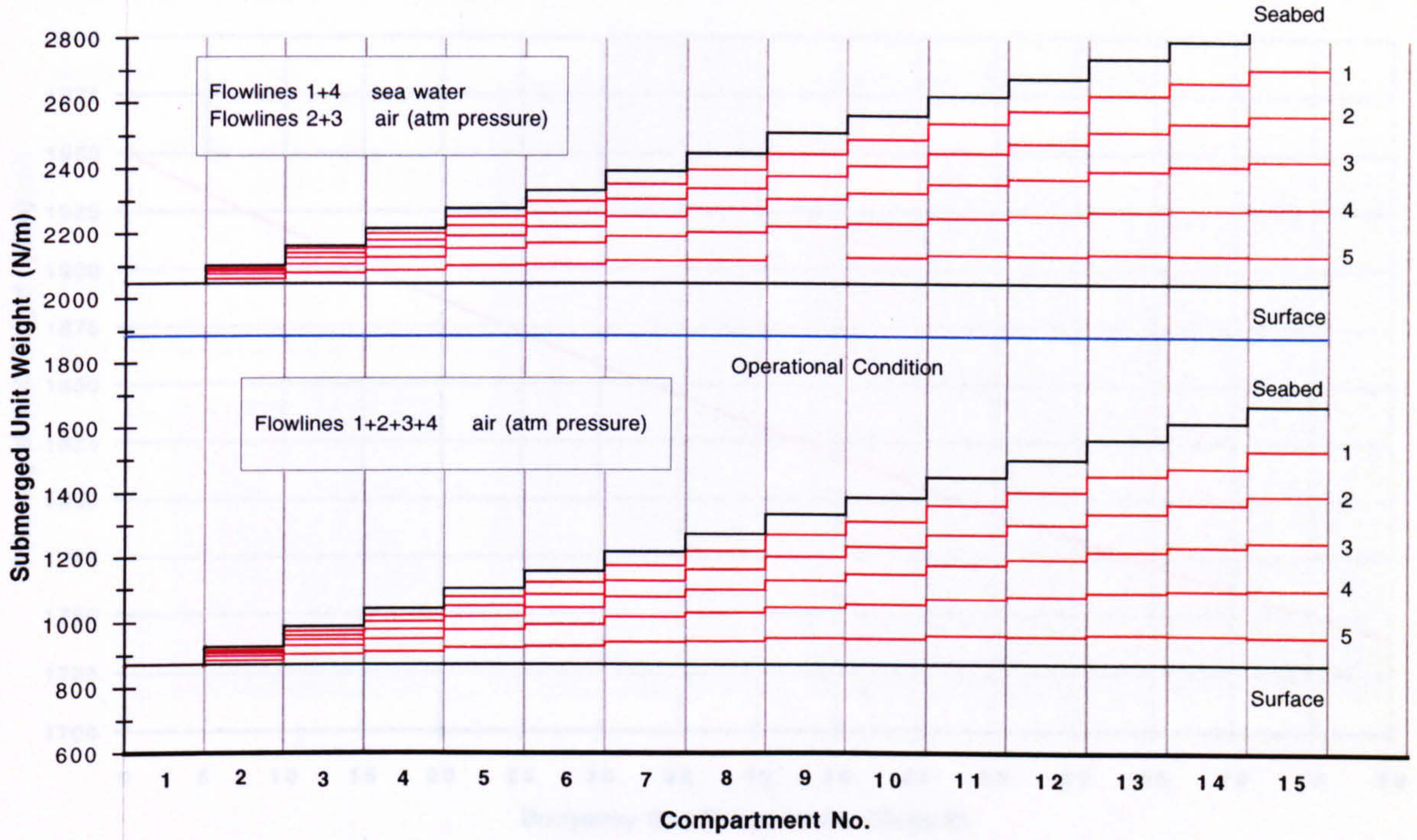

15 Compartments

Carrier Pipe Outer Diameter = 1.1 m

(b)

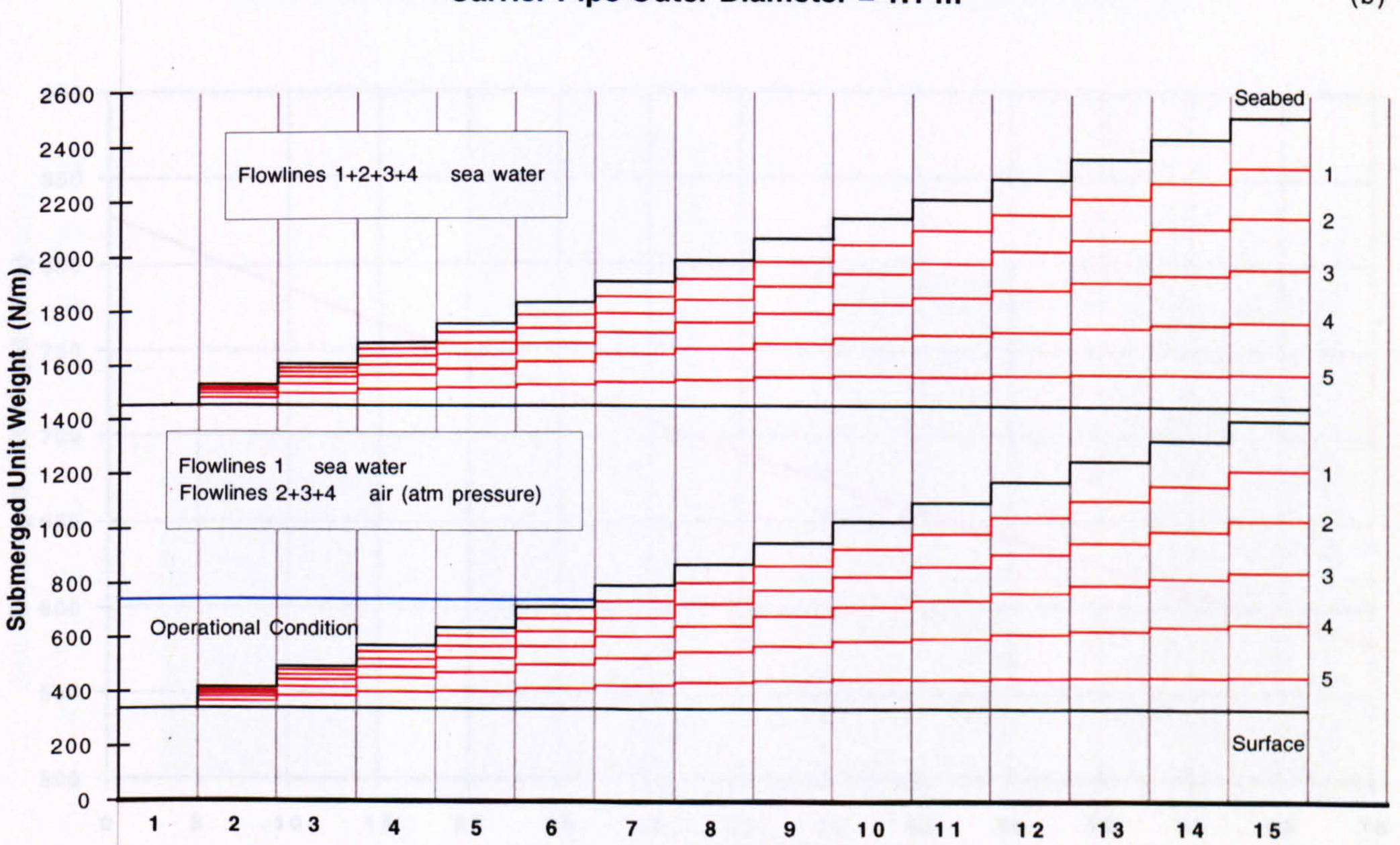

Horizontal Surface Offset = 1500 m

Sea Depth = 1500 m

Carrier Pipe Wall Thickness = 10 mm

Nitrogen Gas Temperature = 0 degs C

Figure 3.37

The Effects of Gas Temperature on Submerged Unit Weight

Carrier Pipe Outer Diameter = 1.0 m (a)

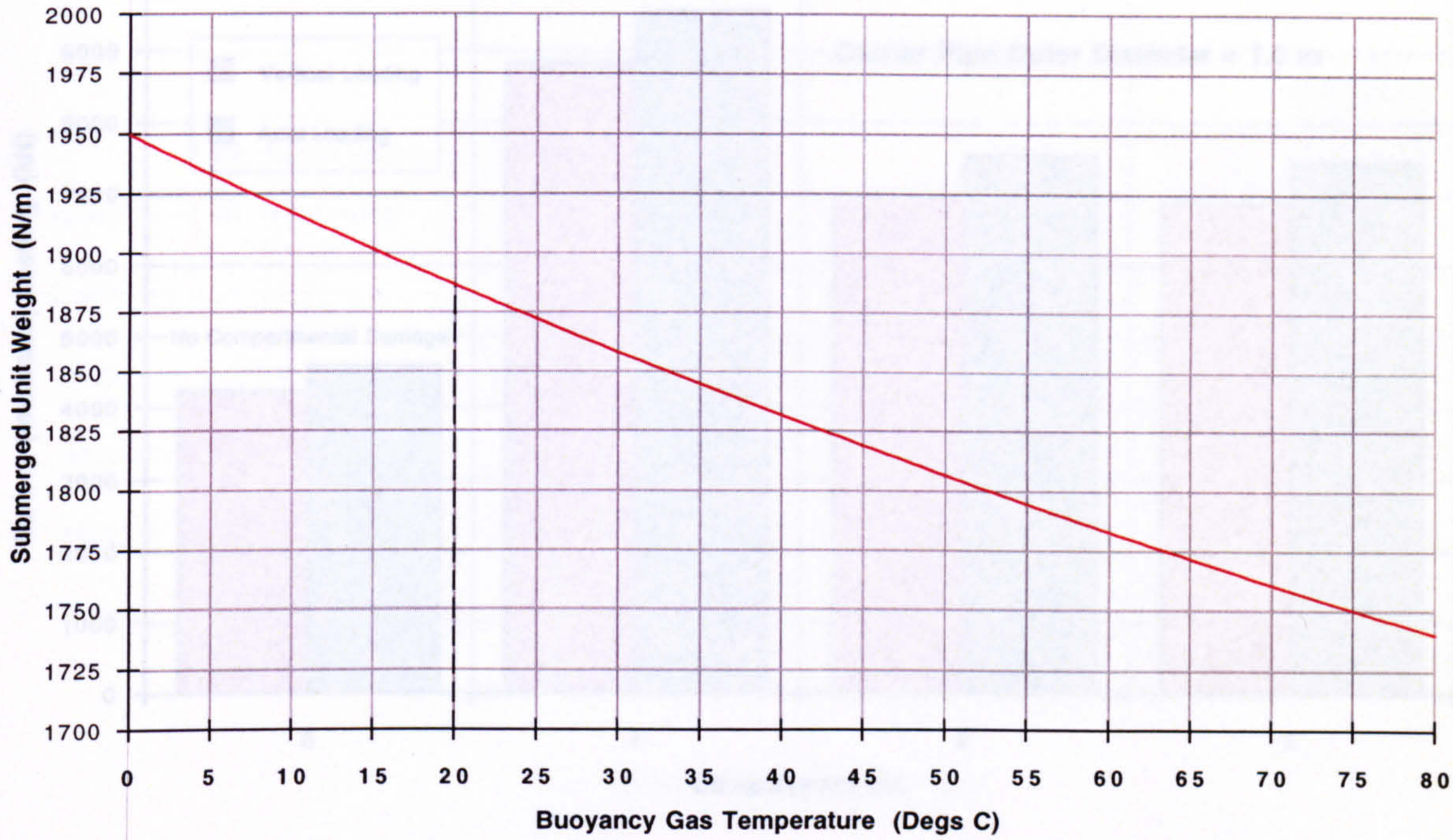

Carrier Pipe Outer Diameter = 1.1 m (b)

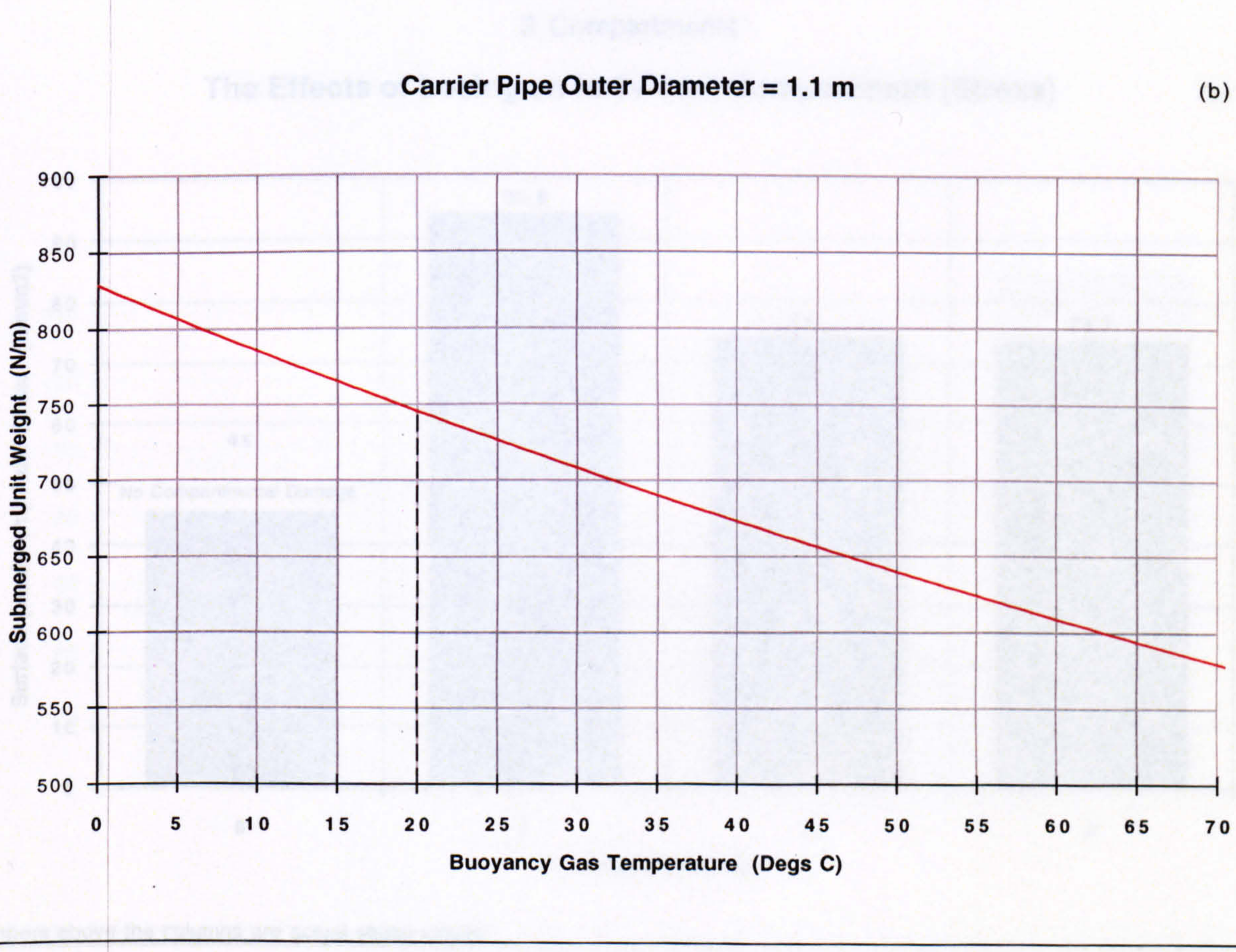

Horizontal Surface Offset = 1500 m

Carrier Pipe Wall Thickness = 10 mm

Sea Depth = 1500 m

Figure 3.38

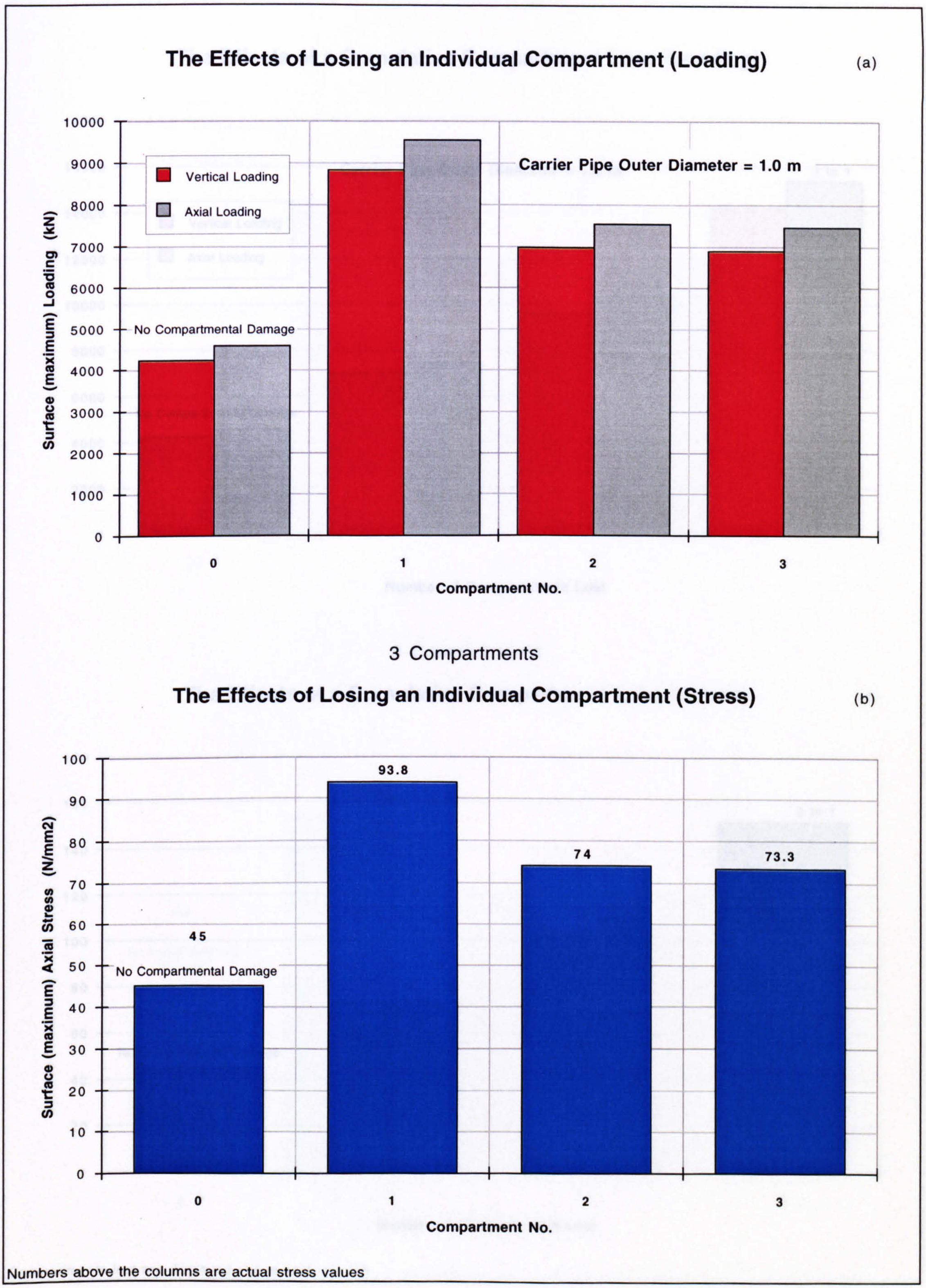

Horizontal Surface Offset = 1500 m

Carrier Pipe Wall Thickness = 10 mm

Sea Depth = 1500 m

Figure 3.39

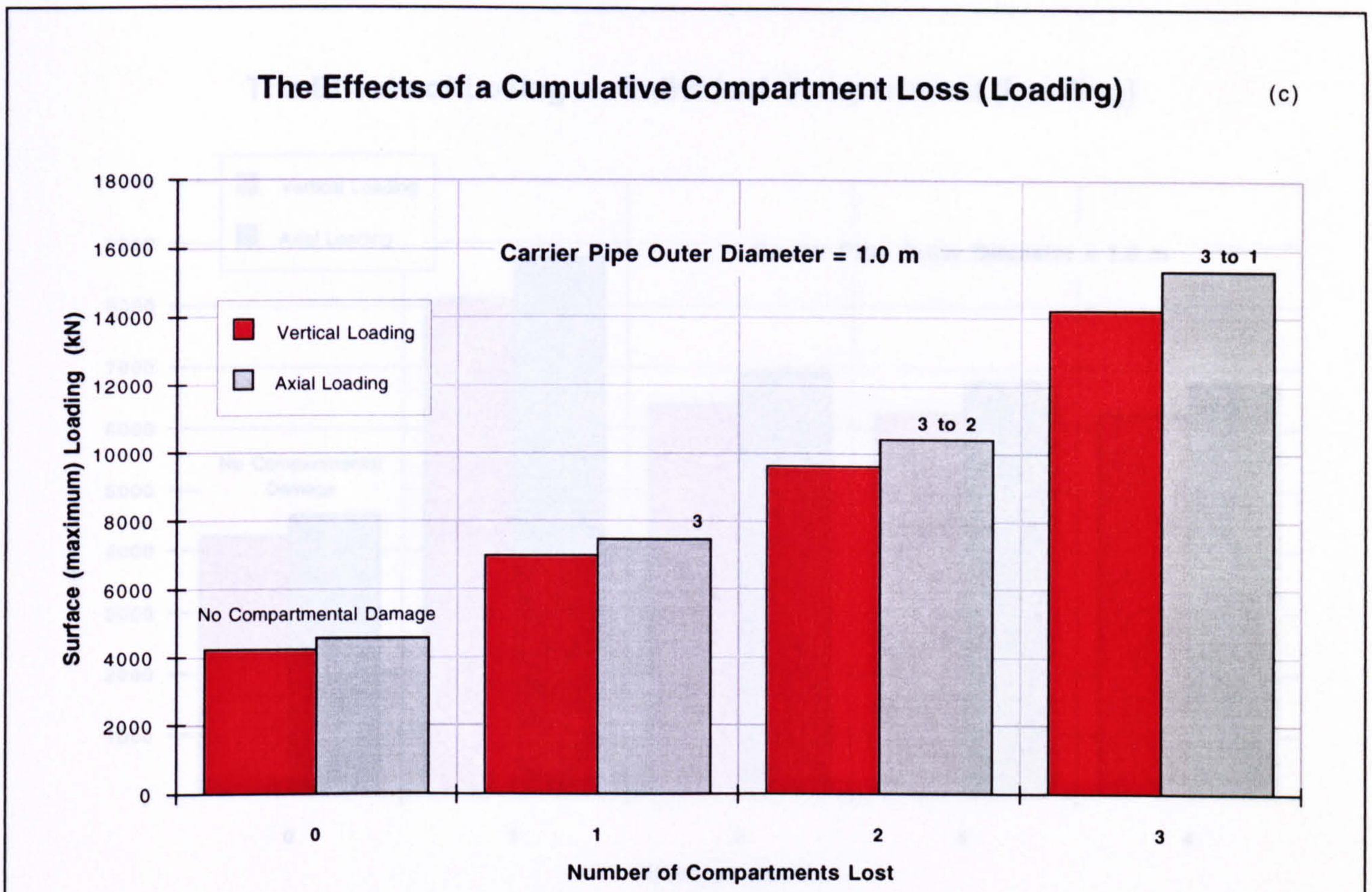

3 Compartments

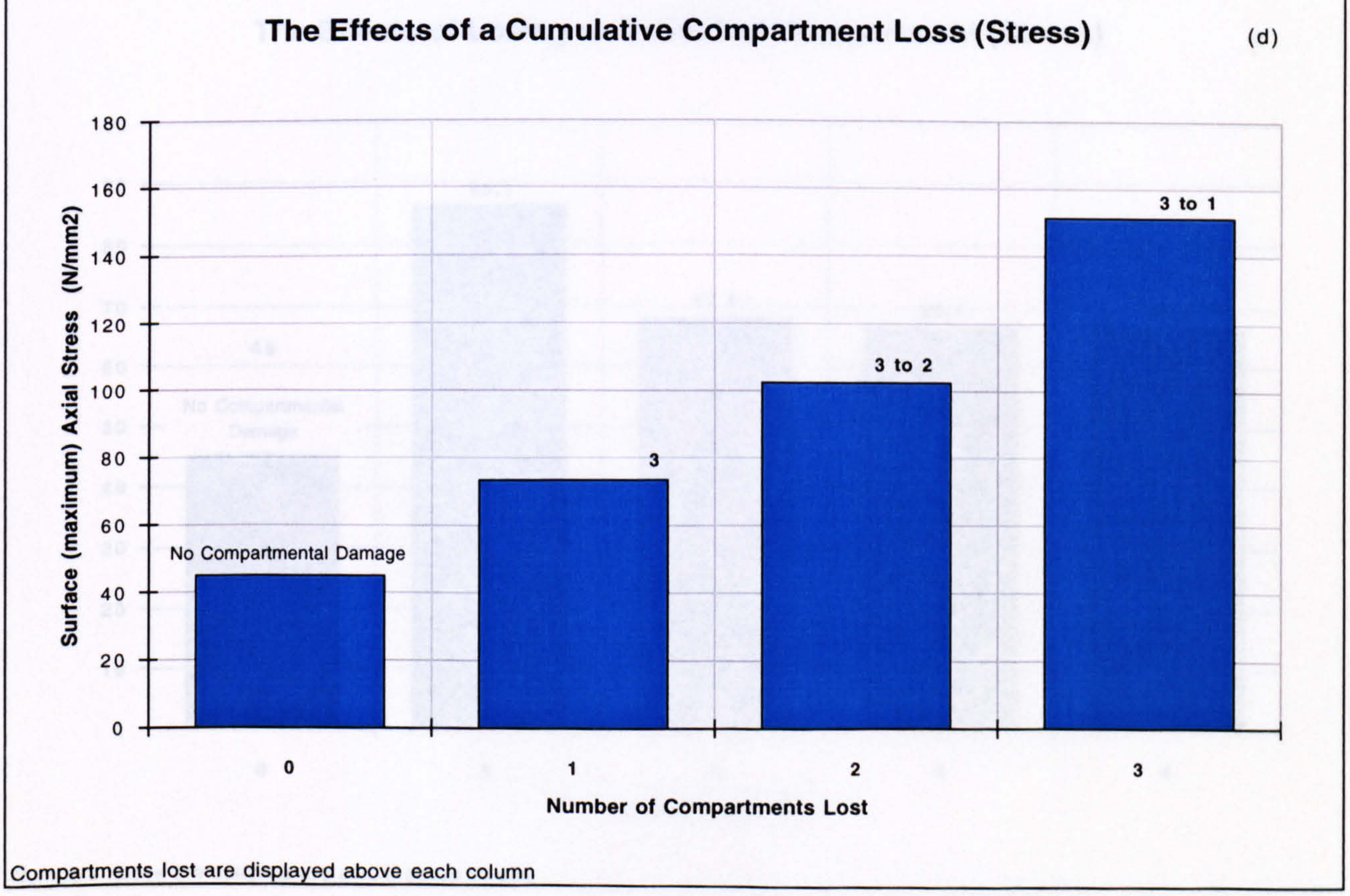

Horizontal Surface Offset = 1500 m

Carrier Pipe Wall Thickness = 10 mm

Sea Depth = 1500 m

Figure 3.39

The Effects of Losing an Individual Compartment (Loading)

(a)

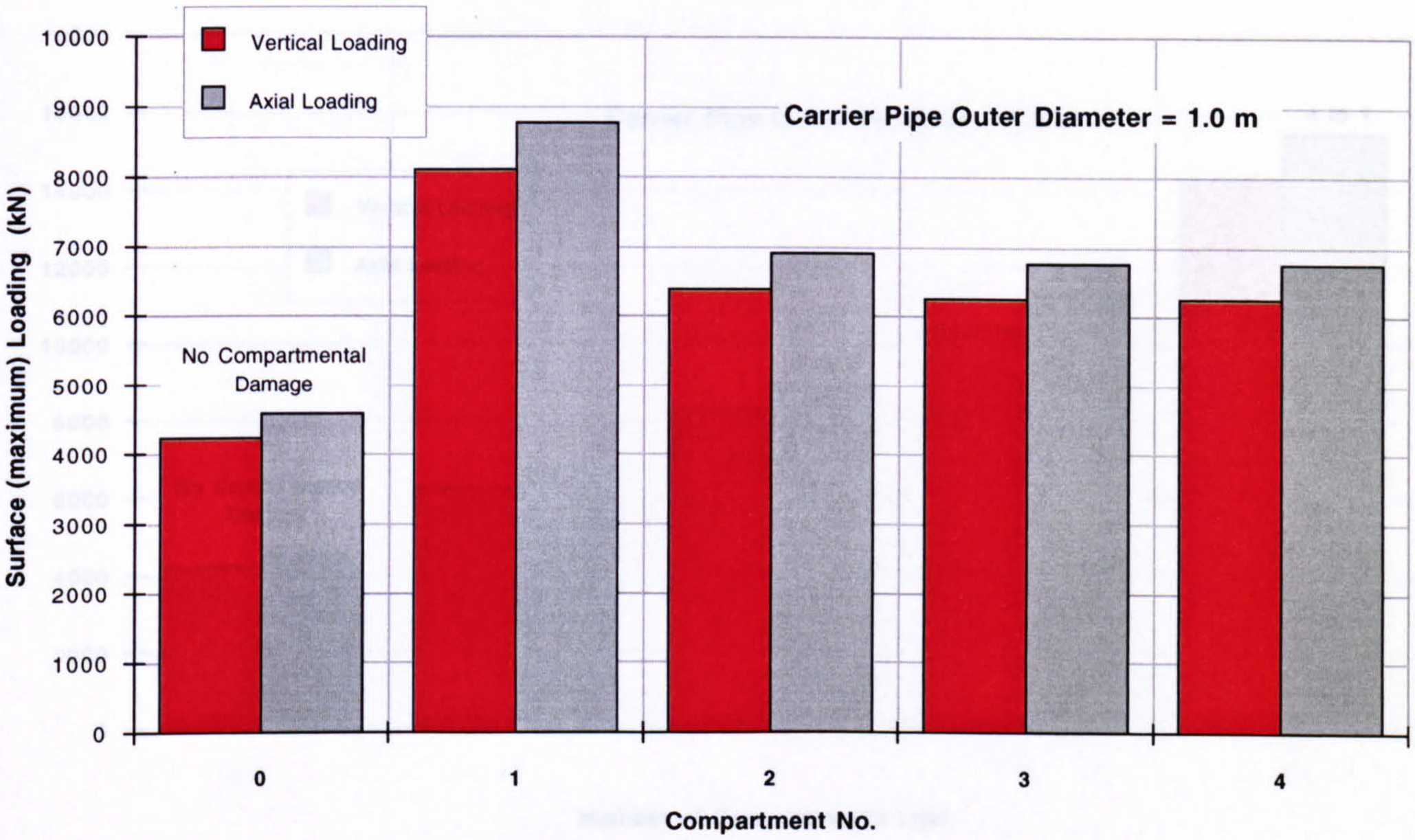

4 Compartments

The Effects of Losing an Individual Compartment (Stress)

(b)

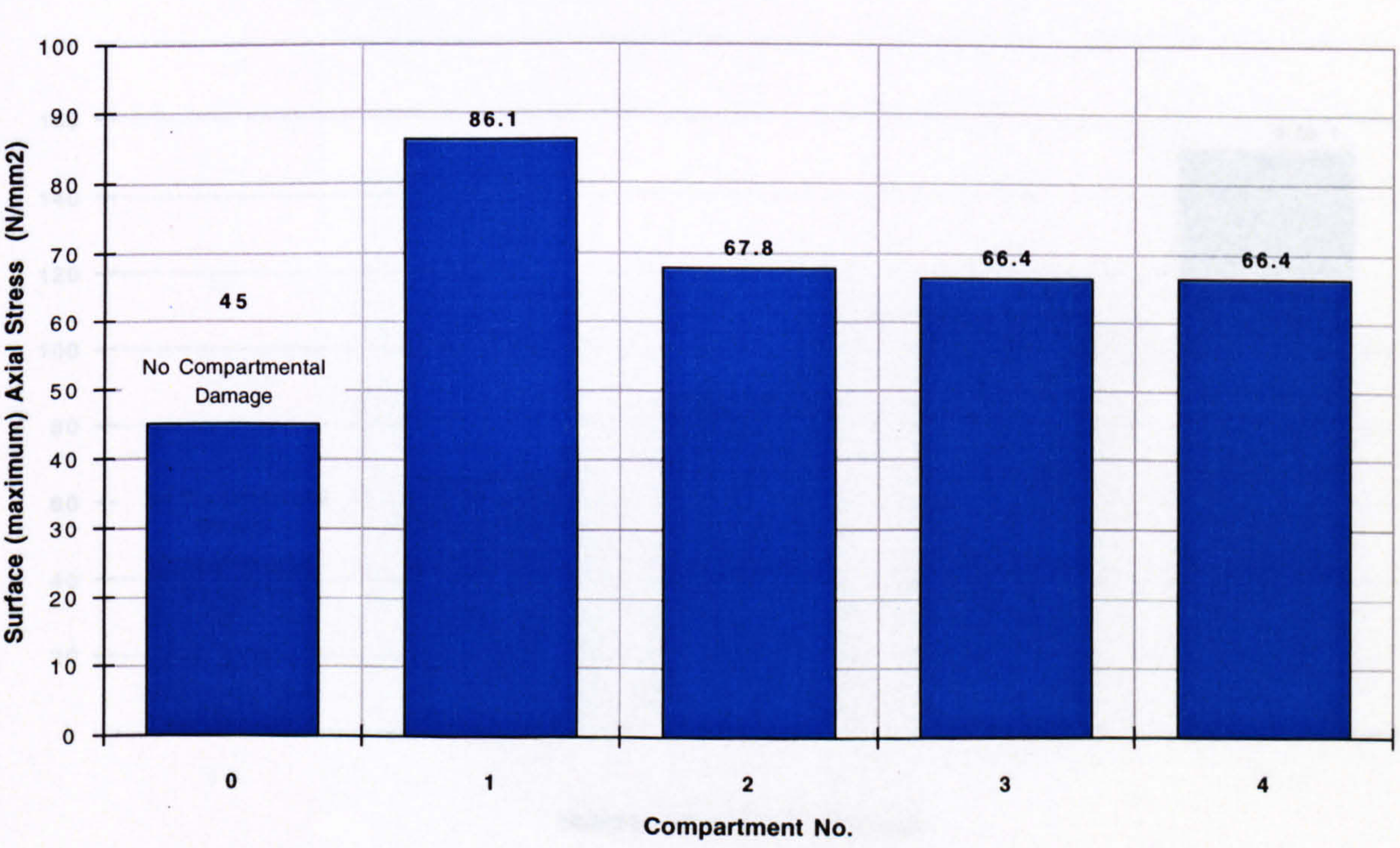

Numbers above the columns are actual stress values

Horizontal Surface Offset = 1500 m

Carrier Pipe Wall Thickness = 10 mm

Sea Depth = 1500 m

Figure 3.40

The Effects of a Cumulative Compartment Loss (Loading)

(c)

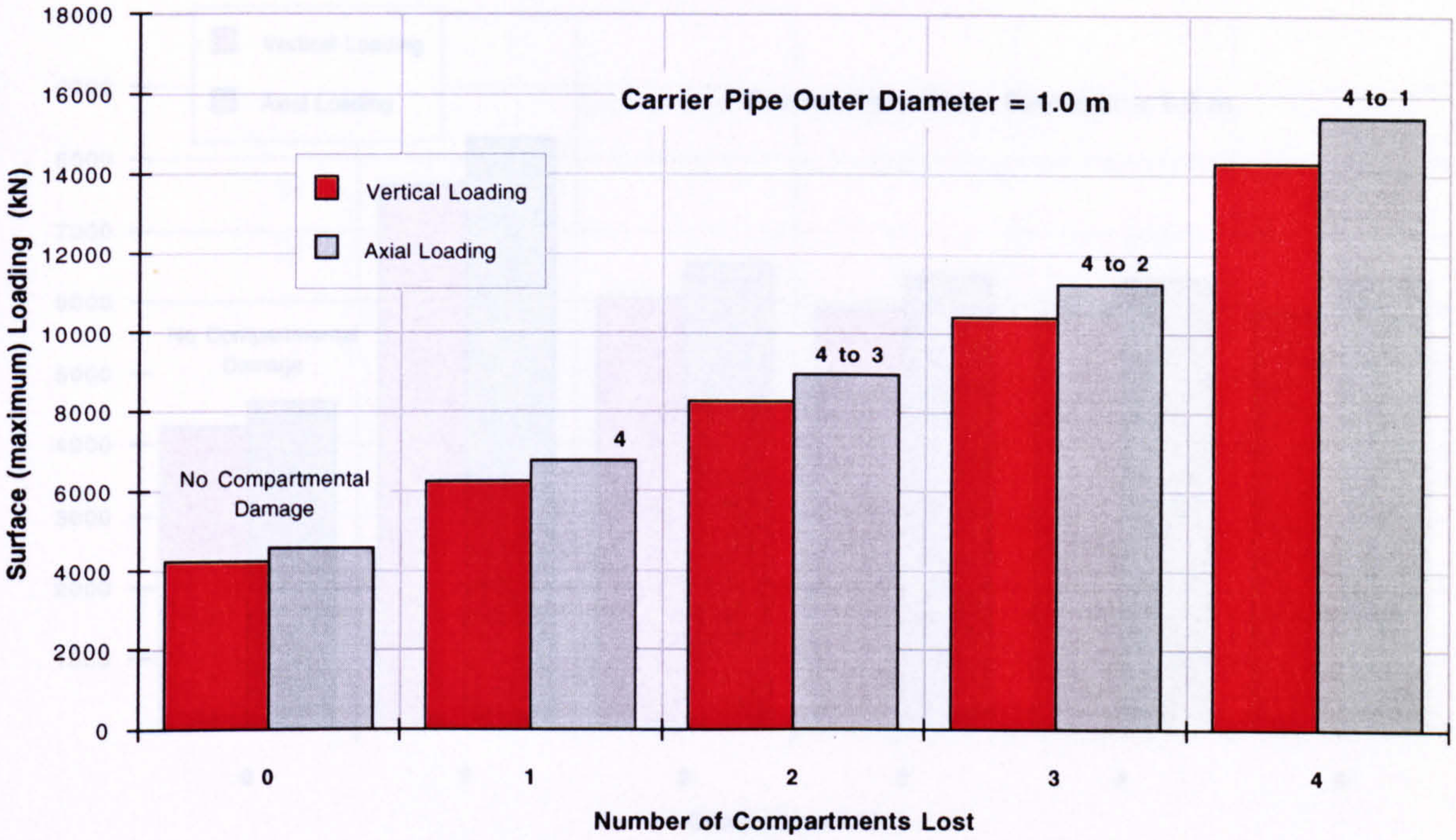

4 Compartments

The Effects of a Cumulative Compartment Loss (Stress)

(d)

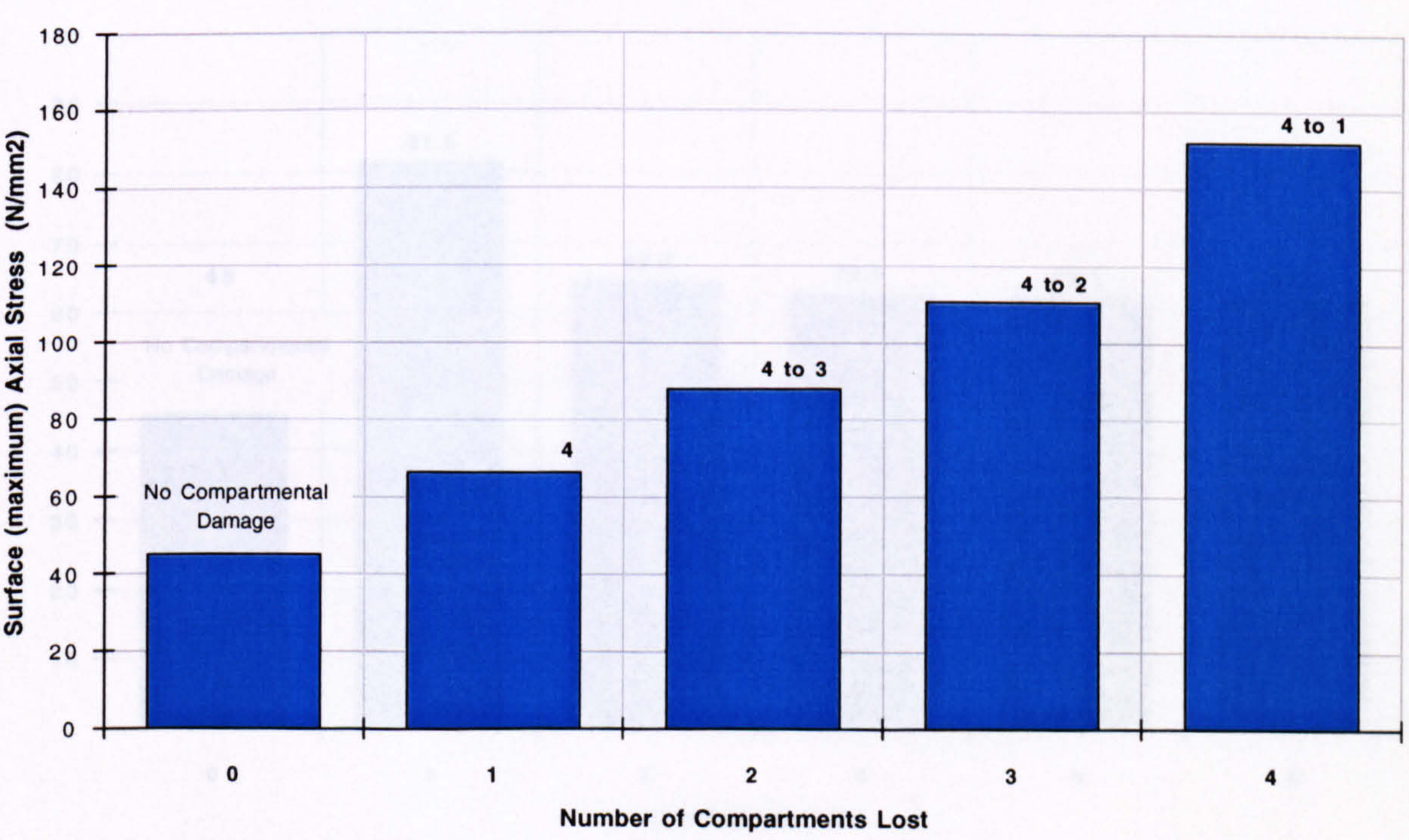

Compartments lost are displayed above each column

Horizontal Surface Offset = 1500 m

Carrier Pipe Wall Thickness = 10 mm

Sea Depth = 1500 m

Figure 3.40

The Effects of Losing an Individual Compartment (Loading)

(a)

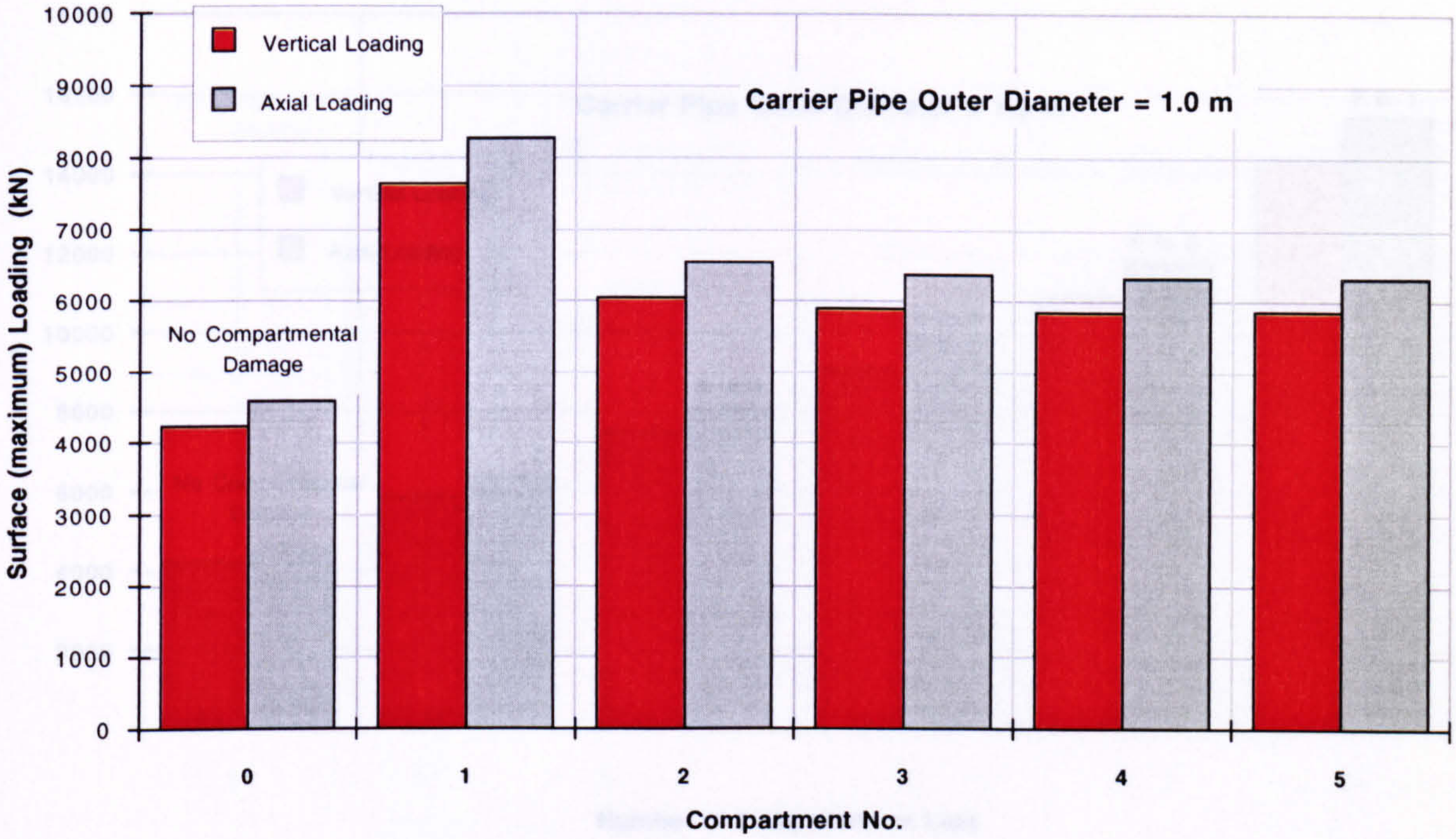

5 Compartments

The Effects of Losing an Individual Compartment (Stress)

(b)

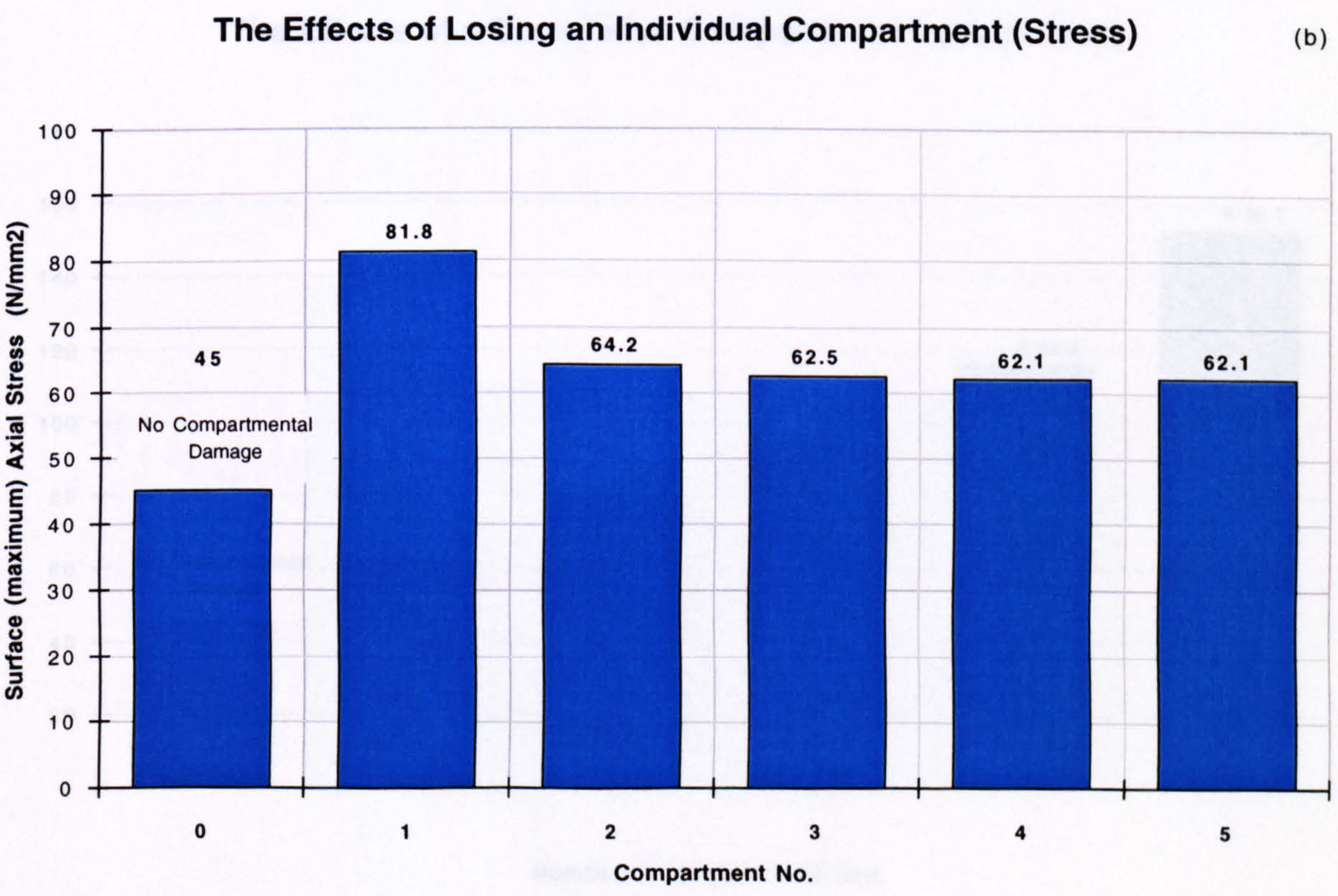

Numbers above the columns are actual stress values

Horizontal Surface Offset = 1500 m

Carrier Pipe Wall Thickness = 10 mm

Sea Depth = 1500 m

Figure 3.41

The Effects of a Cumulative Compartment Loss (Loading)

(c)

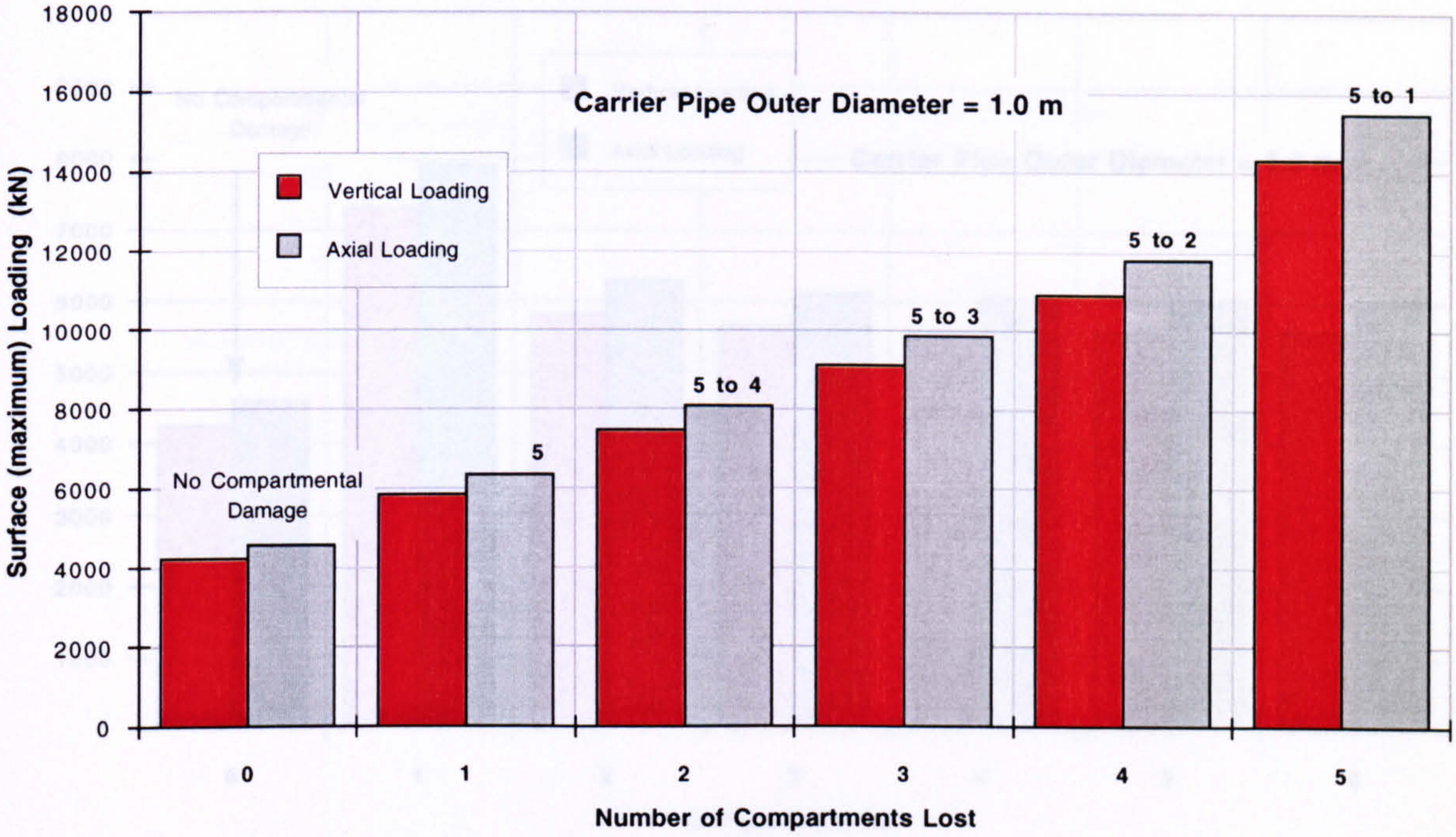

5 Compartments

The Effects of a Cumulative Compartment Loss (Stress)

(d)

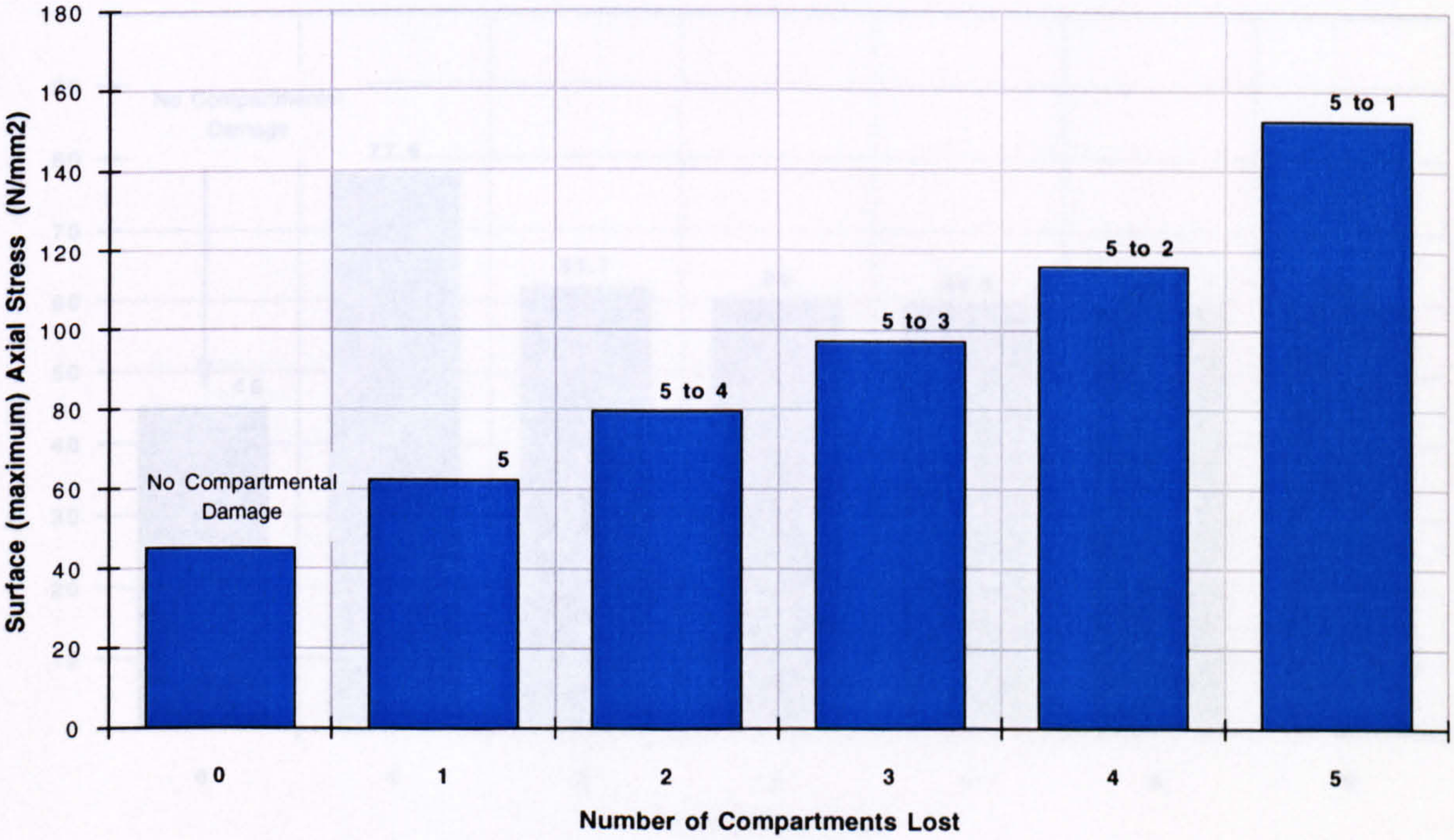

Compartments lost are displayed above each column

Horizontal Surface Offset = 1500 m

Carrier Pipe Wall Thickness = 10 mm

Sea Depth = 1500 m

Figure 3.41

The Effects of Losing an Individual Compartment (Loading)

(a)

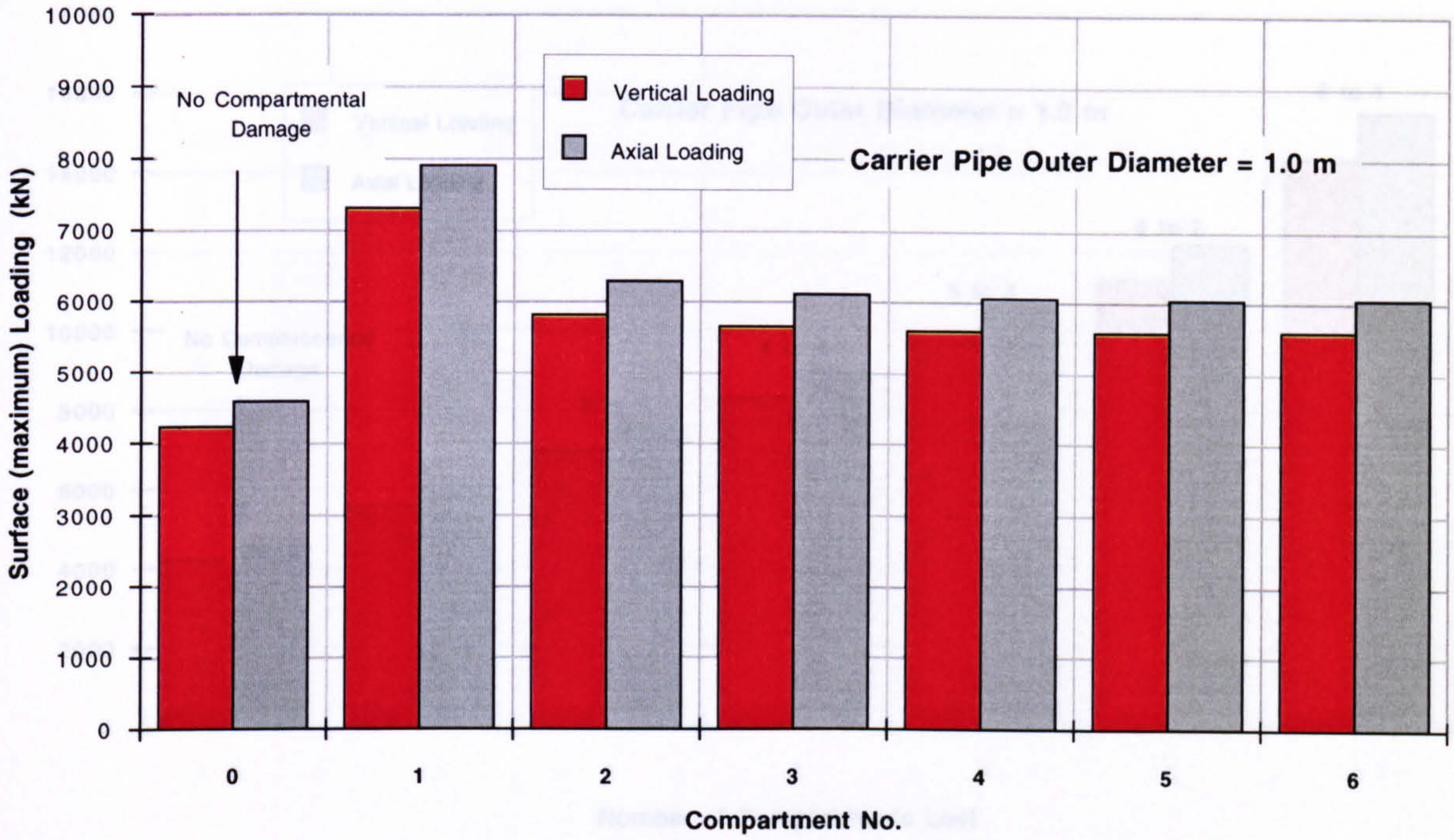

6 Compartments

The Effects of Losing an Individual Compartment (Stress)

(b)

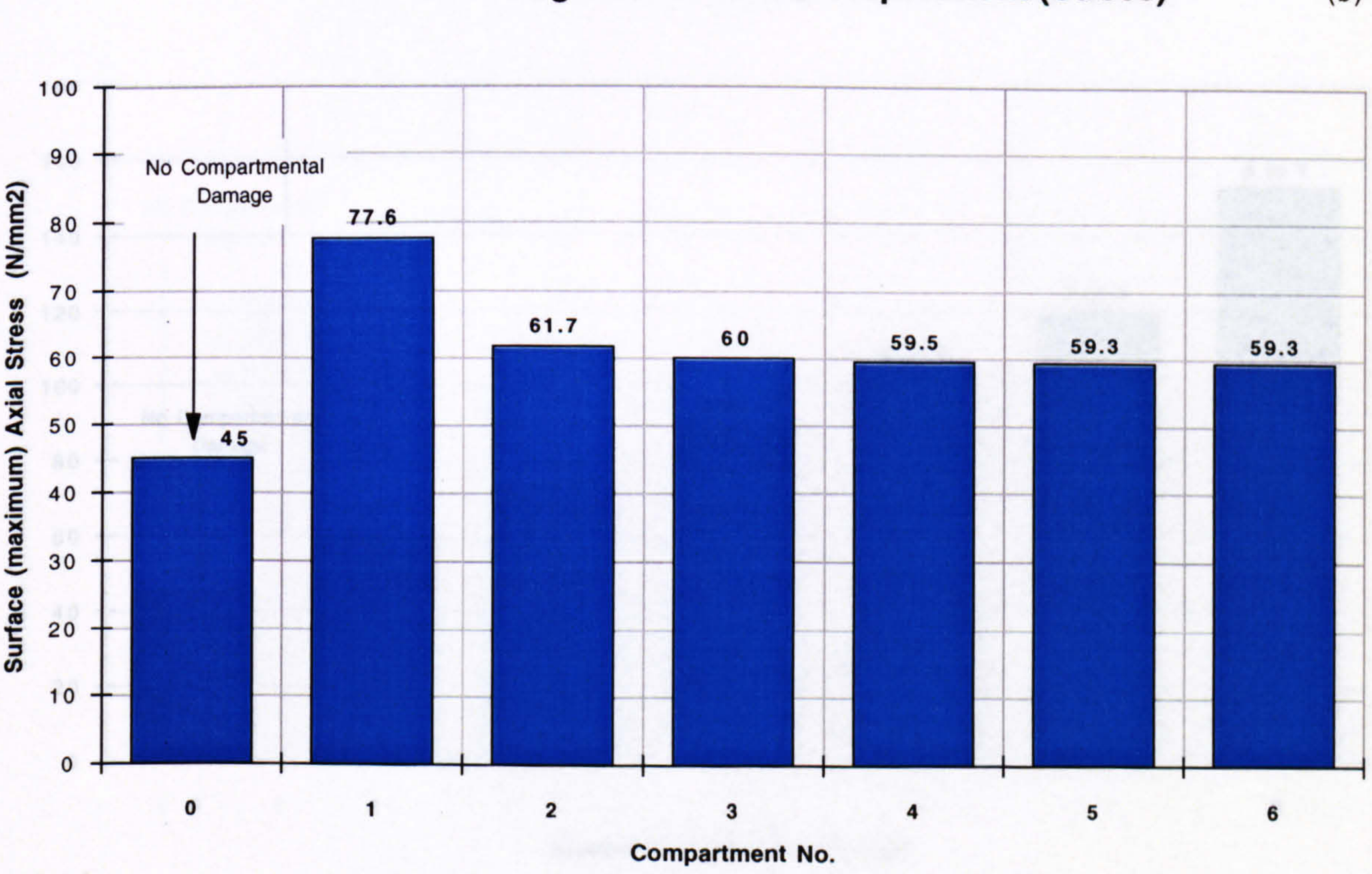

Numbers above the column are actual stress values

Horizontal Surface Offset = 1500 m

Carrier Pipe Wall Thickness = 10 mm

Sea Depth = 1500 m

Figure 3.42

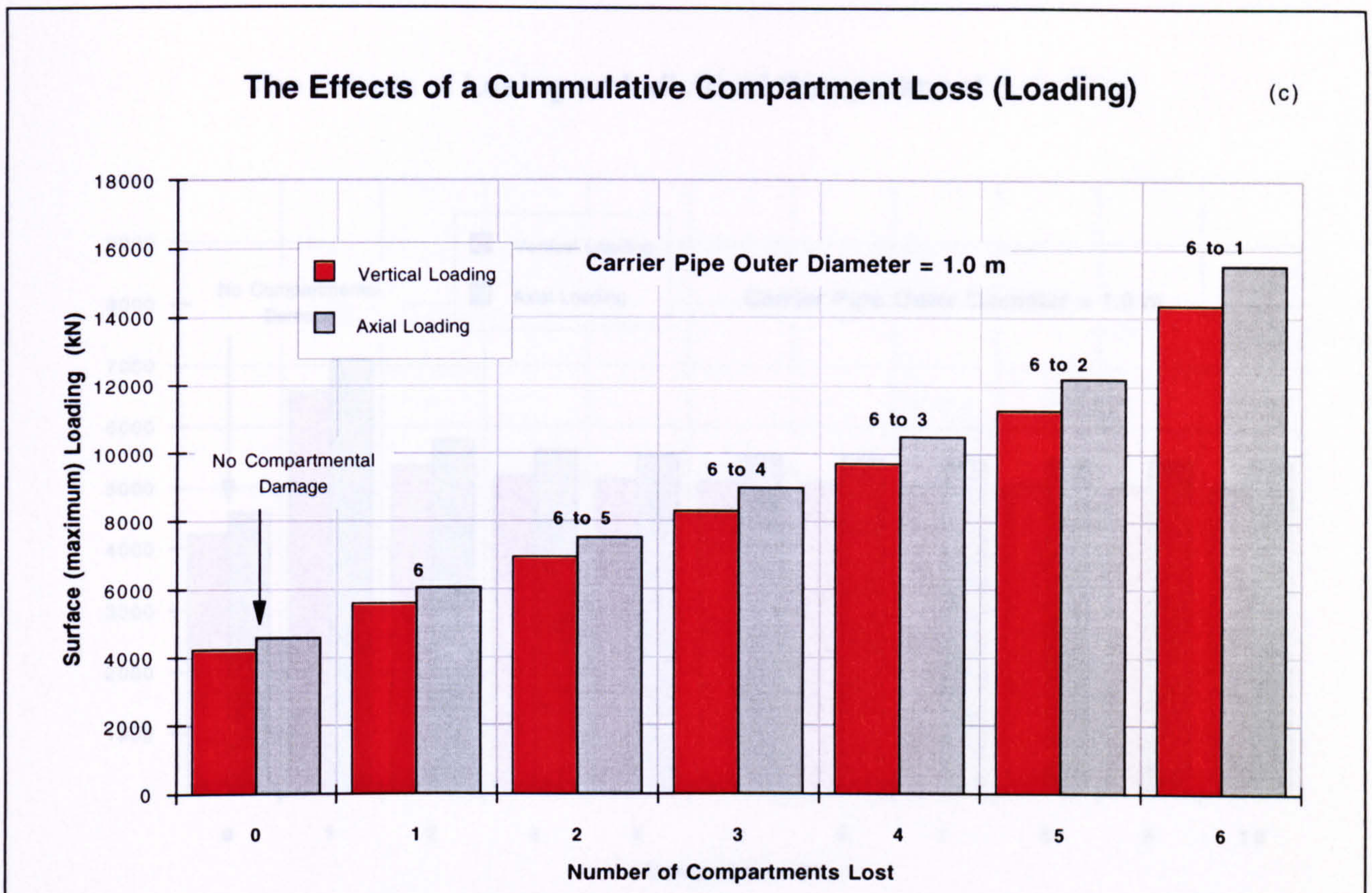

6 Compartments

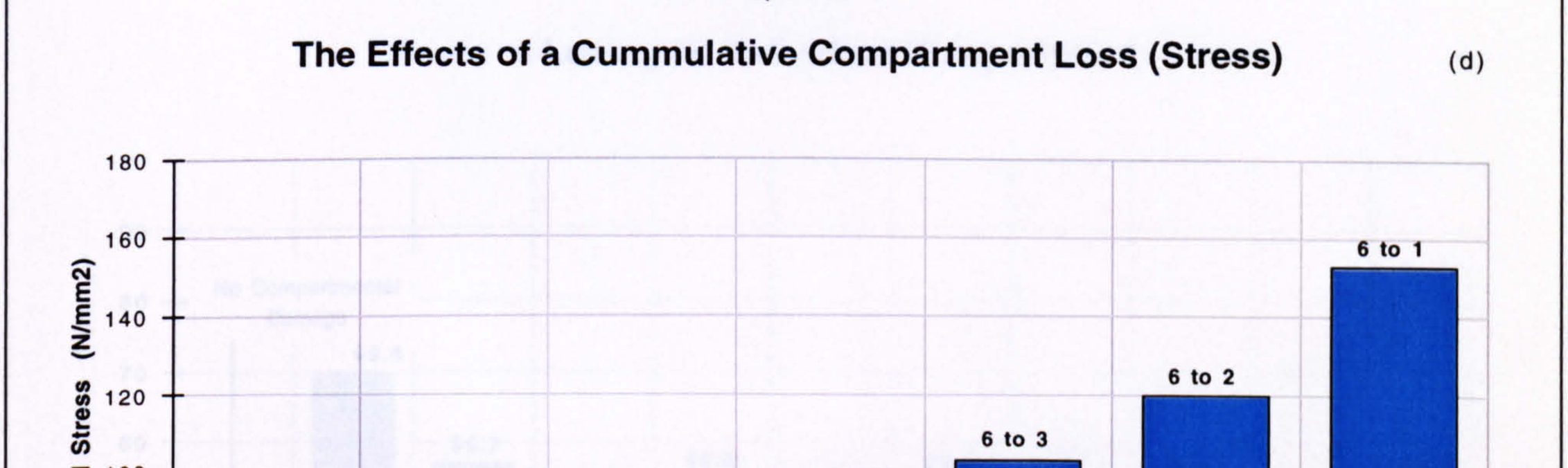

Compartments lost are displayed above each column

Horizontal Surface Offset = 1500 m

Carrier Pipe Wall Thickness = 10 mm

Sea Depth = 1500 m

Figure 3.42

The Effects of Losing an Individual Compartment (Loading)

(a)

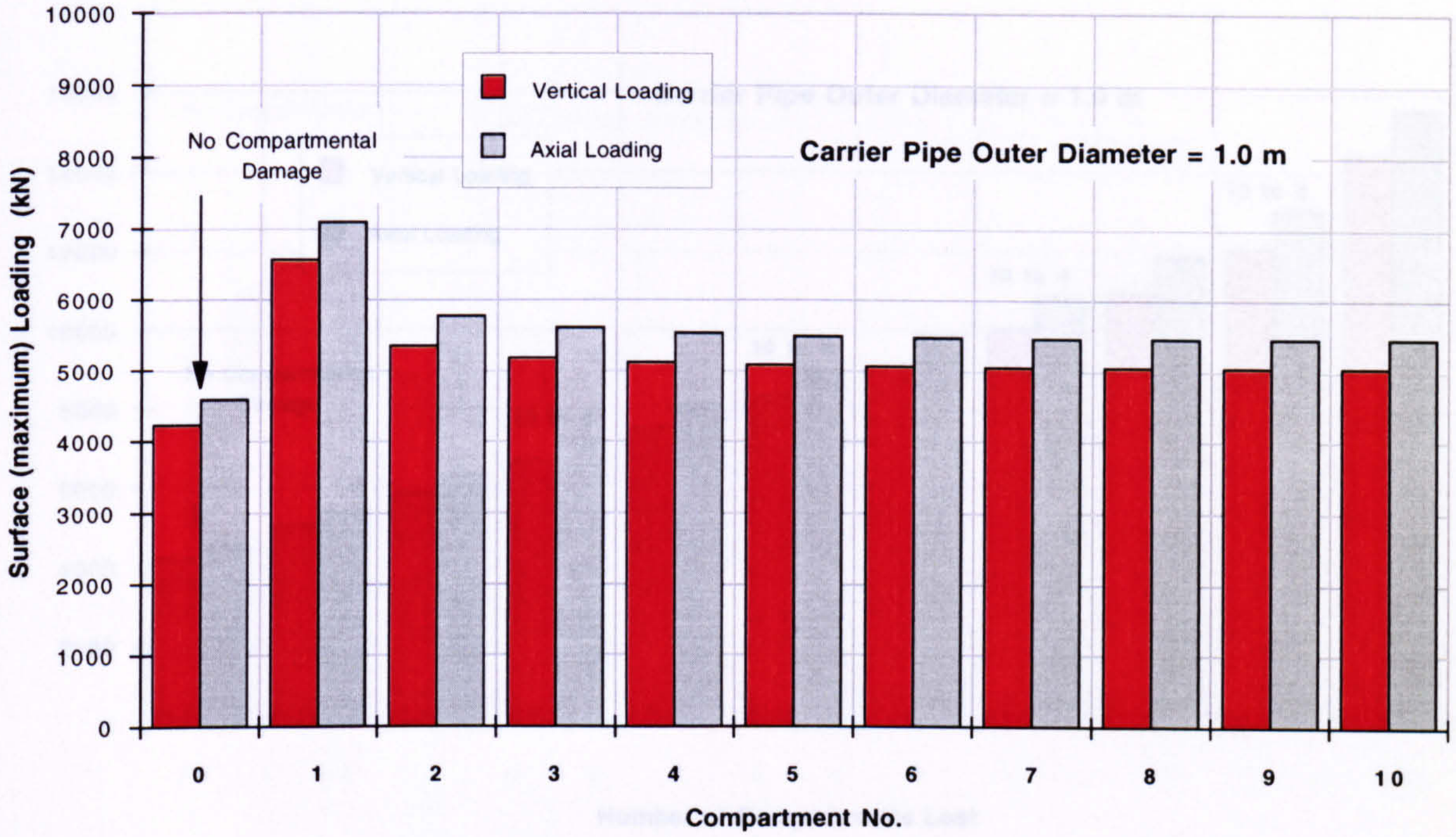

10 Compartments

The Effects of Losing an Individual Compartment (Stress)

(b)

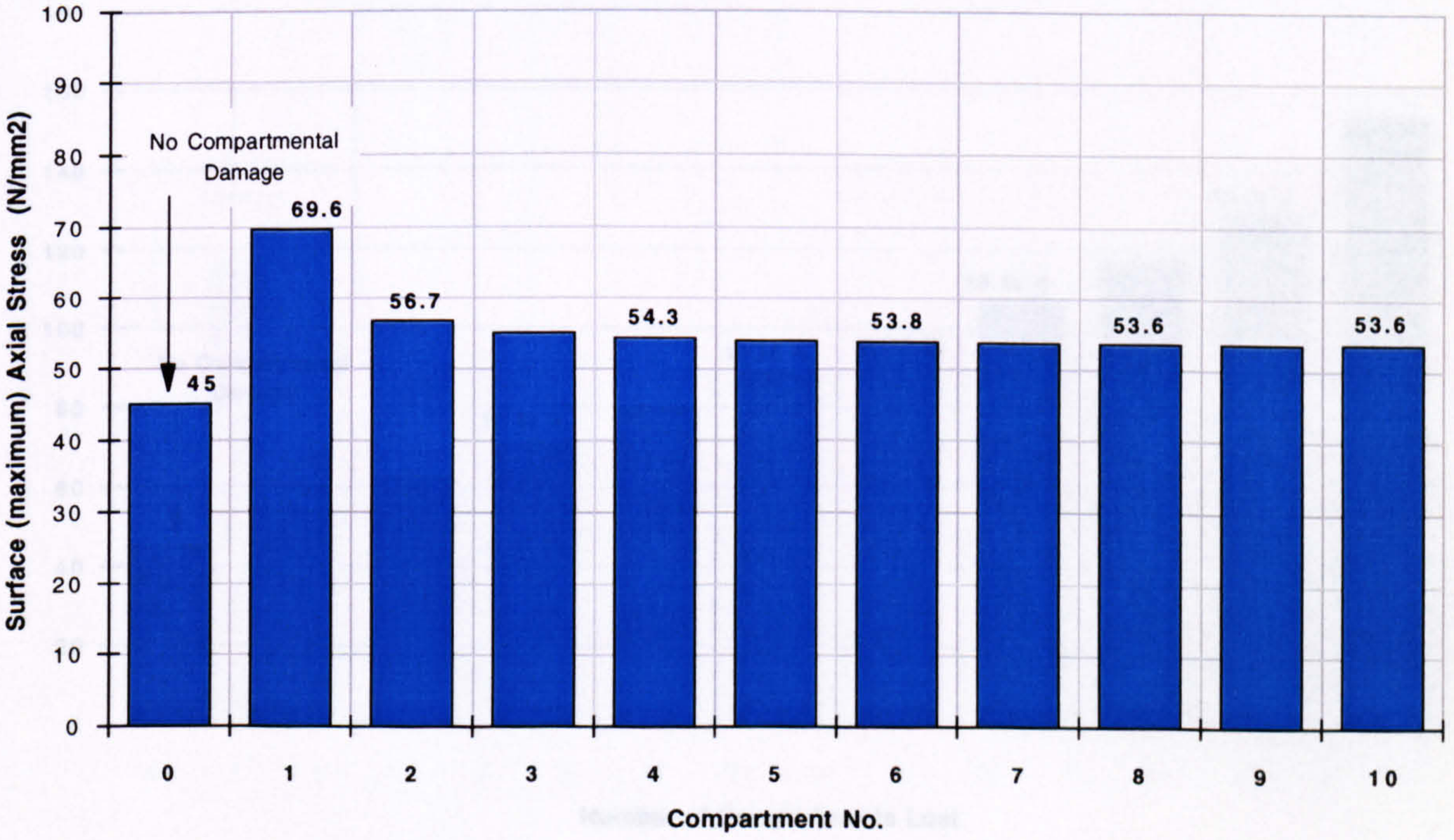

Numbers above the columns are actual stress values

Horizontal Surface Offset = 1500 m

Carrier Pipe Wall Thickness = 10 mm

Sea Depth = 1500 m

Figure 3.43

The Effects of a Cummulative Compartment Loss (Loading)

(c)

10 Compartments

The Effects of a Cummulative Compartment Loss (Stress)

(d)

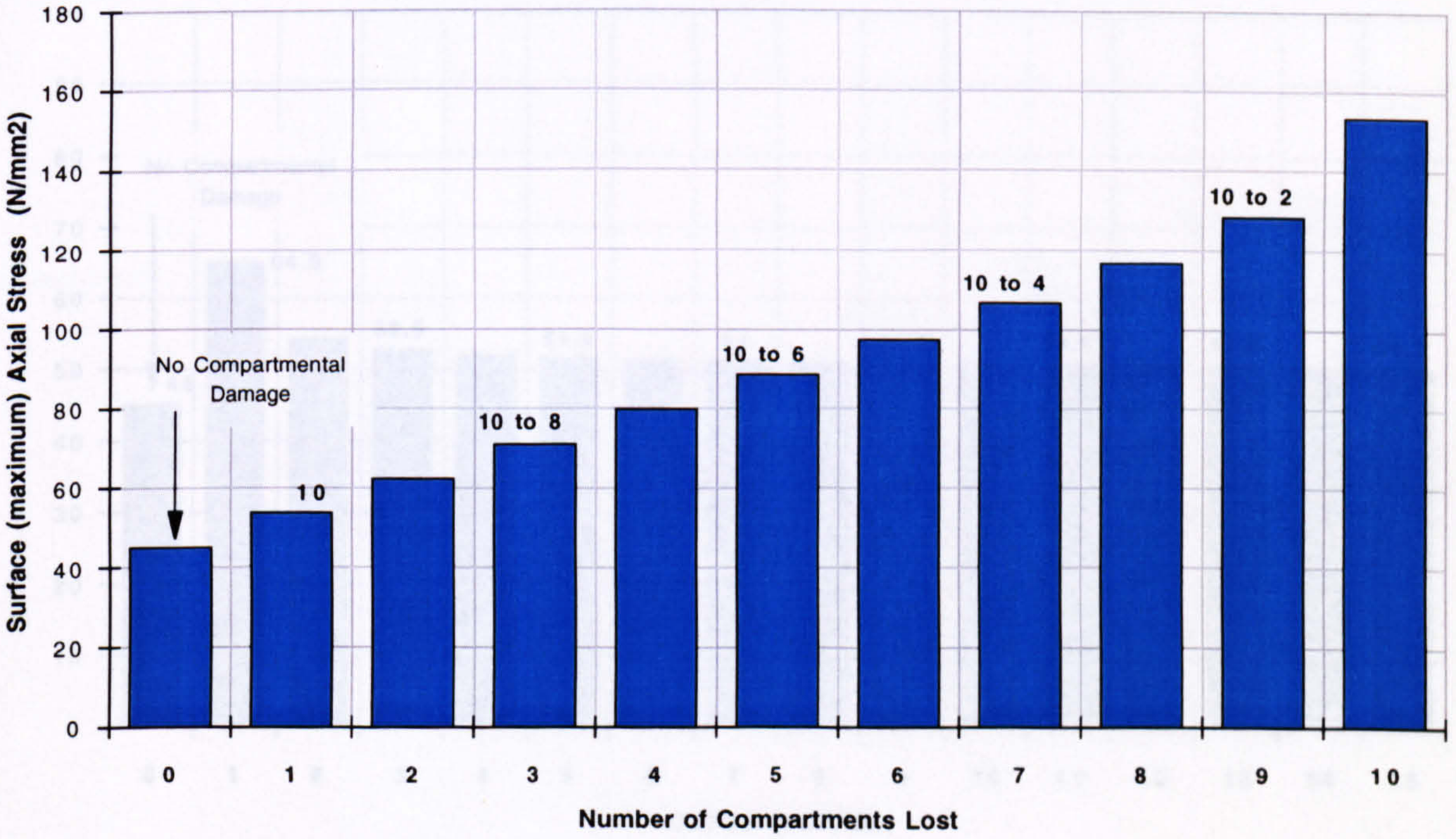

Compartments lost are displayed above each column

Horizontal Surface Offset = 1500 m

Carrier Pipe Wall Thickness = 10 mm

Sea Depth = 1500 m

Figure 3.43

The Effects of Losing an Individual Compartment (Loading)

(a)

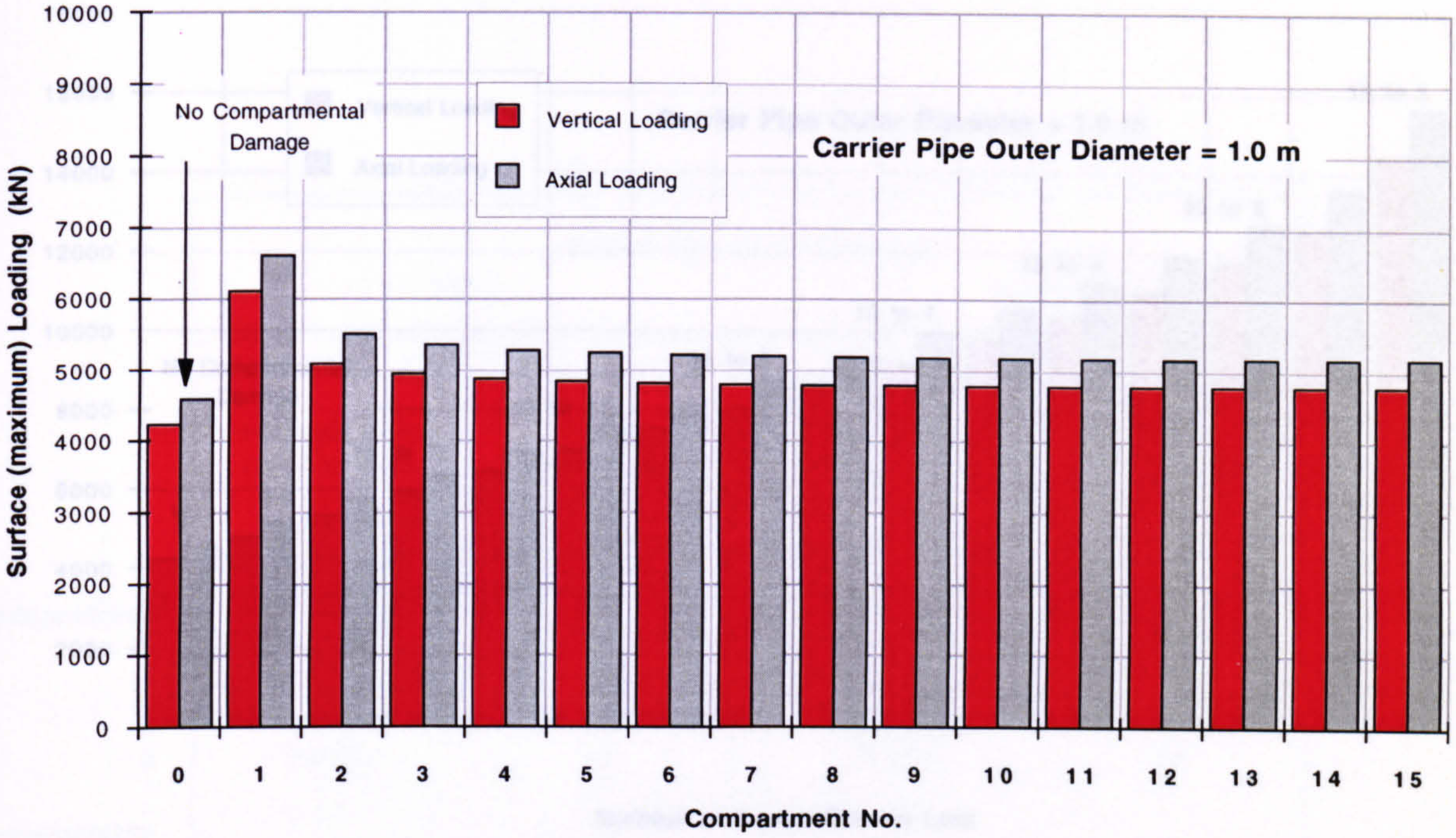

15 Compartments

The Effects of Losing an Individual Compartment (Stress)

(b)

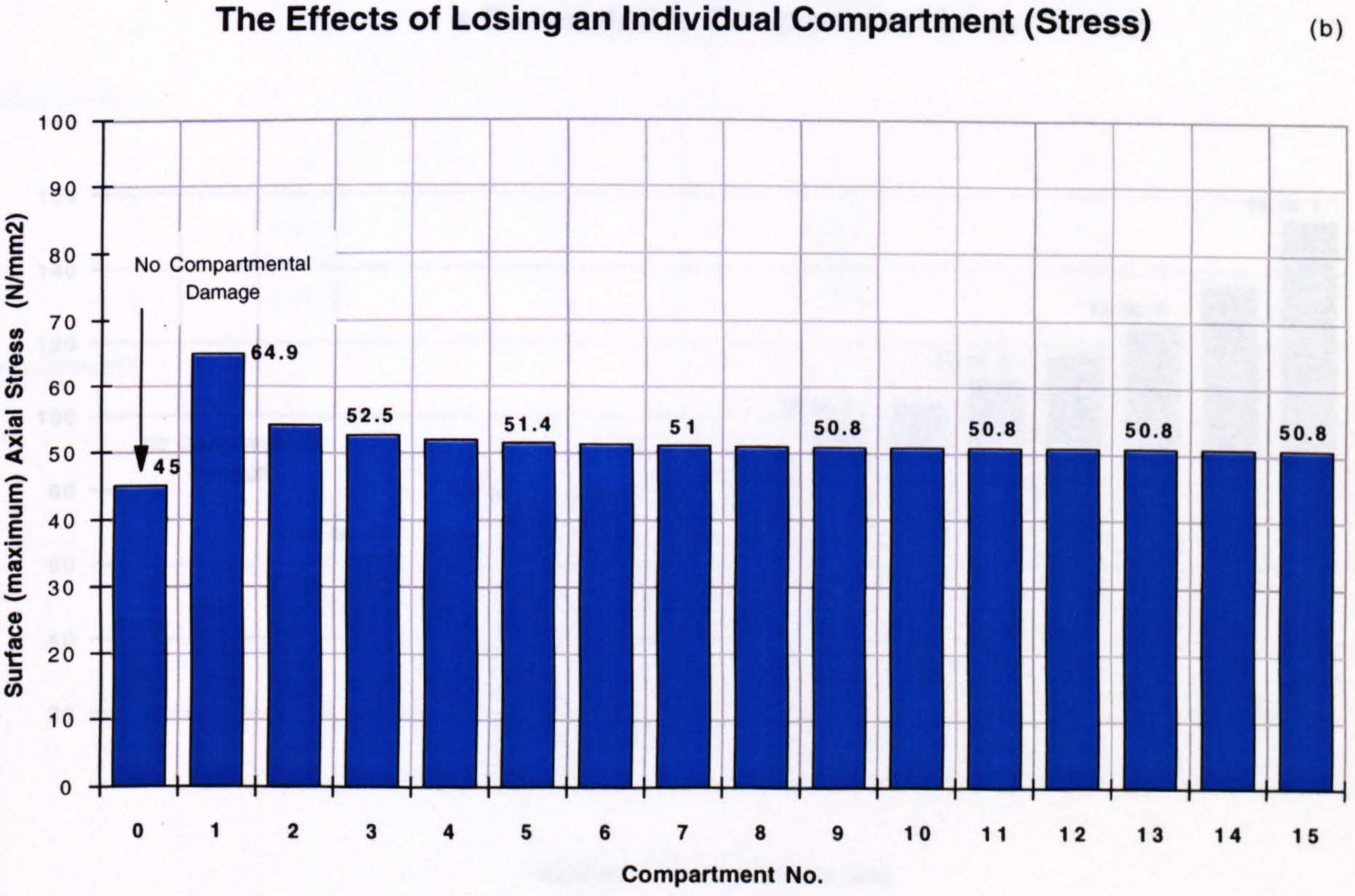

Numbers above the columns are actual stress values

Horizontal Surface Offset = 1500 m

Carrier Pipe Wall Thickness = 10 mm

Sea Depth = 1500 m

Figure 3.44

The Effects of a Cummulative Compartment Loss (Loading) (c)

15 Compartments

The Effects of a Cummulative Compartment Loss (Stress) (d)

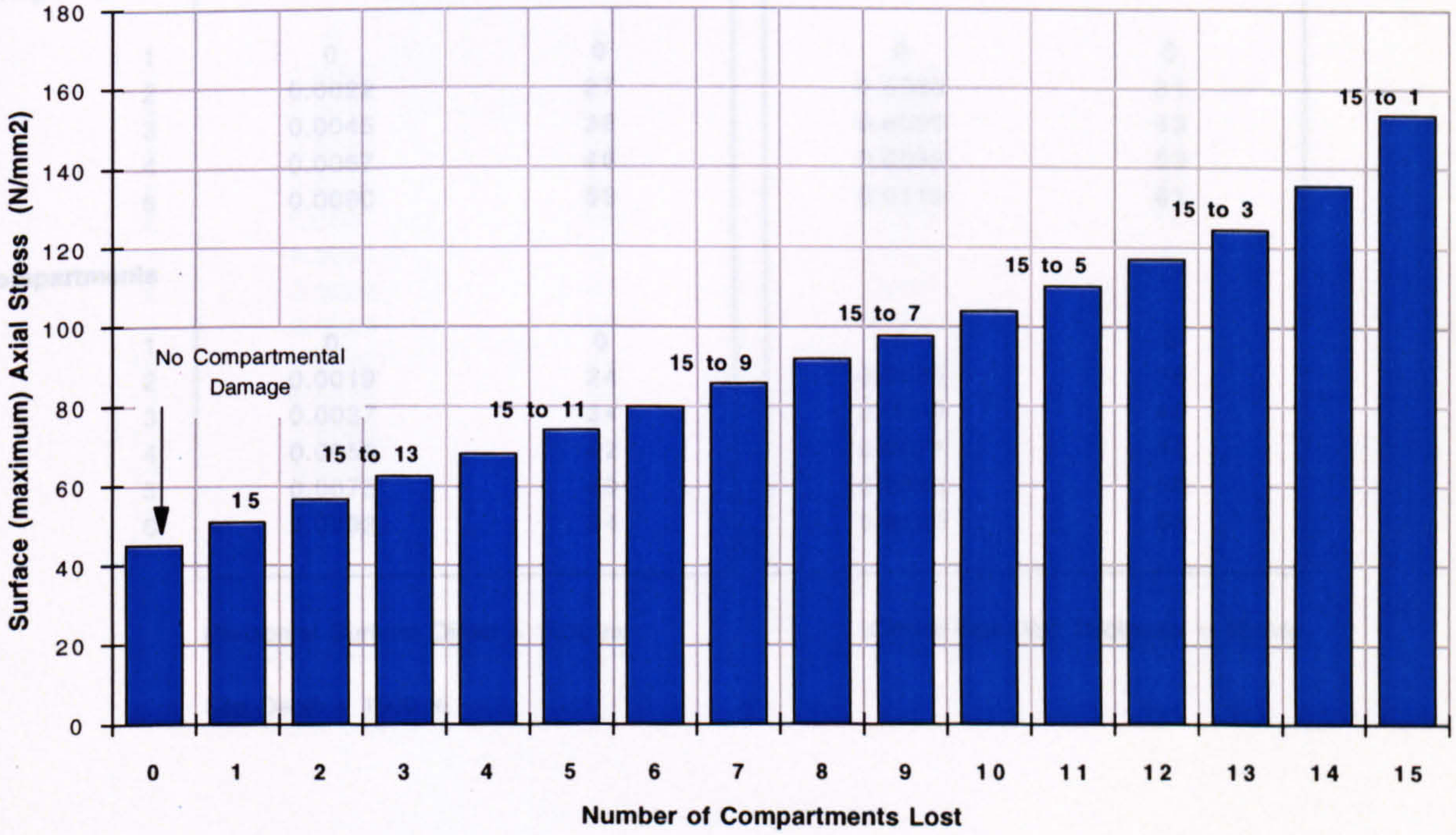

Compartments lost are displayed above each column

Horizontal Surface Offset = 1500 m

Carrier Pipe Wall Thickness = 10 mm

Sea Depth = 1500 m

Figure 3.44

Compartmental Ballast (Steel Rods)

	Carrier Pipe Outer Diameter 1.0 m		Carrier Pipe Outer Diameter 1.1 m	
	Additional Steel C.S.A Required (m2)	Ballast Rod Diameter (mm)	Additional Steel C.S.A Required (m2)	Ballast Rod Diameter (mm)
3 Compartments				
1	0	0	0	0
2	0.0037	34	0.0049	40
3	0.0075	49	0.0098	56
4 Compartments				
1	0	0	0	0
2	0.0028	30	0.0037	34
3	0.0056	42	0.0074	48
4	0.0084	52	0.0111	59
5 Compartments				
1	0	0	0	0
2	0.0022	27	0.0030	31
3	0.0045	38	0.0059	43
4	0.0067	46	0.0089	53
5	0.0090	53	0.0118	61
6 Compartments				
1	0	0	0	0
2	0.0019	24	0.0025	28
3	0.0037	34	0.0049	40
4	0.0056	42	0.0074	48
5	0.0075	49	0.0098	56
6	0.0093	54	0.0123	63

Horizontal Surface Offset = 1500 m

Carrier Pipe Wall Thickness = 10 mm

Sea Depth = 1500 m

Table 3.7(a)

Compartmental Ballast (Steel Rods)

	Carrier Pipe Outer Diameter 1.0 m		Carrier Pipe Outer Diameter 1.1 m	
	Additional C.S.A Required (m2)	Ballast Rod Diameter (mm)	Additional C.S.A Required (m2)	Ballast Rod Diameter (mm)
10 Compartments				
1	0	0	0	0
2	0.0011	19	0.0015	22
3	0.0022	27	0.0030	31
4	0.0034	33	0.0044	38
5	0.0045	38	0.0059	43
6	0.0056	42	0.0074	48
7	0.0067	46	0.0089	53
8	0.0078	50	0.0103	57
9	0.0090	53	0.0118	61
10	0.0101	57	0.0133	65
15 Compartments				
1	0	0	0	0
2	0.0007	15	0.0010	18
3	0.0015	22	0.0020	25
4	0.0022	27	0.0030	31
5	0.0030	31	0.0039	35
6	0.0037	34	0.0049	40
7	0.0045	38	0.0059	43
8	0.0052	41	0.0069	47
9	0.0060	44	0.0079	50
10	0.0067	46	0.0089	53
11	0.0075	49	0.0098	56
12	0.0082	51	0.0108	59
13	0.0090	53	0.0118	61
14	0.0097	56	0.0128	64
15	0.0104	58	0.0138	66

Horizontal Surface Offset = 1500 m

Carrier Pipe Wall Thickness = 10 mm

Sea Depth = 1500 m

Table 3.7(b)

CHAPTER 4

Production Fluid Heat Loss and Insulation Analysis

4.1 General Description

In order to prevent wax deposition, emulsification and hydrate formation oil companies have sought to either chemically inject, insulate or heat the oil within risers and subsea pipelines. This is especially important when crude oil transportation is required through a deep water environment where ambient temperatures are relatively low, or when the oil to be transported is of a low gravity and high viscosity type (heavy oil).

The study presented in this chapter aims to first of all identify and discuss the operational problems associated with subsea oil transportation in terms of crude oil characteristics with a subsequent examination of existing remedies along with corresponding examples and geographic areas of application. However most of the work undertaken within this chapter concentrates on the design of a thermal insulation system for a deep water seabed pipeline and catenary riser as illustrated in Figure 4.1. The objective is to provide an insulation system that will sufficiently maintain product temperature to an extent where the formation of substances within the oil as mentioned above are minimised. The insulation has to posses certain capabilities in order to satisfy geometric, buoyancy and strength constraints which have already been defined. One of the main technical obstacles that must be overcome in satisfying these requirements is hydrostatic pressure since the carrier pipe will not be designed to withstand the high pressure loading experienced in deep water. At a depth of 1500 m, water exerts a pressure of 151 bar or 15 MN/m^2 which greatly exceeds the maximum performance of most insulating materials in terms of compression resistance and generally those that can are of high density which subsequently creates further problems with buoyancy. The final section of this chapter aims to establish the thermal stressing inherent within the system due to the presence of large temperature differences within the structure.

4.2 Crude Oil Characteristics

4.2.1 Viscosity and Gravity

In the analysis of crude oil transportation through subsea pipelines, the viscosity and density of the oil plays an important role and in the case of heavy oil is the major cause of many production problems. Heavy oil is usually referred to as crude with gravities less than 16 °API and with dynamic viscosities greater than 1 kg/m.s at 28 °C and 0.02 kg/m.s at 100 °C.

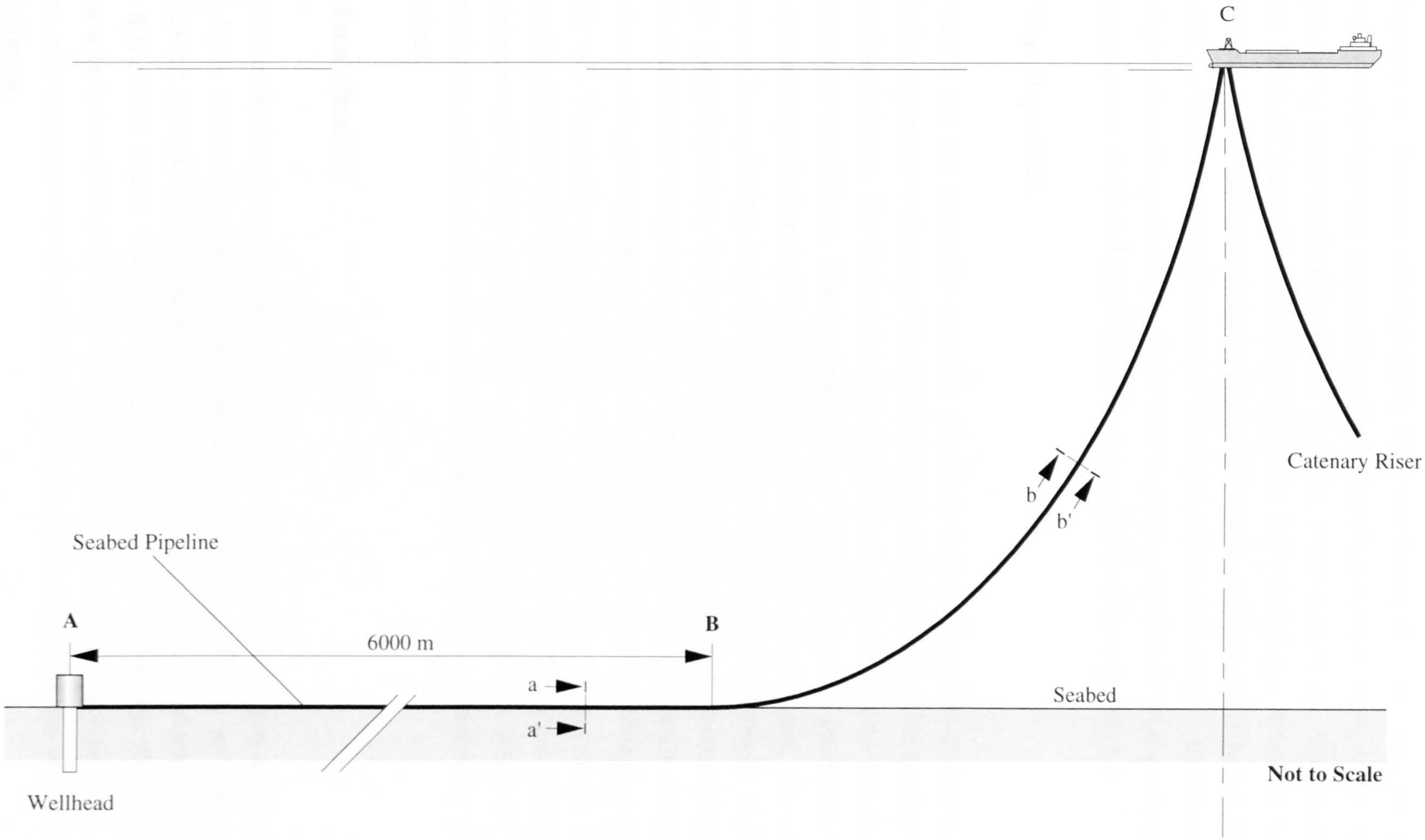

Figure 4.1

Catenary Riser and Seabed Pipeline

This crude lacks the lighter ends and contains heavy metals, particularly vanadium, nickel and sulphur. Although very viscous these crudes do behave as Newtonian fluids in that their viscosity is a function of temperature only (see Figure 4.2) and does not change significantly with shear rate or pumping speed. There are however only a few offshore fields producing heavy crude oil, namely the *Beta, Point Pedernalis, San Miguel and Hueneme* fields off the coast of California plus the *Vega* and *Rospo Mare* fields in the Mediterranean and Adratic respectively. Light oil is more common and is found in places such as the *North Sea*, *Gulf of Mexico* and *West of Shetland.* This study is therefore based upon a light oil and in particular a crude with a gravity of 34 °API whose relationship with temperature is illustrated graphically on a logarithmic scale in Figure 4.2.

4.2.2 Wax Deposition

Crude oils are generally complex chemical systems containing thousands of individual components in the range from low molecular weight to high molecular weight waxes and asphaltenes. The high molecular weight waxes and asphaltenes are dissolved under reservoir conditions. These components may precipitate in pipelines as the thermodynamic equilibrium is disturbed which is caused by the changing pressure and temperature. Precipitation is carried out by several mechanisms namely molecular diffusion, shear dispersion, brownian motion and gravity settling, however it has been shown that molecular diffusion is the main mechanism. The wax crystals which form during the crystal growth process may develop an interlocking 3D - structure that can entrap the oil. This leads to an increase in the viscosity of the transported oil. For the majority of light crude oils wax deposition starts at about 37 °C. Therefore a solution to this problem would include preventing the oil cooling to temperatures below 37 °C by either insulating or heating the crude, utilising wax suppressants or periodically 'pigging' the pipelines.

4.2.3 Emulsification

Emulsification is a problem only associated with crude oil - gas mixtures and studies have shown that unless the temperature of the crude is at least 40 °C emulsification can take place to an extent where separation (on the production platform) can be difficult to attain. This was a problem that was faced by the Cormorant 'A' platform which is a multi-purpose facility that acts as collection and separation, water injection, gas compression and pump-station for its own crude and gas and that from other platforms.

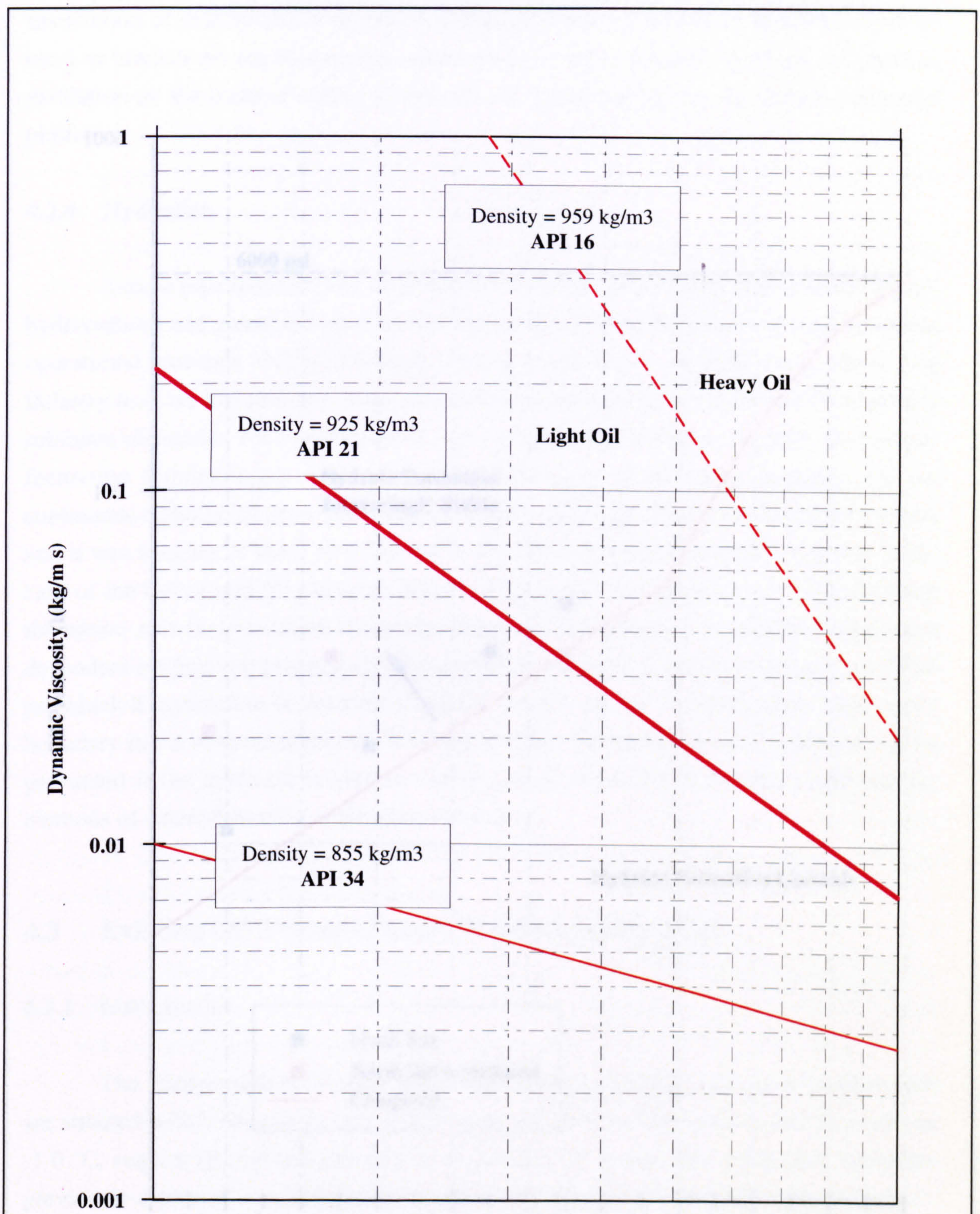

Figure 4.2
Crude Oil Viscosity

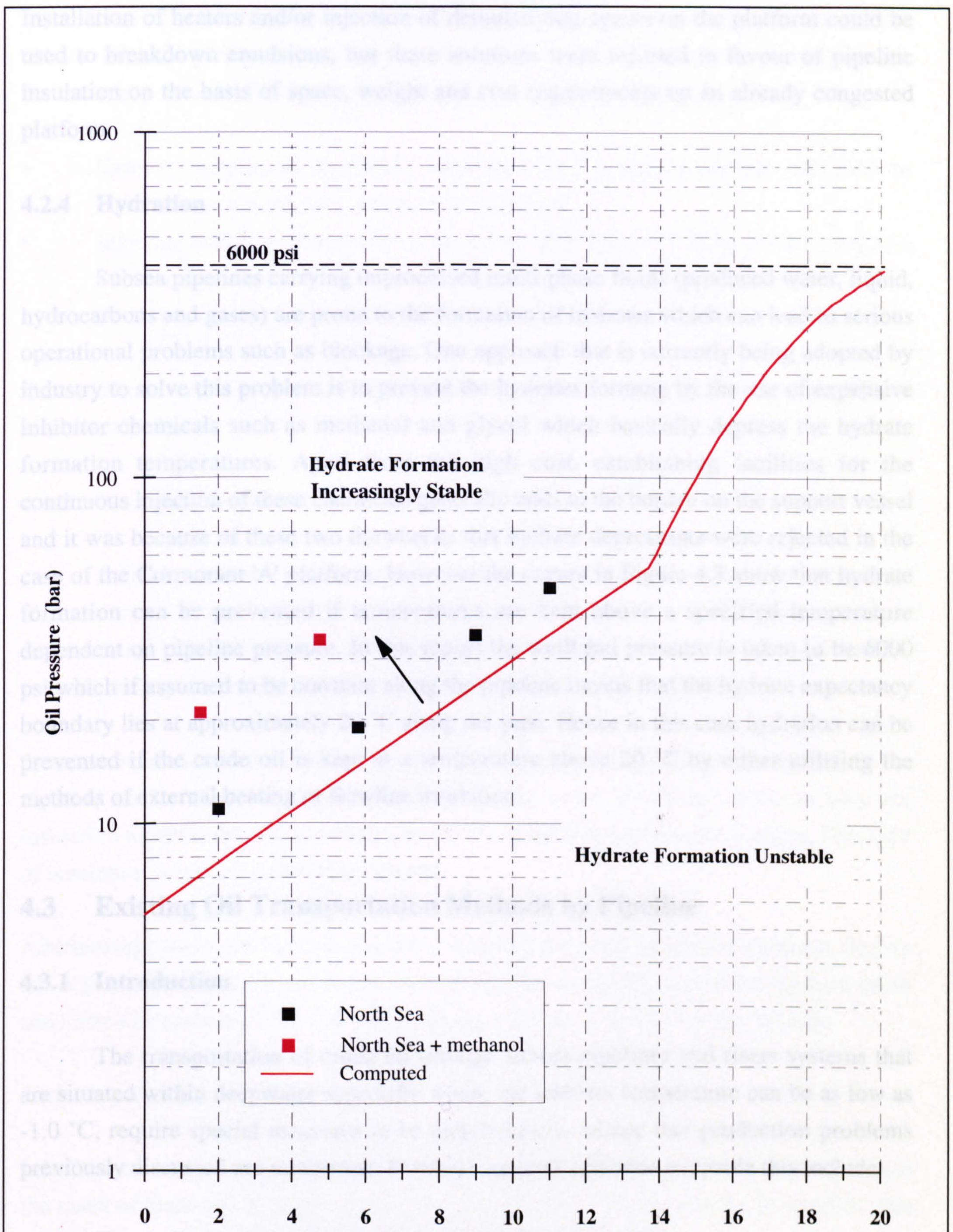

Figure 4.3
Hydrate Stability Boundary Curves

Installation of heaters and/or injection of demulsifying agents on the platform could be used to breakdown emulsions, but these solutions were rejected in favour of pipeline insulation on the basis of space, weight and cost requirements on an already congested platform.

4.2.4 Hydration

Subsea pipelines carrying unprocessed multi-phase fluids (produced water, liquid, hydrocarbons and gases) are prone to the formation of hydrates which can lead to serious operational problems such as blockage. One approach that is currently being adopted by industry to solve this problem is to prevent the hydrates forming by the use of expensive inhibitor chemicals such as methanol and glycol which basically depress the hydrate formation temperatures. Apart from the high cost, establishing facilities for the continuous injection of these chemicals generally adds to the burden on the support vessel and it was because of these two drawbacks that hydrate depressants were rejected in the case of the Cormorant 'A' platform. However the curves in Figure 4.3 show that hydrate formation can be prevented if temperatures are kept above a specified temperature dependent on pipeline pressure. In this report the wellhead pressure is taken to be 6000 psi which if assumed to be constant along the pipeline means that the hydrate expectancy boundary lies at approximately 20 °C along the pipe. Hence in this case hydration can be prevented if the crude oil is kept at a temperature above 20 °C by either utilising the methods of external heating or flowline insulation.

4.3 Existing Oil Transportation Methods by Pipeline

4.3.1 Introduction

The transportation of crude oil through subsea pipelines and risers systems that are situated within deepwater especially where the ambient temperature can be as low as -1.0 °C, require special measures to be undertaken to ensure that production problems previously discussed are minimised. Practical methods available to enable this include:

- Thermally insulating the pipeline (and riser) to retain heat.
- Heating the crude in the pipeline by either pumping a hot liquid through a concentric line or by using electrical coil heating.
- The continuous injection of chemicals to suppress the formation of hydrates, wax and emulsions.

In the case of production from heavy oil fields it is the high viscosity of the oil that causes the main problems especially in terms of pumping. Therefore methods available for the transportation of low gravity, high viscosity crude include:

- External heating or thermally insulating the pipeline to reduce viscosity or maintain the existing low viscosity respectively.
- Injecting water to form a water ring around the crude or to form an emulsion with a lower viscosity.
- Reducing the viscosity of the crude by the addition of a dilutent.

Two methods outlined above, namely thermal insulation and external heating will be discussed further.

4.3.2 Thermal Insulation

A small number of thermally insulated pipelines have been installed offshore in different parts of the world. Most of these lines were installed to either prevent hydrate and wax deposition or to allow the pumping of high pourpoint crudes. Methods that are currently being used or are under development are detailed in Figure 4.4.

Thermal insulation is accomplished by adding insulation material to the outside of the pipeline (or flowline) with the further addition of a steel or plastic sleeve to keep the insulation material dry and prevent it from been crushed by hydrostatic loading. This type of insulation is termed a Jacketing System.

Alternatively there are various insulation systems currently under development that do not depend upon a sleeve and therefore rely upon the insulating material being both crush and corrosion resistant. This type of insulation is termed a Thick Coating System.

Jacketing System

Installations using polyurethane foam inside a polyethylene sleeve have been made off the coast of Gabon and in the Arabian Gulf. However in deeper waters; 30 to 45 m, this method is no longer satisfactory because of the possibility of leaks through the polyethylene sleeve. Once this happens the water pressure will crush the polyurethane foam and make it ineffective as an insulating material. The problem of hydrostatic pressure is overcome by the pipe within a pipe method or steel jacket in which the steel is made sufficiently thick to withstand the compression. The insulation material such as low density polyurethane foam is then placed between flowline and sleeve (or carrier).

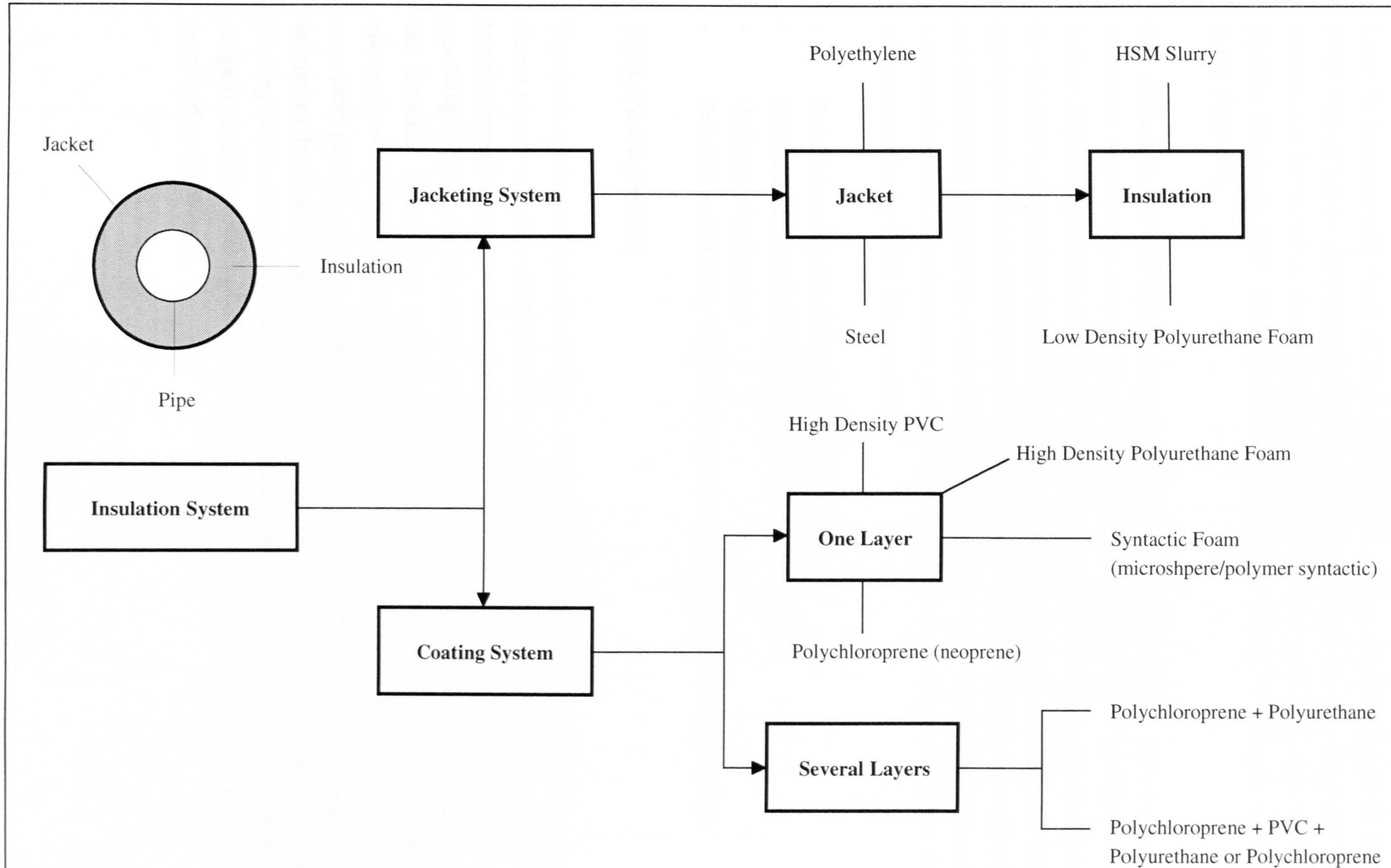

Figure 4.4
Current Methods of Insulating a Pipeline or Riser

Its thermal conductivity value *k* is typically of the order of 0.025 W/m.K, which is close to the thermal conductivity of air. In fact it is the air which is the insulator as the function of the cellular plastic structure is just to prevent the air from convecting. Examples of this method can be found in the Indonesian offshore fields as well as in the case of the pipeline linking the UMC (Underwater Manifold Centre) and the Cormorant 'A' platform in the North Sea.

One method recently introduced into North Sea operations provides a more economical alternative to polyurethane foams by which a pumpable gelling but non-setting slurry of hollow, high-strength silica spheres and sea water is pumped into the space surrounding the flowline(s) and enclosed by the steel carrier pipe. The slurry can be pumped into the pipeline annulus after it has been installed providing a flexibility in insulation application and hence slurry installation can be deferred until the later stages of the productive life of a field when flow rate decreases and thermal conservation is more important. Other advantages of using HSM Slurry include:

- Reduction in capital costs at the fabrication site
- Good thermal conductivity (approximately 0.3 W/m.K)
- Unlimited depth rating
- Provides a stabilising weight to a pipeline system (relatively high density)

Thick Coating System

The thick coating system represents an alternative to the jacketing system whereby the sleeve pipe or carrier is omitted thereby greatly reducing the work at the fabrication site. In this alternative the insulation is provided either in the form of prefabricated half-shell mouldings of High Density Polyurethane Foam (HDPUF) or Syntactic Foam strapped to the flowline. Since these mouldings are exposed to the sea water, they must be encapsulated in a layer of either steel or solid polymer in order to prevent water ingress over long periods of time at high hydrostatic pressures. HDPUF has an approximate maximum depth rating of only 140 m whilst Syntactic Foam has a substantially greater limiting depth of approximately 3000 m, depending upon material density. Densities range from 250 to 500 kg/m^3 with associated thermal conductivity values in the range from 0.05 to 0.1 W/m.K.

Material	Thermal Conductivity (W/m.k)	Density (kg/m3)
Low Density Polyurethane Foam	0.025	70
Nitrogen Gas	0.026	Dependent upon Pressure
Polyurethane + PVC Foam + Polychloropene	0.05	300
High Density Polyurethane Foam	0.057	400
Syntactic Foam	0.085 - 0.1	384.4
High Density PVC	0.15	1400
Asbestos	0.165	577
HSM Slurry Stiffened with Bentonite and Cement	0.3	820
High Density Polyethylene	0.52	950
Concrete	0.86 - 1.3	1900 - 2300
Steel	40	7850

Table 4.1
The Insulating Capabilities of Various Materials

An alternative method involves the application of several coatings of a combination of material including Polyurethane, PVC and Polychloroprene which are usually applied using an automatic machine that also bonds the layers together as well as to the pipe using various heat methods. This type of insulation system has been proposed for the North Alwyn development with the aim of preventing wax deposition problems.

The insulating capabilities of various materials are detailed in Table 4.1

4.3.3 External Heating

External heating is mainly used in the transportation of high pourpoint crude to ensure a sufficiently low viscosity so as not to cause any pumping problems. It is also used to maintain a minimum oil temperature under conditions of no-flow or very little flow, and to reheat the pipeline after a shutdown.

One method which can provide a heat source to a pipeline is to install a concentric pipeline with either the inner line or the annulus serving as the crude carrier with the ability to pump a heated liquid through the other portion of the line. i.e. uses the heat exchanger principle. However such a system is limited to relatively short distances.

An alternative method available to provide external heating is that of electrical means. Again this method is only applicable to short lengths of pipeline. An example of an electrically heated pipe is currently being installed for Statoil and will carry gas and condensate from the *Sleipner West* wellhead platform to the processing platform. The electrical system offers a means of controlling hydrate and wax formation in multiphase flows. It also enables electricity to be delivered to remote subsea facilities. For heating purposes the system uses electrical induction cables inserted along the full axial length of the pipeline. A high frequency alternating current in the cables forms an induction field that generates heat in the ferromagnetic steel pipe, sufficient to raise and maintain the temperature of the pipe material and the pipe contents to a pre-determined level.

4.4 Fundamental Heat Transfer Theory for an Annular Section

4.4.1 Introduction

This section aims to establish the fundamental basis of heat conduction and convection for annular sectional geometries. The theory presented is then applied to a

flowline encapsulated within carrier pipe or jacket with the resulting annular gap filled with either a solid or gaseous insulator, see Figure 4.5.

The objective of this exercise is to formulate heat transfer expressions that can be used to predict:

- the temperature behaviour of a pipe line fluid subjected to radial heat loss
- radial temperature distribution across the annular section

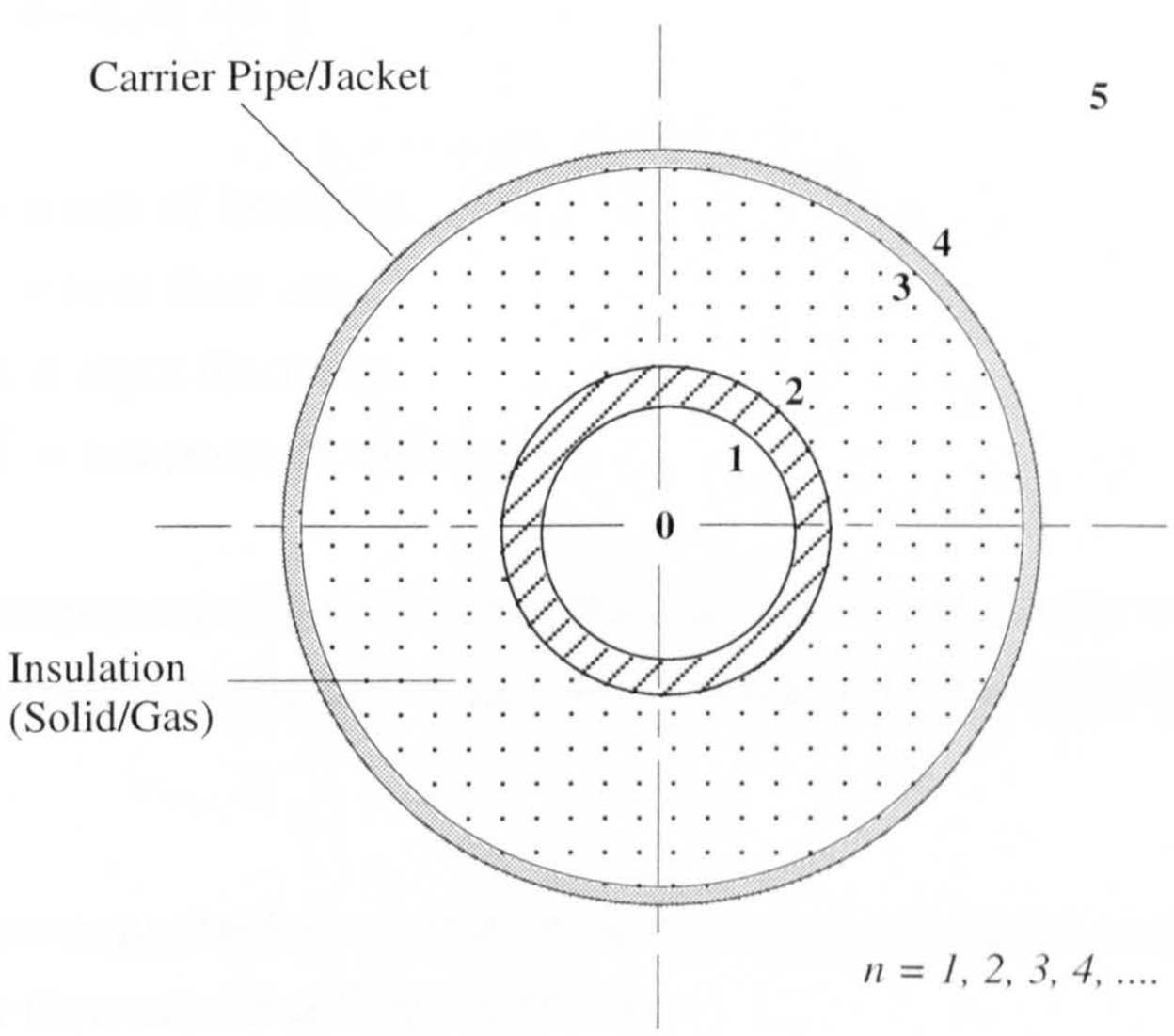

Figure 4.5

An Insulated Flowline

4.4.2 Heat Transfer Mechanisms

In cases involving the radial loss of heat from a liquid or gaseous pipe flow to an ambient environment composed of either liquid or gas, three heat transfer mechanisms must have taken place; conduction, convection and radiation. For the purposes of this study radiation is neglected on the grounds that its influence is small relative to the other two modes of transfer because of the relatively low temperatures involved.

Conduction

Fourier's law forms the fundamental basis of heat conduction and is based upon the empirical observation of one-dimensional steady heat flow through a solid. *One-dimensional flow* implies that the temperature is uniform over surfaces perpendicular to the direction of heat conduction and such surfaces are called *isothermal* surfaces. *Steady*

flow implies that the temperature at any point does not vary with time. It therefore follows from considerations of continuity, that in one-dimensional steady flow the rate of heat flow through successive surfaces is constant.

It is subsequently found that the rate of heat flow is proportional to the area of flow and to the temperature difference across the layer and inversely proportional to its thickness. This is Fourier's law and can be expressed as follows:

$$Q = -k A \left(\frac{dT}{dx} \right) \tag{4.1}$$

where: Q = rate of heat loss
A = heat flow area
dx = layer thickness
dT = temperature difference

The constant of proportionality *k* is called the *Thermal Conductivity* of the material and the negative sign indicates that the heat flow is positive in the direction of temperature fall.

When Fourier's law is applied to a situation involving steady radial conduction through a pipe wall the heat flow can be defined as follows:

$$Q = -2 k \pi r \left(\frac{dT}{dr} \right) L \tag{4.2}$$

where: r = nominal radius of the pipe
L = pipe length

Since Q is independent of r, we obtain through integration

$$q = \frac{2 k \pi}{\log_e \left(\frac{r_{n+1}}{r_n} \right)} \left(T_n - T_{n+1} \right) \tag{4.3}$$

where: q = rate of heat loss per unit length
T_n = temperature of surface *n*
r_n = radial distance to surface *n*

Convection

The mechanism of convective heat flow could theoretically be calculated from Fourier's law as expressed by Eqn (4.1) where dT/dx is the temperature gradient in the fluid and k is the thermal conductivity of the fluid. However dT/dx is a quantity which cannot be easily measured in practice due to its non-linear behaviour and so it is more common to express convective heat transfer by an equation of the form:

$$Q = h A \left(T_n - T_{n+1} \right) \tag{4.4}$$

where: h = convective heat transfer coefficient
$\left(T_n - T_{n+1} \right)$ = the temperature difference across the fluid layer

It must be remembered that h is not a physical constant of the fluid as opposed to the thermal conductivity k and is in fact a function of all the parameters that affect the heat flow, such as viscosity, specific heat capacity and velocity.

When the above expression is applied to cases involving cylindrical geometries the following equation is obtained:

$$q = 2 h \pi r \left(T_n - T_{n+1} \right) \tag{4.5}$$

4.4.3 Temperature Behaviour of a Pipeline Fluid Subject to Heat Loss

The radial passage of heat transfer across the pipeline system can be broken down into its constituent material layers.

$0 \rightarrow 1$ The heat transfer medium is a fluid and hence Eqn (4.5) is applicable due to convection taking place.

$$T_0 - T_1 = \frac{q}{2 \pi r_1 h_{0-1}} \tag{4.6}$$

$1 \rightarrow 2$ The heat transfer medium is a solid (i.e. steel flowline) and hence Eqn (4.3) is applicable due to conduction taking place.

$$T_1 - T_2 = \frac{q}{2 \pi k_{1-2}} \log_e \left(\frac{r_2}{r_1} \right) \tag{4.7}$$

2 → 3 (a) Solid insulation material (i.e. foam) and hence Eqn (4.3) is applicable due to conduction taking place.

$$T_2 - T_3 = \frac{q}{2\pi k_{2-3}} \log_e\left(\frac{r_3}{r_2}\right) \tag{4.8}$$

2 → 3 (b) Gaseous insulation material (i.e. nitrogen gas) and hence Eqn (4.5) is applicable due to convection taking place.

$$T_2 - T_3 = \frac{q}{2\pi r_2 h_{2-3}} \tag{4.9}$$

3 → 4 Solid (i.e. steel carrier pipe) and hence Eqn (4.3) is applicable due to conduction taking place.

$$T_3 - T_4 = \frac{q}{2\pi k_{3-4}} \log_e\left(\frac{r_4}{r_3}\right) \tag{4.10}$$

4 → 5 Ambient fluid (i.e. sea water) and hence Eqn (4.5) is applicable due to convection taking place.

$$T_4 - T_5 = \frac{q}{2\pi r_4 h_{4-5}} \tag{4.11}$$

Since q is constant Eqns (4.6) to (4.11) can be added together:

Case (a) - Solid Insulator

$$T_0 - T_5 = \frac{q}{2\pi}\left[\frac{1}{r_1 h_{0-1}} + \frac{1}{k_{1-2}} \log_e\left(\frac{r_2}{r_1}\right) + \frac{1}{k_{2-3}} \log_e\left(\frac{r_3}{r_2}\right) + \frac{1}{k_{3-4}} \log_e\left(\frac{r_4}{r_3}\right) + \frac{1}{r_4 h_{4-5}}\right]$$

re-arranging to obtain an expression for q:

$$q = \frac{2\pi(T_0 - T_5)}{\left[\frac{1}{r_1 h_{0-1}} + \frac{1}{k_{1-2}} \log_e\left(\frac{r_2}{r_1}\right) + \frac{1}{k_{2-3}} \log_e\left(\frac{r_3}{r_2}\right) + \frac{1}{k_{3-4}} \log_e\left(\frac{r_4}{r_3}\right) + \frac{1}{r_4 h_{4-5}}\right]} \tag{4.12}$$

in which:

$$\frac{2\pi}{\left[\frac{1}{r_1 h_{0-1}}+\frac{1}{k_{1-2}}\log_e\left(\frac{r_2}{r_1}\right)+\frac{1}{k_{2-3}}\log_e\left(\frac{r_3}{r_2}\right)+\frac{1}{k_{3-4}}\log_e\left(\frac{r_4}{r_3}\right)+\frac{1}{r_4 h_{4-5}}\right]} \tag{4.13}$$

can be defined as the *Overall Heat Transfer Coefficient U.*

Case (b) - Gaseous Insulator

$$T_0 - T_5 = \frac{q}{2\pi}\left[\frac{1}{r_1 h_{0-1}}+\frac{1}{k_{1-2}}\log_e\left(\frac{r_2}{r_1}\right)+\frac{1}{r_2 h_{2-3}}+\frac{1}{k_{3-4}}\log_e\left(\frac{r_4}{r_3}\right)+\frac{1}{r_4 h_{4-5}}\right]$$

re-arranging to obtain an expression for *q*

$$q = \frac{2\pi(T_0 - T_5)}{\left[\frac{1}{r_1 h_{0-1}}+\frac{1}{k_{1-2}}\log_e\left(\frac{r_2}{r_1}\right)+\frac{1}{r_2 h_{2-3}}+\frac{1}{k_{3-4}}\log_e\left(\frac{r_4}{r_3}\right)+\frac{1}{r_4 h_{4-5}}\right]} \tag{4.14}$$

in which:

$$\frac{2\pi}{\left[\frac{1}{r_1 h_{0-1}}+\frac{1}{k_{1-2}}\log_e\left(\frac{r_2}{r_1}\right)+\frac{1}{r_2 h_{2-3}}+\frac{1}{k_{3-4}}\log_e\left(\frac{r_4}{r_3}\right)+\frac{1}{r_4 h_{4-5}}\right]} \tag{4.15}$$

can be defined as the *Overall Heat Transfer Coefficient U.*

The overall heat transfer coefficient obtained for each case allows the expression for unit rate of heat loss *q* to be simplified:

$$q = U(T_0 - T_5) \tag{4.16}$$

This can be re-written as:

$$dQ = U\left(T_{0(x)} - T_5\right)dx \tag{4.17}$$

where: x = axial distance along the pipe
dQ = total rate of heat loss over a flowline length of *dx*

$T_{0(x)}$ = flowline fluid temperature (function of x)

It is reasonable to assume that the temperature of the ambient environment T_s which effectively acts as a heat sink remains constant along the pipe length.

In order to eliminate the unknown quantity dQ another equation is required. This can be generated by applying the conservation of energy to a flowline length dx as illustrated below.

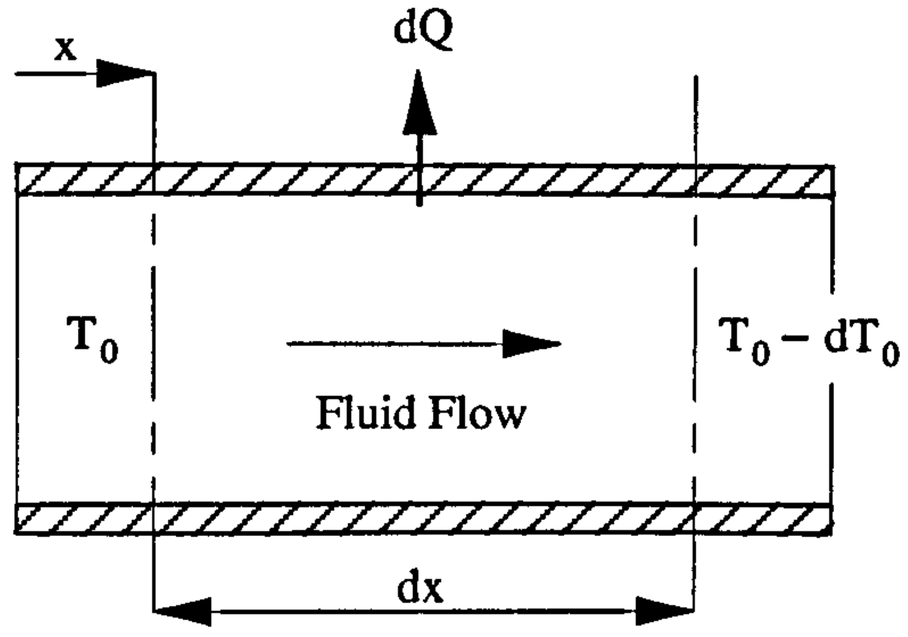

Figure 4.6

Fluid Heat Balance

$$\dot{m} c_p T_0 = \dot{m} c_p (T_0 - dT_0) + dQ \qquad (4.18)$$

where: $\dot{m}$ = fluid mass flow rate
c_p = fluid specific heat capacity

Simplifying Eqn (4.18)

$$dQ = \dot{m} c_p dT_0 \qquad (4.19)$$

however since the ambient temperature T_s is assumed to be constant along the pipeline length this expression can be re-written as:

$$dQ = \dot{m} c_p \, d(T_{0(x)} - T_s) \qquad (4.20)$$

The fluid temperature T_0 can be obtained as a function of x by substituting Eqn (4.17) into (4.20) thereby eliminating the unknown variable dQ.

$$U(T_{0(x)} - T_s) dx = \dot{m} c_p \, d(T_{0(x)} - T_s) \qquad (4.21)$$

Re-arranging Eqn (4.21):

$$\frac{d\left(T_{0(x)}-T_5\right)}{\left(T_{0(x)}-T_5\right)}=\frac{U}{\dot{m}c_p}dx \tag{4.22}$$

$$\int_{T_{0(i)}}^{T_{0(x)}}\frac{1}{\left(T_{0(x)}-T_5\right)}d\left(T_{0(x)}-T_5\right)=\int_0^x\frac{U}{\dot{m}c_p}dx \tag{4.23}$$

Integrating using the initial boundary conditions $x=0,\ T_{0(x)}=T_{0(i)}$ yields the following equation:

$$\log_e\left[\frac{\left(T_{0(i)}-T_5\right)}{\left(T_{0(x)}-T_5\right)}\right]=\frac{U}{\dot{m}c_p}x \tag{4.24}$$

$$\frac{\left(T_{0(i)}-T_5\right)}{\left(T_{0(x)}-T_5\right)}=\exp\left[\frac{Ux}{\dot{m}c_p}\right] \tag{4.25}$$

Re-arranging to obtain $T_{0(x)}$

$$T_{0(x)}=\frac{T_{0(x)}-T_5}{\exp\left(\frac{Ux}{\dot{m}c_p}\right)}+T_5 \tag{4.26}$$

This equation enables the flowline fluid temperature to be calculated at any point along the pipeline. The *overall heat transfer coefficient U* is obtained using either Eqn (4.13) or Eqn (4.15) depending upon whether the annular gap between flowline and carrier pipe is filled with a solid or gas insulator respectively.

It should be noted that Eqn (4.26) demonstrates a characteristic logarithmic decay in fluid temperature along the flowline as a result of heat loss to the ambient environment.

4.4.4 The Calculation of a Heat Transfer Coefficient for a Fully Developed Pipe Flow ($h_{0\text{-}1}$)

In the following section both analytical and empirical correlations recommended for engineering use in terms of a cylindrical geometry are summarised. These are subsequently used to predict an average heat transfer coefficient value for the inner pipe surface assuming a heat transfer condition of forced convection.

Reynolds Number

The first important condition that must be established is whether the internal pipe flow is laminar or turbulent and this is dependent upon Reynolds number. For internal flow it is customary to base the Reynolds number in the internal pipe (or flowline) diameter, D_l as defined below:

$$Re_D = \frac{\rho u_m D_l}{\mu} \tag{4.27}$$

where: ρ = fluid density
u_m = mean fluid velocity
D_l = internal pipe diameter
μ = dynamic viscosity

However a more useful form of the above expression may be found upon the introduction of the mass flow rate $\dot{m}$.

$$\dot{m} = \rho a u_m \tag{4.28}$$

where: a = internal pipe cross-section

If this expression is substituted in to Eqn (4.27):

$$Re_D = \frac{4\dot{m}}{\pi D_l \mu} \tag{4.29}$$

It is difficult to predict with precision when a fully developed pipe flow is laminar or turbulent, however for engineering calculations it is generally agreed that the transition may be expected to occur at a critical Reynolds number of:

$$Re_{critical} \cong 2300$$

As an example the pipeline/riser system under consideration later in this chapter has the following oil and flowline parameters:

$$\dot{m} = 110 \text{ kg/s} \qquad D_l = 0.324 \text{ m} \qquad \mu = 3.20 \times 10^{-3} \text{ kg/ms}$$

This results in a Reynolds number of 1.35×10^5 which greatly exceeds the critical value and hence a condition of turbulent flow exists.

Nusselt Number

The Nusselt number is a dimensionless group, and is a measure of the rate heat transfer by convection. It has been shown that it can be expressed as a function of Reynolds number which describes the flow and Prandtl number which is a property of the fluid. For the purposes of this analysis the following empirical relation is used to calculate the Nusselt number:

$$Nu_D = \frac{f}{2} \frac{Re_D Pr}{\left[1 + 1.99 Re_D^{-1/8} (Pr - 1)\right]} \tag{4.30}$$

where: f = friction factor
Pr = Prandtl number

This relation is the *Prandtl-Taylor modification of the Reynolds analogy* and is applicable to fully developed flow in smooth pipes. The friction factor can be found from the *Friction Law of Blasius* which is an experimental relation that appears to apply reasonably well to Reynolds numbers up to 2×10^5 for developed turbulent flow in a pipe. It can be defined as follows:

$$f = 0.0791 Re_D^{-1/4} \tag{4.31}$$

The Prandtl number Pr is a measure of the ratio of momentum diffusion through the fluid due to viscosity, to heat diffusion by conduction and is calculated as follows:

$$Pr = \frac{\mu c_p}{k} \tag{4.32}$$

Heat Transfer Coefficient

The heat transfer coefficient h can be calculated from the Nusselt number using the following relationship:

$$h_{0-1} = \frac{Nu\, k}{D_1} \tag{4.33}$$

4.4.5 The Calculation of a Heat Transfer Coefficient for an Ambient Fluid ($h_{4\text{-}5}$)

The Convection Process

Fluid motion is the distinguishing feature of heat transfer by convection. Although the process of conduction by molecular exchange is still present in a fluid, the transport of energy is profoundly influenced by the fluid motion. The cause of motion can be attributed to a number of sources:

- When the fluid motion past a body such as a pipe is generated by external forces (i.e. a current) the transfer of heat between the surface and the fluid is termed *forced convection*.
- When no external forces are present, fluid motion may still occur about a body immersed in a fluid at a different temperature as a result of density differences setting up internal buoyancy forces. In this situation the process of heat transfer is termed *free convection*.

In practice both forced and free convection occur simultaneously, however one is usually dominate over the other. One method of establishing the prevailing convection type is outlined below.

Grashof Number

The significance of buoyant convective forces within a flow can be described in terms Grashof number:

$$Gr = \frac{D_4^{\,3} g \beta \Delta T}{\upsilon^2} \qquad (4.34)$$

where: D_4 = outer diameter of the carrier pipe
g = gravity
β = coefficient of thermal expansion
ΔT = temperature difference
υ = kinematic viscosity

The ratio Gr/Re^2 can be used to establish whether a flow has either forced or free convective characteristics:

$Gr/Re^2 << 1$	forced convection
$Gr/Re^2 >> 1$	free convection

Nusselt Number for Free Convection

For free convection around cylinders sufficiently long that end effects may be neglected *Churchill* and *Chu* recommended the following relation which is valid for a wide range of Rayleigh number Ra_D.

$$Nu_D = \left\{0.60 + 0.387 Ra_D^{1/6}\left[1 + \left(\frac{0.559}{Pr}\right)^{9/16}\right]^{-8/27}\right\}^2 \qquad (4.35)$$

valid for: $0 < Pr < \infty$

$10^{-5} < Ra_D < 10^{12}$

where: $Ra_D = Pr.Gr_D$ (4.36)

Nusselt Number for Forced Convection Normal to a Cylinder

Forced convection normal to a pipeline or riser represents a worst case condition as opposed to tangential forced convection, in terms of fluid flow heat loss. In an ocean environment forced convection will be generated by currents and whether the flow is predominantly normal or tangential to the pipeline/riser will depend upon the currents orientation to it. However for the purposes of this study current flow normal to the pipe is assumed be prevalent and hence the worst case condition is applied along the entire pipeline length.

For flow normal to a cylinder (Figure 4.7) *Churchill* and *Bernstein* proposed the following correlation based upon an analysis of data covering wide ranges of Pr and Re_D:

$$Nu_D = 0.3 + \frac{0.62 Re_D^{1/2} Pr^{1/3}}{\left[1 + (0.4/Pr)^{2/3}\right]^{1/4}}\left[1 + \left(\frac{Re_D}{2.82 \times 10^5}\right)^{5/8}\right]^{4/5} \qquad (4.37)$$

valid for: $Re_D . Pr > 0.2$

in which the Reynolds number is based upon the undisturbed freestream velocity normal to the carrier pipe of diameter D_4 :

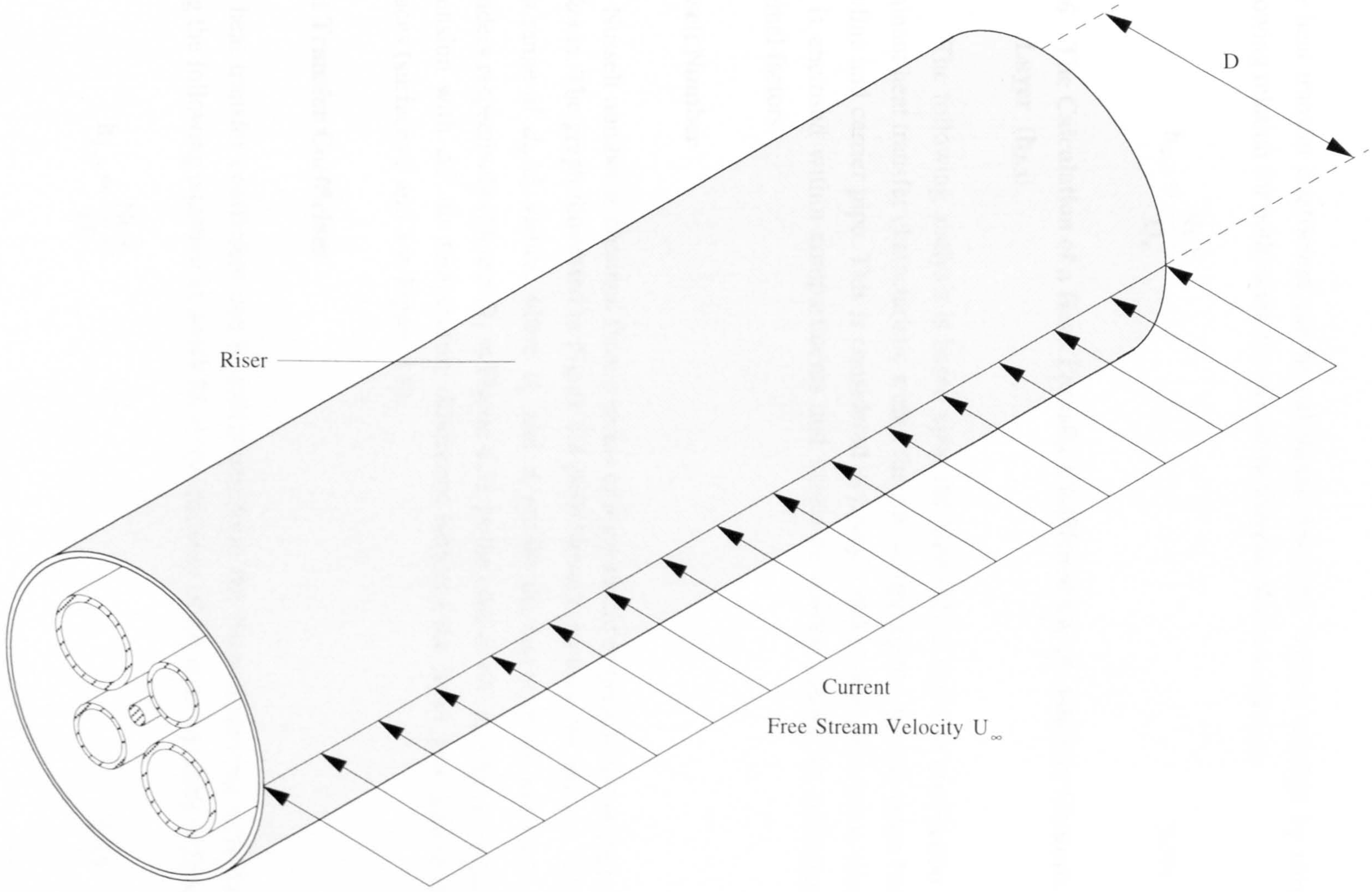

Figure 4.7

Forced Convection - Normal to the Riser

$$Re_D = \frac{U_\infty D_4}{\upsilon} \tag{4.38}$$

Heat Transfer Coefficient

The heat transfer coefficient can be calculated from the Nusselt number by using the following relation for both cases of convective transfer discussed above:

$$h_{4-5} = \frac{Nu\,k}{D_4} \tag{4.39}$$

4.4.6 The Calculation of a Heat Transfer Coefficient for an Annular Gaseous Layer (h_{2-3})

The following analysis is based upon the assumption that free convection is the dominant heat transfer characteristic within the gas occupying the annular space between flowline and carrier pipe. This is considered as being a reasonable assumption since the gas is enclosed within compartments and hence its motion cannot be influenced by external factors.

Nusselt Number

The Nusselt number is obtained from a series of logarithmic empirical curves derived by *Beckman*. The graph illustrated in Figure 4.8 plots Nusselt number Nu against $(Gr_{di}\,Pr)$ for a range of d_o/d_i values, where d_o and d_i are the diameters of the outer and inner cylinders respectively (D_2 and D_3 in Figure 4.5). In the case of Gr, d_i is the characteristic dimension with ΔT the temperature difference between the inner and outer cylinder surfaces (surfaces 2 and 3 in Figure 4.5).

Heat Transfer Coefficient

The heat transfer coefficient can be calculated from the Nusselt number as before by using the following equation in which D_2 is the diameter of the inner cylinder or flowline.

$$h_{2-3} = \frac{Nu\,k}{D_2} \tag{4.40}$$

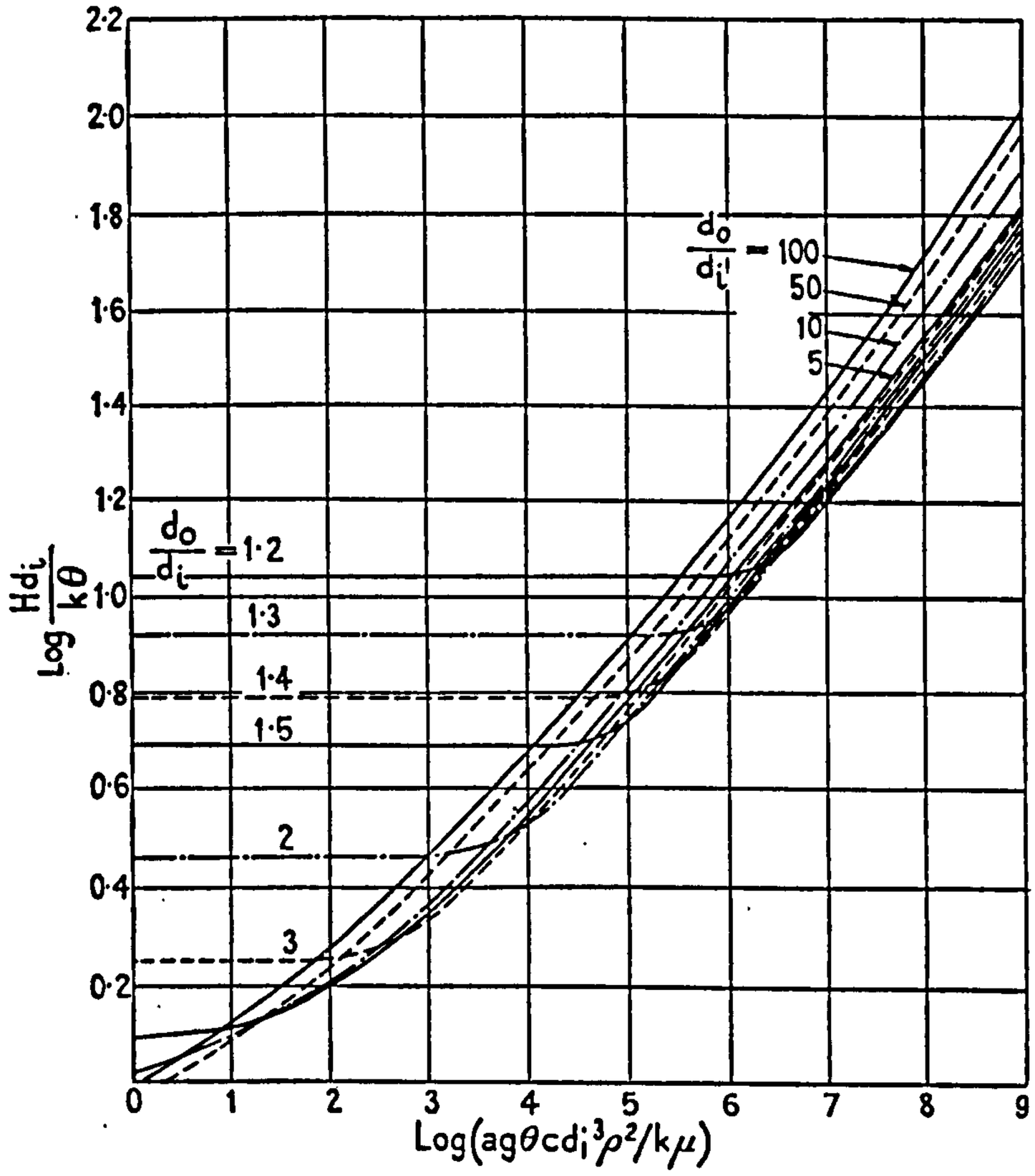

Equivalent Terms:

$$\text{Log}\left(a\,g\,\theta\,c\,d_i^3\,\rho^2/k\,\mu\right) \equiv \text{Log Gr Pr}$$

$$\text{Log}\,\frac{H d_i}{k\theta} \equiv \text{Log Nu}$$

$$\frac{d_o}{d_i} \equiv \frac{D_3}{D_2}$$

Figure 4.8

Beckman's Curves for Free Convection across a Layer of Fluid between Two Concentric Cylinders

4.5 Insulation Design for a Seabed Pipeline and Catenary Riser.

4.5.1 Introduction

This analysis aims to apply the heat transfer relationships detailed in the previous section to first of all establish fluid heat loss and temperature decay behaviour for the proposed riser arrangements as described in Chapter 3. A similar analysis is also conducted upon the pipeline linking wellhead and riser. This section of the production system can be considered to be as critical if not more so than the riser in terms of heat loss due to its considerable length (6000 m) and servere ambient environment (min water temperature at 1500 m is approx. -1.0 °C). The results of both studies should then provide information on whether flowline insulation is required in order to further minimise heat loss and ultimately limit oil transportation problems.

4.5.2 System Modelling

In order to carry out an analytical heat transfer analysis both pipeline and riser are modelled using a simplified cross-sectional geometric arrangement. Oil flow heat loss calculations are then carried out on this model using an EXCEL spreadsheet. The spreadsheet is created so as allow a variety of both fluid and structural parameters to be altered in order for their respective influences on the heat transfer behaviour to be established.

Catenary Riser

Figure 4.9 illustrates the proposed cross-section of the catenary riser as defined in Chapter 3 in which buoyancy is provided by either syntactic foam or pressurised nitrogen gas. The heat transfer model is displayed below in Figure 4.10. This model is created by removing all but one of the flowlines, a single oil flowline, which is centred within the carrier pipe. The cross-section is now of annular geometry and therefore similar to that shown in Figure 4.5, thereby allowing the thermal analysis methods previously outlined to be applied using the catenary riser spreadsheet (Spreadsheet 4.2).

Seabed Pipeline

The cross-sectional arrangement of the seabed pipeline (Figure 4.10) is exactly the same as that of the riser with the exception that in this case the carrier pipe is externally coated with concrete.

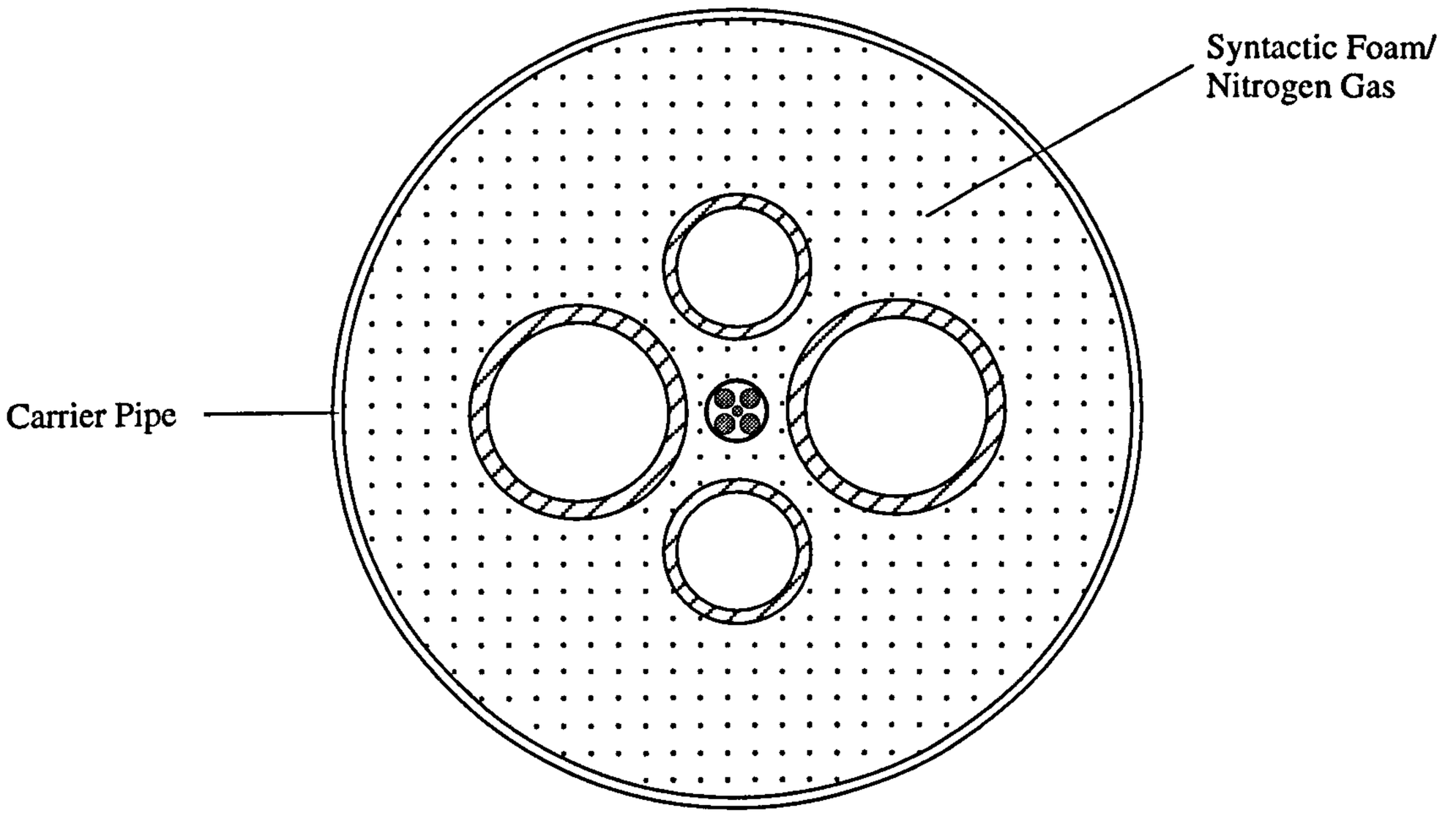

Actual Section b-b' **(a)**

Scale 1:15

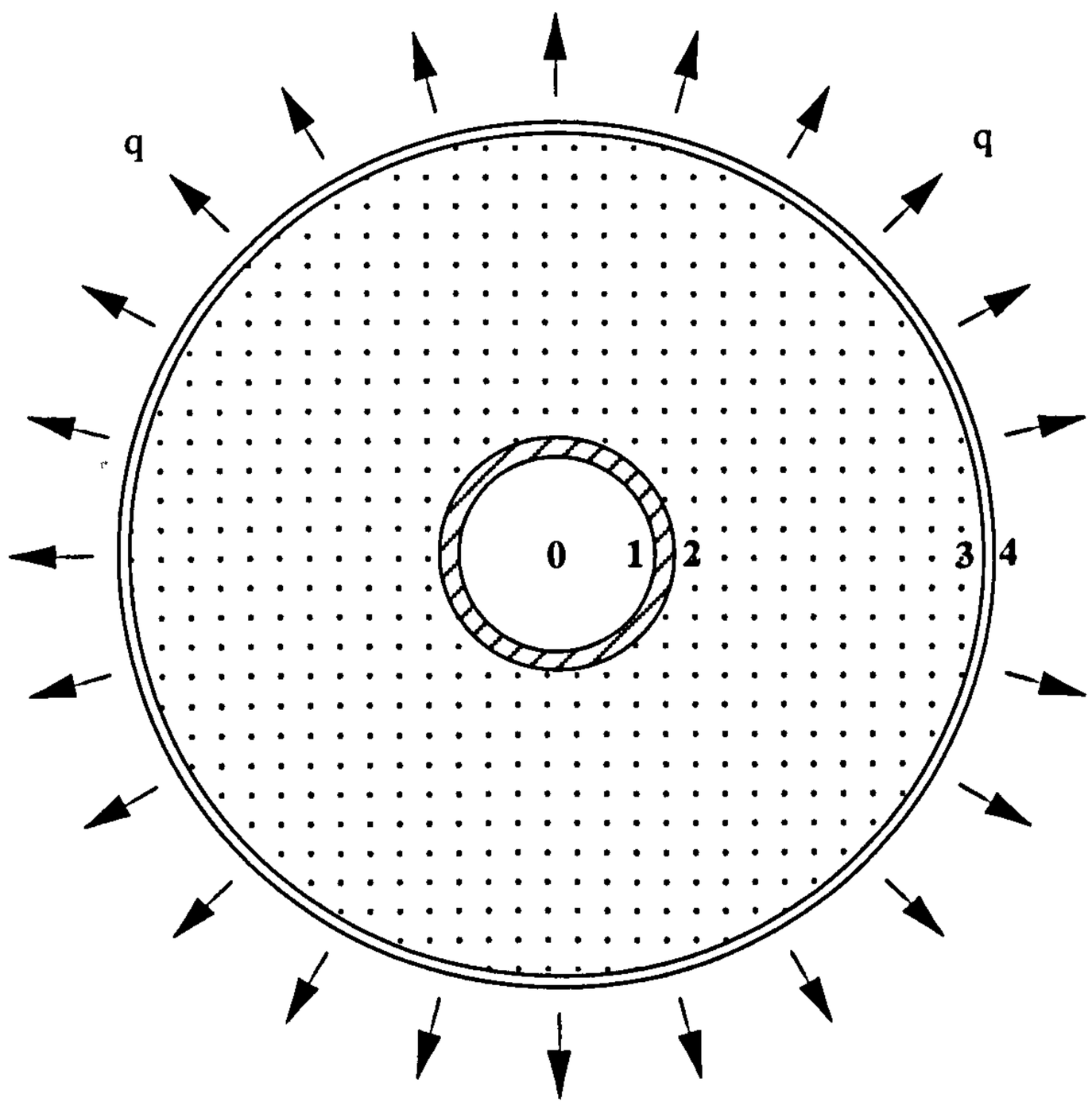

Thermal Model **(b)**

Figure 4.9

Catenary Riser Cross - Section

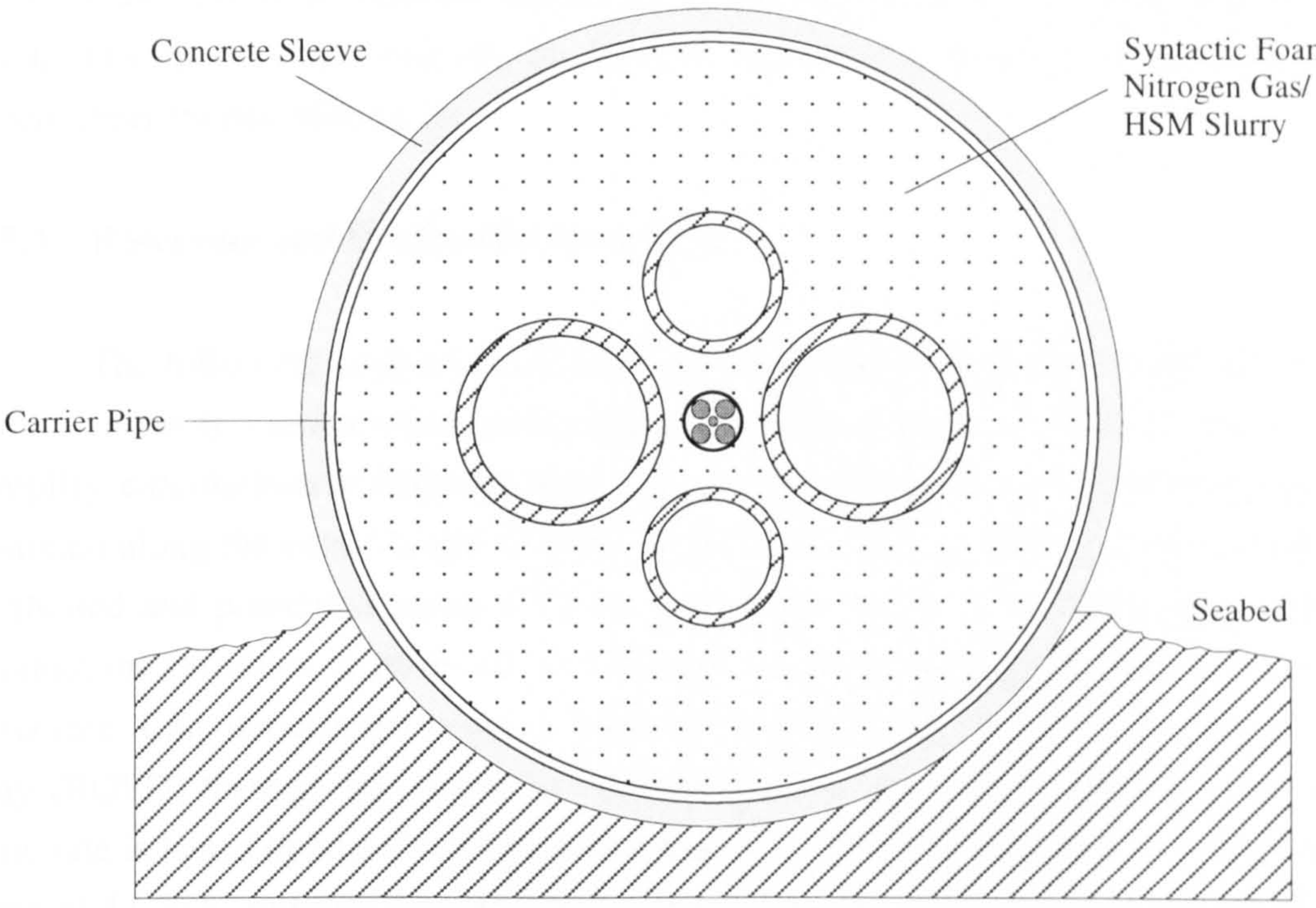

Actual Section a-a' **(a)**

Scale 1:15

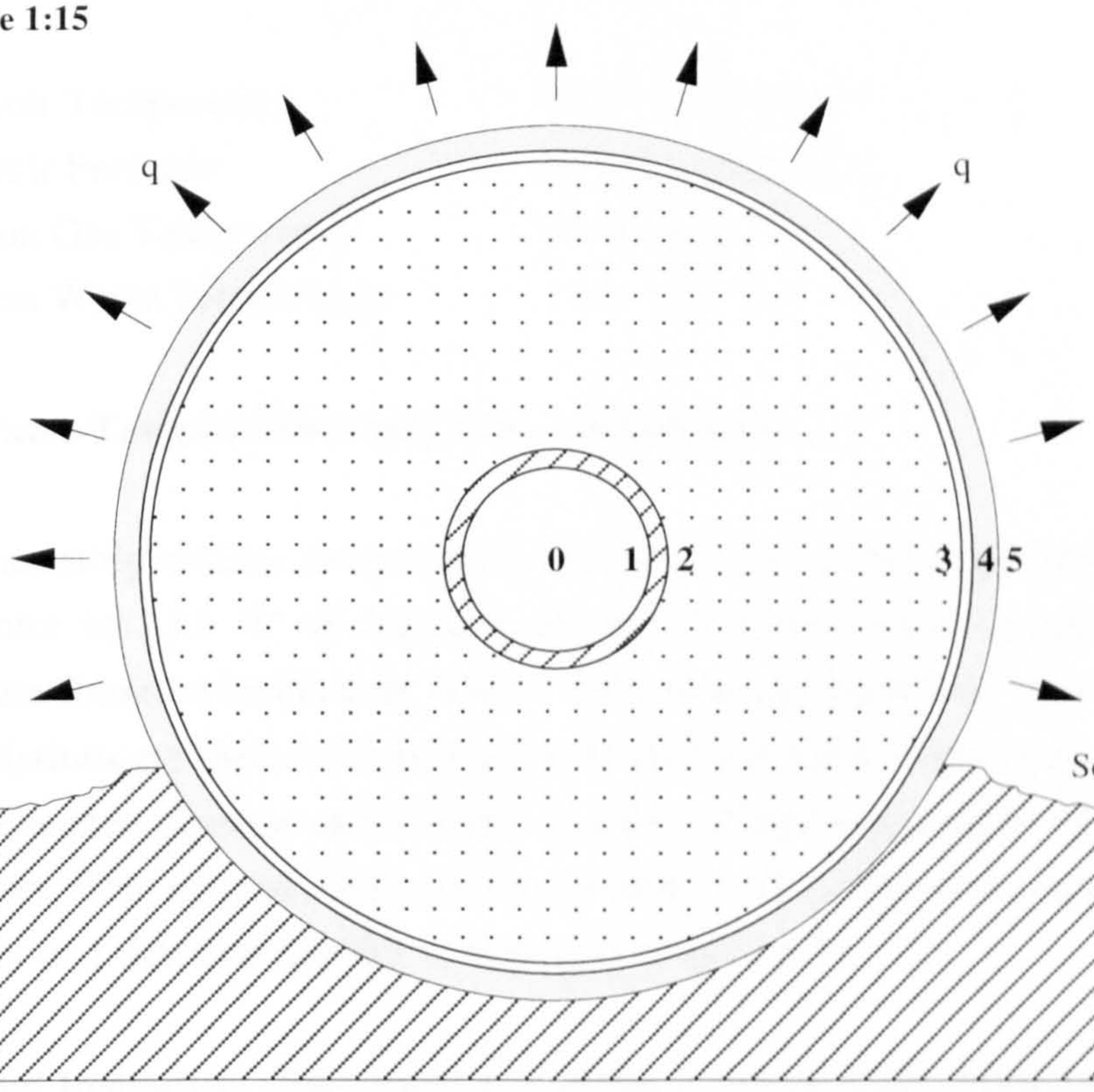

Thermal Model **(b)**

Figure 4.10

Seabed Pipeline Cross - Section

This coating provides the seabed pipeline with a certain degree of lateral and vertical stability as well protection and according to current practices is approximately 40 mm thick. The thermal analysis of the pipeline is carried out using the seabed pipeline spreadsheet (Spreadsheet 4.1).

4.5.3 Reservoir and Production Flow Data

The following analysis is conducted using a single phase light crude oil (34 °API) with a viscosity - temperature relationship as shown in Figure 4.2. However in order to simplify calculations a constant viscosity (corresponding to wellhead temperature) is assumed along the entire length of pipeline and riser. The suitability of this hypothesis is evaluated and presented along with the rest of the results. One of the most important production variables in terms of its influence on fluid temperature decay behaviour is flow rate. Calculations are initially based upon a flow rate of 70,000 Barrels of Oil per Day (BOPD) through the single 12" flowline in the heat transfer model. This specific flow rate is based upon a oil production throughput of 150,000 BOPD for two production lines of 11.375" internal diameter taken from a current engineering design study. Other parameters selected for the purposes of this study are detailed below:

Reservoir Temperature	74 °C (165 °F)
Reservoir Pressure	413 bar (6000 psi)
Injection Gas Temperature	94 °C (200 °F)
Injection Water Temperature	10 °C (50 °F)

4.5.4 Sea Water Temperatures and Current Velocities

Mean monthly surface temperatures over the West of Shetland slope range from 8.0 °C in winter to 12.5 °C in summer. However beyond water depths of 1000 m temperatures are found to be close to -1.0 °C with seasonal variations almost negligible. Thermal calculations are therefore based upon an ambient water temperature of -1.0 °C in the case of the seabed pipeline and a depth averaged winter temperature of 4.5 °C in the case of the riser. The analysis subjects the production pipeline and riser to a normal current velocity of 1 m/s over the full water depth (Figure 4.7).

4.5.5 Thermal Insulation Characteristics of the Existing Riser Arrangement

The decay in production oil temperature along the seabed pipeline and riser is graphically shown in Figure 4.15 for both the syntactic foam and nitrogen gas arrangements. In each case the pipeline is simply an extension of the riser in terms of

construction and internal buoyancy content with the exception of the concrete coating. The actual cross-sectional arrangement along with the corresponding thermal model for both riser and pipeline are illustrated in Figures 4.9 and 4.10 respectively. Utilising either syntactic foam or nitrogen gas in a 6000 m seabed pipeline isn't very practical in terms of economic or technical feasibility, however the results are useful in a purely comparative role.

Syntactic Foam

The *Overall Heat Transfer Coefficient* for the syntactic foam riser can be expressed as follows:

$$U = \frac{2\pi}{\left[\frac{1}{r_1 h_{oil}} + \frac{1}{k_{steel}}\log_e\left(\frac{r_2}{r_1}\right) + \frac{1}{k_{sf}}\log_e\left(\frac{r_3}{r_2}\right) + \frac{1}{k_{steel}}\log_e\left(\frac{r_4}{r_3}\right) + \frac{1}{r_4 h_{sw}}\right]}$$

where:
h_{oil} = production oil heat transfer coefficient (forced convection)
k_{steel} = thermal conductivity of steel
k_{sf} = thermal conductivity of syntactic foam
h_{sw} = ambient sea water heat transfer coefficient (forced/free convection)
r_n = surface radii - defined in Figure 4.11(a)

The results presented in Figure 4.15 clearly illustrate how effective syntactic foam is as an insulating material. The syntactic foam maintains the oil temperature at a level virtually equivalent to its wellhead condition along the entire length of seabed pipeline and riser. The calculated drop in temperature between wellhead and surface is only 1.3 °C representing a 2% reduction from the wellhead condition. This impressive insulating characteristic is also demonstrated in Table 4.2, in which temperatures at specified radial surfaces are tabulated at three different locations (A, B and C, see Figure 4.1) along the seabed pipeline and riser. The fall in temperature (radially) across the foam at each of the locations is approximately equivalent to 99% of the centre flow temperature T_0.

Nitrogen Gas

The *Overall Heat Transfer Coefficient U* for the nitrogen gas riser can be defined as follows:

$$U = \frac{2\pi}{\left[\frac{1}{r_1 h_{oil}} + \frac{1}{k_{steel}} \log_e\left(\frac{r_2}{r_1}\right) + \frac{1}{r_2 h_{ng}} + \frac{1}{k_{steel}} \log_e\left(\frac{r_4}{r_3}\right) + \frac{1}{r_4 h_{sw}}\right]}$$

where: h_{ng} = nitrogen gas heat transfer coefficient (free convection)

r_n = surface radii - defined in Figure 4.11(a)

Although a gas is a very good insulator in terms of conduction with a thermal conductivity of only 0.024 W/m K gases are very poor insulators whenever convection becomes the dominant thermal mechanism. This is confirmed by the results presented in Figure 4.15 which show a considerable decay in oil temperature along both the seabed pipeline and catenary riser. The calculated drop in temperature between wellhead and surface production unit is 44 °C representing a 60% reduction from the wellhead condition (at 74 °C). As a result of this large decrease in temperature the oil in the riser attains a thermal condition in which emulsification and wax deposition can develop ultimately inhibiting efficient oil transportation. When the radial temperature distributions are examined (Table 4.2) only 30 to 55% of the total temperature drop occurs across the annular gas layer, compared to 99% in the case of synaptic foam. Although syntactic foam is mostly air, the fact that it is trapped within tiny hollow particles that are themselves held securely within a resin matrix ensures that heat conduction is the more dominant heat transfer mechanism. Air has a very low thermal conductivity giving rise to the effective nature of syntactic foam as a insulator. If a gas is held in a large compartment un-restrained, it circulates in response to density changes thereby creating convection currents which are considerably more proficient in transporting thermal energy than conduction

The gases heat transfer coefficient as determined from Figure 4.8 is based upon both Prandtl and Grashof numbers as defined in Eqns (4.32) and (4.34) respectively. These in turn are a function of viscosity (dynamic and kinematic) and ultimately gas pressure. Thermal calculations carried out on the seabed pipeline use a gas pressure equal to that experienced at a sea water depth of 1500 m (151 bar) where as the riser calculations are based upon a uniform depth averaged pressure of 75.5 bar along the entire length.

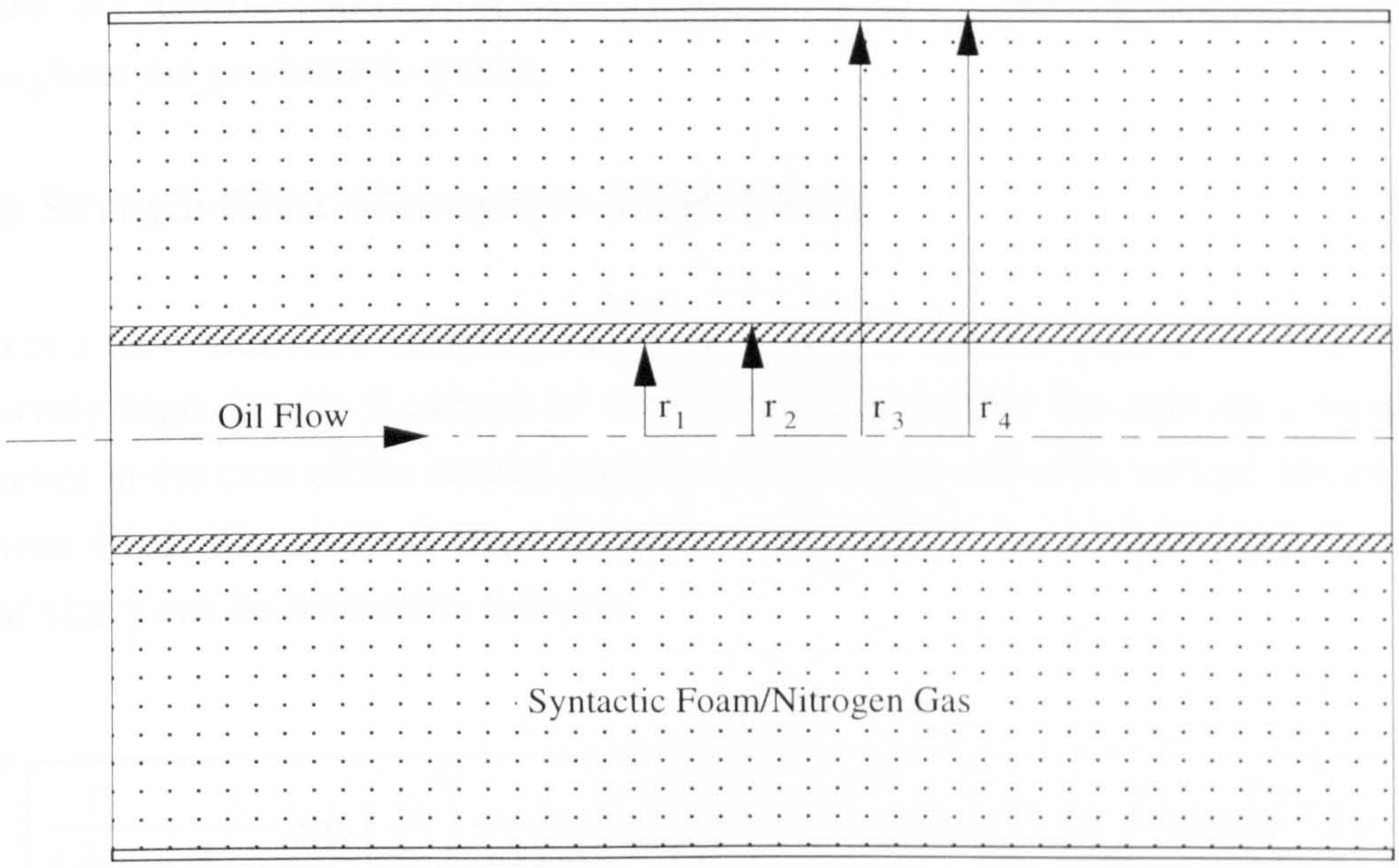

Catenary Riser **(b)**

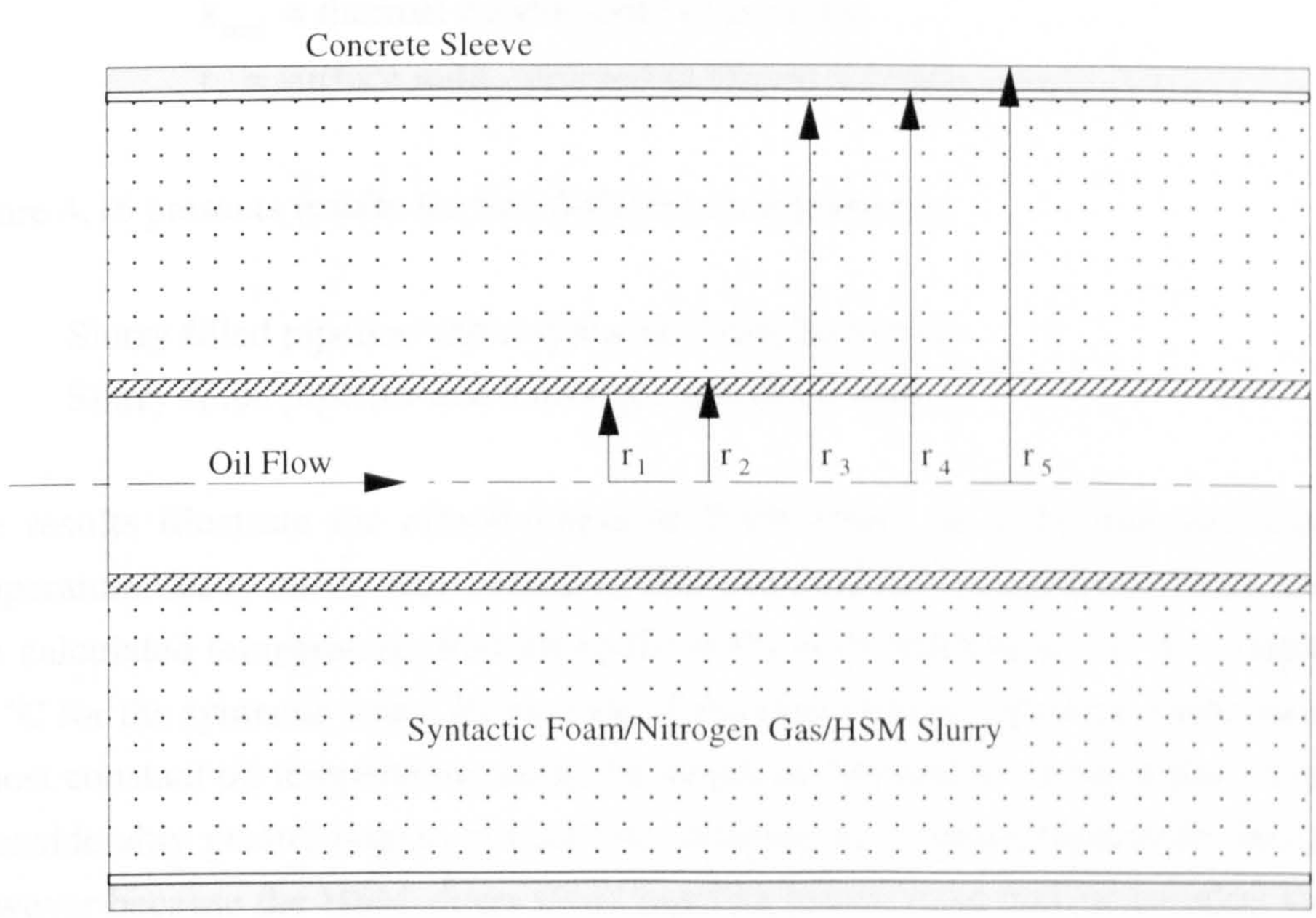

Seabed Pipeline **(a)**

Scale 1:15

Figure 4.11

Thermal Model Longitudinal - Sections

4.5.6 Alternative Methods of Insulation

This section examines alternative methods of insulation which are economic, technically feasible and capable of maintaining the oil temperature at a high enough level throughout the production system.

High Strength-Silica Microsphere (HSM) Slurry

This is a new substance currently being developed at Heriot Watt University. Due to its relatively high density it cannot be considered practical for the riser on a weight basis, however in the case of the seabed pipeline HSM slurry can offer several advantages, see Section 4.3.2. The *Overall Heat Transfer Coefficient U* for a seabed pipeline utilising HSM slurry can be defined as follows:

$$U = \frac{2\pi}{\left[\frac{1}{r_1 h_{oil}} + \frac{1}{k_{steel}}\log_e\left(\frac{r_2}{r_1}\right) + \frac{1}{k_{hsm}}\log_e\left(\frac{r_3}{r_2}\right) + \frac{1}{k_{steel}}\log_e\left(\frac{r_4}{r_3}\right) + \frac{1}{k_c}\log_e\left(\frac{r_5}{r_4}\right) + \frac{1}{r_5 h_{sw}}\right]}$$

where: k_{hsm} = thermal conductivity of HSM slurry
k_{steel} = thermal conductivity of concrete
r_n = surface radii - defined in Figure 4.11(b)

Figure 4.16 presents results for two different arrangements:

- Slurry filled pipeline and a syntactic foam filled riser
- Slurry filled pipeline and a nitrogen gas filled riser

The results illustrate the effectiveness of HSM slurry as a thermal insulator with a temperature decay curve very similar to that obtained for the syntactic foam filled riser. The calculated temperature drop along the 6000 m of pipeline is 1.8 °C compared with 1.0 °C for the syntactic foam. In the case of the riser section, syntactic foam maintains an almost constant oil temperature along the length as opposed to nitrogen gas which allows a considerably greater degree of heat loss resulting in a rapid temperature decay profile. However because the HSM slurry filled pipeline has ensured that oil entering the riser is at a temperature level close to its wellhead condition, the temperature at the sea surface is now well above the level required (≈ 37 °C) to potentially activate any oil flow problems such as emulsification and wax deposition. The calculated oil temperature at the top of the riser is 54.1 °C compared with 30 °C in the case of a nitrogen gas filled seabed pipeline.

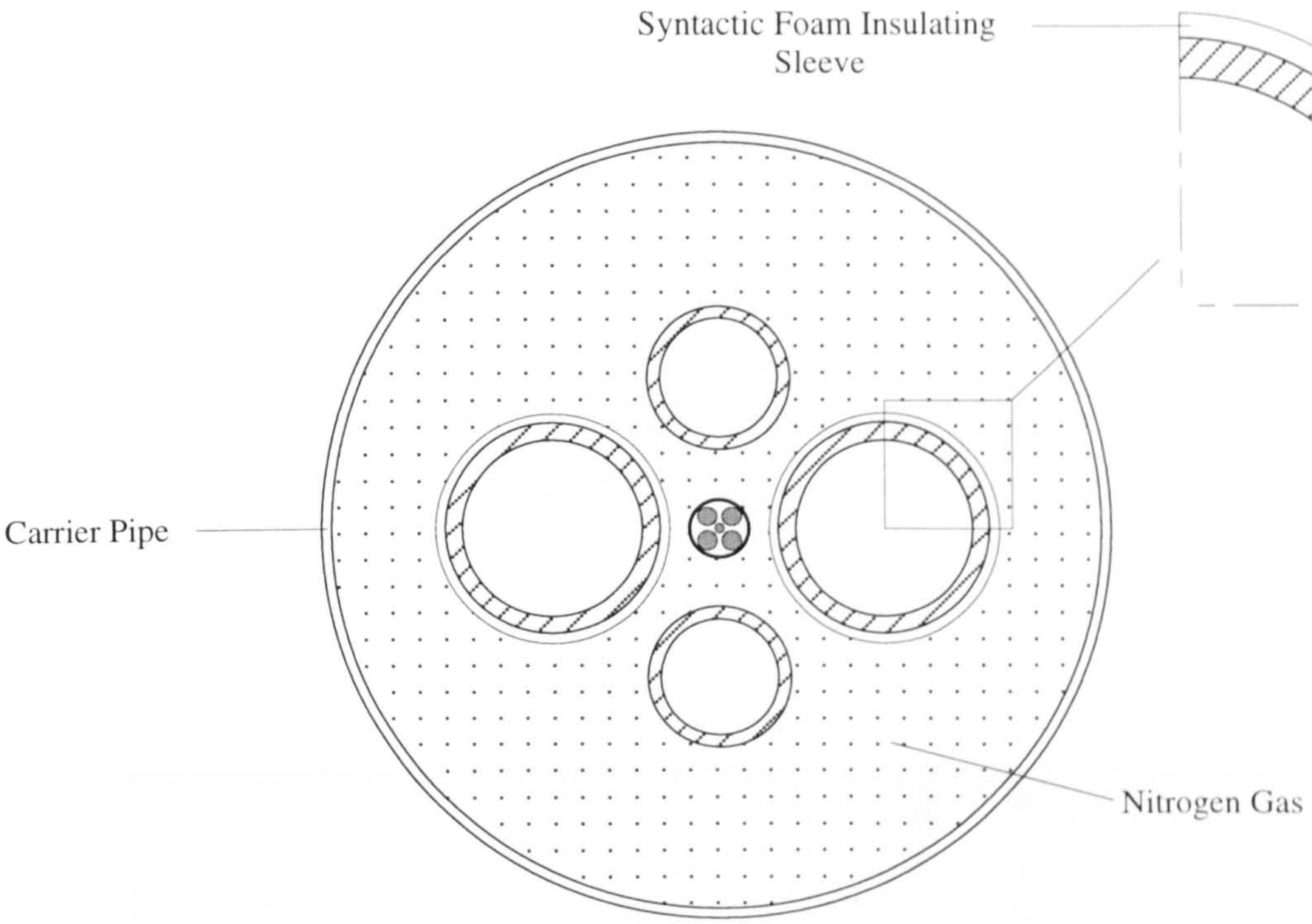

Actual Section b-b' **(a)**

Scale 1:15

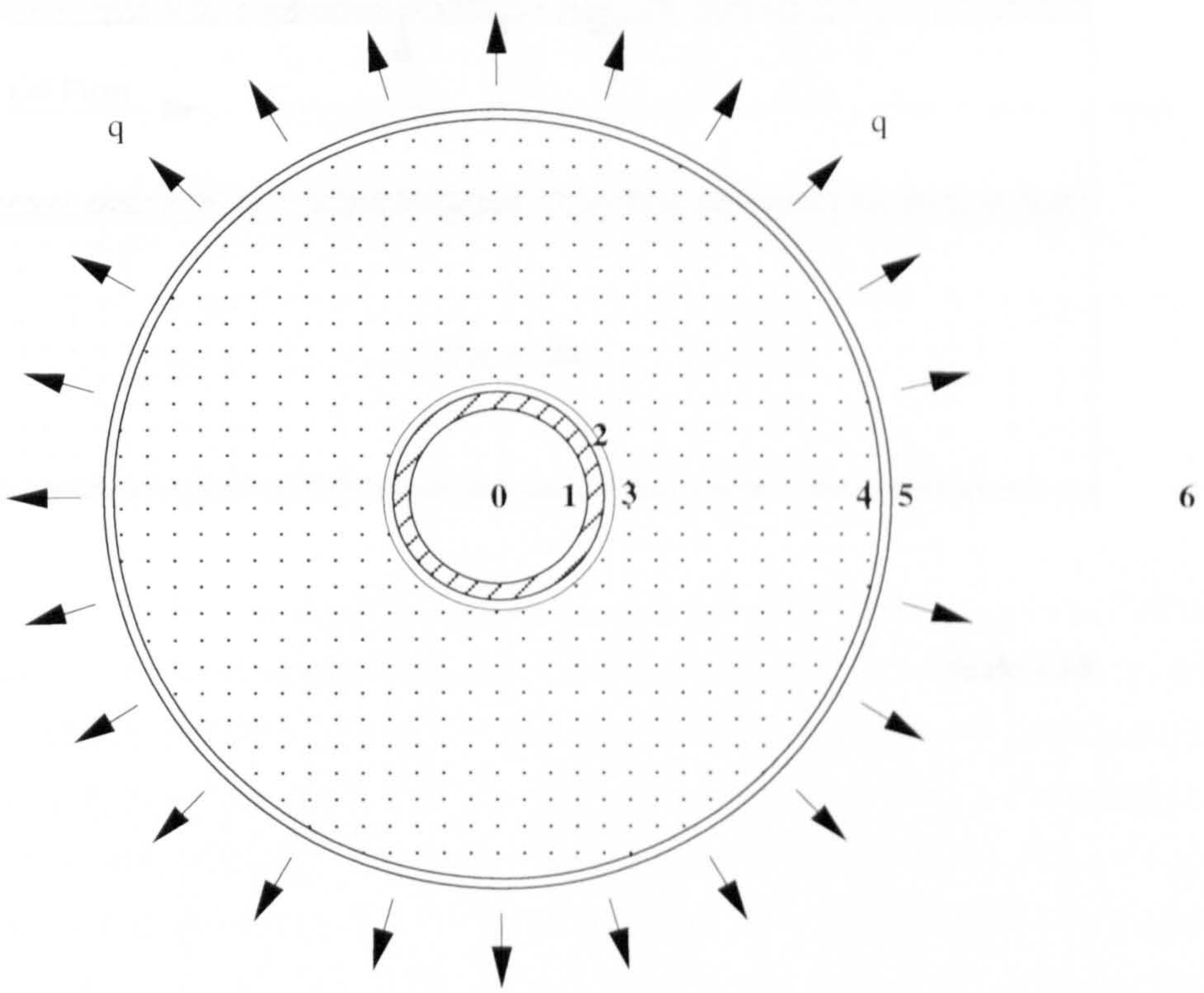

Thermal Model **(b)**

Figure 4.12

Catenary Riser Cross - Section

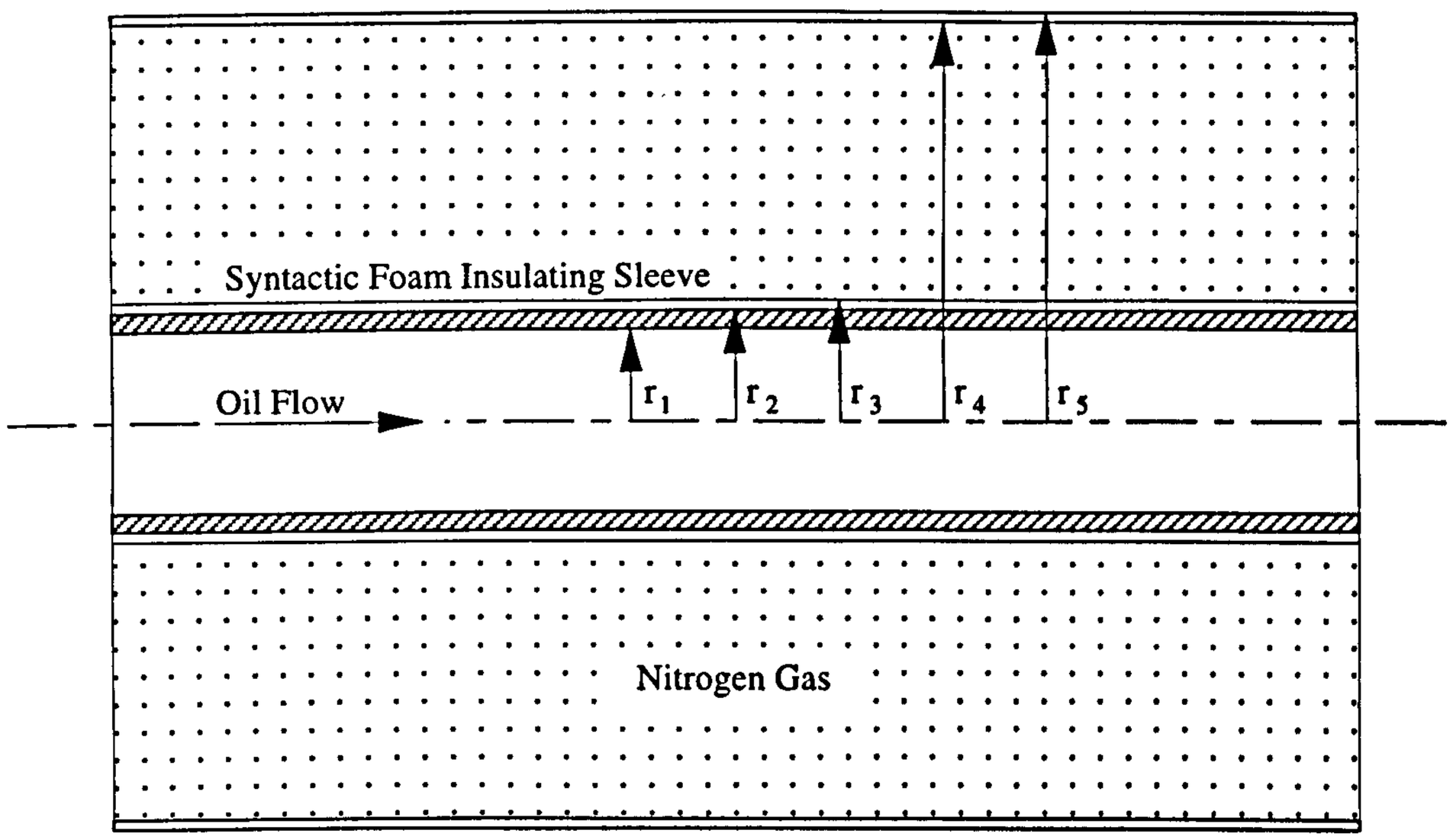

Scale 1:15

Figure 4.13

Thermal Model Longitudinal - Section

Nitrogen Gas with a Syntactic Foam Flowline Sleeve

In order to try and retain even more heat within the riser whilst still using a nitrogen gas based system requires the oil flowlines to be encased within an insulating sleeve (Figure 4.12). This sleeve has to be lightweight, easily fabricated, sufficiently strong under compression as well as possessing good insulating characteristics. This specification can be achieved by using syntactic foam and therefore this section aims to evaluate the thermal characteristics of a nitrogen gas riser with syntactic foam insulated oil flowlines. The *Overall Heat Transfer Coefficient U* for the riser can be defined as follows:

$$U = \frac{2\pi}{\left[\frac{1}{r_1 h_{oil}} + \frac{1}{k_{steel}}\log_e\left(\frac{r_2}{r_1}\right) + \frac{1}{k_{sfl}}\log_e\left(\frac{r_3}{r_2}\right) + \frac{1}{r_3 h_{N_2}} + \frac{1}{k_{steel}}\log_e\left(\frac{r_5}{r_4}\right) + \frac{1}{r_5 h_{sw}}\right]}$$

where: r_n = surface radii - defined in Figure 4.13

The results displayed graphically in Figure 4.17 correspond to a slurry filled seabed pipeline and a 10 mm thick syntactic foam sleeve around the flowline. The added insulation has the effect of increasing the oil temperature at the surface from 54.1 °C to 66.5 °C. The effect of sleeve thickness on heat loss is demonstrated in Figure 4.18(a) in which surface oil temperature is plotted against syntactic foam sleeve thickness. The results show a non-linear relationship with most of the increase in temperature occurring when the thickness is increased from 0 to 20 mm, beyond this the temperature curve tends to a horizontal asymptote as thickness approaches infinity.

4.5.7 The Effect of Oil Flow Rate on Temperature Decay

Besides the overall heat transfer coefficient, temperature decay is also a function of fluid flow rate as demonstrated by Eqn (4.26). The influence of single flowline flow rates between 1,000 and 70,000 Barrels of Oil per Day (BOPD) on oil temperature at locations (B) and (C) are calculated and presented in Figure 4.18(b). The insulation system chosen for this analysis is the nitrogen gas/syntactic foam sleeve (10 mm) arrangement with the seabed pipeline filled with HSM slurry. Both temperature curves show a non-linear response to flow rate, as flow rate is increased so does temperature, however the rate of increase progressively decays with both curves levelling out at about 40,000 BOPD in a similar way to that experienced with the sleeve thickness. At about 12,000 BOPD the oil at the top of the riser (location C) reaches the temperature zone where emulsification and wax deposition become potential problems and at a flow rate of

approximately 7,000 BOPD hydration becomes an issue depending upon the composition of the crude oil.

4.5.8 The Effect of Oil Viscosity on Temperature Decay

All the thermal analysis conducted so far has assumed a constant oil viscosity with respect to temperature. This section aims to justify this assumption by establishing the thermal sensitivity of the system to oil viscosity, this can be achieved by taking practical maximum and minimum values from Figure 4.2 and applying them throughout the production system using the existing thermal models. The results are as follows:

Dynamic Viscosity (74 °C) is 0.0032 kg/m s Oil Temperature at (C) = 66.5 °C

Dynamic Viscosity (10 °C) is 0.01 kg/m s Oil Temperature at (C) = 66.8 °C

For the viscosity range considered the results suggest an almost negligible difference. The insulation system chosen for this analysis is the nitrogen gas/syntactic foam sleeve (10 mm) arrangement with the seabed pipeline filled with HSM slurry.

4.5.9 The Effect of High Temperatures on Syntactic Foam

For the grade of syntactic foam required for deep water operations, most manufacturers suggest a maximum limiting temperature of approximately 90 °C. At about this temperature the foam starts to soften creating a reduction in density and hence strength with the rate of softening being dependent upon the grade of foam used. In the case of the oil flowlines temperatures don't exceed 74 °C (reservoir temperature) and so no problems arise, however injection gas temperatures can reach temperatures of 94 °C, high enough to degrade the foam in the immediate area. A simple and practical solution to this problem would be insert a high density polyurethane sleeve around the injection gas flowline with the aim of sufficiently insulating the syntactic foam from the high temperatures generated by the gas. An illustration of this arrangement can be found in Figures 3.3, 3.4 and 3.5.

4.6 Thermal Stress Analysis

4.6.1 Introduction

The following section attempts to evaluate the effects of temperature on the catenary riser in terms of induced axial stress.

Thermal stress is caused by differences in structural temperature that are inherent within the system. These structural temperature differences are created by materials either expanding or contracting from an initial condition in response to radial temperature gradients set up between the hot flowline fluids and the cold ambient sea water as presented in the previous chapter.

Thermal stress is a direct function of structural temperature difference and so the greatest stresses will occur when the riser has attained it operational condition. All calculations are therefore based upon this condition and the assumption that the flowlines equal the oil temperature and the carrier pipe equals the ambient sea water temperature. The radial temperature distributions tabulated in Tables 4.2 to 4.4 justify this hypothesis.

Thermal strain is based upon a components change in temperature from an initial condition which for the purposes of this study is 20 °C. It is assumed that this corresponds to an ambient average temperature during riser and pipeline onshore fabrication. During oil production the flowlines as shown in the previous section attain a considerably higher temperature and will therefore expand, however the carrier pipe experiences a drop in temperature as it takes on the surrounding temperature and hence it contracts. An important feature about this behaviour is that if the flowlines and carrier pipe were not structurally connected then thermal strain would be unaccompanied by stress i.e. component strain is unrestrained. However the riser design is based upon both the flowlines and carrier pipe being integral parts of the structure and therefore axial strain is restrained resulting in thermal stress. In the cases of both riser and pipeline structural connection between flowlines and carrier pipe is achieved by way of transverse steel bulkheads.

The total strain in a body experiencing restraint and therefore stress may be divided into two components:

- strain resulting from the stress (restriction induced) - expressed as ε_σ
- strain resulting from the temperature change - expressed as ε_T

Therefore:

$$\varepsilon = \varepsilon_\sigma + \varepsilon_T \tag{4.43}$$

or

$$\varepsilon = \frac{\sigma}{E} + \alpha\left(T - T_i\right) \tag{4.44}$$

where: α = coefficient of linear thermal expansion

$\left(T - T_i\right)$ = change in temperature from initial condition

σ = axial thermal stress

The coefficient of linear expansion is a measure of a materials size dependence upon temperature and is therefore a material property.

4.6.2 Thermal Stress Calculations

Figure 4.14 illustrates the basic longitudinal cross-section of a riser or pipeline in which a flowline bundle is encapsulated within a carrier pipe. The annular volume around the flowlines is filled with either pressurised gas, slurry (in the case of the pipeline) or syntactic foam with structural connections between flowlines and carrier pipe provided through the use of transverse bulkheads. These bulkheads act to constrain relative movement between flowlines and carrier pipe ensuring that all structural components acts as an integral unit.

Since there is no externally applied force, the sum of the internal forces in the flowlines and carrier pipe must be zero. Therefore:

$$F_{cp} + F_f = 0 \tag{4.45}$$

or

$$\sigma_{cp} A_{cp} + \sigma_f A_f = 0 \tag{4.46}$$

where: F_{cp} = carrier pipe internal axial force

F_f = flowline bundle internal axial force

σ_{cp} = carrier pipe axial stress

σ_f = flowline bundle axial stress

A_{cp} = carrier pipe steel cross-sectional area

A_f = total steel cross-sectional area of flowline bundle

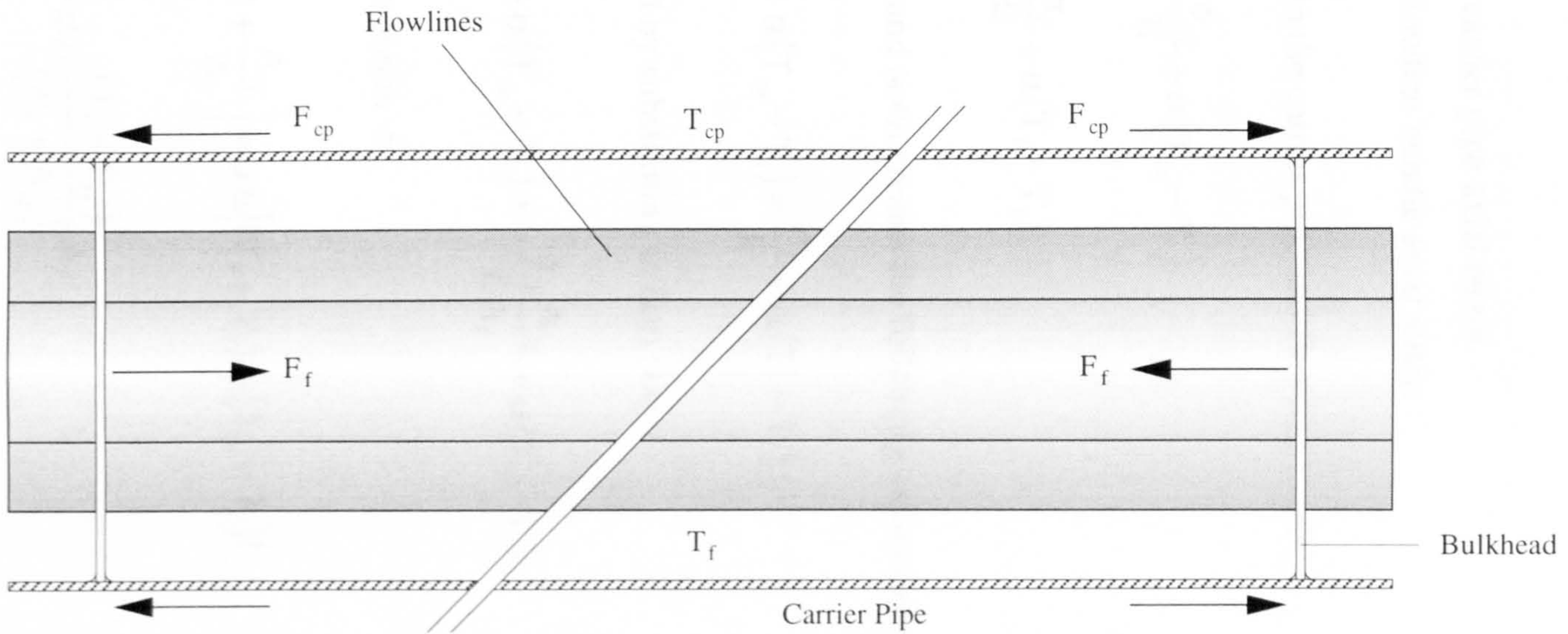

Scale 1:20

Figure 4.14

Thermal Stress Model

Since relative motion between flowlines and carrier pipe is restrained then their respective axial strains are equal:

$$\varepsilon_{cp} = \varepsilon_f \tag{4.47}$$

where: ε_{cp} = carrier pipe axial strain

ε_f = flowline bundle axial strain

Applying Eqn (4.44) to the carrier pipe and flowline bundle:

$$\varepsilon_{cp} = \frac{\sigma_{cp}}{E} + \alpha\left(T_{cp} - T_i\right) \tag{4.48}$$

$$\varepsilon_f = \frac{\sigma_f}{E} + \alpha\left(T_f - T_i\right) \tag{4.49}$$

Equating Eqns (4.48) and (4.49) creates the following expression:

$$\frac{\sigma_{cp}}{E} + \alpha\left(T_{cp} - T_i\right) = \frac{\sigma_f}{E} + \alpha\left(T_f - T_i\right) \tag{4.50}$$

σ_f can be eliminated by substituting in Eqn (4.46):

$$\frac{\sigma_{cp}}{E} + \alpha\left(T_{cp} - T_i\right) = -\frac{\sigma_{cp} A_{cp}}{E A_f} + \alpha\left(T_f - T_i\right) \tag{4.51}$$

Re-arranging so as to obtain σ_{cp}

$$\sigma_{cp}\left(1 + \frac{A_{cp}}{A_f}\right) = \alpha E\left[\left(T_f - T_i\right) - \left(T_{cp} - T_i\right)\right] \tag{4.52}$$

$$\sigma_{cp} = \alpha E \frac{\left(T_f - T_{cp}\right)}{\left(A_f + A_{cp}\right)} A_f \tag{4.53}$$

σ_f can be obtained by substituting in Eqn (4.46):

$$\alpha E \frac{\left(T_f - T_{cp}\right)}{\left(1 + \frac{A_{cp}}{A_f}\right)} + \sigma_f A_f = 0 \tag{4.54}$$

therefore:

$$\sigma_f = -\alpha E \frac{\left(T_f - T_{cp}\right)}{\left(A_f + A_{cp}\right)} A_{cp} \qquad (4.55)$$

The negative sign indicates a compressive stress whilst a positive sign denotes a tensile stress.

The axial loads imposed upon the seabed pipeline and riser as a consequence of temperature differences within the structure are presented graphically in Figures 4.19(a) and (b) respectively for carrier pipe diameters of 1.0 and 1.1 m. In each case it is assumed that the difference in temperature between carrier pipe and ambient seawater is negligible resulting in a pipeline carrier pipe at -1.0 °C and a riser carrier pipe at 4.5 °C.

Both graphs illustrate a linear relationship between flowline temperature and axial stress in both the carrier pipe and flowline bundle. As the temperature of the flowlines is increased, the carrier pipe is forced to expand and the flowlines forced to contract resulting in an increase in axial stress, tensile in the case of the carrier pipe and compressive in the case of the flowlines. If a situation arose in which the flowlines were colder than the surroundings then the opposite would occur i.e. the flowlines would be tension and the carrier pipe in compression, see Figure 4.19(b).

References

1. Visser, R.C. (1987) *Offshore Production of Heavy Oil*, In Proc Offshore Technology Conference, OTC 5494.

2. Woodyard, A.H. (1978) *An Insulated Offshore Pipeline for Deep Water*, In Proc Offshore Technology Conference, OTC 3070.

3. Hamouda, A.A. and Ravnoy, J.M. (1992) *Prediction of Wax Deposition in Pipelines and Field Experiance on the Inf;luence of Wax on Drag-Reducing Performance*, In Proc Offshore Technology Conference, OTC 7060.

4. Qunelle, A. and Gunaltun, M. (1987) *Comparison Between Thermal Insulation Coatings for Underwater Pipelines*, In Proc Offshore Technology Conference, OTC 5500.

5. Nelson, D.O. and Colquhoun, R. (1993) *New Thermal Insulations for CDTM Bundles: Foamed Polyurethanes and Silica Sphere Slurries*, In Proc Offshore Technology Conference, OTC 7313.

6. Costello, G.J. and Henery, D. (1983) *Insulated Pipelines Between the Underwater Manifold Centre and Cormorant A Platform in the Northern North Sea*, In Proc Offshore Technology Conference, OTC 4611.

7. Massey, B.S. (1989) *Mechanics of Fluids*, Sixth Edition, VNR International.

8. Chapman, A.J. (1987) *Fundermentals of Heat Transfer*, Macmillan Publishing Company.

9. Rogers, G.F.C. and Mayhew, Y.R. (1980) *Engineering Thermodynamics, Work & Heat Transfer*, Third Edition, Longman Scientific & Technical.

10. Benham, P.P. and Crawford, R.J. (1987) *Mechanics of Engineering Materials*, Longman Scientific & Technical.

11. *Mobil Riser Study*, Kvaerner Engineering, Project No. 2429

12. Wilson, P.M. *Riser Mooring Design Study*, Basis of Design Document, YD4724, Section

CHAPTER 4

Analysis Spreadsheets

Spreadsheets 4.1 - 4.2

Thermal Analysis - Seabed Pipeline

Material and Fluid Components	Initial Temperature (degs C)	Thermal Conductivity (W/m K)	Kinematic Viscosity (m2/s)	Dynamic Viscosity (kg/m s)	Density (kg/m3)	Specific Heat Capacity (J/kg K)	Volume Flow Rate (BPD)	Gas Pressure (bar)	Beta
Oil	74	0.0825	3.74E-06	3.20E-03	855	2009	70,000		
Sea Water	-1	0.5619	1.79E-06	1.79E-03	1025	4218			0.0052
Steel		36			7850				
Nitrogen Gas		0.034	1.28E-07	2.31E-05	179.83	1047		151	0.0035
Syntactic Foam		0.1			384				
Concrete Lining		1			2000				
HSM Slurry		0.3			820				
Polyurethane		0.057			400				

	Outer Diameter (m)	Wall Thickness (mm)
Carrier Pipe	1.2	10
Flowline	0.324	25.4
Flowline Sleeve		0
Carrier Pipe Sleeve		40

Radius (1)	0.137	m
Radius (2)	0.162	m
Radius (3)	0.162	m
Radius (4)	0.590	m
Radius (5)	0.600	m
Radius (6)	0.640	m

Fluids	Mass Flow Rate (kg/s)	Prandtl No.	Reynolds No.	Friction Factor	Grashof No.	Rayleigh No.	Nusselt No.	Heat Transfer Coefficient (W/m2 K)	Gr/Re2
Oil	110.14	77.92	1.60E+05	0.00395			701.4	211.8	
Sea Water		13.44			2.74E+10	3.69E+11	1018.2	476.8	
Sea Water		13.44	6.70E+05		2.74E+10		2515.5	1177.9	0.06
Nitrogen Gas		0.71			1.27E+12		354.0	37.2	

Forced Convection - Internal Flow
Free Convection - External
Forced Convection - External Flow
Free Convection - Internal

Overall Heat Transfer Coefficient =	1.42	W/m2 K
Initial Rate of Heat Output =	0.11	kW/m2
Oil Temperature at Distance x =	71.2	degs C

Output to Spreadsheet 4.2 ◄ x = 6000 m

Initial Temperatures

T0 =	74	degs C	T5 =	0.1	degs C
T1 =	73.4	degs C	T6 =	-1.0	degs C
T2 =	73.3	degs C	T7 =	-1.0	degs C
T3 =	73.3	degs C			
T4 =	0.1	degs C			

Spreadsheet 4.1

Thermal Analysis - Catenary Riser

Material and Fluid Components	Initial Temperature (degs C)	Thermal Conductivity (W/m K)	Kinematic Viscosity (m2/s)	Dynamic Viscosity (kg/m s)	Density (kg/m3)	Specific Heat Capacity (J/kg K)	Volume Flow Rate (BPD)	Gas Pressure (bar)	Beta
Oil	71.2	0.0825	3.74E-06	3.20E-03	855	2009	70,000		
Sea Water	4.5	0.5619	1.79E-06	1.79E-03	1025	4218			0.0052
Steel		36			7850				
Nitrogen Gas		0.034	2.59E-07	2.31E-05	89.32	1047		75	0.0035
Syntactic Foam		0.1			384				
Concrete Lining		1			2000				
HSM Slurry		0.3			820				
Polyurethane		0.057			400				

Input from Spreadsheet 4.1

	Outer Diameter (m)	Wall Thickness (mm)
Carrier Pipe	1.0	10
Flowline	0.324	25.4
Flowline Sleeve		10
Carrier Pipe Sleeve		0

Radius (1)	0.137	m
Radius (2)	0.162	m
Radius (3)	0.172	m
Radius (4)	0.490	m
Radius (5)	0.500	m
Radius (6)	0.500	m

Fluids	Mass Flow Rate (kg/s)	Prandtl No.	Reynolds No.	Friction Factor	Grashof No.	Rayleigh No.	Nusselt No.	Heat Transfer Coefficient (W/m2 K)	Gr/Re2	
Oil	110.14	77.92	1.60E+05	0.00395			701.4	211.8		Forced Convection - Internal Flow
Sea Water		13.44			1.59E+10	2.14E+11	851.5	478.5		Free Convection - External
Sea Water		13.44	5.58E+05		1.59E+10		2170.5	1219.6	0.05	Forced Convection - External Flow
Nitrogen Gas		0.71			3.76E+11		259.4	25.6		Free Convection - Internal

Overall Heat Transfer Coefficient =	7.24	W/m2 K
Initial Rate of Heat Output =	0.48	kW/m2
Oil Temperature at Distance x =	66.5	degs C
x =	2243.75	m

Initial Temperatures

T0 =	71.2	degs C	T5 =	4.6	degs C
T1 =	68.5	degs C	T6 =	4.6	degs C
T2 =	68.2	degs C	T7 =	4.5	degs C
T3 =	22.1	degs C			
T4 =	4.7	degs C			

Spreadsheet 4.2

CHAPTER 4

Results

Figures 4.15 - 4.19

Tables 4.2 - 4.4

Seabed Pipeline Oil Temperature Profile (N2/SF)

(a)

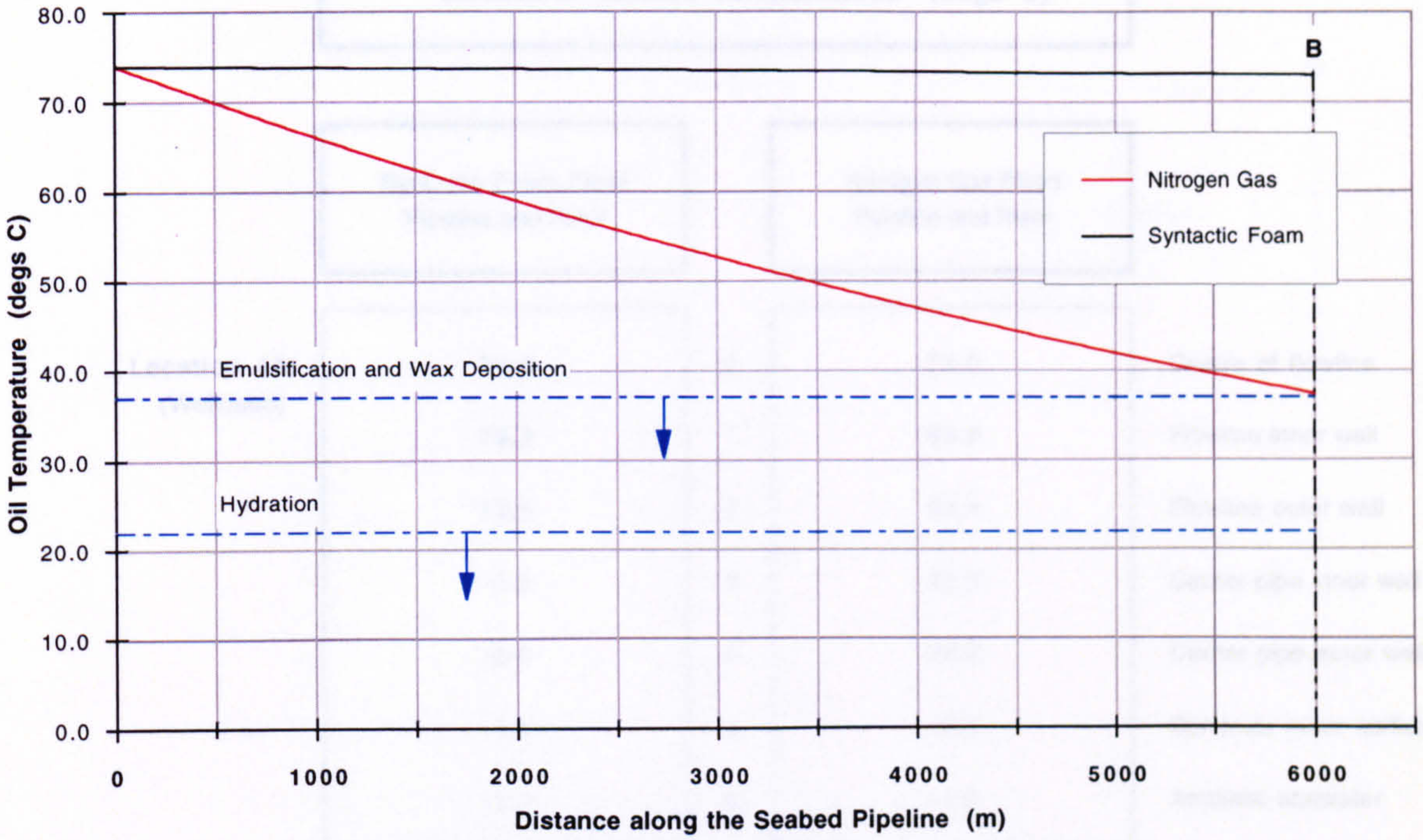

Catenary Riser Oil Temperature Profile

(b)

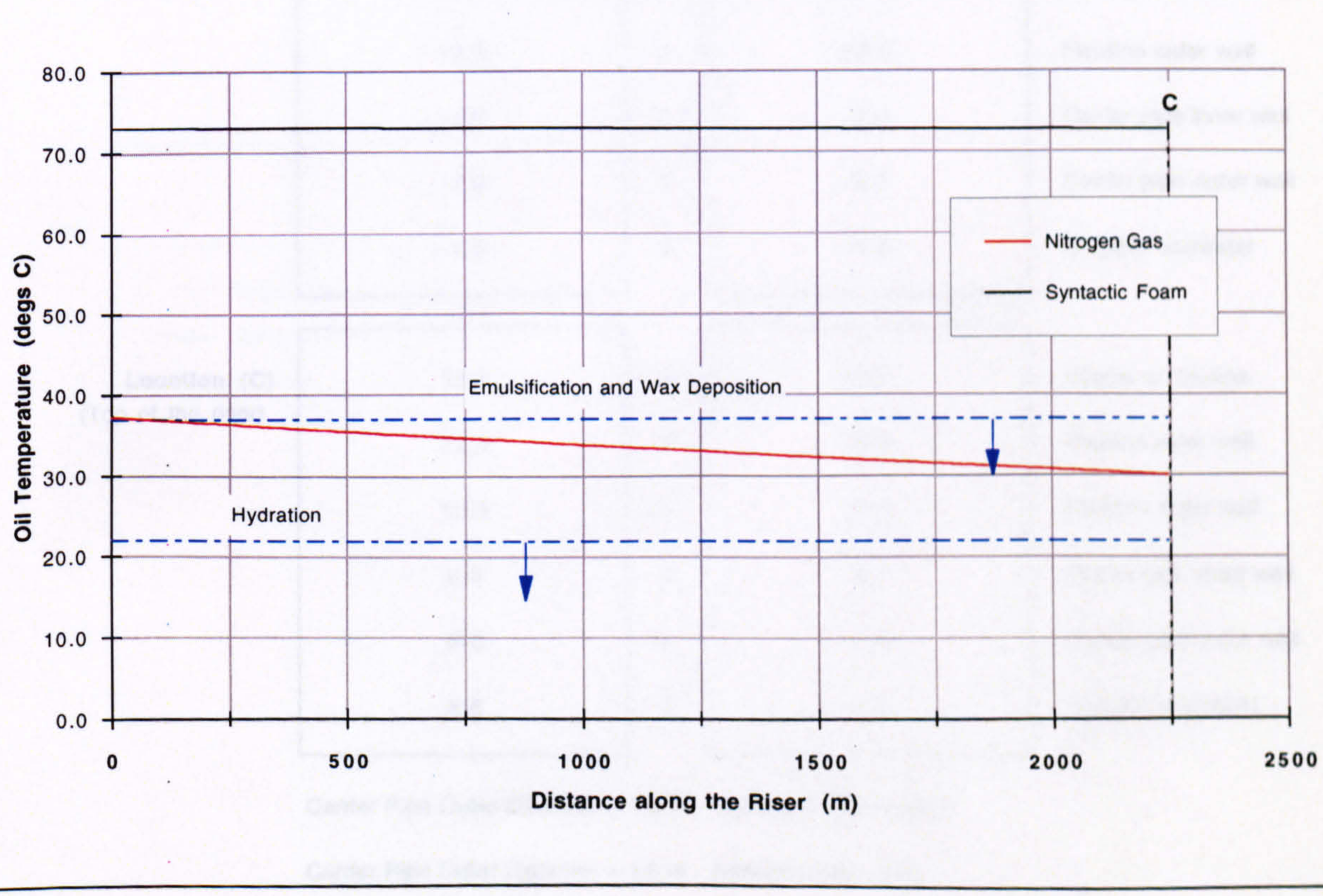

Carrier Pipe Outer Diameter = 1.2 m (Syntactic Foam case)

Sea Depth = 1500 m

Carrier Pipe Outer Diameter = 1.0 m (Nitrogen Gas case)

Figure 4.15

Radial Temperature Distributions (N2/SF)

	Structural Surface Temperatures (degs C)			
	Syntactic Foam Filled Pipeline and Riser		Nitrogen Gas Filled Pipeline and Riser	
Location (A) (Wellhead)	74.0	0	74.0	Centre of flowline
	73.8	1	63.8	Flowline inner wall
	73.8	2	62.4	Flowline outer wall
	-0.6	3	22.3	Carrier pipe inner wall
	-0.6	4	22.2	Carrier pipe outer wall
	-1.0	5	-0.6	Concrete outer surface
	-1.0	6	-1.0	Ambient seawater
Location (B) (Bottom of the riser)	73.0	0	37.3	Centre of flowline
	72.8	1	30.2	Flowline inner wall
	72.8	2	29.3	Flowline outer wall
	-1.0	3	-0.6	Carrier pipe inner wall
	-1.0	4	-0.7	Carrier pipe outer wall
	-1.0	5	-1.0	Ambient seawater
Location (C) (Top of the riser)	72.7	0	30.0	Centre of flowline
	72.5	1	29.6	Flowline inner wall
	72.5	2	29.6	Flowline outer wall
	8.0	3	8.0	Carrier pipe inner wall
	8.0	4	8.0	Carrier pipe outer wall
	8.0	5	8.0	Ambient seawater

Carrier Pipe Outer Diameter = 1.2 m (Syntactic Foam case)

Carrier Pipe Outer Diameter = 1.0 m (Nitrogen Gas case)

Sea Depth = 1500 m

Table 4.2

Seabed Pipeline Oil Temperature Profile (HSM Slurry)

(a)

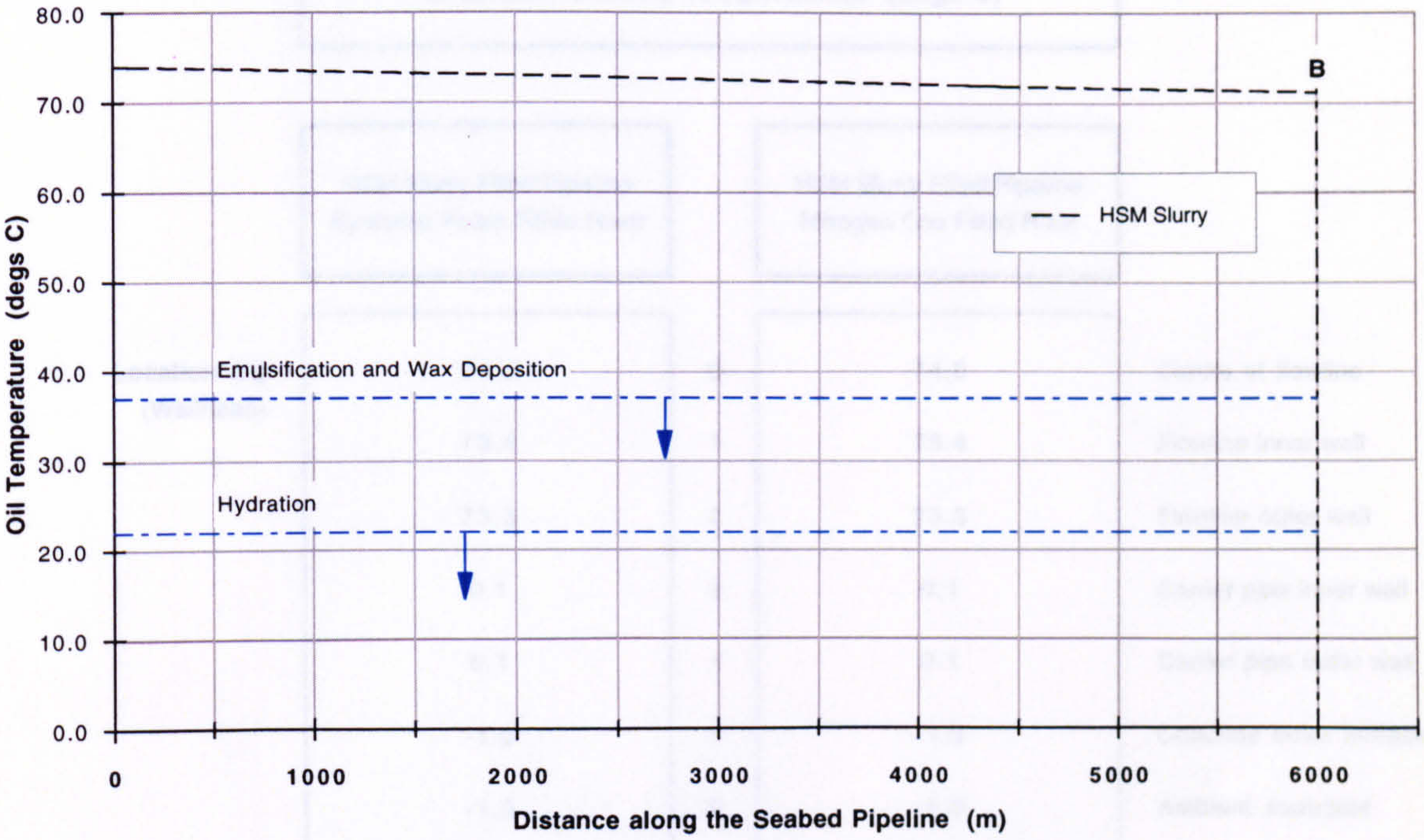

Catenary Riser Oil Temperature Profile

(b)

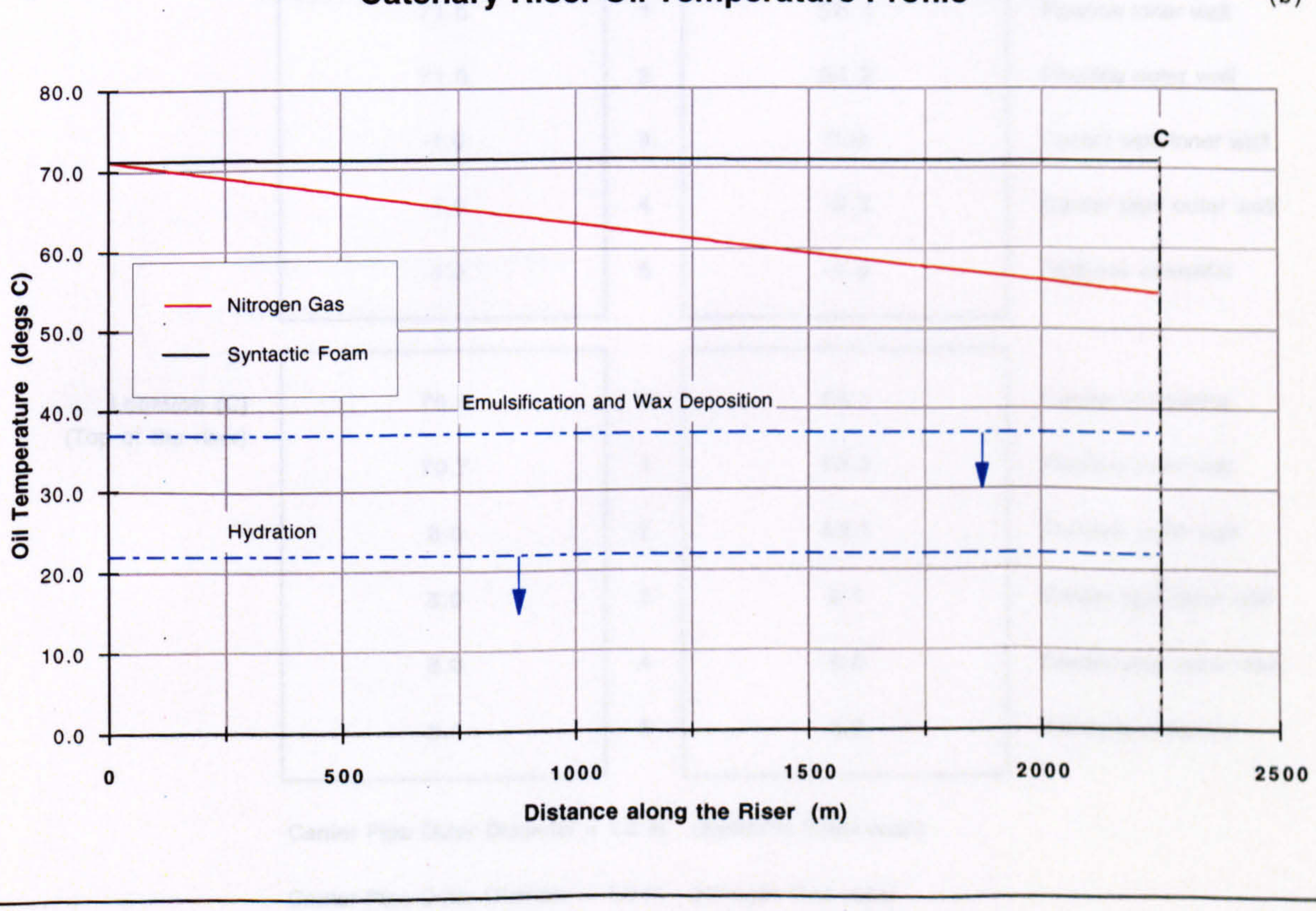

Carrier Pipe Outer Diameter = 1.2 m (Syntactic Foam case)

Sea Depth = 1500 m

Carrier Pipe Outer Diameter = 1.0 m (Nitrogen Gas case)

Figure 4.16

Radial Temperature Distributions (HSM Slurry)

	Structural Surface Temperatures (degs C)			
	HSM Slurry Filled Pipeline Syntactic Foam Filled Riser		HSM Slurry Filled Pipeline Nitrogen Gas Filled Riser	
Location (A) (Wellhead)	74.0	0	74.0	Centre of flowline
	73.4	1	73.4	Flowline inner wall
	73.3	2	73.3	Flowline outer wall
	0.1	3	0.1	Carrier pipe inner wall
	0.1	4	0.1	Carrier pipe outer wall
	-1.0	5	-1.0	Concrete outer surface
	-1.0	6	-1.0	Ambient seawater
Location (B) (Bottom of the riser)	71.2	0	71.2	Centre of flowline
	71.0	1	56.3	Flowline inner wall
	71.0	2	54.2	Flowline outer wall
	-1.0	3	0.0	Carrier pipe inner wall
	-1.0	4	-0.3	Carrier pipe outer wall
	-1.0	5	-1.0	Ambient seawater
Location (C) (Top of the riser)	70.9	0	54.1	Centre of flowline
	70.7	1	53.2	Flowline inner wall
	8.0	2	53.1	Flowline outer wall
	8.0	3	8.1	Carrier pipe inner wall
	8.0	4	8.0	Carrier pipe outer wall
	8.0	5	8.0	Ambient seawater

Carrier Pipe Outer Diameter = 1.2 m (Syntactic Foam case)

Carrier Pipe Outer Diameter = 1.0 m (Nitrogen Gas case)

Sea Depth = 1500 m

Table 4.3

Seabed Pipeline Oil Temperature Profile

(a)

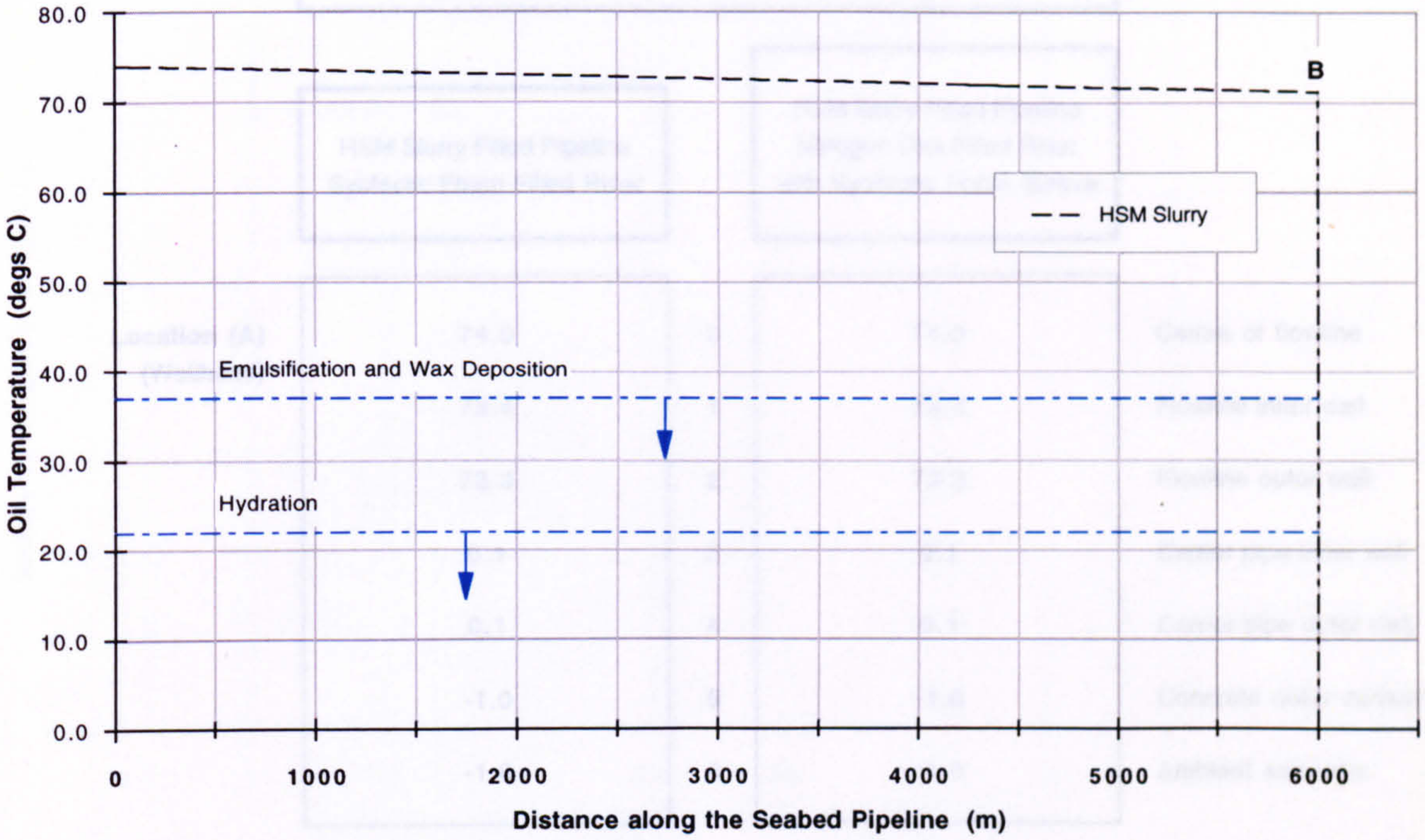

Catenary Riser Oil Temperature Profile (SF Sleeve)

(b)

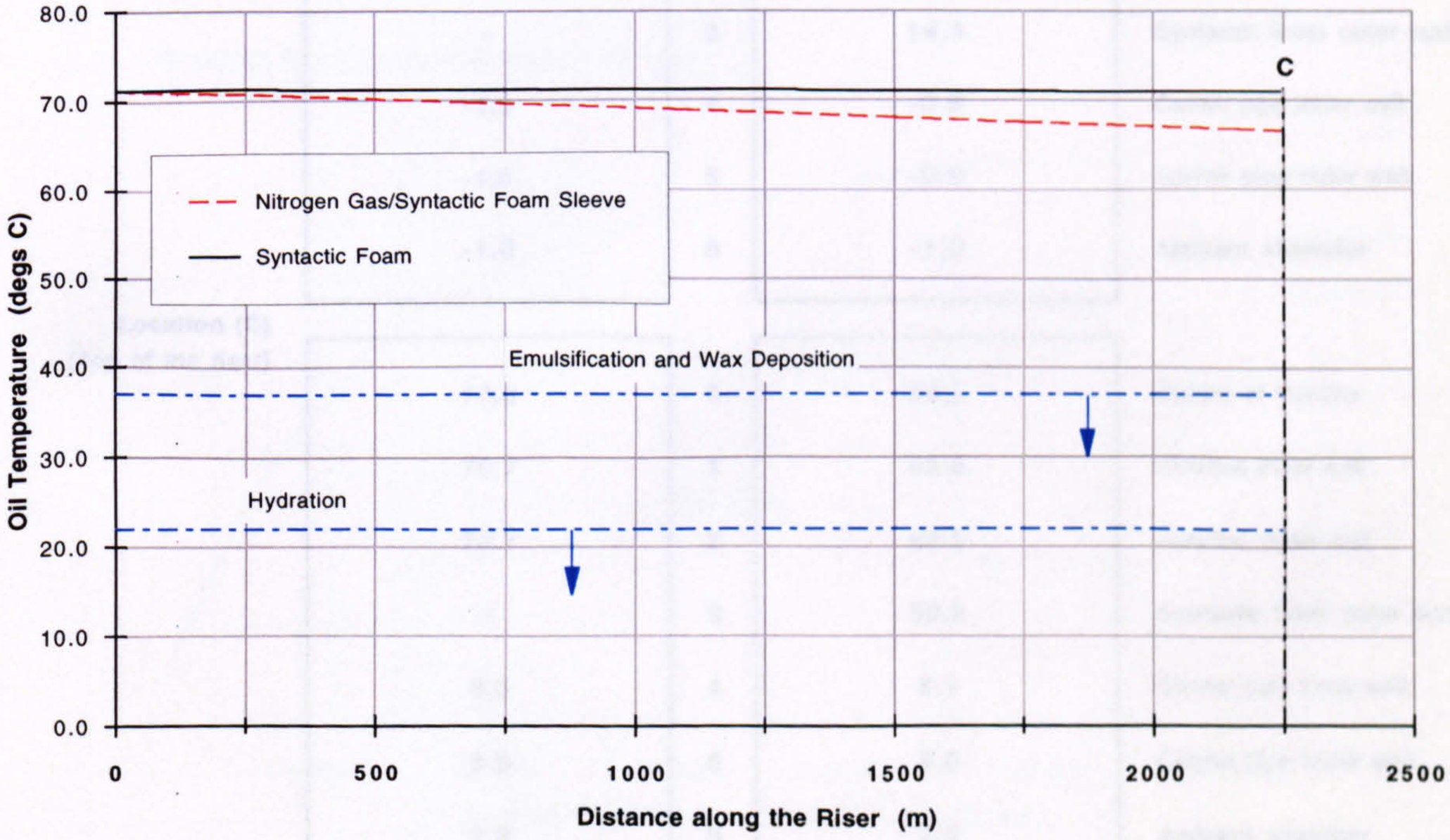

Carrier Pipe Outer Diameter = 1.2 m (Syntactic Foam case)

Sea Depth = 1500 m

Carrier Pipe Outer Diameter = 1.0 m (Nitrogen Gas/Syntactic Foam Sleeve case)

Syntactic Foam Sleeve Thickness = 10 mm

Figure 4.17

Radial Temperature Distributions (SF Sleeve)

	Structural Surface Temperatures (degs C)			
	HSM Slurry Filled Pipeline Syntactic Foam Filled Riser		HSM Slurry Filled Pipeline Nitrogen Gas Filled Riser with Syntactic Foam Sleeve	
Location (A) (Wellhead)	74.0	0	74.0	Centre of flowline
	73.4	1	73.4	Flowline inner wall
	73.3	2	73.3	Flowline outer wall
	0.1	3	0.1	Carrier pipe inner wall
	0.1	4	0.1	Carrier pipe outer wall
	-1.0	5	-1.0	Concrete outer surface
	-1.0	6	-1.0	Ambient seawater
Location (B) (Bottom of the riser)	71.2	0	71.2	Centre of flowline
	71.0	1	68.1	Flowline inner wall
	71.0	2	67.7	Flowline outer wall
	-	3	14.1	Syntactic foam outer surface
	-1.0	4	-0.8	Carrier pipe inner wall
	-1.0	5	-0.9	Carrier pipe outer wall
	-1.0	6	-1.0	Ambient seawater
Location (C) (Top of the riser)	70.9	0	66.5	Centre of flowline
	70.7	1	65.6	Flowline inner wall
	70.7	2	65.5	Flowline outer wall
	-	3	50.2	Syntactic foam outer surface
	8.0	4	8.1	Carrier pipe inner wall
	8.0	5	8.0	Carrier pipe outer wall
	8.0	6	8.0	Ambient seawater

Carrier Pipe Outer Diameter = 1.2 m (Syntactic Foam case)

Carrier Pipe Outer Diameter = 1.0 m (Nitrogen Gas case)

Table 4.4

The Effect of S-Foam Sleeve Thickness on Oil Temperature

(a)

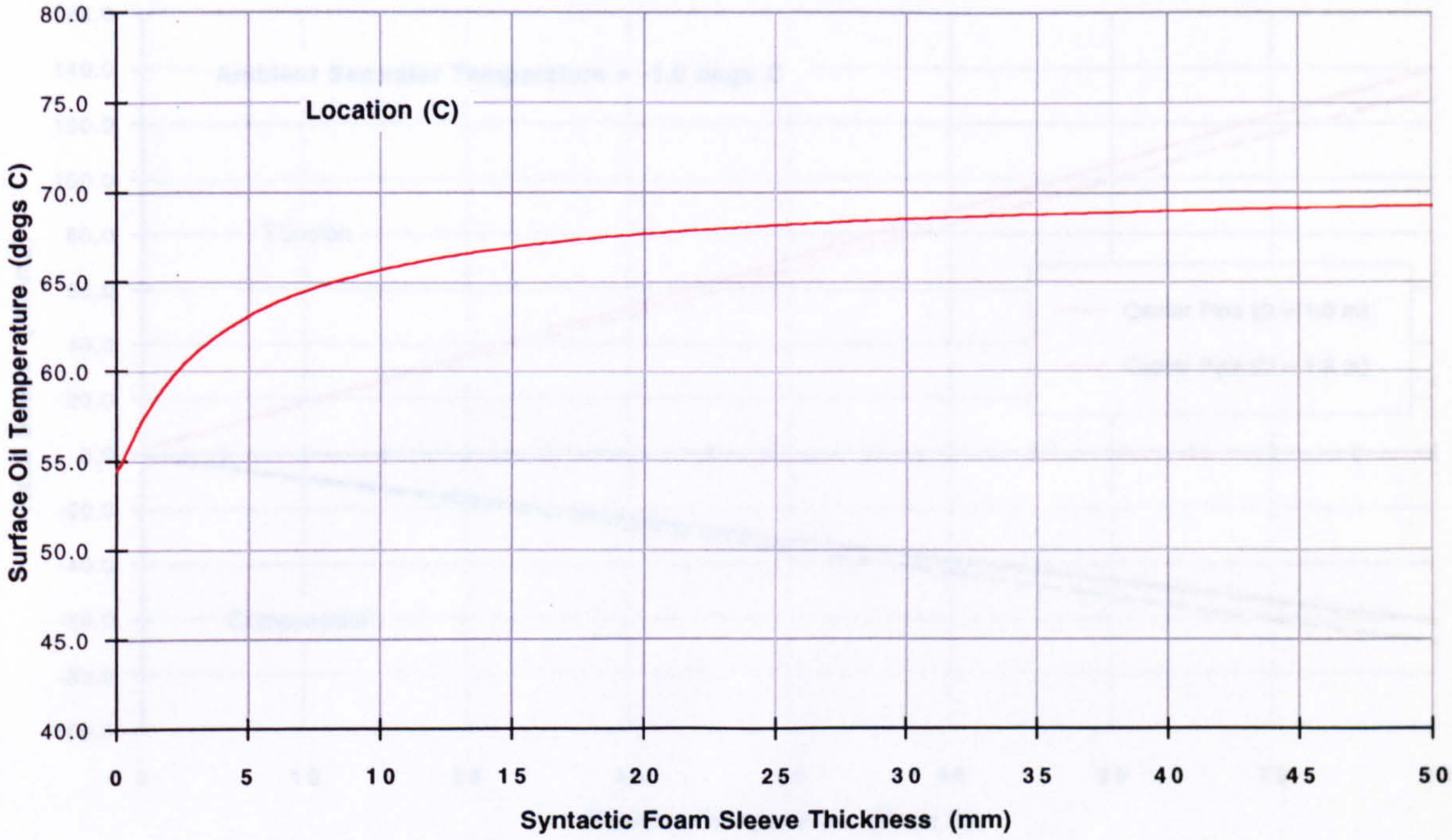

The Effect of Flow Rate on Oil Temperature

(b)

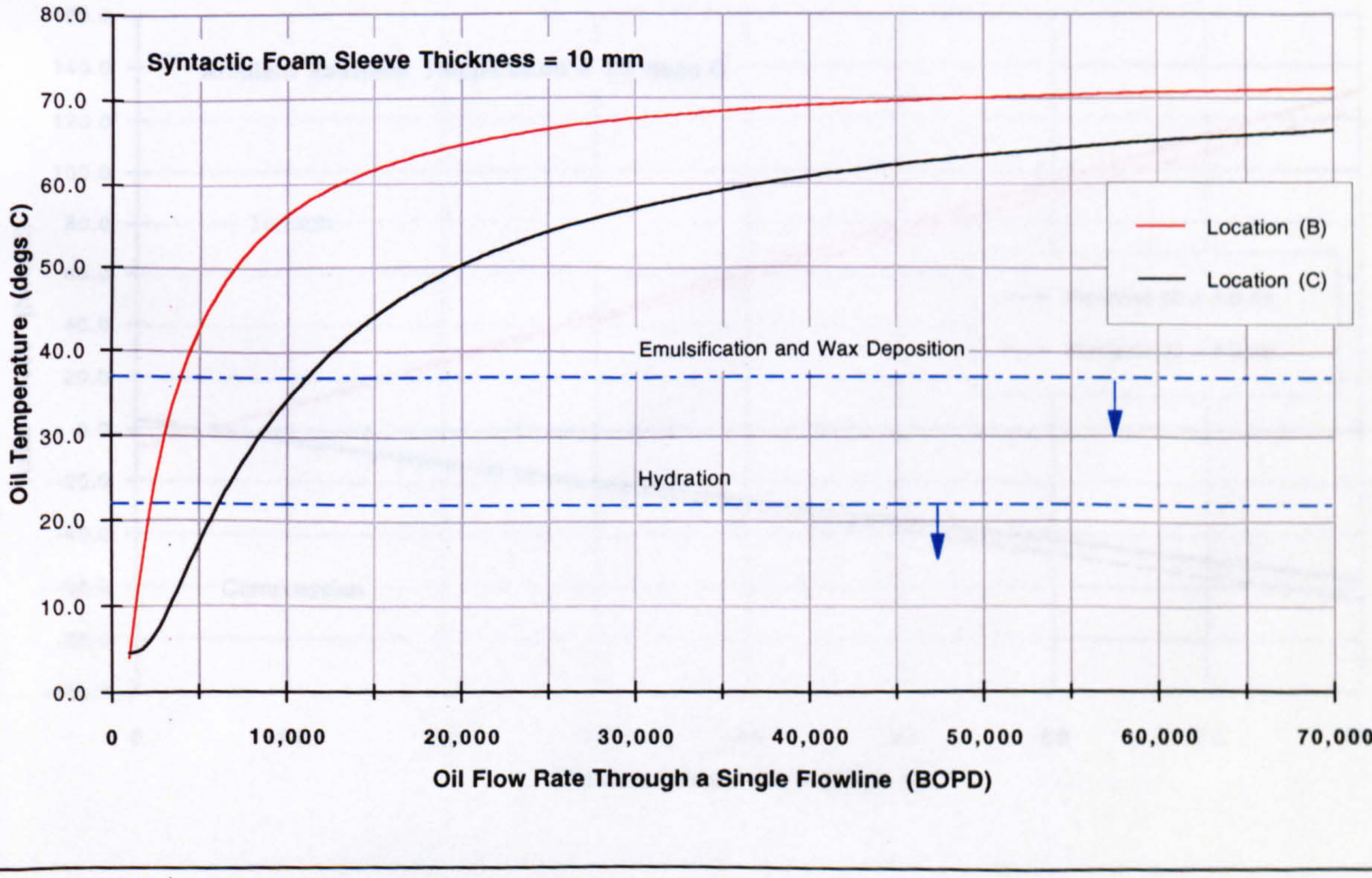

Seabed Pipeline - HSM Slurry

Sea Depth = 1500 m

Catenary Riser - Nitrogen Gas/Syntactic Foam Sleeve

Figure 4.18

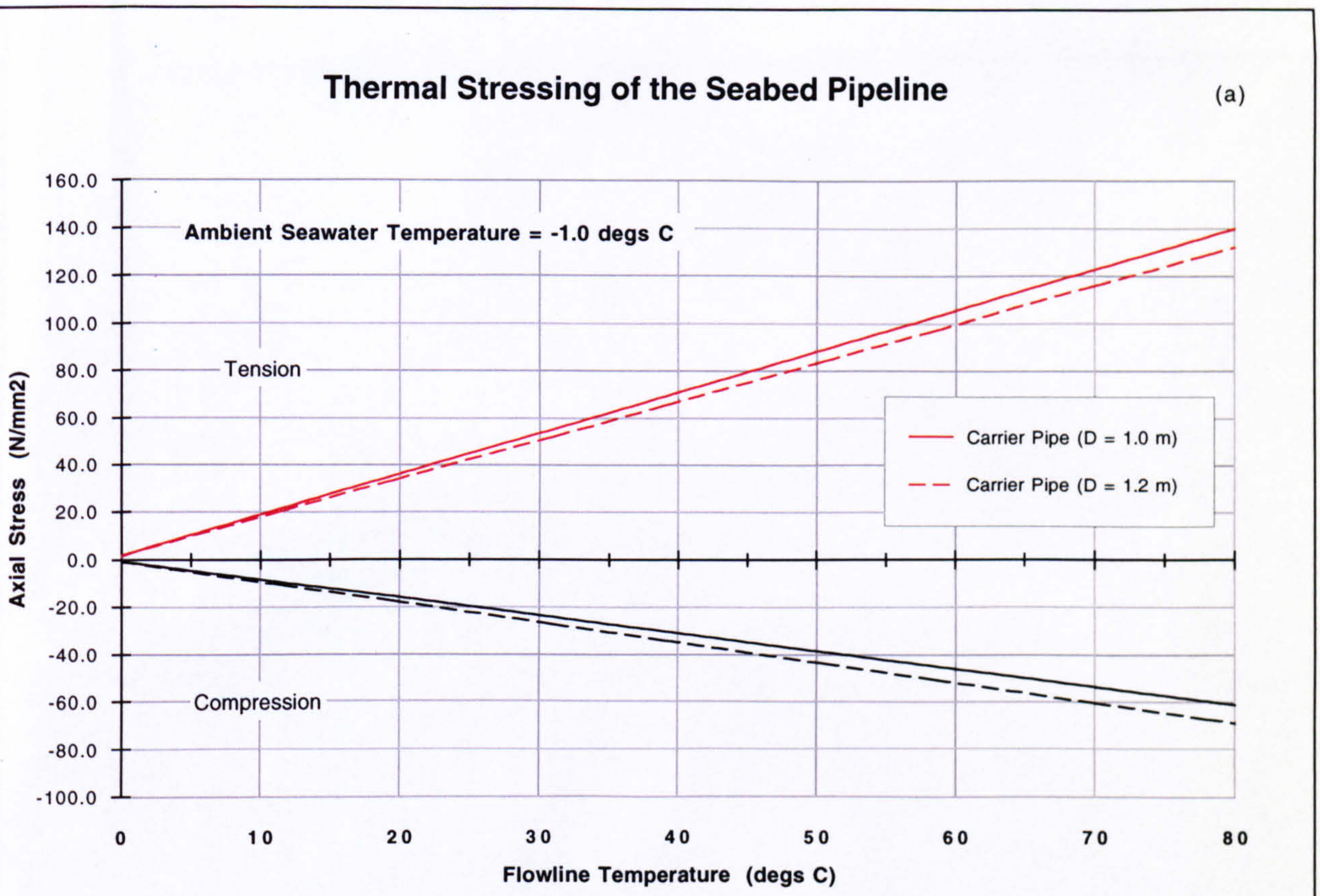

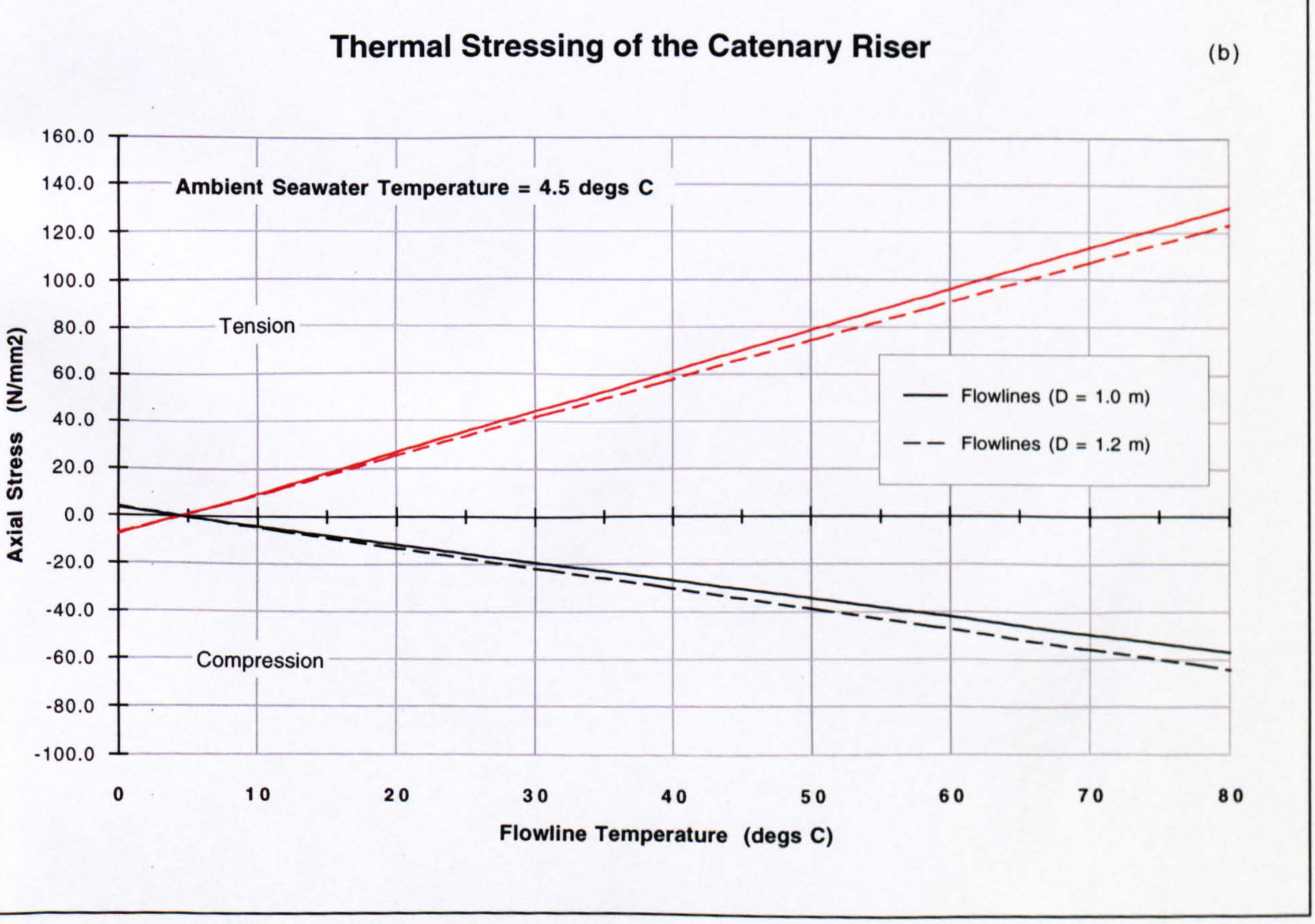

Carrier Pipe Wall Thickness = 10 mm

Coefficient of Linear Thermal Expansion = 1.20 E-05 1/degs C

Figure 4.19